Safety Regulation Group

Civil Aviation
Authority

CAA Paper 2009/02

The Aerodynamics of Gyroplanes

www.caa.co.uk

Safety Regulation Group

CAA Paper 2009/02

The Aerodynamics of Gyroplanes

August 2010

ISBN 978 0 11792 234 1

Published August 2010

List of Effective Pages

Part	Page	Date	Part	Page	Date
	iii	August 2010		25	August 2010
	iv	August 2010		26	August 2010
	v	August 2010		27	August 2010
	vi	August 2010		28	August 2010
Contents	1	August 2010		29	August 2010
Contents	2	August 2010		30	August 2010
Contents	3	August 2010		31	August 2010
CAA Introduction	1	August 2010		32	August 2010
CAA Introduction	2	August 2010		33	August 2010
List of Figures and Tables	1	August 2010		34	August 2010
List of Figures and Tables	2	August 2010		35	August 2010
List of Figures and Tables	3	August 2010		36	August 2010
List of Figures and Tables	4	August 2010		37	August 2010
List of Figures and Tables	5	August 2010		38	August 2010
List of Figures and Tables	6	August 2010		39	August 2010
List of Figures and Tables	7	August 2010		40	August 2010
Executive Summary	1	August 2010		41	August 2010
Glossary	1	August 2010		42	August 2010
Glossary	2	August 2010		43	August 2010
Glossary	3	August 2010		44	August 2010
Glossary	4	August 2010		45	August 2010
Glossary	5	August 2010		46	August 2010
	1	August 2010		47	August 2010
	2	August 2010		48	August 2010
	3	August 2010		49	August 2010
	4	August 2010		50	August 2010
	5	August 2010		51	August 2010
	6	August 2010		52	August 2010
	7	August 2010		53	August 2010
	8	August 2010		54	August 2010
	9	August 2010		55	August 2010
	10	August 2010		56	August 2010
	11	August 2010		57	August 2010
	12	August 2010		58	August 2010
	13	August 2010		59	August 2010
	14	August 2010		60	August 2010
	15	August 2010		61	August 2010
	16	August 2010		62	August 2010
	17	August 2010		63	August 2010
	18	August 2010		64	August 2010
	19	August 2010		65	August 2010
	20	August 2010		66	August 2010
	21	August 2010		67	August 2010
	22	August 2010		68	August 2010
	23	August 2010		69	August 2010
	24	August 2010		70	August 2010

Part	Page	Date	Part	Page	Date
	71	August 2010		119	August 2010
	72	August 2010		120	August 2010
	73	August 2010		121	August 2010
	74	August 2010		122	August 2010
	75	August 2010		123	August 2010
	76	August 2010		124	August 2010
	77	August 2010		125	August 2010
	78	August 2010		126	August 2010
	79	August 2010		127	August 2010
	80	August 2010		128	August 2010
	81	August 2010		129	August 2010
	82	August 2010		130	August 2010
	83	August 2010		131	August 2010
	84	August 2010		132	August 2010
	85	August 2010		133	August 2010
	86	August 2010		134	August 2010
	87	August 2010		135	August 2010
	88	August 2010		136	August 2010
	89	August 2010		137	August 2010
	90	August 2010		138	August 2010
	91	August 2010		139	August 2010
	92	August 2010		140	August 2010
	93	August 2010		141	August 2010
	94	August 2010		142	August 2010
	95	August 2010		143	August 2010
	96	August 2010		144	August 2010
	97	August 2010		145	August 2010
	98	August 2010		146	August 2010
	99	August 2010		147	August 2010
	100	August 2010		148	August 2010
	101	August 2010		149	August 2010
	102	August 2010		150	August 2010
	103	August 2010		151	August 2010
	104	August 2010		152	August 2010
	105	August 2010		153	August 2010
	106	August 2010		154	August 2010
	107	August 2010		155	August 2010
	108	August 2010		156	August 2010
	109	August 2010		157	August 2010
	110	August 2010		158	August 2010
	111	August 2010		159	August 2010
	112	August 2010		160	August 2010
	113	August 2010		161	August 2010
	114	August 2010		162	August 2010
	115	August 2010		163	August 2010
	116	August 2010		164	August 2010
	117	August 2010		165	August 2010
	118	August 2010		166	August 2010

Part	Page	Date	Part	Page	Date
	167	August 2010	Appendix 4	3	August 2010
	168	August 2010	Appendix 4	4	August 2010
	169	August 2010	Appendix 4	5	August 2010
	170	August 2010	Appendix 4	6	August 2010
	171	August 2010	Appendix 4	7	August 2010
	172	August 2010	Appendix 4	8	August 2010
	173	August 2010	Appendix 4	9	August 2010
	174	August 2010	Appendix 4	10	August 2010
	175	August 2010	Appendix 4	11	August 2010
	176	August 2010	Appendix 4	12	August 2010
	177	August 2010	Appendix 4	13	August 2010
	178	August 2010	Appendix 4	14	August 2010
	179	August 2010	Appendix 5	1	August 2010
	180	August 2010	Appendix 5	2	August 2010
	181	August 2010	Appendix 5	3	August 2010
	182	August 2010	Appendix 5	4	August 2010
	183	August 2010	Appendix 5	5	August 2010
	184	August 2010	Appendix 5	6	August 2010
	185	August 2010	Appendix 5	7	August 2010
	186	August 2010	Appendix 6	1	August 2010
	187	August 2010	Appendix 6	2	August 2010
	188	August 2010	Appendix 6	3	August 2010
	189	August 2010	Appendix 6	4	August 2010
	190	August 2010	Appendix 6	5	August 2010
	191	August 2010	Appendix 7	1	August 2010
	192	August 2010	Appendix 7	2	August 2010
	193	August 2010	Appendix 7	3	August 2010
	194	August 2010	Addendum 1	1	August 2010
	195	August 2010	Addendum 1	2	August 2010
Acknowledgements	1	August 2010	Addendum 1	3	August 2010
References	1	August 2010	Addendum 1	4	August 2010
References	2	August 2010	Addendum 1	5	August 2010
References	3	August 2010	Addendum 1	6	August 2010
References	4	August 2010	Addendum 1	7	August 2010
References	5	August 2010	Addendum 1	8	August 2010
References	6	August 2010	Addendum 1	9	August 2010
Appendix 1	1	August 2010	Addendum 1	10	August 2010
Appendix 1	2	August 2010	Addendum 2	1	August 2010
Appendix 1	3	August 2010	Addendum 2	2	August 2010
Appendix 1	4	August 2010	Addendum 2	3	August 2010
Appendix 2	1	August 2010	Addendum 2	4	August 2010
Appendix 2	2	August 2010	Addendum 2	5	August 2010
Appendix 2	3	August 2010	Addendum 2	6	August 2010
Appendix 2	4	August 2010	Addendum 2	7	August 2010
Appendix 3	1	August 2010	Addendum 2	8	August 2010
Appendix 3	2	August 2010	Addendum 2	9	August 2010
Appendix 4	1	August 2010	Addendum 2	10	August 2010
Appendix 4	2	August 2010	Addendum 2	11	August 2010

Part	Page	Date	Part	Page	Date
Addendum 3	1	August 2010	Addendum 3	49	August 2010
Addendum 3	2	August 2010	Addendum 3	50	August 2010
Addendum 3	3	August 2010	Addendum 3	51	August 2010
Addendum 3	4	August 2010	Addendum 3	52	August 2010
Addendum 3	5	August 2010	Addendum 3	53	August 2010
Addendum 3	6	August 2010	Addendum 3	54	August 2010
Addendum 3	7	August 2010	Addendum 3	55	August 2010
Addendum 3	8	August 2010	Addendum 3	56	August 2010
Addendum 3	9	August 2010	Addendum 3	57	August 2010
Addendum 3	10	August 2010	Addendum 3	58	August 2010
Addendum 3	11	August 2010			
Addendum 3	12	August 2010			
Addendum 3	13	August 2010			
Addendum 3	14	August 2010			
Addendum 3	15	August 2010			
Addendum 3	16	August 2010			
Addendum 3	17	August 2010			
Addendum 3	18	August 2010			
Addendum 3	19	August 2010			
Addendum 3	20	August 2010			
Addendum 3	21	August 2010			
Addendum 3	22	August 2010			
Addendum 3	23	August 2010			
Addendum 3	24	August 2010			
Addendum 3	25	August 2010			
Addendum 3	26	August 2010			
Addendum 3	27	August 2010			
Addendum 3	28	August 2010			
Addendum 3	29	August 2010			
Addendum 3	30	August 2010			
Addendum 3	31	August 2010			
Addendum 3	32	August 2010			
Addendum 3	33	August 2010			
Addendum 3	34	August 2010			
Addendum 3	35	August 2010			
Addendum 3	36	August 2010			
Addendum 3	37	August 2010			
Addendum 3	38	August 2010			
Addendum 3	39	August 2010			
Addendum 3	40	August 2010			
Addendum 3	41	August 2010			
Addendum 3	42	August 2010			
Addendum 3	43	August 2010			
Addendum 3	44	August 2010			
Addendum 3	45	August 2010			
Addendum 3	46	August 2010			
Addendum 3	47	August 2010			
Addendum 3	48	August 2010			

Contents

CAA Introduction

List of Figures and Tables

Executive Summary

Glossary

    Abbreviations

    Nomenclature

Report

Flight Testing

Model Validation

Parametric Studies of Configurational Effects

Review of BCAR Section T

Assessment of Rotor Blade Torsion Effects

A Simulation Study of Air Command Autogyros

Investigation of Gyroplane Rotor Teeter Motion

Overall Conclusions

Acknowledgements

References

Appendix 1

Appendix 2

Appendix 3

Appendix 4

Appendix 5

Appendix 6

Appendix 7

Addendum 1

Addendum 2

Addendum 3

INTENTIONALLY LEFT BLANK

CAA Introduction to Glasgow University Report

1 Foreword

Five fatal accidents to Air Command Gyroplanes between April 1989 and March 1991 resulted in CAA requesting that AAIB undertake an Airworthiness review of the Air Command. AAIB produced report EW/101/06 Airworthiness Review of Air Command Gyroplanes dated 12 September 1991. Recommendation 4 of the report (see 2.0 below) was the driver that led to the initial research contract with Glasgow University, requesting CAA to explore the possibility of assisting the gyroplane fraternity in a research programme on aerodynamic and airworthiness characteristics of gyroplanes.

2 AAIB Recommendation

AAIB Report EW/101/06 dated 12th Sept 1991, Airworthiness Review of Air Command Gyroplanes made the following recommendations.

Recommendations:

1 It is recommended that the approved syllabus for prospective gyroplane pilots includes training on a dual control gyroplane.

2 It is recommended that the Authority review its procedures for establishing that an aircraft type has accumulated satisfactory service experience in its country of origin when assessing it for a Permit to Fly

3 It is recommended that the CAA examine the possibility of some devolution of Gyroplane modification approval. This will be facilitated by incorporation of Section T into BCARs at the earliest opportunity.

4 It is recommended that the CAA explore the possibilities of assisting the gyroplane movement to commission a programme of research into aerodynamic and airworthiness characteristics.

3 Report Findings

This comprehensive report represents a significant step forward in the understanding of the aerodynamics of gyroplanes. The conclusions presented are the scientific results of the tests and studies carried out on a limited number of gyroplane designs. The report does not cover all configurations of gyroplane designs and therefore the conclusions may not be directly appropriate to gyroplanes not specifically addressed by the report. It is important to appreciate that it represents the scientific findings of the areas addressed and does not attempt to extrapolate beyond those boundaries as this would be speculation and not appropriate for a scientific research report. Various conclusions have been made in the report and are noted below:

1 CG / Thrustline offset. The recommendation that the vertical location of the centre of mass is within 2 inches of the propeller thrust line is a result of the study and therefore is reported as such. CAA accepts that closer alignment of the CG and the thrustline is a sensible design aim to achieve pitch dynamic stability (phugoid mode) but also has flight test experience of a gyroplane design that achieves good stability but is well outside of the 2 inch criteria. CAA Flight Test Specialist qualitative assessment implies that pitch dynamic stability may not be solely a function of CG/Propeller Thrust alignment for all types of Gyroplane. It is appreciated that in paragraph 8.3.1 (page 152) of the report it is stated that other factors can affect the phugoid mode.

MPD 2005-08 was issued 24 August 2005 mandating, in part, restrictions on pilot experience, V_{NE} and wind/gust speeds for single seat a/c. These could be removed if acceptable evidence was presented to show that the CG/thrustline offset was within ± 2 inches. However other restrictions noted in the MPD would still apply.

Advisory material to BCAR Section T.23 now includes ± 2" criteria.

2   Effect of tailplanes. The report also concludes that horizontal tailplanes are largely ineffective in improving the long term response of pitch dynamic stability (phugoid mode). This is the result of studies primarily on narrow tandem cockpit enclosures. A CAA Flight Test Specialist qualitative evaluation of the effects of a horizontal tailplane on a single side-by-side configuration gyroplane type indicated a degree of improvement in the phugoid characteristics at higher speed. It is appreciated that in paragraph 8.3.1 (page 152) of the report it is stated that other factors can affect the phugoid mode.

3   Teeter Margins. Due to the possibility of excessive teeter angles under certain phases of flight, that can lead to blade strike with the prop, pod or mast, flight tests were undertaken. Flight instrumentation revealed small teeter angles in steady flight conditions, but in one instance during a particularly extreme manoeuvre, the angle reached 8 deg within an 11 deg safe envelope. Testing was limited, and it is difficult to draw meaningful conclusions from the data, other than to recognise that certain more extreme flight conditions will produce teeter angles that may go outside of the safe envelope, and so could lead to a strike on some part of the aircraft.

Advisory material to BCAR Section T.143 (a) is to be revised to require satisfactory control margin and rotor clearance up to $1.1V_{NE}$.

4   Rotor aeroelasticity. One aspect of the fatal accidents over the past two decades that has not been well understood is the sudden loss of rotor speed under certain circumstances. To address this a study was undertaken to review rotor aeroelastic instability. This is a study of the design parameters of the blade (e.g. bending stiffness, torsional stiffness, cg position, lift characteristics, etc.) that affect the behaviour of the blade in certain flight conditions. For gyroplanes the blade is not mechanically driven, but generates lift in an autorotative process, relying on air passing through the disc. Should the blade slow down, lift is reduced. The research modelled the rotor and varied these design parameters to investigate their sensitivity on aeroelastic instability (flutter and divergence). Their research analysed a NACA aerofoil shape supplemented by physical data from a McCutcheon blade.

Results noted that the key parameter to blade instability is the torsional dynamic behaviour. To this end the research concluded that a safe rule of thumb would be to ensure the blade chordwise cg was always forward of the 25% chord. This would allow for the most pessimistic case of a blade with zero torsional stiffness, and supports the current Section T 659 (b) requirement. CAA accepts this finding yet notes that the stabilising affect of a number of other parameters was not exhaustively investigated during this limited research, which would allow for CAA acceptance of alternate means of compliance to this requirement that demonstrates blade stability.

BCAR Section T 659 currently requires blades to have chordwise cg at or forward of 25% chord.

List of Figures and Tables

Appendix 3

Appendix 4

Appendix 5

Appendix 6

Appendix 7

INTENTIONALLY LEFT BLANK

Executive Summary

This report describes all work undertaken for the Civil Aviation Authority between November 1993 and June 2008 under the study entitled "Aerodynamics of Gyroplanes" and whose genesis is to be found in the 1991 Air Accidents Investigation Branch review of the airworthiness of Air Command series of gyroplanes. One recommendation of that review was the commissioning of a programme of research into the aerodynamic and airworthiness characteristics of light gyroplanes in general. Accordingly, the Authority tasked the University of Glasgow with this work, and subsequent associated studies, by means of analytical, wind tunnel and flight test activities.

The fundamental approach to such problems is to build a mathematical engineering model of the aircraft so that design features, changes or hypothetical situations can be examined in safety. However, such a model requires validation against actual flight test data in order that a degree of confidence in its predictive capability can be established. This methodology is consistent with contemporary industry practice, and was the one adopted here. Accordingly, much of the work undertaken focussed on checking the fidelity of the model against flight test data gathered during a number of campaigns using two fully instrumented light gyroplanes: a VPM M16 Tandem Trainer; and a Montgomerie-Parsons Two-Place (Modified) aircraft. These trials used specialised flight test techniques involving stylised and, to the lay pilot, unusual control inputs. The resulting data were then analysed using sophisticated mathematical analysis techniques, again typical of that used in industry and national research laboratories worldwide.

The resulting validation confirmed that the model offered very good to excellent fidelity in most aspects associated with the prediction of vehicle behaviour, certainly well up to the level obtained by other agencies with helicopter modelling. As a result the model was deemed suitable for use in a parametric study that posed a range of questions; e.g. what if the tailplane is removed; what if the mass is increased; what if the rotor is raised on the airframe. It was discovered that the static and dynamic stability, and hence compliance with BCAR Section T, is sensitive to the vertical location of the centre of mass in relation to the assumed propeller thrust line and this was found to be the case across the speed range. No other parameter had any significant effect on the aircraft's likelihood of satisfying BCAR Section T. The simulation study, together with an analysis of BCAR Section T made in the context of the VPM M16 flight trials, resulted in the advisory recommendation that light gyroplanes certified against Section T should ensure that the vertical location of the centre of mass is within 2 inches of the propeller thrust line. A handling study of five single-seat gyroplanes was made independently by the Civil Aviation Authority, and it was found that only one satisfied Section T dynamic stability requirements - that was the machine that was specifically modified to comply with the 2 inch recommendation thereby providing independent verification of this recommendation. These data are also included in this report.

The Report also presents results from a number of associated studies. First, a literature review highlights a body of work that has increased during the 16 years this research has taken place, indicating a growing interest in the gyroplane configuration although there remains little indication that rigorous scientific or engineering investigation of airworthiness has occurred. Second, a study of teeter margin is truly unique in terms of the instrumentation design and installation, the flight trial itself and the data analysis. Coming as it did at the end of the work is testament to growth in the confidence with which gyroplane problems can be tackled, and indicates that adequate teeter margin exists in all but the most extreme dynamic response situations. Finally an assessment of blade flexibility on rotor and aircraft stability, and a review of BCAR Section T completes the Report.

INTENTIONALLY LEFT BLANK

Glossary

1   Abbreviations

AAN	Airworthiness Approval Note
AIAA	American Institute of Astronautics and Aeronautics
BCAR	British Civil Airworthiness Requirements
CAA	Civil Aviation Authority
DOF	Degrees of Freedom
FAA	Federal Aviation Administration
ISA	International Standard Atmosphere
NACA	National Advisory Council on Aeronautics
NASA	National Aeronautics and Space Administration
NASA STAR	NASA Scientific and Technical Aerospace Reports
RAE R and M	Royal Aeronautical Establishment, Research and Memoranda
RASCAL	Rotorcraft Aeromechanics Simulation for Control Analysis
VZLU	Czech National Aeronautical Research and Test Institute

2   Nomenclature

A	System matrix	
a_x, a_y, a_z	Absolute accelerations measured by accelerometers	m/s^2
B	Control matrix	
c	Effective damping	
c_{crit}	Critical damping (i.e. $\zeta = 1$)	
CL	Aircraft rolling moment coefficient from wind tunnel data	
CM	Aircraft pitching moment coefficient from wind tunnel data	
CN	Aircraft yawing moment coefficient from wind tunnel data	
CX	Aircraft thrust coefficient from wind tunnel data	
CY	Aircraft side force coefficient from wind tunnel data	
CZ	Aircraft normal force coefficient from wind tunnel data	
CD	Drag coefficient	
CL	Lift coefficient	
C_{Lmax}	Maximum lift coefficient	
C_m	Pitching moment coefficient	
C_{m_0}, C_{m_a}	Coefficients of pitching moment expression	
C_t	Propeller thrust coefficient	
D	Rotor diameter	m
d	Propeller diameter	m
g	Acceleration due to gravity	m/s^2
h	Altitude	m
I	Identity matrix	
$\mathbf{I}_{xx}$	Aircraft moment of inertia about x-axis	kg m^2
$\mathbf{I}_{yy}$	Aircraft moment of inertia about y-axis	kg m^2
$\mathbf{I}_{zz}$	Aircraft moment of inertia about z-axis	kg m^2
$\mathbf{I}_{xz}$	Aircraft product of inertia	kg m^2
J	Advance ratio	
k	Scale correction factor	
l	Distance from nose wheel to main undercarriage	m
L, M, N	External moments (roll, pitch, yaw)	Nm
m	Mass of aircraft	kg
N_g, N_r	Measured propeller and rotor speeds	rev/min
P	Roll rate (+ve roll to starboard)	rad/s
p	Perturbation in roll rate from reference trim state	rad/s
Q	Pitch rate (+ve nose up)	rad/s

q	Perturbation in pitch rate from reference trim state	rad/s
Q	Main rotor torque	Nm
R	Yaw rate (+ve nose to starboard)	rad/s
r	Perturbation in yaw rate from reference trim state	rad/s
R	Rotor Radius	m
R_e	Reynolds number	
T	Rotor thrust	N
T	Period of an oscillatory mode	s
t_{half}	Time to half amplitude of stable mode	s
t_{double}	Time to double amplitude of unstable mode	s
U	Fore and aft component of velocity (+ve forward)	m/s
u	Perturbation in fore and aft component of velocity	m/s
$\underline{u}$	Control vector	
u_{probe}, v_{probe}, w_{probe}	Component air velocities measured by air data probe	m/s
V_f	Indicated airspeed	m/s
V_w	Wind tunnel flow velocity	m/s
V	Lateral (sideslip) component of velocity (+ve to starboard)	m/s
v	Perturbation in lateral (sideslip) component of velocity	m/s
v_0, v_{1s}, v_{1c}	Component of rotor inflow	m/s
W	Vertical component of velocity (+ve downwards)	m/s
w	Perturbation in vertical component of velocity	m/s
W	Weight of aircraft (c.g. calculation)	N
W_{nose}	Weight measured by load cell under nose wheel (c.g. calc)	N
W_L, W_R	Weights measured by load cells under left and right wheels (c.g. calculation)	N
X, Y, Z	External forces	N
$\underline{x}$	State vector	
x_{cg}, z_{cg}	Position of aircraft centre of gravity w.r.t. reference point	m
x_{probe}, y_{probe}	Positon of tip of air data probe with respect to fuselage	m
x_E, y_E, z_E	Aircraft position as measured by GPS	m
z_{probe}	datum point	m
α	Angle of attack (+ve nose up)	rad
α_{vane}	Angle of attack measured by air data probe vane	rad
β	Sideslip angle (+ve to port)	rad
β_{1c}, β_{1s}	Rotor disc orientation (long, lat) in multi-blade co-ords	rad
β_{vane}	Angle of sideslip measured by air data probe vane	rad

γ_t	Teeter angle		rad
δ	bias or offset correction		
δ_r	Rudder deflection	(+ve to port)	rad
$\delta_e, \delta_a, \delta_t$	Control inputs for fixed wing aircraft (elevator, aileron, throttle)		rad
ε	Error function		
η_s, η_c	Longitudinal and lateral stick displacement		rad
η_p	Pedal displacement		
$\eta_\square$	Throttle position		
Φ	Bank angle	(+ve roll to starboard)	rad
ϕ	Perturbation in bank angle from reference trim state		rad
λ	eigenvalue		
Θ	Pitch angle	(+ve nose up)	rad
θ	Perturbation in pitch angle from reference trim state		rad
θ	Keel inclination angle in c.g. calculation		rad
μ	Absolute viscosity of air		kg/ms
Ψ	Aircraft heading (+ve to starboard, measured from North)		rad
ψ	Blade azimuth position		rad
ρ	Density of air		kg/m3
ω_n	Natural frequency		rad/s
ω_d	Damped natural frequency		rad/s
Ω	Rotorspeed		rad/s
Ω_{ss}	Rotorspeed in steady state (trimmed) flight		rad/s
ζ	Damping ratio		

Subscripts

b	Body fixed axes set
cg	Centre of gravity
e	Equilibrium flight state (reference trim state)
E	Earth fixed axes set
ph	Phugoid Mode
probe	Located at the pressure transducer in air data boom
sp	Short period mode
vane	Located at the vane on air data boom

Stability Derivatives

Stability (or aerodynamic) derivatives are expressed in the form: A_b, where:

$$A_b = \left(\frac{\partial A}{\partial b} \right)_e$$

that is the change in an external force or moment A with respect to a small perturbation in a state or control b, evaluated at a reference trim state (denoted by the subscript e). For example:

$$X_u = \frac{\partial X}{\partial u}$$

= perturbation in X- force due to perturbation in forward velocity, u (known as speed damping)

$$M_q = \frac{\partial M}{\partial q}$$

= perturbation in pitching moment, M due to a perturbation in pitch rate q (known as pitch damping),

$$Q_\Omega = \frac{\partial Q}{\partial \Omega}$$

= perturbation in rotor torque, Q due to a perturbation in rotorspeed Ω

INTENTIONALLY LEFT BLANK

The Aerodynamics of Gyroplanes

1   Introduction

1.1   Background

The emergence of the gyroplane aircraft in the 1920's and '30's paved the way for the development of the helicopter in the 1940's. Many of the technical problems associated with rotary wing flight had been discovered and rectified by the early gyroplane pioneers, most notably Juan de la Cierva's solution of installing flapping hinges to accommodate non-symmetric lift from the rotor blades. The development of the gyroplane receded as the helicopter became more popular and successful. In recent years, however, there has been a resurgence of interest in this type of aircraft both as a recreational aircraft and as a low cost alternative to the helicopter with companies such as Groen and Cartercopter both seeking to market gyroplane configurations to commercial and military operators.

In the UK the gyroplane is very much the domain of the private hobby flyer where the aircraft is often purchased in kit form and built by the owner. Although the number of gyroplanes registered in the UK is relatively small compared to, say, microlights or light aircraft, gyroplane owners are often extremely enthusiastic and the UK gyroplane community is a very active one. Despite (or in some part due to) the popular belief that these aircraft are naturally stable, and that flying them was no more difficult than piloting a light aircraft, a series of accidents between 1989 and 1991 occurred in the UK. The statistics show 6 fatalities per 1000 hours of flying time during this period for this type (compared to 0.015 per 1000 flying hours for general aviation). Given the small number of aircraft of this type registered in the UK, this was clearly an unacceptable situation.

Investigation of these accidents was hindered by a lack of contemporary published research into this type of vehicle, particularly in its aerodynamic characteristics, its flight dynamics and flying qualities. The Air Accidents Investigation Branch recommended that the CAA undertake appropriate research in these areas to support a major review of the British Civil Airworthiness Requirements for gyroplanes (BCAR Section T). The aim was to improve the design standard of gyroplanes in the UK and so improve their safety. A contract was awarded to the Department of Aerospace Engineering, University of Glasgow in 1993. As the project developed, it became clear that additional research was necessary, and over the period from 1993 to 2008 a series of related research projects were commissioned by the CAA. The findings of the various research projects have been fully reported in individual contract reports. The purpose of this report is to set the various individual projects into context with the main findings presented in an accessible manner, and to provide a single source of reference for all of the research. This report has been structured to provide the most logical route through the research, rather than a chronological list of project descriptions.

1.2   Fundamental Research

Early efforts at investigating the gyroplane accidents mentioned above were hampered by insufficient contemporary research material being available. In particular, there were suggestions that some of the accidents might have been caused by dynamic instability. Further, some of the accidents involved aircraft which had been modified by the owner; for example, the fuselage pod removed to give an open framed vehicle. One of the first tasks undertaken in 1993 was a literature

review. This was updated in 2007, and the results are presented in Section 2, with the papers found listed in the references. This review showed an almost complete lack of material on the flight dynamics of gyroplanes, and no detail whatsoever on the aerodynamic properties. It was clear then that wind tunnel tests would be required to establish, in the first instance, whether changes to the basic configurational design of a gyroplane (tailplane, fin, pod etc.) might have any significant effect on its aerodynamic characteristics. The results from an extensive series of wind tunnel tests (see Appendix 1 for the test matrix) using a model of a typical gyroplane configuration are presented in Section 3.

The approach used to study the dynamic stability characteristics of the gyroplane was to modify an existing rotorcraft mathematical model to represent a gyroplane configuration. This required creating a data set of parameters representing the gyroplane to be simulated (mass, inertia, geometry etc.) – see Appendix 2. An important parameter is the location of the centre of gravity, and a practical method of achieving this is detailed in Appendix 3. The aerodynamic coefficients measured in the wind tunnel tests also form part of this data set. There were therefore two reasons for performing the wind tunnel tests described in Section 3; to investigate whether configurational changes can have any substantial influence on aerodynamic loading, and to provide data for the simulation.

1.3   Simulation and Model Validation

The simulation used for this study, RASCAL, was developed in a modular and generic form and so its conversion from primarily helicopter simulation to gyroplane simulation was a relatively straightforward process, which is described in Section 4. The resulting model is nonlinear and includes all body, rotor speed, teeter (flap) and inflow degrees of freedom. Each blade on the rotor and propeller is represented as an individual component with its own degrees of freedom. The model is used to calculate trim states, response to controls and dynamic stability characteristics. It is appreciated that many readers will be unfamiliar with the theory involved, and the terminology used, and so Section 4 is supported by a "tutorial" in the theoretical calculation of dynamic stability, given in Appendix 4. It is recommended that Appendix 4 be read before Section 4.

An essential element of any simulation development is its validation. This involves comparing the results from the simulation with those measured from the real system. In the case of the gyroplane, validation is achieved by comparing results from RASCAL with data measured in flight. As described in Section 5, a total of 3 flight test campaigns were carried out to collect sufficient data to successfully validate the model. In the first trials, data from a VPM M16 aircraft was collected. Then, to provide dissimilar data, a Montgomerie-Parsons aircraft was tested. In a third series of trials, the focus was on the rotor teeter dynamics (see Section 11) and, again, the Montgomerie-Parsons aircraft was used. The flight test instructions for this final trial are given in Appendix 5.

The validation process itself is discussed in Section 6 of the report with comparisons made between trim states, aircraft response to controls, and stability derivatives. Significant post processing of flight data is necessary before validation can take place, and the theory behind this is presented in Appendix 6 and Appendix 7.

1.4   Application of Research

Having discussed the development of the mathematical model and established its validity, it is now possible to use the simulation to investigate specific issues relating to the flight characteristics of gyroplanes. As mentioned above, during the period in the early 1990's when the gyroplane accident rate was at its highest, there was a

certain level of evidence (often anecdotal and always unsubstantiated) that changes to basic configuration had contributed to some of the accidents. Armed with the results of the wind tunnel trials described in Section 3, it was possible to carry out parametric studies varying many of the key design parameters which define the gyroplane configuration. The results from the parametric studies are given in Section 7. This research has identified the vertical location of centre of gravity with respect to the propeller thrust line as the parameter which is most influential in the dynamic stability of gyroplanes. This result, and much of the other research carried out in this study, has fed into the development of the airworthiness requirements for light gyroplanes, BCAR Section T. A review of these requirements, and a description of the contributions of this research to their formulation is given in Section 8. Two technical papers supporting this work are included as Addenda to this report. Rotor blade torsional effects are included in the mathematical model, and the influence this has on the simulation results is discussed in Section 9. A third Addendum is provided giving further insight into aeroelastic properties of gyroplane rotors. An investigation of a specific gyroplane type, the Air Command, is presented in Section 10, whilst unique results from tests to measure blade teeter angle in flight are given in Section 11. This report is concluded with a discussion of the main conclusions which have emerged from the research in Section 12.

2   Literature Survey

It was clear from the very early stages of the research in 1993 that there was little contemporary published research into gyroplane aerodynamics or flight dynamics. The aim of the literature survey was to identify as much relevant information as possible. Having obtained this information, the next task was to acquire copies of the identified literature where possible. During the course of the research from 1993 – 2006, further relevant research has been published, perhaps stimulated by the activities at Glasgow University, but certainly due to a resurgence in interest in the use of the gyroplane in commercial and military roles. A second, internet-based literature review was therefore undertaken in 2007, and these results are also incorporated here.

2.1   Methodology

The initial survey was carried out in 1993 and was composed of three main sources of information - a PC based CD ROM database available in Glasgow University Library, a computer search of the main technical archives, and a search of the Department of Aerospace archives. A more recent survey in July 2007 was conducted using internet resources. Brief details of the methodology adopted are given below.

a) **CD ROM Database**

   This database contains citations from all of the major science and engineering journals (including all of the AIAA publications and the Journal of the American Helicopter Society). Discs for the years 1987 - 1993 are available in Glasgow University Library and these were searched using appropriate keywords (gyroplane, gyrocopter, autogyro etc.) and various citations recorded.

b) **Computer Search**

   A wider computer search was undertaken with the assistance of library staff. This included accessing databases such as the NASA STAR archives and, as with the CD ROM search, appropriate keywords were entered and a series of citations recorded.

c) **Departmental Archive**

Until the mid 1970's the Department of Aerospace Engineering at Glasgow University maintained a comprehensive collection of NACA/NASA and RandM/RAE technical reports. The catalogues of these collections are still largely intact and were used to obtain references to a series of gyroplane related documents.

d) **Internet Search**

The most popular search engines (Yahoo, Google Scholar) were used with appropriate keywords to obtain lists of references. More specialised sites such as AIAA and the NASA Technical Report Server were also used. This search returned many of the papers previously found in the earlier reviews carried out in 1993, however a number of additional papers were also discovered dating from before 1993 which had not been uncovered in the original search. Many papers published after the original search were, of course, also found.

2.2 **Results of Literature Review**

2.2.1 **General**

The gyroplane helped to pave the way for the development of the helicopter, introducing cyclic pitch control and blades attached to the rotor hub by means of a hinge. Unfortunately the literature available before the current research was undertaken did not specifically address vehicle stability and control. The literature on gyroplanes is nonetheless considerable. However, in a contemporary context, much of the early work is now primarily of historical significance. It provides the basis of the understanding of gyroplane flight but does not address the issues of stability and control. Examination of the literature shows a logical development of the study of gyroplanes, from the elementary theory of gyroplane flight to an analysis of aerodynamics and performance and ultimately rotor behaviour, but only for steady flight. Interest then apparently waned and the next logical stage in the study of the gyroplane, i.e. stability and control, was not examined.

2.2.2 **Published work pre–1940**

The early work on the dynamics and aerodynamics of rotary wings was mainly in support of the development of gyroplanes. Most notable amongst the early work is that of Glauert [3, 5, 7] who developed methods for calculating rotor loadings and also investigated the flapping motion of the blades. The rotor theory produced by Glauert (which is still widely used today) was complemented by wind tunnel tests of gyroplane rotors by Lock [4, 6, 7]. The work of Glauert and Lock in the 1920s was advanced in the U.S.A. by Wheatly who, between 1932 and 1937, again concerned himself primarily with the aerodynamics and dynamics of the rotor and also included some wind tunnel testing [8–21]. The greater potential of the helicopter saw the emphasis shift from unpowered to powered rotors from the late thirties onwards, and NACA's interest in the gyroplane then seemed to wane, with only Bailey [22, 23] continuing the work initiated by Wheatley. A couple of review papers written for NACA also appeared during this era, Bregeut [24] and Schrenk [25]. The natural progression from aerodynamics and dynamics through to stability and control seems therefore not to have been made for the case of the gyroplane. Consequently there appears to be no definitive study of the flight mechanics of a gyroplane. Likewise, although there were many wind tunnel studies of gyroplane rotors there appear to have been few of a gyroplane fuselage and empenage.

2.2.3   **Published work 1941–1959**

Towards the 1940s as the helicopter became a practical proposition, rotorcraft research really focused on helicopter issues, and there is almost no mention in published literature of the gyroplane aircraft again until the 1960s.

2.2.4   **Published work 1960–1993**

Perhaps due to increased use as a sport or recreational vehicle, technical papers specifically dealing with gyroplane issues began to re-emerge during the 1960s. One of the main exponents of the gyroplane was, of course, Wallis who published details of his design in the Aeronautical Journal in 1963 [26]. Later in 1965, Schad [27] published details of performance trials of Bensen and Avian gyroplanes, whilst interest from academia appeared in the form of a Masters Thesis by Niemi [28]. Also around this time Mouille [29] published a detailed analysis of the Turbogyre 330 gyroplane for Agard. Also in this era, the notion of using autorotation to decelerate spacecraft on re-entry into the earth's atmosphere was proposed, and papers by Levin and Smith [30] and by Barzda [31] presented details of proposed systems.

Little appeared in the literature again until 1974 when Liss [32] published a theoretical analysis of the deformation of a rotor blade in autorotative flight. The first indication of handling problems associated with gyroplanes was reported by Przybylski et al [33] at the 2nd European Rotorcraft Forum in 1976. They report on an investigation into the lack of responsiveness of a light gyroplane to nose down inputs at certain rotorspeeds. Johnson [34] used data gathered in flight tests using a gyroplane to validate a wake model by comparing lateral flapping angles. The only other works of interest are that of Nicholls et al [35] on the nature of gyroplane accidents which had been occurring in Australia, and that of McKillip [36] who reports on the instrumentation required to record data from a rotor of a towed gyroplane.

Due to the historical significance of the gyroplane there are citations in many rotorcraft and aeronautical textbooks [37 - 40]. Mainly, these citations are concerned with the evolution of rotorcraft rather than dealing specifically with the gyroplane.

2.2.5   **Published work 1994–present**

During the course of this research the popularity of the gyroplane as a sport aircraft has increased. It is its re-emergence as a potentially useful vehicle for commercial or military operations, however, which has led to an upsurge in the volume of published literature. Shippen [41, 42] published his findings from a flight test programme to record control stick forces in flight. The aim was to determine the reason for a previous in-flight failure. Interest in the gyroplane in Spain led to an analytical review by Lopez-Diez et al [43] of aspects of the control of the Cierva C30 gyroplane, which led to a more topical study of possible applications for the gyroplane by comparing its performance to that of the helicopter in various roles [44]. Rapp et al [45] also reported on an experimental measurement of blade loads in flight in 2000. Various other authors [46–51] have used contemporary techniques to analyse various aspects associated with gyroplanes: rotor aerodynamics [46, 47], performance [48], and aircraft design [49–51].

As in other areas of aviation, the idea of an unmanned gyroplane has received some attention in the past few years [52–55]. Further, and as mentioned above, there is a re-emergence of interest in the gyroplane concept for commercial and military use, most notably from the Groen Brothers and Carter Aviation Technologies in the USA. Both companies have produced a small number of publications of a technical nature with most of their output naturally being of a promotional nature [56–58]. There have also been a couple of papers reflecting on historical aspects of the gyroplane [59–60], most notably the work by Leishman [60] which is rich in technical content as well as historical background.

2.2.6 **Publications Arising from this Study**

A number of papers reporting work arising directly and indirectly from this study have been published. Their content will be discussed in detail throughout this report however, for convenience, they are listed together in the references [61–78]

2.3 **Conclusions**

In the early days of this study there was very little useful information concerning the dynamic stability of gyroplanes available in published works. Similarly, there was no literature available pertaining to the aerodynamics of the gyroplane as a complete vehicle. Through the course of this study the available literature has grown in no small part through the efforts of the researchers, but also due to resurgence of interest in the gyroplane configuration. Although the more recent material is of interest, none of it has been of direct relevance to the current study which remains unique in its breadth and depth of investigation into gyroplane aerodynamics and flight dynamics. The policy adopted throughout by the researchers of publishing their findings in learned, refereed journals has been a very important and significant outcome of the work as it has greatly enhanced the quantity and quality of openly available technical information on the gyroplane, particularly in relation to the location of the propeller thrust line relative to the centre of gravity.

3 Wind Tunnel Testing

3.1 **Introduction**

A scale model of a VPM M14 gyroplane was tested in the 3m low speed wind tunnel at the Aeronautical Research and Test Institute (VZLU) in Prague in the Czech Republic. The results from this test series were analysed and then utilised in the mathematical model used throughout this study.

The wind tunnel test programme described below had two distinct aims. The first was to provide basic aerodynamic data on the effects of gyroplane configurational characteristics with a view to assessing the degree to which specific design features, such as cowlings and tailplanes, are beneficial to gyroplane performance. Secondly, it was intended to provide aerodynamic data for input to mathematical models to facilitate parametric studies of static and dynamic stability.

3.2 **Wind Tunnel Facility**

The tests were conducted in the VZLU 3m Low Speed Wind Tunnel. This institute has provided high quality wind tunnel facilities for the Czech aircraft industry for many years and is highly regarded throughout the world. The particular wind tunnel used in this study is an atmospheric open-section, closed return, Gottigen style tunnel with a maximum velocity of around 60m/s. Forces and moments were measured on a six component fully-automatic overhead gravitational balance which is accurate to between 0.01% and 0.05% full scale.

3.3 **Wind Tunnel Model**

The model used in this study was a powered, one-third scale model of a VPM-M14 gyroplane minus rotor. It is normal, in rotorcraft testing, to carry out wind tunnel tests without the rotor since scaling considerations of a combined rotor-fuselage configuration would require the use of a very large test facility and would be prohibitively expensive. A VPM M16 model ideally would have been used, however there were no sufficiently accurate engineering drawings of this vehicle available. Accurate drawings of the M14 were available and the decision to build this model was taken on the grounds that the basic configuration of the VPM M14 was typical of light

gyroplanes of this type, and the two vehicles used in this study (the VPM M16 and Montgomerie-Parsons) were so similar that there would be no major differences in their aerodynamic properties from those of the VPM M14.

The basic model frame was constructed from metal box-section on which was mounted a water-cooled motor. This motor was connected by a toothed-belt to the propeller drive system. The removable tailplane assembly was fabricated in aluminium as were the representations of the aircraft wheels and wheel-covers. A scaled representation of the VPM-M14 cowling was made from glass fibre. In addition to the basic features of the aircraft, it was necessary to model the aerodynamic effect of the pilot. This was achieved by creating a representation of the pilot's upper-body which was mounted in an appropriate position on the model frame. The pilot's lower body was adequately represented by the motor which was positioned just above the main spar. A diagram of the model is shown in Figure 3.1, whilst Figure 3.2 shows a photograph of the complete model, and Figure 3.3 shows the installation of the motor.

3.4   Test Set-up

The model was mounted in inverted mode on the wind tunnel balance via a series of connecting wires as shown in Figure 3.4. Services to and from the motor were provided by a shrouded conduit which was located centrally above the model. This conduit not only provided a power supply for the model but also housed the water pipes necessary for the motor cooling system. The angle of attack and sideslip settings were automatically adjusted using the balance control system. Rudder deflection was achieved manually.

The model was tested in both power on and power off modes. In the latter case, the propeller was removed from the model during testing as it would contribute unrealistically to the measured drag of the model. For powered tests, the model propeller operating conditions were appropriately matched to the cruise performance of the full scale VPM-M14 propulsion unit. In particular, both the thrust coefficient and advance ratio of the two propeller systems were matched by adjustment of the blade pitch on the model propeller. The settings used were:

Advance Ratio

$$ J = \frac{V_w}{\Omega D} = 0.431 $$

Propeller Thrust Coefficient

$$ C_t = \frac{T}{\rho V_w^2 d^2} = 0.317 $$

All tests, including power off tests, were conducted at a test Reynolds number of:

$$ R_e = \frac{\rho V_w R}{\mu} = 2.5 \times 10^6 $$

which corresponds to a wind tunnel flow velocity of 31 m/s. The test Reynolds number is approximately 40% of that of the full scale vehicle during cruise. This discrepancy in the Reynolds number was a consequence of the model size and was necessary to achieve propeller advance ratio matching between the model and the full-scale vehicle. It is unlikely that the reduced Reynolds number of the tests would

produce any significant differences between the measured force and moment coefficients and those experienced by the full-scale aircraft. This is primarily because the basic gyroplane structure is non-streamlined and, consequently, insensitive to Reynolds number changes. In addition, the surfaces which are streamlined, such as the cowling and tail surfaces, all operate at test Reynolds numbers well in excess of the generally accepted threshold (R_e = 250 000) for low Reynolds number flows. Hence, it unlikely that their performance would be adversely affected by the test conditions.

All force and moment coefficients presented in the following sections were measured with respect to the fuselage reference point and coordinate system shown in Figure 3.5. The non-dimensional coefficients were calculated using the rotor radius as the basic characteristic length. Thus, for example, the normal force and pitching moment are given by:

$$Z = \frac{1}{2} \rho V_w^2 \pi R^2 CZ$$

and

$$M = \frac{1}{2} \rho V_w^2 \pi R^3 CM$$

respectively.

3.5   **Test Matrix**

In total, one hundred and fourteen data polars were measured during the wind tunnel test programme. These tests considered the performance of four different gyroplane configurations over a range of incidence, sideslip and rudder angles for both power on and power off settings. These four basic configurations were as follows:

Configuration 1: Cowling on, full tail on

Configuration 2: No Cowling, full tail on

Configuration 3: Cowling on, vertical fin on, no horizontal tail or end-plates

Configuration 4: No Cowling, vertical fin on, no horizontal tail or end-plates

In addition to these four basic configurations, individual tests were conducted on two other configurations. These were

Configuration 5: Cowling on, full tail on, extended tail boom

Configuration 6: Cowling on, vertical fin on, horizontal tail on, no end-plates

The full test series, detailing sideslip and rudder angles, is outlined in Appendix 1.

3.6   **Wind Tunnel Test Results**

In the following sections, the main features of the results from the wind tunnel test programme are presented and analysed. For clarity, only data which highlight the salient features of the full dataset are presented in this report. The results are given in graphical form and it should be noted that results labelled "tail off" relate to the removal of the horizontal tail surfaces and associated end plates only.

3.6.1   **Basic Configurational Aerodynamics**

Of particular interest in this study is the extent to which the physical configuration of a gyroplane can influence its aerodynamic performance. One of the primary objectives of the wind tunnel test programme was, therefore, to obtain a quantitative assessment of the effects which the addition of a cowling and/or tailplane would have on the vehicle aerodynamics. This was achieved by measurement of the performance of the four different gyroplane configurations described previously.

a) **Zero sideslip**

In Figure 3.6, the variations of the three force coefficients with incidence are presented for the case of zero sideslip and power on. What is immediately apparent from this figure is that, as may be expected, both CX and CY are relatively insensitive to gyroplane configuration. It is noticeable, however, that there is a greater difference between the four configurations at high negative angles of attack.

In the case of CX, the most interesting effect is the higher drag at negative incidence due to the horizontal tail surfaces in both power on and power off (Figure 3.7) modes. The insensitivity of the effect to power setting excludes the possibility of increased tailplane performance due to the propeller wash and points more towards an induced incidence effect resulting from forebody shielding. Forebody shielding occurs when, at negative incidence, the tail moves into the wind shadow of the gyroplane forebody. This does not happen at positive incidence where, as the angle of attack is increased, the tail moves progressively further into clear air and ultimately stalls. The effect of tail stall is particularly clear in the power off case where, above 20 degrees incidence, the values of CX produced with no tail exceed those of the tail-on configuration. In power off mode, the significant increase in thrust produced by the cowling across the entire incidence range is due to an additional thrust component from the cowling itself. This behaviour is consistent with that which would be expected of any streamlined body but is masked in the power-on case by the interference effect of the cowling on the propeller.

In the power off mode, the value of CY should ideally be zero over the entire incidence range when the gyroplane is at zero sideslip. As may be observed in Figure 3.7, the measured values of CY are very small for all configurations but not exactly zero. This may be a result of a slight misalignment of the model on the balance wires or a small flow angularity in the test section. It is also apparent that the addition of the cowling at high negative incidence causes a marked increase in the side force. One likely reason for this could be the effect of the flow which is channelled into the open cowling at high negative incidence. Under these conditions, the cowling acts like a scoop and, as may be observed in the CZ graph, produces considerably more downforce. It is likely that this 'scoop' effect would also contribute significantly to the sideforce if the cowling were not exactly aligned with the fuselage.

In the power on case, CY also exhibits the cowling effect described above but the general trend of the data comes from two specific effects. The first is due to the basic propeller effect which is a combination of the sideforce produced at the fuselage reference point by the propeller torque and the sideforce due to the asymmetric loading on the propeller. On a fixed pitch propeller, a finite gross inflow angle produces a blade angle of attack variation around the propeller disc and so leads to a force imbalance. The second effect is the interaction of the vertical tail surface with the swirl from the propeller. As is clearly visible in the figure, this effect becomes more significant as the tail moves into the propwash at negative angles of attack.

The variation in the normal force coefficient, CZ, with gyroplane configuration is much more marked than the other two force coefficients. In both power on and power off cases the effects of the cowling and tailplane are quite clear. The increase in wetted area of the cowling increases the effective drag, in relation to the onset flow, which is produced by the gyroplane forebody. Thus, at positive angles of attack the upforce is increased and the opposite occurs at negative angles. In addition, the 'scoop' effect of the cowling, at negative incidence, increases the downforce further. The effect of the tail is, if anything, more significant with the general effect being in the same sense as the cowling. At positive incidence, there is clear evidence of tailplane stall at around 20 degrees. The fact that stall is not obvious at negative incidence may be a consequence of the forebody shielding effect discussed earlier.

Much of the information contained in the force coefficient plots translates directly to the moment coefficient plots presented in Figures 3.8 and 3.9. In the power off case, both CL and CN are almost zero over the entire angle of attack range. The small moments which have been measured are probably due to slight model misalignment or flow angularity as discussed earlier. In power on mode, both of these coefficients are influenced by the propeller. The rolling moment, CL, is almost constant and is produced by the reaction torque from the propeller and CN varies according to the effect of the propwash on the vertical tail and the asymmetric loading on the propeller disc as discussed in relation to CY above.

The pitching moment, CM, is the most sensitive of the three moments to the gyroplane configuration. This is a direct consequence of the effects described in relation to the normal force, CZ, above. In particular, it may be observed that the general effect of the tailplane is to longitudinally stabilise the aircraft, whilst the cowling has a destabilising effect. In this respect, the positive gradient of the CM curve for the cowling on, tail off case indicates that this configuration is unstable. It is also apparent that the onset of tail stall has significant influence on the stability of the aircraft with the aircraft becoming marginally unstable above 20 degrees incidence. The basic airframe plus pilot but without cowling or tail surfaces has almost neutral stability.

b) **-15 Degrees Sideslip**

As may be observed from the tables in Appendix 1, power-off tests were only conducted at negative sideslip angles. This is because, in all power-off configurations, the gyroplane is symmetric about the XZ plane and so positive sideslip angle results can be inferred from those measured at negative angles. In the power-on mode, the influence of propeller rotation and swirl is significant and, consequently, both positive and negative sideslip angle measurements were made. In this section, the results for -15 degrees sideslip in power on mode are compared to those measured with power off. The results not only highlight the basic configurational effects, but also serve to illustrate the influence of the propeller.

Figures 3.10 and 3.11 present the force coefficients measured in power on and power off mode at -15 degrees sideslip. Examination of the results presented in both of these figures indicates that the tailplane has almost no effect on the developed thrust (CX) except at high negative incidence with the power on. This is quite unlike the zero sideslip case where the shielding effect of the gyroplane forebody resulted in increased thrust from the tail at negative incidence in both power on and power off modes. It is therefore clear that, as may be expected, the forebody shielding effect is reduced with increasing sideslip angle. Consequently, the increased thrust from the tailplane in power on mode is due entirely to the influence of the propeller wake on the tail as the aircraft incidence becomes more negative.

The effect of the cowling on CX is unusual in that the influence which the cowling has is different in the power on and power off modes. In Figure 3.11, it may be observed that the effect of the cowling removal in power off mode is to reduce the thrust. As discussed in the zero sideslip case, this is probably due to an additional component of thrust developed by the streamlined shape of the cowling itself when the aircraft is in yaw. In power on mode, however, there is little effect from the cowling at positive incidence but a marked increase in thrust when the cowling is removed at negative incidence. There was, in fact, some evidence of this at zero sideslip, but in this case the effect is more pronounced. A probable cause of this could be that the increased effective area of the cowling is reducing the mass flow to the propeller and, so, reducing thrust.

It is immediately apparent from Figures 3.10 and 3.11 that the general variations in sideforce are little affected by the power setting. It is also clear that a general increase in sideforce is achieved in the tail-on case. Bearing in mind that "tail off" refers only to the removal of the horizontal tail and end-plates, it is appears likely that the inclusion of end-plates in this particular design was necessitated by lateral stability considerations rather than any desire to enhance tail lift.

The cowling appears to have little influence on the sideforce at negative incidence but is responsible for a substantial increase at positive angles of attack. This effect on the sideforce would appear to be produced by the effective difference in shape which the cowling presents to the onset flow in the two cases.

The normal force variations produced at -15 degrees sideslip are very similar in trend to those of head-on flow. As before, the effect of the tail is to enhance the absolute value of the normal force produced by the aircraft. In this case, however, tail stall is not as well defined due to the strongly three-dimensional flow. The effect of the cowling is, again, to increase the absolute normal force experienced by the aircraft. This effect is more pronounced at negative angles of attack where, as discussed previously, the open cowling acts like an air scoop.

Figures 3.12 and 3.13 present the moment coefficients measured at -15 degrees sideslip for both power on and power off cases. Both figures exhibit the same general trends for the rolling moment curves. In both cases, only small variations are apparent across the incidence range with the most significant effect being the change in the magnitude of the rolling moment between power on and power off modes due to propeller reaction torque.

As in the head-on case, the pitching moment, CM, is very sensitive to gyroplane configuration. Again, the tailplane and cowling have opposing effects with the cowling acting to destabilise the aircraft and the tailplane providing an element of stability. As before, the cowling on, tail off configuration is unstable with the 'scoop' effect of the cowling at negative incidence being particularly influential.

Apart from the change in magnitude due to the propwash on the vertical tail and the propeller disc loading, the yawing moment curves for the power on and power off modes are remarkably similar in form. In particular, the effects of the cowling and tailplane are clearly in opposition in both cases. Given the position of these two elements with respect to the fuselage reference point, and also in the light of the preceding discussion on sideforce, this is not surprising. It is, however, important to note that reduction in CN due to the removal of the tailplane and the addition of the cowling may have an adverse effect on lateral stability.

3.6.2 **Synthesis of Configuration Four Results**

In flight mechanics modelling, it is common to supply input aerodynamic data in the form of basic fuselage coefficients plus increments for any optional configurational components. Thus, in the case of the gyroplane, the basic configuration could be taken as cowling off, tail on and increments to each coefficient could be applied if, for example, a cowling was added or the tail removed. This approach, however, relies heavily on minimal aerodynamic interference between the constituent parts of each aircraft configuration. In wind tunnel testing it is also possible to use this technique to synthesize data if the subject of the test programme is suitable.

In the particular case of the gyroplane wind tunnel test programme, staff from Glasgow University and VZLU were confident that the technique could be applied successfully. For this reason, a full series of tests were conducted on three configurations to establish cowling and tailplane increments and only a limited series of tests were carried out for the tail off, cowling off case. This section compares the measured tail off, cowling off results with those synthesized from the results obtained for the other three configurations.

Figure 3.14 represents the most difficult case for the synthesis method; i.e. that of zero sideslip where the cowling effectively shields the tail from the onset flow. In the figure, the synthesized normal force, thrust and pitching moment coefficients are compared to those measured. It is immediately apparent that, at positive angles of attack, the level of agreement between the two datasets is exceptional. The same is not true, however, at negative angles of attack when the tail moves into the shadow of the cowling. Here, both CX and CZ show discrepancies whereas CM is well modelled.

In Figure 3.15, a similar comparison is presented for the 15 degree sideslip case. Again, the agreement at positive angles of attack is substantial. In this case, however, the level of forebody shielding at negative incidence is much reduced and, consequently, the agreement between the two datasets is considerably improved. A similar quality of agreement is achieved for the remaining coefficients which are not presented here.

Despite the anomalies at high negative incidence, the synthesis technique has been shown to be suitable for the calculation of the tail off, cowling off coefficients within the normal operating range of the gyroplane. The performance of the tail off, cowling off configuration can, thus, be inferred from the discussion of configurational aerodynamics given above.

3.6.3 **Effect of Power Setting**

In this section the results measured for the cowling on, tail off configuration are used to illustrate the basic effects which the propeller has on the measured coefficients.

Figure 3.16 presents the measured force coefficients for the power on and power off settings. The effect of the operating propeller on the thrust coefficient, CX, is to simply shift the curve in the positive direction. Otherwise, the shapes of the two curves are almost identical and there is little evidence of any change in the propeller thrust with incidence.

The sideforce coefficient (CY) curves are again offset from each other but, this time, the curves are not parallel. This is due to the previously discussed effect of the propwash on the vertical tail and the forces generated as a result of the torque and sideforce on the propeller itself.

Unlike the two previous coefficient variations, the normal force coefficient (CZ) curves for the power on and power off cases do not exhibit large differences. It could be expected that the power on case should produce greater downforce as a result of the two degree offset in the thrust axis. This, however, is not borne out by the measured data and, in fact, the power on case appears to produce less downforce over the measured incidence range than the power off case. At positive incidence, this is a consequence of the inflow angle to the propeller which determines the direction in which thrust is developed on the propeller disc. At negative angles, however, the opposite behaviour should be observed, but is not. Again, this is most likely a result of the blocking effect of the aircraft forebody at negative angles of attack.

The three moment coefficient comparisons of the power on and power off cases are presented in Figure 3.17. As may be expected, the rolling moment coefficient (CL) curves are merely displaced from each other by a nearly constant amount when power is applied. This effect is purely due to the reaction torque produced by the propeller.

The pitching moment coefficient (CM) curves are offset from each other as a result of the displacement of the thrust axis from the fuselage reference point. A divergence is, however, apparent between the two curves as the gyroplane incidence is increased. This behaviour is entirely consistent with that of the normal force coefficient (CZ) described above. It has been established that the propeller produces an upforce which increases as the angle of attack increases. Since the propeller is located behind the fuselage reference point, a nose down pitching moment will be produced. The increasing strength of this moment as the gyroplane incidence becomes higher is responsible for the different gradients of the power on and power off curves. It should be noted that the general effect of the propeller is a longitudinally stabilising one.

The yawing moment (CN) effect of the propeller is very evident from the comparison of the power on and power off cases. Again, it is clear that the influence of the propwash on the vertical tail is substantial but reduces as the tail moves clear of the forebody at positive angles of attack.

Figures 3.18 and 3.19 show the force and moment coefficient curves, in power on and power off modes, for the same gyroplane configuration at -15 degrees sideslip. Generally speaking, the observed trends are much the same as the zero degree sideslip case although some differences are apparent. In particular, the sideforce coefficient (CY) curves are almost parallel in the yawed case. In addition, the behaviour of the power on and power off curves of CZ are more in line with that which was originally anticipated. This would indicate that, as expected, the blocking effect of the aircraft forebody is reduced as the sideslip angle increases. One consequence of this result is a slightly more beneficial effect of the propeller on the pitching moment characteristics.

3.6.4   **Rudder Effectiveness**

The influence of the rudder is illustrated for the cowling on, tail off configuration in Figures 3.20 and 3.21. As may be observed in Figure 3.20, the effect of rudder deflection on CX is to marginally reduce the overall thrust. At positive angles of attack, this effect seems almost linear. At negative angles of attack, where the forebody shields the tail and the propwash becomes more significant, the effect is most noticeable between 0 and 10 degrees of rudder deflection.

The effects which the rudder have on the side force and yawing moments are, of course, the most significant feature of these graphs. It is clear that the rudder effect on side force is almost linear at a given angle of attack. It is also apparent that there is a slight reduction in the effectiveness of the rudder as the absolute angle of attack of the gyroplane increases and the tail is subject to strongly three-dimensional flow.

In light of the above, it is not surprising that the yawing moment also exhibits linear behaviour with rudder deflection. In addition, the offset of the rudder centre of pressure from the fuselage reference point results in a rolling moment when the rudder is deflected. Again, the characteristics of this particular behaviour are benign.

The response of the aerodynamic characteristics of the gyroplane to rudder deflection described above are indicative of those observed on all gyroplane configurations over the range of sideslip measured in this study.

3.6.5   **The Effect of Sideslip**

Many of the effects of sideslip have already been addressed in previous sections. Here, however, the effects which configurational changes have on lateral stability in yaw will be examined.

In Figures 3.22 to 3.25, the sideforce and yawing moment coefficient variations for the four basic gyroplane configurations, in power off mode, at three different sideslip angles are presented. In Figure 3.25, the data for configuration four is synthesized from the other three datasets. Examination of these four figures indicates that, in all cases, the variation of sideforce (CY) with yaw angle shows no unusual characteristics. The yawing moment coefficient (CN) variation with sideslip angle is, however, particularly sensitive to gyroplane configuration. From a stability stand-point, it is important that there exists a gradient in yawing moment with respect to sideslip angle. In these figures the magnitude of this gradient can be inferred from the spacing between each curve. It is clear that those configurations in which the cowling is present appear to lack stability between 0 and -7.5 degrees of sideslip at positive angles of attack. Indeed, the cowling on, tail off configuration is affected over a wider range of sideslip angles. It is also particularly noticeable that the end plates on the horizontal tail do have a beneficial effect on the lateral stability characteristics of the aircraft.

In isolation, the above features would be particularly detrimental to the aircraft handling characteristics. In practice, however, the stability of the aircraft is aided by the relatively large propeller. This is illustrated in Figure 3.26. which presents the corresponding power on measurements on the cowling on, tail on configuration. It is clear from this figure that the effect of the propeller is to stabilise the configuration by increasing the absolute magnitude of the yawing moment as the sideslip angle is increased.

3.6.6   **The Horizontal Tail**

The configuration of the tail sections of the VPM M14 and M16 aircraft are quite unusual in terms of the large endplates on the horizontal tail surfaces. It has already been established that these endplates are beneficial for lateral stability but it was unclear what effect, if any, they would have on the lifting effectiveness of the tailplane. To investigate this, a single test was carried out with the cowling on, tail on configuration but without the endplates. The measured normal force and pitching moment coefficient curves are compared with those from the corresponding test with the endplates on in Figure 3.27.

By preventing the flow of air around the tips of the horizontal tail, the end plates restrict the flow over the horizontal tail to an almost two-dimensional state. This should allow the tail to develop higher lift than a conventional tail at moderate incidence but will result in a sharper stall. This is illustrated in Figure 3.27 where the loss of normal force due to tail stall is apparent at around twenty degrees when the endplates are on but there is a much more gradual loss when the endplates are removed. There is no clear indication in the CZ curve of any increase in lift at moderate incidence but the gradient of the CM curve is obviously greater between -20 and +20 degrees when the endplates are on. This is indicative of increased tailplane effectiveness.

The effect of increasing the length of the tail boom by approximately 0.3m (on the full scale vehicle) was also examined. The results of this study are presented in Figure 3.28 and were very much as expected with almost no change in the normal force coefficient curve, but a substantial change in the gradient of the pitching moment coefficient curve. This is simply due to the increased offset of the tail from the fuselage reference point. It also appears, however, that the stall angle of the tail at positive incidence is reduced with movement away from the gyroplane forebody. This is undoubtedly a result of a change in the effective angle of attack experienced by the tail due to reduced interference between the tail and the forebody.

Perhaps the most significant observation associated with the tailplane is the lift-curve slope. This is a measure of efficiency and also an indicator of its likely impact on the complete aircraft and it can be extracted from these data readily. For example Figure 3.7 compares Z-force coefficient with tail on and off; analysis shows that the lift-curve slope is 2. A typical value for a blade is 5.7; for a helicopter horizontal tailplane 3.7; and the theoretical maximum for a finite wing is 2π. When combined with the short moment arm of the typical pusher configuration it can be seen that tailplane effectiveness is likely to be limited at anything other than high speed. Note that with power on, where even the low-set tailplane might be expected to experience some slipstream benefit, the lift-curve slope increases only by a relatively small amount to a value of 2.7 - still well below even helicopter values.

3.7   Configurational Differences Between the VPM M14 and M16 Variants

The mathematical model used to generate all of the simulation results presented in this report incorporates the aerodynamics data gathered for the VPM-M14 configuration. It is worthwhile noting that the aircraft flight tested was in fact a VPM-M16 which differs slightly from the M14 variant (refer to Figures 3.1 and A2.1). The use of M14 aerodynamic data in a simulating the M16 vehicle requires some justification. However, there are only three significant differences between the two variants:

a) the M16 is 738mm longer than the M14 - due to a longer cowling and tail boom;

b) the horizontal tailplane of the M16 is 20% larger than the M14 (the vertical tailplane areas are almost identical);

c) the cowlings are different in shape, although the wetted areas are almost identical.

Given the geometric similarity of the two variants it is unlikely that their general aerodynamic characteristics (coefficients) will differ substantially. It is therefore reasonable to use the data for the M14 to simulate the M16 with suitable adjustments made to account, for example, for the larger horizontal tail surface. Further, the data collected for the VPM M14 should give a fair representation of other similar aircraft, given the very minor differences in overall configuration between types: most light gyroplanes consist of keel, pod, mast, horizontal and vertical tail surfaces and a pusher propeller. Finally, the relatively low operating speed of these aircraft implies that any minor differences in aerodynamics characteristics would manifest themselves in very small differences in aerodynamics loads.

3.8   Concluding Remarks

The aerodynamic characteristics of the gyroplane configurations considered in this study are generally benign. It is, however, pertinent to note that there are several effects associated with the cowling that are detrimental to stability. Although the cowling on the VPM-M14 is particularly large, it is likely that any 'open' cowling design will be subject to similar effects in the longitudinal mode. Additionally, the length of the VPM cowling is substantial; extending from well in front of the pilot up to the rotor support column. The increased wetted area which this presents to the onset flow in sideslip acts to oppose the stabilising effect of the tail. The tail itself benefits from the additional sideforce produced by the endplates on the horizontal surfaces.

An important assumption also made here is that the VPM M14 and M16 variants are sufficiently similar that their aerodynamic properties will be insignificantly different. The implication is that it is reasonable to use M14 data in a flight dynamics model of the M16 and other similar aircraft (such as the Montgomerie-Parsons) without greatly affecting (if at all) the overall assessment of its dynamic stability characteristics.

It is worth noting that the modification proposed to solve the stability problems which led to the grounding of the Air Command gyroplane type comprised principally, in aerodynamic terms, of the addition of a pod and a tailplane. These tests suggest that this modification would not be very effective and, indeed, this proved to be the case.

CAA Comment

The remarks concerning the addition of a tailplane to the Air Command are noted, however CAA Flight Test Specialist qualitative evaluation of the effects of a horizontal tailplane on the RAF 2000 indicated a degree of improvement in the phugoid characteristics at higher speed.
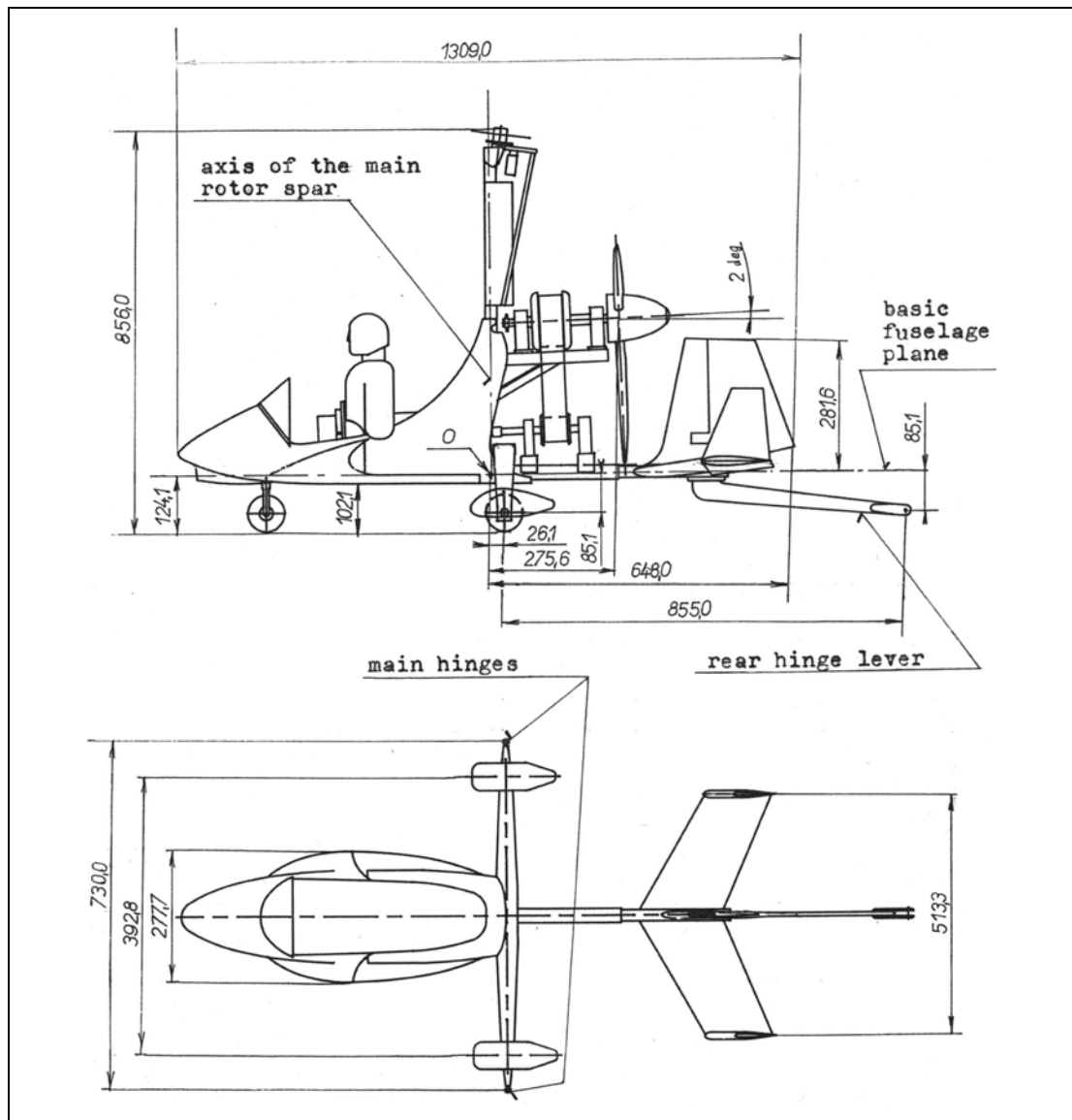
Figure 3.1   VPM M14 One Third Scale Wind Tunnel Model (dimensions in mm)

Figure 3.2   One Third Scale Wind Tunnel Model of a VPM M14 Gyroplane
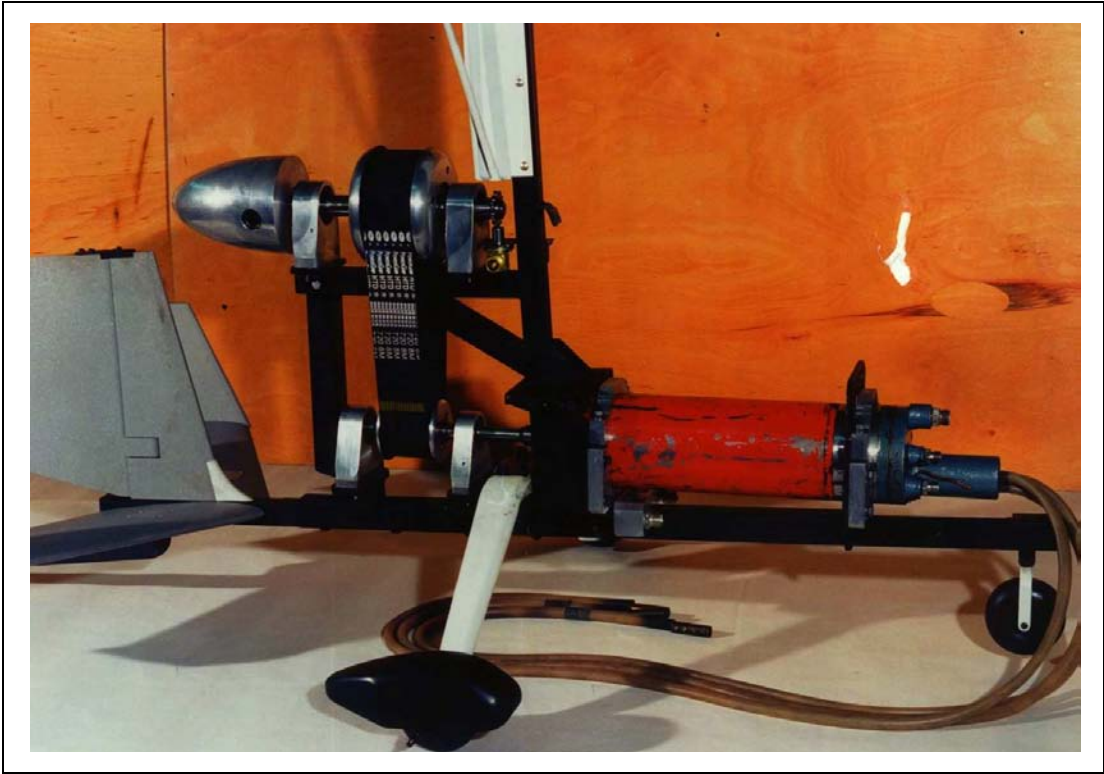
Figure 3.3   The VPM M14 Model Without Cowling

Figure 3.4 a)   VPM M14 Model in VZLU Wind Tunnel (Front View)

Figure 3.4 b)   VPM M14 Model in VZLU Wind Tunnel (Rear View)
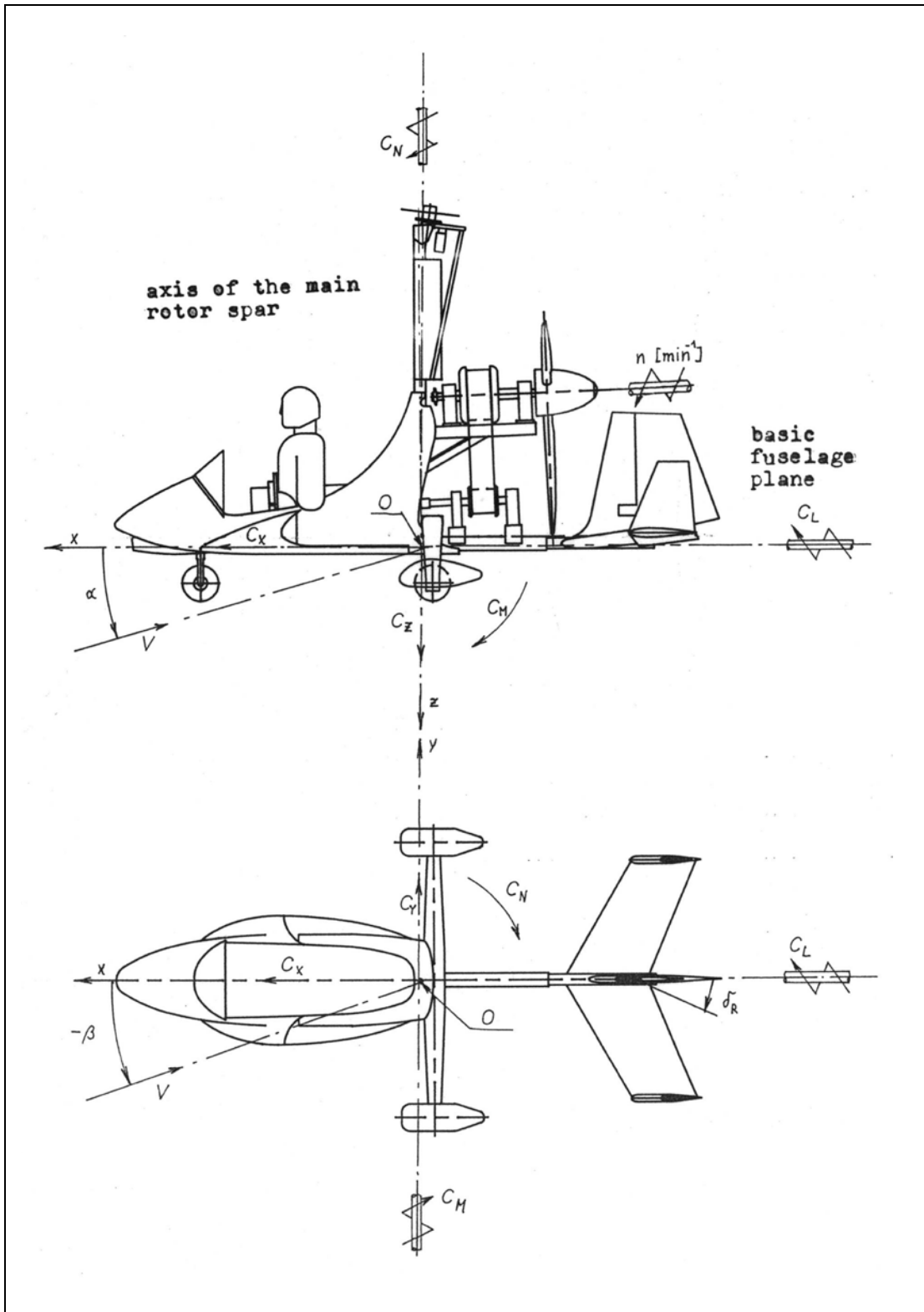
Figure 3.5   Co-ordinate System for Aerodynamic Coefficients
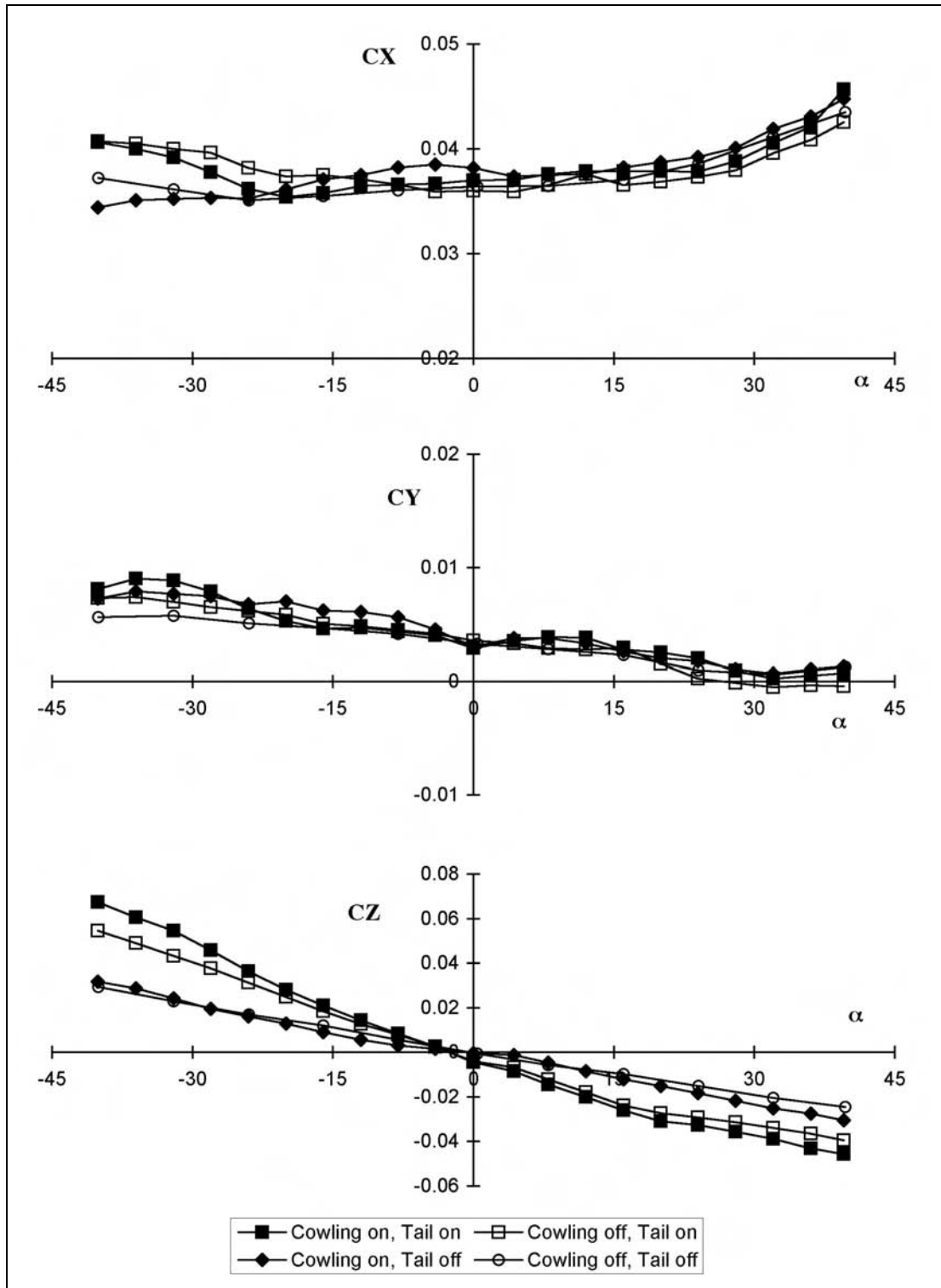
Figure 3.6　　Force Coefficient Variations ($\beta = 0$, Power On)
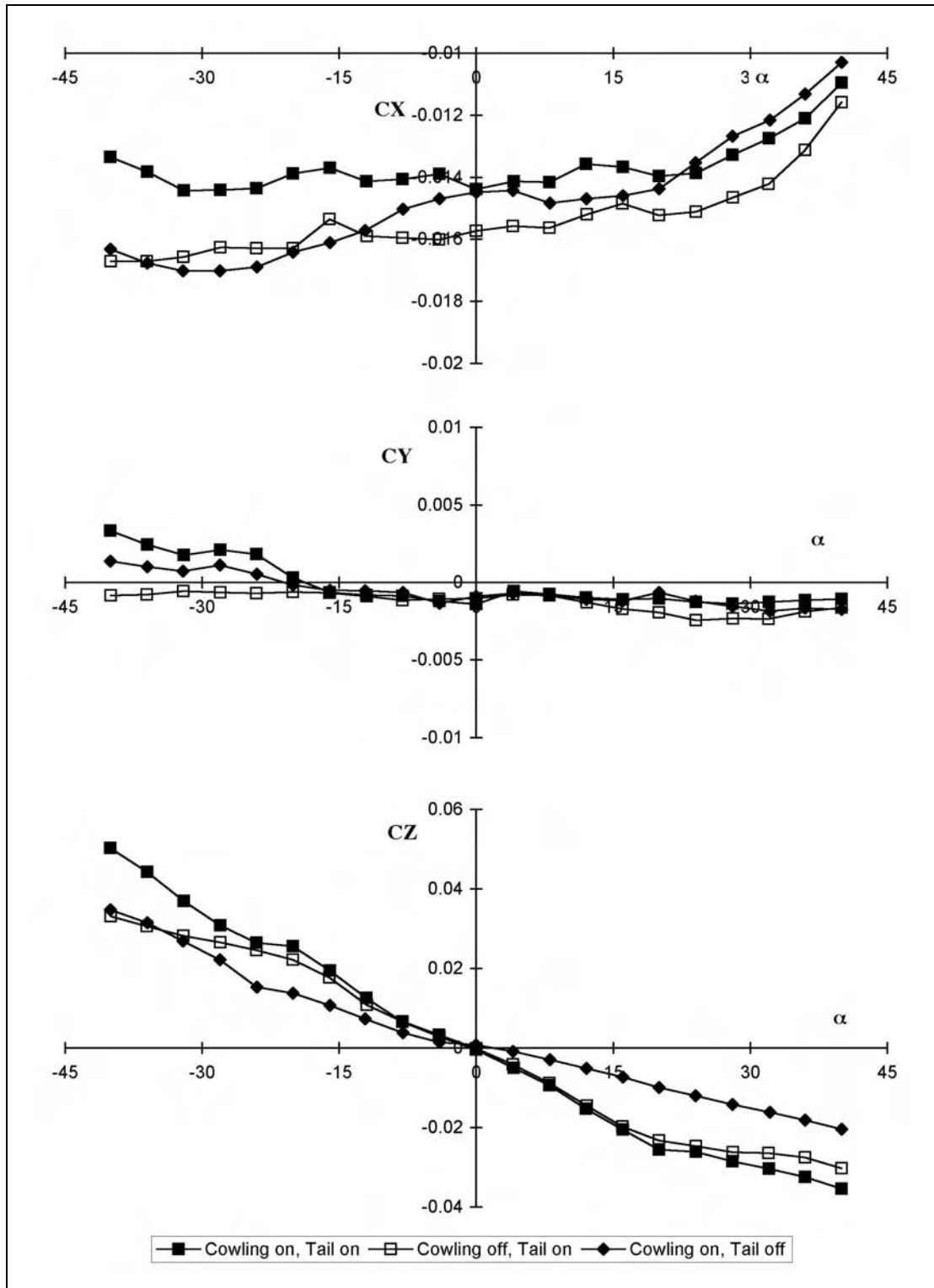
Figure 3.7   Force Coefficient Variations (β = 0, Power Off)
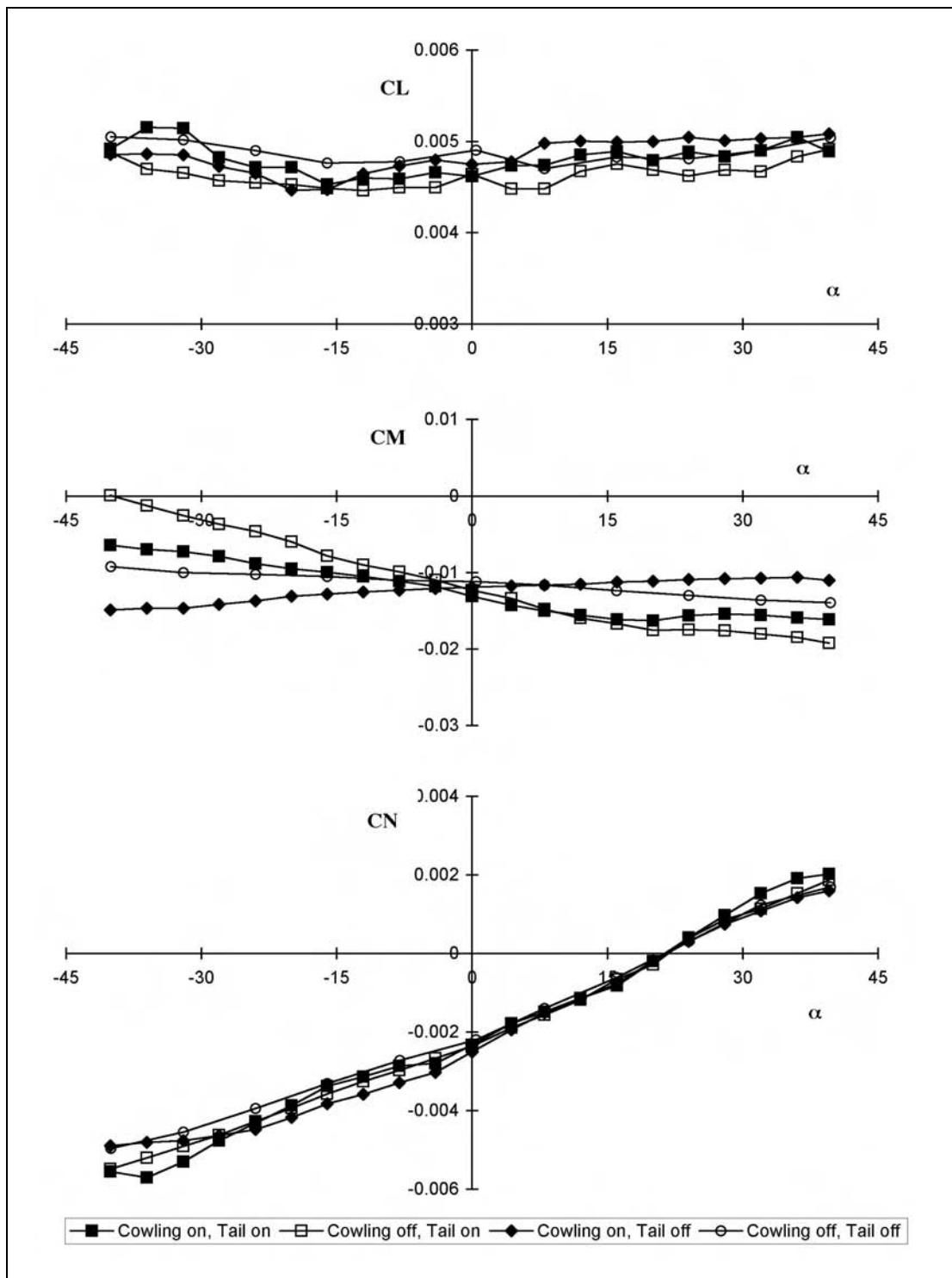
Figure 3.8   Moment Coefficient Variations (β = 0, Power On)
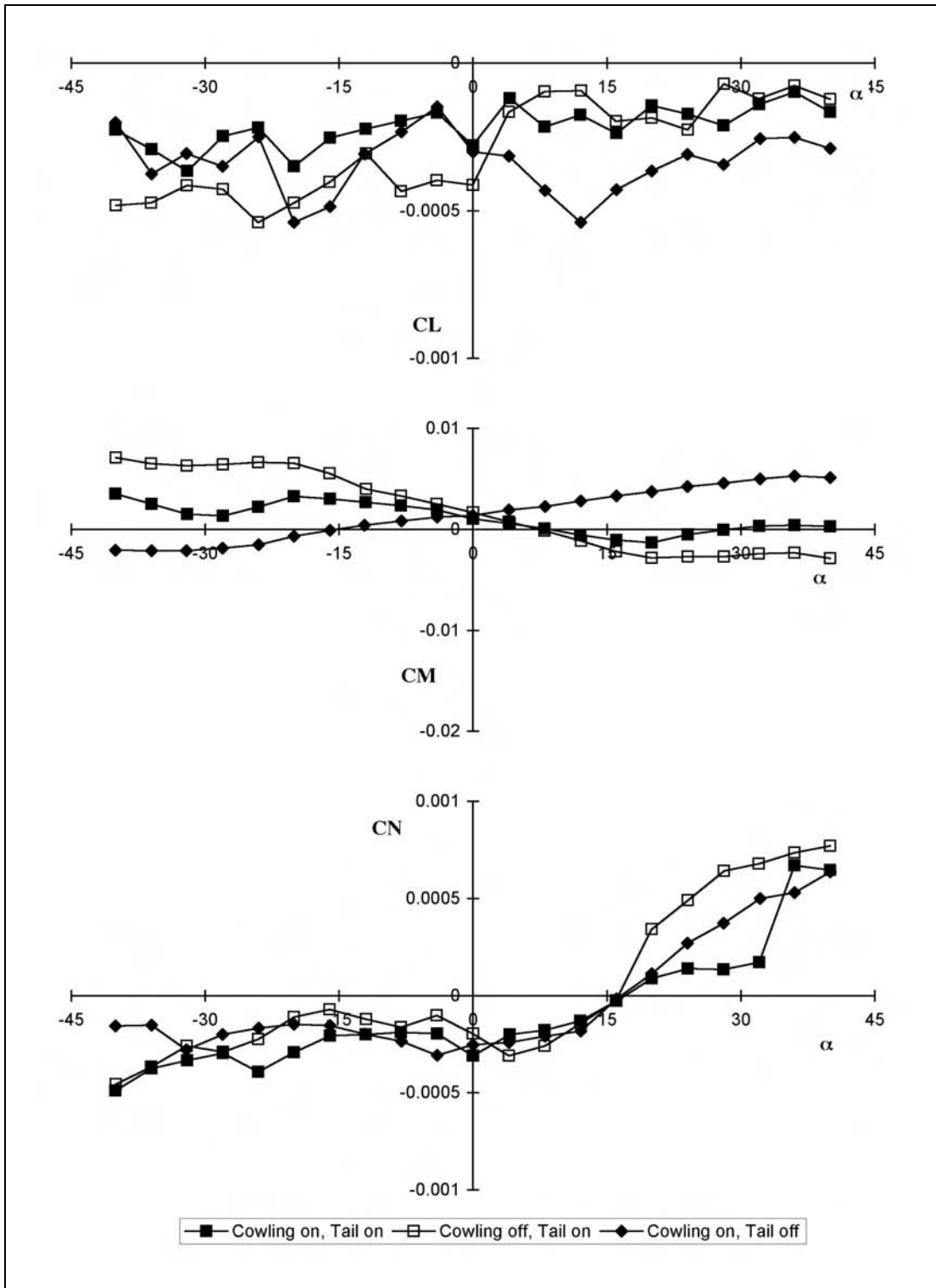
Figure 3.9   Moment Coefficient Variations (β = 0, Power Off)
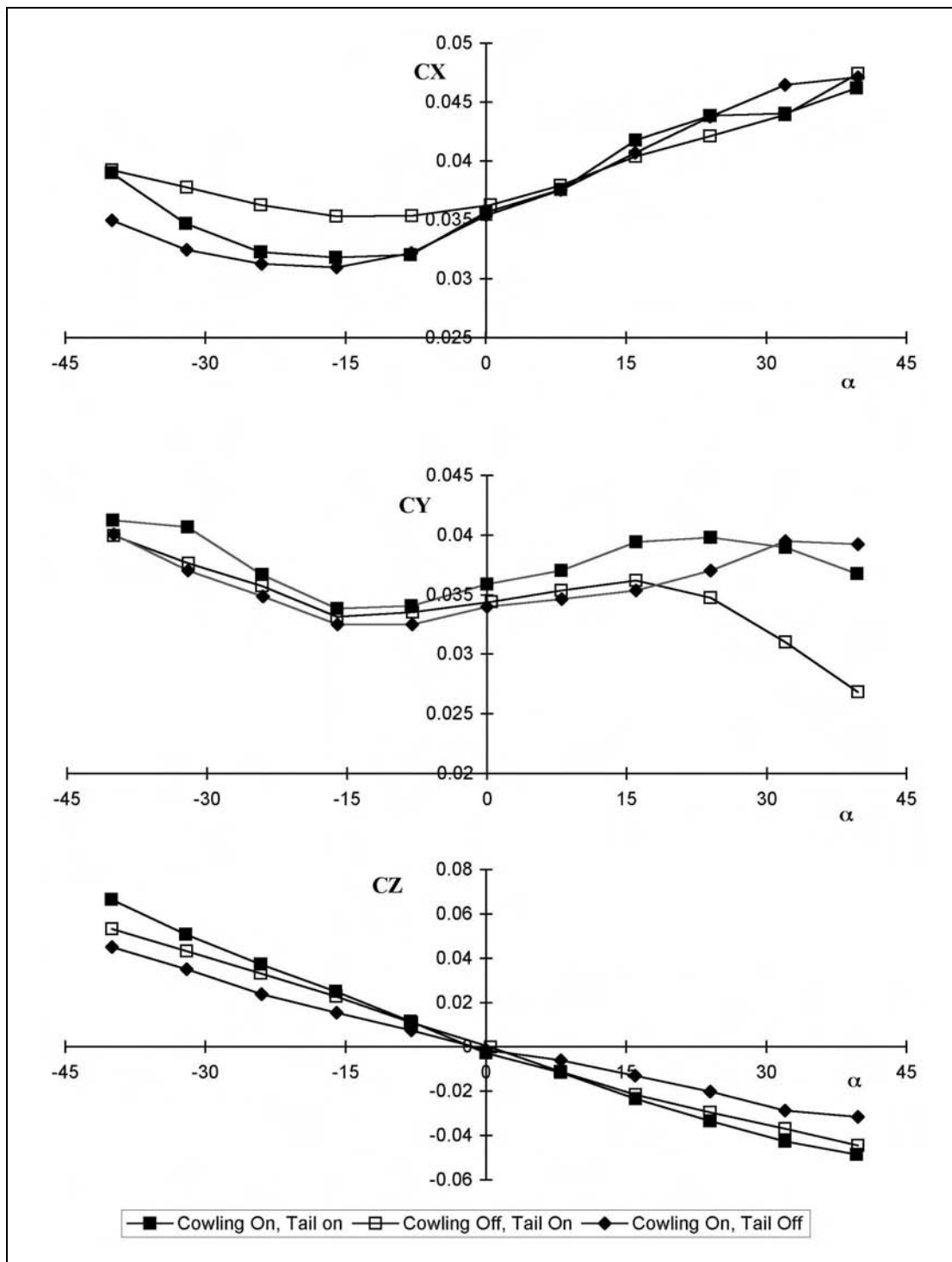
Figure 3.10   Force Coefficient Variations (β = -15 deg, Power On)
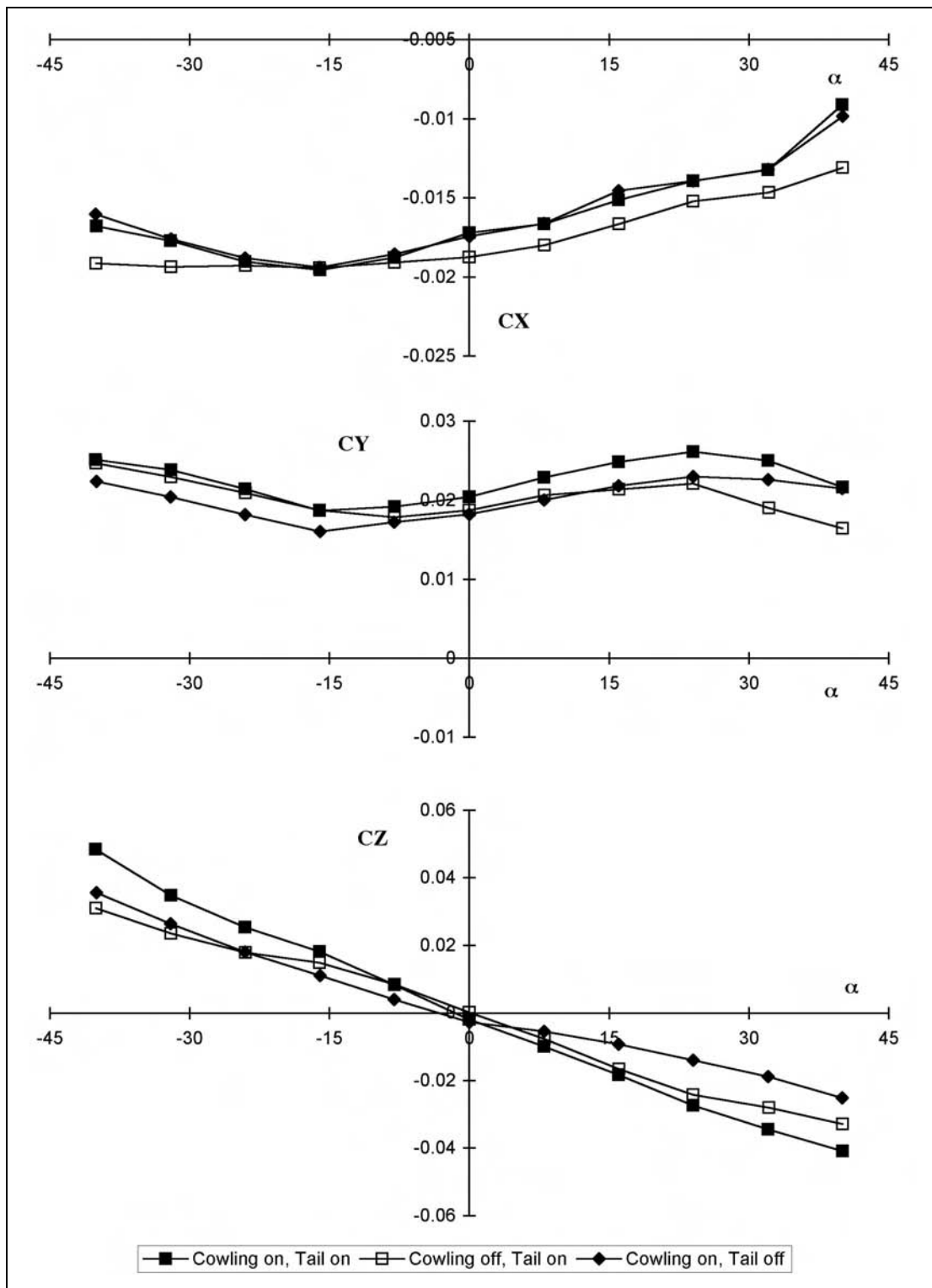
Figure 3.11   Force Coefficient Variations (β = -15 deg, Power Off)
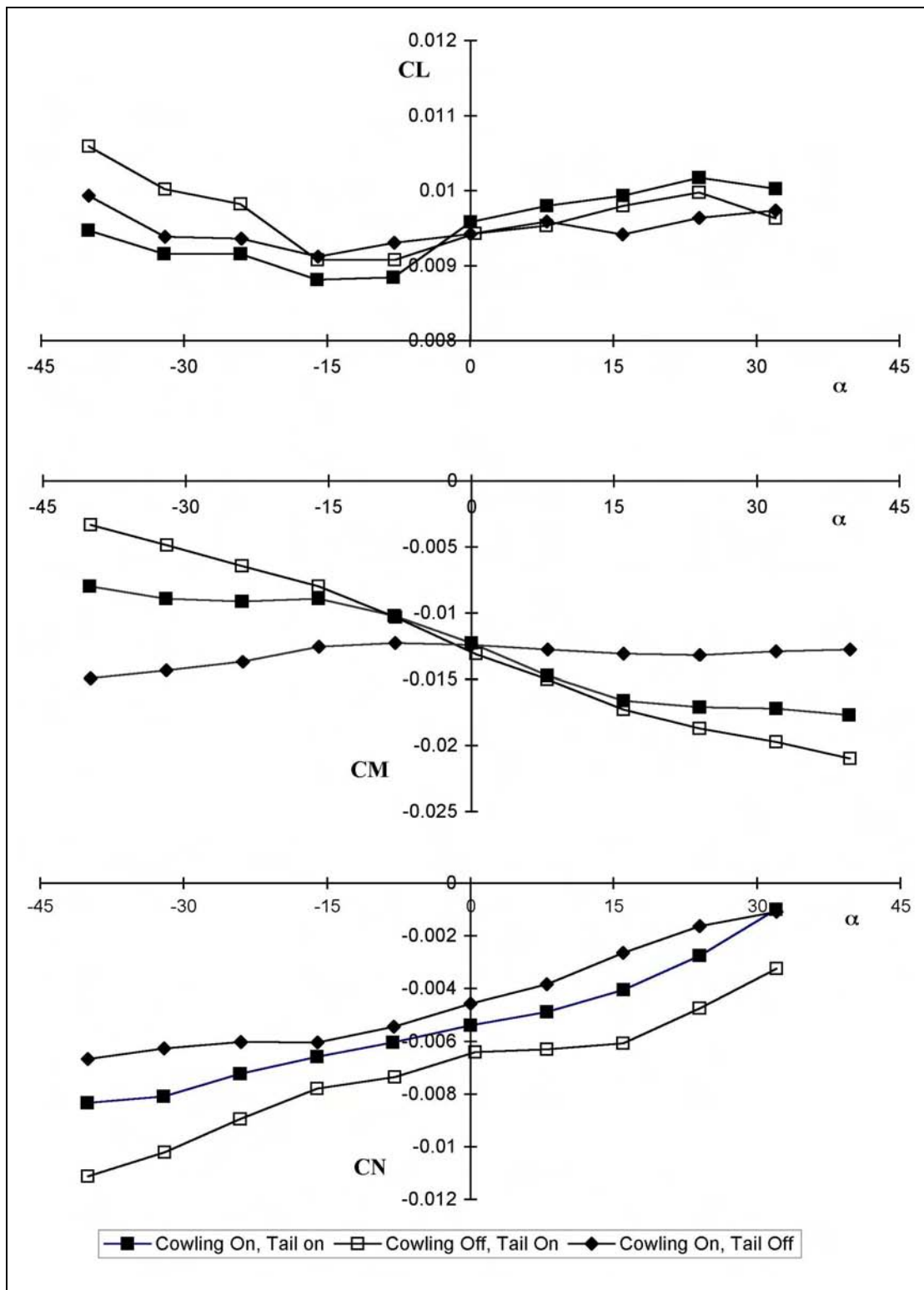
Figure 3.12   Moment Coefficient Variations (β = -15 deg, Power On)
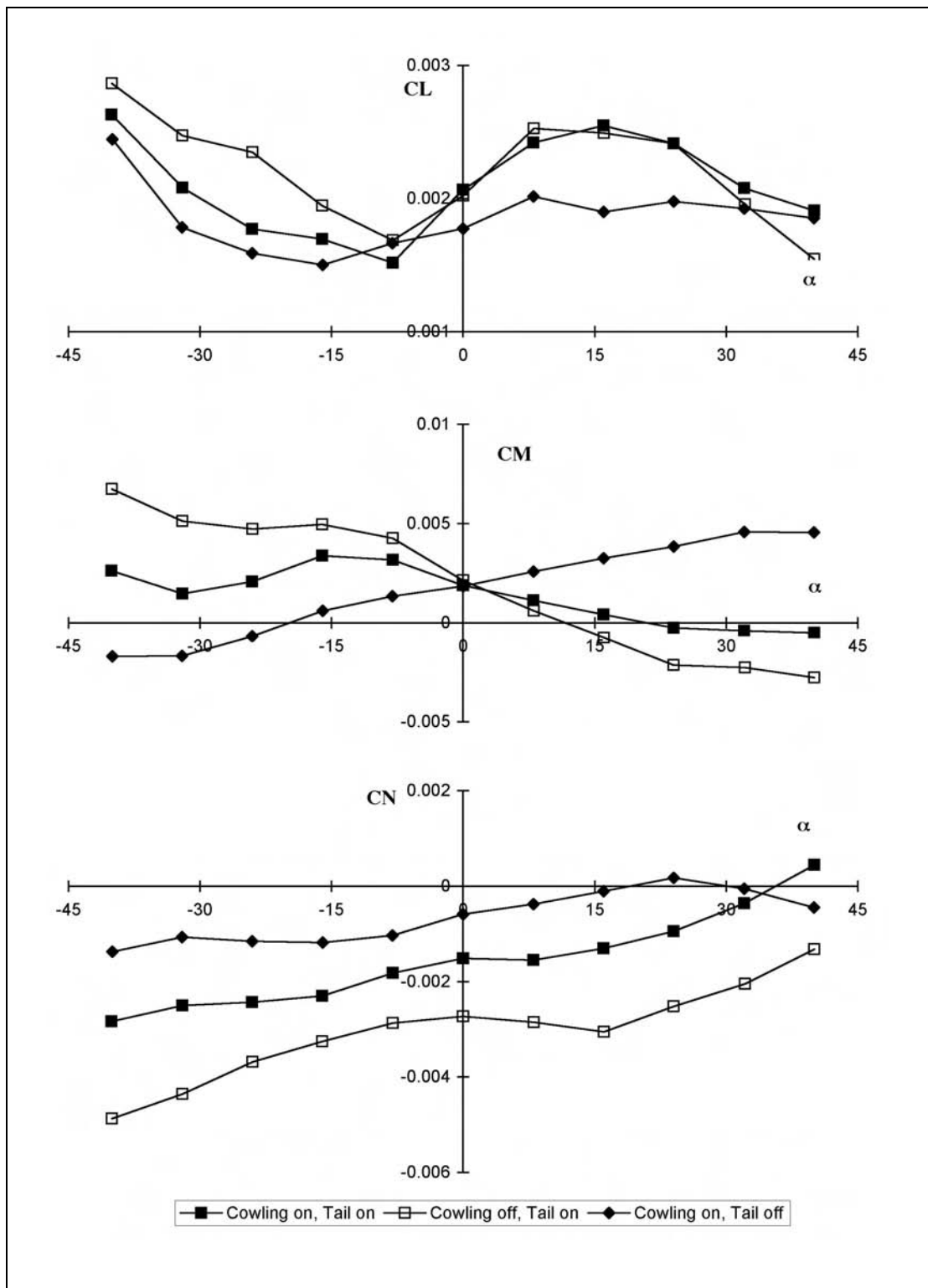
Figure 3.13   Moment Coefficient Variations (β = -15 deg, Power Off)
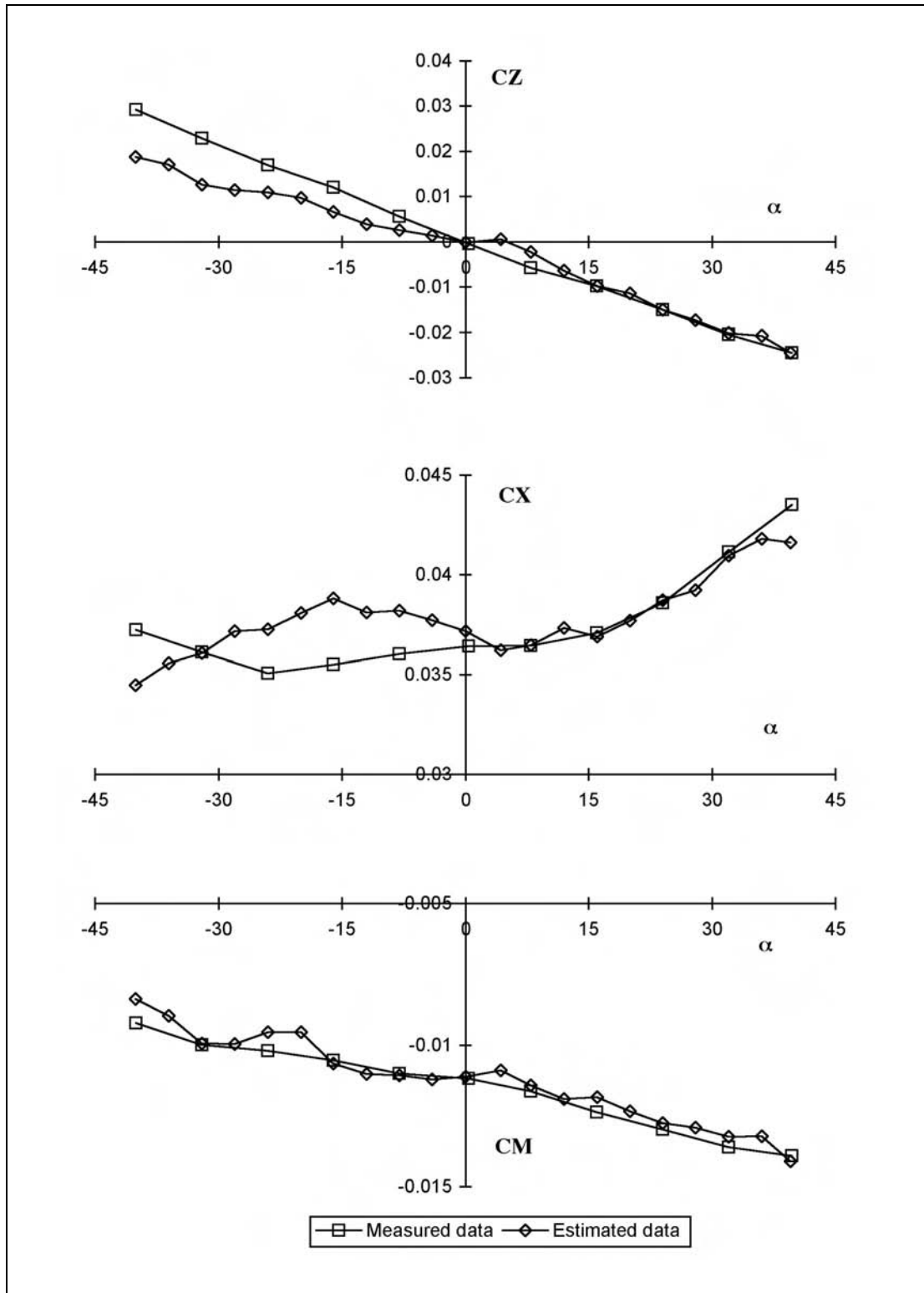
Figure 3.14   Comparison of Measured and Estimated Cowling Off, Tail Off Results for $\beta = 0$, Power On
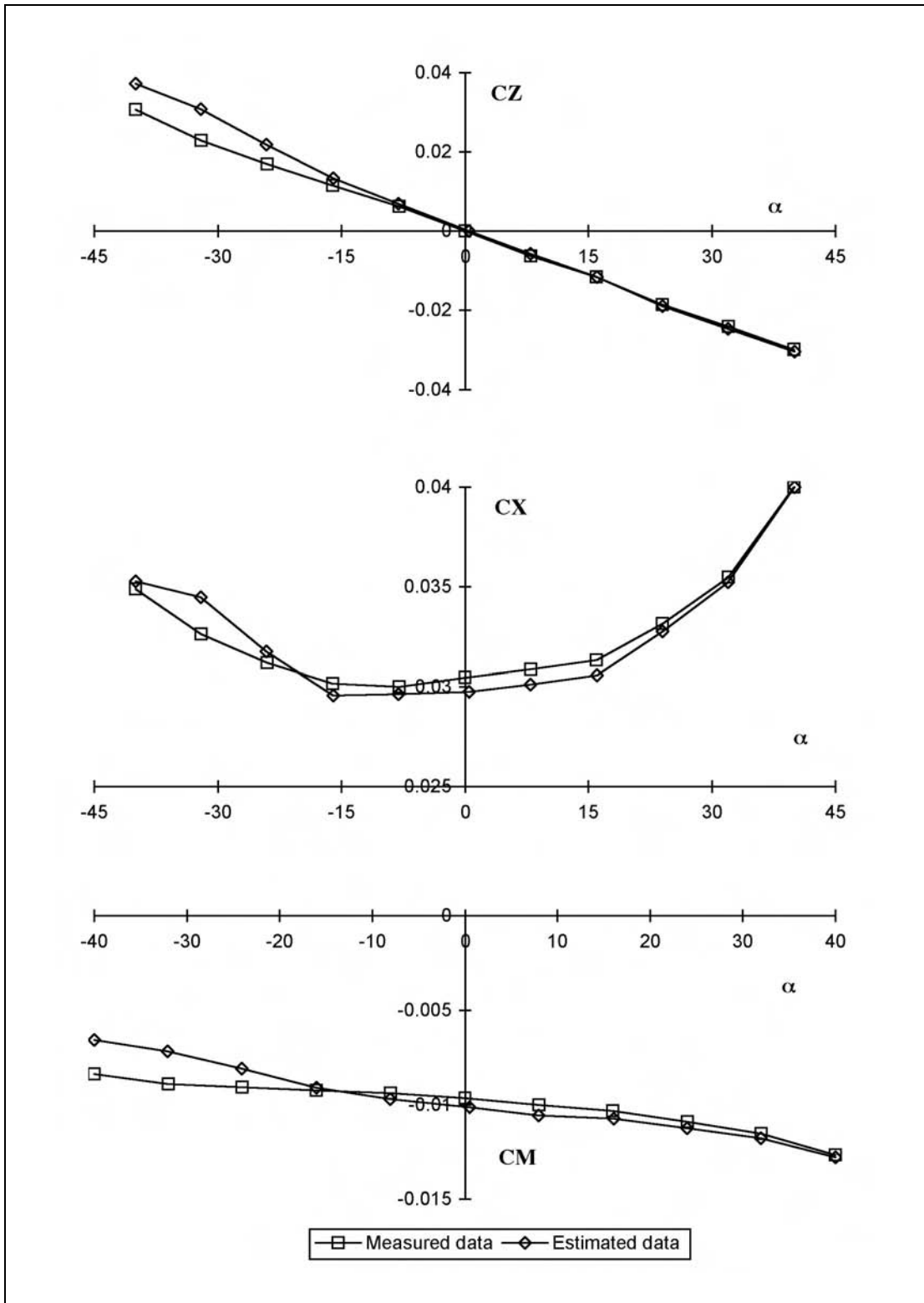
Figure 3.15   Comparison of Measured and Estimated Cowling Off, Tail Off Results
for β = 15 deg Power On
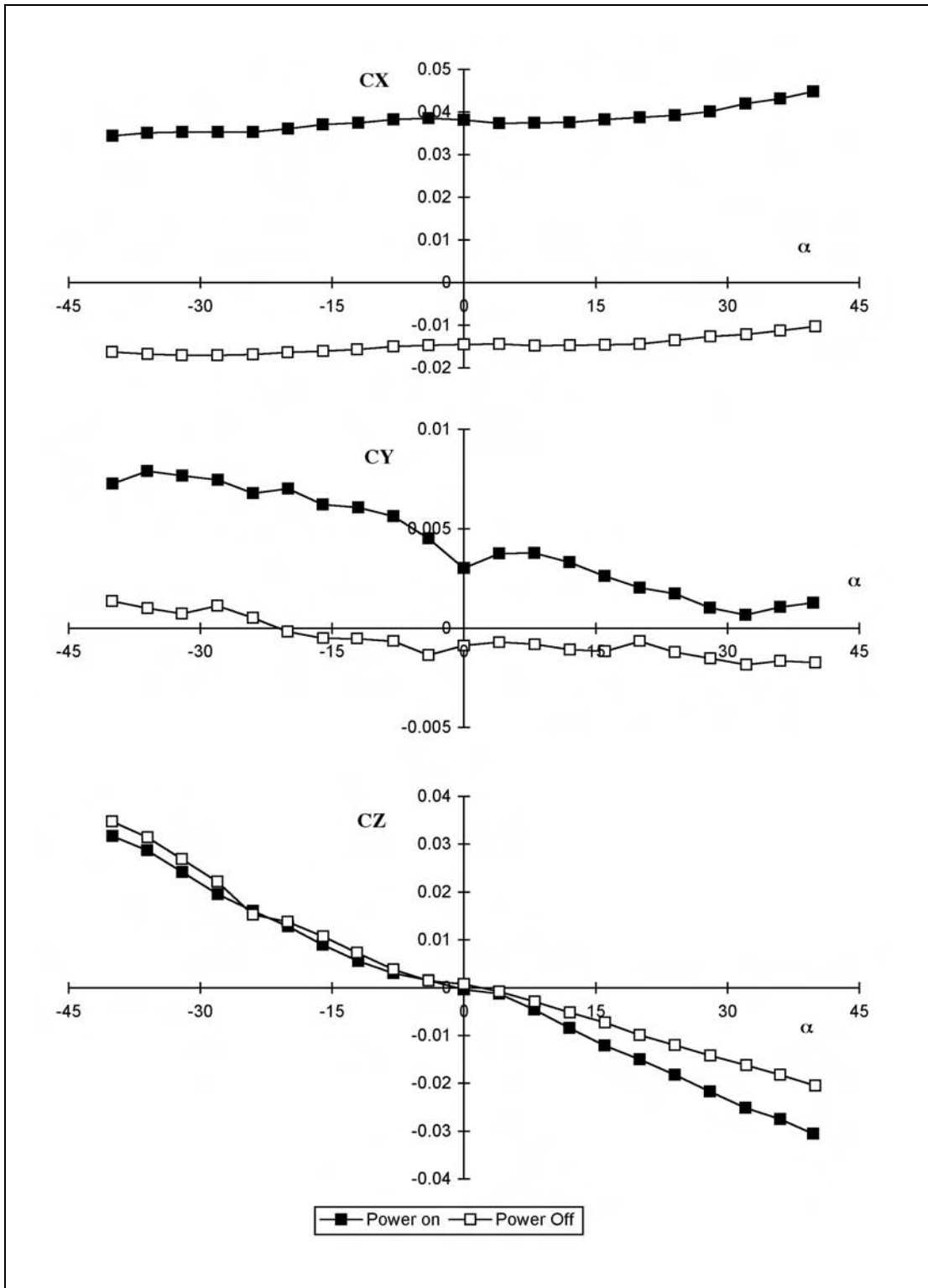
Figure 3.16   Comparison of Power On and Power Off Force Coefficients,
                  β = 0, Configuration 3
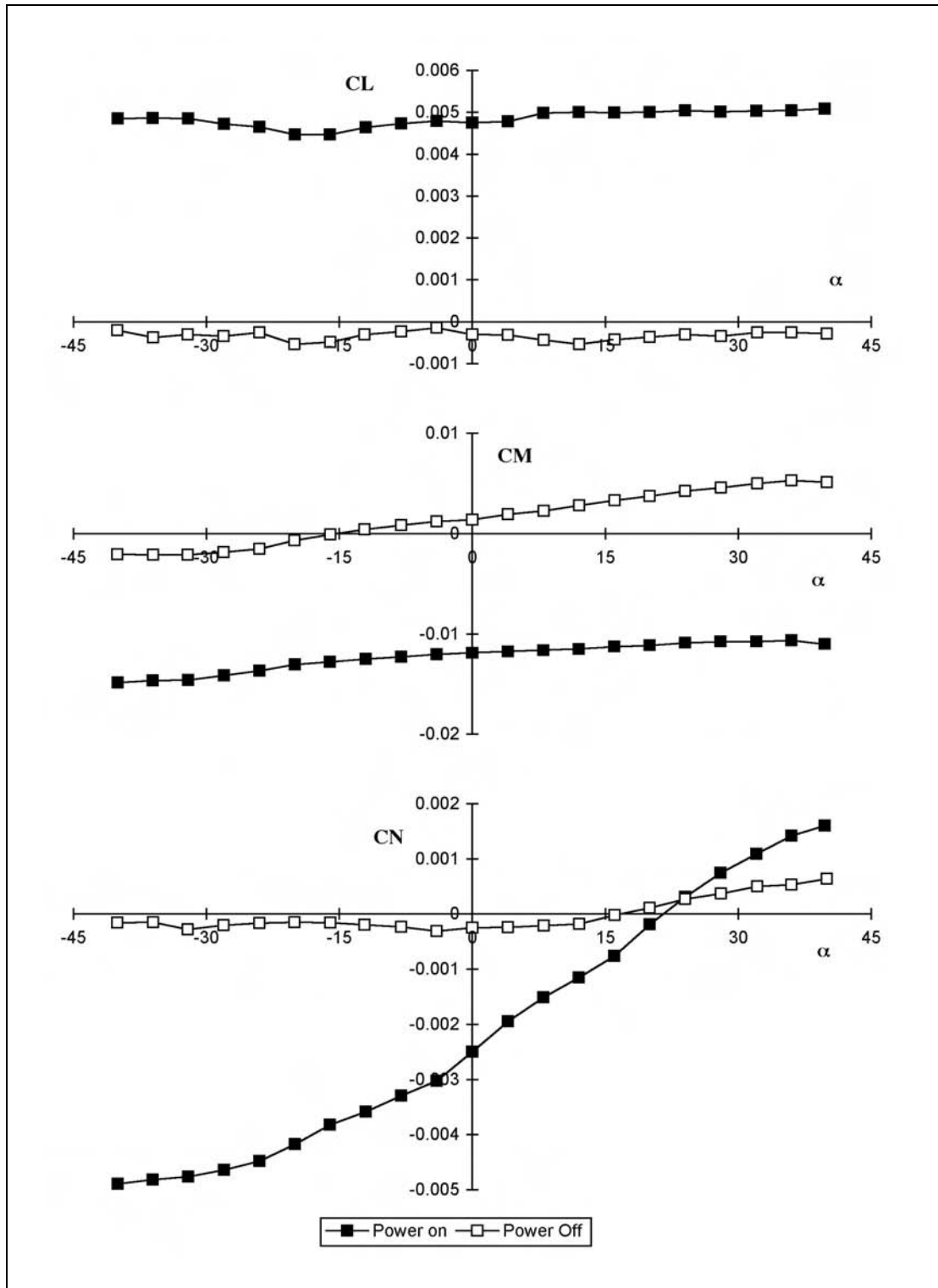
Figure 3.17   Comparison of Power On and Power Off Moment Coefficients,
β = 0, Configuration 3
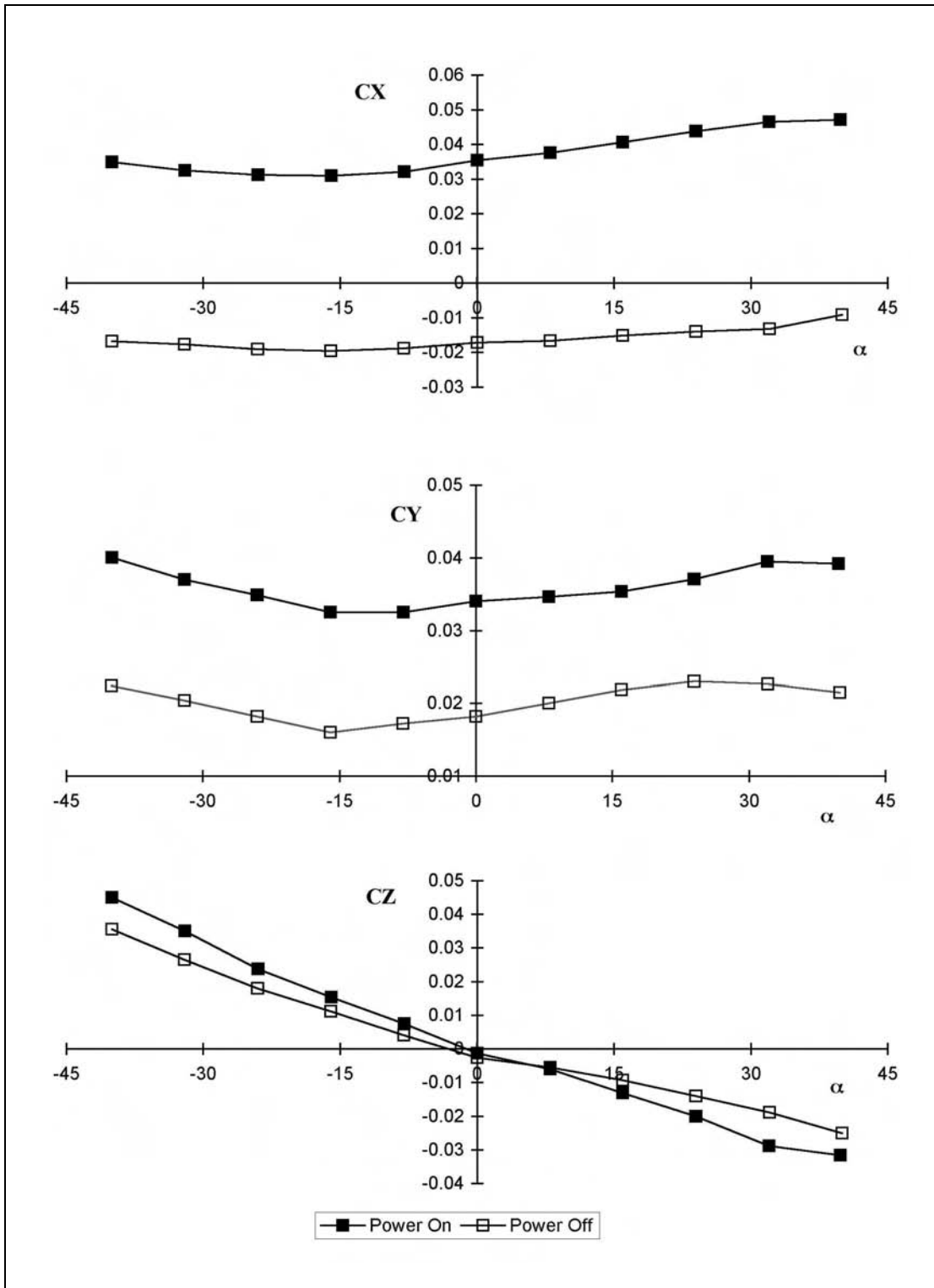
Figure 3.18　　Comparison of Power On and Power Off Force Coefficients, β = -15 deg, Configuration 3
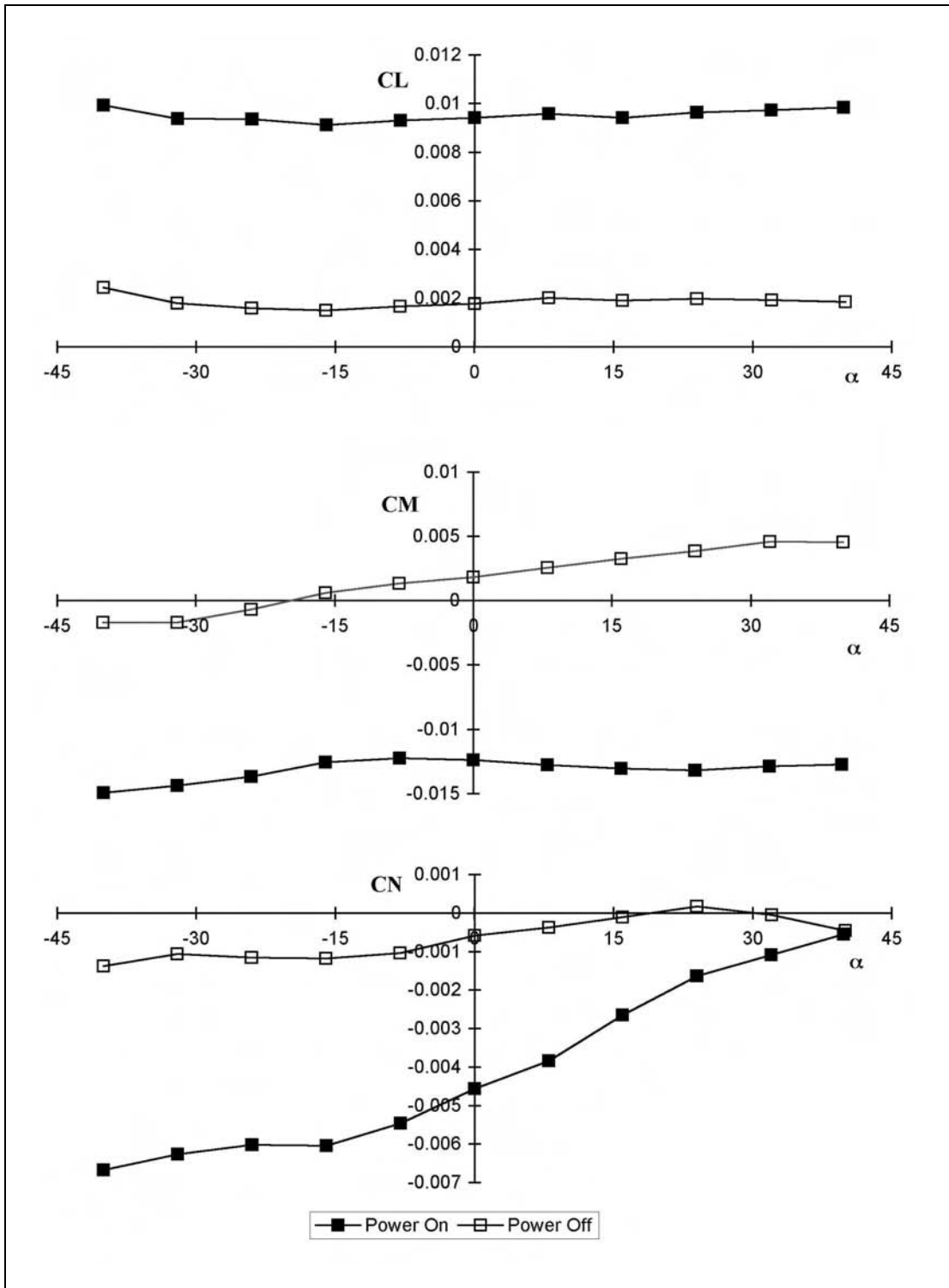
Figure 3.19   Comparison of Power On and Power Off Moment Coefficients,
                   β = -15 deg, Configuration 3
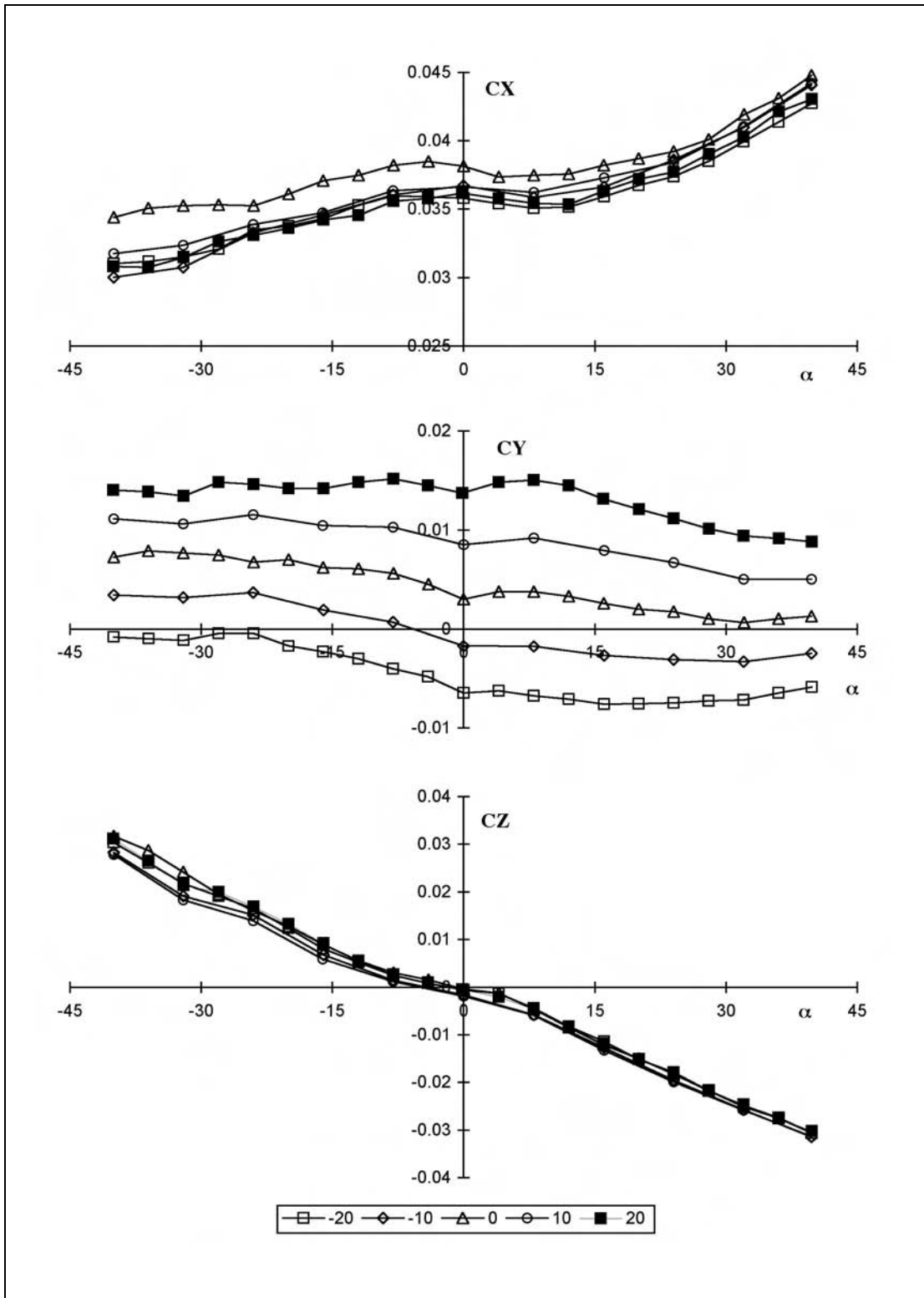
Figure 3.20 Effect of Rudder Setting on Force Coefficients,
β = 0, Configuration 3
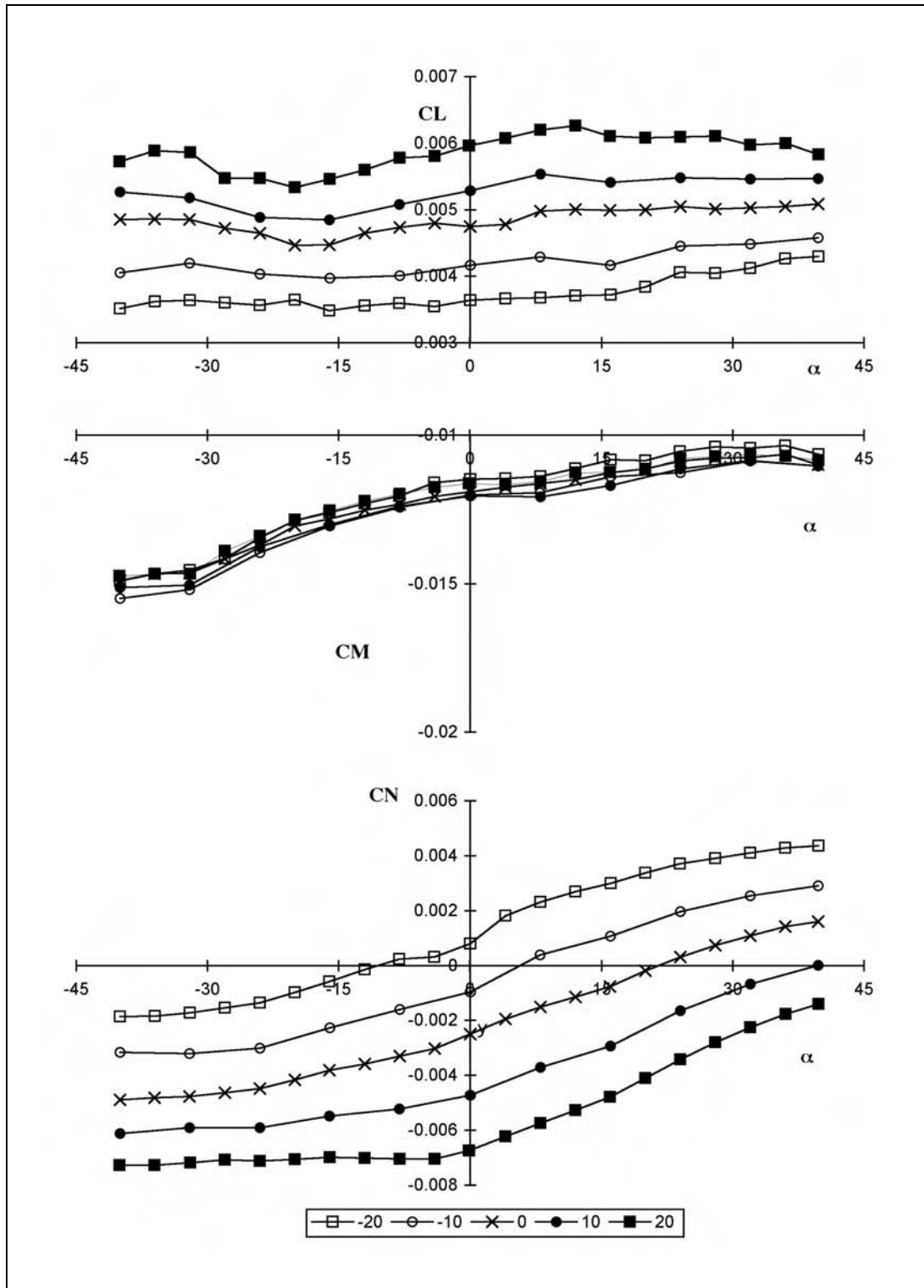
Figure 3.21   Effect of Rudder Setting on Moment Coefficients,
                   β = 0, Configuration 3
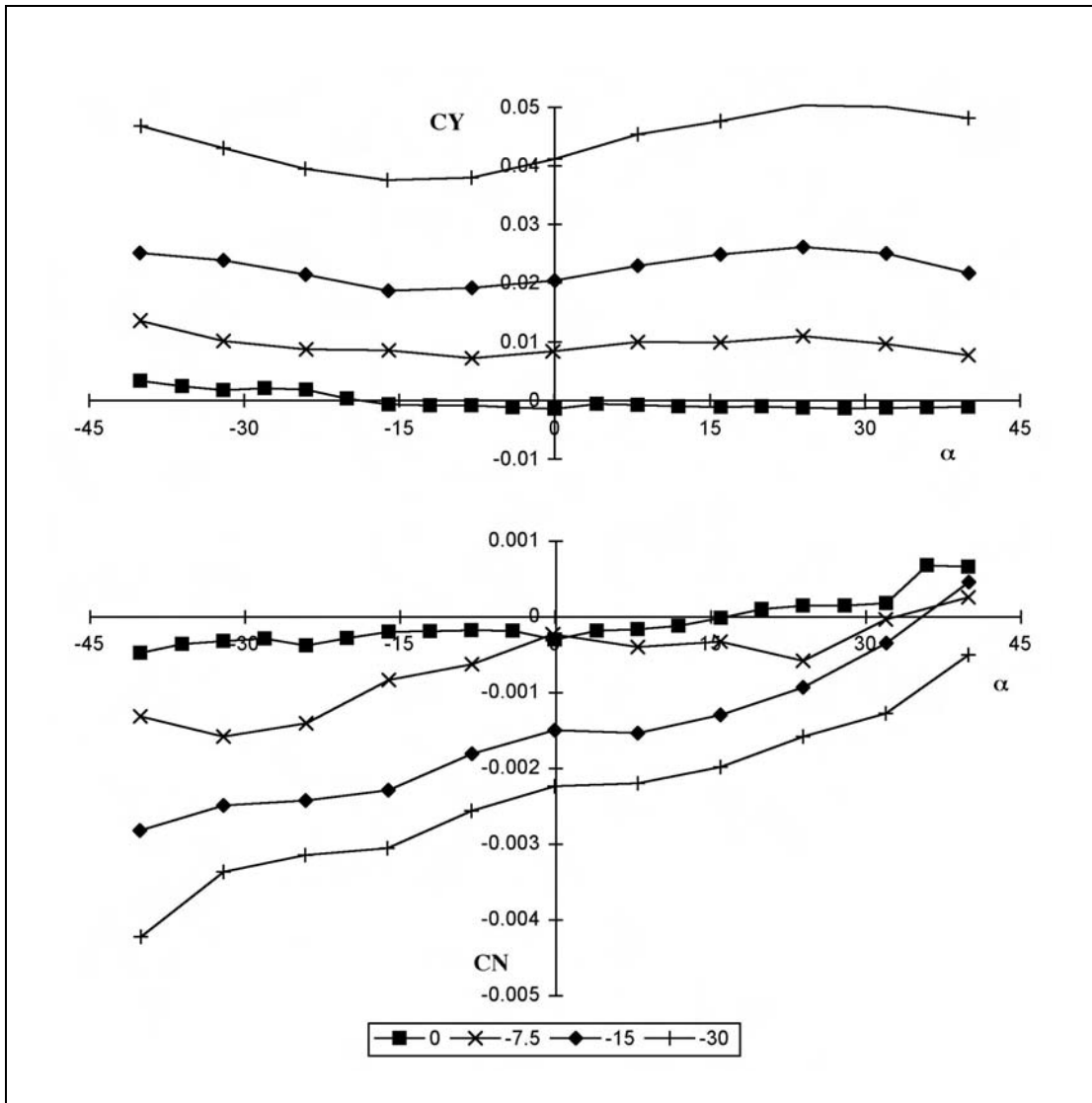
Figure 3.22   Effect of Sideslip Angle on Cowling On, Tail On Configuration
(Power Off)
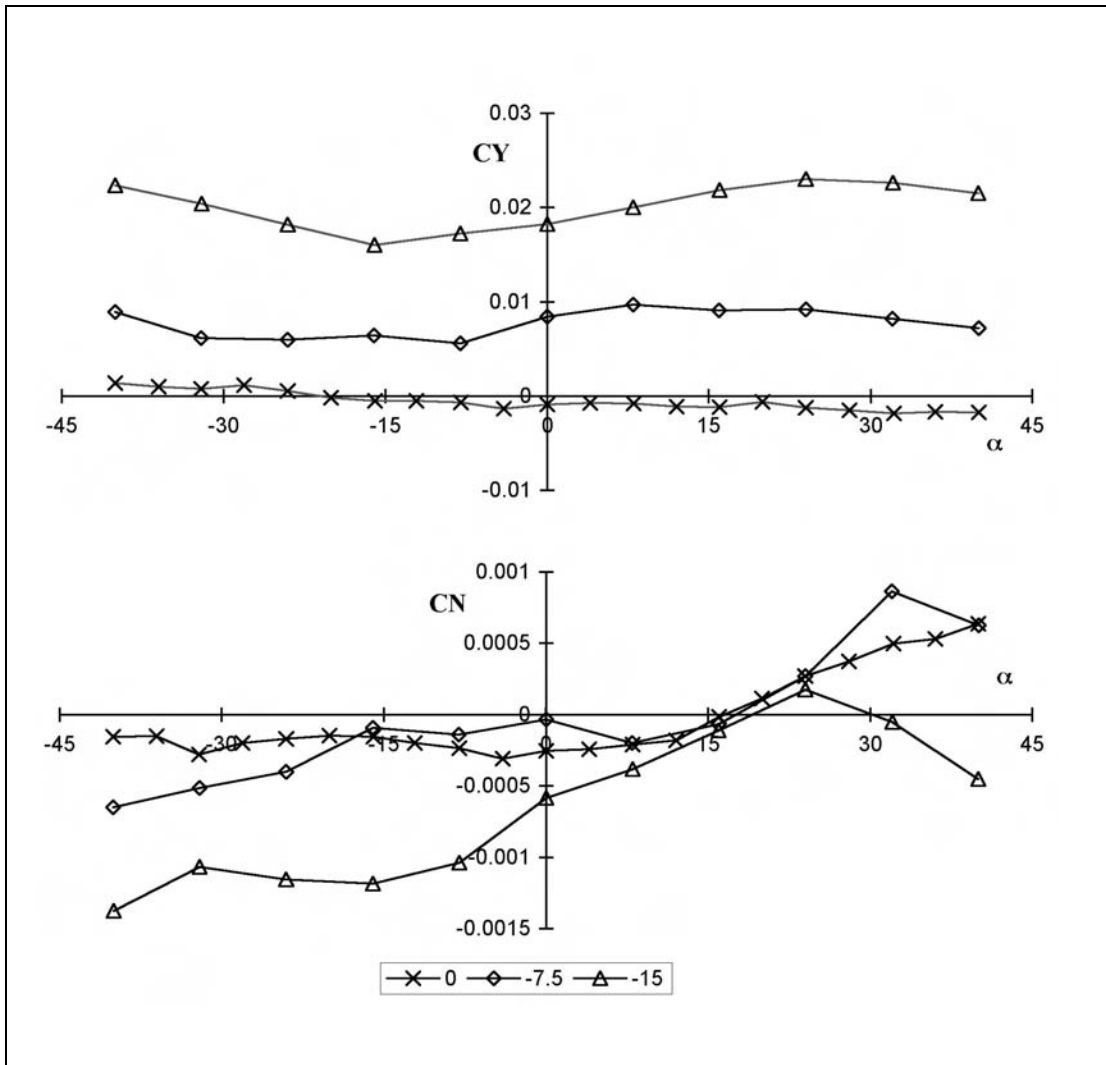
Figure 3.23   Effect of Sideslip Angle on Cowling On, Tail Off Configuration
(Power Off)
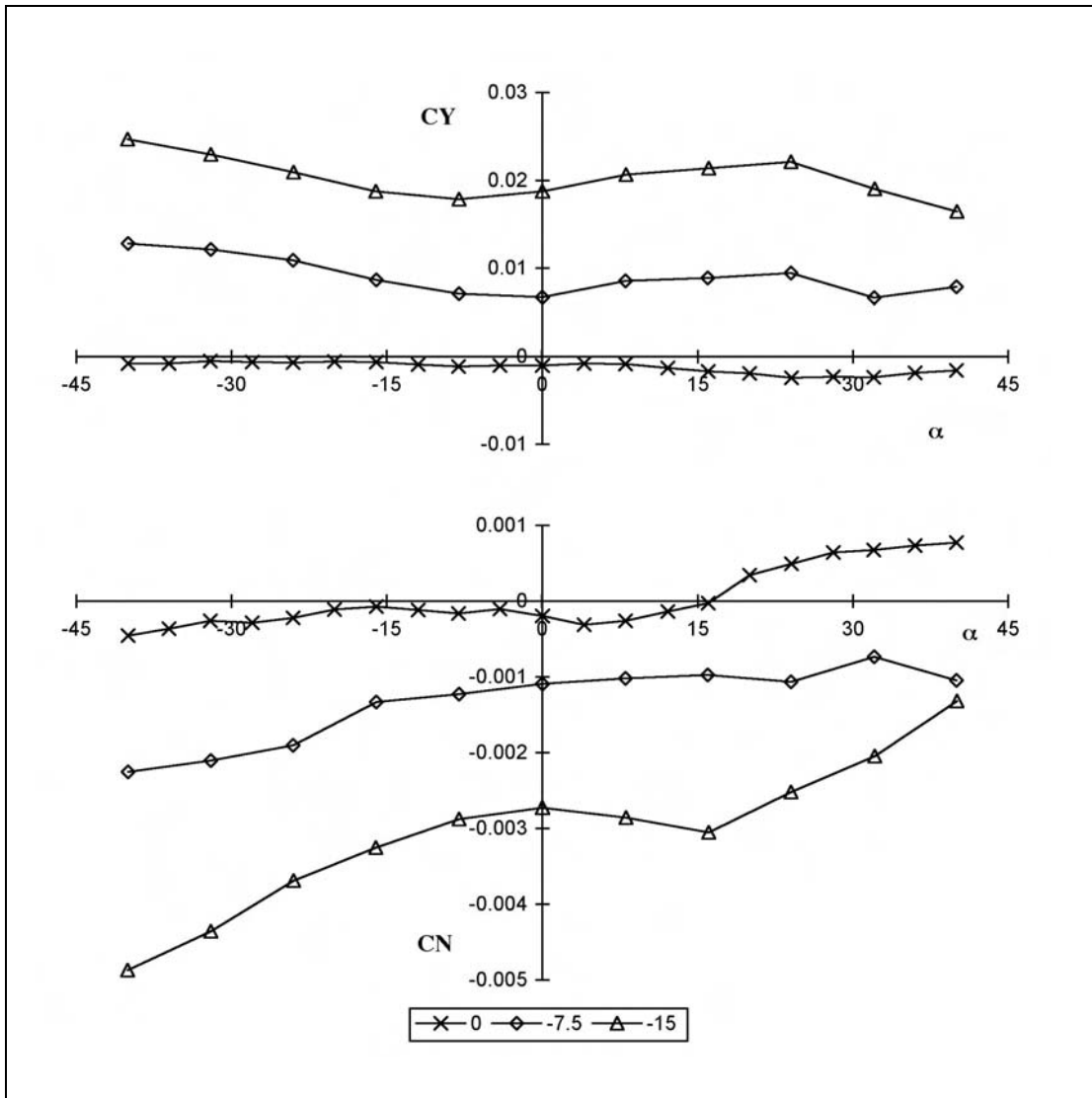
Figure 3.24   Effect of Sideslip Angle on Cowling Off, Tail On Configuration
                   (Power Off)
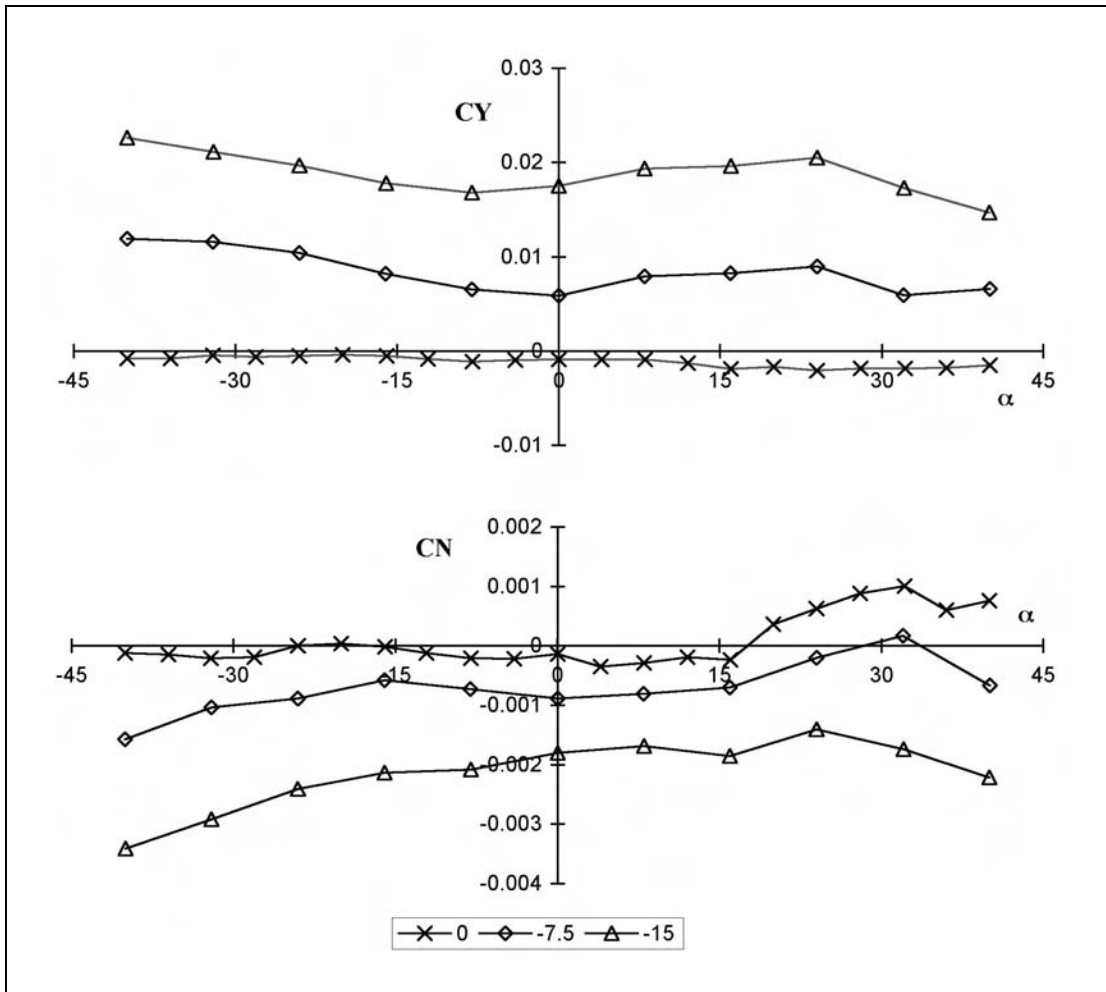
Figure 3.25   Effect of Sideslip Angle on Cowling Off, Tail Off Configuration
(Power Off)
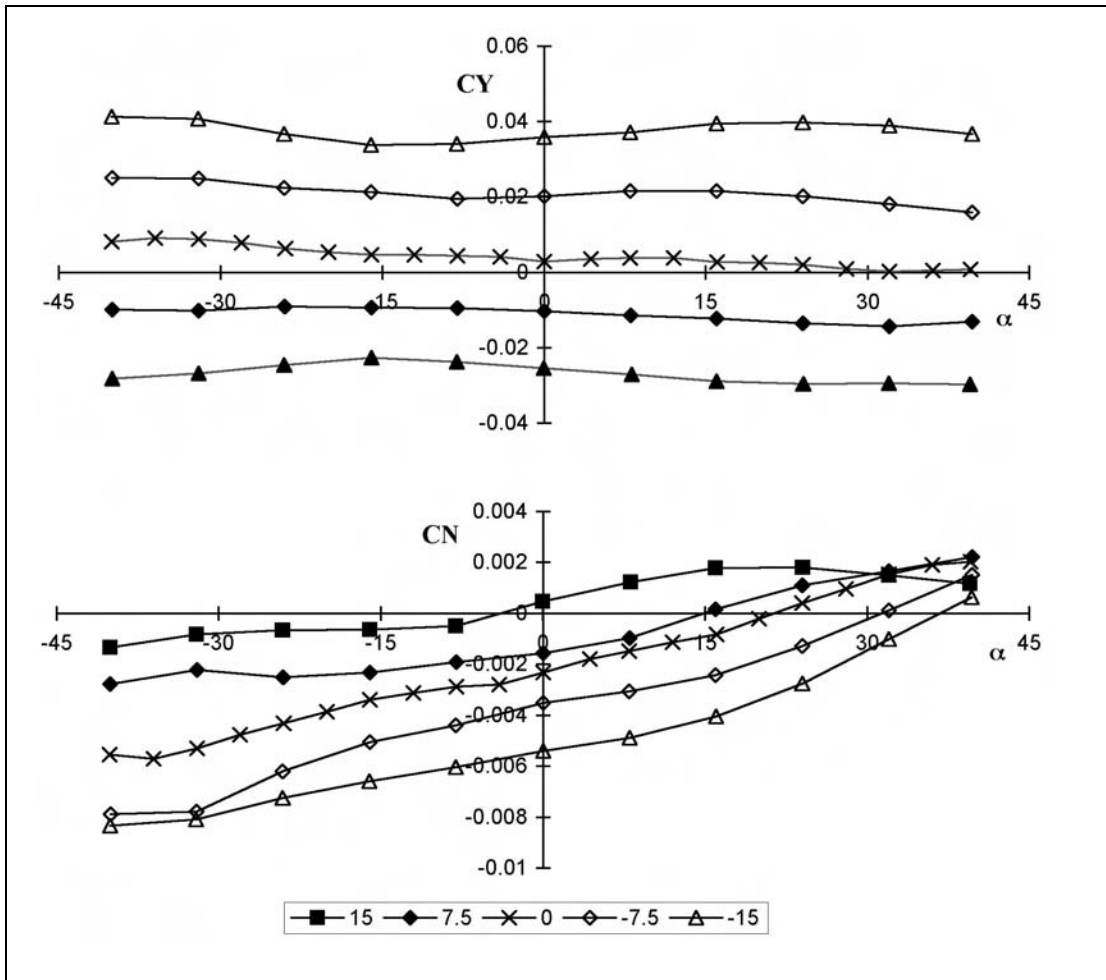
Figure 3.26   Effect of Sideslip Angle on Cowling On, Tail On Configuration
(Power On)
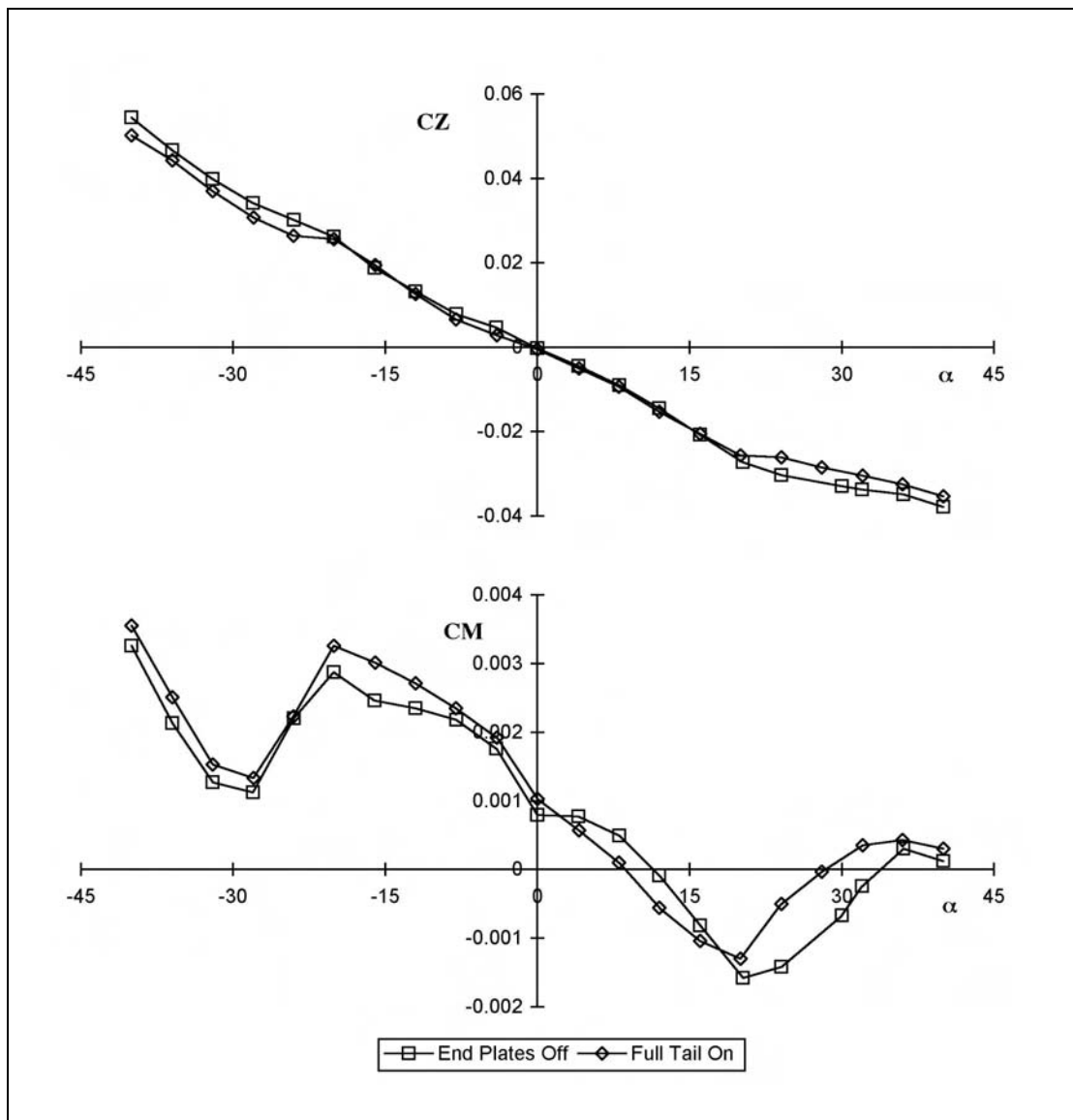
Figure 3.27   Effect of Tailplane Endplates on CZ and CM, β = 0, Power Off, Cowling On
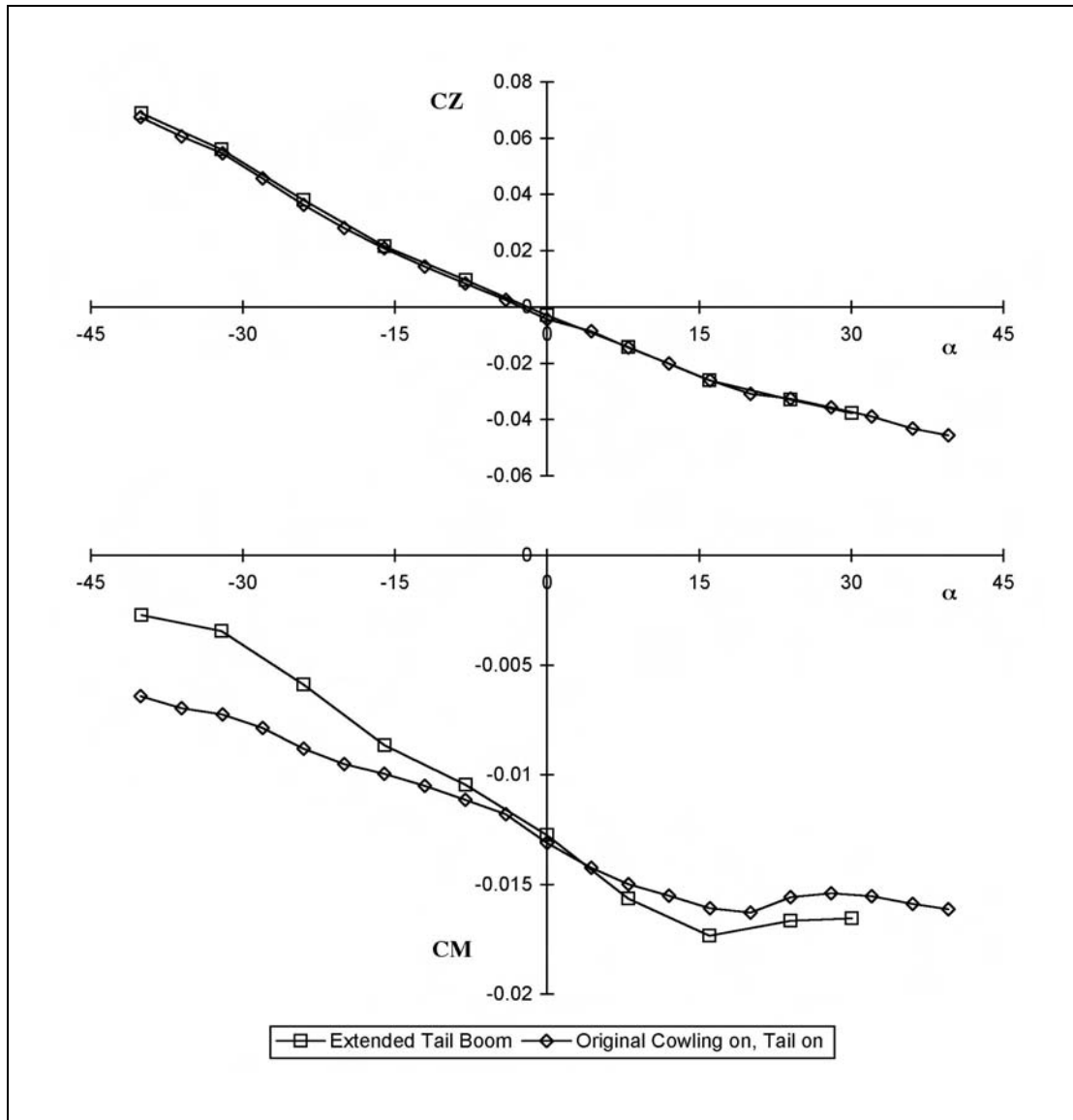
Figure 3.28   Effect of an Extended Tail Boom on the Cowling On,
Tail On Configuration (Power On)

4   Development of a High Fidelity Gyroplane Simulation

4.1   Aims

Before developing any mathematical model it is important to be clear on the purposes to which it will be put. For the current study there are three distinct uses for the model. Firstly, there is clearly a gap in the understanding of the fundamental dynamic characteristics of the gyroplane configuration. The aim will be to use the model to put the stability characteristics of this configuration into context alongside those of fixed wing aircraft and other rotorcraft. Secondly, the model can be used to undertake parametric studies of the configuration to identify any key configurational parameters which might strongly influence the stability characteristics. Third, it is anticipated that the model might be useful in predicting the characteristics of new or modified vehicles, highlighting the possibility of characteristics which might be detrimental to airworthiness. This last aim, of course, can only be considered once the validity of the model has been established (see Section 6).

In the following section the RASCAL mathematical model, and its reconfiguration for use in simulating gyroplanes, will be discussed in some detail. Readers unfamiliar with the basic concepts of rotorcraft mathematical modelling, and the methods used to determine the dynamic stability of aircraft are referred to Appendix 4 for background information.

4.2   Background

Mathematical modelling of rotorcraft dynamic characteristics is considerably more challenging than that of fixed wing aircraft. This is due mainly to the additional degrees of freedom from the rotor but also due to the nonlinearities present and the coupling between the longitudinal and lateral/directional dynamics. The equations of motion are expressed in the form:

$$m(\dot{U} + QW - VR) = X - mg\sin\Theta$$
$$m(\dot{V} + RU - PW) = Y + mg\cos\Theta\sin\Phi$$
$$m(\dot{W} + PV - QU) = Z + mg\cos\Theta\cos\Phi$$

$$(4.1)$$

$$I_{xx}\dot{P} - I_{xz}\dot{R} + QR(I_{zz} - I_{yy}) - PQI_{xz} = L$$
$$I_{yy}\dot{Q} + RP(I_{xx} - I_{zz}) + (P^2 - R^2)I_{xz} = M$$
$$I_{zz}\dot{R} - I_{xz}\dot{P} + PQ(I_{yy} - I_{xx}) + QRI_{xz} = N$$

where U, V, and W are the components of translational velocity in the x, y, and z body axis directions, and P, Q, and R are the angular velocities about the axes. The roll and pitch attitudes are given by Φ and Θ respectively, m is the aircraft mass, and I_{xx} etc. are its moments of inertia.

The real effort in modelling a rotorcraft (or any other rigid body) is in the development of suitable methods of calculating the external forces and moments, X, Y, Z and L, M and N. In general the procedure would be to break down the vehicle into a number of subsystems or components so that in the case of a gyroplane, for example:

$$X = X_{Rotor} + X_{Prop} + X_{Fuselage} + X_{Tailplane} + X_{Rudder}$$

(4.2)

Components such as those from the fuselage and the tailplane are simply the aerodynamic loads which, for the current study, are readily obtained directly from the wind tunnel data described in section 3. The real complexity lies in establishing the rotor components for a given flight condition.

The loads generated by a rotor are calculated using the well understood approach of blade element theory. The blade is divided into a number of elements, the normal and tangential components of velocity at these elements is derived from the blade kinematics allowing the angle of attack of each element to be established. A look-up table of aerodynamic properties of the blade section used (NACA 8H12, for example) is then used to calculate the lift and drag of the element. The component forces and moments acting on the blade are then obtained by summing the contributions from all of the elements, and making appropriate transformations into body axes. The loads on a given element vary with its position around the azimuth giving a periodic forcing with time. Some mathematical models essentially average the load over one complete revolution to give steady values for loading, however, higher fidelity representations such as the model used here, retain the periodicity of the rotor's motion. It is clear that in order for this scheme to be accurate, the kinematics of the blade motion must be accurately represented. This involves considering each individual blade and fully representing its motion as a function of azimuth and vehicle state. The geometry of the rotor system - position of the teeter hinge for example, is therefore important. The position of a particular blade element will be dependent on the bending of the blade as well as its teetering, and a simple structural model which assumes that the blade is attached to the hub by a stiff torsional spring may also be included. It is also worthy of note that if the rotor model is expressed in a generic manner, then the same model can be used to represent the propeller, albeit with different representative data, and this is the approach adopted here.

The description above gives the reader a basic idea of the nature of the mathematical model used in this study. Further background information on rotorcraft modelling can be found in the many excellent text books available on the subject [39, 40, 82–6]. The mathematical model used in this study, RASCAL, was developed in a manner which allowed it to be configured for any rotorcraft type, although it had mainly been used for helicopter simulation [87–89]. Details of the model are summarised in the following section, the reader being referred to the published literature for more extensive information.

4.3   **A Description of the RASCAL Model**

The RASCAL model was developed primarily to study the flight dynamics of helicopters but with sufficient generality to allow it to be modified to capture other rotorcraft types. In this section, it is introduced in its most fundamental form, whilst its reconfiguration to represent a generic gyroplane configuration is detailed in the next section. The model has been influenced strongly by the literature in the field, taking account of the significance of research by others into individual blade/blade element modelling, and dynamic inflow modelling [90]. The key features of the model used are summarised in Table 4.1.

Table 4.1 RASCAL Mathematical Model Description

Model item	Characteristics
Rotor dynamics (main, tail, or propeller)	• up to 10 individually-modelled rigid blades • fully-coupled flap, lag and pitch motion • blade attachment by hinges and springs • lag damper
Rotor loads	• aerodynamic and inertial loads represented by up to 10 elements per blade
Blade aerodynamics	• lookup tables for lift and drag as function of angle-of-attack and Mach number
Wake model	• momentum-derived dynamic wake model • uniform and harmonic components of inflow • rudimentary interaction with tail surfaces • ground effect
Transmission	• coupled rotorspeed and engine dynamics • up to 3 engines • geared or independently-controlled rotor torque
Airframe	• fuselage, tailplane and fin aerodynamics by lookup tables or polynomial functions
Atmosphere	• International Standard Atmosphere • provision for variation of sea-level temperature and pressure

The model takes the form

$$A\underline{\dot{x}} = f(\underline{x}, \underline{u})$$

(4.3)

where the state vector $\underline{x}$ contains the airframe translational and angular velocity, blade flap, lag and pitch angles and rates for each blade on each rotor (in the context of gyroplanes this implies a main rotor and a propeller), the induced velocity states for each rotor wake as well as the angular velocity of both rotors, and the engine torque. Elements of the control vector are the four controls, which vary with aircraft type, e.g. single main and tail rotor configurations will have three main rotor controls and one tail rotor control. Depending on the number of blades on each rotor, there can be up to 100 non-linear, periodic ordinary differential equations describing the coupled rotor/airframe behaviour. The body dynamics are represented by equations (4.1). Note that the matrix contains off-diagonal terms not simply associated with airframe products of inertia, but which also include terms associated with the dynamic inflow and blade equations of motion.

The model has been used previously for helicopter validation and simulation studies, [87–89], and simulation of gyroplanes [62, 66, 67, 91].

4.4 **Configuring the RASCAL Model to Represent a Gyroplane**

As described above, the RASCAL model was written to represent a generic rotorcraft, and configuration as a gyroplane required synthesis of an appropriate aircraft data file. The data files for the VPM M16 and the Montgomerie-Parsons are given in Appendix 2.

4.4.1 **Aircraft Measurements**

Accurate measurements of the aircraft's principle dimensions were made. These included blade chord and length, propeller location, and teeter bolt location. The aircraft was also weighed with and without fuel. Lists of the measured data are given in Appendix 2. Note that the body axes frame of reference to which all geometric measurements are referred is the point at which the mast and keel lines intersect (rear mast in the case of the Montgomerie-Parsons).

The centre of mass position was identified as a key parameter and care was taken in every set of tests to ensure that its position was known accurately. In the first campaign the centre of gravity location was established by hanging the aircraft (G–BWGI) from its teeter bolt (at a known location). An inclinometer was placed on the aircraft keel and masses added at a known point until the keel became level. The centre of mass location could then be established by simple geometry. For the trials involving G–UNIV an alternative method of locating centre of gravity involving the use of a calibrated aircraft weighing system was employed (see Appendix 3).

The aircraft pitching and yawing moments of inertia, I_{yy}, and I_{zz} were obtained by hang tests. A single-point suspension method (from the teeter bolt) was used for the former, and a bifilar method for the latter [39]. Periods of oscillation were taken and converted into the moments of inertia. Note that I_{xx} could not be measured due to the nature of the suspension point provided. The most likely lowest estimate was made, based on rotor and pilot masses.

4.4.2 **Aircraft Aerodynamic Data**

The VPM M16

The aerodynamic data from the wind tunnel tests was incorporated into the RASCAL model for the VPM M16 in the form of look-up tables. These look-up tables contained body axis fore-and-aft, lateral and vertical forces, and roll pitch and yaw moments at five angles of attack within the range ± 40 deg and five sideslip angles within the range ± 40 deg. Linear interpolation is used to estimate coefficient values at general intermediate points between measured data values. The data from the tests with power off was used, as this was thought to give the worst case in terms of the fin / rudder effectiveness. Without the benefit of the propeller flow field, the forces and moments arising from these components are likely to be less than might otherwise be the case.

It should be noted that the data obtained from the wind tunnel tests was for a VPM M14 gyroplane despite our wish to simulate the M16 variant. In aerodynamic coefficient terms, the differences between the two aircraft are largely superficial, the general shape and dimensions of both aircraft are similar. The use of M14 data to simulate the M16 should not significantly compromise the validity of results, particularly as the gyroplane operates at low speed.

The Montgomerie-Parsons

As it was not possible to test a Montgomerie-Parsons model in the wind tunnel, the strategy adopted was to adapt the data available for the VPM to suit. The premise was that both aircraft types are largely similar in basic configuration and so it is likely that their aerodynamic characteristics would be alike. Account of differences in size were easily incorporated by scaling based on appropriate planar areas. Some additional synthesis of the VPM data was required to obtain pod lift and drag coefficients, CL and CD. The pitching moment was estimated from the simple expression:

$$C_m = C_{m_0} + C_{m_\alpha} \alpha$$

where the coefficients C_{m_0} and C_{m_α} were estimated using the synthesised C_L and C_D values and an assumed moment arm.

4.4.3 **Blade Airfoil Section Data**

It is a feature of an individual blade/blade element model that a comprehensive description of the blade section aerodynamic properties can be included. For both aircraft, the manufacturer describes the rotor blade section as a NACA 8H12 and data for this profile was obtained [92]. It became apparent when comparing the 8H12 profile with that of the actual blade on the VPM that there were some differences. There was the possibility that these differences may have a significant effect on the predicted properties of the blades and hence may have an effect on the simulation results. In particular, there is an obvious relationship between poor prediction of drag properties and resulting poor prediction of rotorspeed. An aerodynamic assessment of the actual blade was made by GKN Westland Helicopters Ltd., [93] and its main recommendations were as follows:

a) The low drag characteristics of the 8H12 may be diminished as spanwise flow and centrifugal effects will prevent laminar flow.

b) The actual aerofoil has a greater CL_{max} at lower Mach numbers than the 8H12 but at high Mach numbers the performance reduces rapidly.

c) The NACA 8H12 exhibits positive pitching moment coefficient and a negative gradient. The VPM M16 aerofoil has a similar pitching moment coefficient but its gradient is much less marked.

The results from this study were used to modify the existing 8H12 data set in order to make it more representative of the actual blade used on the VPM aircraft. The data was also used for the Montgomerie-Parsons model as blades from the same manufacturer are used in this vehicle. Data for the 8H12 section is available for a variety of surface roughness conditions. Initially data for zero roughness was applied, however the resulting rotorspeed and Q_Ω derivative comparisons suggested that higher drag was present in the real aircraft. Section data for greater roughness (and hence higher drag) was therefore applied which halved the rotorspeed error and improved the correlation in Q_Ω. When a comprehensive validation exercise is performed, as in this case, one of the main aims is to identify where it is possible to adjust the model to improve the fidelity of the predictions. Any changes to the model must of course be physically justifiable. In this case, the validation exercise (Section 6) has highlighted the need to increase the drag of the blade section, and the independent information available on this blade section, which indicates a sensitivity to surface roughness, certainly provides the necessary justification for this action.

4.5   **Results from the Mathematical Model**

The mathematical model can be used to provide 3 related sets of data. Firstly the model can be configured to provide trim data. The body accelerations a   made zero so that there are no resultant unsteady forces on the aircraft (essentially $\underline{\dot{x}}$, on the left hand side of equation 4.3 is set to zero), and the equations solved to provide the control positions and resulting body attitude to achieve trimmed flight for a given flight velocity, for example. Next it is possible to obtain the vehicle's response to a particular pilot input by using equation 4.3. This time the control vector $\underline{u}$, is perturbed to simulate a pilot input (a step change, from the trim value, of one or more of the controls, for example) and a numerical integration scheme (Runge-Kutta, for example) used to calculate the response of the vehicle. The output is a set of time histories showing how the various states of the aircraft change in response to the input. Finally, it is possible to linearise the nonlinear equations of motion given by equations (4.3). The linearization process is described by Padfield [89], however for the purposes of this report it is sufficient to say that the nonlinear set of equations (4.3) when linearised are expressed in state-space form as:

$$\underline{\dot{x}} = \mathbf{A}\,\underline{x} + \mathbf{B}\,\underline{u}$$

(4.4)

where the symbols and their meaning are as follows:

$\underline{x}$ The linearization process is defined from a known reference point - usually taken to be a trim state. The vector $\underline{x}$ is known as the state vector and contains the n states which represent the dynamic characteristics of interest expressed as perturbations from the trim state.

$\underline{u}$ This is the control vector and contains the *m* control variables (again as perturbations from trim).

A   This is a square matrix of dimension *n* which has a series of constants known as the stability derivatives which again are referred to a particular trim state, and represent the dynamic characteristics of the vehicle.

B   This is the control matrix which is of dimension *n x m* and contains the control derivatives.

One structure of model which has been found to be useful for gyroplane flight dynamics is an extension of the classical longitudinal set of equations familiar for fixed wing flight, which includes the rotor speed degree of freedom. For this model we have:

$$\underline{x} = \begin{bmatrix} u \\ w \\ q \\ \theta \\ \Omega \end{bmatrix}, \quad \underline{u} = \begin{bmatrix} \eta_s \end{bmatrix}, \quad \mathbf{A} = \begin{bmatrix} X_u & X_w & X_q & X_\theta & X_\Omega \\ Z_u & Z_w & Z_q & Z_\theta & Z_\Omega \\ M_u & M_w & M_q & M_\theta & M_\Omega \\ 0 & 0 & 1 & 0 & 0 \\ Q_u & Q_w & Q_q & Q_\theta & Q_\Omega \end{bmatrix}, \quad \mathbf{B} = \begin{bmatrix} X_{\eta_s} \\ Z_{\eta_s} \\ M_{\eta_s} \\ 0 \\ Q_{\eta_s} \end{bmatrix}$$

(4.5)

Note that the convention is that lowercase characters are used in the linearised equations. For example, in the nonlinear equations (4.1), U is the translational velocity in the direction of the x-axis whilst in the linearised equations u is defined as the (small) perturbation from the reference trim state, U_e, that is $U = U_e + u$. The main limitation of these equations is that they are only valid for small perturbations from the trim state. As they are linear, however, they are extremely useful in determining the aircraft's stability characteristics, as discussed in Appendix 4.

As an example of how the simulation may be used, consider the case of the VPM aircraft in its nominal configuration described in Appendix 2. Figure 4.1 shows the variation in the trim values of the controls, rotor speed, and pitch and roll attitude over the speed range from 30 to 70mph (IAS). The decrease in longitudinal hub tilt with increasing airspeed is equivalent to the disc tilting forward, and a forward migration of the stick. As would be expected, this is accompanied by the pitch attitude of the aircraft reducing from about 6° at low speed to 1° at higher speeds. At all flight speeds the aircraft sits "left wing down", as indicated by the negative roll attitude. Given that the full travel of lateral tilt is equivalent to 18° (i.e. ±9°), the lateral tilt for trim over the speed range of 2° is significant. Finally, rotor speed is also shown, and from this plot it is apparent that there is only a slight increase in the rotor speed for trim over the speed range. Figure 4.1 represents a small subset of the data which is produced by the trim calculation; all of the aircraft and rotor states are calculated along with performance related parameters such as power required and propeller thrust.

Consider now the use of the model to calculate response to control inputs. As an example, Figure 4.2 shows the response of the VPM M16 to a longitudinal stick input (shown in the first plot). The aircraft is initially in trim at a velocity of 40mph then, after 3 seconds, a step input of longitudinal stick equivalent to an aft hub tilt of 1° input is applied. This is maintained for 5 seconds after which the stick is returned to its original trim position. This input is typical of one used in BCAR Section T compliance tests. Initially the short period mode is excited, which can be characterised by a heavily damped oscillation in pitch rate, which is visible in the first few seconds of the pitch rate response. Whilst the aft stick is held the pitch rate is positive and the pitch attitude is nose up, reaching around 20° before the forward stick step input is applied, arresting the motion. The longer term response, the phugoid, becomes apparent with the periodic variation in airspeed (and attitude). Note that the high frequency oscillations on the pitch rate plot are due to the teetering motion of the rotor that is captured by the model through its representation of the individual blade dynamics. They are not visible on the pitch attitude plot, for example, as the high frequency content of the pitch rate response will, effectively be filtered by the integration process used to obtain pitch displacement.

Finally, the nonlinear model can be linearised as described above to produce the simplified representation given by equation (4.4). Using the structure shown in equation (4.5) it is possible to predict the stability characteristics of the aircraft over its speed range by calculating the stability derivatives (X_u, X_w, …, Q_Ω) at each trim speed, to form a system matrix **A** at each speed. The eigenvalues (see Appendix 4) can then be plotted on the complex plane to examine the aircraft's stability characteristics. The results for this exercise are shown in Figure 4.3 where the eigenvalues are plotted again from flight speeds in the range 30–70mph, as indicated. As in fixed wing aircraft, the characteristic modes are a short period mode which is a heavily damped oscillation in pitch, and the phugoid which is a longer period mode characterised by oscillations in airspeed and attitude. The third mode is a rotor speed mode which is aperiodic and varies very little over the speed range. The short period mode damping varies from around 0.85 at low speed to 0.6 at higher speeds. The phugoid is unstable at low speeds (i.e. the eigenvalues are to the right of the

frequency axis, see Figure A4.3, Appendix 4), but stabilises as speed is increased (the eigenvalues move over to the left of the axis). The point of neutral stability occurs at about 40mph, and the frequency here is approximately 0.04cycles/sec (equivalent to a period of 25 seconds). Figure 4.4 is equivalent to Figure 4.3 however the eigenvalues are plotted in an alternative form as frequency vs. damping ratio (see Appendix 4), which is a more convenient format when investigating compliance with BCAR Section T. As explained in Appendix 4, one consequence of plotting eigenvalues in this way is that the stable region of the plot is now to the right of the vertical axis. The short period mode is now on the right hand side of the plot as positive damping ratio indicates a decaying amplitude of oscillation (i.e. stability). Note that the rotor speed mode, cannot be displayed on this plot (damping ratio cannot be defined for aperiodic modes), which is another consequence of plotting eigenvalues in this way.

Figure 4.2 shows the response of the aircraft calculated using the nonlinear version of RASCAL for a flight case initiated at a trim speed of 40mph. Examining the pitch attitude plot it is apparent that the period of the phugoid oscillation is indeed around 25s. It should be appreciated that in this case the linear and nonlinear models are in agreement as the perturbations from trim experienced are small. The linear model (developed from the nonlinear model) would not be suitable for simulating larger scale manoeuvres.

Although the results from the RASCAL simulation presented here can all be discussed qualitatively and logically, the issue of just how representative these values are with respect to those of the actual aircraft can only be established by a full model validation exercise. Such an exercise is discussed fully in Section 6.
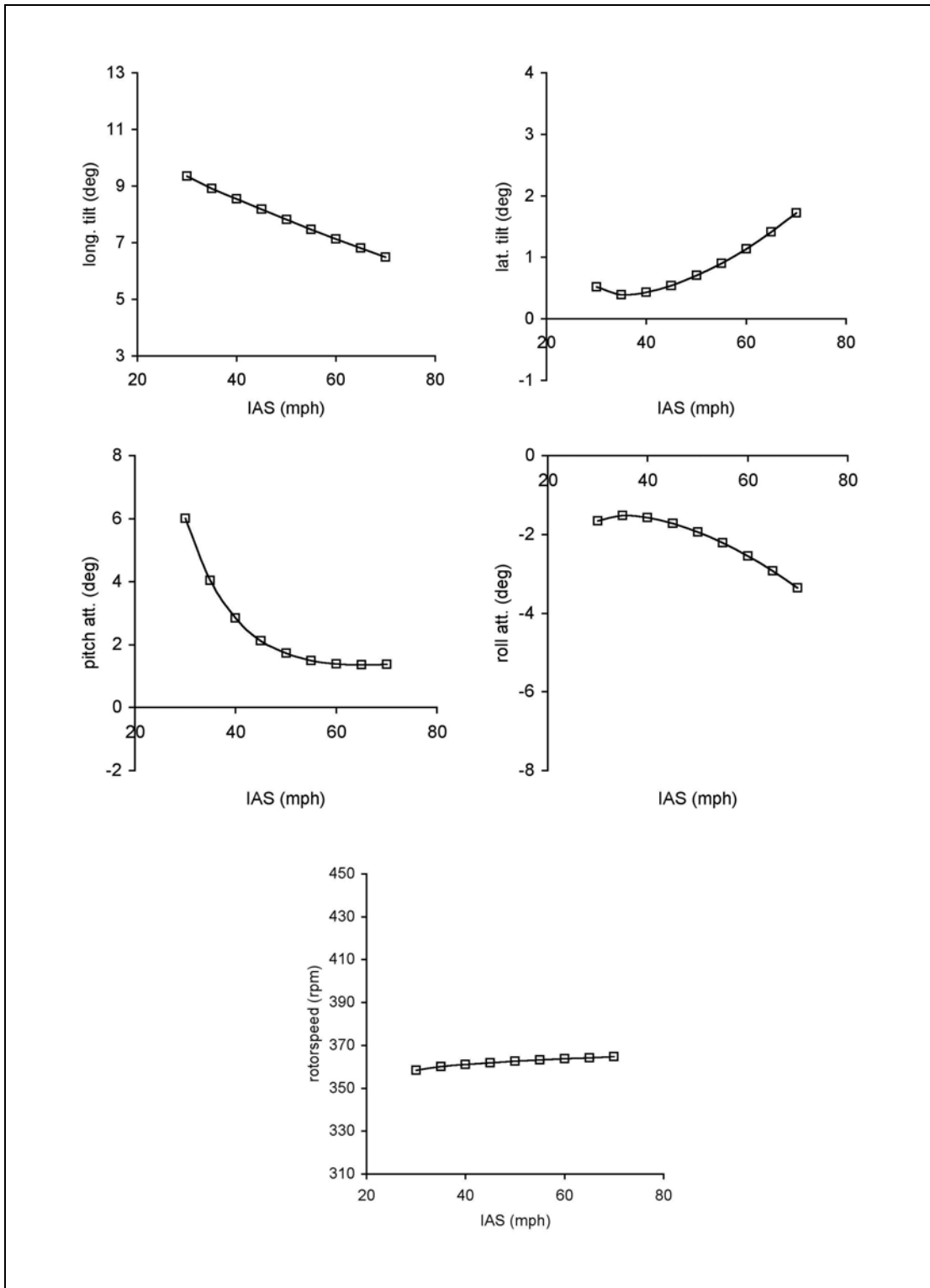
Figure 4.1   Trim Results from RASCAL Mathematical Model for VPM M16
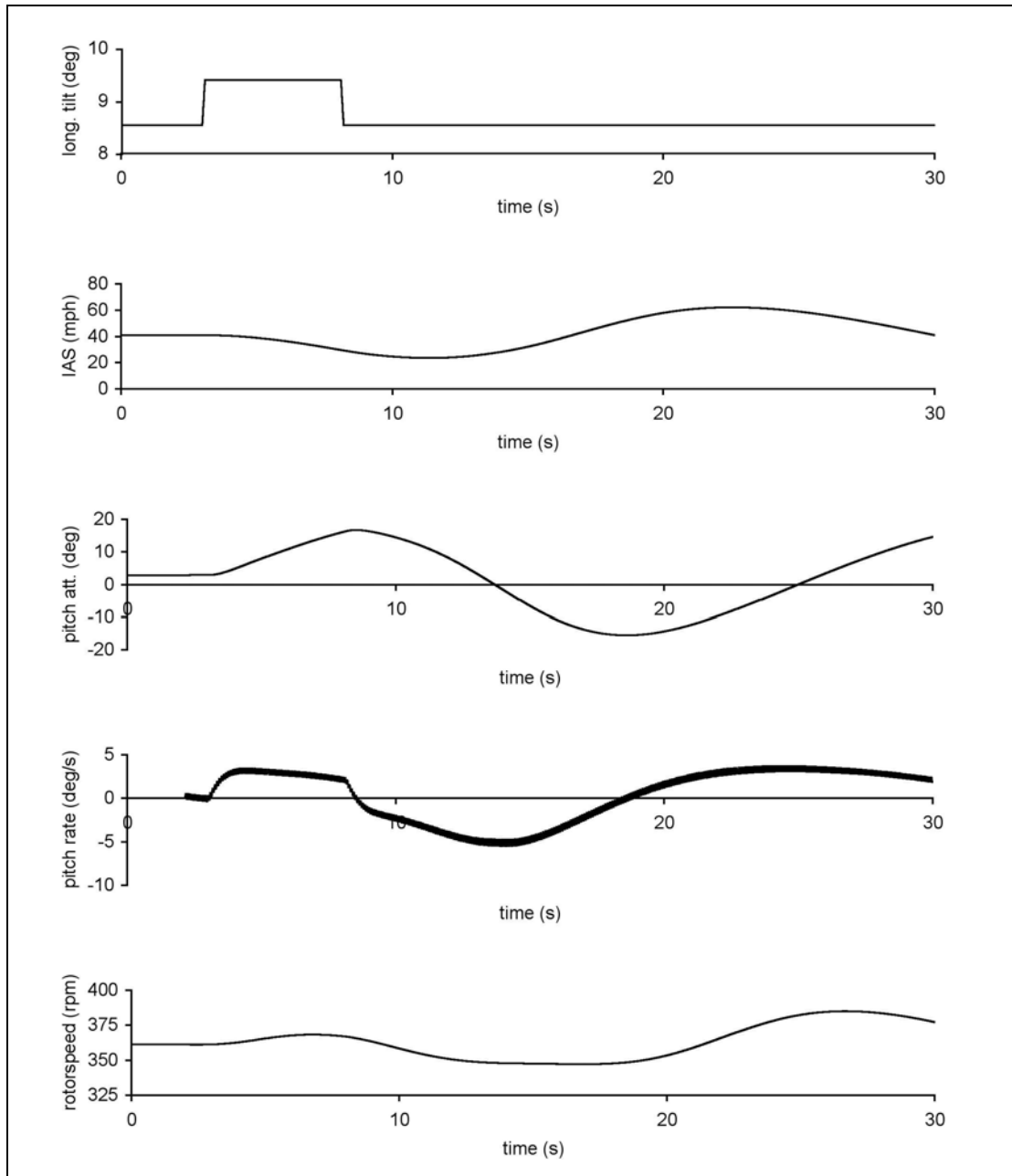
Figure 4.2   Response of VPM M16 to a 5s Pulse in Longitudinal Stick (40mph, IAS)
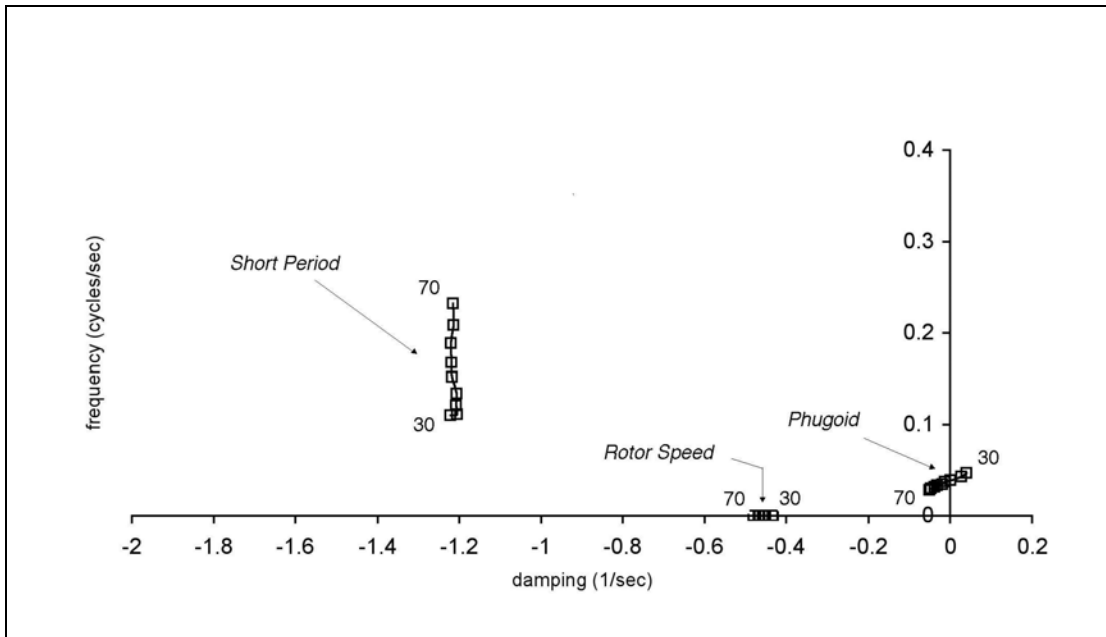
Figure 4.3   Eigenvalues for VPM M16
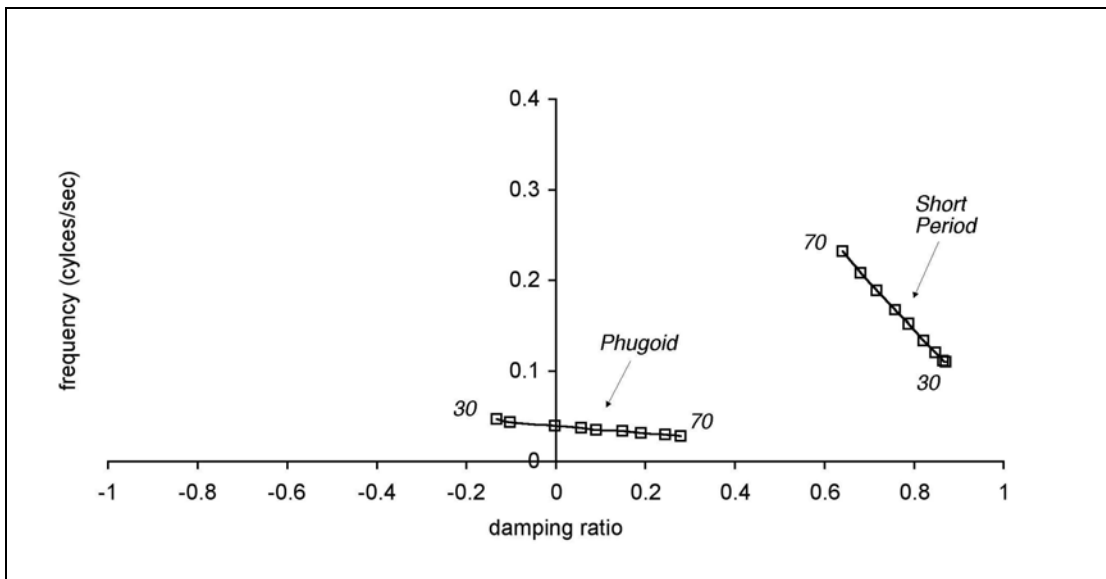
Figure 4.4   Eigenvalues for VPM M16 Plotted Against Damping Ratio

5 Flight Testing

5.1 Background

Flight testing, as with any experimental activity, is a vital component of aeronautical engineering studies requiring understanding of real behaviour. It is important however to recognise that there are various categories of flight test as described by Bailey [79]. Since the design of the experiment and the resulting data is tuned exactly to the nature of the specific application, the activity may appear abstract and obscure to the lay person or pilot. The application for which data is required here, is model validation. The flight testing is therefore best described as 'experimental' or 'research' flying and by Bailey's definitions means that the nature of the tests are unusual.

Three test campaigns were undertaken. The first, using VPM M16 G-BWGI, was conducted in 10 hours of flying based at Flight Refuelling Ltd's Bournemouth base in October 1996, Figure 5.1. The second, using Montgomerie-Parsons Two-Place G-UNIV, took place at Bournemouth (October 2000) and Carlisle (February 2001), Figure 5.2. The third and final trial was conducted at Perth in July 2005, again using G-UNIV.

The first two trials were designed specifically to gather data that could be used to validate the mathematical model used for simulation studies. It was felt necessary to undertake two sets of validation trials to gather data on different aircraft of the same class to confirm the general applicability of the model. The third trial was designed to gather rotor teeter data in steady and manoeuvring flight, with a view to making an assessment of the behaviour of an actual rotor. It was hoped that these data could also be used to further support mathematical model validation, but this was not the primary aim. The first two trials were conducted under Flight Refuelling Ltd's 'B' conditions approval; the third campaign was conducted under a Permit to Fly for Test Purposes, with close CAA supervision and direction. Tables 5.1 – 5.3 summarise the content of these three campaigns.

Table 5.1 Summary of VPM M16 Flight Trials

Flight number	Airspeed (mph)	Nature	Location
1 - 4	-	Pre-trials test flights	Bournemouth
5	25 - 75	Steady, level flight. Zero sideslip	Bournemouth
6	25 - 75	Steady, level flight. Sideslip angles ±5°, ±10°	Bournemouth
7	30, 50, 70	Longitudinal stick doublets; phugoid (step) inputs	Bournemouth
8	30, 50, 70	Longitudinal stick doublets; phugoid (step) inputs	Bournemouth
9	30, 50, 70	Lateral stick and rudder doublets, steps, frequency sweeps (70mph only)	Bournemouth
10	70	Longitudinal, lateral and rudder frequency sweeps	Bournemouth

Table 5.2 Summary of Montgomerie-Parsons Two-Place Flight Trials
(Model Validation)

Flight number	Airspeed (mph)	Nature	Location
1 , 2	-	Pre-trials test flights	Bournemouth
3	60	Steady, level flight.Phugoid (step) and doublets, all controls	Bournemouth
4	60	Steady, level flight.Phugoid (step) and doublets, all controls	Carlisle
5	60	Frequency sweeps, all controls	Carlisle
6	40	Phugoid (step) and doublets, all controls	Carlisle
7	40	Longitudinal frequency sweeps	Carlisle
8	50	Phugoid (step) and doublets, all controls	Carlisle
9	40, 50, 60	Phugoid (step), doublets and frequency sweeps (longitudinal stick only)	Carlisle

Table 5.3 Summary of Montgomerie-Parsons Two-Place Flight Trials
(Teeter Angle Measurement)

Flight number	Airspeed (mph)	Nature	Location
1	-	Permit test flight	Perth
2	30-70	Steady, level flight. Steady, turning flight (up to ±30°bank)Climb/descent various power settings	Perth
3	40, 50, 60	Longitudinal stick; phugoid (step) inputs	Perth
4	40, 60	Steady, level flight. Sideslip angles ±5°, ±10°	Perth

5.2   **Flight Test Procedures and Techniques**

It is important to understand the terminology and purpose of these individual tests. A general, steady flight condition can be defined in terms of airspeed; turn rate; rate of climb or descent; and sideslip angle. Steady, level flight is therefore an equilibrium condition at a constant airspeed and altitude. Nominally conducted with zero sideslip (i.e. balanced flight), some tests were flown in an unbalanced condition with up to 10 deg of sideslip. The simulation model can then be set up in exactly the same flight condition and a direct comparison made of the control positions, roll and pitch angles, rotorspeed etc. required to hold that equilibrium condition. The control input cases (step, doublet, frequency sweep and phugoid) perturb the aircraft from this

equilibrium condition, producing non-steady (i.e. time-varying) changes in the measured parameters. These resulting 'time histories' can be used to characterise the aircraft behaviour, or be compared directly with the simulation model disturbed by exactly the same control input, or be compared mathematically in exactly the same form as the model giving a direct comparison of the mathematical framework of the simulation.

The fundamental objective when flight testing to provide data that characterises an aircraft's response is to excite it in frequency and amplitude. Amplitude is straightforward - the test pilot simply applies larger inputs with the appropriate flying control. Frequency testing is less easy, or straightforward. It may be required to excite a particular frequency or a range of frequencies. Airworthiness and flight safety considerations are paramount. Large inputs may cause departure from controlled flight or over-stress; certain frequencies may excite structural modes rather like flutter in fixed-wing aircraft. These inputs must be applied from a steady flight condition to have any meaning. Samples of what they should look like are shown in Figure 5.3. These are not examples from flight but illustrate a mathematically perfect input that the pilot needs to replicate as closely as possible. The first is called a step; the second is a doublet; and finally a frequency sweep is shown.

The frequency sweep clearly excites over a range of frequencies. It is normal to start at low frequency and build up to the faster cycles. The sweep shown here starts with a 24 sec period, followed by 20 then 16, 12, 8, 4 and 2. The input then moves on to higher frequencies up to a limit defined by flight safety considerations. The doublet looks like a square sine wave and, indeed, in terms of frequency of excitation this is how it impacts on the aircraft - doublets excite at a particular frequency. In this case it is about 0.5 Hz (the frequency is not exactly the same as the sine wave analogue). Finally, the step excites the aircraft at a range of low frequencies, although it is obviously difficult to see any 'wave' content in the data (sophisticated mathematical and numerical analysis tools [80], are required to see the frequency content of any waveform, and will be referred to later in the data analysis).

5.3   Instrumentation

A range of parameters were recorded during each flight trial, and the instrumentation used is summarised in Table 5.4. The fundamental flight mechanics data consists of airspeed, angle of attack and sideslip; roll, pitch and yaw rates; roll, pitch and yaw (heading) attitudes; longitudinal, lateral and normal acceleration (these with reference to a set of axes fixed in the aircraft); rotor and propeller rotational speeds; and the positions of the flying controls (control column pitch and roll, rudder and throttle positions). These parameters were common to all three flight test campaigns. A selection of the sensors used across the first two campaigns is shown in Figures 5.4 and 5.5.

The aircraft used for the first campaign of test flying was a privately owned VPM M16 gyroplane (G-BWGI). It is shown in unmodified form in Figure 5.1. The aircraft was modified to carry appropriate measurement instrumentation by FR Aviation at their Bournemouth Airport site. Additional specialised sensors were fitted for this trial in the form of 5 strain gauges applied to various elements of the flying control system. These had no part to play in this study but were fitted at the request of the CAA to be analysed in-house as part of a follow-up investigation to the incident involving G-YRAT, [81].

Table 5.4   Instrumentation Used in Flight Tests

Parameter	Description	Units	Measurement Device
a_x	Longitudinal Acceleration	m/s^2	Accelerometer
a_y	Lateral Acceleration	m/s^2	Accelerometer
a_z	Normal Acceleration	m/s^2	Accelerometer
P	Roll Rate	rad/s	Rate Gyro
Q	Pitch Rate	rad/s	Rate Gyro
R	Yaw Rate	rad/s	Rate Gyro
Φ	Pitch Attitude	rad	Attitude Gyro* Angle Indicator**
Θ	Roll Attitude	rad	Attitude Gyro* Angle Indicator**
Ψ	Heading	rad	Pick-up from existing sensor* Angle Indicator**
V_f	Indicated Airspeed	knots	Air Data Probe
h	Altitude	m	Air Data Probe*
β	Sideslip Angle	rad	Air Data Probe
α	Angle of Attack	rad	Air Data Probe
η_s	Longitudinal Stick Position	%	Displacement Transducer
η_c	Lateral Stick Position	%	Displacement Transducer
η_p	Pedal Position	%	Displacement Transducer
η_t	Throttle Position	%	Displacement Transducer**
N_g	Propeller Speed	rpm	Induction coil* Optical sensor**
N_r	Rotor Speed	rpm	Pick-up from existing sensor* Optical sensor**
x_E, y_E, z_E	Aircraft position	m	GPS**
γ_t	Teeter Angle	rad	Rotary Transducer**
ψ	Blade Azimuth	rad	Rotary Transducer**

* VPM M16 (G-BWGI) ** Montgomerie-Parsons (G-UNIV)

For the second set of trials the University of Glasgow-owned Montgomerie-Parsons gyroplane, G-UNIV was used, Figure 5.2. This two seat aircraft was modified by the manufacturer to accommodate the necessary instrumentation, essentially by removing the second seat. The sensor and recording system was designed and built by University of Glasgow technical staff using "off the shelf" components.

The third campaign (the second involving G-UNIV) involved measurement of teeter angle and this required a newly-manufactured rotor head assembly. Considerable investigation was undertaken to establish the best means of doing so with regard to robustness of signal with minimum impact on the existing rotor head design as shown in Figure 5.6 a) The teeter angle was measured by means of an angular displacement transducer driven by a gear secured to the teeter bolt, Figure 5.6 b). As the transducer drive gear is made of plastic, any malfunction of the sensor would result in the gear teeth being stripped thereby having no effect on the controllability of the aircraft. This philosophy was applied consistently throughout the design of the new instrumentation to ensure that the airworthiness and flight safety of the vehicle were not compromised. The rotary transducer is mounted on a modified teeter bolt support plate, which was extended to carry the transducer mounting bracket and a plate holding circuitry for signal conditioning and amplification. During flight this circuitry is protected by a plastic cover, Figure 5.6 c). Note that the modification to the support plate extended above the teeter bolt and so did not weaken the overall head assembly. It should also be stressed that all modifications to the rotor head were conducted after consultation with the aircraft manufacturer, Jim Montgomerie to ensure the appropriate material specifications and manufacturing standards were maintained.

It was decided to use slip rings to transfer data from the rotating to non-rotating frame of reference rather than using any form of telemetry. The slip ring arrangement is shown in Figure 5.6 d). Four slip rings were bonded to the underside of the pre-rotator ring gear, one of these carried the signal from the teeter sensor which was then picked up by the non rotating contacts before being recorded by the on-board computer. Again great care was taken to ensure that the instrumentation, wiring contacts etc. did not interfere with the normal working of the aircraft and its systems. The contacts were mounted on a modified hub bar. The modification involved extending the hub bar beyond its original pivot point. There is therefore no change to the load path or the loads carried by the bar. The final modification to the aircraft was a display of vane sideslip for the pilot to assist accurate setting of test points.

A key choice to be made with a digital recording system is the sample rate used. High sample rates can be good for frequency resolution with long record lengths (such as frequency sweeps) but demanding of storage capacity. Low sample rates can adversely affect frequency resolution and introduce aliasing in the recorded data, i.e. introduction of 'ghost' or 'spoof' frequencies. As usual, a compromise is required. The sample rate for the VPM M16 trial was set at 10 samples per second; for the two Montogmerie campaigns it was variable but for flight mechanics parameters such as air data and inertial measurements a sample rate of 50 per second was used. A much faster sample rate, 200kHz, was required for the teeter angle campaign.

5.4   Conduct of Flight Trials

In each campaign, once the instrumentation had been installed and ground tested, the aircraft was weighed and the new centre of mass position determined. All appropriate documentation was completed, and there was close consultation with the CAA at all times to ensure that the tests were carried out in a completely safe manner. The tests were carried out in an incremental manner with replay facilities to examine the recorded data available immediately after landing. There were some specific issues which arose with each trial, and these are documented briefly below.

5.4.1 **VPM M16 (G-BGWI) Trial**

For the VPM M16 trial, mass and centre of mass position were determined for the aircraft in standard condition, as well as modified. It was necessary to calculate the latter for airworthiness and flight safety reasons as the aircraft would be flown from the rear seat, normally prohibited solo. It was decided that, provided the weight and balance of the aircraft in modified form lay within the (undefined) envelope for normal operation, then the likelihood of the aircraft handling being changed would be minimised. This normal operational envelope was calculated from hang-test measurements taking into account the mass of fuel (from minimum to maximum) and the pilot.

During the trials, engine management problems, particularly at low power settings, resulted in frequent stoppages and poor running, and resulted in the decision not to apply frequency sweep or multi-step inputs to the throttle. It was felt by the test pilot that this might compromise engine integrity and hence flight safety, given his growing concerns with the serviceability of the engine.

5.4.2 **Montgomerie-Parsons (G-UNIV) Model Validation Trials**

a) Carlisle, July 2000, Pre-Trials Verification of Aircraft and Instrumentation

Before the main series of trials took place it was considered prudent to undertake a series of "shakedown" flights primarily to test the functionality of the instrumentation suite, but also to practice procedures for downloading data from the onboard computer. These trials were funded by the Department of Aerospace Engineering, University of Glasgow and took place during the month of July 2000. The tests were restricted to steady trimmed flight and simple manoeuvres to gather performance data (steady climbs etc.). A problem with an incorrectly installed roll rate sensor became apparent and was immediately rectified. Thereafter the aircraft and instrumentation proved to be reliable, and a procedure for recovery and initial processing of data was developed and perfected. Inspection of the recorded results provided confidence in the ability of the aircraft system to generate the data required to fulfil the objectives of the main test programme.

b) Bournemouth, 16th - 27th October 2000

A number of test flights were flown to ensure that the aircraft was ready before it was then handed over to FRA and placed under B conditions. However, the following day the aircraft developed a fuel tank leak. The aircraft was grounded and the instrumentation system removed to allow repair of the fuel tank. Following the repair, one flight was then performed to record data in trim, and responses to step and doublet inputs at 60 mph. Inspection of the data from this flight also highlighted a problem involving mis-wired pitch and yaw rate gyros (pitch rate data being recorded to the yaw rate channel on the PC and vice versa). This problem, which had not been detected in the earlier shake-down trials as these involved relatively benign steady flight manoeuvres, was easily rectified.

Bad weather caused a short delay in flying, and when the weather improved a further leak in the fuel tank was discovered. The aircraft was grounded and the flight trials were postponed until a replacement tank could be obtained. It was agreed, with the approval of the CAA, to complete the test flying at Carlisle airfield as soon as a replacement fuel tank could be sourced and at a date agreeable to all concerned. Operations at Carlisle were to remain under FRA's B conditions.

c) Carlisle, 19th - 23rd February 2001

   The remainder of the data required was to be generated during trials from Carlisle Airport during the week 19th - 23rd February, 2001. Carlisle was seen as a sensible choice because, due to the relatively low volume of air traffic in the area, it was possible to perform the tests close to the airfield minimising transit time and thereby increasing the number of flights possible in a day. This was particularly significant when considering the very low temperatures encountered that week. By the end of the period all scheduled tests had been flown, and the test programme had been completed.

5.4.3   **Montgomerie-Parsons (G-UNIV) Teeter Trials**

The flight test programme was carried out at Perth Airport on the 20th and 21st of July 2005. Before proceeding with the experimental flights, a Flight Trials Instruction was drawn up by the CAA Flight Test Engineer, agreed by the University of Glasgow team and the pilot - see Appendix 5, before finally being authorised by the CAA. Details of personnel involved, and the various operational aspects are also given in the Appendix. Particular care was taken in this trial in reviewing the recorded data after each flight as this trial represented the first ever measurement of gyroplane rotor teetering motion and there was, naturally, a degree of uncertainty as to what would be encountered.

5.5   **Processing of Recorded Data**

During each set of trials, data was recorded for the complete duration of each flight. The first stage of processing was to download the data from the onboard recording system to a PC, converting it to engineering units, and formatting it into a convenient form (Matlab or Mircosoft Excel). The second stage of processing was to extract only the events of interest. Both aircraft were equipped with event markers to indicate specific test points on the data records to facilitate identification.

Data quality can be assessed in a rudimentary fashion by inspection and, as happened during the trials, minor errors such as incorrectly labelled data streams were easily rectified. Drop-outs or spikes can be identified for smoothing, typically using an averaging process based on neighbouring points. Magnitudes and signs can be checked using engineering judgement as well as knowledge of the calibrations applied, however, a formalised method of checking the quality of rate and attitude sensors, and air data and inertial sensors, can be employed. This is called kinematic consistency, and details of its nature and use are given in Appendix 6.

5.6   **Sample Flight Test Results**

Typical results are shown in Figures 5.7 - 5.9. Figure 5.7 shows a longitudinal stick frequency sweep conducted during the VPM M16 trial. Figure 5.8 shows a longitudinal stick doublet input applied to the Montgomerie-Parsons. Figure 5.9 shows teeter angle measurement in steady, level flight, taken from the Montgomerie-Parsons trial during the third flight test campaign. These data are really designed for analysis using mathematical techniques to 'tease out' the dynamic features of interest. Nonetheless, it is the case that best practice demands that the data be 'eyeballed' and engineering judgement applied as much can be learned about the status of the instrumentation system, and the nature of the aircraft itself, which can shape consideration of airworthiness issues in relation to the experiments underway. Figure 5.7 is typical in this regard. Notice the presence of 'dropouts', or spikes. This is an electrical phenomenon, and clearly is not the result of aircraft behaviour. Dropouts are a feature of older, analogue systems, such as the one used in the VPM M16. The Montgomerie-Parsons data does not suffer from dropouts which are in any case easily corrected numerically. Note that the frequency sweep is

similar to the ideal shown in Figure 5.3, although it is difficult for the pilot, as frequency increases, to keep the amplitude constant. This can have airworthiness implications as imposing large-amplitude inputs at high frequency can accelerate fatigue damage despite the fact that at these frequencies the airframe response diminishes greatly. The frequency sweep is therefore an input that needs application with care. However, the benefits of the frequency sweep input can be seen, even without mathematical analysis, if the records between 100 and 200 s are examined. The rotorspeed variation is at its greatest, ±40 rpm, when the magnitude of the control input is at its smallest. This is indicative of a resonance, or mode, that might not be obvious in normal operation.

The Montgomerie-Parsons sample shown in Figure 5.8 is of a doublet input. This aircraft proved a particular challenge to flight test using these specialised flight test control inputs. Note that the shape of the doublet lacks the sharp edges of the idealised sample shown in Figure 5.3. The fundamental problem with this aircraft is the undamped pitch oscillation, most clearly seen in the pitch rate time history. The case shown here, at 40mph, is benign in this regard but at higher speeds this oscillation is intrusive. The aircraft has a very lightly damped mode that rendered accurate inputs difficult to make. Note also that the airspeed time history is meaningless, being unrealistically low. The air data system proved prone to blockage by moisture and airspeed time histories had to be reconstructed from inertial data using the kinematic consistency approach. The rotorspeed time history also suffers from lack of resolution, making the dynamic behaviour difficult to identify. However, the sensor was changed for the teeter angle trial, Figure 5.9 where it can be seen to produce a much 'cleaner' signal.

The teeter trial data shown in Figure 5.9 illustrates the quality of data taken from the rotor head using the slip ring assembly. Two sensors were used, the second being provided for redundancy. Only the master is shown. The rotor azimuth position is vital to interpret teeter data. For example, the maximum teeter angle of approximately 2.5° occurs when the blades are approximately 40° from the fore-and-aft position. To aid the understanding of the teetering motion an individual to multi-blade transformation can be made. This has the effect of replacing individual blade motion by a disc oriented at particular longitudinal and lateral tilt angle. This transformation can be expressed mathematically as:

$$\beta_{1_c} = \gamma_t \cos \psi \quad \text{and} \quad \beta_{1_s} = \gamma_t \sin \psi$$

The teeter angle γ_t, represents the orientation of the hub bar relative to the shaft which is then transformed to disc co-ordinates β_{1c}, being the longitudinal tilt and β_{1s} being the lateral tilt of the disc. The blade azimuth position, ψ, is taken to be zero when the blade lies on the centre-line of the aircraft ahead of the pilot, and the teeter angle γ_t, is taken to be positive when the hub bar is tilted forward. This gives aft longitudinal disc tilt as being negative, and for a rotor rotating in an anti-clock wise direction (when viewed from above), a positive lateral disc tilt indicates a tilt to the right. Referring again to Figure 5.9, a maximum teeter angle of 2.5° means that the tip-path plane is therefore tilted aft by approximately 1.9° (= 2.5 cos 40°), and to the left by about 1.6° (= 2.5 sin 40°). Data from the teeter trial is of extremely high quality and forms a rich and unique resource.

Figure 5.1   VPM M16 G-BWGI in Unmodified Form

Figure 5.2   G-UNIV at FRA Bournemouth Airport for Initial Trials (October 2000)
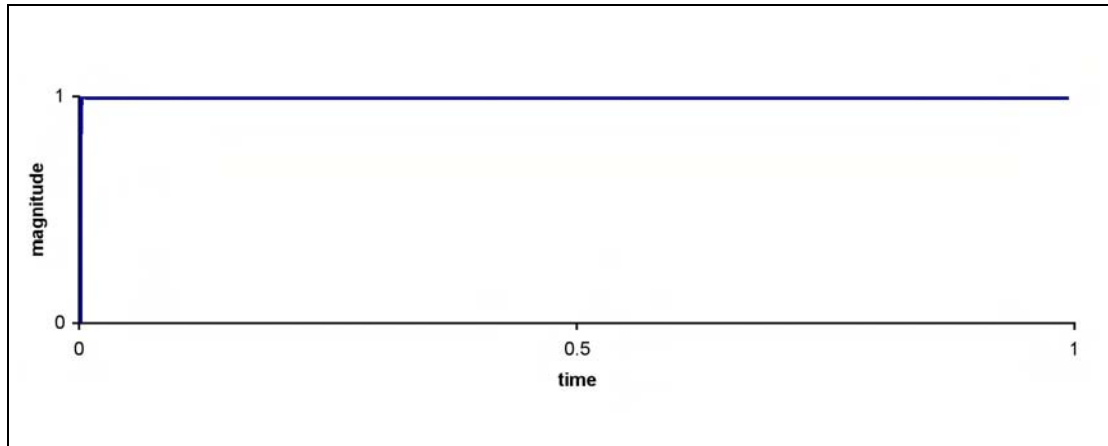
Figure 5.3 a)   Standard Test Inputs (A Step Input)
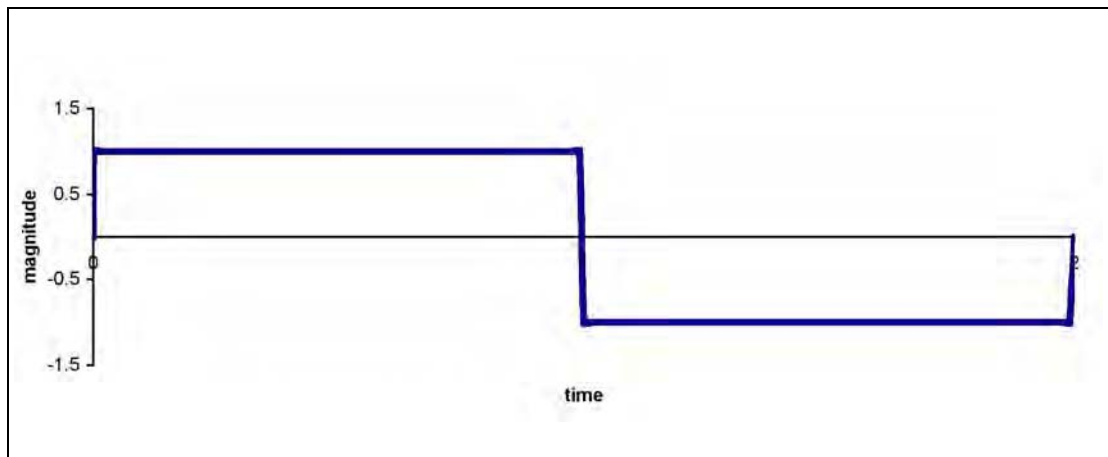
Figure 5.3 b)   Standard Test Inputs (A Doublet Input)
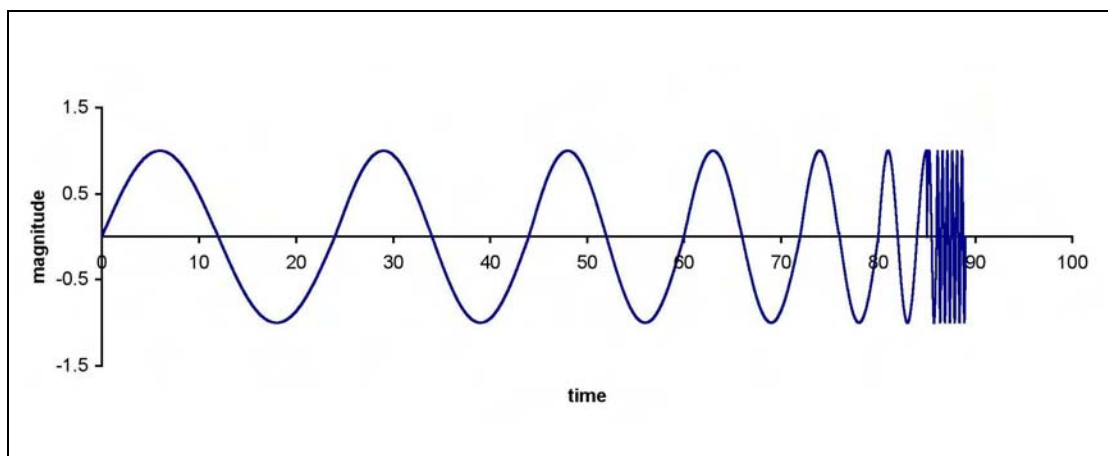
Figure 5.3 c)   Standard Test Inputs (A Frequency Sweep)

Figure 5.4 a) Flight Test Instrumentation for VPM M16 G-BWGI Flight Trials
(G-BWGI in Modified Form for Flight Trials)
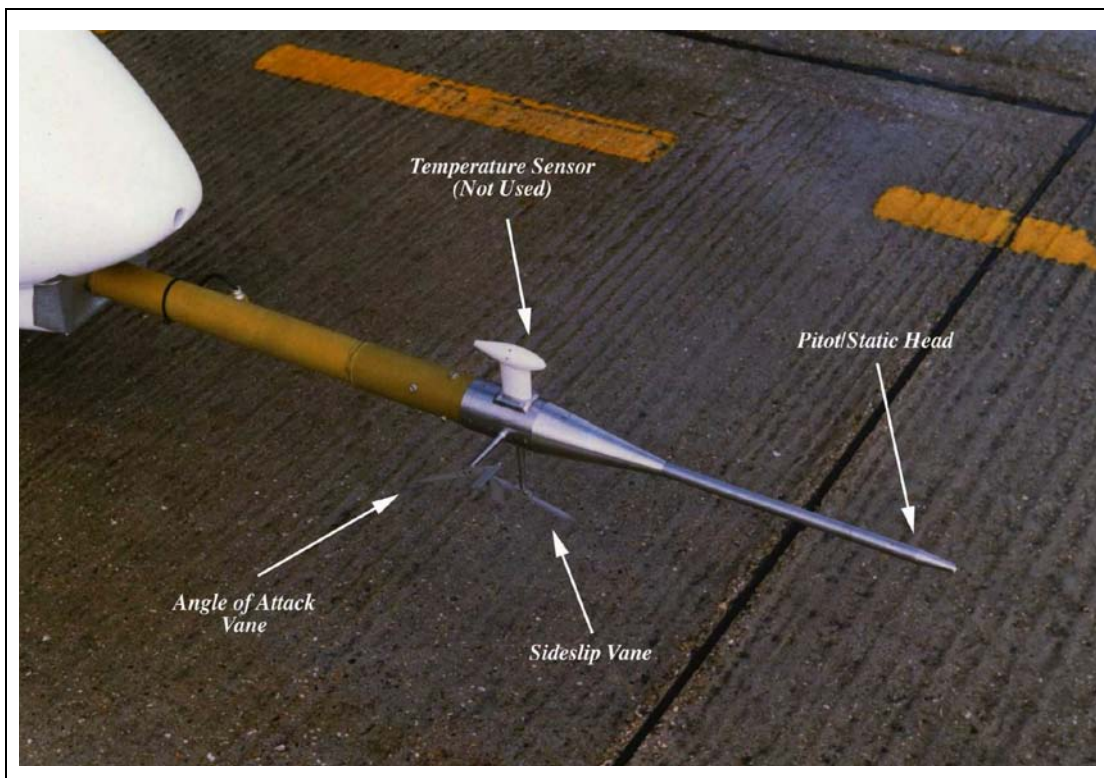
Figure 5.4 b) Flight Test Instrumentation for VPM M16 G-BWGI Flight Trials
(Air Data Probe)
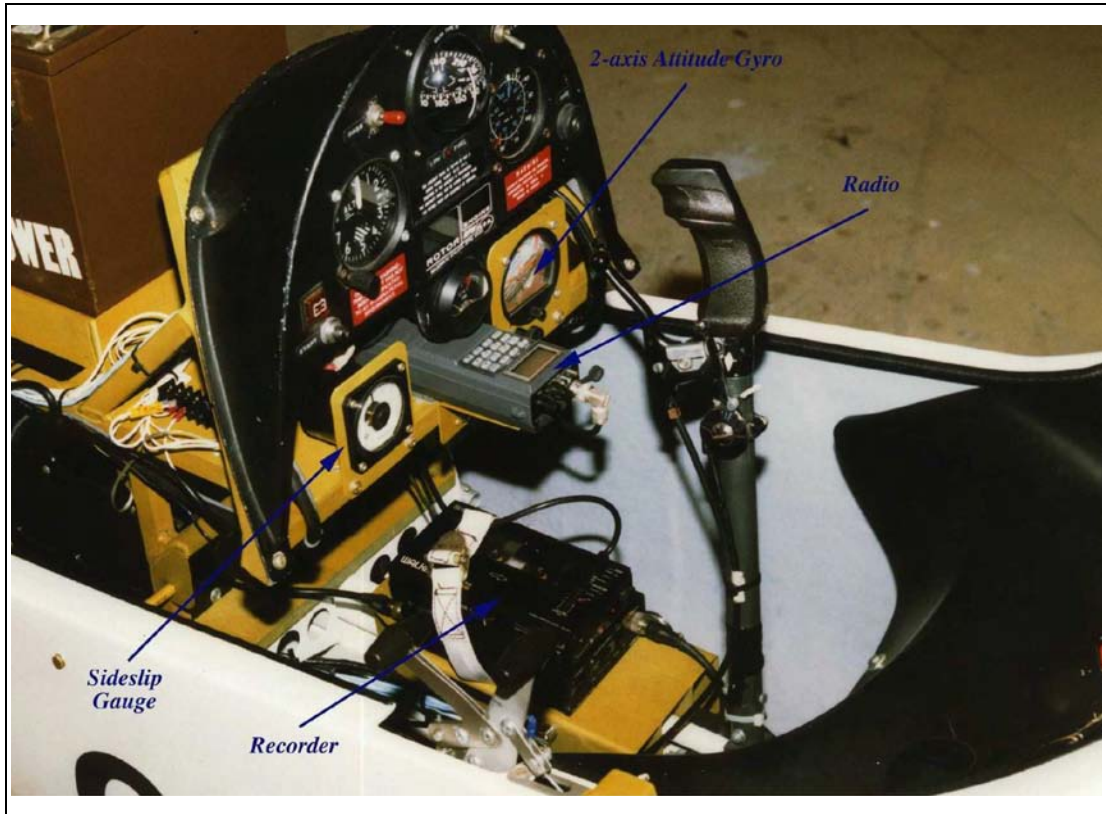
Figure 5.4 c) Flight Test Instrumentation for VPM M16 G-BWGI Flight Trials
                  (Rear Cockpit)
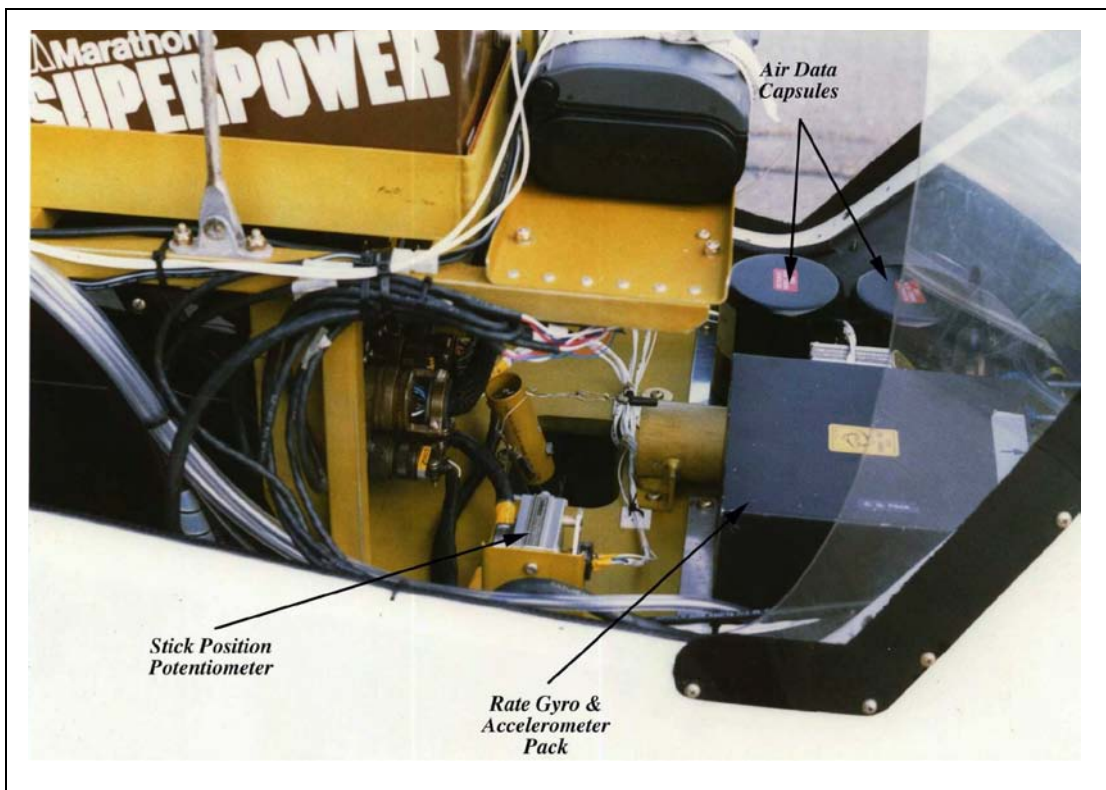
Figure 5.4 d) Flight Test Instrumentation for VPM M16 G-BWGI Flight Trials
                  (Inertial Unit)
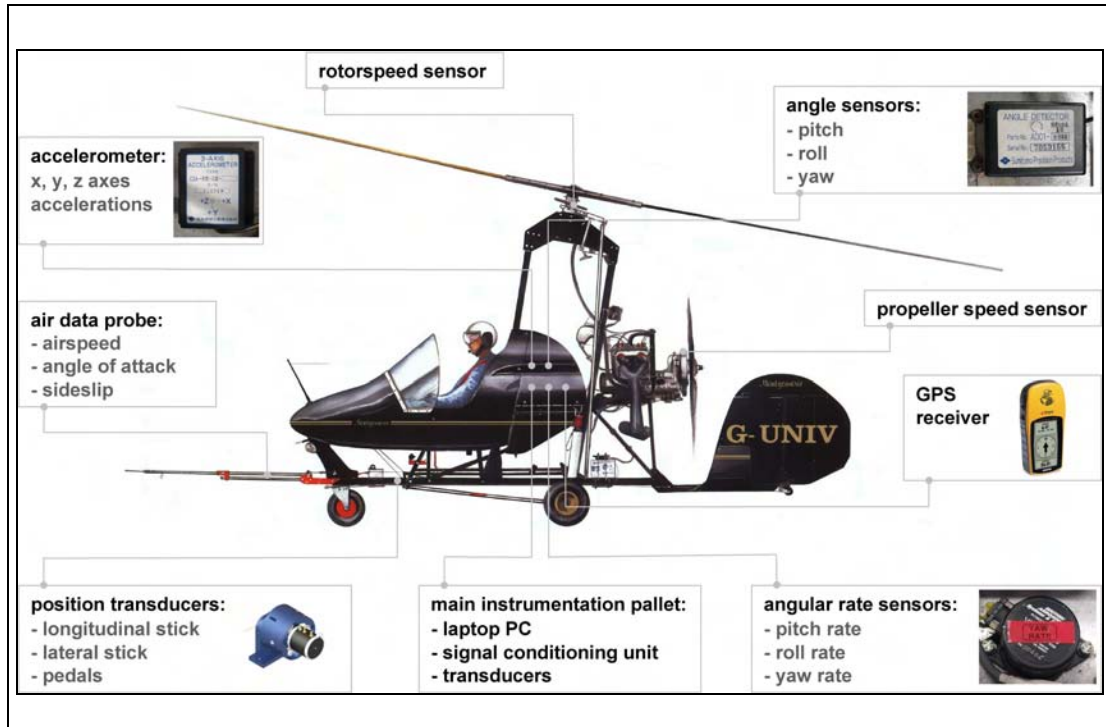
Figure 5.5 a) G-UNIV Flight Test Instrumentation
(General Layout of Instrumentation)
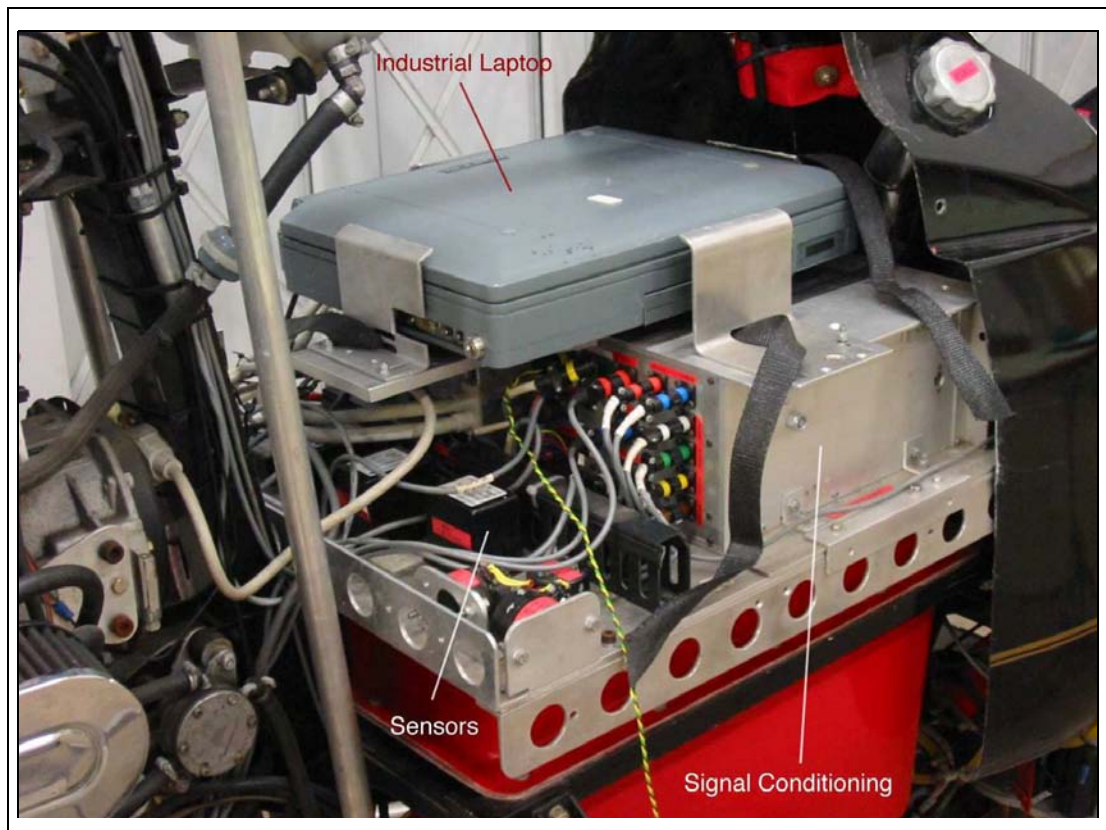
Figure 5.5 b) G-UNIV Flight Test Instrumentation
(Main Instrument Pallet)

Figure 5.5 c) G-UNIV Flight Test Instrumentation
(Sensors On-board Main Instrumentation Pallet)

Figure 5.5 d) G-UNIV Flight Test Instrumentation
(Displacement Transducers for Measurement of Stick Position)
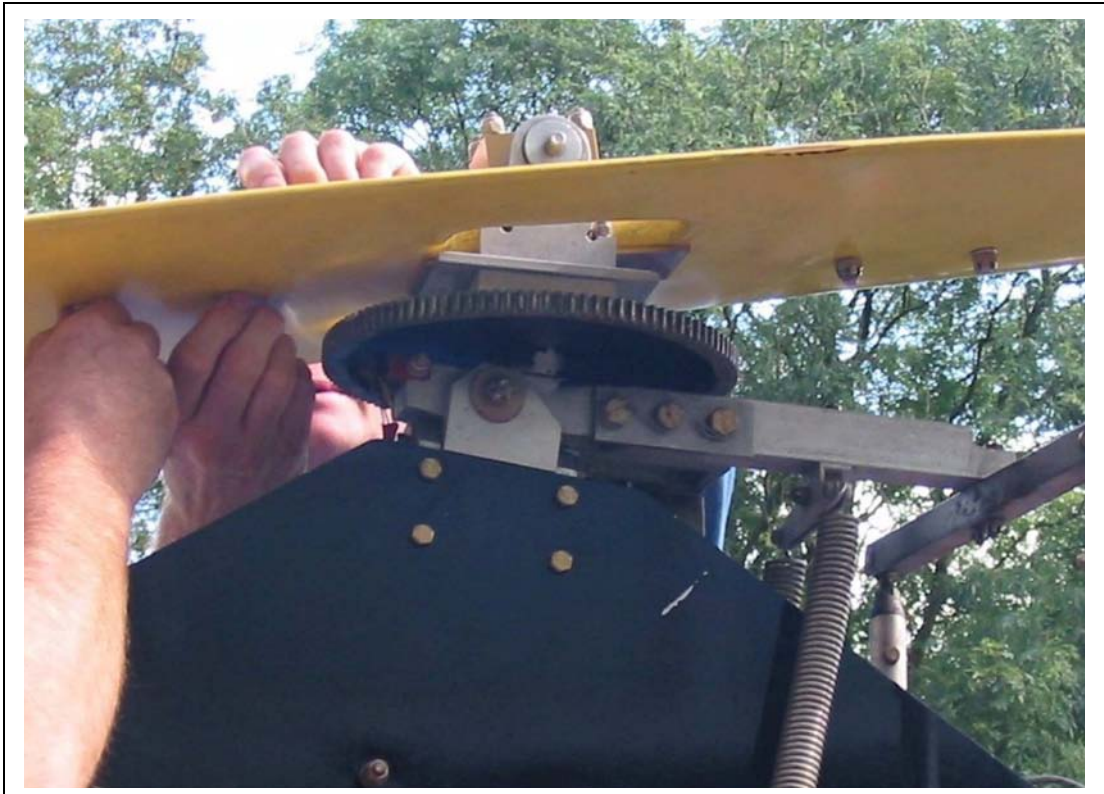
Figure 5.6 a) Additional Modification of G-UNIV for Teeter Angle Measurement
(Rotor Head Prior to Installation of Teeter Angle Instrumentation)
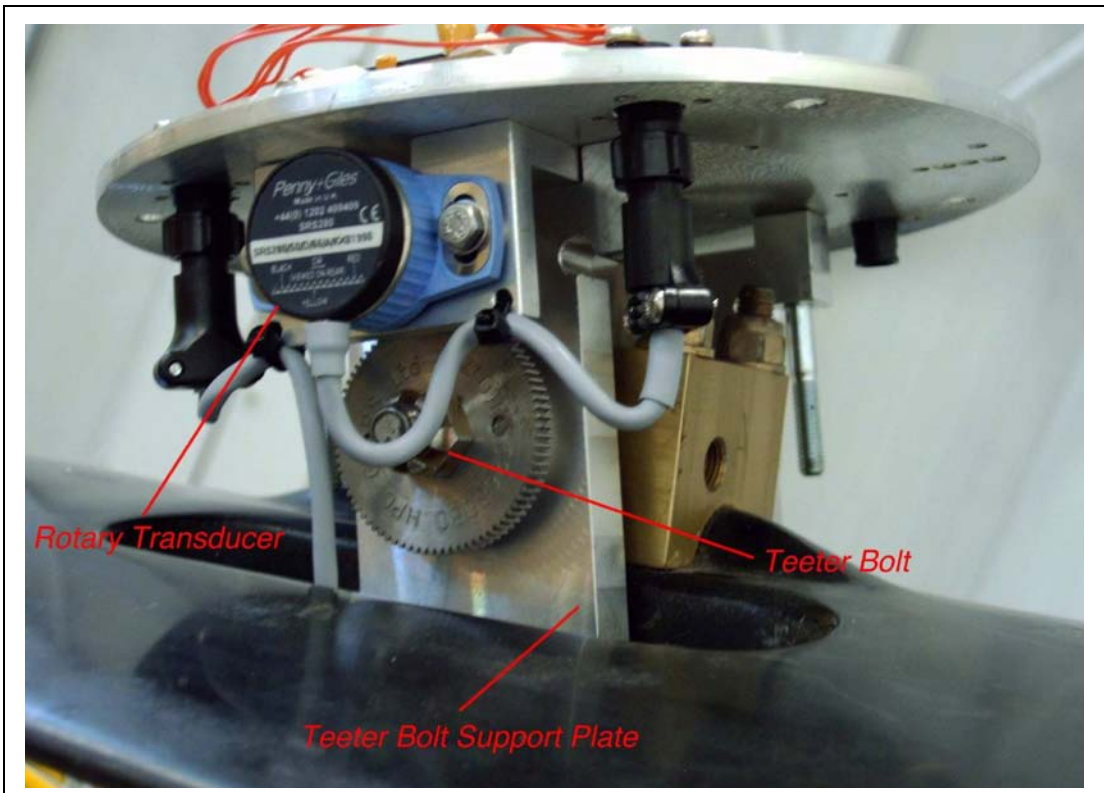
Figure 5.6 b) Additional Modification of G-UNIV for Teeter Angle Measurement
(Additional Modification of G-UNIV for Teeter Angle Measurement)
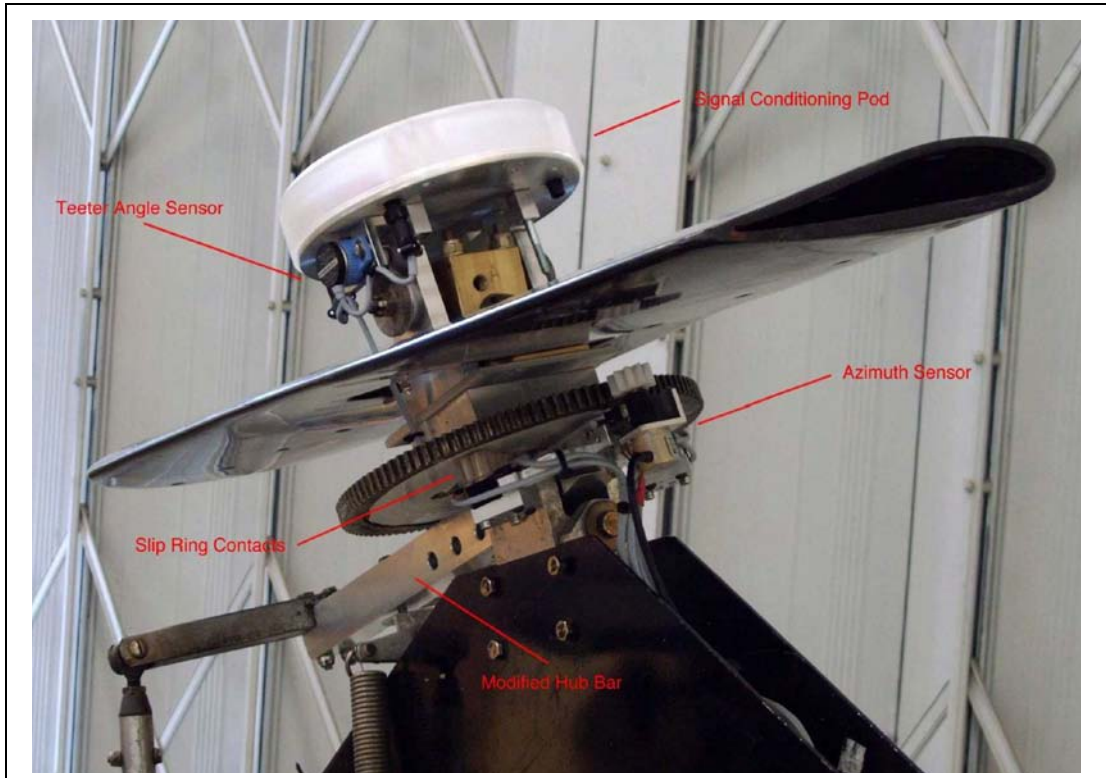
Figure 5.6 c) Additional Modification of G-UNIV for Teeter Angle Measurement
(Rotor Head Assembly After Modification)
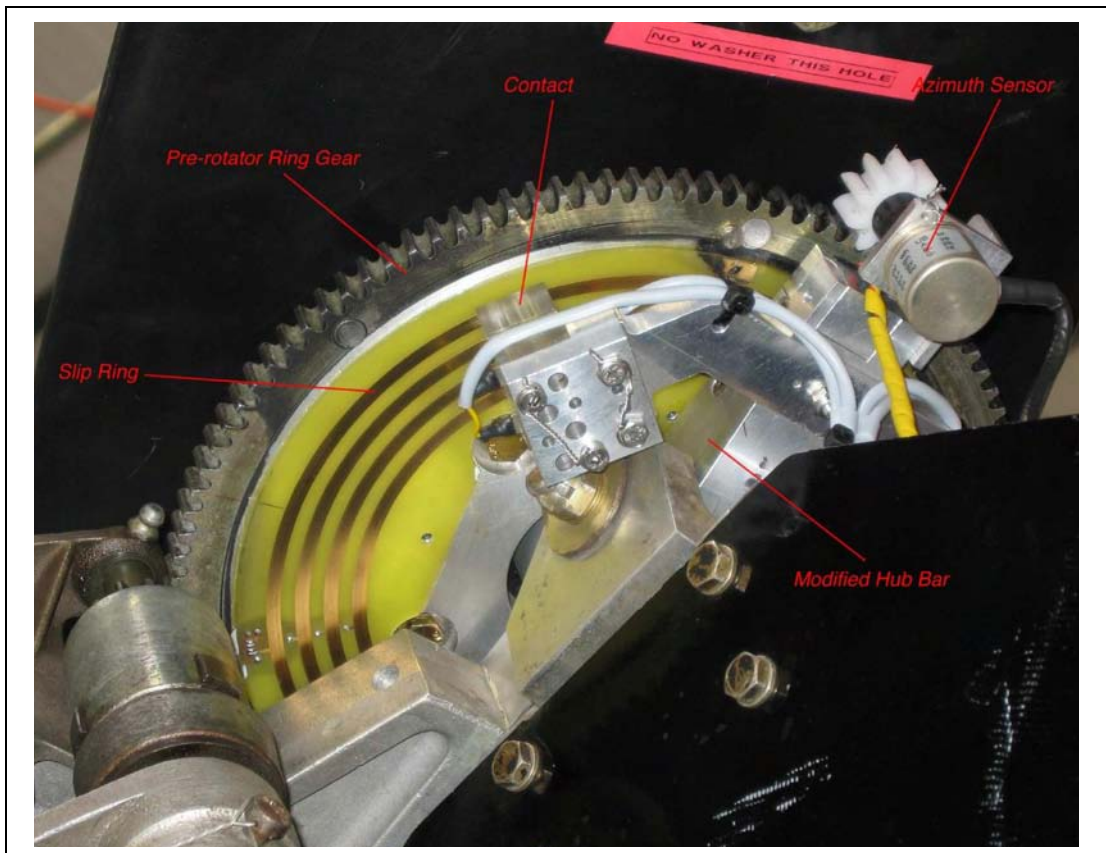
Figure 5.6 d) Additional Modification of G-UNIV for Teeter Angle Measurement
(Slip Ring and Teeter Bar Assembly)
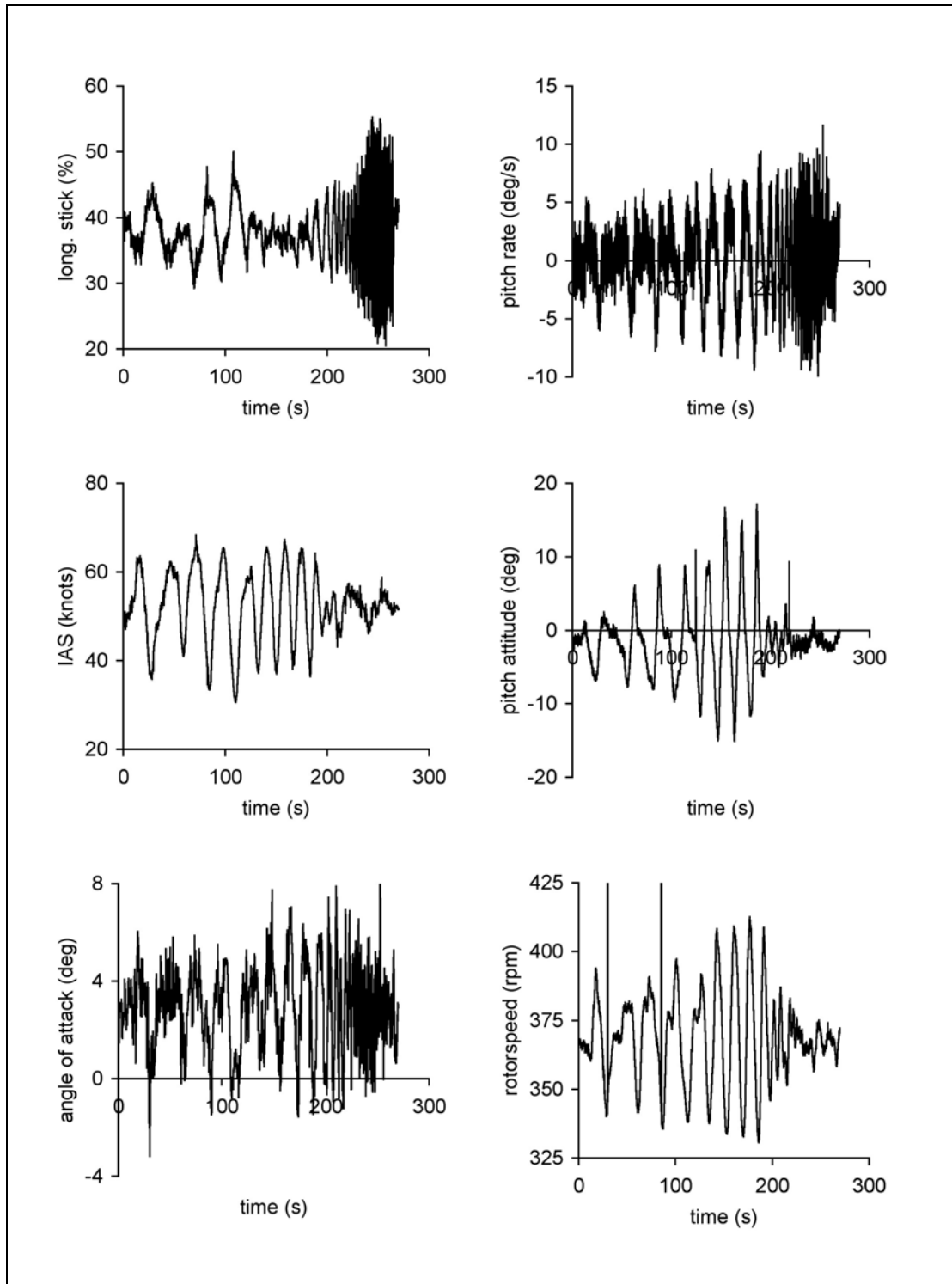
Figure 5.7   Longitudinal Stick Frequency Sweep (VPM M16)
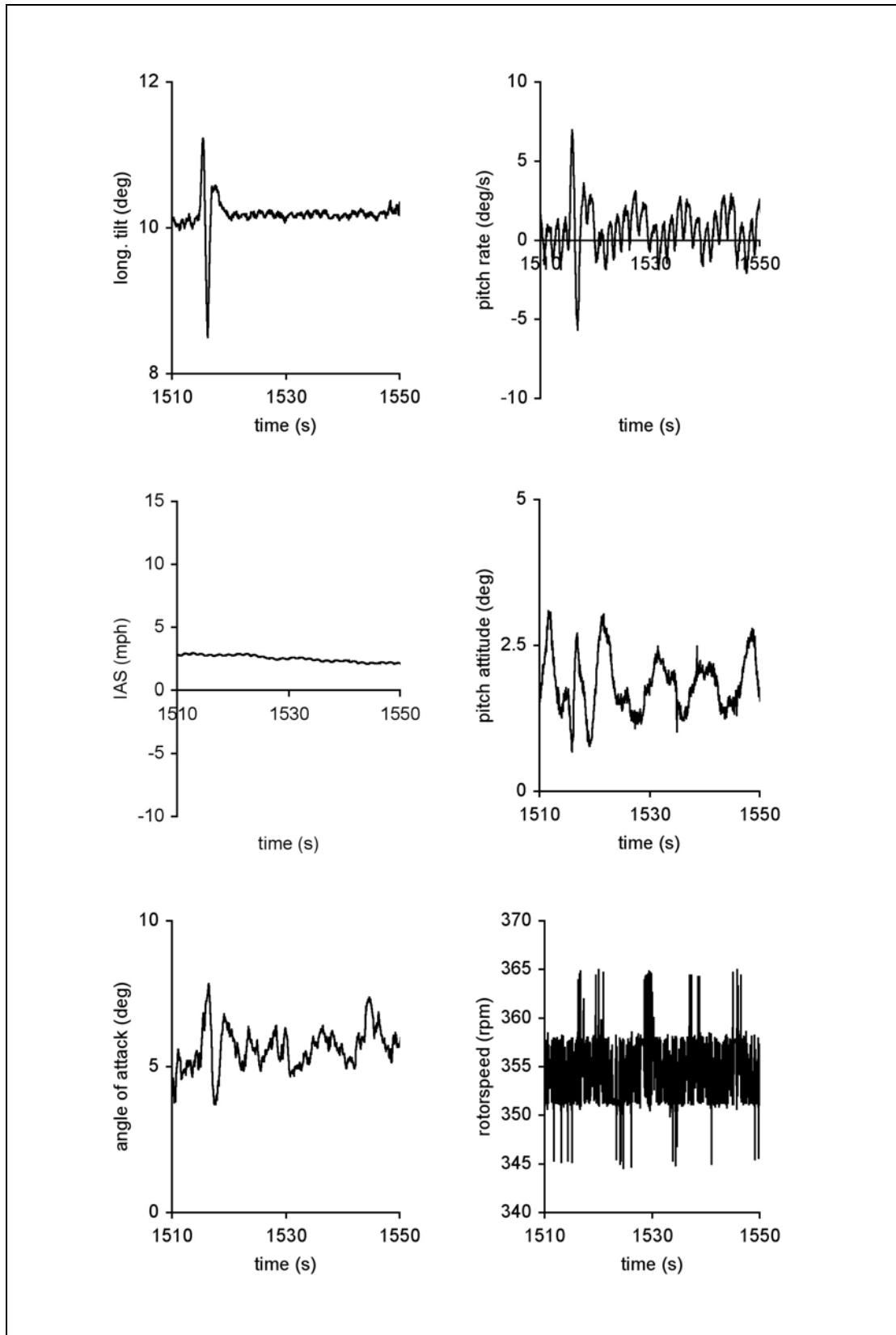
Figure 5.8 Longitudinal Stick Doublet (Montgomerie)
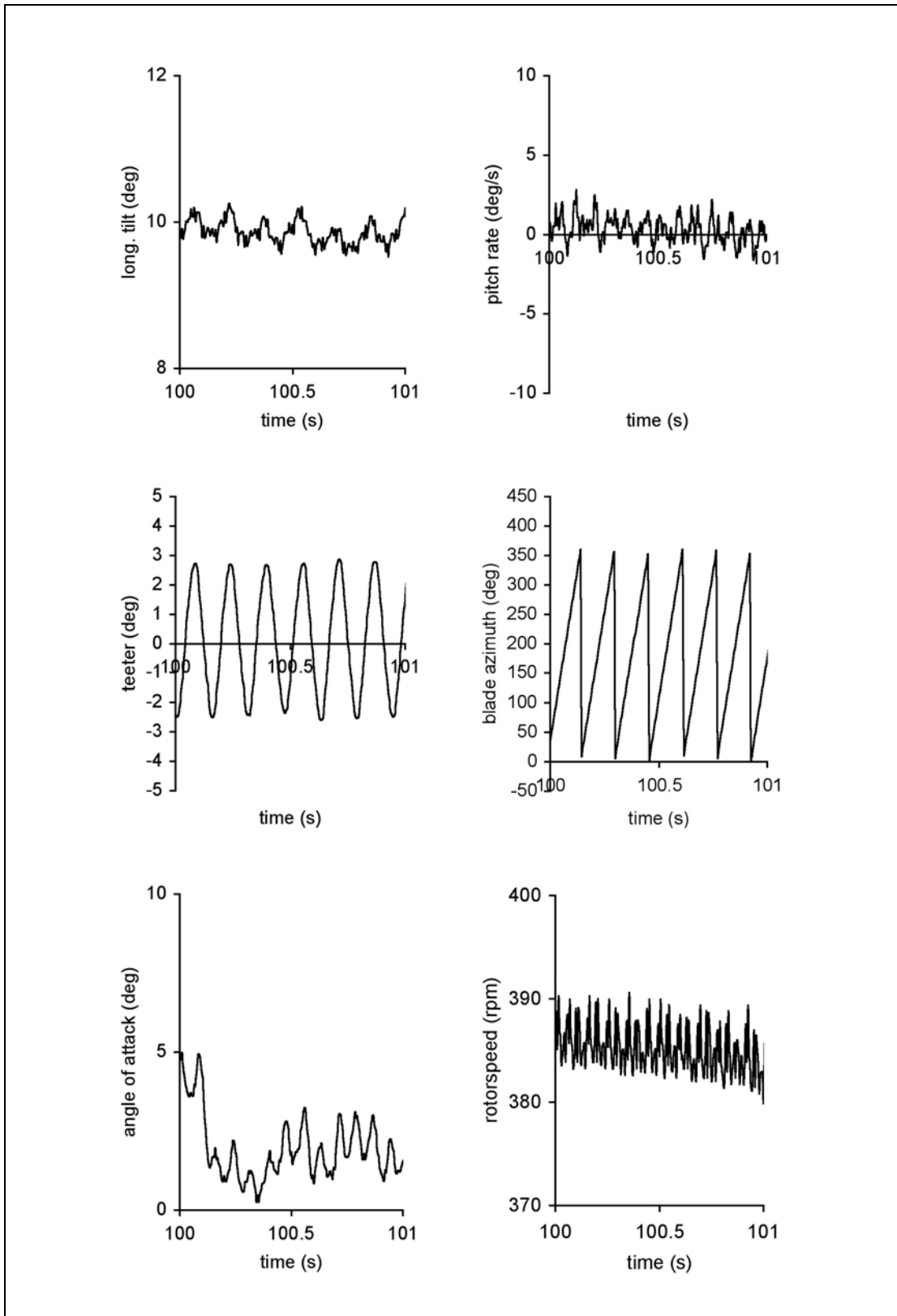
Figure 5.9   Trim with Teeter Measurement (Montgomerie)

6 Model Validation

An engineering model is a powerful tool for supporting studies into aircraft stability, control and handling qualities but confidence in the results can only be quantified if the model has a known level of validity. An important precursor to validation is verification. The verification process involves determining whether the simulation is functioning correctly, that is, are the numerical processes within the computer code working, is the computer code "bug free", and most importantly, can the results be interpreted in a sensible manner when considered in the context of the known physics of the actual system. This process is often performed by comparison of results with other simulations, or in the case of a simulation undergoing development, with results from a previous version. A successful verification gives sufficient confidence in the functionality of the simulation to allow validation (that is comparison of simulated data with real life data) to proceed. Verification is an important process as it eliminates the possibility of a deficient (computational) implementation being the cause of any mismatch between simulated and test data at the validation stage.

Validity, at its simplest level, describes whether or not a model is 'good enough' for predicting behaviour. Hence validation must involve comparison, in some way, with flight. A valid criticism of the process is that if the model compares well with a specific test case, then it is only valid for those flight conditions or control input. In an attempt to generalize any comparison to give confidence in wider applicability, model fidelity is generally described in terms of amplitude and frequency, and here this is addressed by comparing the model's trim, linearised small perturbation derivatives and the response to large amplitude control inputs, with corresponding results from flight test data. Note that what constitutes 'good enough' depends very much on the engineering judgment of the user - formal approaches to the general problem of validation do not exist.

Notwithstanding this, the overall objective remains the definition of the predictive capability across a wide range of operating conditions from steady flight, to the transient response to large control inputs. Note that the mathematical model is regarded as generic, and is configured as a specific gyroplane type by means of a data file that defines the model as that type. In principle then, the model can be used for any gyroplane and if validated against a specific type, should exhibit the same level of fidelity when used to simulate other aircraft. It is accepted that this may not be the case due to type-specific attributes of particular aircraft and, to this end, the model was validated against both the VPM M16 and Montgomerie-Parsons gyroplanes.

Although gyroplanes have been simulated previously [93, 94], the models and the results obtained were severely limited in their applicability. For example, simple disc representations of the main rotor were used, and analytical expressions for linearised stability and control derivatives were formulated. Reference 94 was further limited by using data for a generic aircraft type, i.e. a specific aircraft was not modelled. No validation was attempted in either case.

6.1 Methodology

Comparison of model with flight for trim cases is very straightforward - measurements of parameters such as stick position or pitch attitude made in flight are compared with the calculations made by the model. Even in 'trim', the flight measurements tend to vary with time, so an average over a period such as 10 seconds is taken to define 'trim'. Generally, however, the quality of the trim flight results are excellent, and even visual inspection confirms that the aircraft is in steady flight. Nevertheless an average over 10 seconds is calculated and the average is taken to represent trim.

Validation in the dynamic or manoeuvre cases is much less clear-cut. The lay reader might expect that comparison of model and flight time histories is all that is required. This is an attractive prospect as time histories are intuitive. Time history comparison does indeed have a role to play, particularly when inputs of varying amplitude are applied. However, any particular input and resulting time history has a very specific frequency characteristic, as the input itself has specific frequency content. The objective is therefore to find a means of validating the model that is less input-specific. The derivatives (see Appendix 4) form the basis of this analysis as, in combination, they define the response characteristics across a range of frequencies.

Appendix 7 describes the method by which these derivatives are extracted from flight test data. Since they are going to be used as validation metrics against the model, it is important that they are verified (note, not validated) by assessing how they predict the behaviour of the real aircraft to a control input. Note that in this process it is important to use an input that was not used to identify the derivatives, in order that a degree of independence in the verification is preserved.

The derivatives identified from a flight test input are used to create a linearised model of the aircraft (see Appendix 4). The fundamental linearised model structure is:

$$\underline{\dot{x}} = \mathbf{A}\,\underline{x} + \mathbf{B}\,\underline{u}$$

with the derivatives filling the rows and columns of A and B. Typical results are shown in Figures 6.1 to 6.3, all for the VPM M16. Figure 6.1 is for 30mph, and the responses are represented as perturbations from trim (linearised models can only represent perturbations). The M16 displays no real separation of the traditional short-period and phugoid modes at lower speeds, and hence the combined response is presented. However, Figures 6.2 and 6.3 show short-period and phugoid-type responses at 70 mph where these modes do apparently separate into their traditional forms. In all three cases the close similarity between the flight response and that predicted by a model, itself derived from another flight response, give confidence that the derivatives accurately represent the behaviour of the real aircraft and hence can be used to assist model validation. Note that where discrepancies do exist (most notably in the VPM M16 rotorspeed short-period response at 70mph), these tend to be where the response diverges significantly from trim and, since the identified model is linear, it is therefore only really suitable for use with small perturbations.

6.2 Results

The RASCAL simulation model was configured with data appropriate to the flight condition for each test point. Mass and inertia information was available from ground-based measurements. The aircraft mass for each test point was influenced only by fuel state which could not be measured accurately. Accordingly, simulation results were obtained for the two limiting conditions of full fuel (maximum weight) and zero fuel (minimum weight).

6.2.1 Equilibrium Flight

Comparison of the model with measurements taken in steady, level flight for the VPM M16 and Montgomerie-Parsons is shown in Figures 6.4 and 6.5, respectively. Generally, there is very good or excellent agreement between model and flight. The longitudinal parameters (stick position, pitch attitude, rotorspeed) show excellent correlation between flight and theory. The lateral variables (lateral stick position and roll attitude) are less good. However, correlation of these parameters is sensitive to sideslip and blade torsional effects (see Section 9). The model (both its physical

formulation and the engineering data used to configure it as a specific type) can therefore be assessed to offer a realistic facsimile of the actual aircraft in trim flight. Often in rotorcraft model validation it can be difficult to achieve this level of fidelity. Note that with regard to the longitudinal parameters in particular, this level of fit easily satisfies the requirements stipulated by the FAA for Level D (i.e. zero flight-time) piloted flight simulators [95].

6.2.2   **Small-Perturbation Flight**

The RASCAL simulation model can be linearised using either the process used to extract derivatives from the flight test data, or by a simple but quite effective numerical process called forwards and backwards differencing [88]. The latter is used in this case. Figure 6.6 shows comparisons of key longitudinal stability and control derivatives for the VPM M16. The method of extracting the derivatives from flight test produces bounds on the confidence level with which the derivative has been estimated. Here, the flight-derived values are presented as 95% confidence bounds, while the model results are those for minimum and maximum mass. Note that if the 95% bounds are far apart the method has estimated that particular derivative with low confidence, and vice-versa.

Some simulation and flight derivatives show a consistent trend with speed. Simulation values can lie within, or overlap, the uncertainty bounds of the flight results. It is argued that in such cases, model and flight can be said to be in agreement within the limitations of derivative identifiability and modelling uncertainty. Some comparisons are worthy of consideration. For example, the drag damping term X_u, which is of paramount importance in phugoid mode damping, is predicted by the model to lie just on or outside the lower boundary of the flight result. However the flight boundaries are fairly wide, indicating that X_u is estimated with low confidence, except at high speed. Heave damping Z_w plays an important role in short-period mode damping, but its magnitude is substantially over-estimated by the simulation model. This is a difficult result to reconcile, and it is not a result specific to the RASCAL model - even simple theory [83] gives a result very similar to RASCAL. If the flight result is accurate and simple theory is correct, this suggests that the blade lift-curve slope of the real aircraft is unrealistically small. Of less concern, however, is the mismatch in M_w. The model results appear simply shifted relative to the flight values; significantly, the model captures the unusual result for unaugmented rotorcraft, that $M_w < 0$. A physical reason for this result is given by Houston [66]. Coupling of rotorspeed with the pitch degree of freedom, manifested in terms of $M\Omega$, is well-represented by the simulation model.

The simple forms of the derivatives given by Bramwell, [83] can give some indication as to the engineering source of any modelling deficiencies and this is where derivatives have a pivotal role to play in insight. For example, M_w and $M\Omega$ are influenced by the vertical location of the c.g. [66] so a good match in both indicates that this parameter is correctly modelled. However, M_w is also influenced by pod and tailplane aerodynamics (and given the apparent weakness of the tailplane lift-curve slope suggested by the wind tunnel model, it is the pod that dominates), hence the pod aerodynamic data is possibly responsible for the apparent offset between flight and model. Note that the correlation in M_w and M_q could be improved if the pitch moment of inertia was some 50% greater, but this would then worsen correlation in M_u and $M\Omega$. These deliberations are typical of any model validation exercise and serve, if not to highlight errors in the model, then certainly the detailed role that derivatives and only derivatives can play.

The rotor torque derivatives (the Q derivatives) are unique to rotors in autorotation, and are therefore of major importance to simulation of gyroplanes. It is believed that this work is the first time that rotorcraft torque derivatives have been identified in autorotation so there is no body of work against which either the estimation or calculation can be compared. In addition, given the sensitivity of rotorspeed to a multiplicity of factors, good modelling of these terms gives confidence that the physical modelling is accurate. Some of the key derivatives are presented in Figure 6.6, which shows that the simulation model results exhibit excellent agreement with flight. In particular Q_Ω is proportional to blade drag coefficient (in simple modelling, [62]), so the match here is a good indication that the detailed blade element drag modelling is correct in terms of overall effect.

Figure 6.7 presents comparable results for the Montgomerie-Parsons aircraft. The exercise was repeated with this aircraft in an attempt to provide corroboration of modelling assessments made with the VPM M16. It should be remembered that, at the time, the VPM data were unique; there was no body of literature that provided alternative evidence as to how well rotorcraft models performed (in terms of their validity) as gyroplanes, unlike the helicopter literature which is well-populated with case studies. The Montgomerie-Parsons comparisons were therefore undertaken as a check on the VPM study, in an attempt to enhance confidence in the use of the RASCAL code. However the Montgomerie-Parsons flight trials and modelling differ from the VPM case. First, the rotorspeed sensor fitted to the Montgomerie-Parsons lacked resolution (as can be seen by inspection of Figures 5.8 and 5.9, for example), and this adversely influenced the confidence with which rotor torque (Q) estimates could be extracted from the flight data. Second, the airframe aerodynamics used in the RASCAL code were gross simplifications relative to the high quality tunnel-derived data used for the VPM modelling. This was because no tunnel testing of the Montgomerie-Parsons configuration was carried out. The consequences of these aspects can be seen in Figure 6.7 - there is generally poorer correlation between flight and theory in terms of trend and matching of values. However, there is some consistency with the VPM results, in that the Montgomerie-Parsons flight results show low values for X_u and Z_w.

6.2.3 Large-Amplitude Response

The derivatives summarise the small-amplitude or linearised response of the mathematical model. For all their utility and power they represent a view of the model that is limited in amplitude and frequency. Time response of the full, non-linear individual blade/blade element model from which the derivatives can be extracted, is itself limited in frequency and amplitude to the characteristics of the control input applied, yet is viewed usually by the lay reader as the ultimate test of a mathematical model - if it can predict the response to a control input, it's an accurate representation of flight. It is re-iterated however that because we can only ever test one or two cases, response to control inputs is part of the validation process, not a validation process in its own right, and the following cases illustrate this.

Figure 6.8 shows comparisons of response to a longitudinal stick input for the VPM M16. The longer-term rotorspeed response, i.e. greater than 10 seconds, is more heavily damped in simulation model than in flight. This is entirely consistent with linearised model validation which revealed that the real aircraft has little drag damping, X_u, and consequently little phugoid or long-term damping. The opposite is true with the linearised simulation model. The pitch rate response is simulated fairly well, the only anomalous period in time being around 10 sec, consistent with the mismatch in rotorspeed. However, the off-axis response in roll rate displays behaviour familiar to helicopter flight dynamicists, where the amplitude is reasonably predicted in magnitude, but not in phase.

Figure 6.9, 6.10 and 6.11 show the response of the RASCAL code configured as the Montgomerie-Parsons aircraft, when compared with flight test data. Three separate control input responses are shown: the first is a BCAR Section T compliance demonstration case, where it is desired to excite the phugoid or low-frequency mode; the second and third are doublet inputs designed to excite only the short-period or higher-frequency mode. In Figure 6.9 (phugoid response) the model is adequate only for about 5 sec after the input has been made, capturing pretty well the angle of attack, pitch rate and rotorspeed response during this time. From 15 sec onwards, the aperiodic instability that is predicted by the model takes over and it can be seen that all three model responses diverge rapidly, whereas the flight data does not. Figure 6.10 shows the response to a doublet input, where it is to be expected that the longer-term response is not excited, and this is indeed seen to be the case for both model and flight. Short-period pitch rate response is captured well, the angle of attack less so. Rotorspeed judgment is less easy to make due to the limitations of the sensor alluded to earlier, but the model and flight correlate at least in that the magnitude of the rotorspeed response is small. Figure 6.11 shows a very similar input however, in this case, the longer-term response is quite dissimilar to that shown in the previous figure despite the input being very similar (the nominal airspeed is only 5 mph greater and has no bearing on the dynamic response). In this case both the short-period pitch rate and angle of attack are captured accurately. However there is a longer-term, neutrally-damped oscillation not present in the previous case despite the similarity of pilot control input but which is nonetheless captured accurately by the model, at least in terms of damping and frequency if not phase. While this is of credit to the model, the difference in the long-term response between Figure 6.10 and 6.11 is perplexing until one inspects the respective control inputs - note that in the case of Figure 6.11 the pilot control input varies sinusoidally, driving the oscillation seen in the response, whereas in Figure 6.10 the control is held rigidly fixed after the doublet input is made. This emphasizes that comparing only the response to control inputs does not constitute model validation in the widest sense, but only narrowly verifies that the model can capture a specific control input response.

6.3   Discussion

The criteria used to assess whether or not the rotorcraft model can adequately simulate the gyroplane are necessarily subjective, relying on engineering judgement since there are no formal criteria for gyroplane simulation. However, comparisons with FAA Level D simulator requirements for helicopters, [95], can be instructive. They are expressed in terms of trim and time response comparisons, and the model generally satisfies the requirements for control position prediction to be within 5%, and attitude to be within 1.5 deg. Primary axis time responses would fall within acceptable envelopes, although the cross-coupling would not. The criteria for rotorspeed simulation in autorotation is not pertinent to the gyroplane.

Although there are no criteria for derivative comparisons, Tischler, [96], is developing criteria for frequency response validation. It is accepted that the linearised 6 DOF model structure is of limited utility in the context of frequency response methods, being applicable to a much narrower bandwidth. However, the validation envelope defined by the approach taken in this report is consistent with pilot control strategy for gyroplanes, which is essentially low-frequency. In addition, the derivative allows a high degree of insight into the causes of specific modelling deficiencies, such as the heavily damped phugoid (X_u).

Notwithstanding the lack of formal criteria, it is argued that validation discrepancies are typical of that obtained for helicopter models, [97]. For example, the poorly-predicted directional characteristics are determined largely by airframe aerodynamics which are obtained from wind tunnel tests. However, discrepancies in the drag and

heave damping derivatives X_u and Z_w could be directly attributed to modelling of physical phenomenon unique to the gyroplane, specifically the induced velocity in autorotation. However, the functionality of the Peters wake dynamic inflow model for the gyroplane appears acceptable and, given that no previous gyroplane model validation has taken place, a definitive statement cannot be made until the predictive ability of the model for simulating other types reveals whether or not errors in X_u and Z_w in this case are indicative of a generic problem or are type-specific. Note that if the model can simulate gyroplane flight, it should in principle be capable of simulating helicopters in this flight regime as well. It is therefore important that it is capable of being used without major modification to the underlying physical modelling.

Assessment as to whether or not the model is suitable for studies of gyroplane flight is ultimately a matter of engineering judgment, relying upon assessment as to whether or not the model is 'good' enough. Given its use for parametric studies, i.e. to establish trends or tendencies with respect to changes in configuration parameters, it is judged that the modelling is at least as good as if not better than contemporary helicopter mathematical modelling practice.
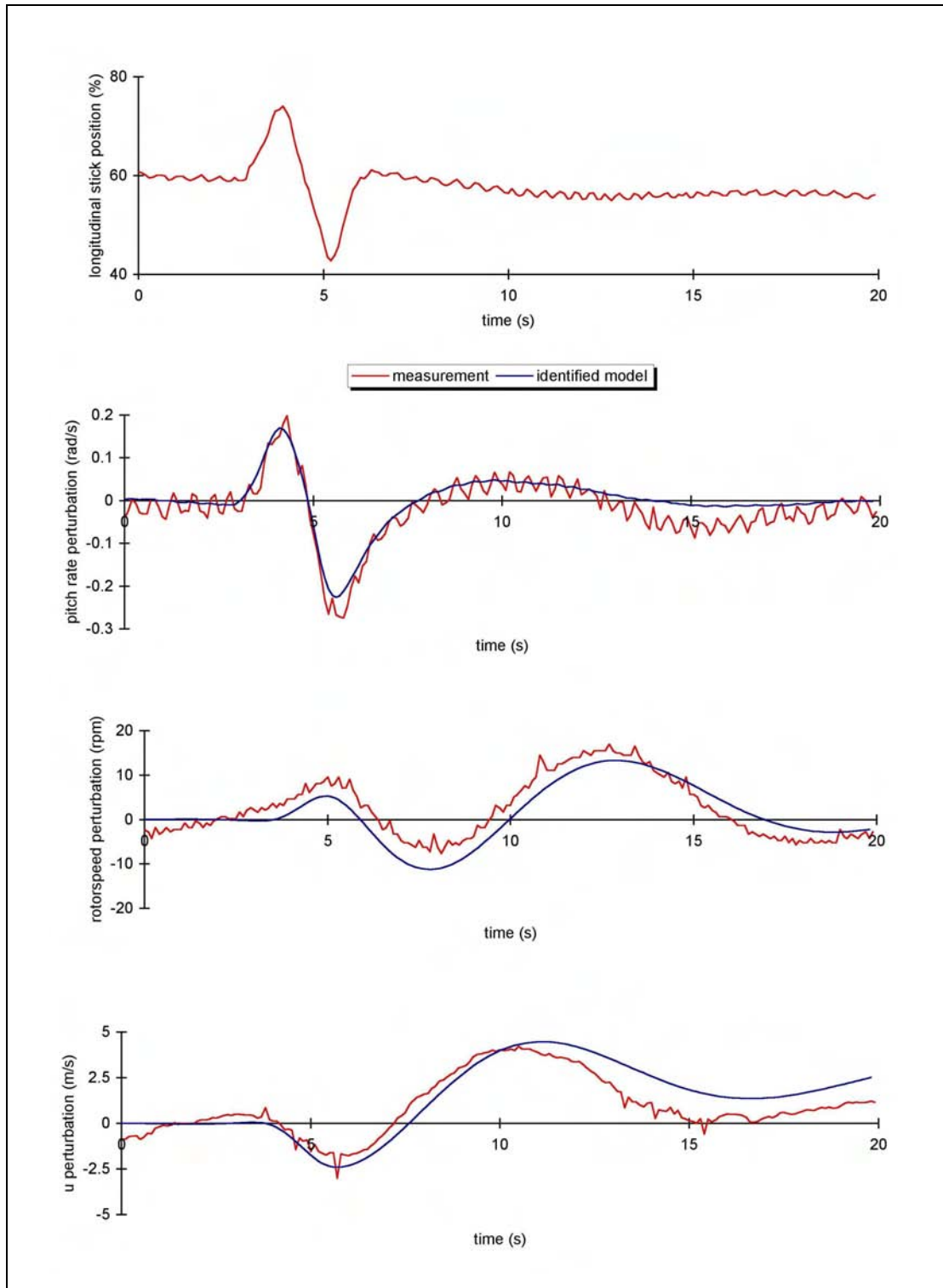
Figure 6.1   VPM M16, Identified Model Verification, 30mph
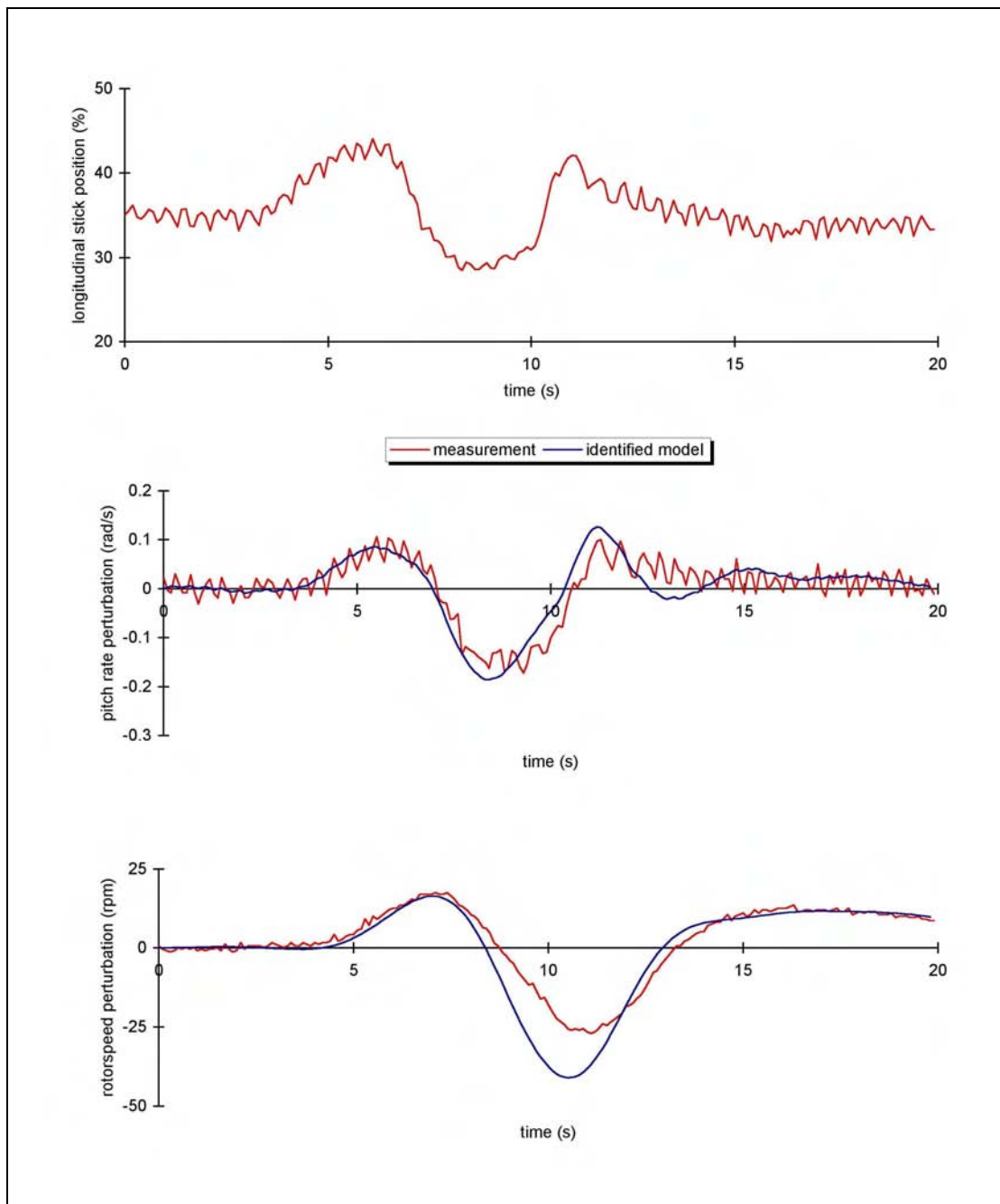
Figure 6.2   VPM M16, Identified Model Verification, 70mph Short Term Response
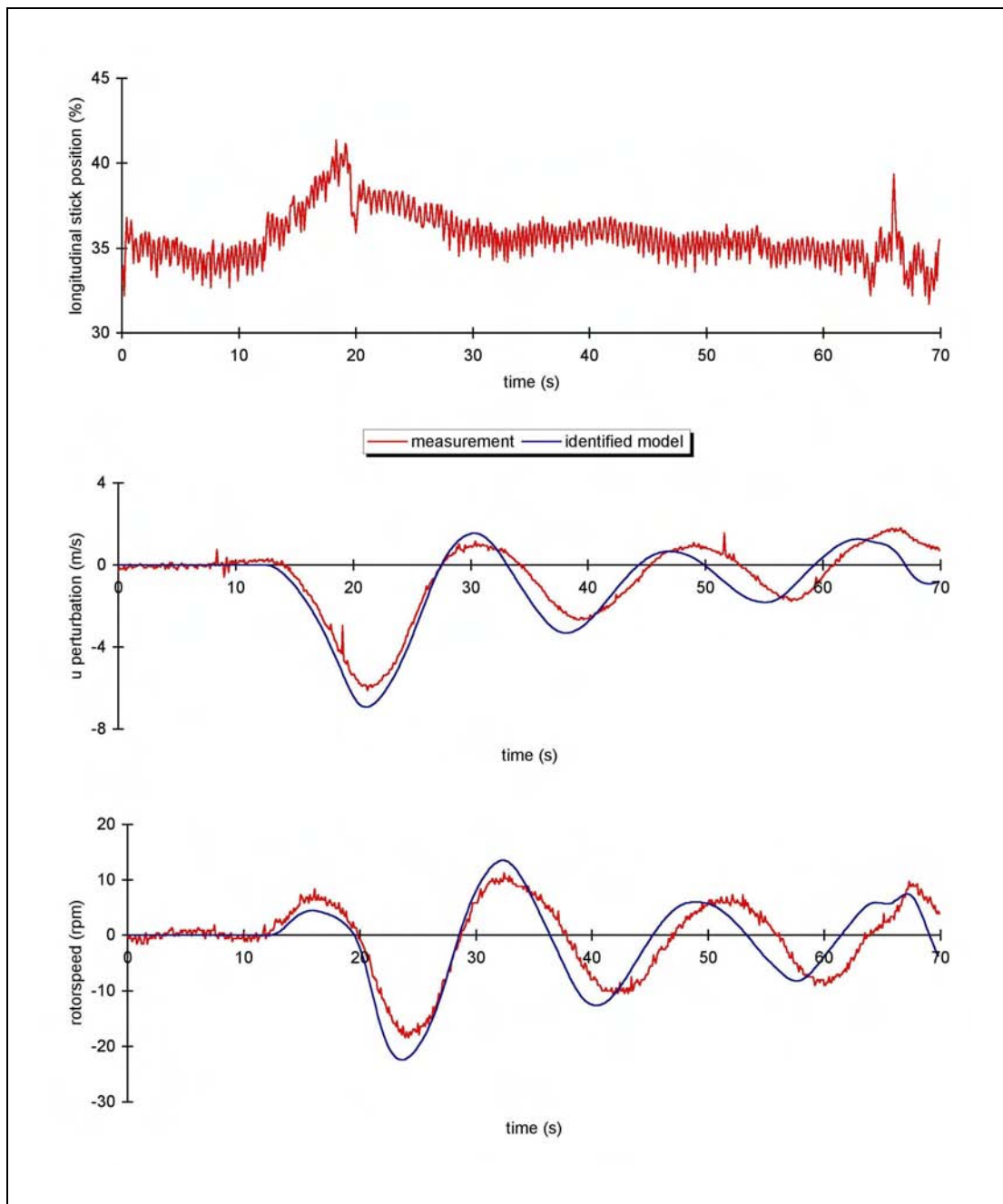
Figure 6.3   VPM M16, Identified Model Verification, 70mph Long Term Response
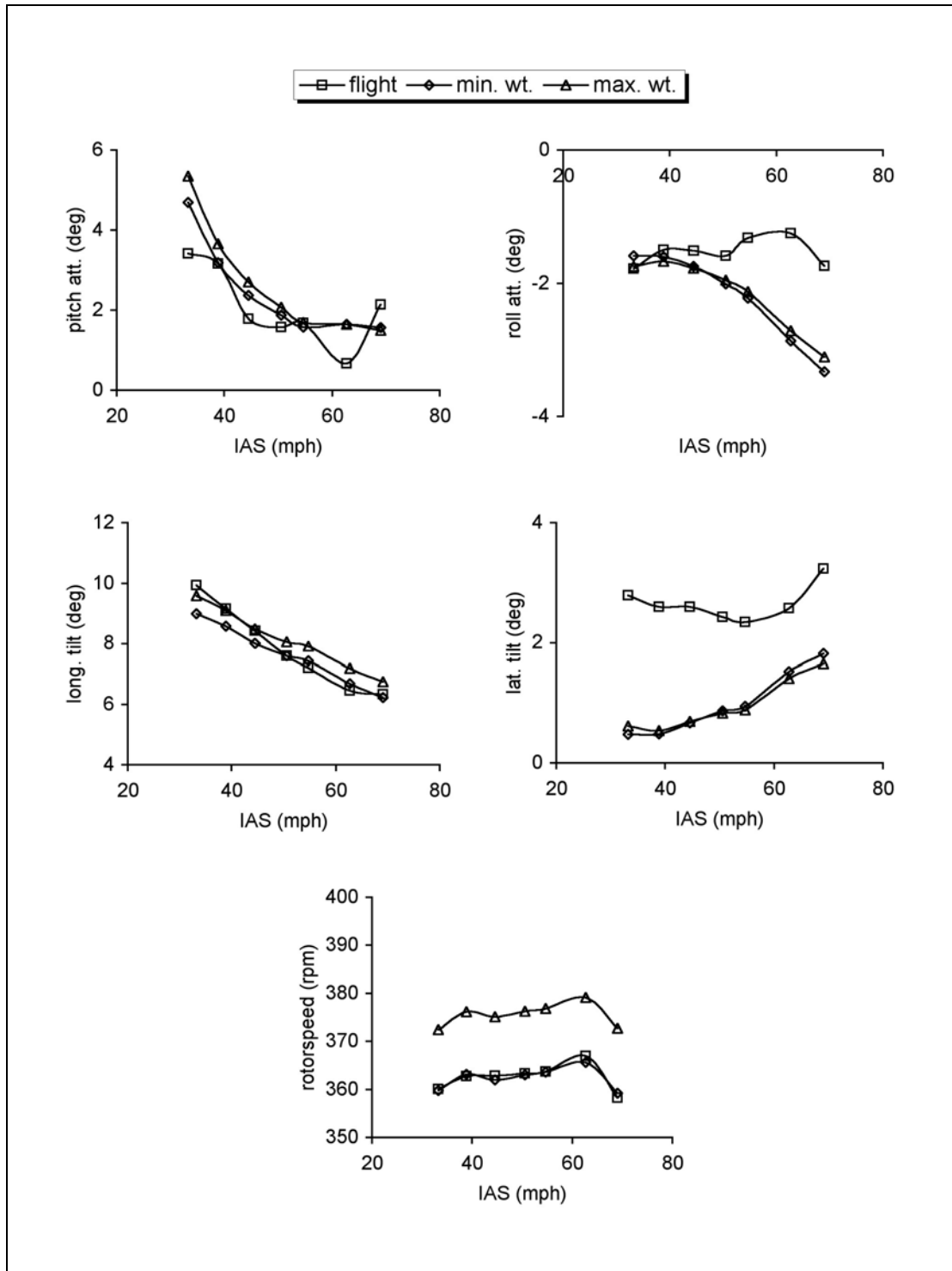
Figure 6.4   Comparison of Flight and Model Data (VPM M16, Trim)
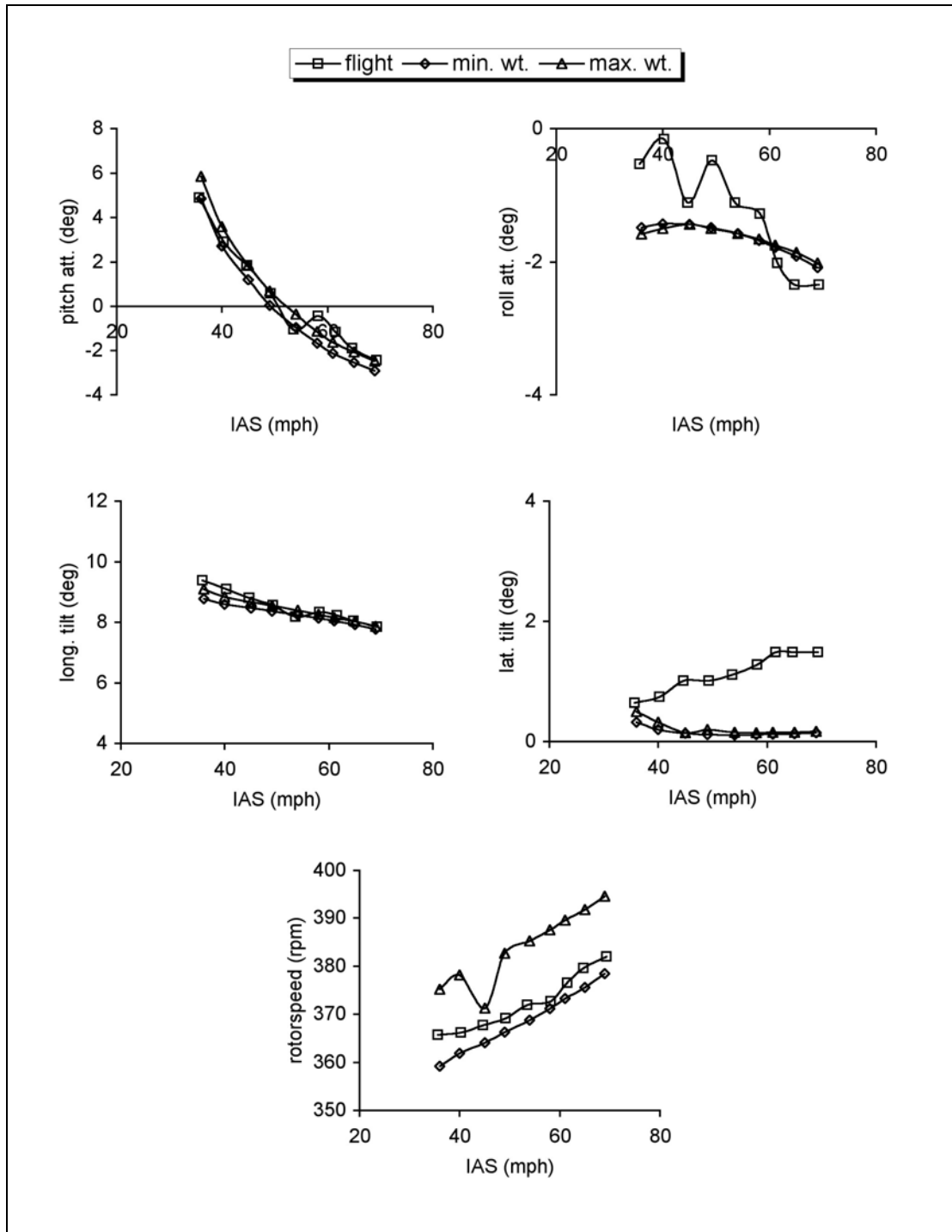
Figure 6.5   Comparison of Flight and Model Data (Montgomerie, Trim)
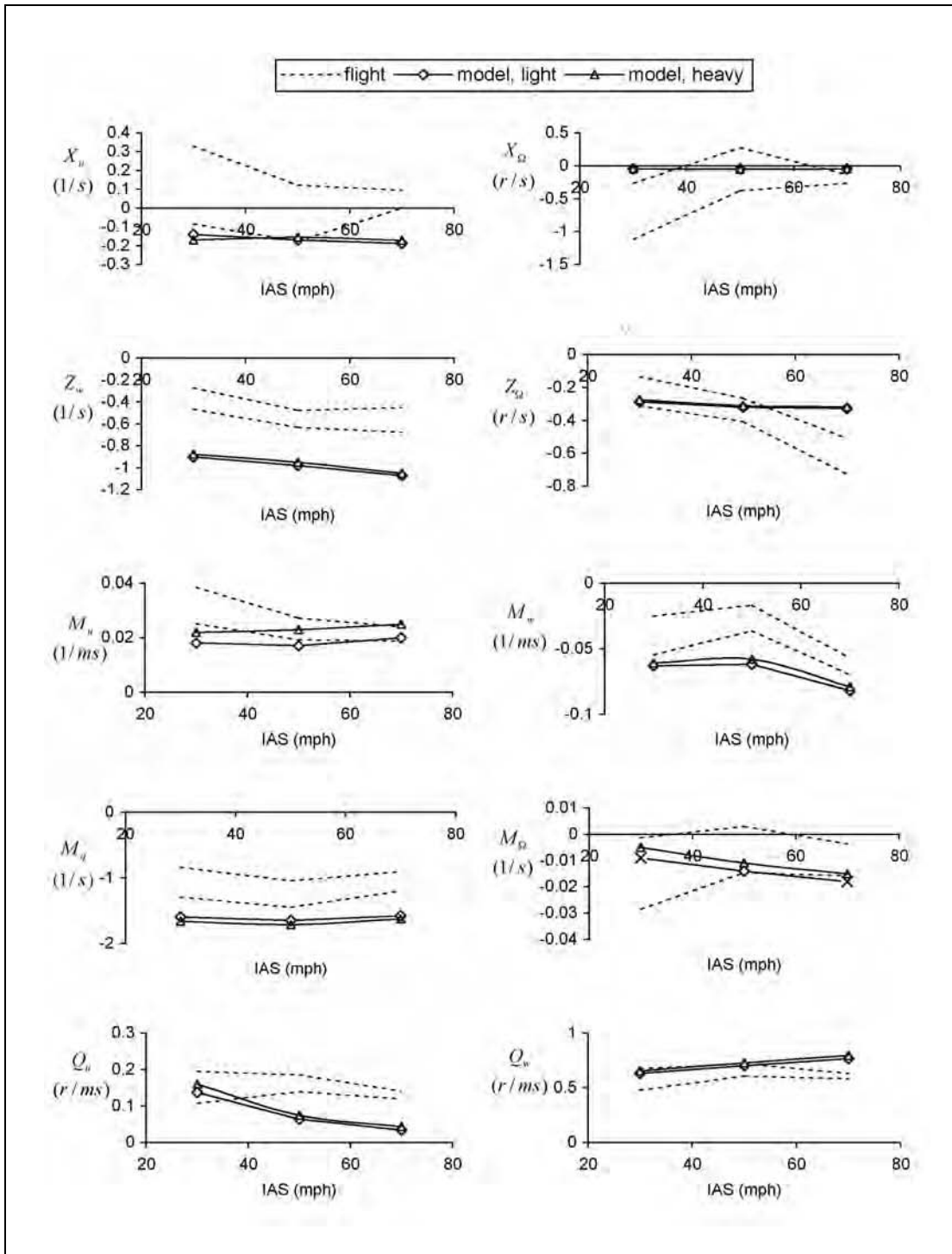
Figure 6.6   Comparison of Flight and Model Data, Derivatives, VPM M16
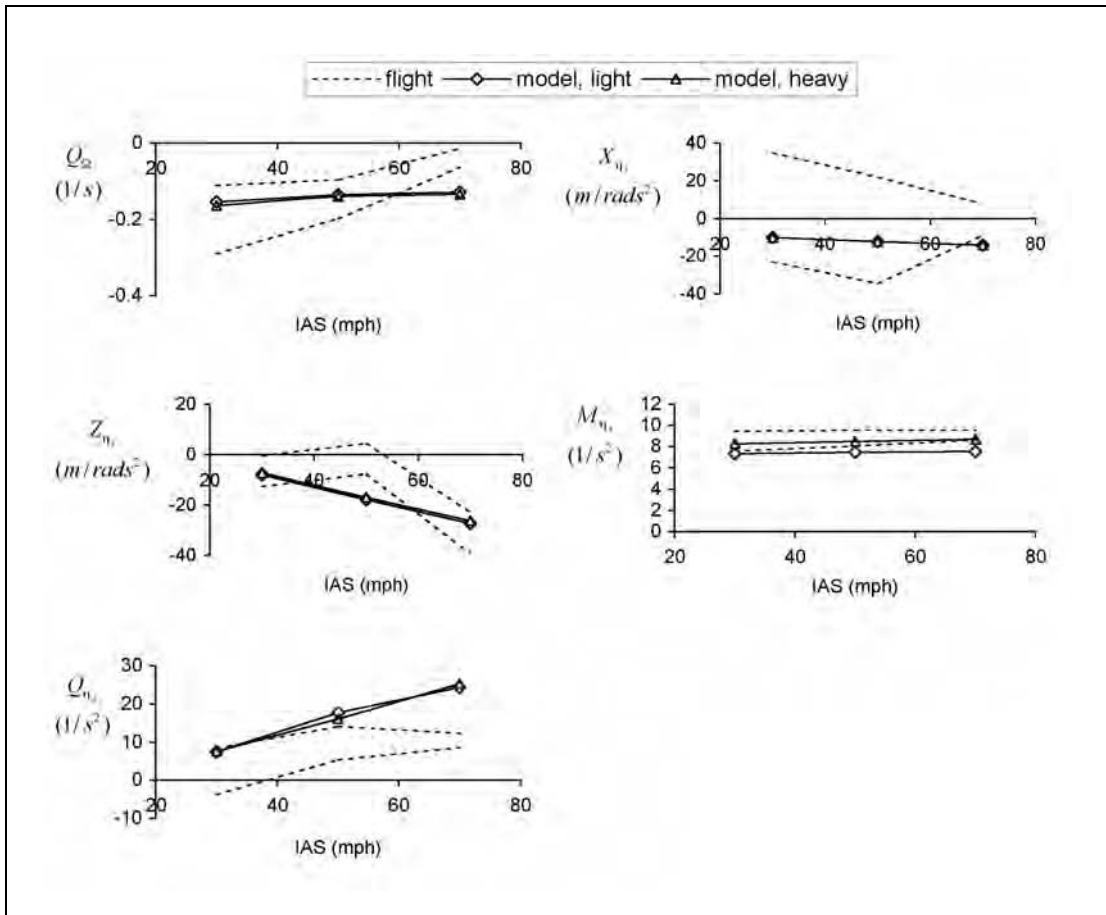
Figure 6.6   Comparison of Flight and Model Data, Derivatives, VPM M16
(continued)
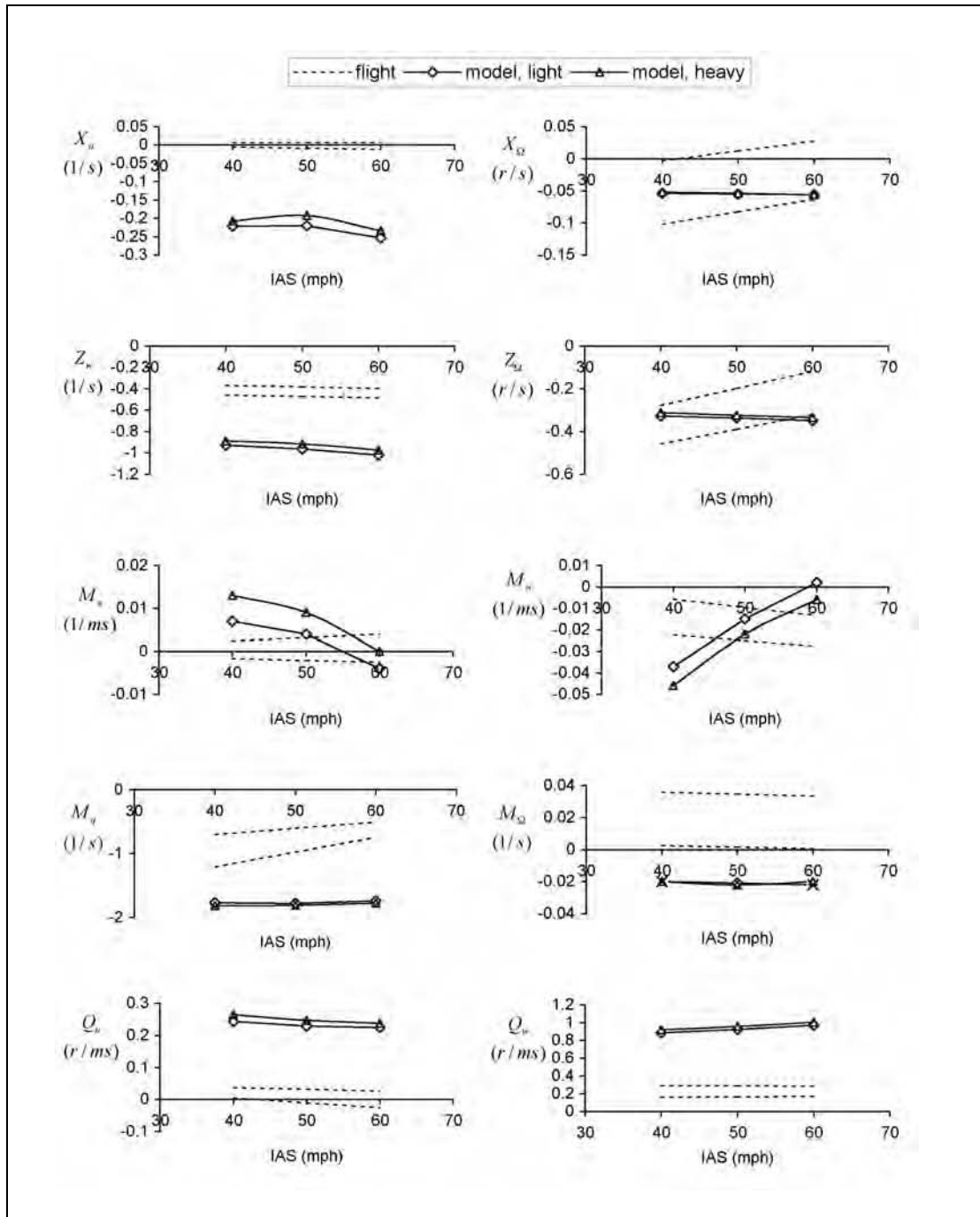
Figure 6.7   Comparison of Flight and Model Data, Derivatives, Montgomerie
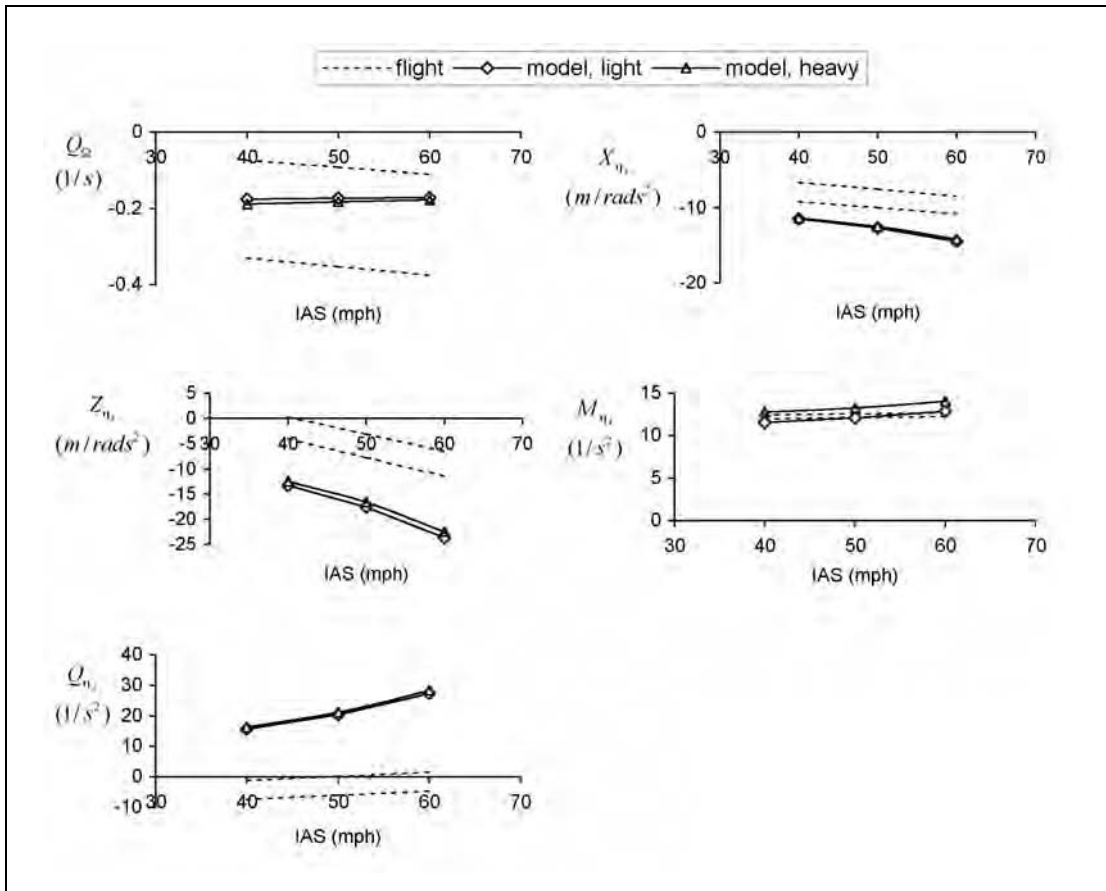
Figure 6.7   Comparison of Flight and Model Data, Derivatives, Montgomerie (continued)
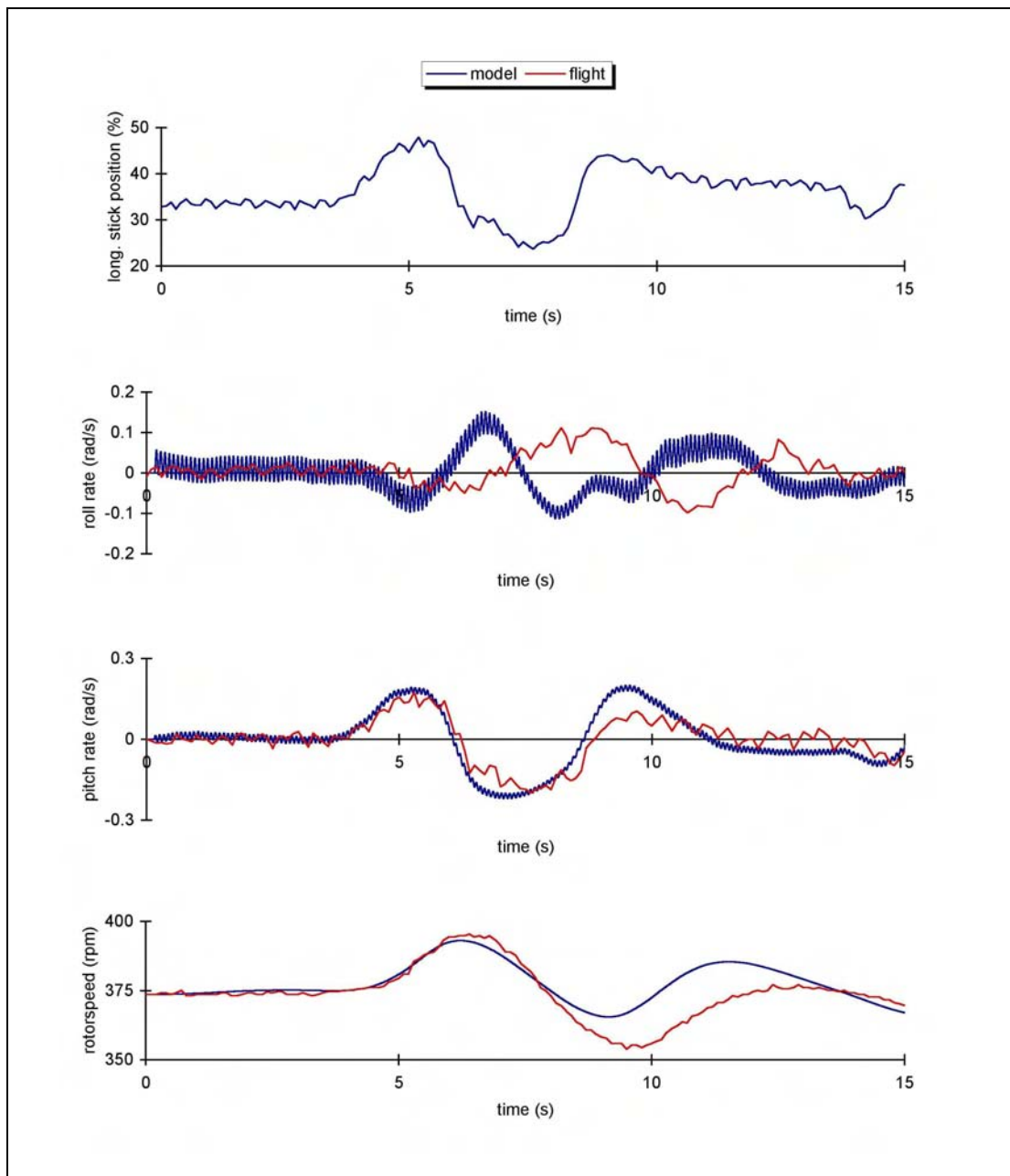
Figure 6.8   Non-linear Model Comparison with Flight Test (VPM M16, doublet input, 70mph)
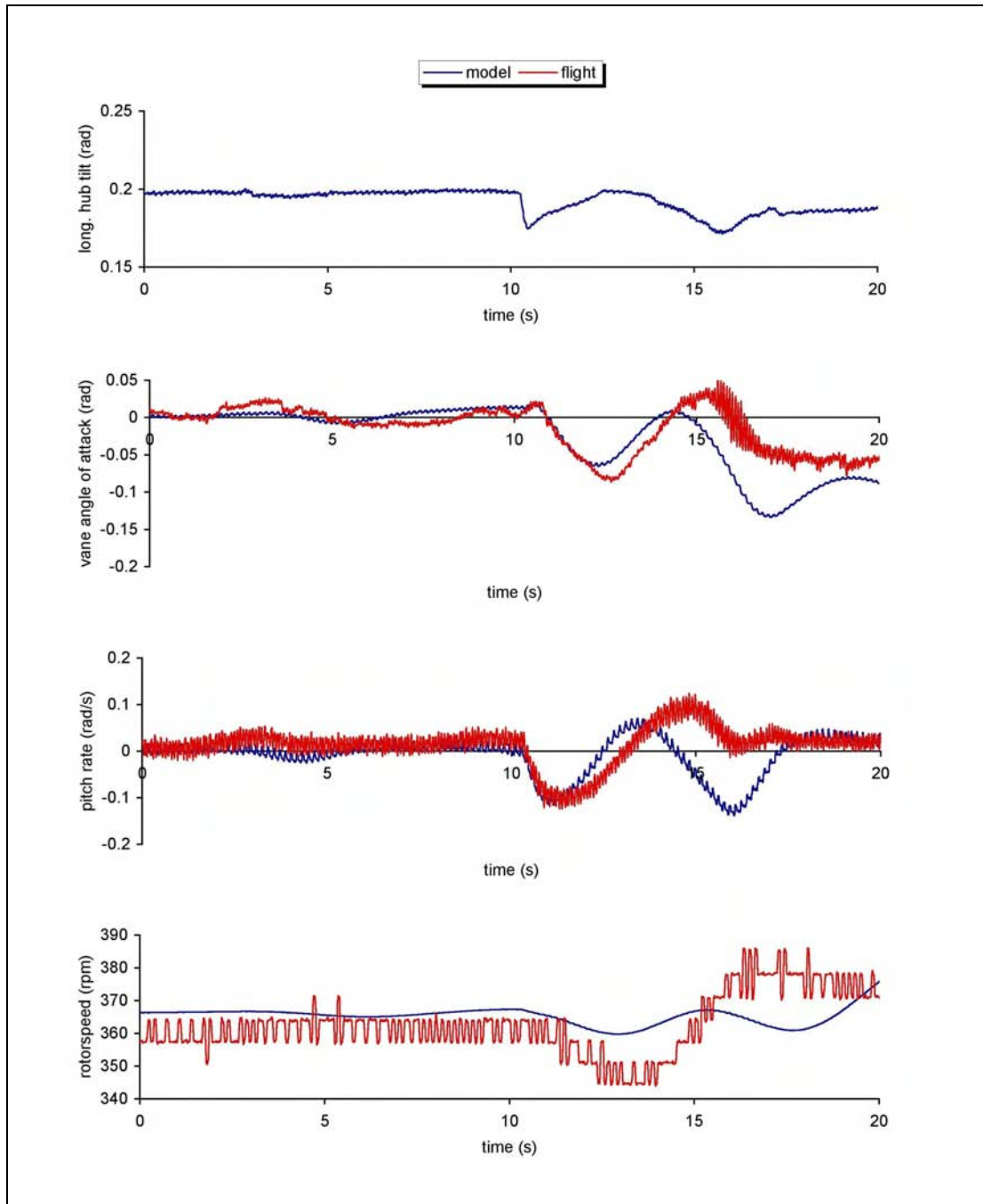
Figure 6.9   Non-linear Model Comparison with Flight Test (Montgomerie, Phugoid Input, 50mph)
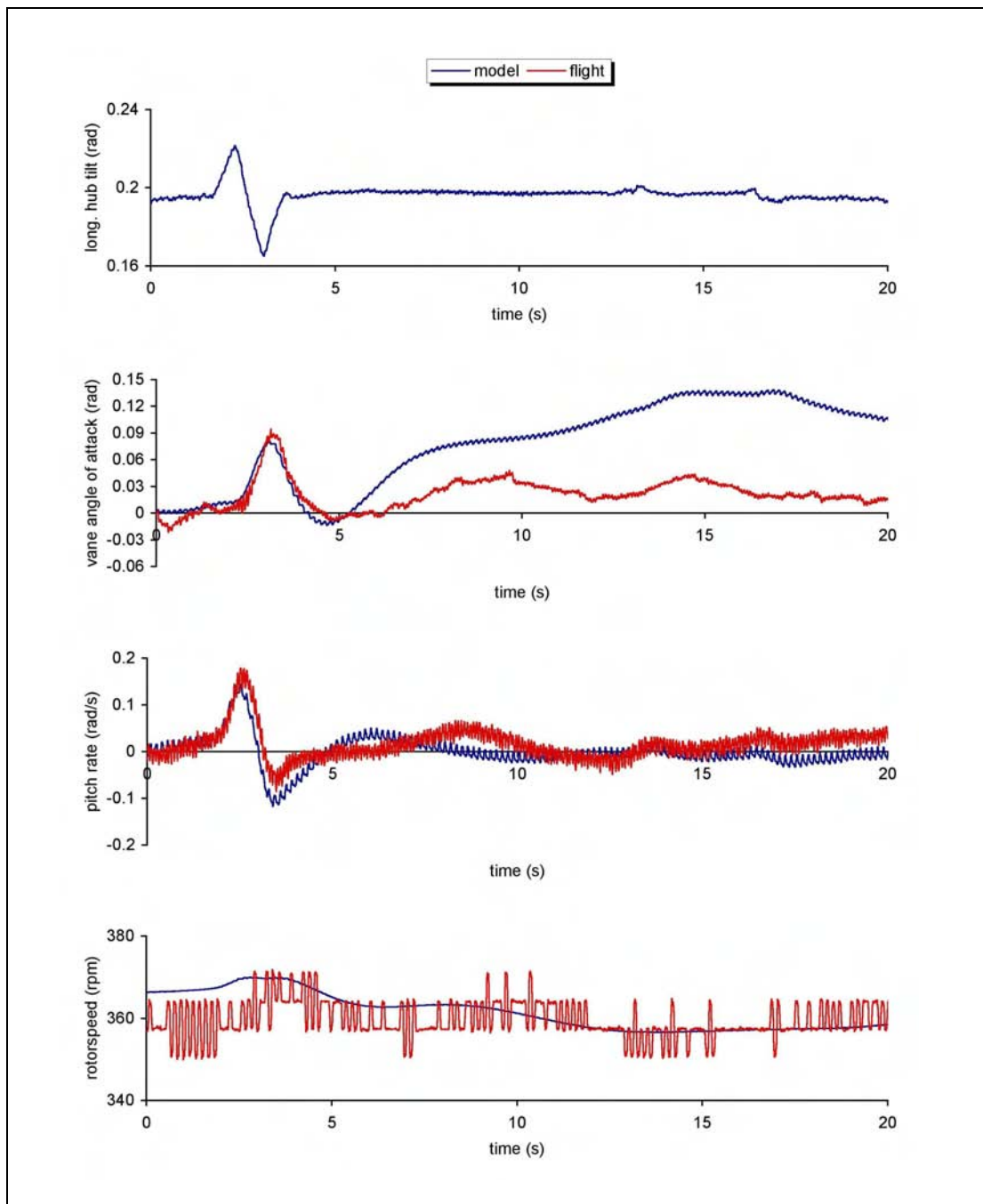
Figure 6.10   Non-linear Model Comparison with Flight Test (Montgomerie, Doublet Input, 50mph)
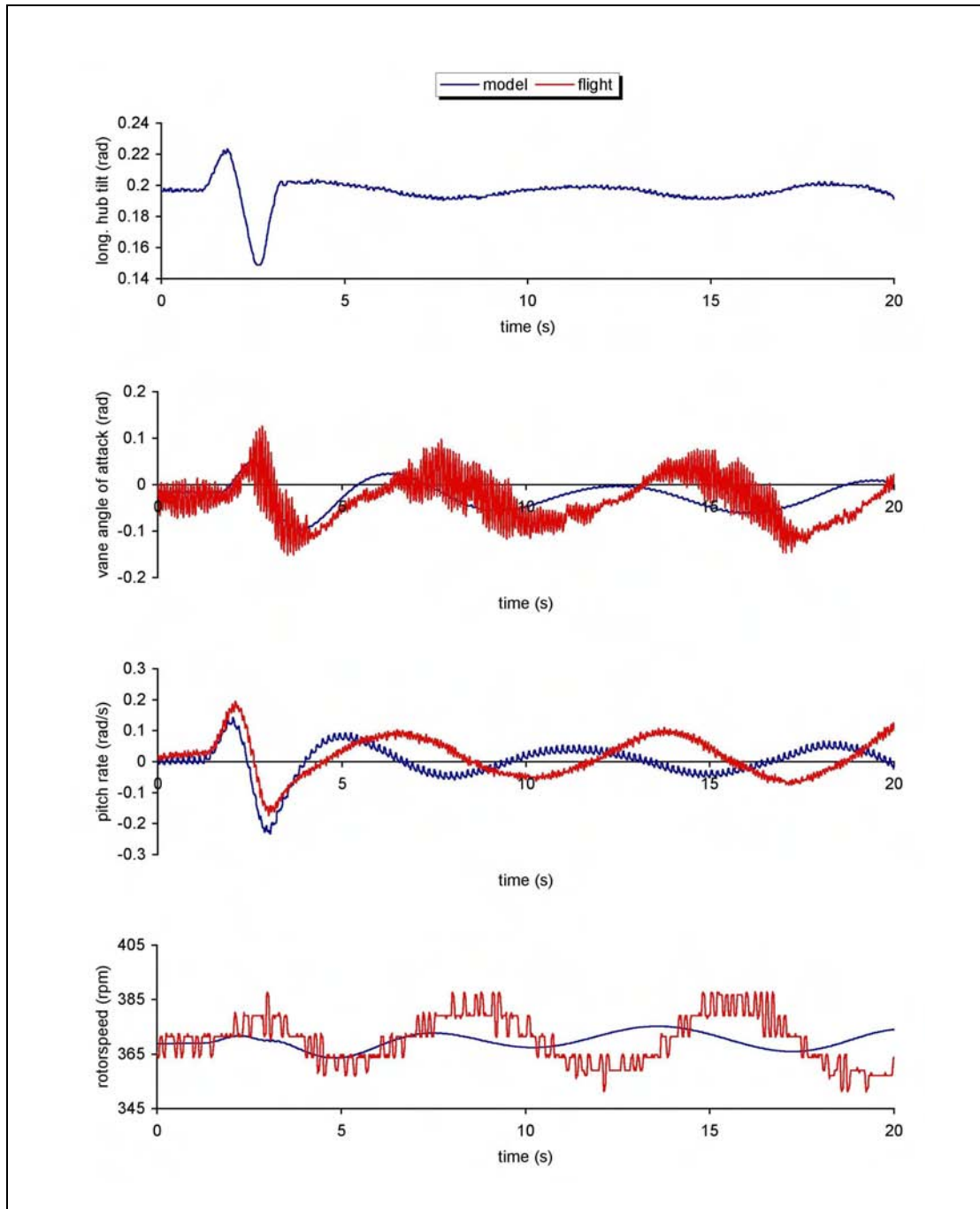
Figure 6.11   Non-linear Model Comparison with Flight Test (Montgomerie,
                   Doublet Input, 55mph)

7   Parametric Studies of Configurational Effects

The RASCAL mathematical model was used to examine the sensitivity of the behaviour of a typical aircraft to a range of design and operational variations. The design variations in particular are those that are either impractical or potentially unsafe to examine in actual flight test. A baseline, or default, configuration was selected and variations applied by modifying the aircraft datafile that defines that configuration. Simulated differences between the modified aircraft and the default then allow an assessment to be made of the importance of the design or operational difference. The objective is to catalogue these changes with a view to determining which ones are likely to have the greatest impact on the airworthiness of the aircraft.

The model was validated against VPM M16 and Montgomerie-Parsons Two-Place flight test data (see Section 6), and demonstrated good predictive ability in both cases so either can be chosen as the basis of the parametric study. However, the default configuration chosen was the VPM M16 modified for flight test, Figure 5.4 a), since more robust and detailed airframe aerodynamic data is available from wind tunnel testing. It also has a much larger tailplane than the Montgomerie-Parsons and so it is somewhat easier to interpret the scale of this parametric variation.

Table 7.1 shows the range of configurations simulated. The 13 configurations or flight conditions examined can be broadly classified as airframe geometry; airframe aerodynamic; rotor system; and operational variations. Engineering analysis then typically takes the form of comparison of steady (equilibrium, or trim) flight, dynamic stability and control response. Much can be learned from such comparisons but the specific form that they take can seem esoteric to the lay reader, hence a particular presentation of the results is made here. First, the trim comparisons are made against airspeed for airframe (roll and pitch attitudes, and flying control positions) and rotor (flapping angles and rotorspeed) parameters. Second, the dynamic stability comparisons are normally expressed in terms of stability and control derivatives, and aircraft modes of motion. Derivatives in particular can have little relevance to a pilot although great insight can be gained from their consideration. The modes of motion can also appear mathematically abstract. However, they can be converted to the form required of BCAR Section T dynamic stability compliance demonstration, and hence compared directly with those boundaries. Finally, the time response to controls, while adding little to an engineering analysis, can serve to illustrate how the aircraft actually behaves in a very specific case. Here, a control input is simulated that a pilot might typically use in demonstrating compliance with BCAR Section T

Table 7.1 Summary of Simulation Model Parametric Variation

Variation type	Parameter	Variation	Figure No.
Airframe geometry	Mass	426, 459 kg	7.1–7.3
Airframe geometry	Vertical c.g.	+6 in	7.4–7.6
Airframe geometry	Longitudinal c.g	±3 in	7.7–7.9
Airframe geometry	Mast height	±3 in	7.10–7.12
Airframe geometry	Propeller thrust line	±3 in	7.13–7.15
Airframe aerodynamics	Pod	Pod on and off	7.16–7.18
Airframe aerodynamics	Tailplane	Tailplane on and off	7.19–7.21
Airframe aerodynamics	Combination	Pod and tailplane on and off	7.22–7.24
Rotor system	Blade section	NACA 8H12 and 0012	7.25–7.27
Rotor system	Blade radius	±1 foot	7.28–7.30
Rotor system	Spindle offset	Nominal, zero	7.31–7.33
Operational	Temperature	ISA and ISA+20	7.34–7.36
Operational	Altitude	Nominal, 13000 feet	7.37–7.39

7.1   **Mass Variation (Figures 7.1 – 7.3)**

It is instructive to consider one example in detail before examining all other comparisons. Figures 7.1 – 7.3 show the trim, stability and time response comparisons of the default configuration with the high-mass case across the speed range. Speeds are given in mph, and are indicated or equivalent airspeeds. The default case is the aircraft as illustrated in Figure 5.4, with pilot but zero fuel giving an all-up mass of 426 kg. The 'high mass' case is obtained by simulating full fuel (33 kg) giving an all-up mass of 459 kg. Figure 7.1 suggests that there is little difference between the two configurations; the heavier aircraft requires a more aft tilt of the main rotor and a greater rotorspeed as might be expected, but the differences are small. Note the very small flapping angles required, as might be expected from a rotor system that has no cyclic pitch applied. The change in stick position is only about 5% of the available travel, or just over 0.5 in. At high speed there is little difference in the pitch attitude between the two cases.

The dynamic stability results are shown in Figure 7.2 presented as eigenvalues, (see Appendix 4 for further explanation). The three modes are present, the short period mode (cluster of points to the left) the phugoid mode (the cluster of points around the vertical axis), and the rotorspeed mode (the series of points on the real, or damping axis). The stable region of the plot is to the left of the vertical axis, and hence we see that the short period is stable over the whole speed range, whilst the phugoid is unstable at lower speeds. The BCAR Section T boundaries consistent with T181 period and cycles to damp are also plotted. Any point to the right of, or above, this boundary is non-compliant. The cluster of points farthest to the left is analogous to what aeronautical engineers would recognise as the 'short-period' mode. It is important to recognise that this mode is the one that determines whether or not a pilot finds aircraft handling qualities to be acceptable or not and, if acceptable, just

how good they are. This mode will tend to be compliant with Section T requirements, as evidenced by the fact that it is so far from the boundary. Yet the handling qualities may be poor if this mode has inappropriate damping and/or frequency. As can be seen, Section T is designed not to prescribe good short-period handling qualities, but rather to protect the pilot from unacceptable 'phugoid' mode characteristics, and in this case the phugoid mode is the one that is on the borderline of Section T compliance. Points to the right of the vertical axis represent unstable aircraft, but Section T allows a degree of instability. In this case, the model is predicting that stability of this phugoid mode improves with increasing speed (the points move right to left). Both configurations are non-compliant at 30 mph but as speed is increased the eigenvalues cross the boundary into the compliant region. Note that relative to a fixed-wing aircraft, this mode is faster (i.e. further up the vertical axis), and this is the attribute that makes the gyroplane airworthiness more problematic if unstable - hence the Section T focus on it. Although the short-period mode plays no part in Section T compliance, it is worthwhile to note that it moves up the plot with increasing speed, so the mode in effect becomes faster and more responsive.

In general through all of the results presented in this section, the 70 mph cases show the greatest difference between default and modified configurations (this is indeed the case for default and heavy cases here), and so are chosen for time history comparisons presented in Figure 7.3. The exception is the comparison of default with ISA+20 where the lowest speed case is used, as it is borderline compliance with Section T and therefore of use in illustrating what the response of such a configuration might look like. The control input is a 5 sec pulse of the longitudinal rotor tilt, similar to that which should be used in Section T compliance demonstration. Again, the default (light) and heavy aircraft show very similar characteristics. These plots help the reader to visualise the response of the configurations shown in Figure 7.2. As described in Appendix 4, the damping, natural frequency, period and time to half (or double) amplitude of a particular mode can be calculated from the eigenvalue. The eigenvalues plotted in Figure 7.2 for 70 mph (m = 426 kg) give the following:

Phugoid $\lambda = -0.0318 \pm 0.0313i$ Damping Ratio = 0.1597,   Period = 31.9s

Short Period $\lambda = -1.2201 \pm 0.188i$ Damping Ratio = 0.7185,   Period = 5.32s

Rotorspeed $\lambda = -0.5126$

The overall response is influenced by all 3 modes. However, as the phugoid is the longer period mode, its influence is much more obvious.

7.2   Vertical c.g. (Figures 7.4–7.6)

The dominant effect of this parameter is on the angle of attack stability derivative M_w. While the derivatives are not being compared in the parametric study, the reader should appreciate that this term will have powerful effects on both the short-period and phugoid modes. This can be seen in Figure 7.5 - lowering the c.g. will reduce the frequency of the short-period mode and, although this mode is deep within the compliance region, the aircraft will tend to feel more sluggish in manoeuvres which can adversely affect handling qualities. The phugoid mode frequency, however, is increased to the point where a number of the speed cases move out of compliance. Whilst this is only just outside in this case, it is intuitive that any marginally-stable mode that becomes faster (and this is what increased frequency means) will require greater pilot attention, compensation and workload.

The time responses, Figure 7.6, particularly the pitch attitude, highlight this clearly. The case shown is for 70 mph where both cases are Section T compliant, but the case with the low c.g. has a phugoid mode frequency considerably greater that of the default case where the c.g. is close to the propeller thrust line (see Figure 7.5 b). The longer-term (phugoid) response is visually much faster than that of the default case.

Whilst the VPM M16 simulations illustrate the general trend effect of lowering c.g. on angle of attack stability and hence these modes of motion, it is the case that of all the simulations conducted during 15 years of study this aircraft requires a fairly large c.g. offset to drive it non-compliant. As will be seen in later in Section 10 dealing with the Air Command series of gyroplanes this is not generally the case, and for the Air Command a 4 in offset produces a gross change in dynamic stability of short-period and phugoid modes.

7.3   **Longitudinal c.g. Variation (Figures 7.7–7.9)**

Longitudinal c.g. position is an important consideration in the stability and controllability of fixed-wing aircraft, and the range of c.g. position allowed is, in relation to the overall size of the aeroplane, quite small indeed. The stability and controllability of rotorcraft on the other hand is much less sensitive to longitudinal c.g. position. Rather, it is the longitudinal control required to trim that is the consideration, where c.g. must not compromise control margins. This is clearly illustrated in Figure 7.8, where an excessive (at least for an aircraft of the VPM M16's size, geometry and payload) longitudinal c.g. variation of 6 in is seen to have a very small impact on Section T compliance modes of motion, the short-period mode and the response to the compliance control input. Trim on the other hand is considerably different (Figure 7.7) with the 6in change in position changing the pitch attitude to trim by 4-5 deg, and the corresponding rotor tilt by 5-6 deg. A comparison of time responses is shown in Figure 7.9.

7.4   **Rotor Mast Height (Figures 7.10–7.12)**

The height of the mast (to the pivot where the pitch and roll control inputs are transferred to the hub) was varied by 3 in. Note that in reality this will raise or lower the c.g. but this effect is not included, hence it is purely the aerodynamic impact of moving the rotor vertical location that is being examined.

Trim, stability and control response plots show that this parameter has an insignificant impact on the flight mechanics of the aircraft.

7.5   **Propeller Hub Height (Figures 7.13–7.15)**

It should be expected that moving the propeller height on the airframe (assuming that the c.g. is in a fixed position and that there is no airframe/propeller interference) would have a broadly similar outcome to that obtained by raising or lowering the c.g. The trim curves (Figure 7.13) show that this is indeed the case, although the pitch attitude and rotor tilt angle differences between these two configurations are about 2 deg whereas the comparisons for vertical c.g. movement showed only a 1 deg difference.

The dynamic stability results (Figure 7.14) are however consistent with lowering the c.g. - raising the propeller hub and therefore thrustline tends to make the short-period mode more sluggish and the phugoid to be of higher frequency. This is shown in the time history (Figure 7.15) where the configuration with a raised propeller thrust line has faster and more oscillatory response.

7.6   **Pod on/Pod off (Figures 7.16–7.18)**

Airframe pods are generally regarded as destabilising, adding as they do a lifting surface ahead of the c.g., and given that the force is a function of dynamic pressure it is expected that pod effects will increase with increasing airspeed.

The trim plots (Figure 7.16) show a clear airspeed effect on both the pitch attitude and the longitudinal tilt of the rotor required to trim. Since the aircraft flies nose-up, i.e. with a positive angle of attack, the pod is lifting across the speed range and hence producing a nose-up moment. This is why without the pod the nose is lower and a more aft rotor tilt is required. The lift force is not, however, significant enough to unload the rotor by an amount sufficient to reduce the rotorspeed.

The dynamic stability results, Figure 7.17, show a short-period mode little affected by having a pod fitted, but a phugoid that perversely is more stable with pod fitted. This counter-intuitive result is clarified when it is considered that while the pod in isolation does indeed confer a degree of instability, the nose-up aerodynamic moment is sufficient to require having the rotor thrust vector placed sufficiently farther aft (i.e. more stabilising) relative to the c.g. to more than overcome the destabilising tendency.

The time histories, Figure 7.18, quantify the degree of difference that might be seen at 70mph and this is consistent with the stability diagram.

7.7   **Tailplane (Figure 7.19–7.21)**

The issue of horizontal tailplanes, or stabilisers, is foremost in the mind of the gyroplane community. While nothing of archival note has come to light, internet forums and association magazines and newsletters have focussed on whether or not to have a tailplane (although the majority seem to agree that to include one in a design is a good thing), where it should be located, the impact of propeller slipstream on effectiveness, etc. It is certainly the case that the Glasgow University work has, and continues to, come in for a degree of criticism for promulgating the view in the early days of the study that tailplanes, while having a role to play, really were insignificant in terms of providing a safe gyroplane. It is hoped that the results presented here, and this brief debate, will clarify and justify the position taken by the University team many years ago.

The results compare a VPM M16 with and without a horizontal tailplane. This is exactly the role for which an engineering model is ideally suited as to conduct actual flight trials would be expensive and have airworthiness implications that, in terms of approval, might be difficult to resolve. The M16 has perhaps one of the largest tailplanes fitted to a light gyroplane, and the reader concerned with fitment of anything smaller should consider any technical judgement in that context. Trim is insignificantly affected by the tailplane - at most there is a 1 deg difference in pitch attitude and rotor longitudinal tilt at 70 mph; less at lower airspeeds (Figure 7.19).

Dynamic stability shows (Figure 7.20) that the absence of the tailplane has an enormous impact on those modes that are of short-period, or 'fast'. However, these modes easily comply with Section T and come nowhere near the boundaries. It is certainly the case that their character changes and, perhaps because of this, gyroplane pilots will indeed feel a difference with and without a stabiliser. However, the phugoid mode is negligibly affected by the presence of a tailplane at low to medium speeds. Even at 70 mph where one might expect the greatest impact, the time to half amplitude of the mode is 7 sec without the tailplane, and 14 sec with. The latter is still a well-damped mode in the context of aircraft phugoid motions; both with and without the tailplane configurations easily satisfy Section T compliance; and at low speed there is no benefit at all, the phugoids for both configurations being nearly identical. The counter-intuitive result that the phugoid is less damped with the tailplane, is specific to the VPM and is a consequence of the pod generating such a significant lift force at high speed due to the nose-up pitch attitude without the tailplane, that the main rotor thrust vector is placed in a more favourable (stabilising) location to trim this increased moment. If the aircraft flew nose-down at high speed, the pod would generate a downforce and the result is reversed. The conclusion is reached that in terms of Section T compliance and the dynamic stability of the mode that is likely to be marginally stable (the phugoid), a tailplane offers no overall benefit. Remember, that is not to say that a pilot will not feel that his aircraft has better handling qualities with a tailplane fitted, as the short-period mode comparisons testify.

Other aircraft with smaller stabilisers are likely to experience less benefit. The fundamental problem, as illuminated by the wind tunnel results, is that the lift-curve slope is weak at around 2 per radian. Typical helicopter values are 3-3.5, an aeroplane overall (including fuselage etc.) may be around 5.5, and finite wing theory limits this parameter to per radian. Combine this with the very short moment arm of the pusher configuration and it can be seen that very large tailplanes will be required and, as the results above show, even then it will only be the short-period mode that is affected.

There is some debate in the gyroplane community over the optimum location for a stabiliser in relation to the propeller wake. The wind tunnel chapter discusses this point and indicates that, for the VPM M16 configuration, there is little benefit to be obtained from the propeller wake. If the tailplane can benefit from the full value of the slipstream velocity by being appropriately placed, simple momentum theory allows an assessment to be made of its potential effectiveness. At 30 mph, the tailplane would experience an airspeed of 43 mph, while at 70 mph it would be 73 mph. This assumes a uniform distribution of induced velocity.

The time histories, Figure 7.21 confirm that there is little difference in the response of the two configurations to the control input at 70 mph, where the difference in the phugoid mode is greatest. (Note that this input fails to excite the short-period mode, indeed it is designed to avoid exciting it, and hence the gross changes seen in the compliance diagram are hidden in the time response plots).

7.8   Pod and Tailplane On/Off Figures 7.22–7.24)

Simulation of pod and tailplane removed shows little difference in the trim variables relative to the standard aircraft (Figure 7.22) or in the phugoid mode, and hence compliance with Section T is not influenced by airframe aerodynamics. However, the short-period mode is significantly different (Figure 7.23) much more so than in any of the parametric variations seen previously. Further, the small control input in this case produces large excursions from trim where the linearised analysis that underpins the stability diagram is of dubious value, as seen from the time response, (Figure 7.24).

7.9   Blade Section (Figures 7.25–7.27)

The VPM M16 blade section is cambered, while the NACA 0012 is symmetrical and was for a number of years the section of choice for helicopter rotor blades. The gyroplane community fly with a number of different blade sections but this comparison was chosen because the 0012 is dissimilar to the majority of sections in use; it is intended therefore as an 'extreme' comparison. The trim results (Figure 7.25) show fairly small differences in rotor tilt and airframe attitude (no more than about 1 deg). The rotor with the 0012 section, however, turns some 40 rpm faster.

The dynamic stability results (Figure 7.26) show for the 0012 a short-period mode similar at low speeds but more lightly damped at high speed. The phugoid mode is of similar frequency to the standard aircraft, but is slightly less well damped. This is clear from the time histories (Figure 7.27).

7.10   Disc Loading (Figures 7.28–7.30)

Disc loading was varied by reducing blade radius by 0.3 m; and increasing it by the same amount relative to the standard aircraft. This results in very considerably different rotor and blade loadings. The small rotor has a blade loading in these simulations of 248.4 kg/m2, and a disc loading of 9.1 kg/m2. By contrast the large rotor blade and disc loadings are 214.6 kg/m2 and 6.8 kg/m2. The scale of the following differences should therefore be seen in this context.

The trim results (Figure 7.28) show, as might be expected, a large difference in the rotorspeed of 60 rpm, and a 2 deg difference in pitch attitude; the more lightly loaded rotor operates at a lower angle of attack.

The dynamic stability results (Figure 7.29) show that the aircraft with the smaller loadings has better short-period mode damping, but poorer phugoid damping to the extent that it only becomes Section T compliant above 40 mph. The better short-period mode damping is due to the greater pitch damping which comes from a lower rotorspeed (the disc will precess more in response to pitch rate disturbances). The time histories (Figure 7.30) quantify the magnitude of the difference in phugoid damping, showing that the response is more oscillatory with the larger and therefore more lightly-loaded rotor.

7.11 Spindle Offset (Figures 7.31–7.33)

All light gyroplanes fly with what are basically slight variations in the design of the Bensen rotor head. A feature of the design is that the teeter mechanism is not mounted directly above the rotor hub pivot point, but is displaced aft by a few centimetres. This endows the aircraft with a degree of stick-free stability when disturbed by, say, atmospheric changes. All the analysis conducted here assumes stick-fixed, and it is the case that stick-free the aircraft is more stable. Trim differences (Figure 7.31) are limited to pitch attitude and rotor tilt, while Section T compliance (Figure 7.32) and time responses (Figure 7.33) both confirm that this parameter has a negligible impact on the dynamic stability and response of the aircraft.

7.12 Environmental Parameters - Density Altitude (Figures 7.34–7.39)

The density altitude is affected by temperature and the height at which the aircraft is flown. The results for ISA+20 deg C (Figures 7.34–7.39) show that the density changes resulting from high temperature at low altitude have an insignificant impact on trim, stability or control response.

Flight at 13,000 feet, however, produces more variability. Overall the results hint at proximity to retreating blade stall. The trim curves (Figure 7.37) differ by only a degree or so, but the dynamic stability (Figure 7.38) shows a short-period mode highly sensitive to flight at altitude. This can be attributed directly and mathematically to the influence of true air speed (rather than indicated air speed) at altitude. The phugoid mode is slightly less stable across the speed range. The time responses (Figure 7.39) confirm that there is little difference in the long-term response, but odd behaviour that appears to be non-linear in nature (most likely the model capturing dynamic stall effects) afflicts the short-term response to the control input.

7.13 Concluding Remarks

Consideration of these results, particularly in the context of design advice or airworthiness considerations in general, requires careful interpretation and insight. For example at face value the design or operational parameter that has the greatest relative impact is a change in disc loading (rotor blade radius). A relatively small change (0.3 m) drives a considerable change in the control angles and rotorspeed required to trim the aircraft, as well as the damping of the phugoid mode (and hence Section T compliance). However, damping alone is only one of the parameters considered when assessing dynamic stability; frequency is also important and while pilots can cope with a degree of phugoid mode instability, that ability is compromised if the mode becomes faster (i.e. the period becomes shorter). The parametric study shows that the relative location of the propeller thrust line in relation to the centre of gravity is the only parameter investigated that produces a significant variation in the period of the phugoid mode for a relatively small change in distance - Figure 7.14 b) for example shows that the frequency of the mode can be doubled, while Figure 7.15 clearly shows a livelier pitch attitude response with a thrust line only 3 in higher than the datum aircraft. Of particular note is that this change occurs across the speed range. Addenda 1 and 2 provide independent experimental validation of the importance to dynamic stability of the relationship between propeller thrust line and c.g. location.

The tailplane effect on Section T compliance, by comparison, is limited. It fails to change the frequency of the phugoid across the speed range; improves the damping only with speed; but has a gross effect on the short-period mode (Figure 7.20 a)). The Section T compliance mode is therefore negligibly affected by a horizontal tailplane at low speeds (consistent with the poor aerodynamic efficiency identified in tunnel test), whereas propeller thrust line location has an impact across the speed range. Heresay evidence from the gyroplane community however is that tailplanes are significant components for the improvement in gyroplane stability. This perception is probably associated with their impact on the short-period mode seen in Figure 7.20 a) – the short-period mode is not an issue for compliance demonstration, but it is the mode that pilots excite to manoeuvre their aircraft and hence the mode that determines how handling qualities are perceived.

CAA Comment

CAA accepts that closer alignment of the CG and the thrustline is a sensible design aim to achieve pitch dynamic stability (phugoid mode) and whilst conclusive Flight Test evidence has supported this and directly led to the issue of MPD 2005-08 for single seat gyroplanes, other flight tests provide evidence of a gyroplane design that achieves good stability whilst being outside of the 2 inch criteria. CAA Flight Test Specialist qualitative assessment implies that pitch dynamic stability may not be solely a function of CG/Propeller Thrust alignment for all types of Gyroplane.

The report also concludes that horizontal tailplanes are largely ineffective in improving the long term response of pitch dynamic stability (phugoid mode). This is the result of studies primarily on narrow tandem cockpit enclosures. CAA Flight Test Specialist qualitative evaluation of the effects of a horizontal tailplane on a single side-by-side configuration gyroplane type indicated a degree of improvement in the phugoid characteristics at higher speed.
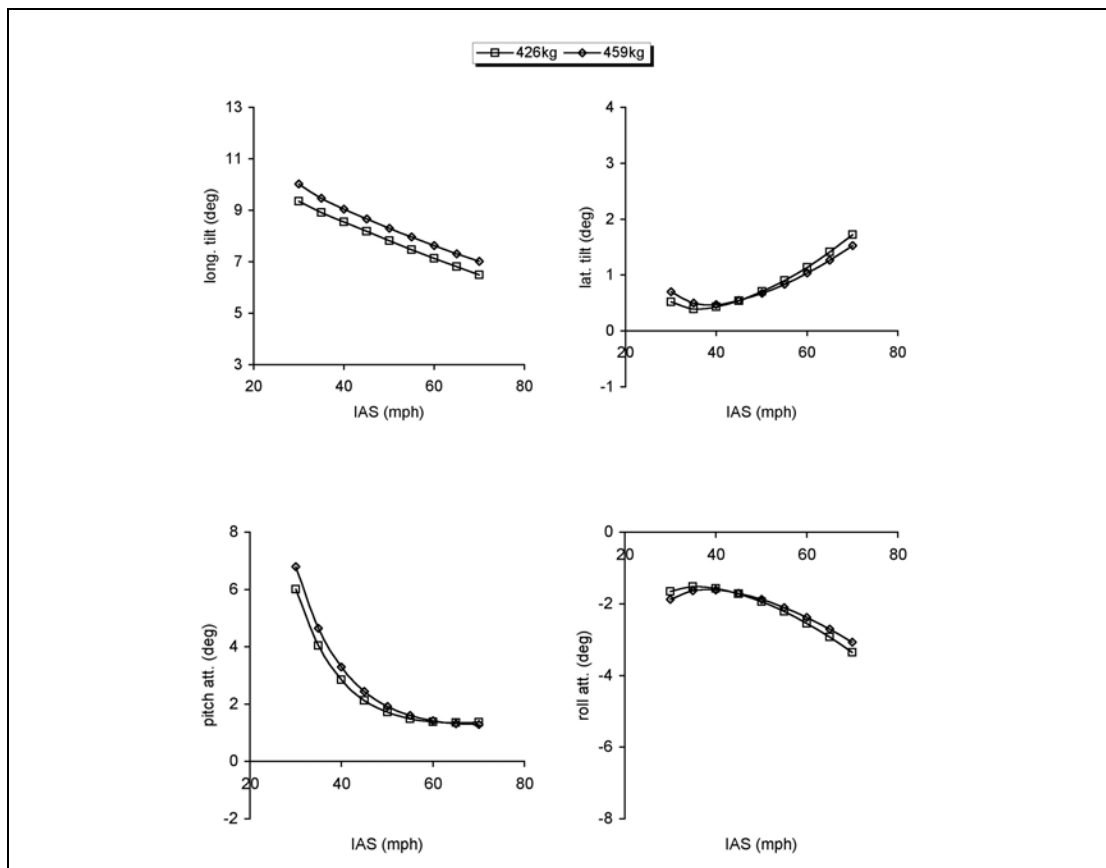
Figure 7.1a   Trim Comparison for Mass Variation (Airframe Parameters)
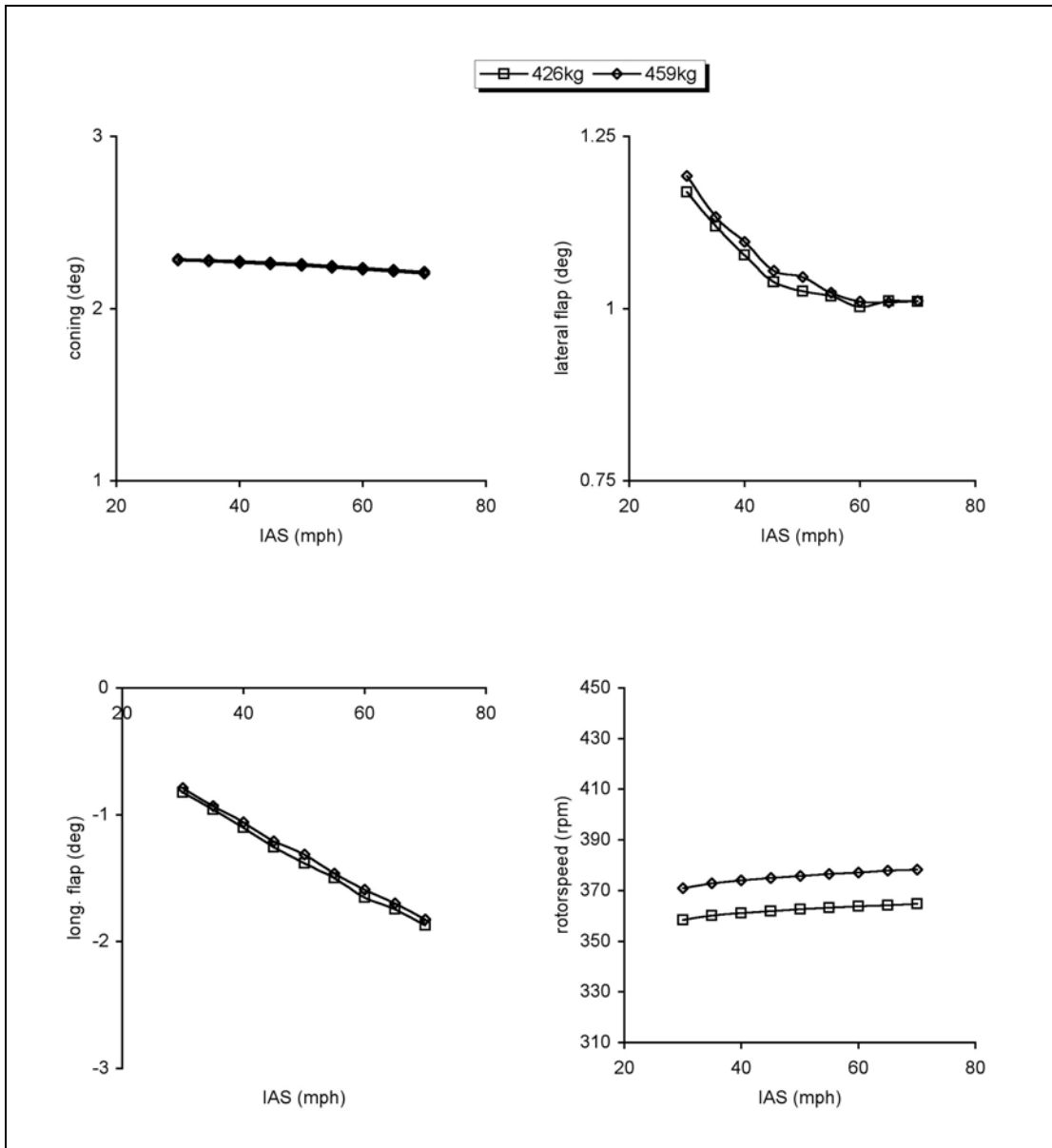
Figure 7.1b   Trim Comparison for Mass Variation (Rotor Parameters)
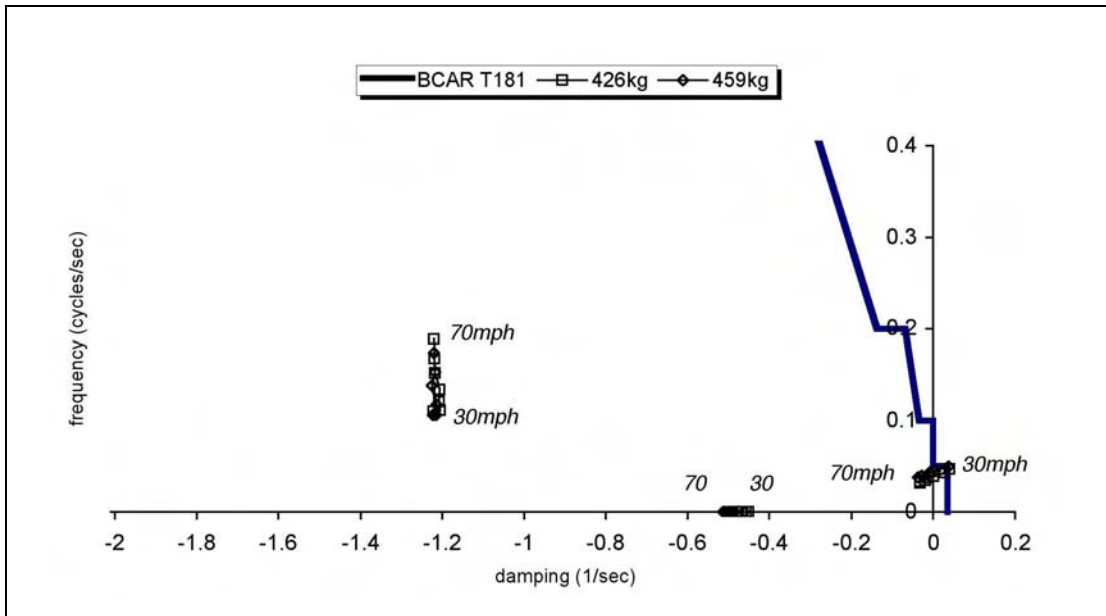
Figure 7.2a   Comparison of Stability Modes (Mass Variation)

Figure 7.2b   The Phugoid Mode (Mass Variation)
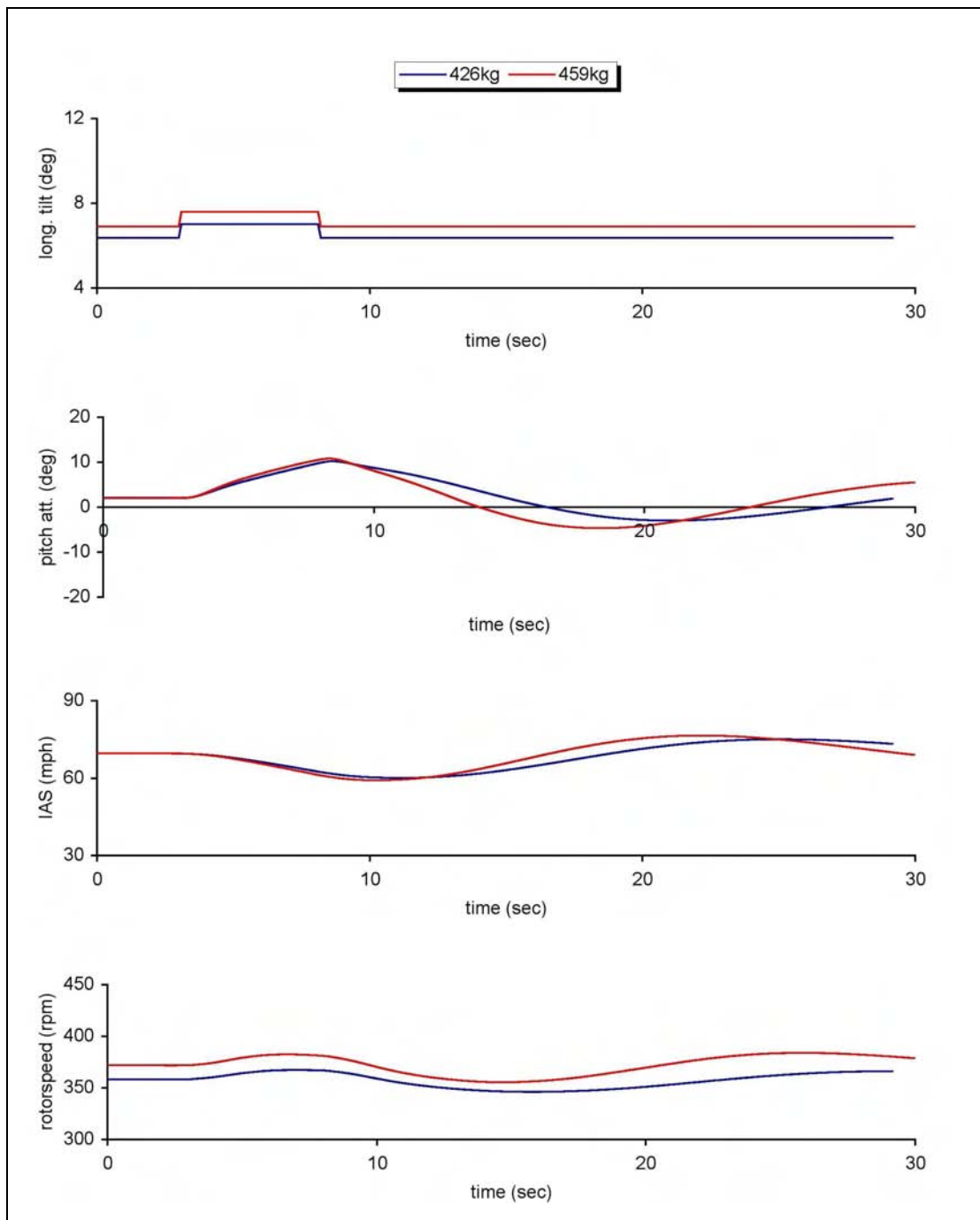
Figure 7.3   Aircraft Response to 5s Pulse of Longitudinal Rotor Tilt - Phugoid
(Mass Variation)
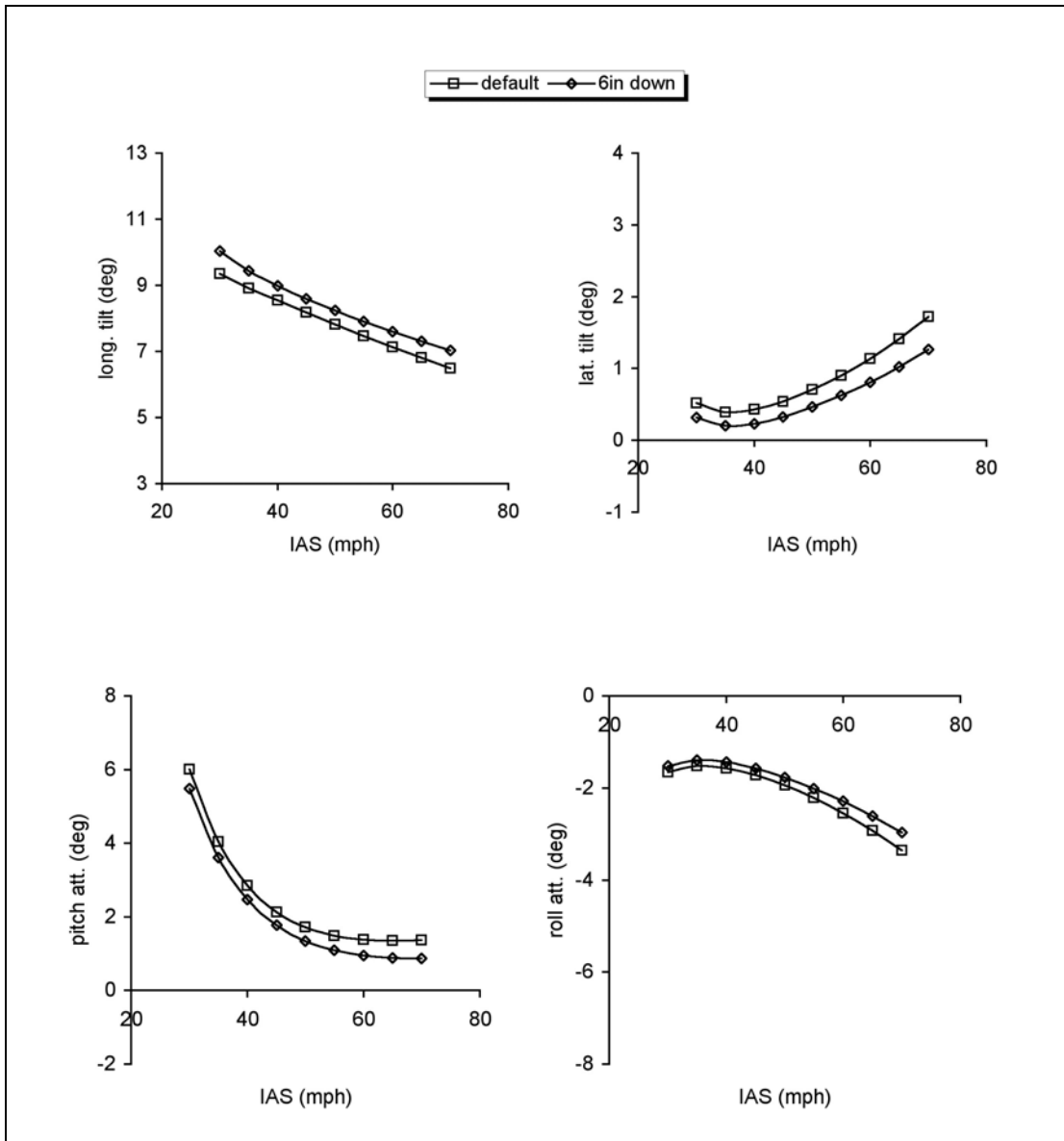
Figure 7.4a   Trim Comparison for Vertical c.g. Variation (Airframe Parameters)
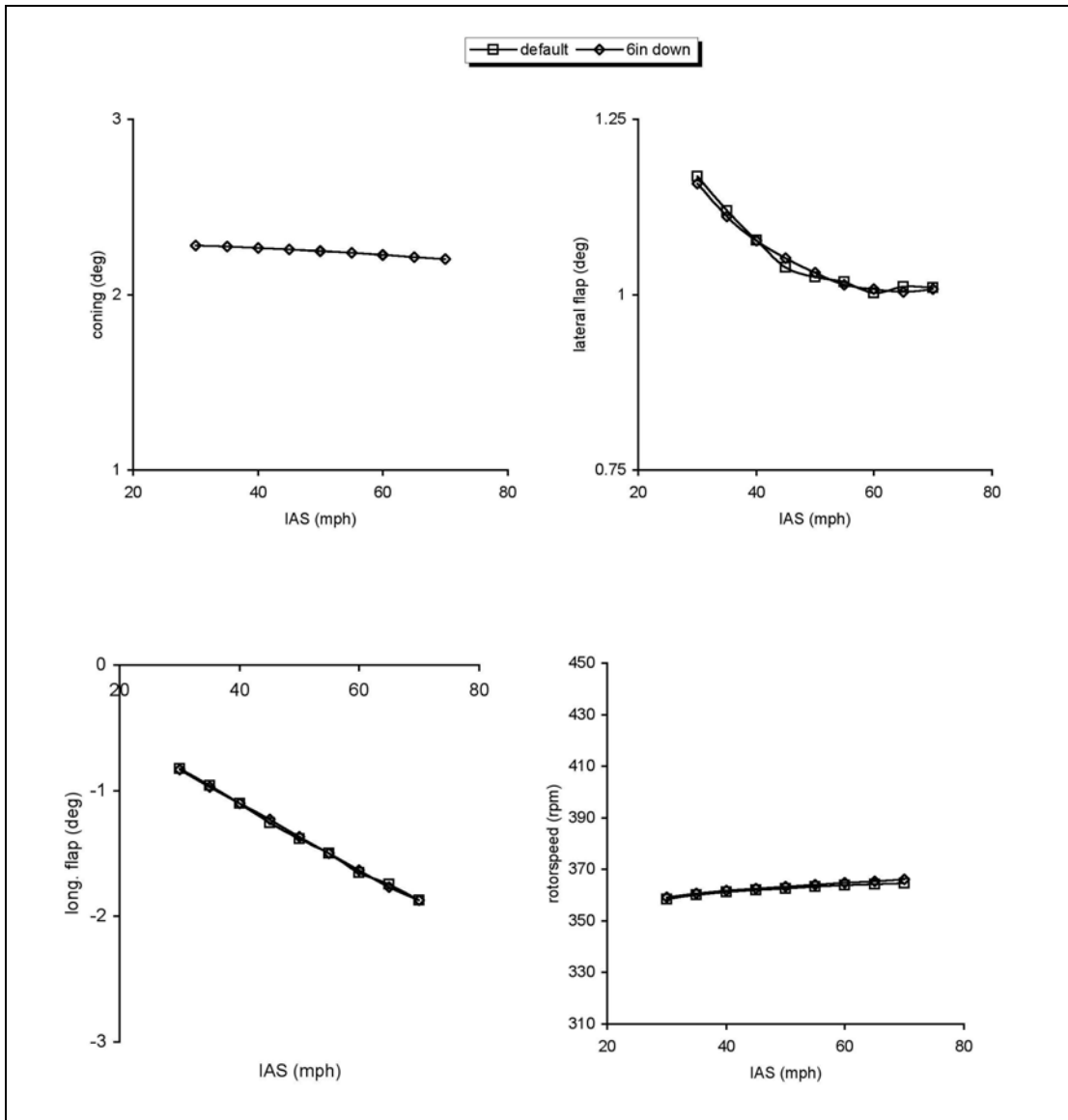
Figure 7.4b   Trim Comparison for Vertical c.g. Variation (Rotor Parameters)
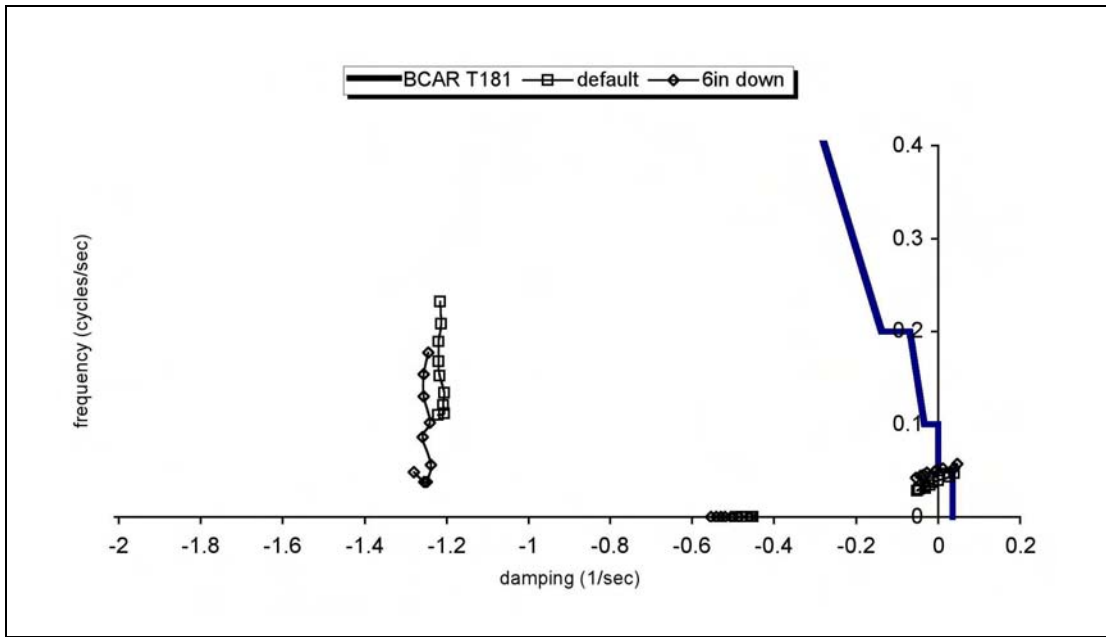
Figure 7.5a Comparison of Stability Modes (Vertical c.g. Variation)

Figure 7.5b The Phugoid Mode (Vertical c.g. Variation)
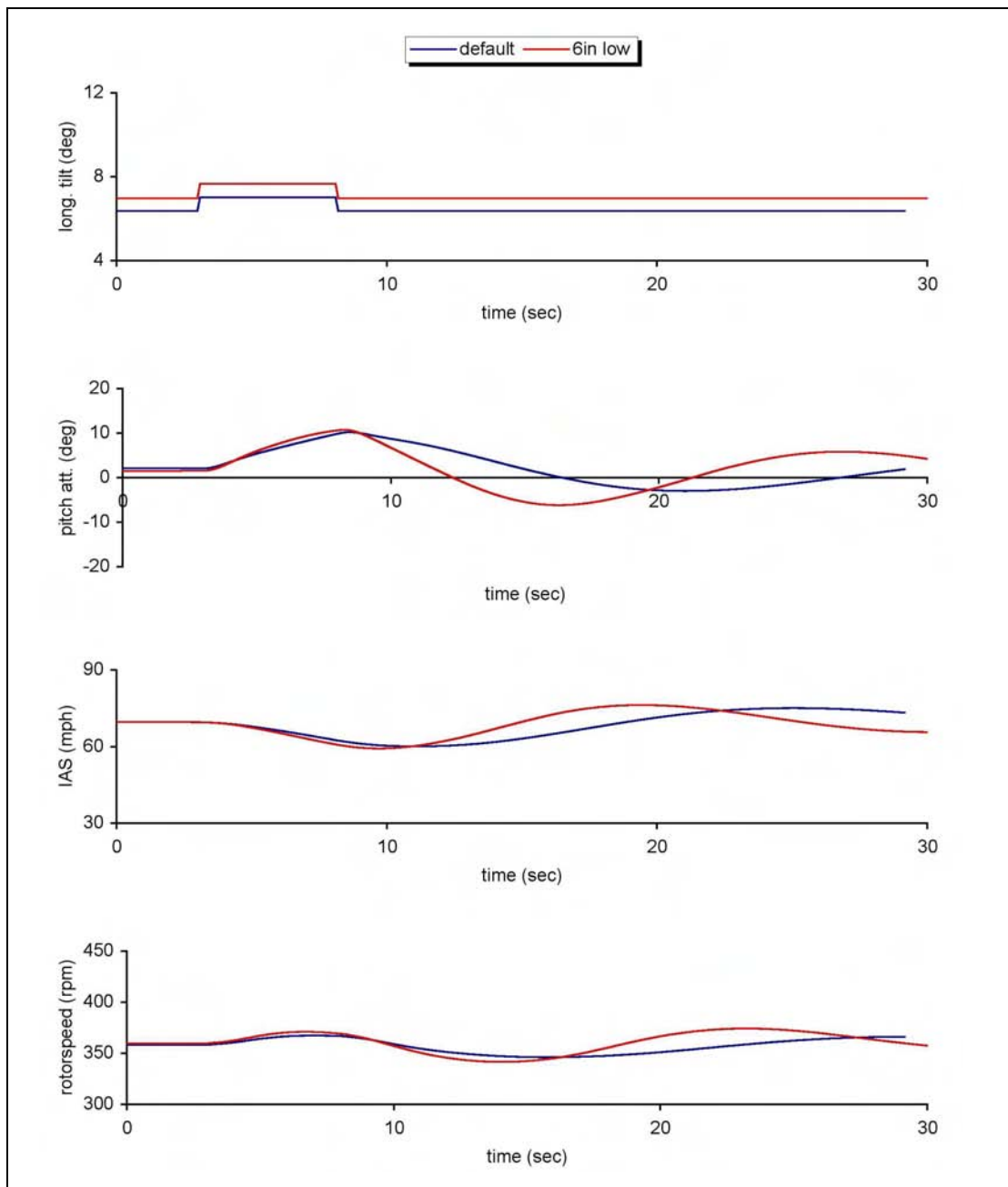
Figure 7.6   Aircraft Response to 5s Pulse of Longitudinal Rotor Tilt - Phugoid
(Vertical c.g. Variation)
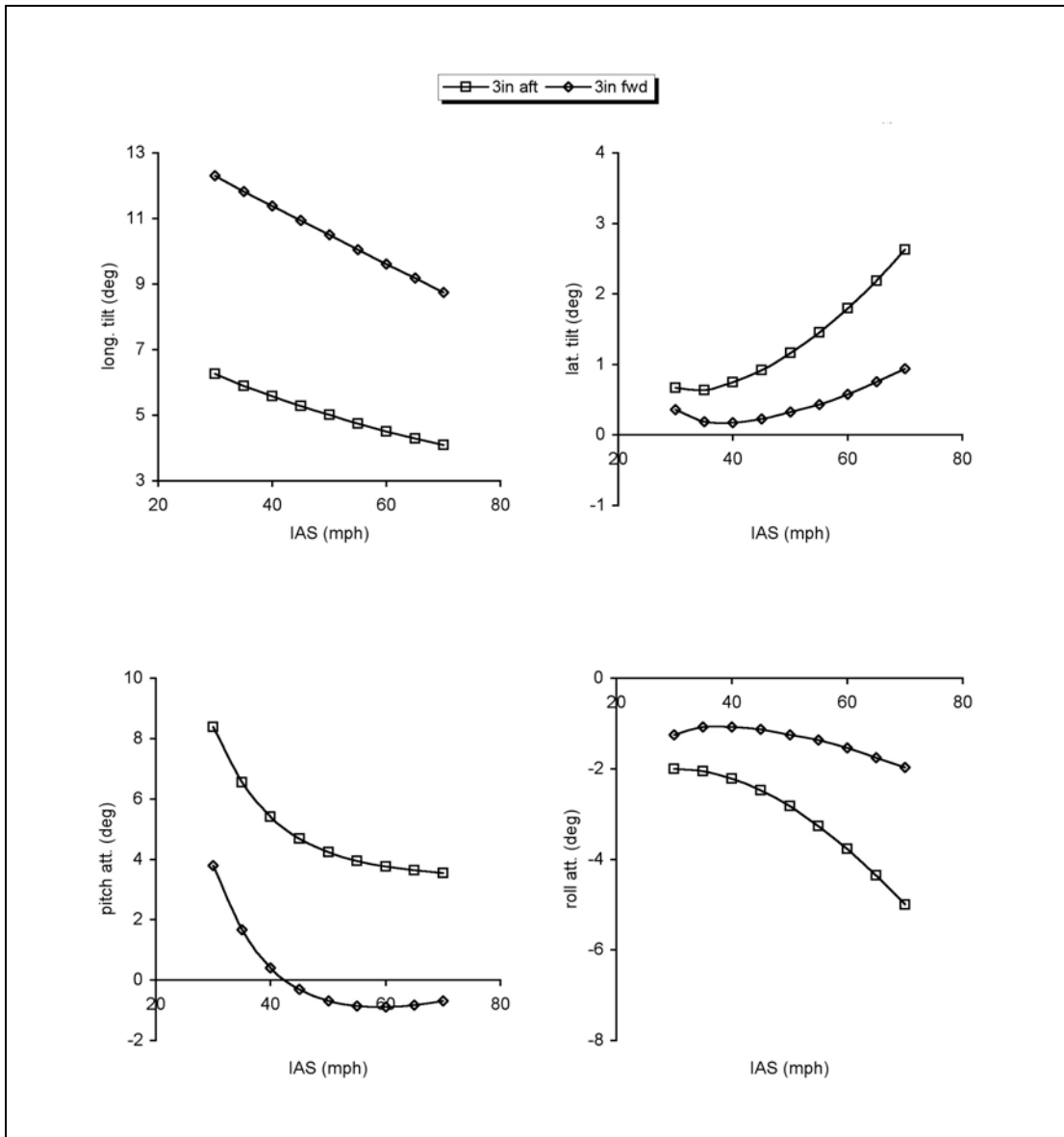
Figure 7.7a   Trim Comparison for Longitudinal c.g. Variation
                        (Airframe Parameters)

Figure 7.7b   Trim Comparison for Longitudinal c.g. Variation
(Rotor Parameters)

Figure 7.8a   Comparison of Stability Modes (Longitudinal c.g. Variation)

Figure 7.8b   The Phugoid Mode (Longitudinal c.g. Variation)

Figure 7.9   Aircraft Response to 5s Pulse of Longitudinal Rotor Tilt - Phugoid
(Longitudinal c.g. Variation)
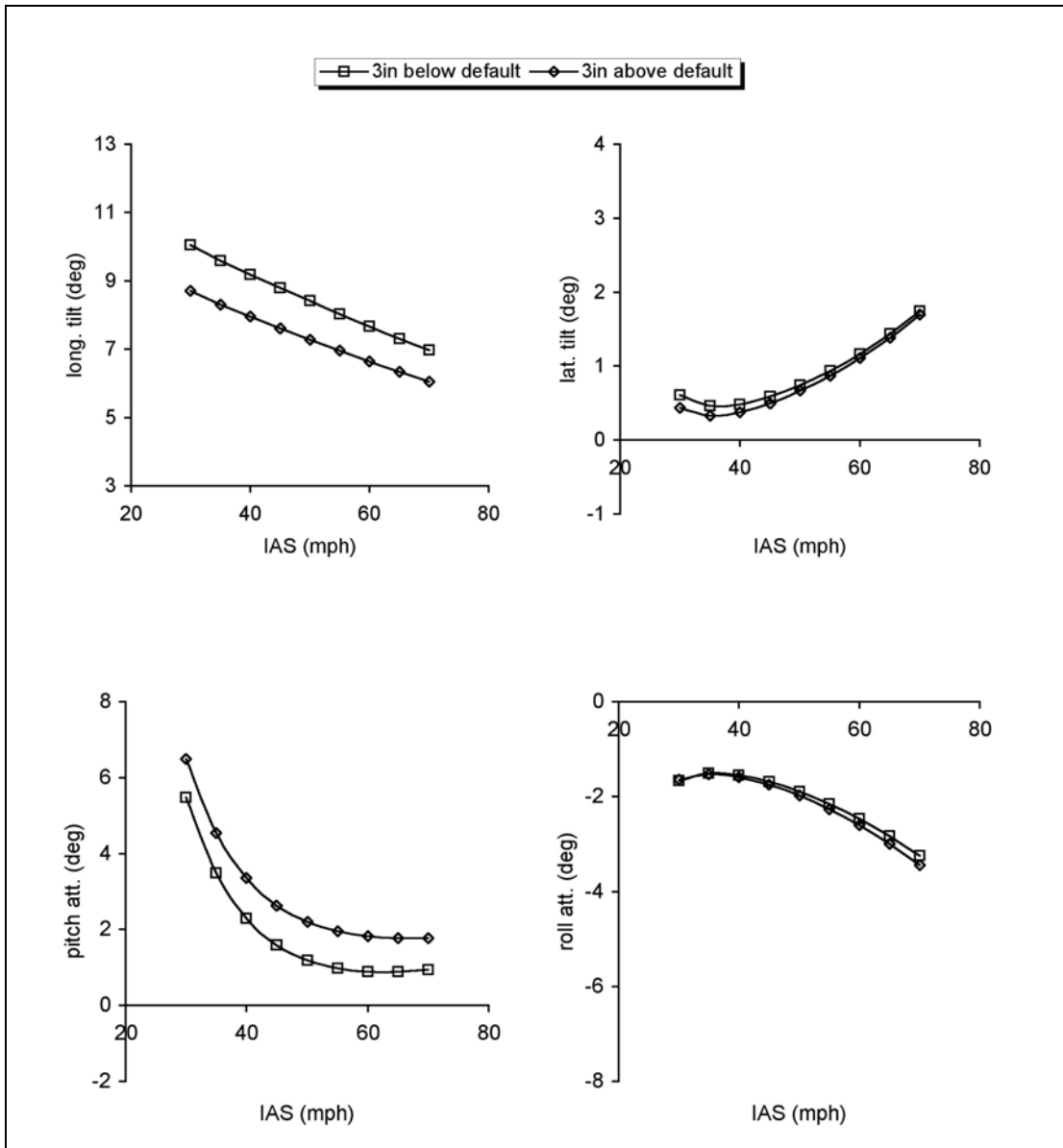
Figure 7.10a Trim Comparison for Mast Height Variation (Airframe Parameters)

Figure 7.10b Trim Comparison for Mast Height Variation (Rotor Parameters)

Figure 7.11a Comparison of Stability Modes (Mast Height Variation)
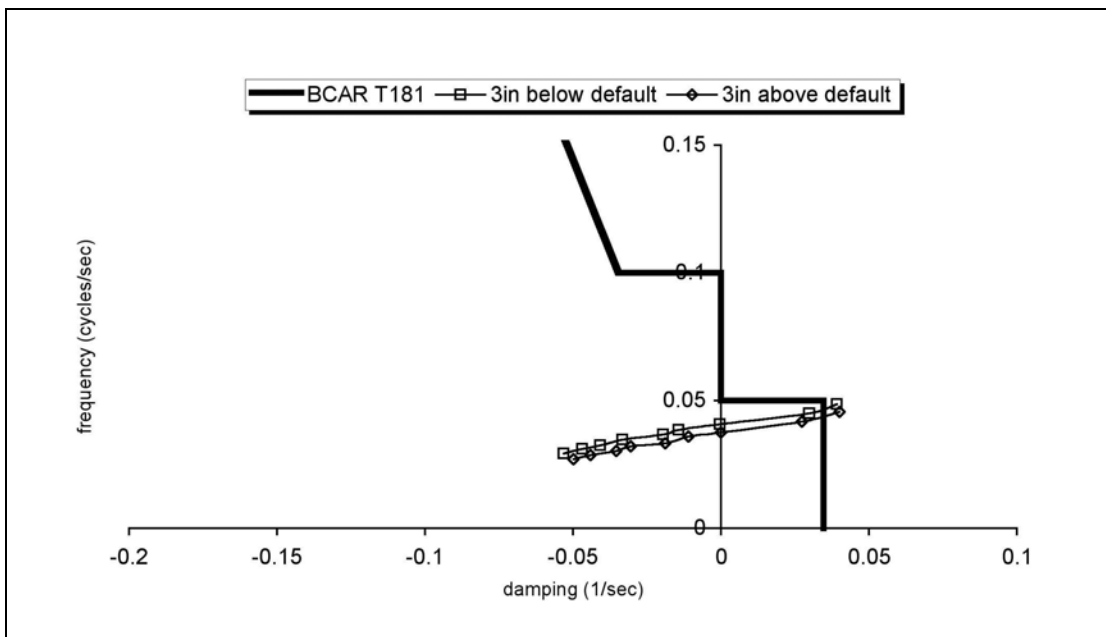
Figure 7.11b The Phugoid Mode (Mast Height Variation)
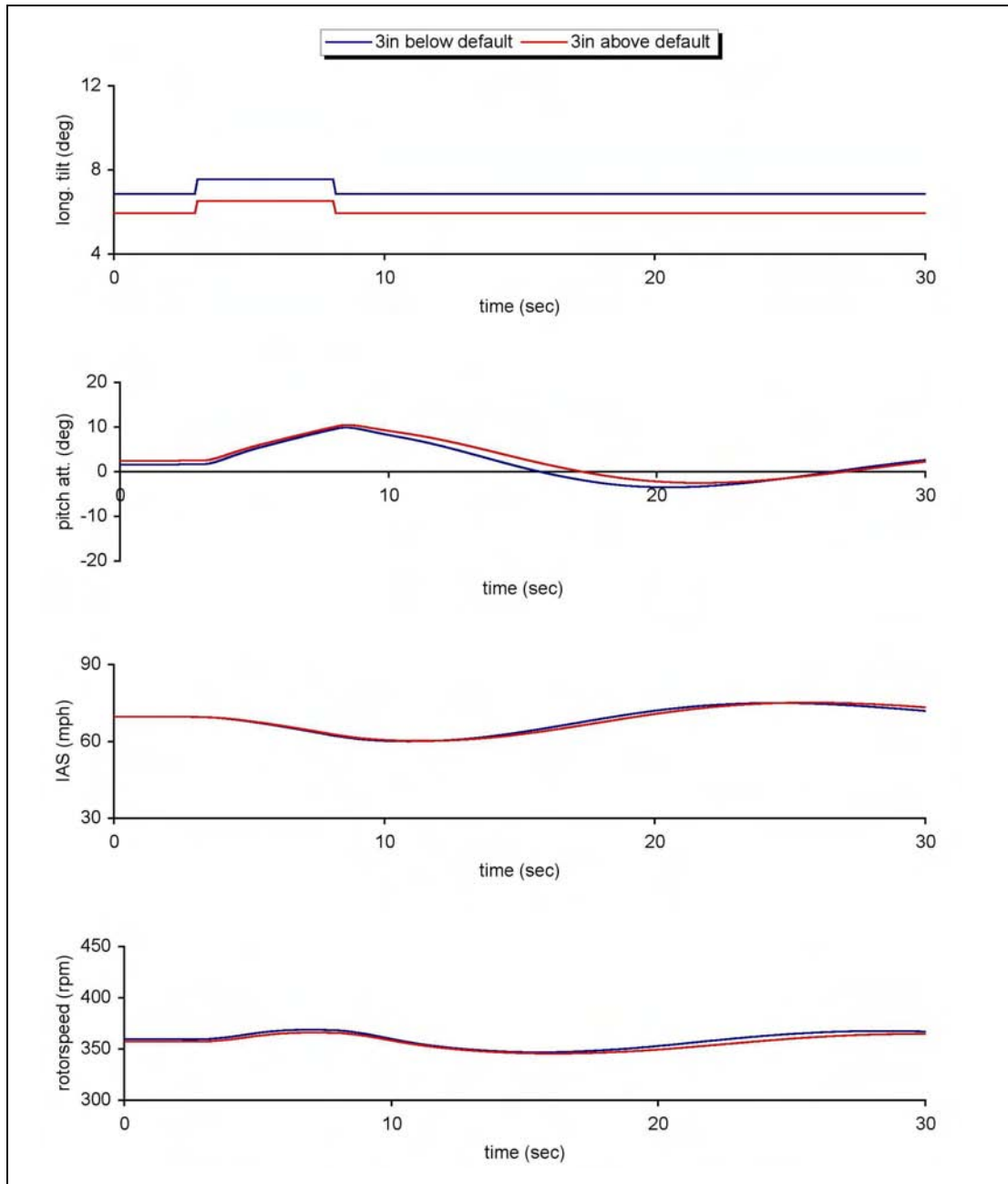
Figure 7.12   Aircraft Response to 5s Pulse of Longitudinal Rotor Tilt - Phugoid
(Mast Height Variation)
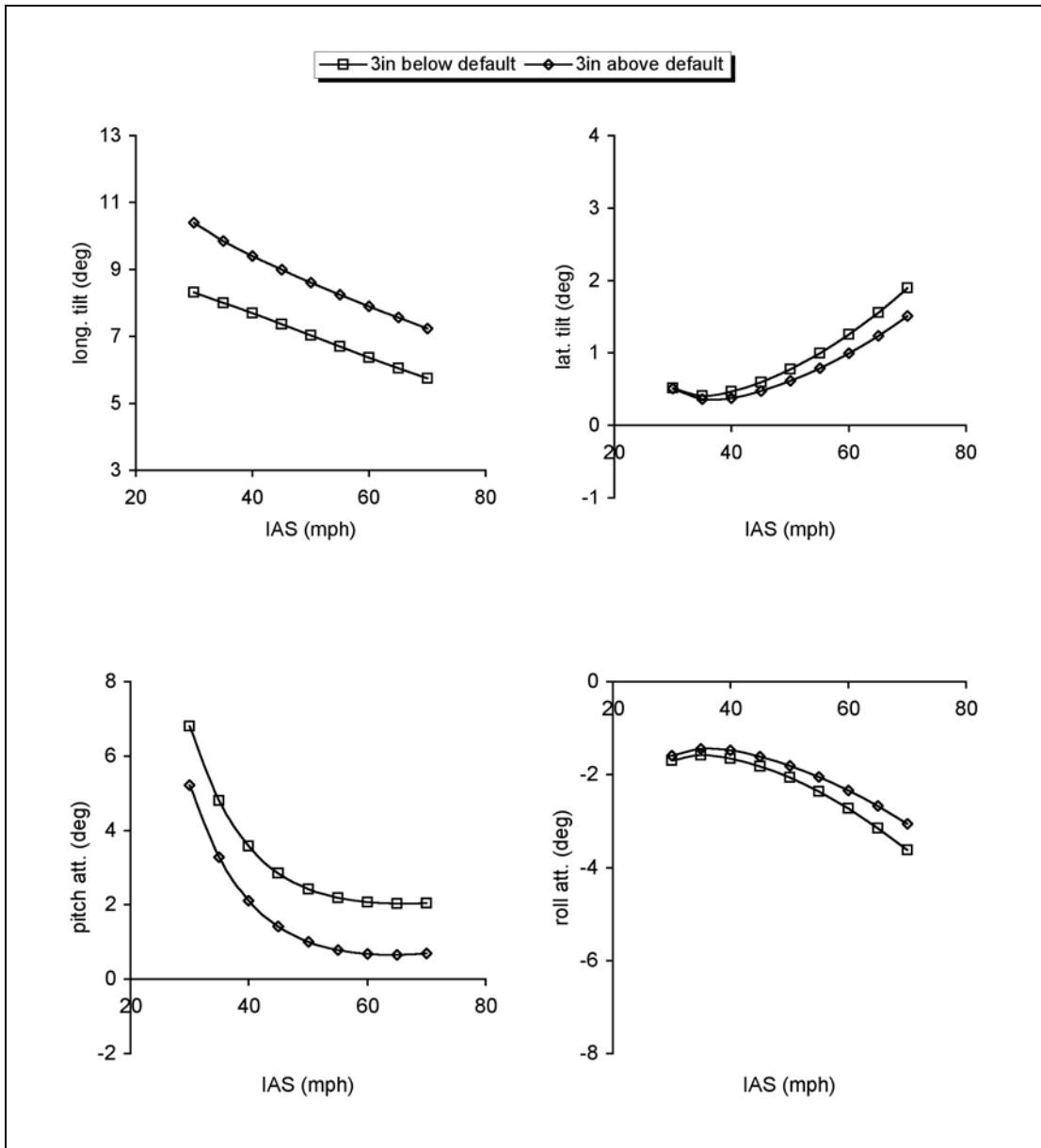
Figure 7.13a Trim Comparison for Propeller Thrust Line Variation
(Airframe Parameters)
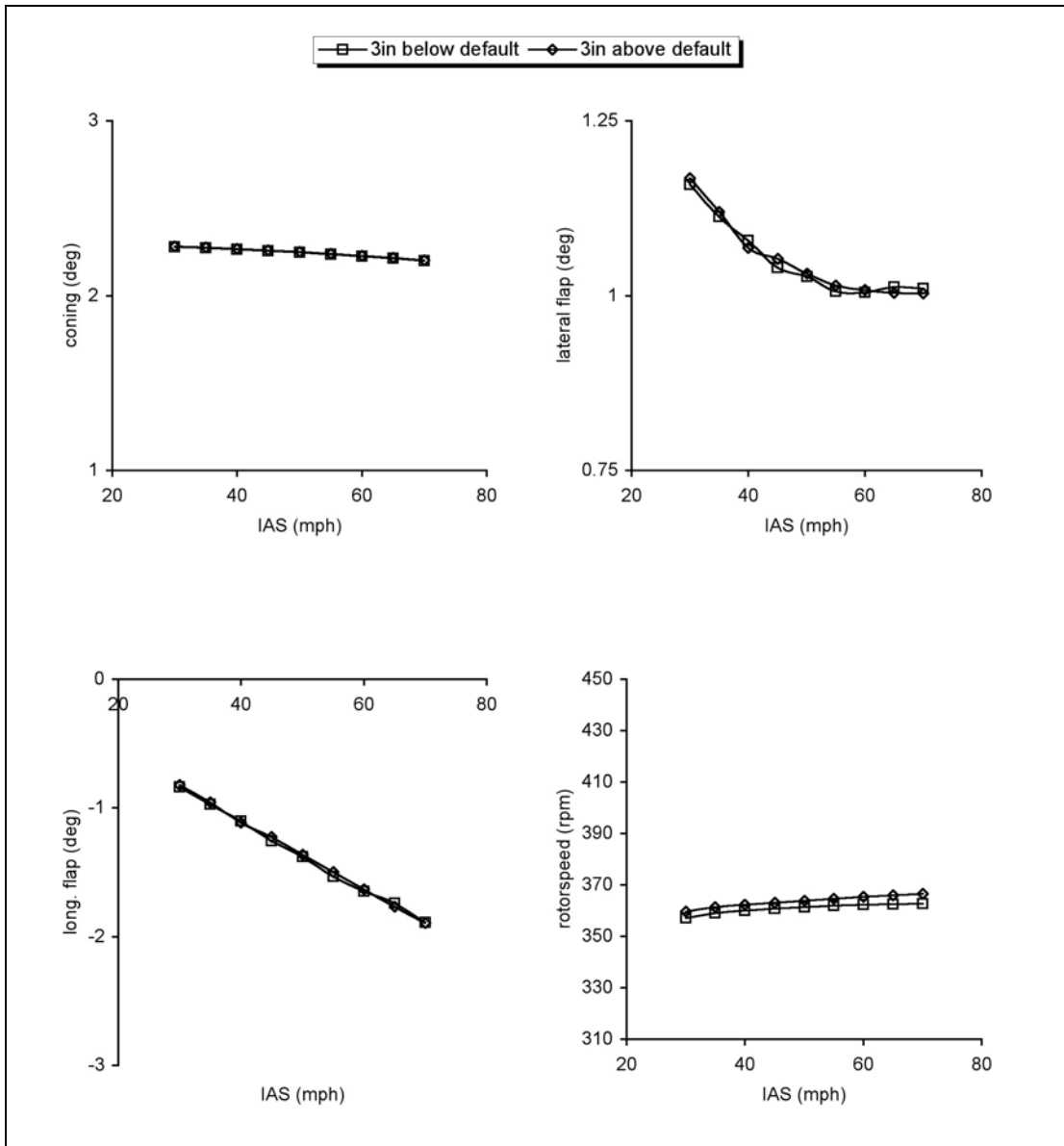
Figure 7.13b Trim Comparison for Propeller Thrust Line Variation
(Rotor Parameters)
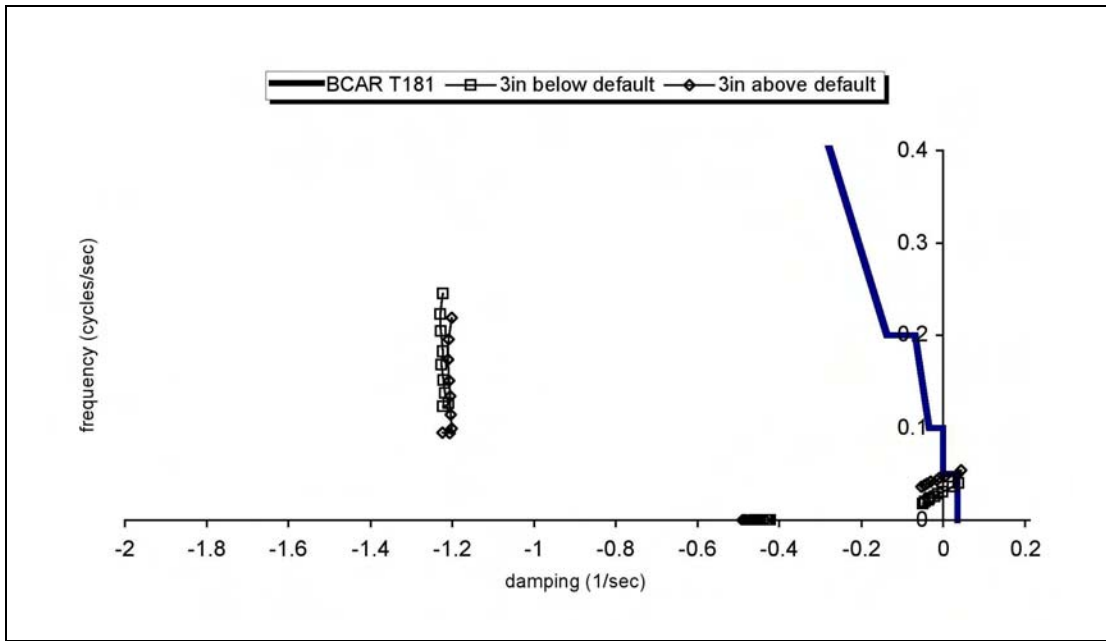
Figure 7.14a Comparison of Stability Modes (Propeller Thrust Line Variation)
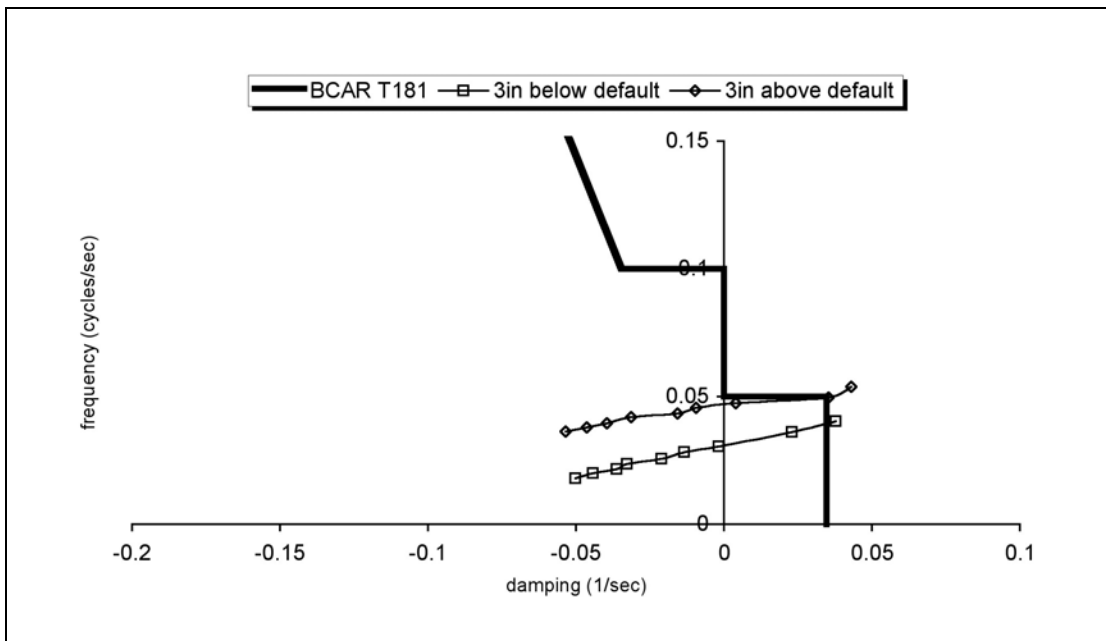
Figure 7.14b The Phugoid Mode (Propeller Thrust Line Variation)
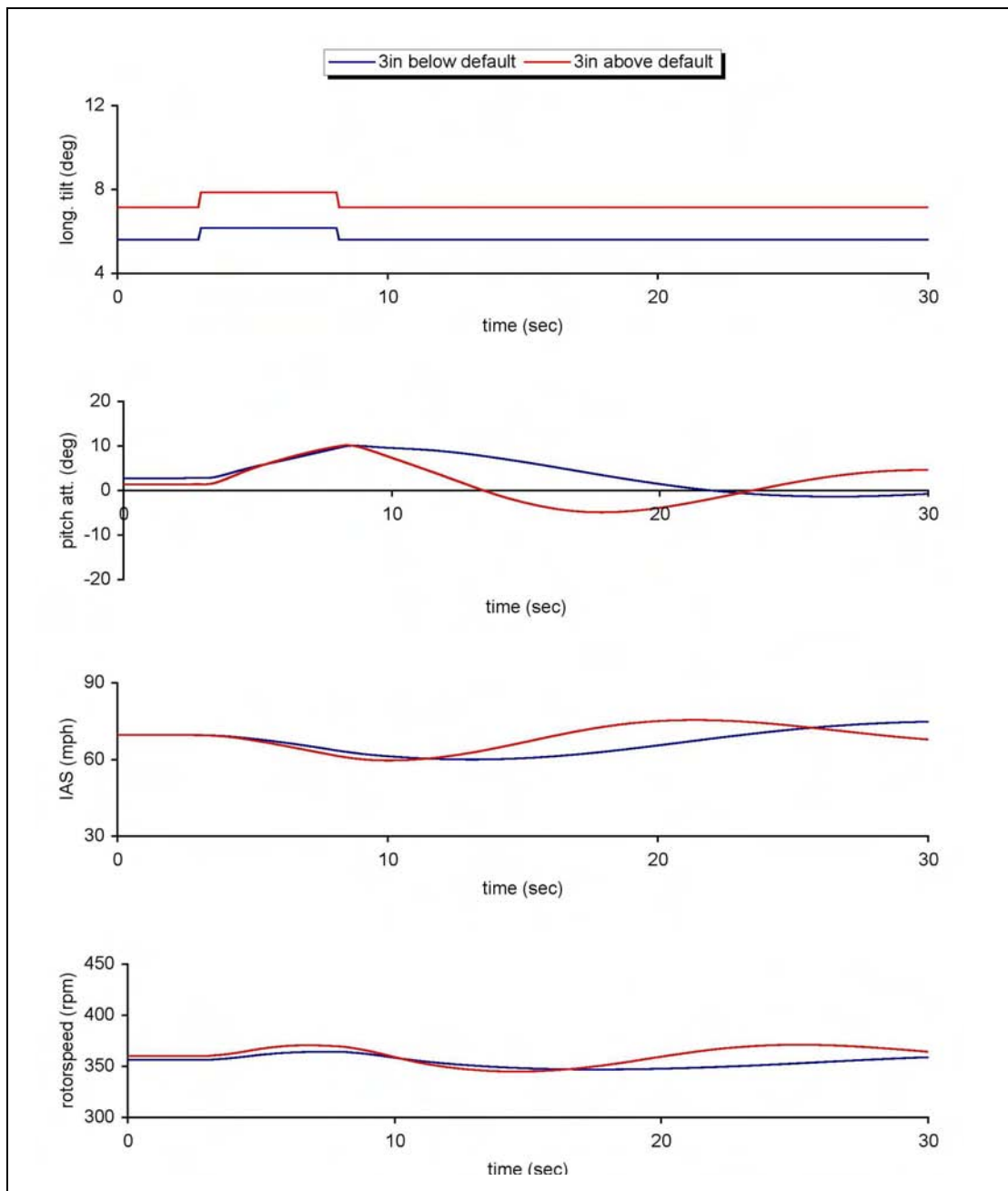
Figure 7.15   Aircraft Response to 5s Pulse of Longitudinal Rotor Tilt - Phugoid
(Propeller Thrust Line Variation)
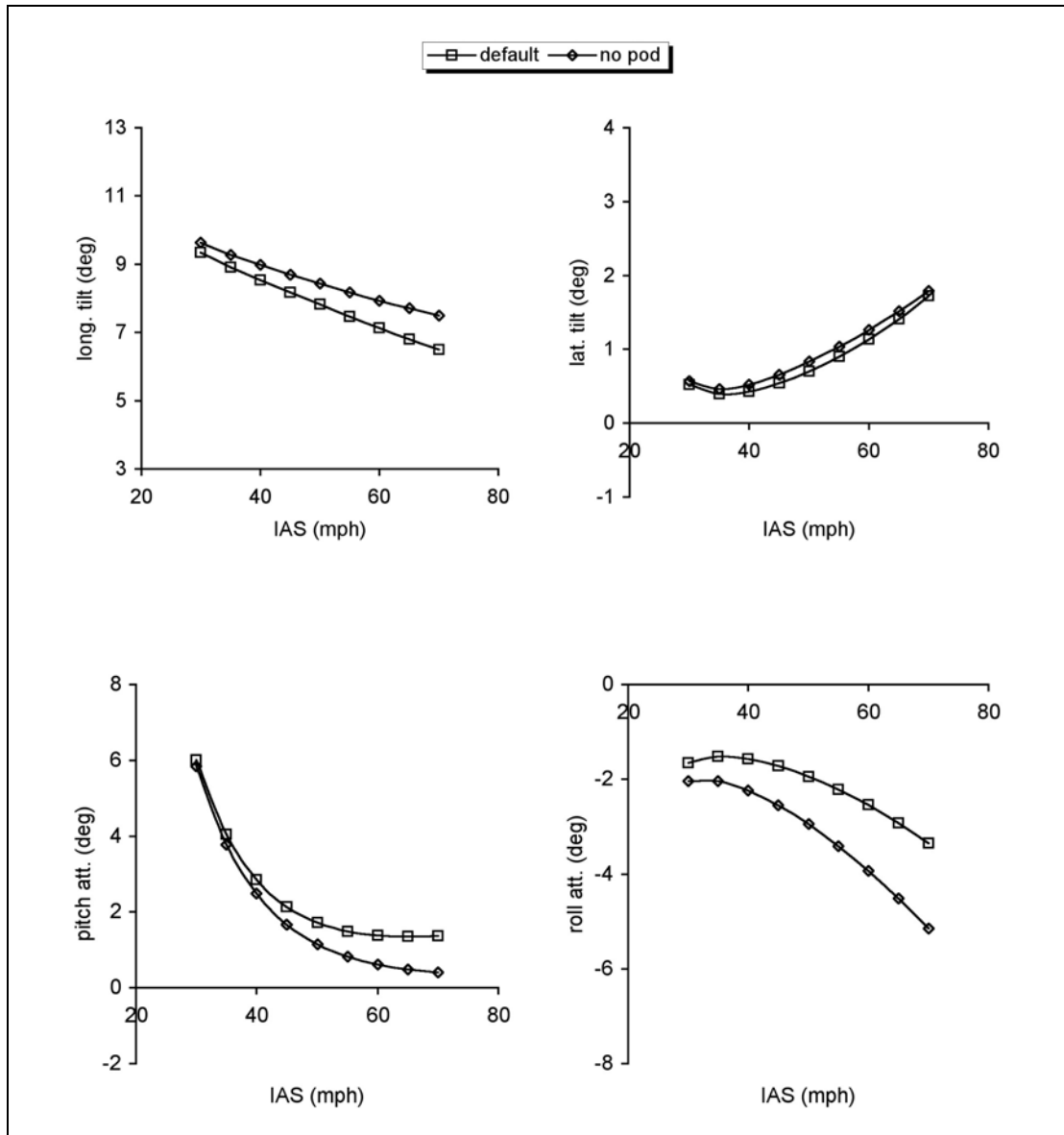
Figure 7.16a Trim Comparison for Pod On/Pod Off (Airframe Parameters)
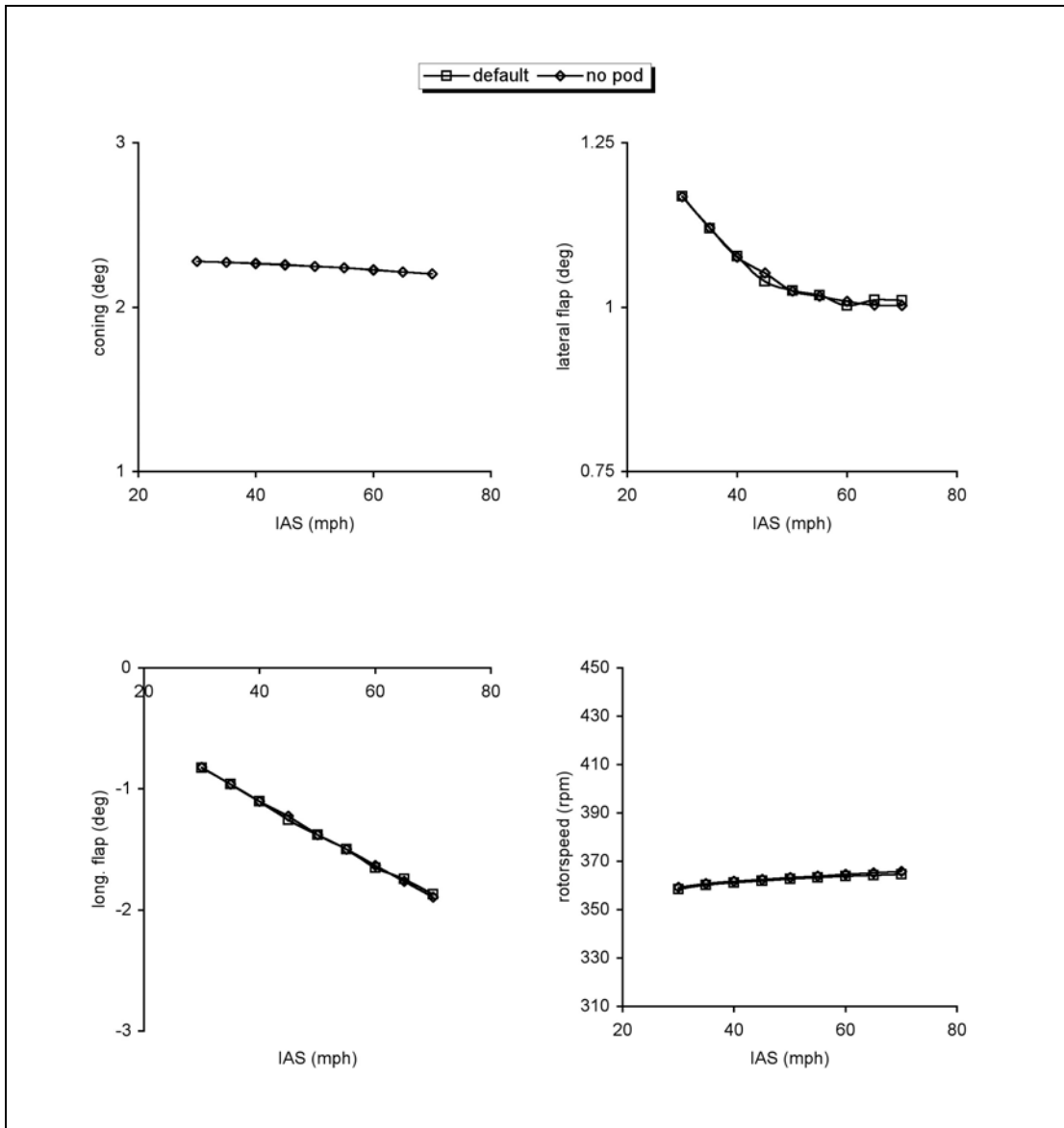
Figure 7.16b Trim Comparison for Pod On/Pod Off (Rotor Parameters)
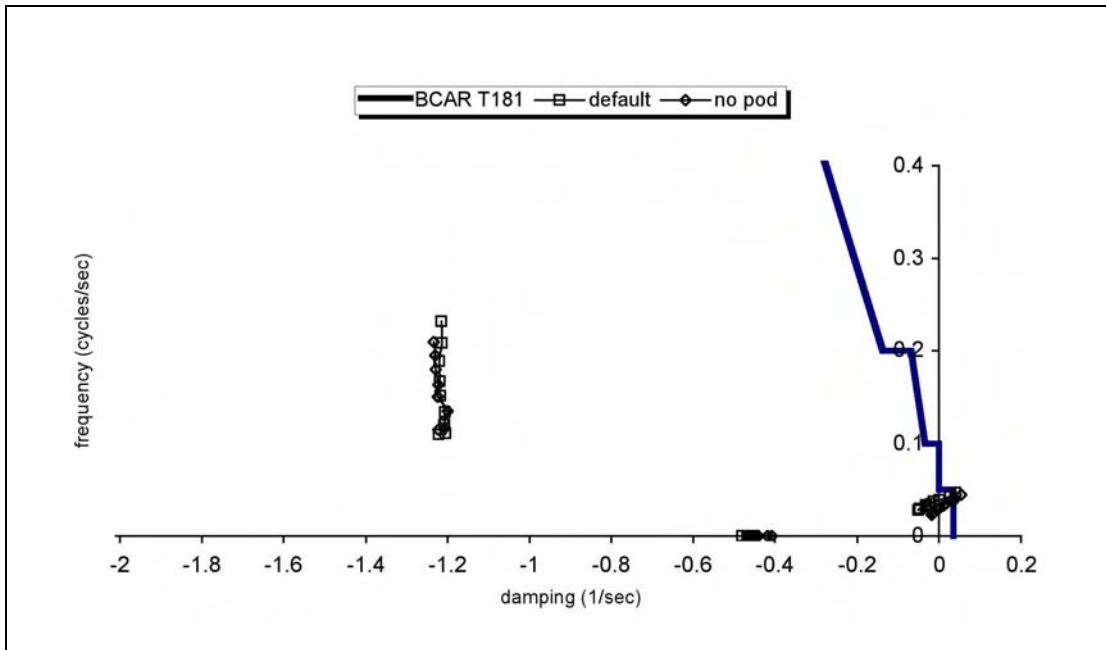
Figure 7.17a   Comparison of Stability Modes (Pod On/Pod Off)
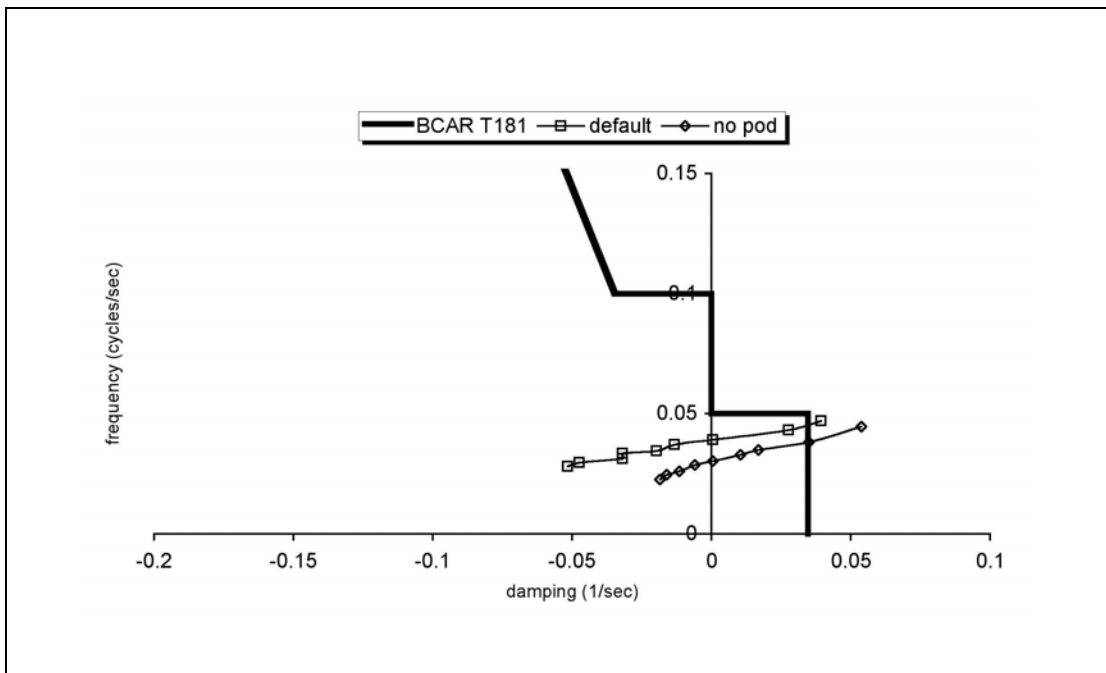
Figure 7.17b The Phugoid Mode (Pod On/Pod Off)
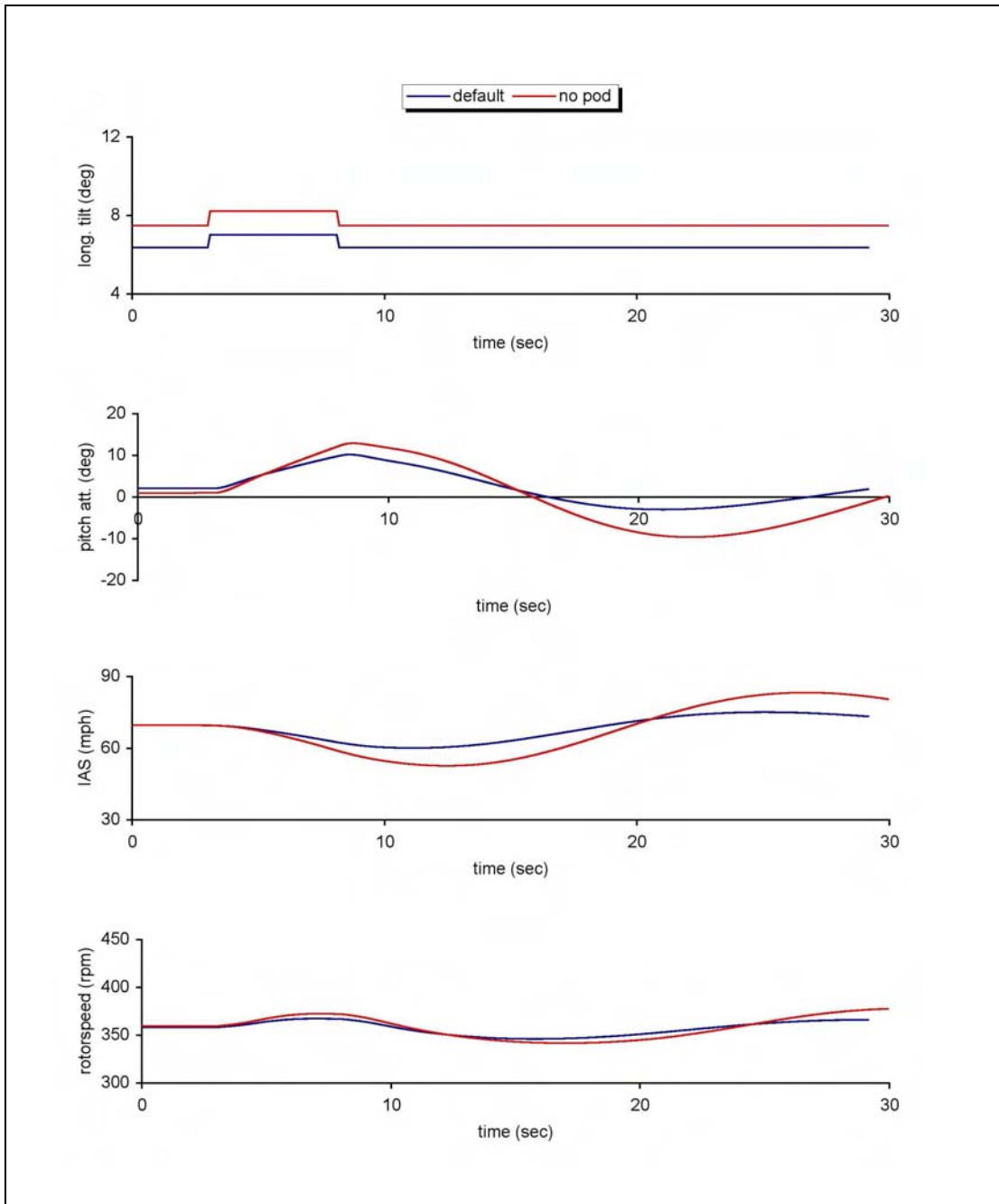
Figure 7.18   Aircraft Response to 5s Pulse of Longitudinal Rotor Tilt - Phugoid
(Pod On/Pod Off)
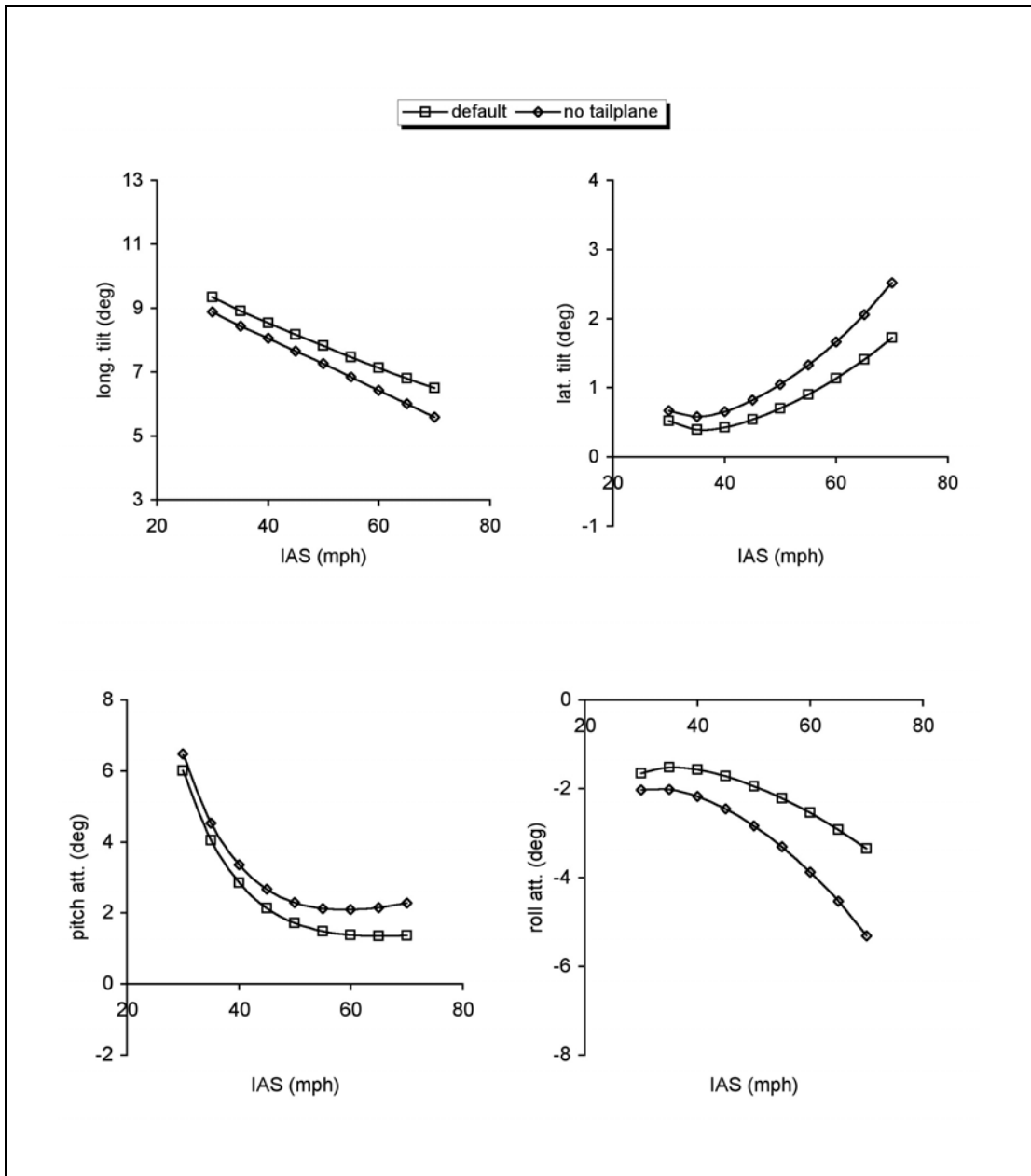
Figure 7.19a Trim Comparison for Tailplane On/Tailplane Off
(Airframe Parameters)
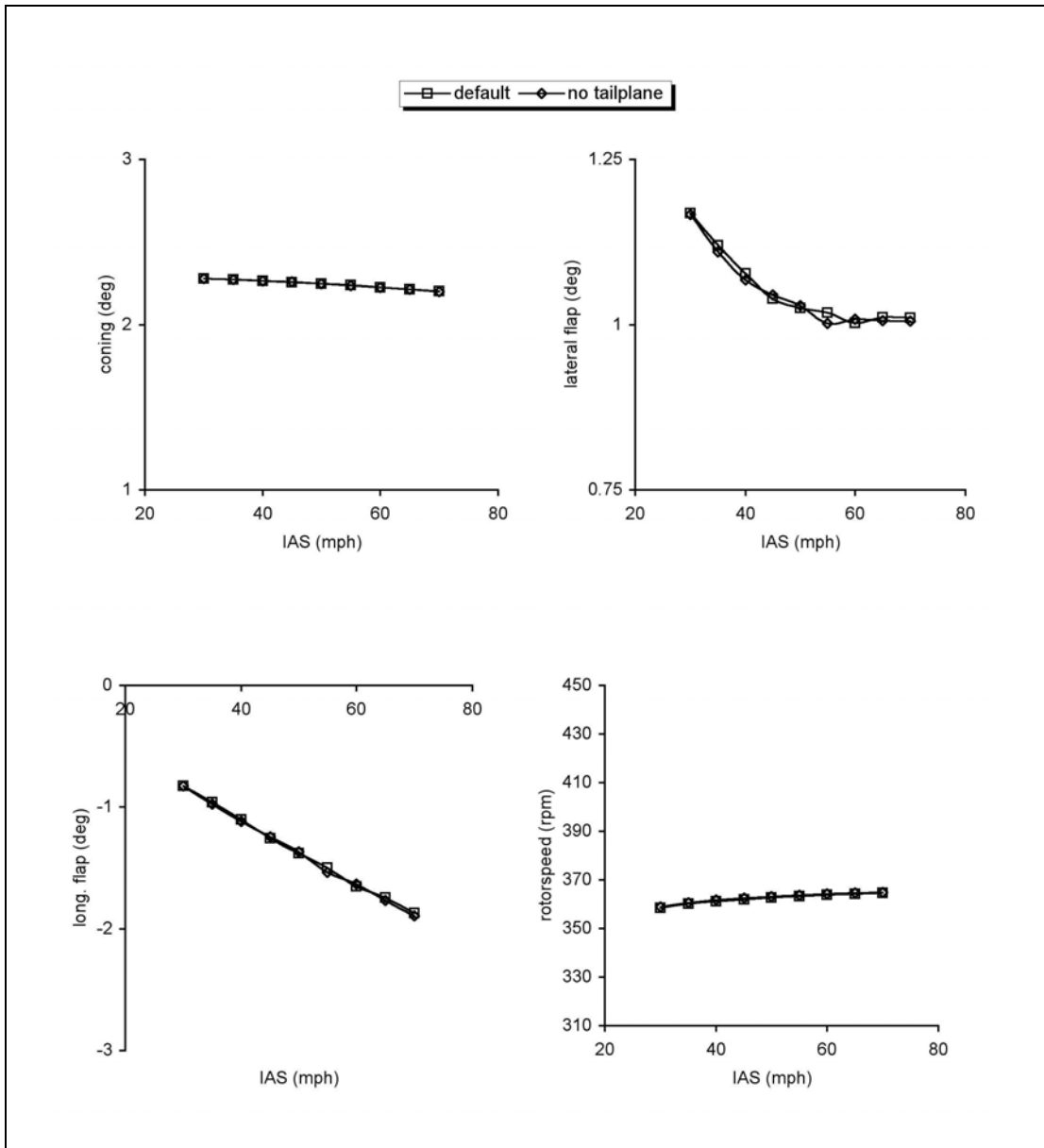
Figure 7.19b Trim Comparison for Tailplane On/Tailplane Off (Rotor Parameters)
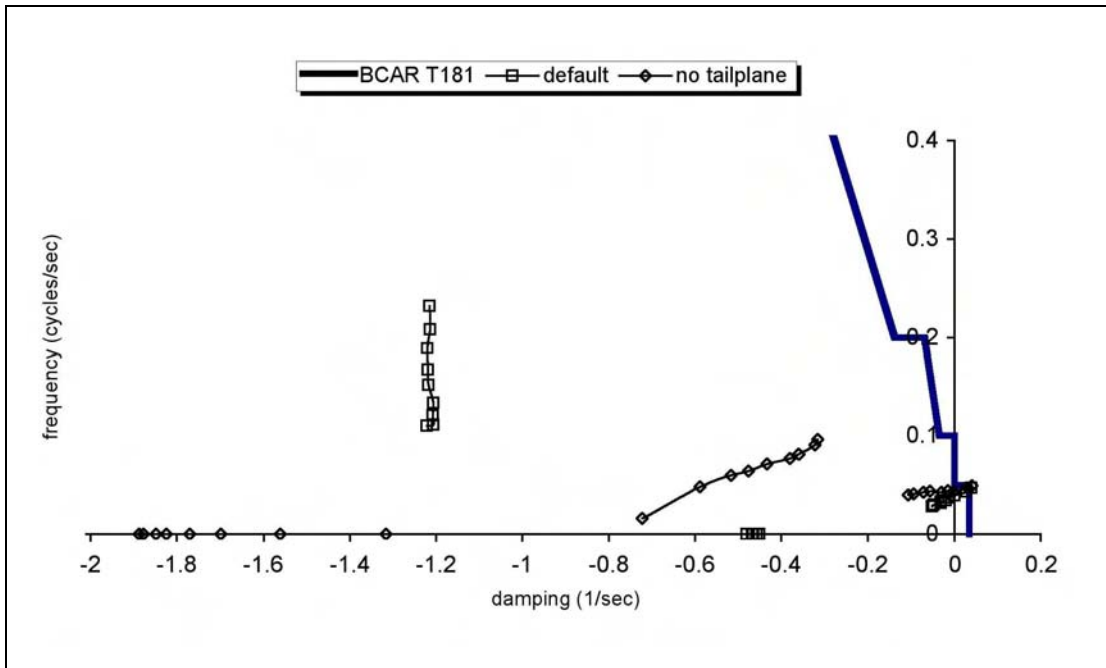
Figure 7.20a Comparison of Stability Modes (Tailplane On/Tailplane Off)
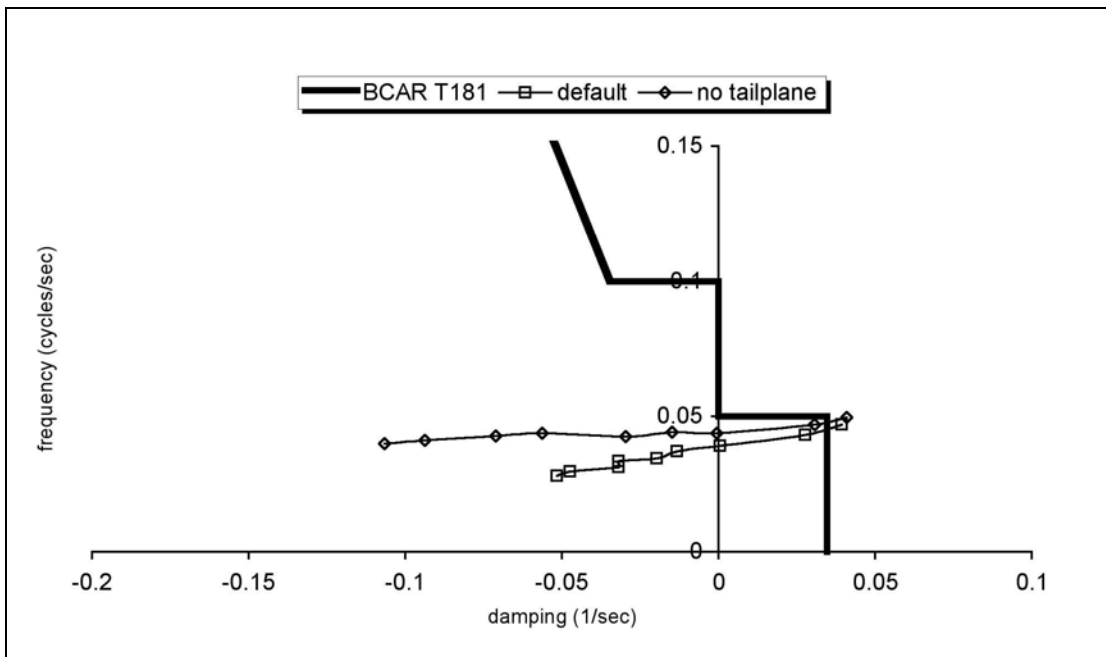
Figure 7.20b The Phugoid Mode (Tailplane On/Tailplane Off)
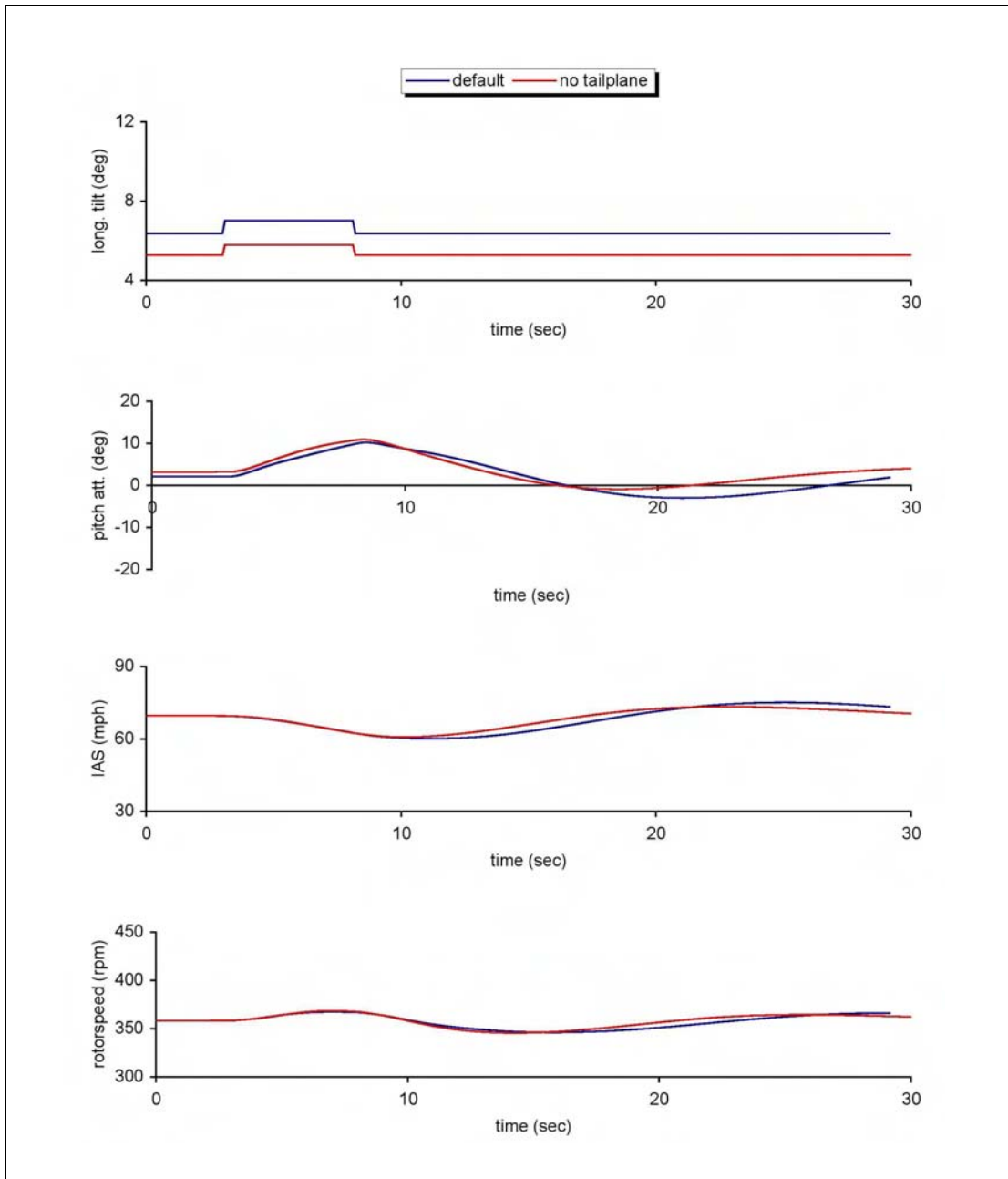
Figure 7.21   Aircraft Response to 5s Pulse of Longitudinal Rotor Tilt – Phugoid
(Tailplane On/Tailplane Off)
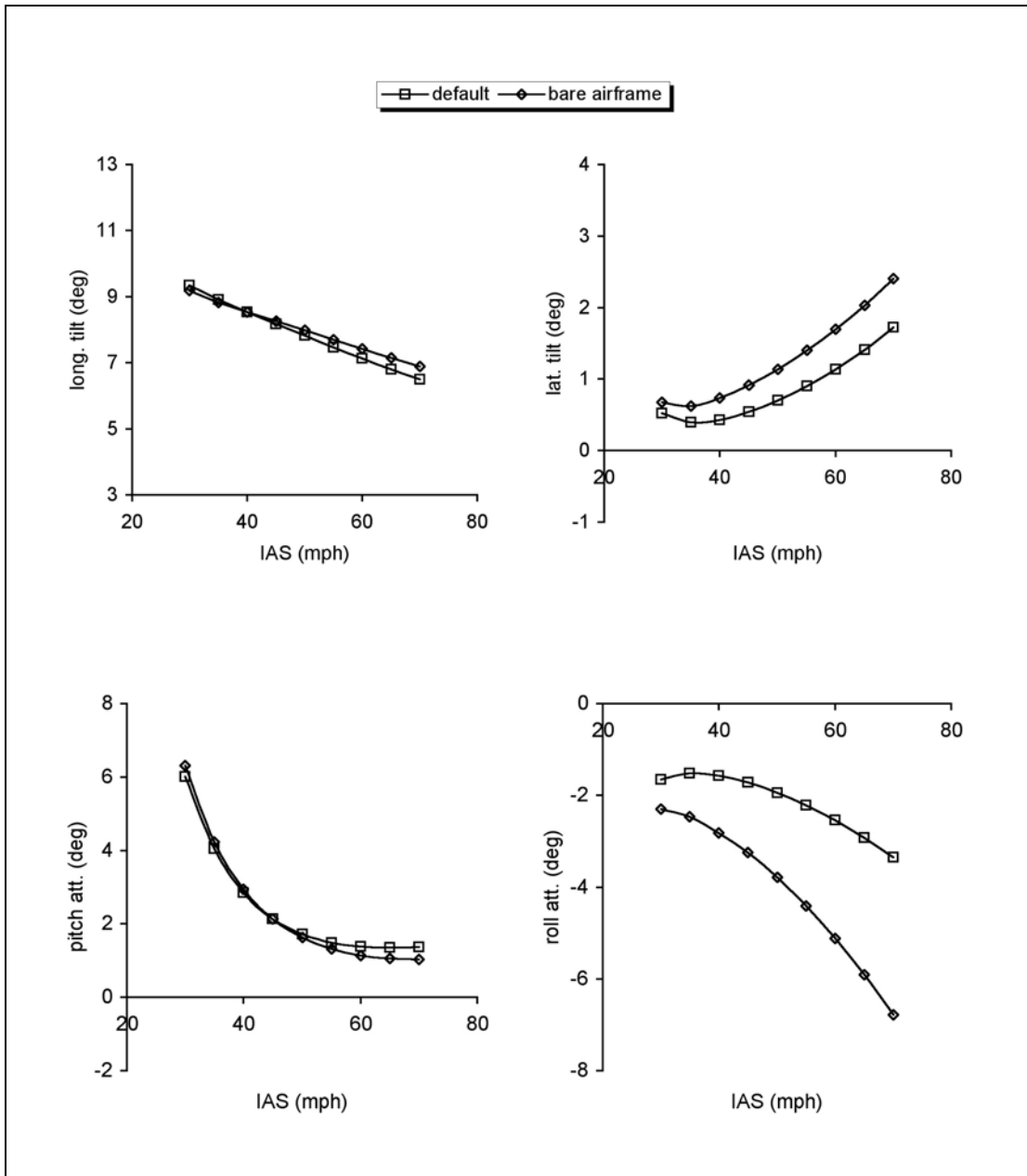
Figure 7.22a Trim Comparison for Pod and Tailplane On/Pod and Tailplane Off
(Airframe Parameters)
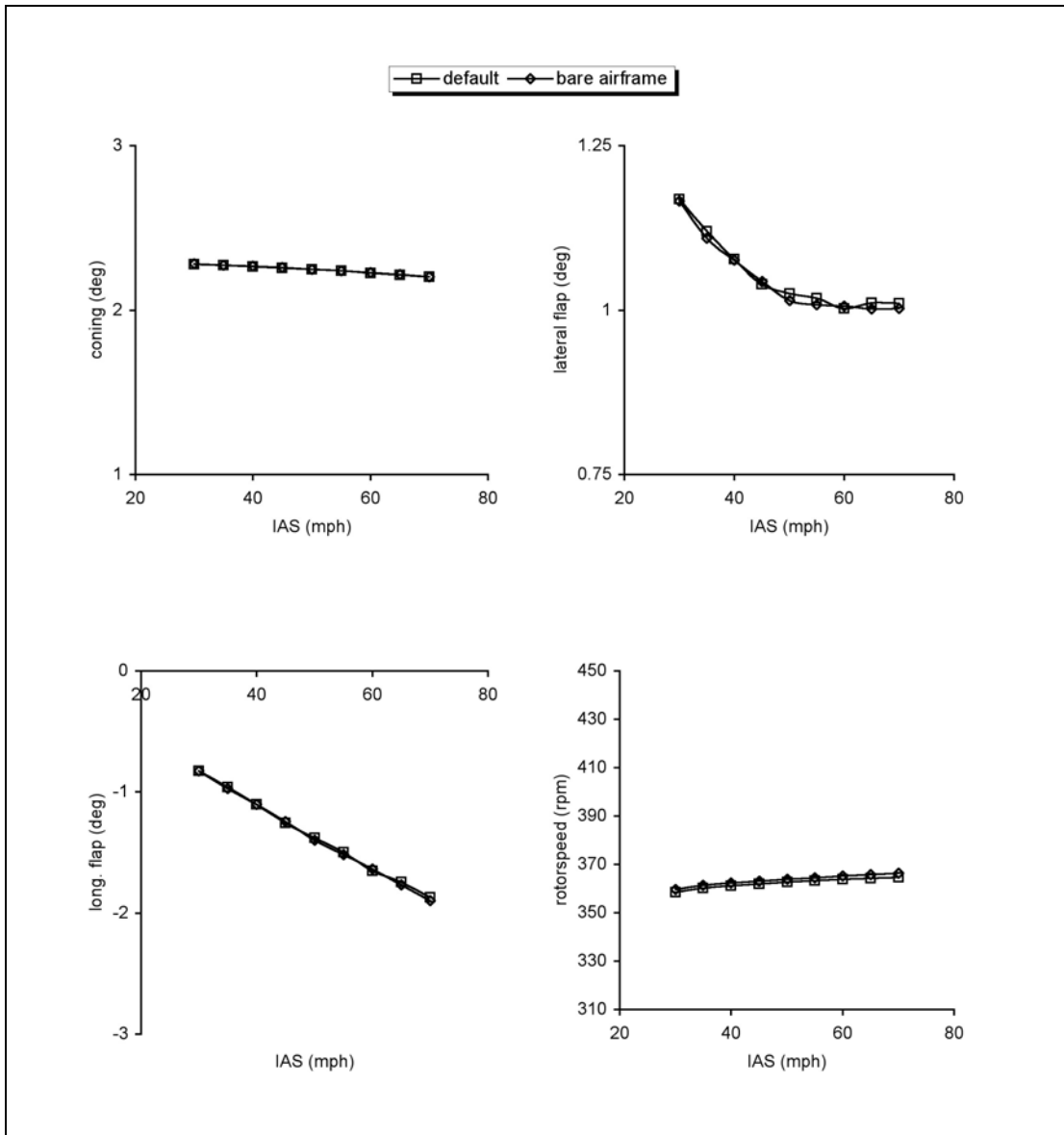
Figure 7.22b Trim Comparison for Pod and Tailplane On/Pod and Tailplane Off
(Rotor Parameters)
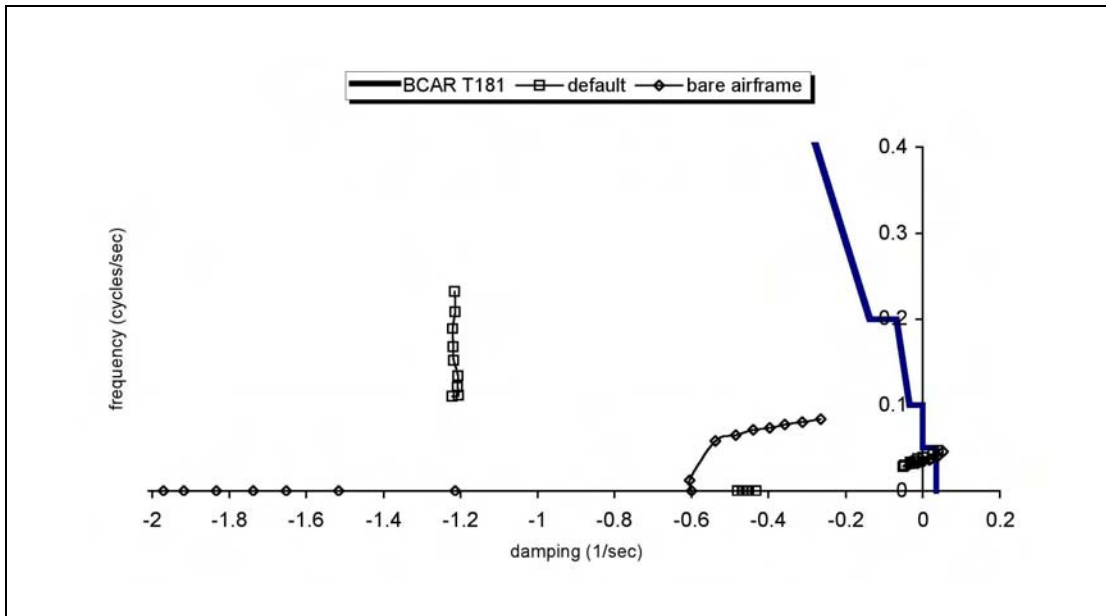
Figure 7.23a   Comparison of Stability Modes
                  (Pod and Tailplane On/Pod and Tailplane Off)
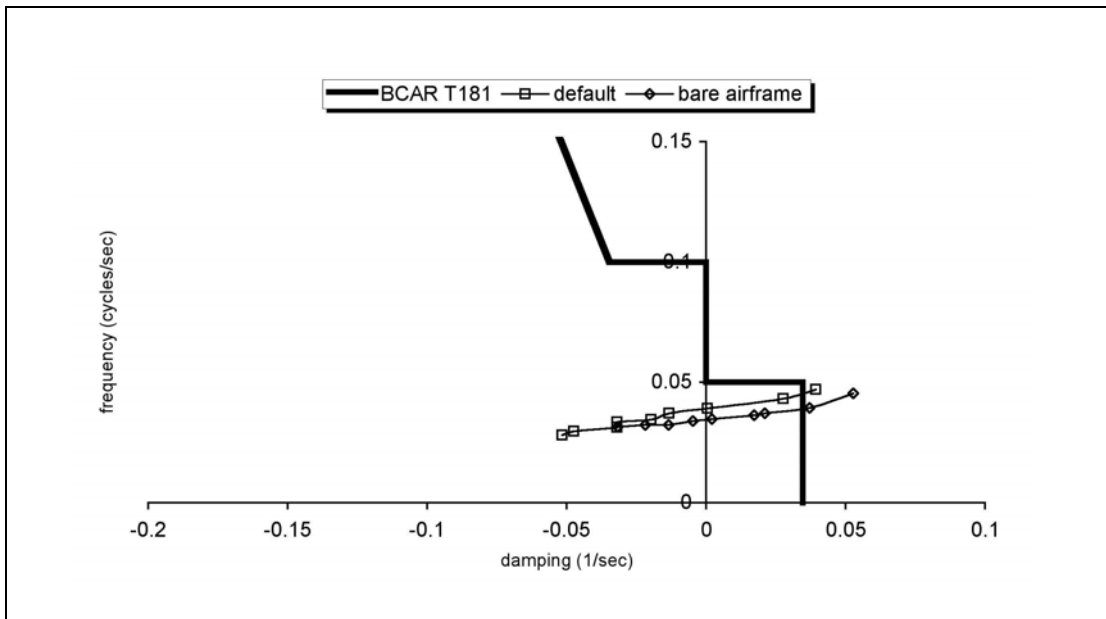
Figure 7.23b The Phugoid Mode (Pod and Tailplane On/Pod and Tailplane Off)
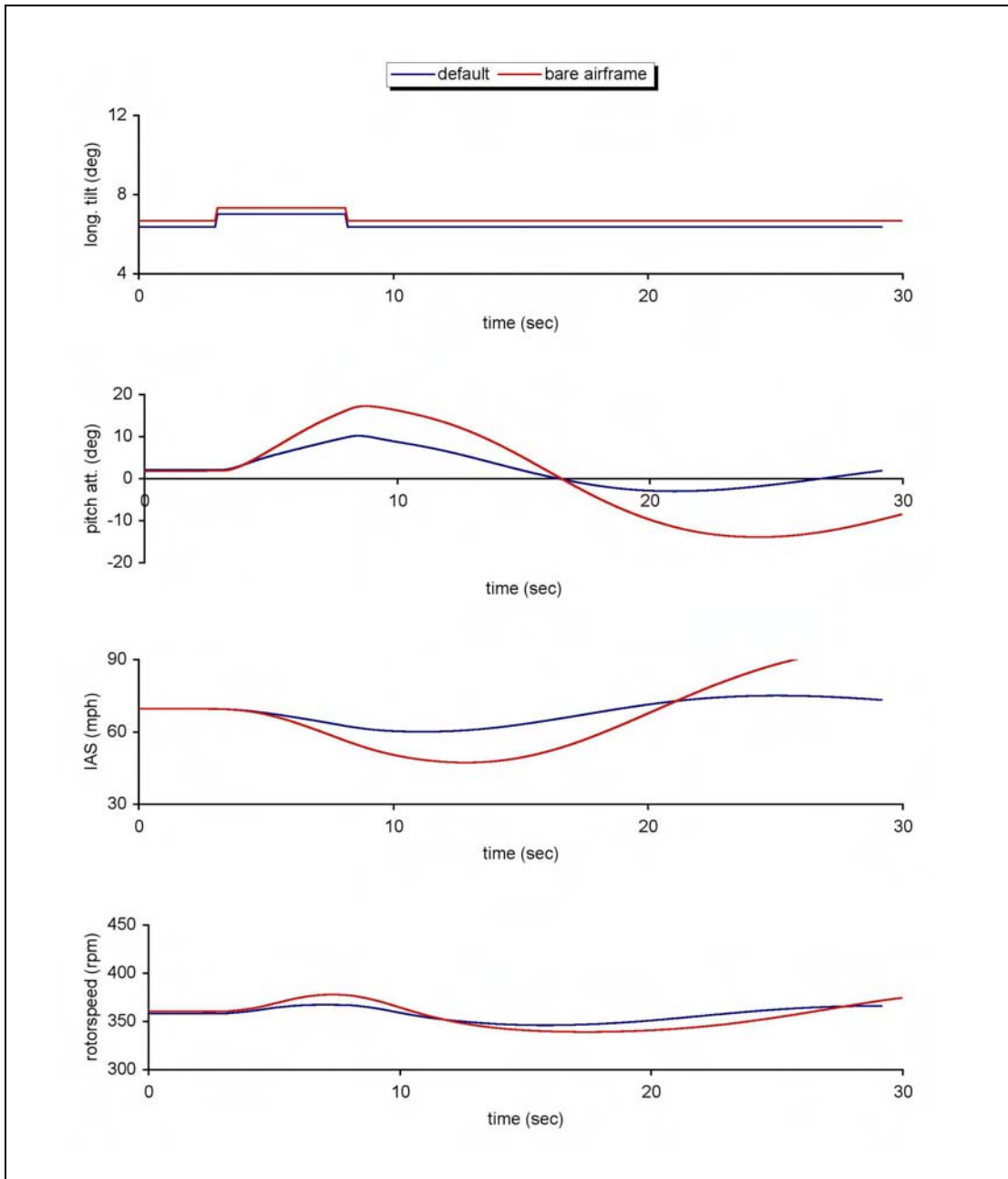
Figure 7.24   Aircraft Response to 5s Pulse of Longitudinal Rotor Tilt - Phugoid
(Pod and Tailplane On/Pod and Tailplane Off)
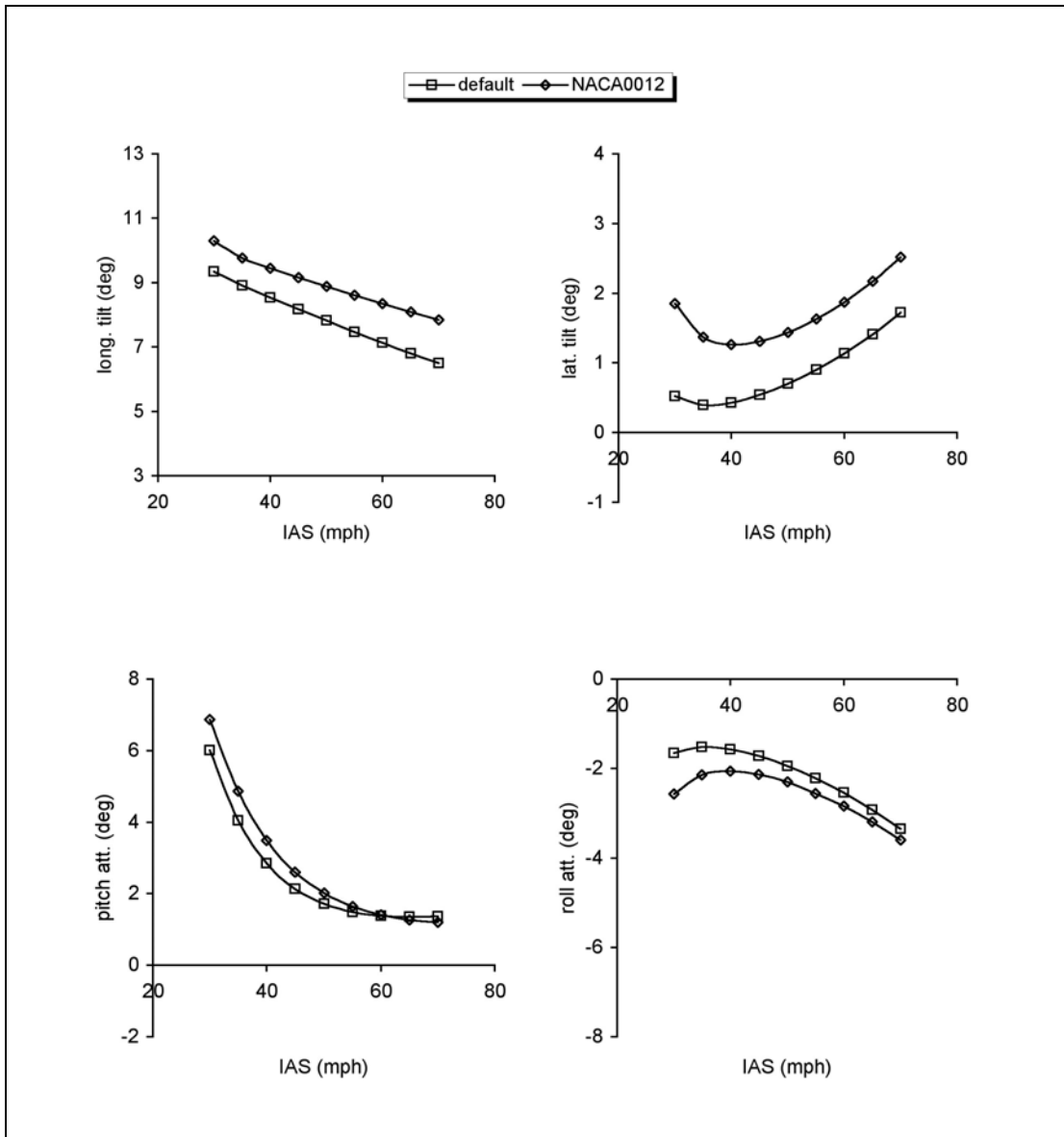
Figure 7.25a Trim Comparison for Different Blade Sections
               (Airframe Parameters)
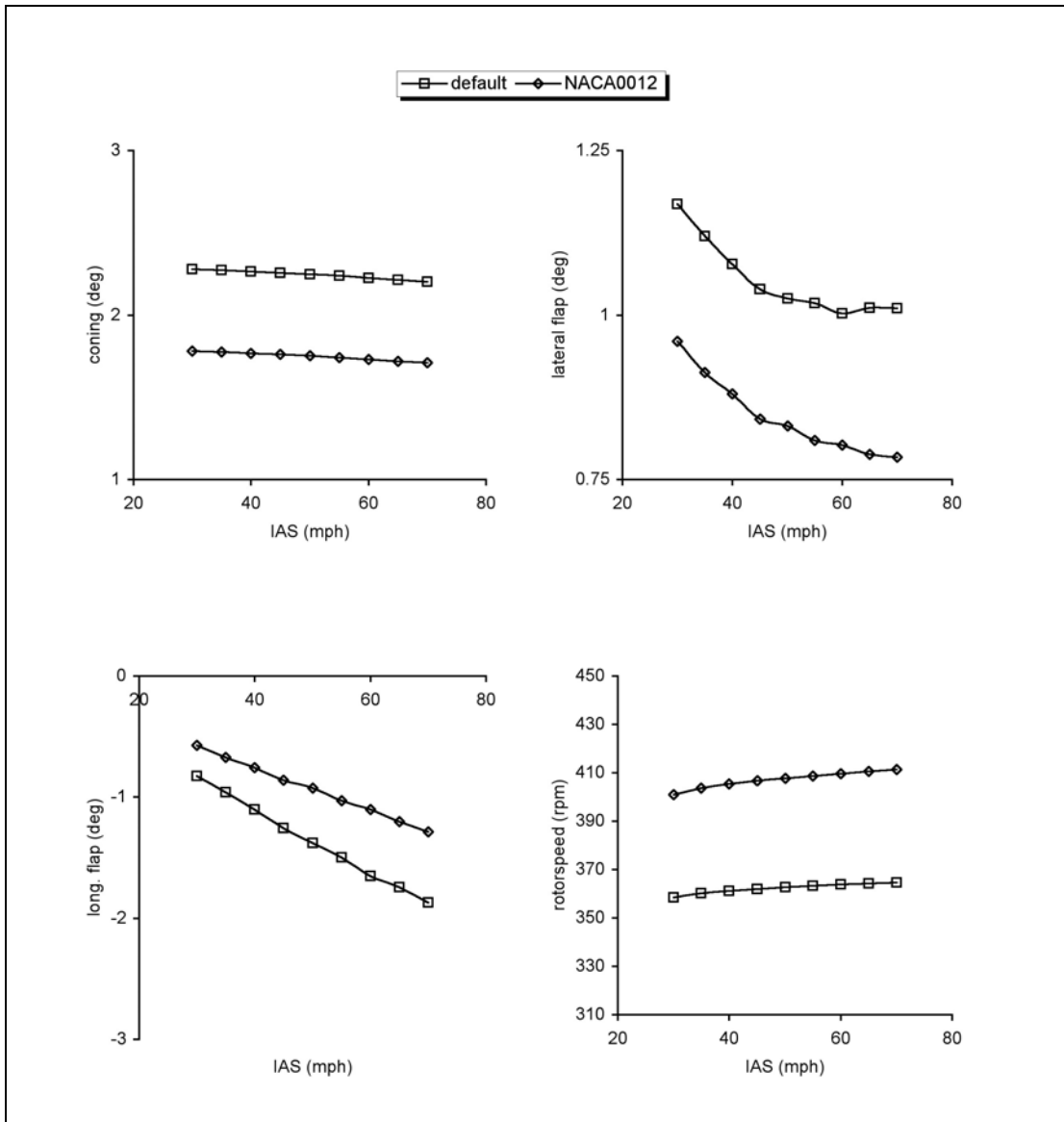
Figure 7.25b Trim Comparison for Different Blade Sections (Rotor Parameters)
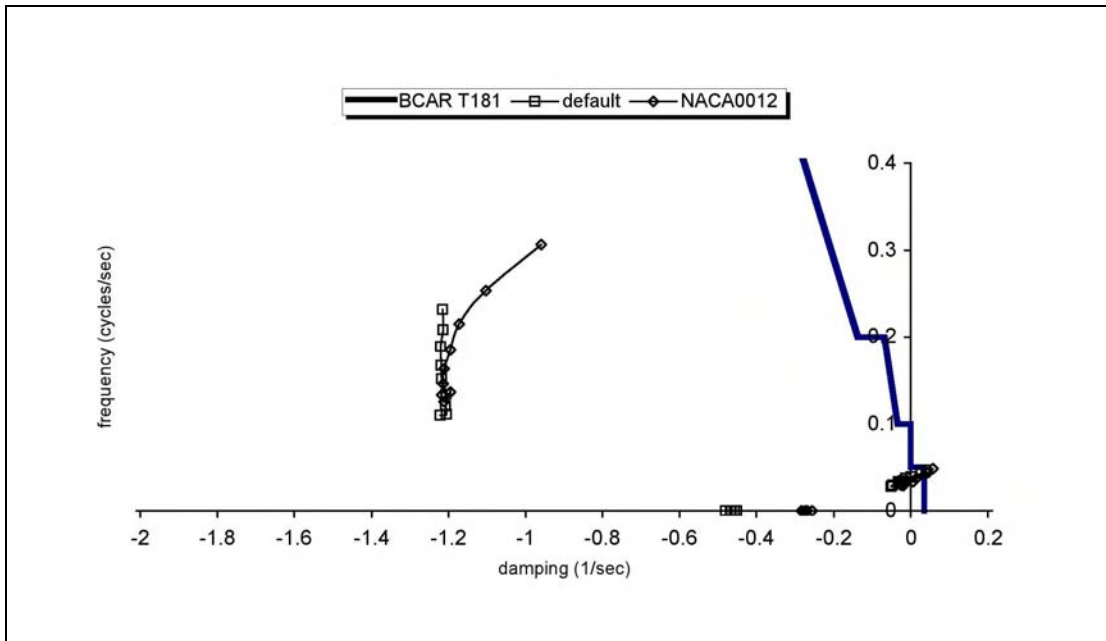
Figure 7.26a Comparison of Stability Modes (Different Blade Sections)
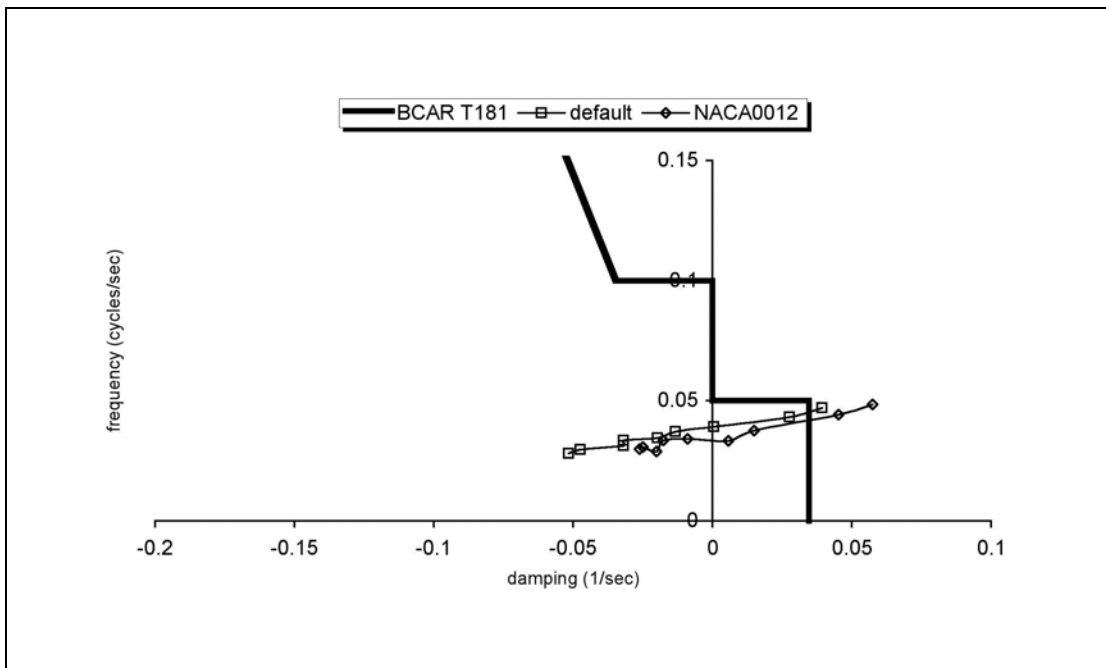
Figure 7.26b The Phugoid Mode (Different Blade Sections)
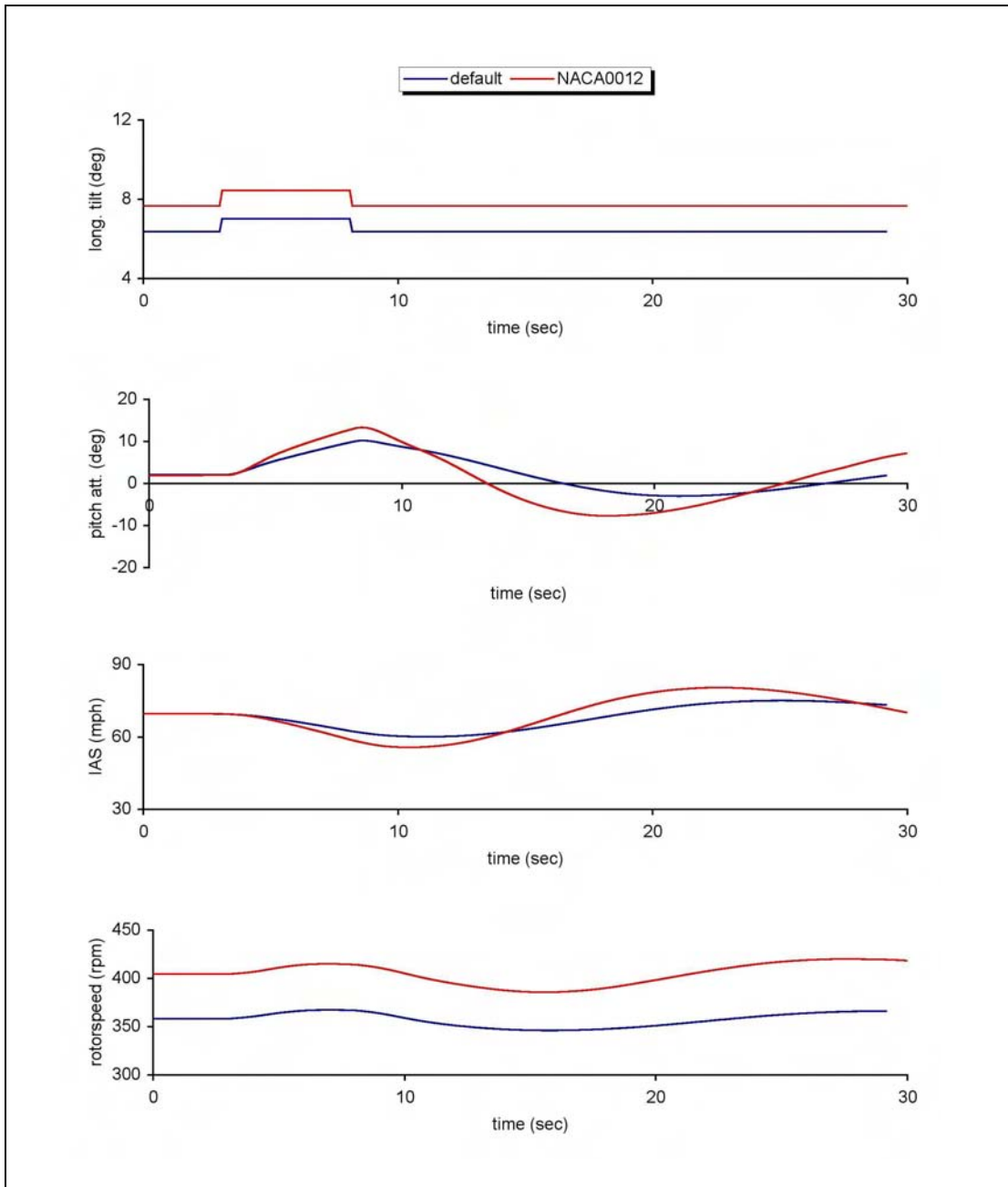
Figure 7.27   Aircraft Response to 5s Pulse of Longitudinal Rotor Tilt - Phugoid
(Different Blade Sections)
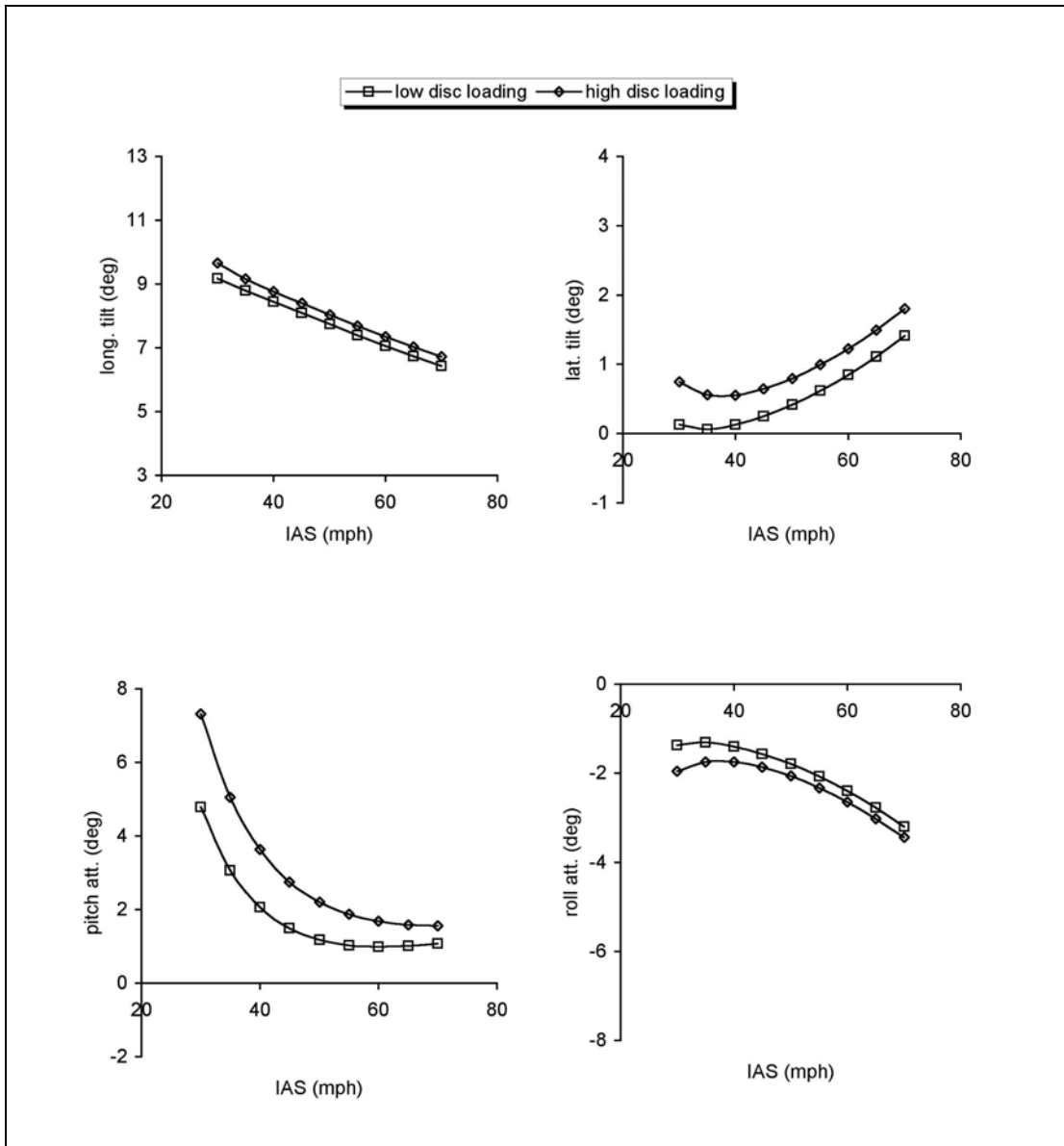
Figure 7.28a Trim Comparison for Disc Loading Variation (Airframe Parameters)
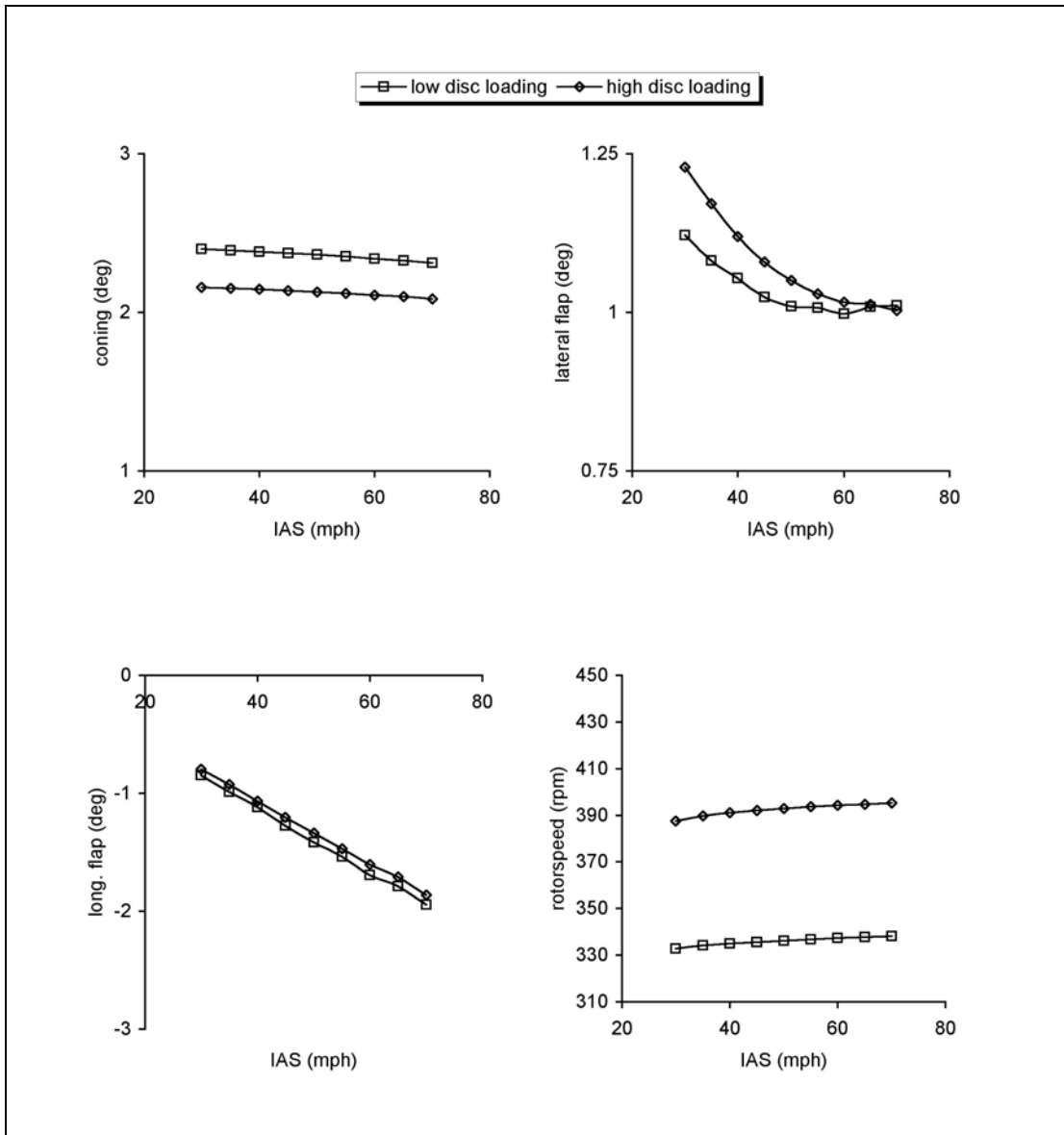
Figure 7.28b Trim Comparison for Disc Loading Variation (Rotor Parameters)
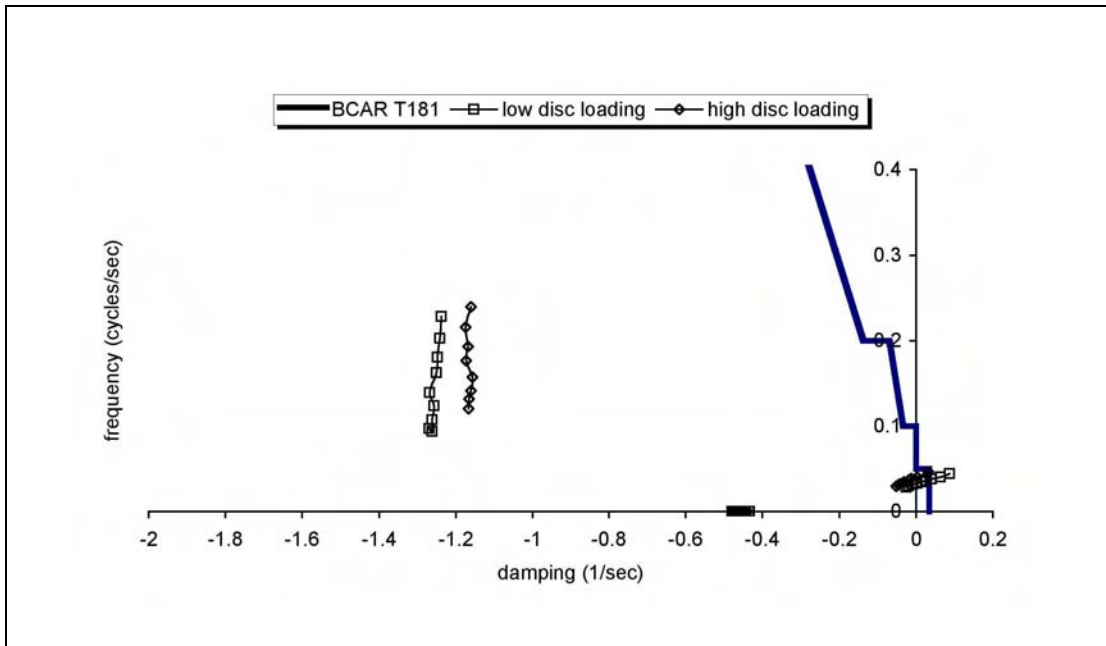
Figure 7.29a Comparison of Stability Modes (Disc Loading Variation)
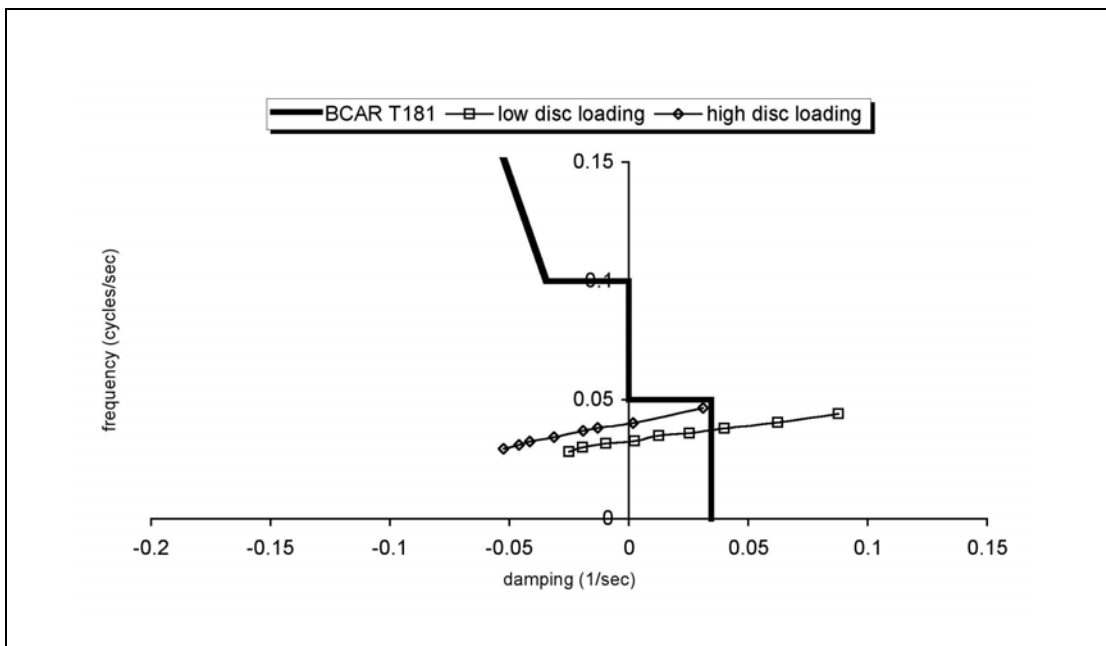
Figure 7.29b The Phugoid Mode (Disc Loading Variation)
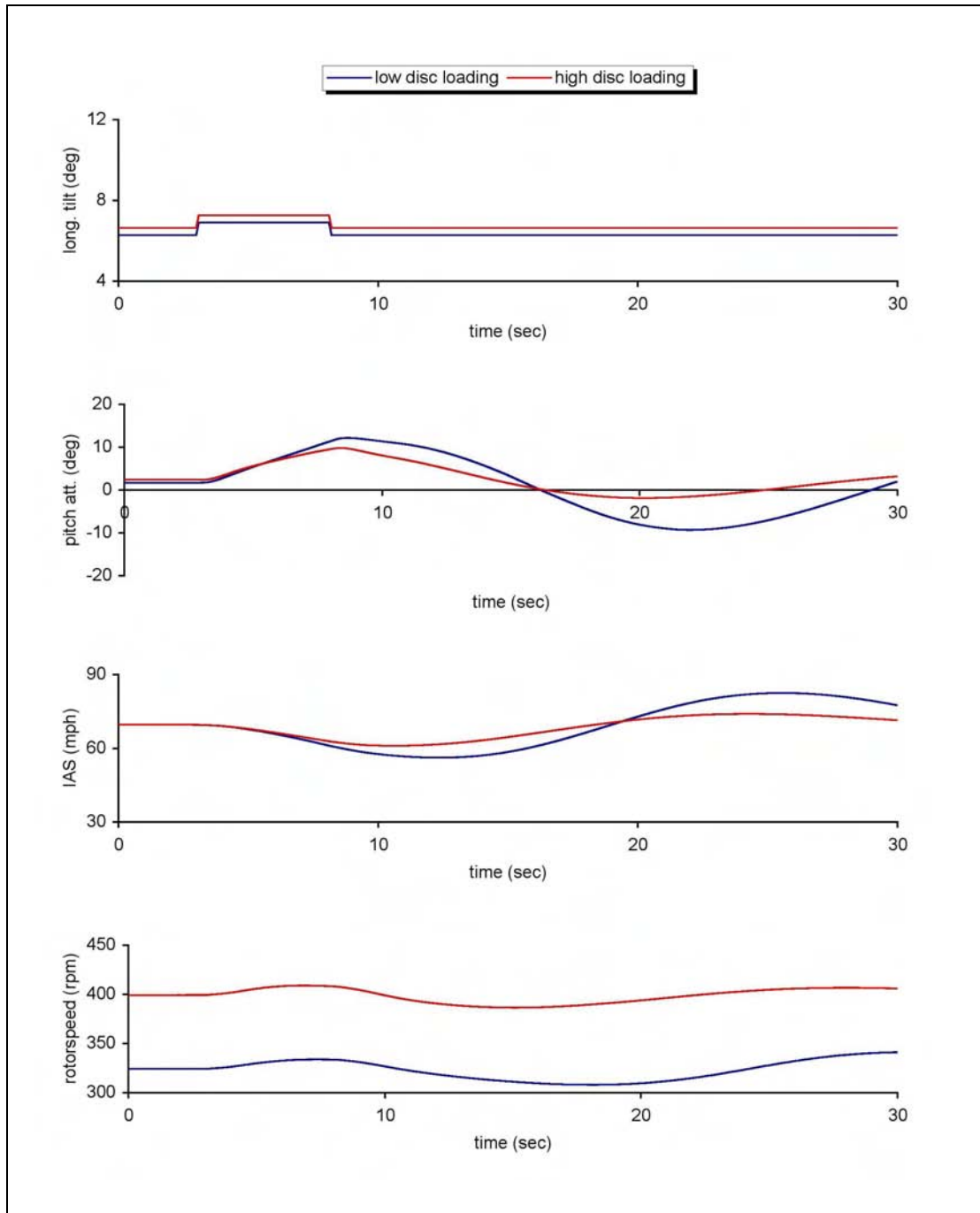
Figure 7.30   Aircraft Response to 5s Pulse of Longitudinal Rotor Tilt - Phugoid
(Disc Loading Variation)
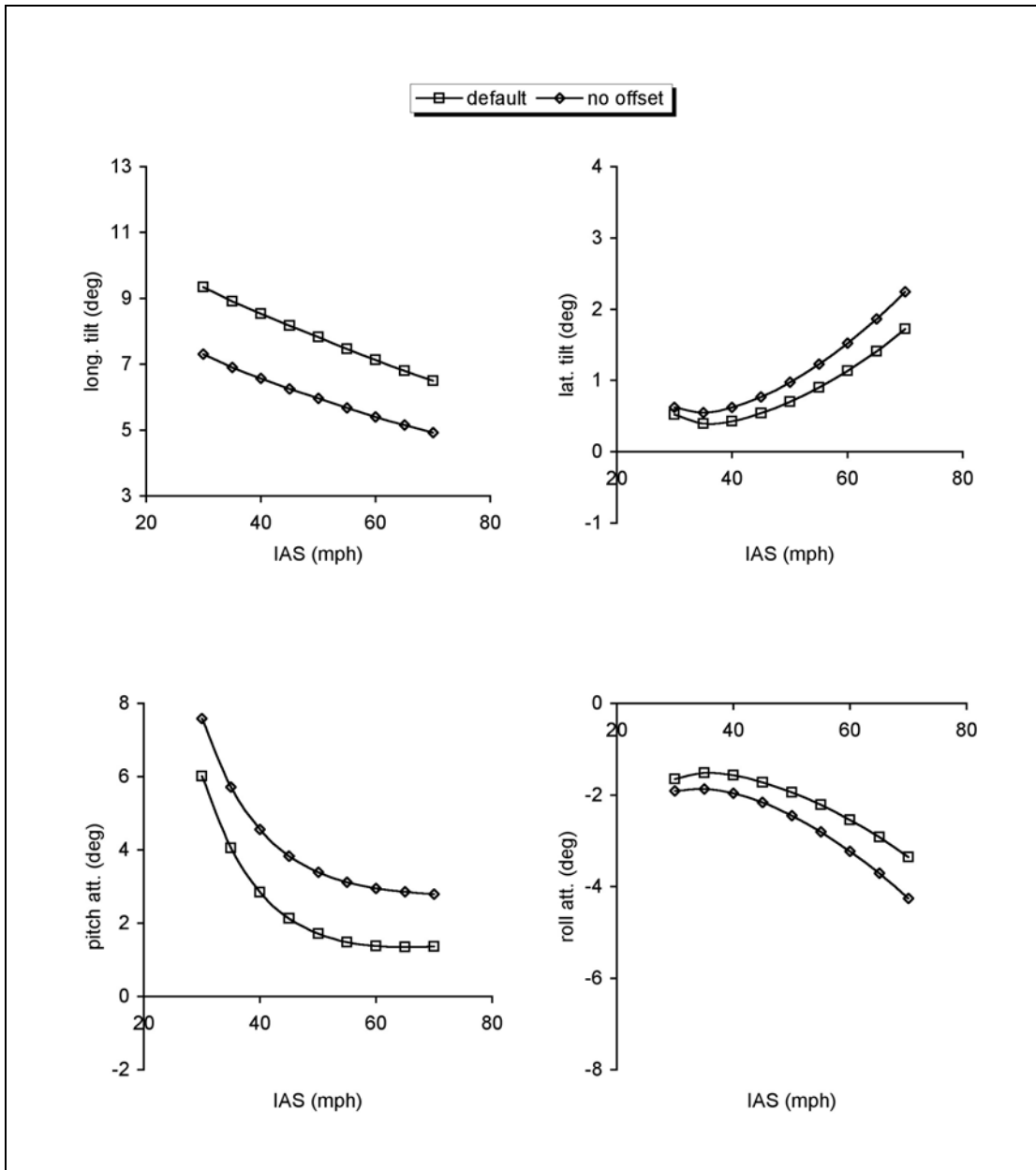
Figure 7.31a   Trim Comparison for Spindle Offset Variation (Airframe Parameters)
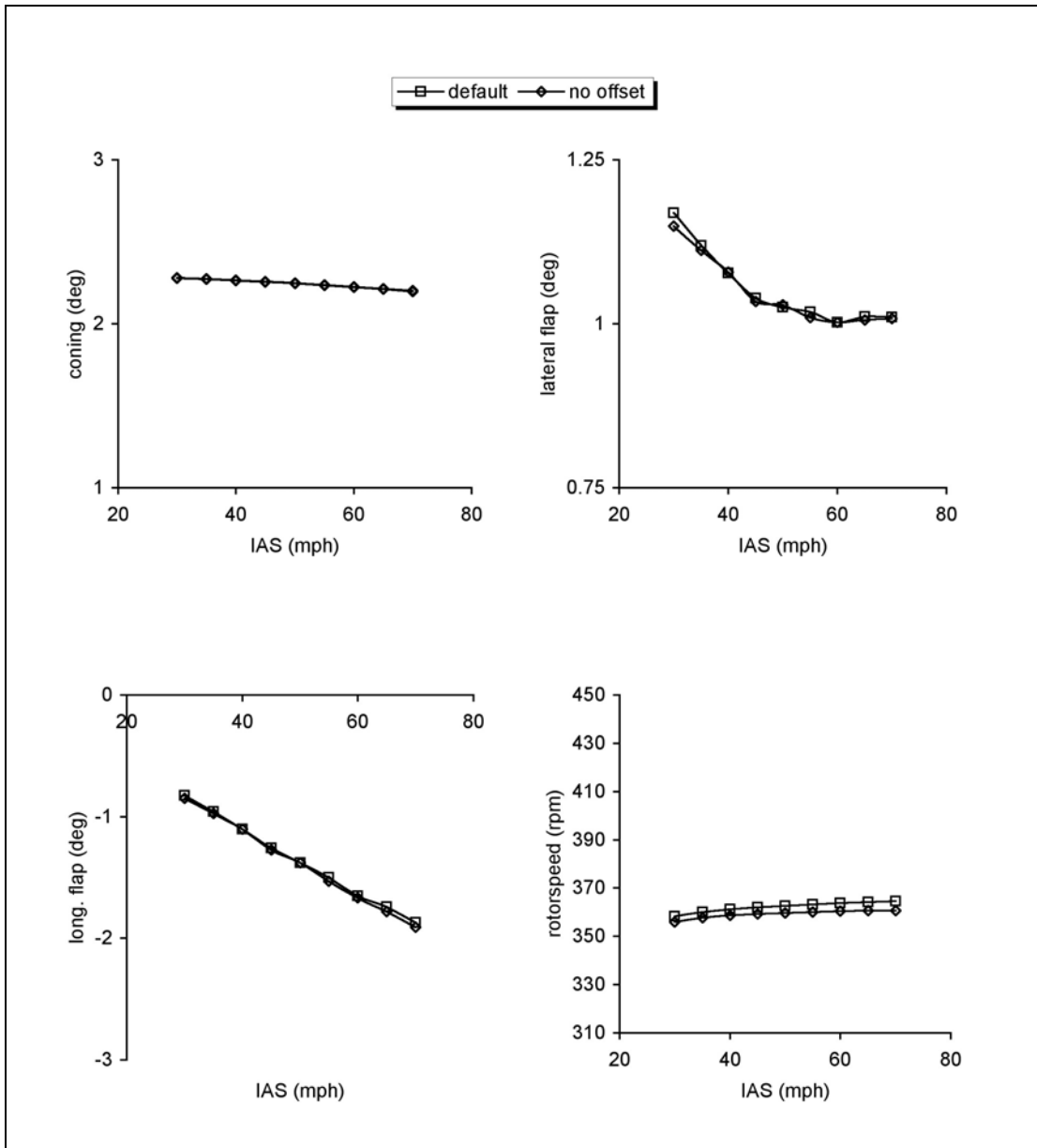
Figure 7.31b Trim Comparison for Spindle Offset Variation (Rotor Parameters)
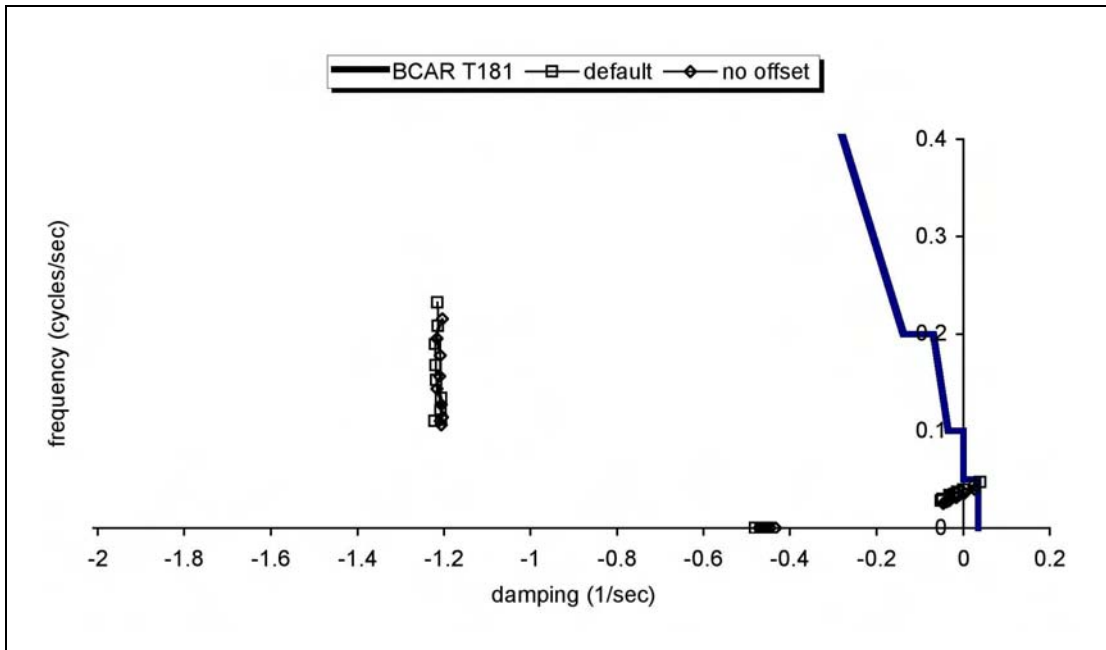
Figure 7.32a Comparison of Stability Modes (Spindle Offset Variation)
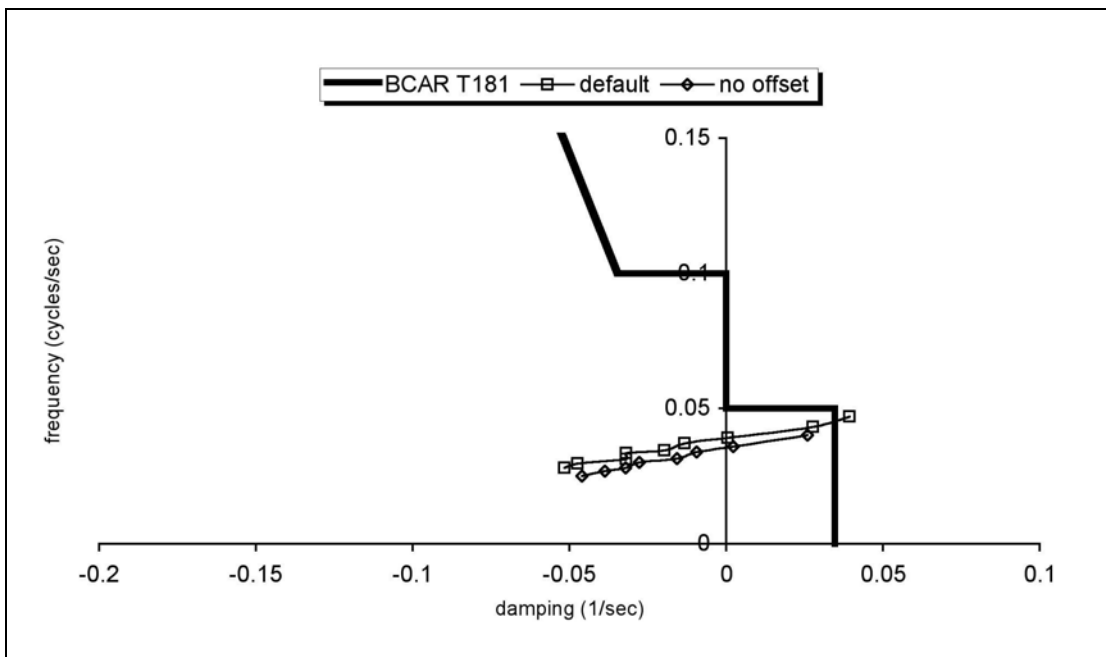
Figure 7.32b The Phugoid Mode (Spindle Offset Variation)
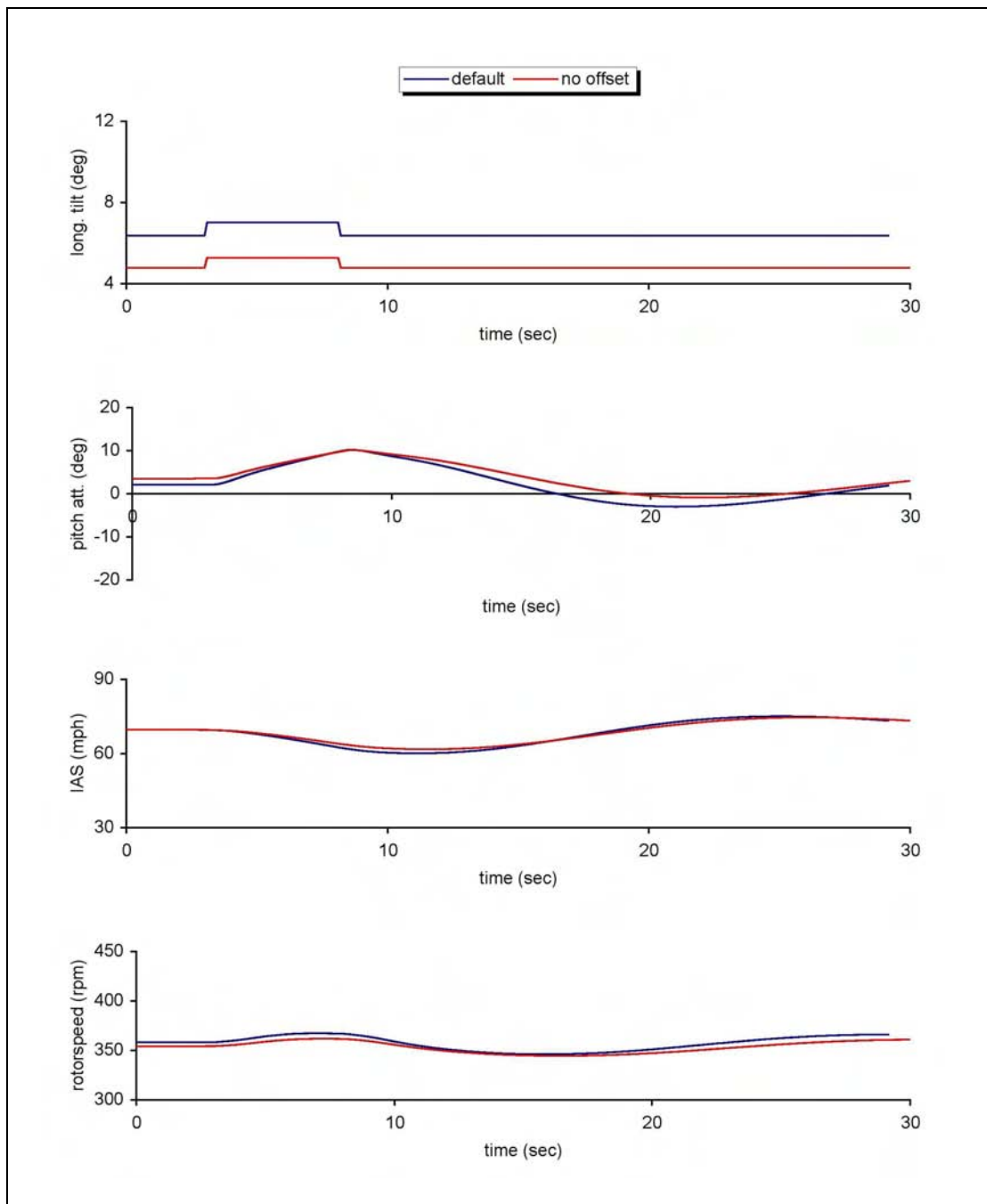
Figure 7.33   Aircraft Response to 5s Pulse of Longitudinal Rotor Tilt - Phugoid
                   (Spindle Offset Variation)
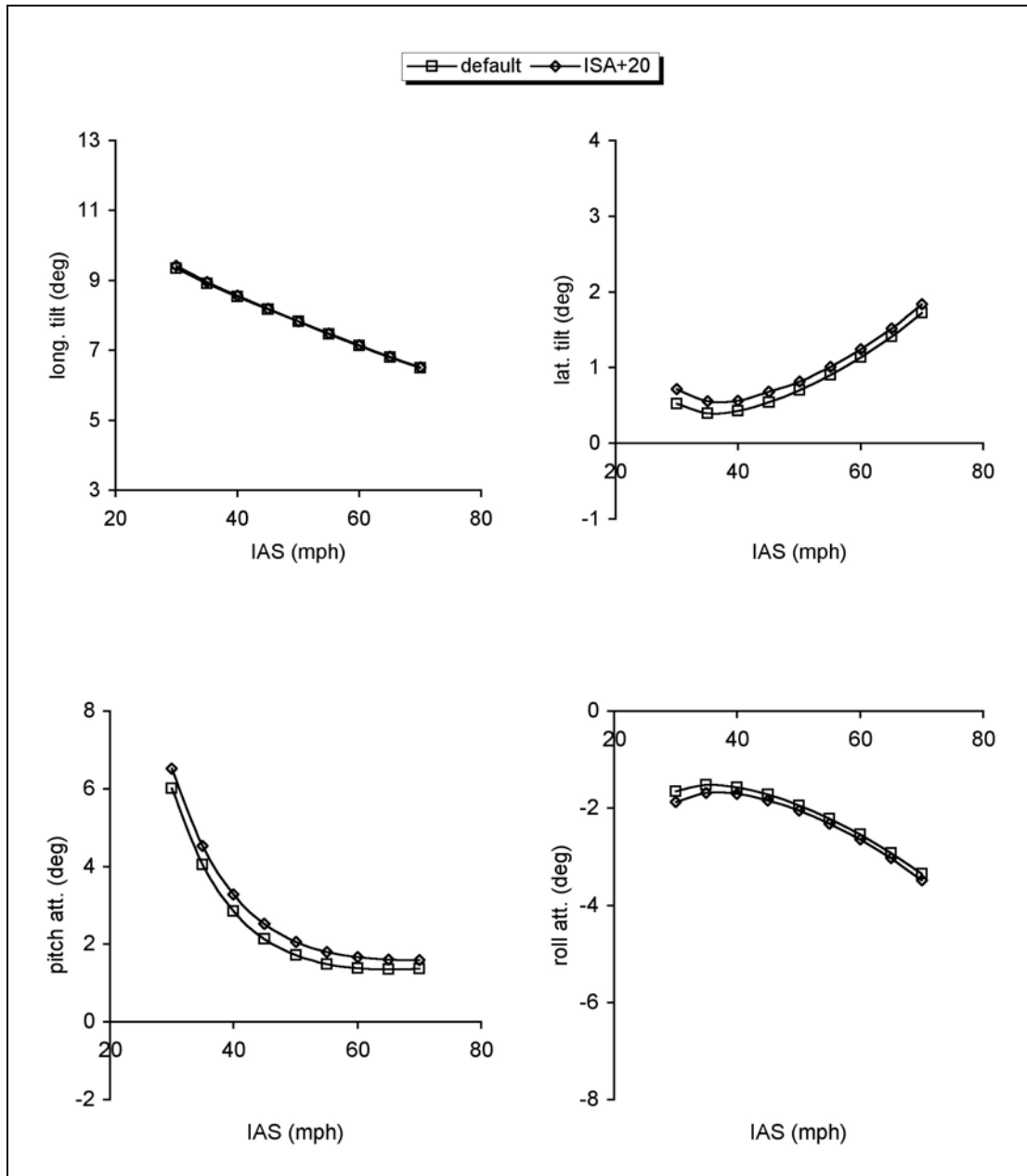
Figure 7.34a Trim Comparison for Temperature Variation (Airframe Parameters)
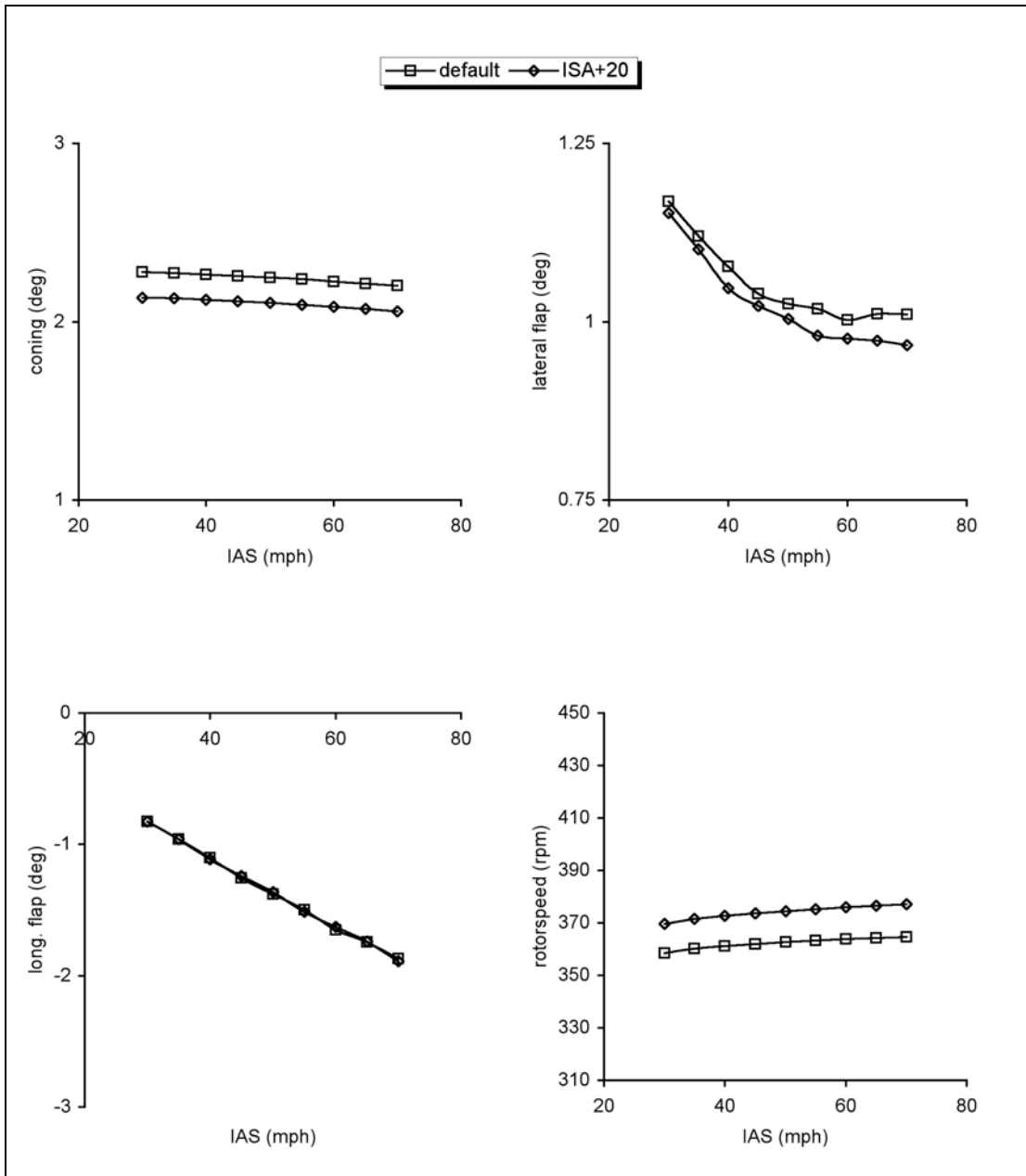
Figure 7.34b   Trim Comparison for Temperature Variation (Rotor Parameters)
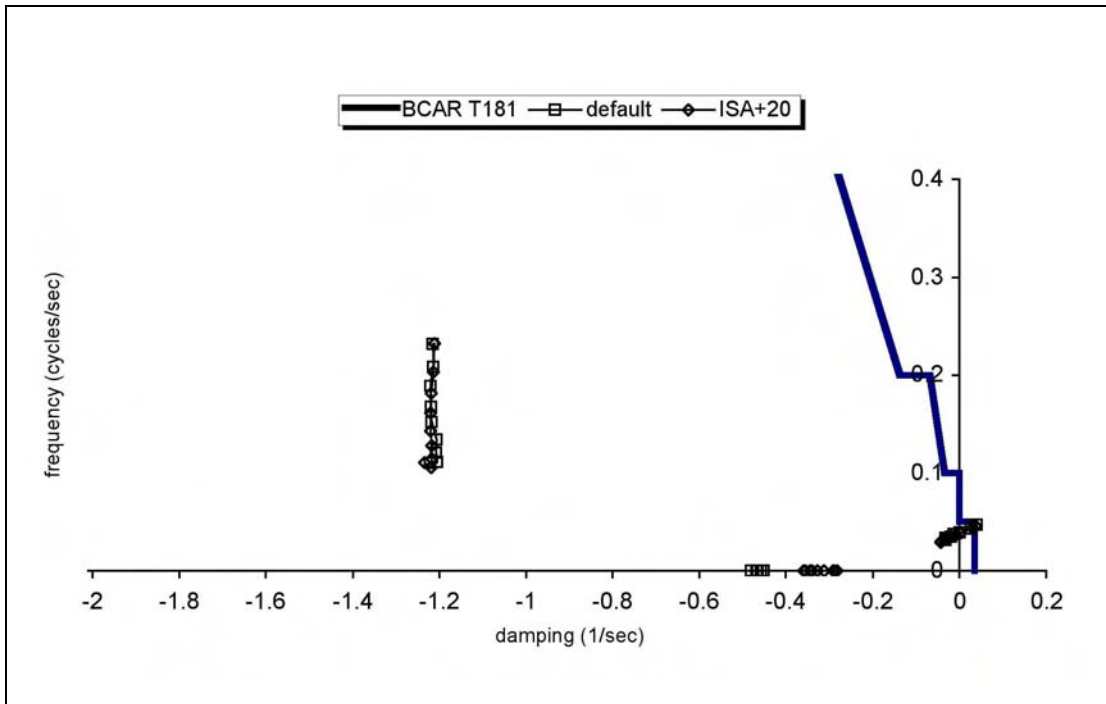
Figure 7.35a Comparison of Stability Modes (Temperature Variation)
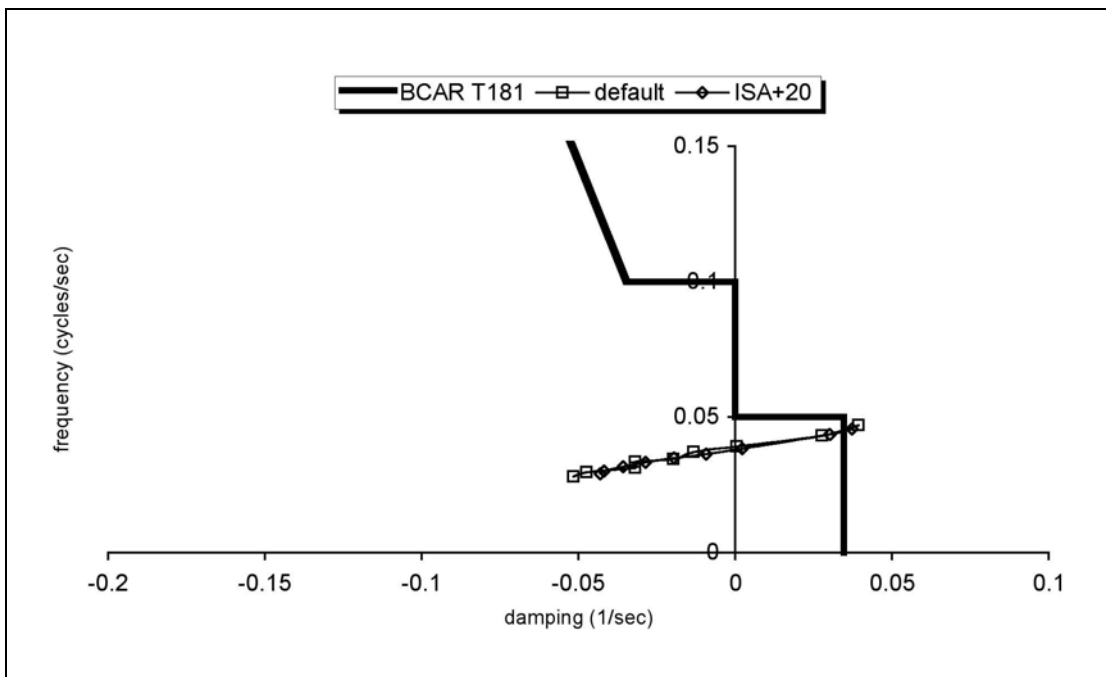
Figure 7.35b The Phugoid Mode (Temperature Variation)
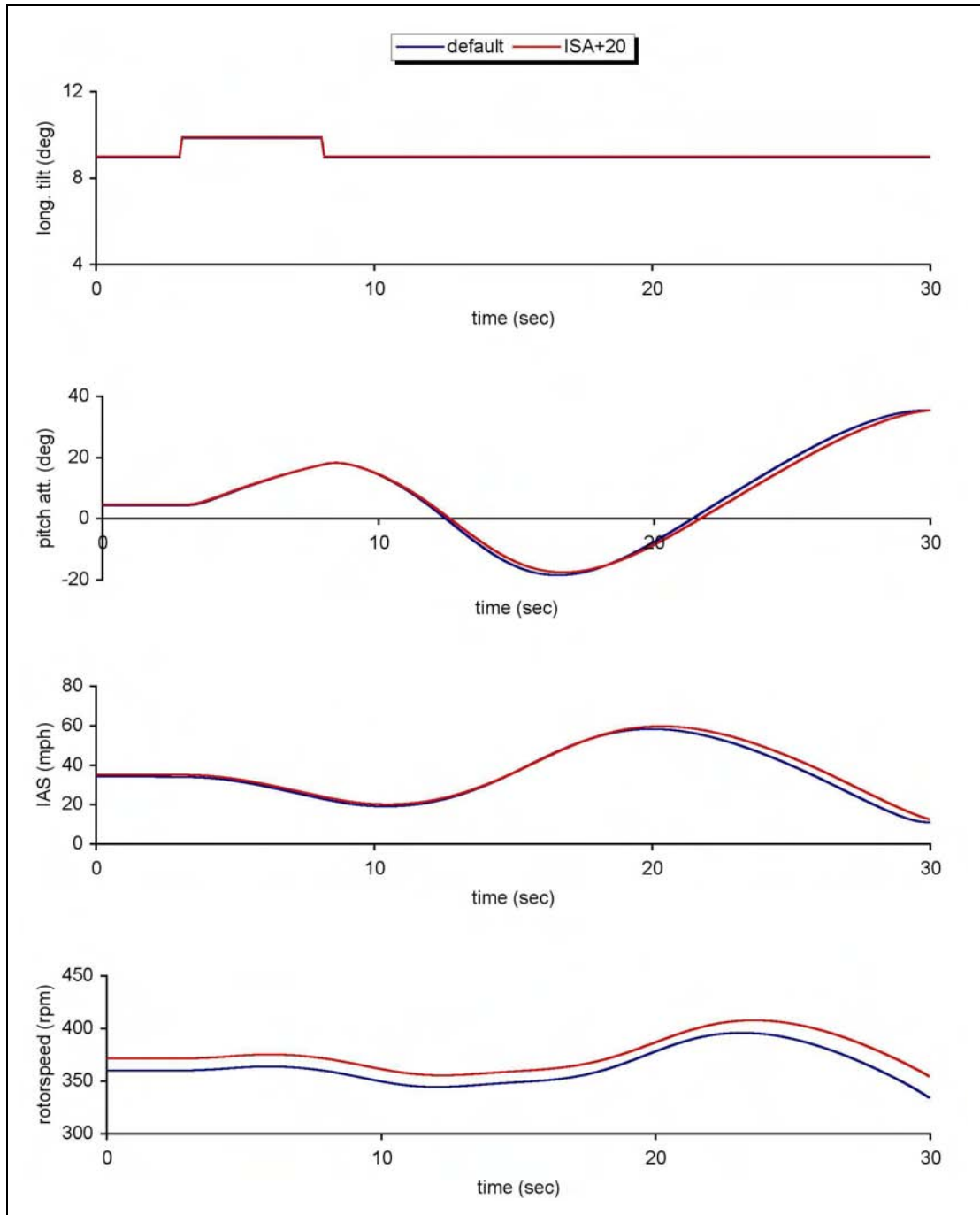
Figure 7.36   Aircraft Response to 5s Pulse of Longitudinal Rotor Tilt - Phugoid
(Temperature Variation)
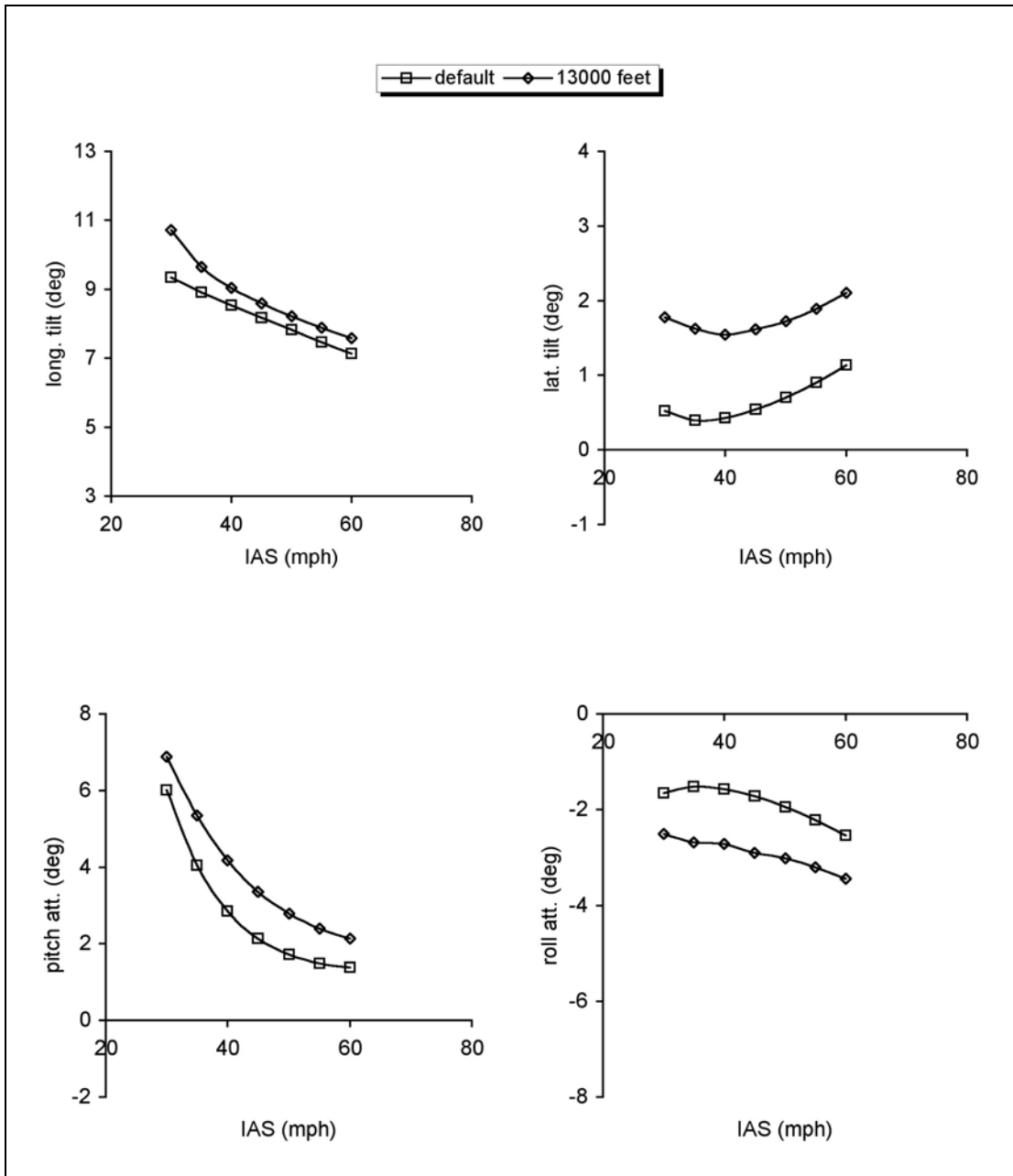
Figure 7.37a　Trim Comparison for Altitude Variation (Airframe Parameters)
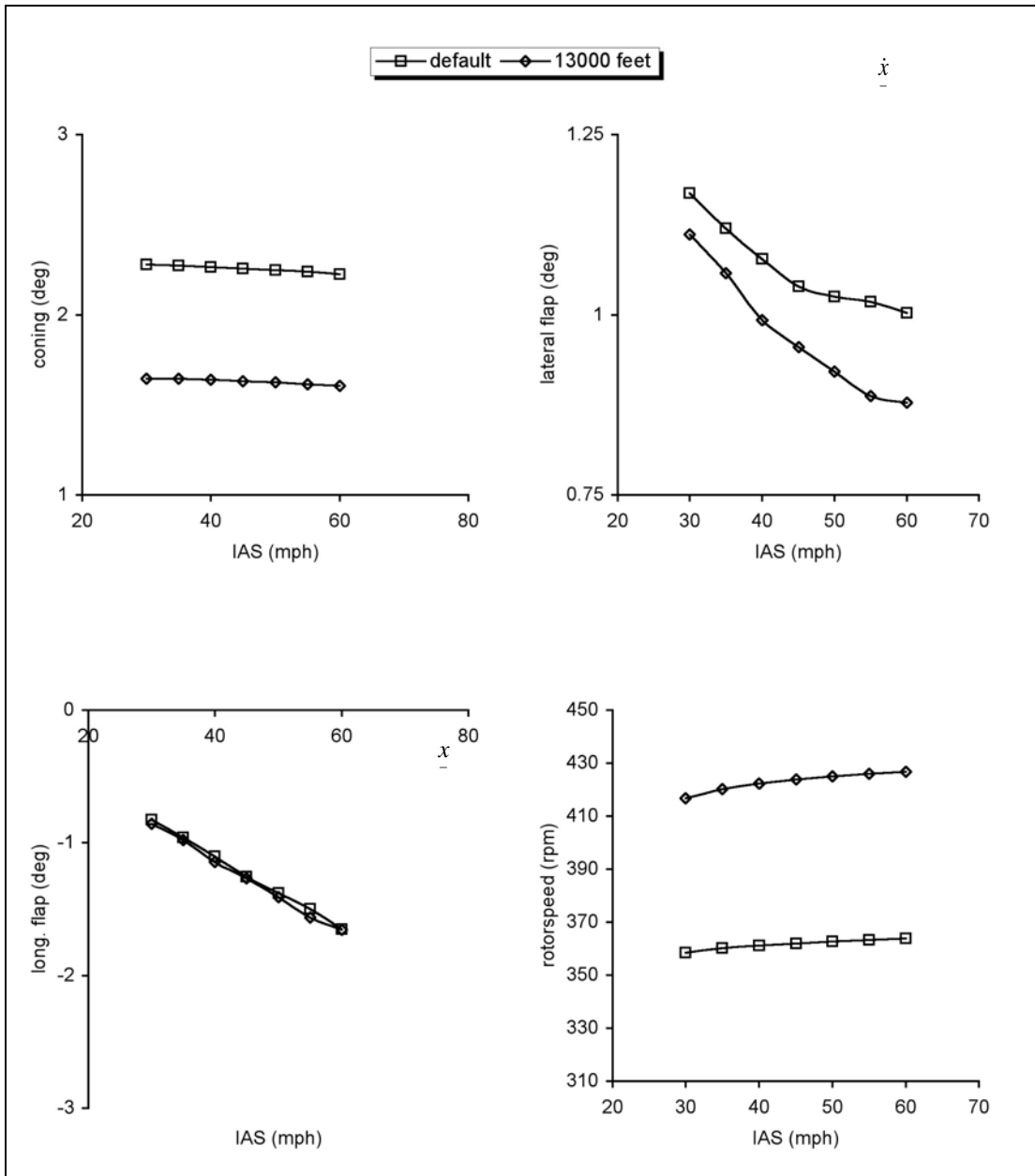
Figure 7.37b Trim Comparison for Altitude Variation (Rotor Parameters)
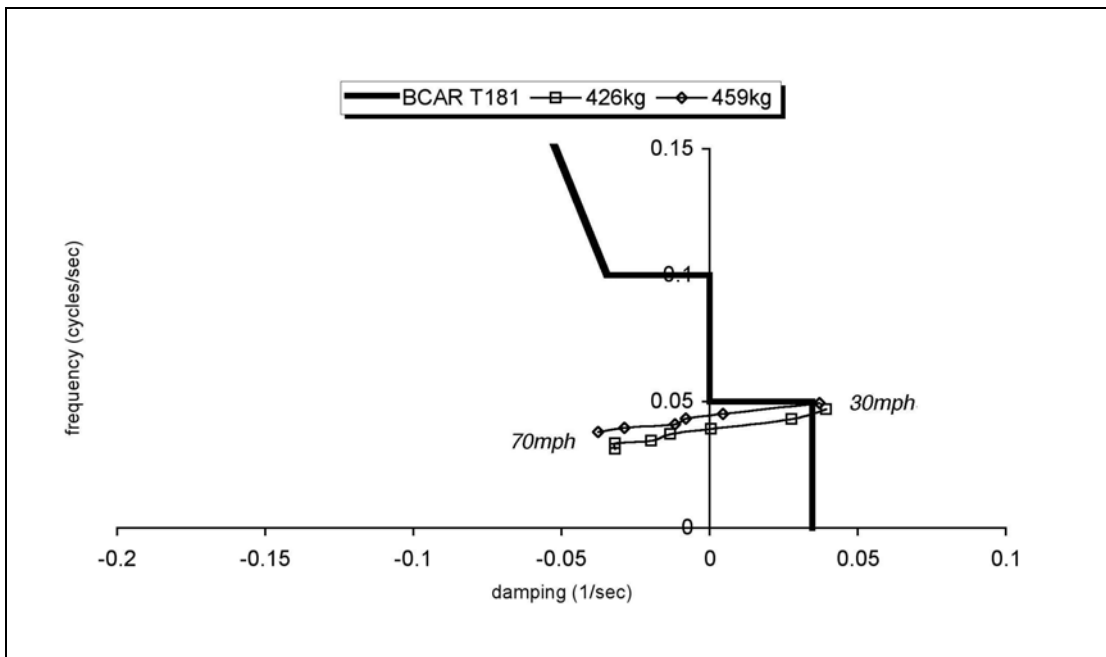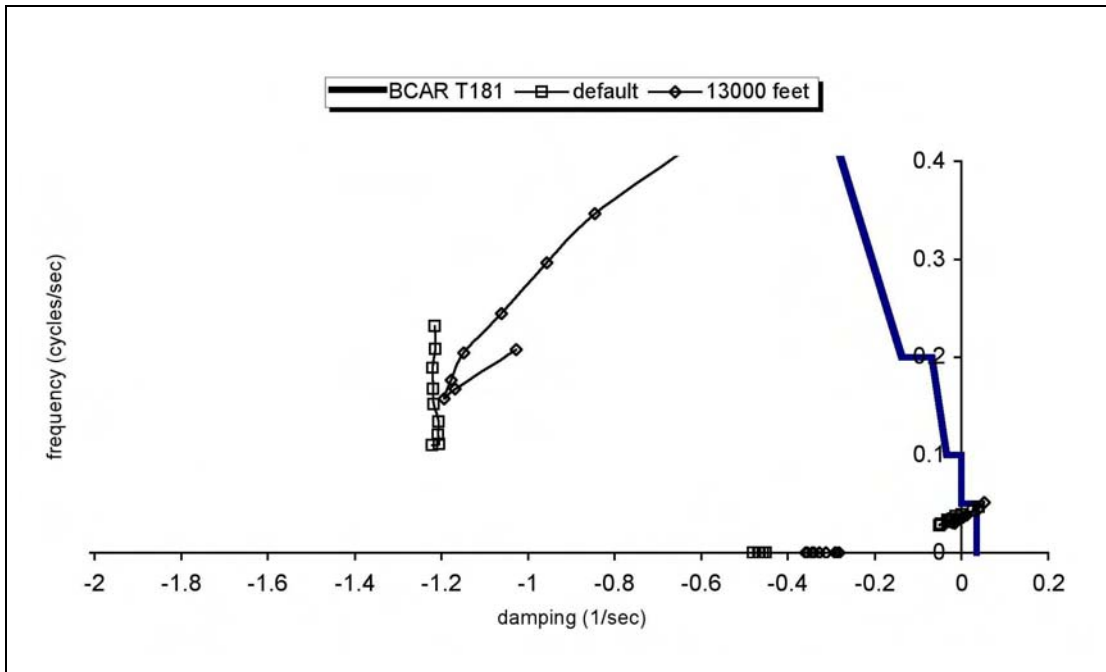
Figure 7.38a Comparison of Stability Modes (Altitude Variation)
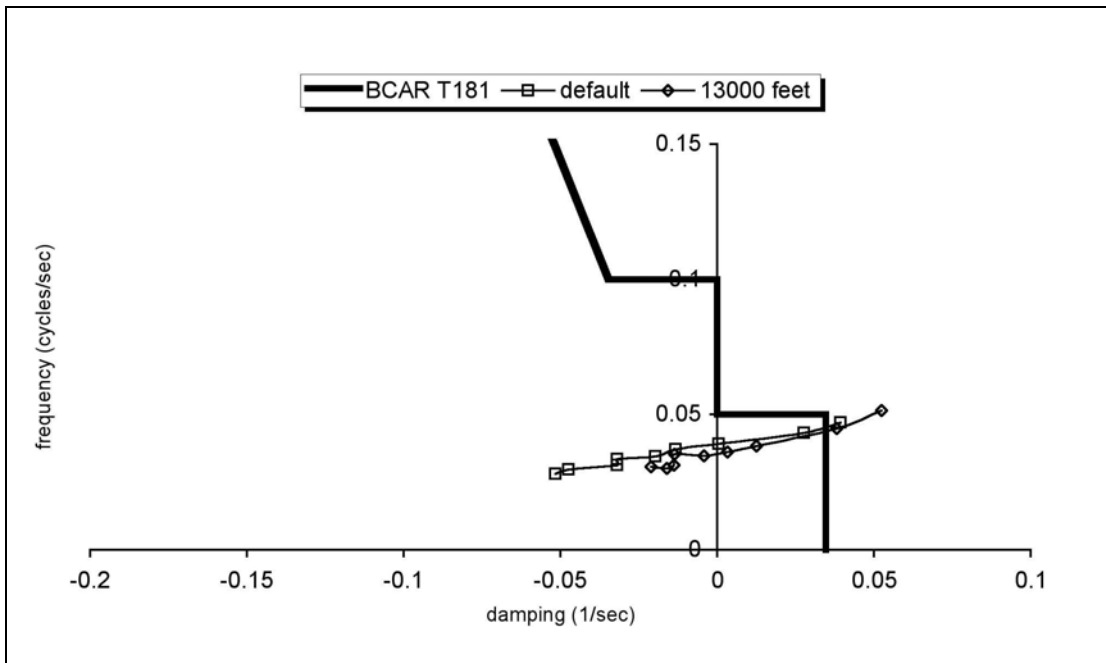
Figure 7.38b The Phugoid Mode (Altitude Variation)

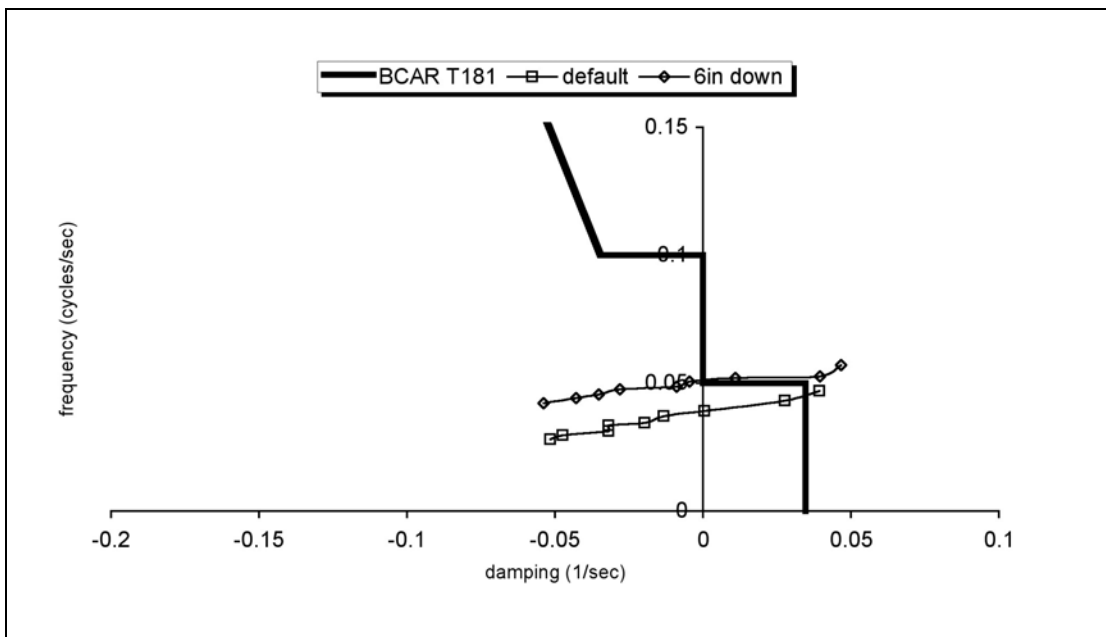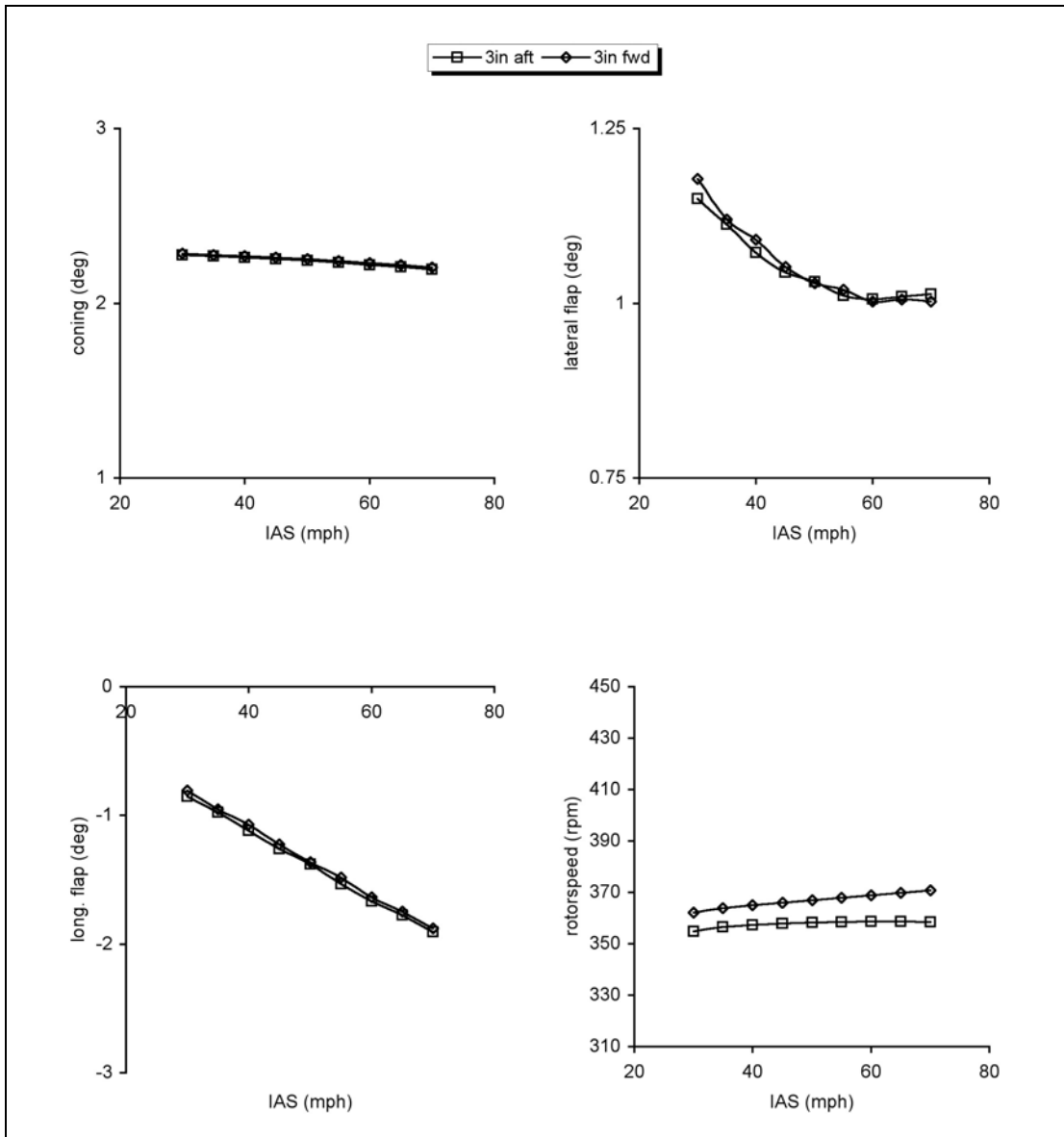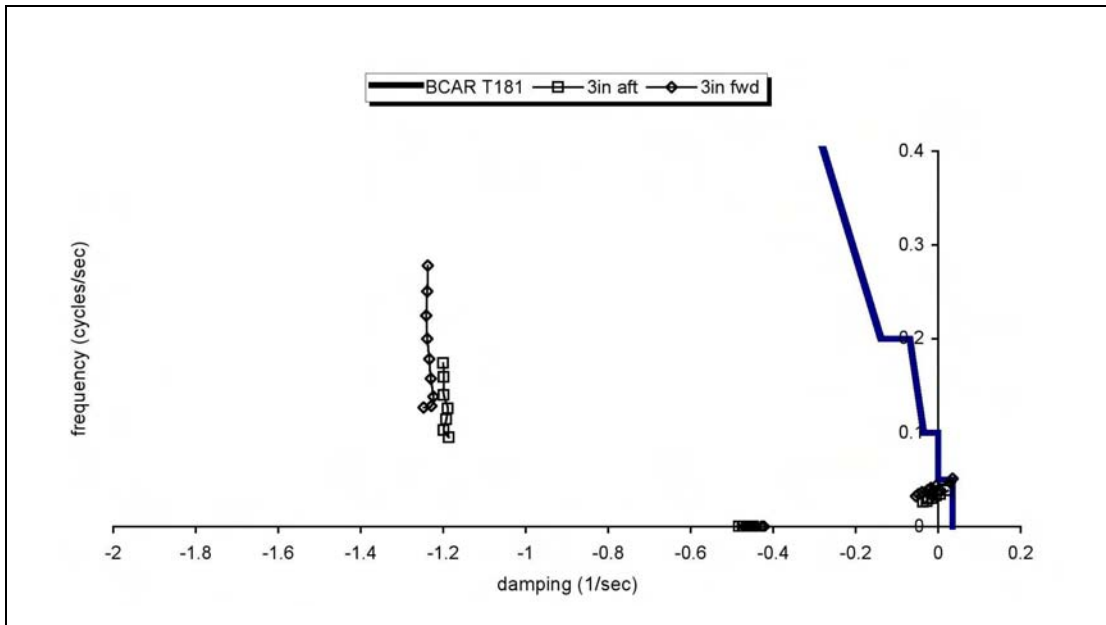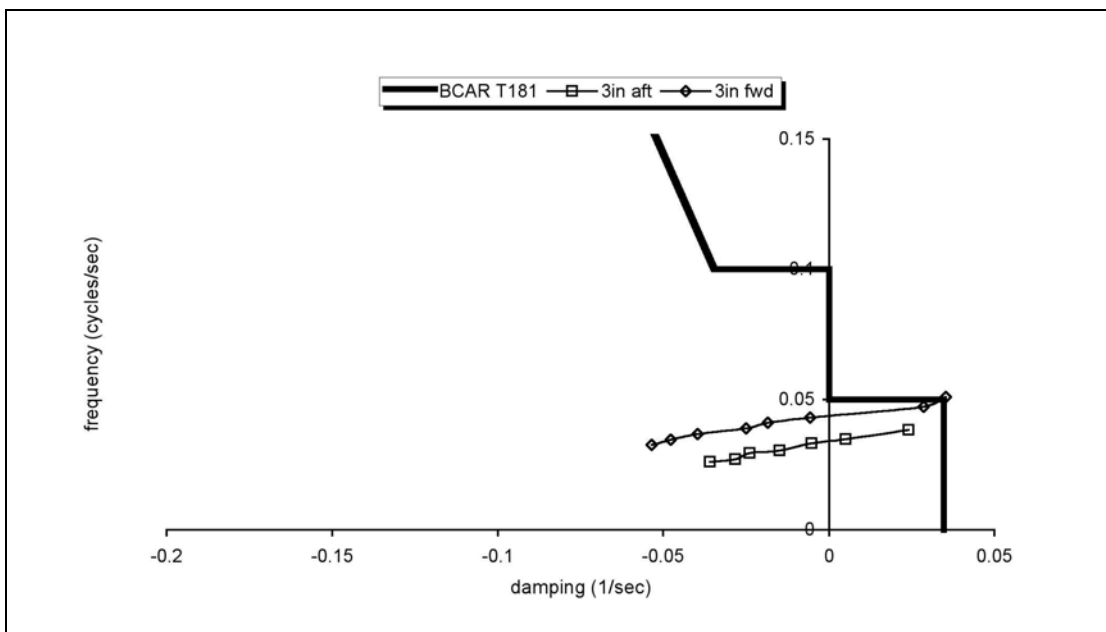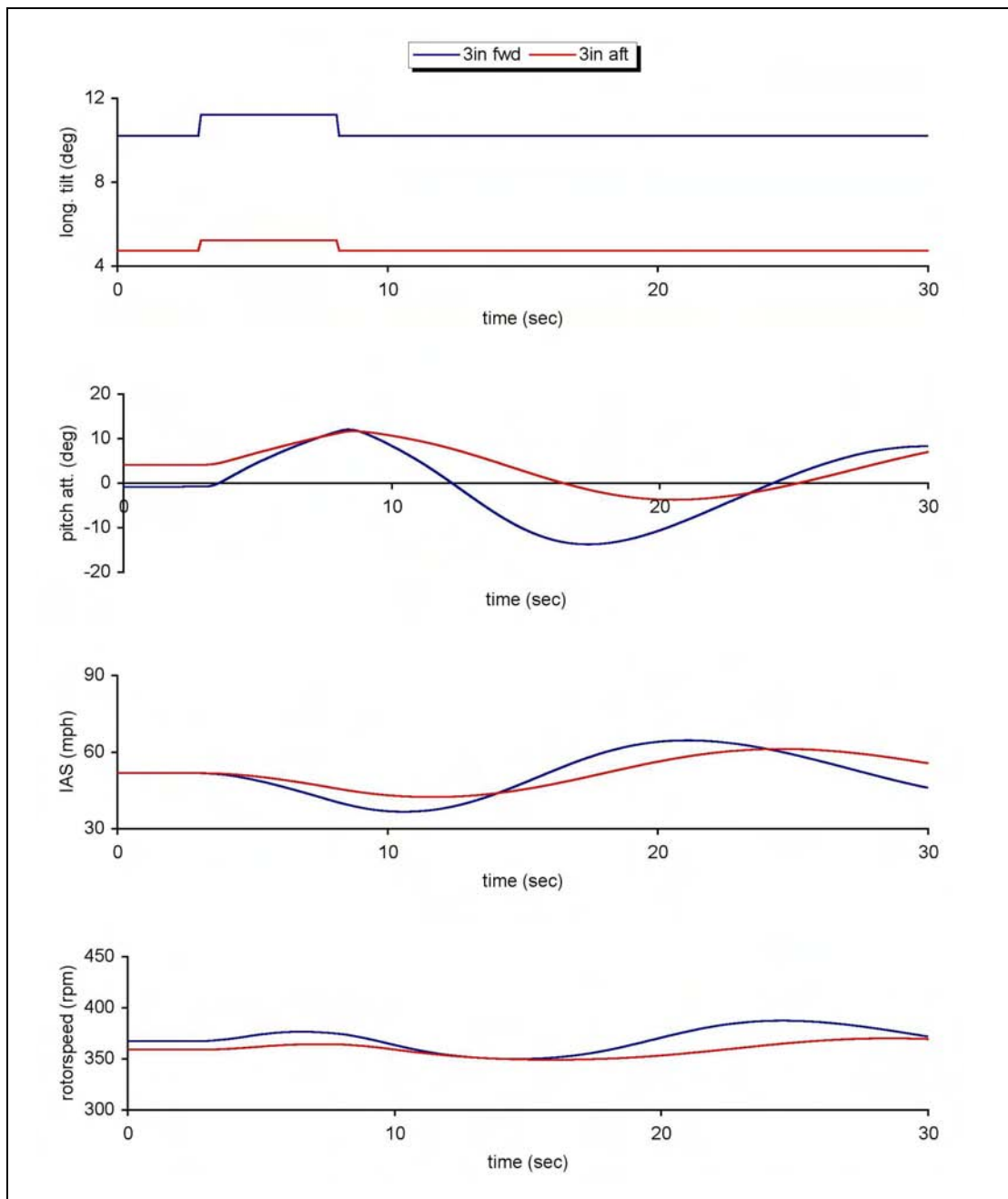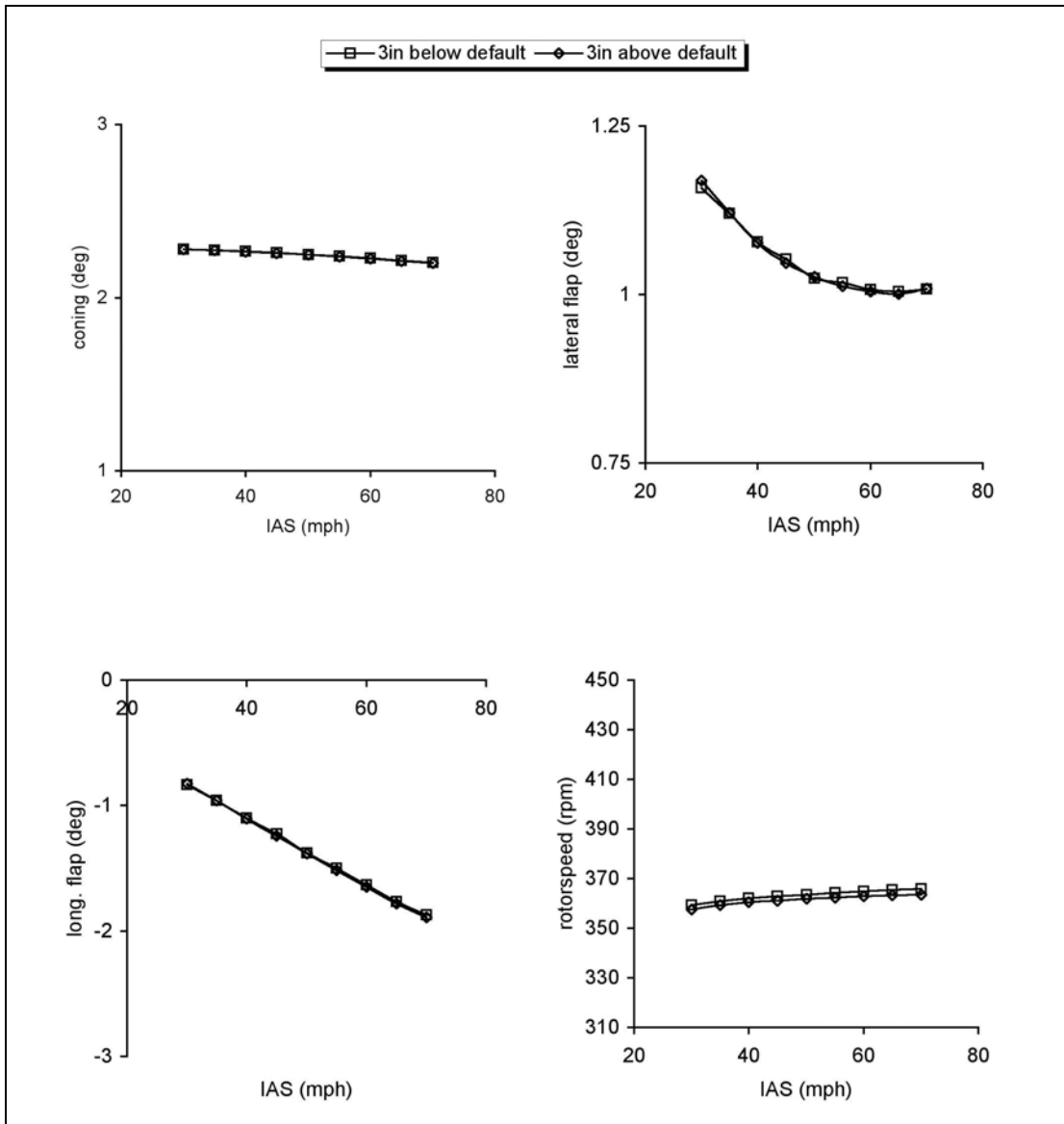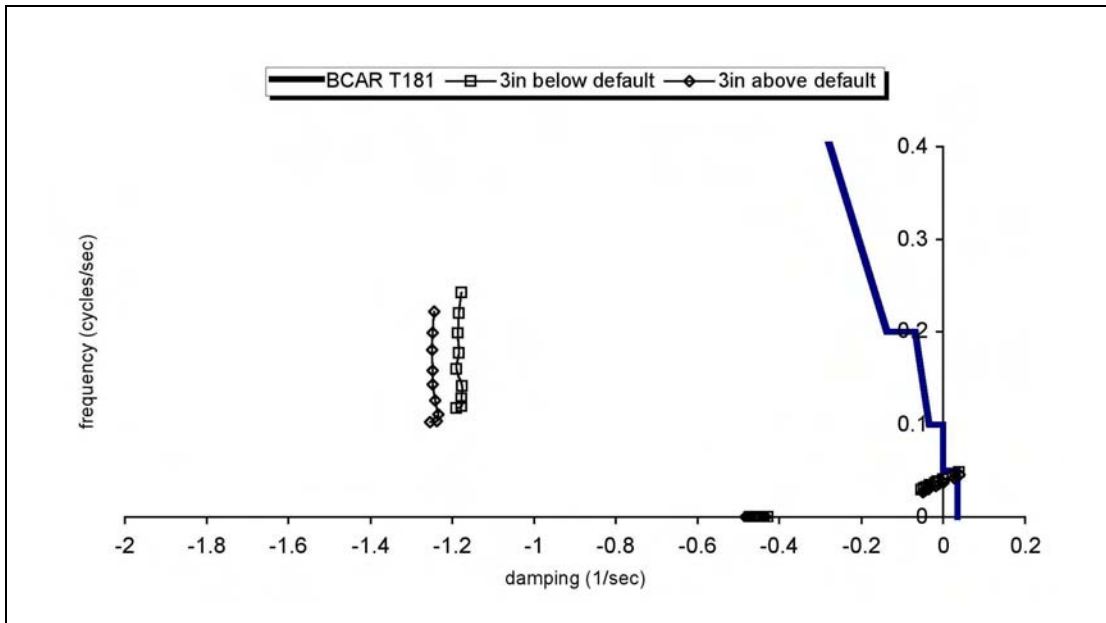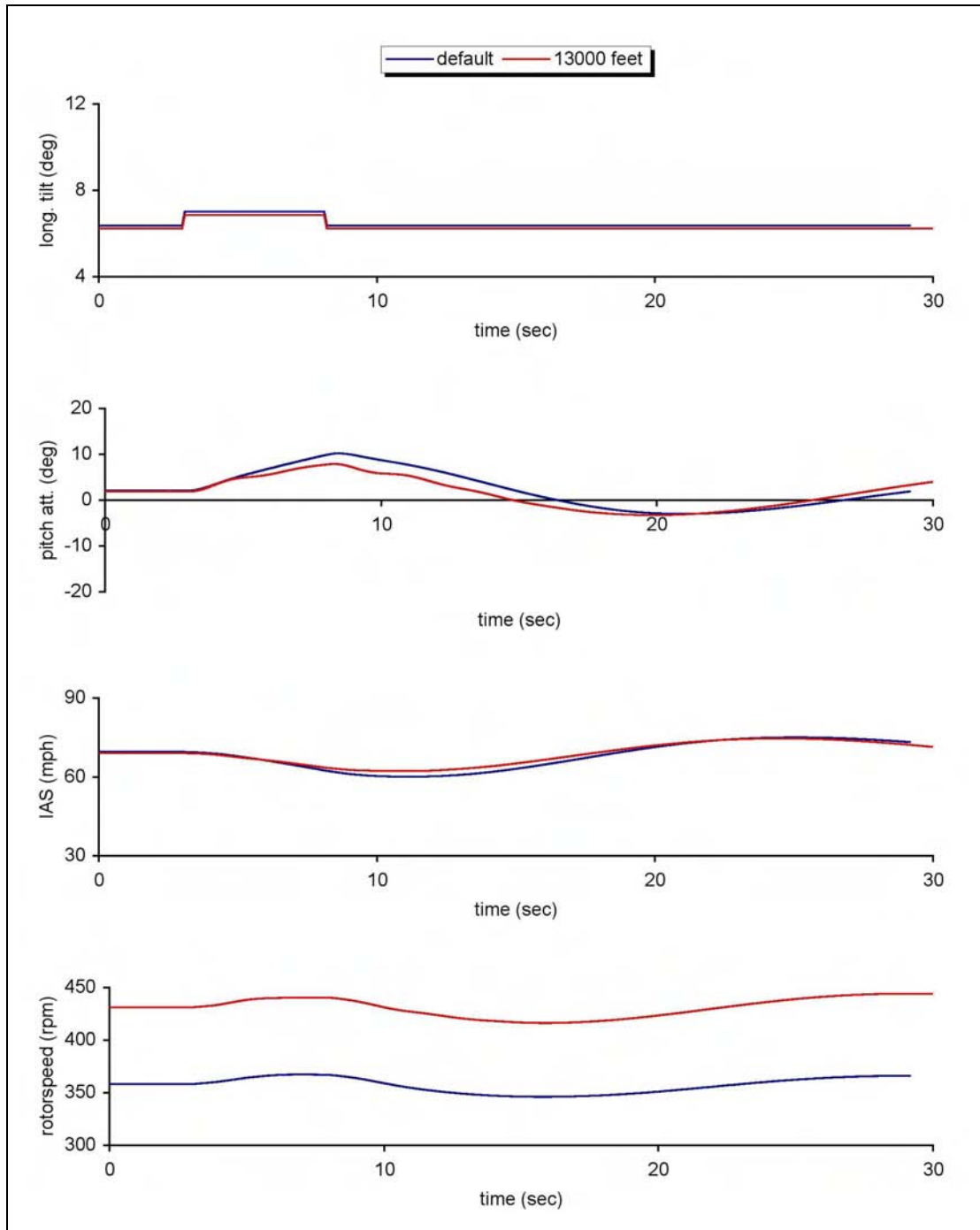**Figure 7.39**   Aircraft Response to 5s Pulse of Longitudinal Rotor Tilt - Phugoid
(Altitude Variation)

8   Review of BCAR Section T

8.1   **Inroduction**

Although there is now a broad literature on the subject of gyroplanes, there is little substantive, validated data available to use for making informed judgement to guide the analysis or development of BCAR Section T. There is an extensive body of experience in the UK, but this resides largely in the knowledge of few individuals who have formed their opinions as pilots or homebuilders, and without the benefit of a rigorous and objective analysis of gyroplane aerodynamics.

The work described in this report has produced an extensive database of results from mathematical modelling, wind tunnel and simulation experiments. In addition, flight tests with two fully-instrumented gyroplanes have been used to generate insight into actual aircraft behaviour by performing highly specialised control inputs and then processing the resulting data using contemporary analysis techniques.

These data, whether derived from simulation or flight tests, are unique. As such, they provide a benchmark for testing BCAR Section T. Perhaps the most important aspect, however, is that these data are objective and quantitative. Opinion, experience and knowledge gained by pilots and homebuilders is essentially subjective and qualitative. It is argued then, that these data can be viewed with a greater degree of confidence than the existing body of experience, and are therefore ideally suited for use in assessing Section T.

8.2   **Background**

8.2.1   A review of Section T [99] was conducted in 1997, with specific reference to the material affected by the study of the Aerodynamics of Gyroplanes, [98]. Accordingly it focused on the following:

a) Subpart B Paragraph T23 "Load distribution limits";

b) Subpart B Paragraph T173 "Static Longitudinal Stability";

c) Subpart B Paragraph T181 "Dynamic stability".

That review was simply intended as a survey of Section T in the context of new information generated subsequent to the Code's initial development from Section S, for which only sparse levels of handling and stability guidance was available. The only substantive, quantitative information that had then been generated was from the modelling and testing described earlier in this report. (No further literature review was conducted to determine if other pertinent studies had generated complementary results. The current, up-to-date review in Section 2 confirms that this remains the case).

8.2.2   Item c) above is directly relevant to handling qualities and, as a result, other material was used in support of the review, [100 - 102]. The 1997 review made the following recommendations:

a) It is recommended that Subpart B Paragraph T23 "Load distribution limits" be modified to specify that weight and balance envelopes be determined that encompass fore-and-aft and vertical centre-of-mass positions for all possible loading configurations. For clarity this recommendation should be expressed as a requirement for the propeller thrust line to pass through the c.g. envelope defined by limiting loading conditions; or that the normal distance between propeller thrust line and c.g. be no more than 2 inches.

b) It is recommended that Subpart B Paragraph T173 "Static Longitudinal Stability" be amended to require stick position as well as force gradients be demonstrated.

c) It is recommended that Subpart B Paragraph T181 "Dynamic stability" be amended to state that short-period oscillations be "damped" and not "heavily damped", unless "heavily" can be further quantified.

8.2.3   These recommendations were adopted and are incorporated in BCAR Section T, [103], as follows:

a) T23 (a) and AMC T23;

b) T173 (a);

c) AMC T181.

The analysis that led to these recommendations is developed in the following section.

8.3   **Analysis**

Note that paragraph references in this section refer to the original CAA BCAR Section T paper, [98].

8.3.1   **Subpart B Paragraph T23 "Load distribution limits"**

Paragraph T23 interprets load distribution limits purely in terms of the conventional (for gyroplanes) hang check. This is done, effectively, to determine that known control limits are not compromised. There is no requirement for a conventional weight and balance schedule to be determined. Aeroplanes require this to be done primarily to ensure that the longitudinal position of the centre-of-mass (known to have a direct impact on static and dynamic stability) is kept within set limits. Simulation has shown that longitudinal centre-of-mass position does not have the same impact on dynamic stability for gyroplanes as it does for aeroplanes so, at first inspection, it may seem reasonable not to require a conventional weight and balance schedule.

However, a theoretical study of gyroplane longitudinal stability, [62], indicates that the vertical location of the centre-of-mass of the aircraft, in relation to the propeller thrust line, may have a significant impact on dynamic stability. Analysis of the flight test data, [104], produced evidence to support this theory. Simulation of the impact of varying this parameter indicates that the phugoid mode can be destabilised, resulting in unstable rotorspeed response to control inputs, controls fixed. Results in Section 7 show significant movement (towards non-compliance) of the phugoid mode with changes to propeller thrust line and vertical c.g. location. The mechanism for this effect is described in Refs. 62 and 104. Strictly speaking, if the propeller thrust line is canted at some angle to the longitudinal axis of the aircraft, it is the normal distance between thrust line and centre-of-mass, i.e. the propeller thrust moment arm, that is the significant parameter.

There is further uncorroborated evidence that this parameter may be an issue in gyroplane stability. The Air Command accidents, [105], are largely unexplained but are thought to have their root in handling problems. The final fatal Air Command accident in the UK to G-BOVP joins this category, although the community seems to think that structural issues and poor post-accident repair had a role to play, despite the AAIB report to the contrary. In 1997 weight and balance information were available for two Air Commands. The owner of one, unregistered in the UK, wrote to the CAA in 1992 stating that the centre-of-mass for his aircraft was 11.5 in below the propeller thrust line. In [62] an early version of the VPM M16 simulation became unstable when the centre-of-mass was only 3.9 in below the propeller thrust line. Data for Modac 503 G-BMZA, dated May 1993, shows the propeller thrust line passing through a calculated centre-of-mass envelope, that was very small. Heresay evidence suggests that this aircraft represents a significant improvement in terms of handling qualities over other Air Commands.

These data were the evidence used in 1997 to propose that the relationship between propeller thrust line and centre-of-mass position can have an impact on longitudinal stability and handling qualities. This parameter can tend to de-stabilise the phugoid mode: whether or not this mode actually becomes unstable depends on other factors such as the drag damping (rotor as well as fuselage), pod and tailplane effectiveness and airspeed. If Paragraph T23 is modified to require determination of the fore-and-aft and vertical centre-of-mass positions, then the difficulty arises as to what quantitative information to supply as interpretative material.

The normal distance between the propeller thrust line and the centre-of-mass, i.e. the moment arm about which the propeller thrust acts, was calculated to be 2.44 in at minimum weight (zero fuel), and 3.36 in at maximum weight (full fuel) for the VPM M16 used for flight trials, when modified with instrumentation and with a pilot in the rear seat. These distances result in the propeller thrust line being above the centre-of-mass. The VPM M16 tested had a marginally stable phugoid oscillation, (see Figure 6.3) so this seems consistent with the study in [62] where the configuration became unstable when the centre-of-mass was 3.9 in below the propeller thrust line.

It would therefore seem reasonable to modify Paragraph T23 to require determination of a centre-of mass envelope for all possible loading configurations. It was suggested that material could be included to specify that the propeller thrust line ought to pass through this envelope, and a conservative figure (in an effort to capture "safe" values for all types addressed by Section T) is that it should not be a normal distance of more than ±2 in from the centre-of-mass at any loading condition. This is indeed the course of action that was adopted by the CAA.

It is fair to say that this recommendation came in for a very considerable degree of criticism from the UK gyroplane community. However, two studies conducted since then serve, in retrospect, to confirm the validity of that original analysis. First, a weight and balance study of two Air Commands (single and twin-seat) was conducted for the CAA as part of a wider simulation study of the type [106], which confirmed that the type had a low centre-of-mass position. Second, and arguably more important, a weight and balance survey of five single-seat machines [107] was carried out in support of the CAA flight tests, [108]. These data validate the earlier recommendation, in that only one of the five aircraft tested satisfied the Section T handling criteria, and it was the aircraft modified to meet the proposed ±2in propeller thrust line/c.g. offset limit. For clarity, Reference 107 and 108 are included in this document as Addendum 1 and Addendum 2 respectively. Note that the tests reported in Reference 108 were conducted separately and independently (and after) the flight tests reported in Reference 107. They were conducted to validate the flight test conclusions.

8.3.2 **Subpart B Paragraph T173 "Static Longitudinal Stability"**

This paragraph expressed static stability in terms of stick force. For completeness, it was recommended that stick position should be included as well. Stick position may be easier to measure accurately and repeatably given the rudimentary nature of light gyroplane trim systems.

8.3.3 **Subpart B Paragraph T181 "Dynamic stability"**

This paragraph is perhaps the most difficult to deal with, for a variety of reasons. It offers a particular challenge in seeking to find easy to apply criteria that are rigorous, complete and consistent. The emphasis on oscillation characteristics may indicate that the intention of the criteria is to deal with the potential for pilot-induced-oscillation (PIO). PIO is difficult to predict, particularly from elementary dynamic response criteria of the type given in T181. Other issues, such as pilot control strategy, task demands

and aircraft frequency response characteristics all have a role to play. Notwithstanding this, T181 can be examined in the context of results from flight test experiments conducted on G-BWGI and the existing literature on handling qualities prediction from dynamic response criteria.

8.3.3.1　Short-period oscillations

T181 (a) states that any short-period oscillations should be "heavily damped". The interpretative material places this in context, that an oscillation with a period of less than 5 sec should damp to half amplitude in not more than one cycle. Consider the limiting case: a 5 sec oscillation, damping to one half amplitude in one cycle, i.e. 5 sec. This gives an oscillation with a damping ratio of 0.11. Critically-damped systems have a damping ratio of 1, and "well-damped" systems, 0.35. The interpretative material is therefore inconsistent with the requirement "heavily damped". Even an oscillation with a 1 sec period, damping to half-amplitude within 1 sec, will have a damping ratio of 0.11, still not "heavily" damped (generally, a damping ratio greater than about 0.6 would indicate "heavy" damping). If the interpretative material were to be modified to read "...should damp to one half amplitude in not more than half a cycle", then the damping ratio increases to 0.22 in these limiting cases, still not even "well" damped. Any further modification to the criteria will then result in compliant aircraft having dynamic characteristics that could call into question the test pilot's ability to identify any oscillation of this sort quantitatively.

Additional information may help in deciding what, if anything, should be done with these requirements. First, the VPM M16 G-BWGI, as identified, has the short-period mode characteristics described in Table 8.1. The aircraft easily satisfies T181 interpretative material at both speeds but the damping, particularly at 70 mph, cannot be described as "heavily damped". Note that MIL-F-8785C, a now obsolete fixed-wing, essentially fighter, handling criteria states that damping ratios of 0.35 and above are required for "satisfactory" handling qualities, 0.25 being the lower limit for Level 2 ("acceptable") handling qualities, [101]. The relevance of MIL-F-8785C to gyroplanes is not clear, however.

However, the undamped natural frequency is also important and, combined with the damping requirement MIL-F-8785C criteria, predicts VPM M16 handling qualities to be borderline poor/unacceptable. Yet it satisfies the criteria in Section T. Further, in previous performance and handling assessments, the aircraft is well-regarded, [109]. There seems little point in changing the interpretative data without any further handling qualities research specific to the gyroplane.

The review therefore recommended that the word 'heavily' be removed from the description of the short-period damping requirement (T181), and this was accepted.

Table 8.1　Identified G-BWGI Short-period Mode Characteristics

speed (mph)	damping ratio	undamped natural frequency (rad/s)
30	0.75	0.59
70	0.38	1.40

8.3.3.2　Long-period oscillations

The interpretative material for longer-period oscillations was contained in App. T 181 (b) and (c), the former dealing with stable and the latter with potentially unstable, oscillations. Identified results for G-BWGI are given in Table 8.2. Note that this oscillation is very lightly damped even in a machine that is well regarded in the community. These data are converted in terms of Section T in Table 9.

Table 8.2 Identified G-BWGI Long-period Mode Characteristics

speed (mph)	damping ratio	undamped natural frequency (rad/s)
30	0.042	0.58
70	0.042	0.40

App. T181 (c) is then the relevant section, and the aircraft passes, as the requirement is only for the oscillation to be damped. However, at 30 mph, the aircraft only just misses App. T181 (b) being the relevant section, where it would fail, as the number of cycles to half amplitude is greater than 2. Again, previous flight test work does not indicate poor handling qualities as a result of long-period oscillations. (It is interesting to note that in this previous work, [109], the test pilot used his judgement and skill to measure phugoid characteristics. Interpretation of this previous data gives a damped natural frequency of 0.5 rad/s, and a damping ratio of about 0.1-0.2, quite different to that identified using parameter estimation methods – it is argued that this is an indication of how challenging the compliance demonstration against Section T can be).

Table 8.3 Identified G-BWGI Long-period Mode Characteristics, Section T

speed (mph)	No. of Cycles to Half Amplitude	Period (s)
30	2.6	10.9
70	2.6	15.6

Some previous, now dated work, [100] suggests that phugoid damping ratios of 0.042, as identified for G-BWGI, will give marginally acceptable, tending to poor, pilot opinion. However, these data were for a period of 50 sec, i.e. quite slow, whereas the VPM M16 has a much faster phugoid oscillation than this. Intuitively one might expect an even higher level of damping is required for satisfactory or acceptable handling qualities.

8.4 Comparison between VPM M16 and Montgomerie-Parsons

The foregoing analysis was developed at a time when only VPM M16 flight test data were available with which to evaluate the compliance demonstration criteria proposed for BCAR Section T. The aircraft complies with the dynamic stability requirements and, since the heresay opinion of the aircraft is good, it can be taken that the boundaries are in the right place. However, corroboration of this assessment requires comparison of other types, and only the Montgomerie-Parsons Two-Place G-UNIV has been subjected to a rigorous flight test programme that allows dynamic characteristics to be identified mathematically from the flight test data.

The Section T compliance boundaries given in T181 are best rendered graphically as shown earlier, rather than as a narrative as given in BCAR Section T. The diagram is by now familiar, and is shown in Figure 8.1. Note that as the x-axis is "damping ratio" and not "damping" as in previous plots presented in this report, the stable region is now to the right of the vertical axis (see Appendix 4). The aircraft have three longitudinal modes: short-period, long-period (more colloquially known as the phugoid), and rotorspeed. The data are for two speeds, 30 and 70 mph IAS in the case of the VPM, 40 and 70 mph IAS in the case of the Montgomerie-Parsons. Arrows against each mode show the progression from low to high speed.

As described above the VPM M16 meets the compliance demonstration criteria. Only the long-period (phugoid) mode is close to the boundary, but is nonetheless compliant. The Montgomerie-Parsons on the other hand fails compliance by virtue of the fact that the long-period mode is placed too far to the left at low speed. This result is broadly consistent with pilot opinion of the aircraft, which was a challenge to fly when conducting specialized inputs such as steps, doublets and especially frequency sweeps where the inadequacy of the handling required an alternative approach to be adopted by the pilot.

A formalized approach correlating these data with Cooper-Harper rating of each aircraft in applied flying tasks would be required to confirm this assessment. Such flying never featured as part of any flight test campaign. Nonetheless, the results tend to confirm the validity of the criteria for predicting handling qualities in the broadest sense.

8.5   Analysis of BCAR Section T Chordal Balance Requirement

A study of the aeroelastic properties of gyroplane rotors has been undertaken in parallel with the work reported here [78], and a full report on this is provided as Addendum 3 to this report. From this work it is clear that aeroelastic instabilities do exist. Occurrence of a type of flutter that is unique for autorotating rotors was predicted by the model developed, both during axial descent in autorotation and autorotative forward flight. This aeroelastic instability is driven by blade pitch / bending / rotor speed coupling and differs from both flutter of a helicopter rotor and flutter of a fixed wing. The instability results in catastrophic decrease of the rotor speed and significant increase of speed of descent. Given this result, it is considered prudent to verify (or otherwise) that the requirements for chordal balance currently in BCAR Section T are appropriate. Specifically, BCAR Section T (light gyroplanes) paragraph T 659 states:

Mass balance

b)   The chordwise balance of the blades must be at, or forward of, the 25% chord. The chordwise balance of each blade in a pair must be the same, or within a tolerance to be agreed with the CAA.

The research looked in detail at this requirement in the light of the identified aeroelastic instability issues. Addendum 3 concludes that BCAR T 659 provides a safe rotor, in terms of pitch flap flutter and divergence, for conventionally designed light gyroplanes with teetering rotors. In addition, the offset gyroplane hub was shown to be slightly stabilizing in forward flight. The predicted flutter frequency for low stiffness control systems is around 1/rev. This low frequency, and the fact that the dominant (low stiffness) degrees of freedom are longitudinal and lateral disc tilt, means that any flutter phenomenon arising from an aft c.g. will manifest itself as a 1/rev varying disc tilt.

8.6   Discussion

The essential fact is that the technical ability of the gyroplane community and the test and analysis facilities available to them, may severely compromise or inhibit the collection of meaningful, or even correct data with which to demonstrate compliance. Any recommendations that might be made in respect of Section T, therefore, may be only of academic consequence, and do little to enhance Section T and therefore airworthiness.

For example, the previous, largely subjective analysis conducted by the CAA's approved gyroplane test pilot, [109], estimated short-period frequencies of the order of 2.5 Hz, or 15 rad/s. The parameter estimation exercise conducted on G-BWGI identifed short-period frequencies, depending on airspeed, of between 0.5 and 1.5 rad/s, i.e. a full order of magnitude less. The phugoid frequency estimated previously was 0.5 rad/s at 70 mph. The exercise conducted on G-BWGI identified 0.4 rad/s so, although test pilot judgement was better in the latter case, it was still in error by 20-25%. With regard to phugoid mode damping, the identification exercise indicates that the damping is less than half of that subjectively measured in the previous exercise. Thus, locating the c.g. appropriately relative to the propeller thrust line offers the best prospect for acceptable handling qualities across the speed range.

Relative to appropriate handling qualities criteria in the literature, the VPM M16 fares badly, with Level 2/3 (acceptable/poor) predictions of short-period and phugoid mode characteristics, [100, 101]. This is at odds with subjective and heresay evidence; the aircraft handling qualities are regarded as an enhancing feature of the type, particularly for the training role. Despite this inconsistency, the aircraft possesses longitudinal dynamics that, for other aircraft performing other tasks, would be unacceptable.

However, there is some consistency with Section T in regard to long-period (phugoid) oscillations, where the aircraft is only marginally acceptable at 30 mph. Given that the VPM M16 may "set the standard" (it certainly, by virtue of the flight test programme conducted on it, benchmarks the understanding of gyroplane stability and control), it is difficult to see how other types will then satisfy Section T's stability requirements. In essence, based on experience with the VPM M16, other gyroplanes of similar configuration and with two-bladed teetering main rotors, will find demonstrating compliance with the stability criteria of Section T a challenge.
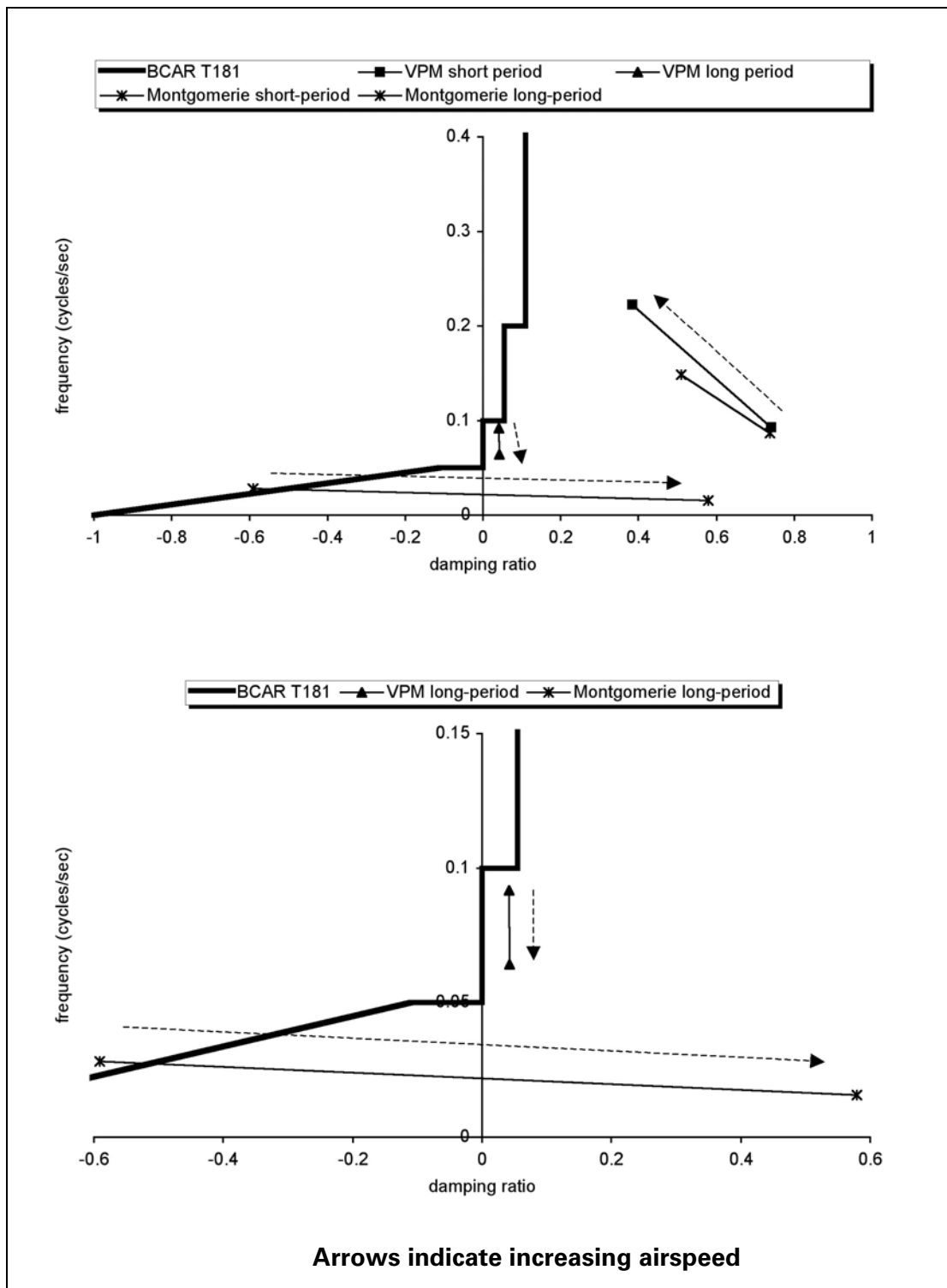
Figure 8.1   Comparison of Flight Identified Modes. VPM and Montgomerie

9   Assessment of Rotor Blade Torsion Effects

9.1   Introduction

The mathematical modelling of rotor blade behaviour and the resulting forces and moments transmitted to the aircraft employed for the studies reported here has embodied a rigid, rather than flexible, representation of the blade. The blades are of course free to flap or teeter, but outboard of the hinge or teeter bolt are regarded as rigid. This is consistent with contemporary approaches to flight modelling of rotorcraft. It is rare indeed to find a rotorcraft flight mechanics model that includes blade flexibility.

The phenomena that arguably have the greatest impact on aircraft behaviour are those that generate changes in angle of attack at a blade element. These include aircraft motions, blade flap velocity, inflow and control inputs. However, if a blade is flexible then the bending of the blade can further change its angle of attack and hence the loads generated. Bending can certainly produce such effects but tends to have a small impact by comparison with elastic twisting, or torsion, of a blade. This produces a direct geometric change in a blade element angle of attack as opposed to that from bending which results from small fast vertical movement of the blade. The total blade motion can then be seen to be a complex and complicated mix of rigid blade motions with elastic deformations in torsion and bending superimposed.

It is possible to couple a simplified representation of torsion with the rigid blade model, but it must be appreciated that it fails to couple the dynamics of torsion such as the time-varying response of the blade's twist with applied load. Instead the blade is assumed to twist instantaneously to an appropriate angle given by the applied load, resulting in a quasi-steady rather than truly dynamic response. However, the relationship between load and twist is predicated on the results from the quite separate and sophisticated model of torsion that, for its part, does not capture the flight behaviour of the whole aircraft. There is nothing in the technical literature that indicates this has been attempted previously but, in principle, it can be expected that this approach offers an appreciation of at least the gross effects of blade torsion on flight mechanics.

9.2   Background

Interest in the effects of blade flexibility as it affects gyroplane rotors is driven by two principle questions: first, can bending be sufficiently large during benign manoeuvres as to cause airframe/rotor strikes or propeller/rotor strikes; secondly, can torsion as a consequence of loading cause a rotor to speed up or slow down sufficiently to cause a flight safety problem. Relatively early studies on the first of these concerns has taken place, [110, 111]. Interest in the torsion problem is fairly recent and was driven by the CAA interest in Wallis gyroplane rotors which anecdotal and circumstantial evidence suggest are torsionally 'soft' and therefore likely to strongly couple rotorspeed and elastic twist effects, perhaps beneficially, [112]. However, the very limited application of blade flexibility models in helicopter flight mechanics modelling does not suggest that blade elasticity has a seminal impact in the fidelity of the modelling, [113]. In this latter study an attempt to resolve poor modelling of cross-coupling by detailed finite-element modelling of blade flexibility, coupled with a more complex wake model, produced at best inconclusive results with regards the modelling improvements obtained. This modelling, and the comparison with flight test data, benefited from a comprehensive flight test database obtained using a fully-instrumented UH60 helicopter.

9.3   **Modelling**

The implementation of blade elastic deformation is enabled by modifying the static twist distribution (normally zero for a gyroplane blade which is typically untwisted). This elastic twist is derived from a blade torsion mode 'shape', and this is shown in Figure 9.1. This shape is the twist adopted by the blade under any load. To derive the actual twist at any position, this shape is correlated with the deflection at the tip, itself a function of the blade load. Calculation of a blade load is an integral part of any flight mechanics code, rigid blade or otherwise, and is therefore readily available in the flight model.

Figure 9.2 shows the relationship between the tip torsional deflection and the total load acting on the blade. So, the torsional deflection (twist) from elastic deformation under load is obtained by multiplying Figure 9.1 by 9.2, scaled to the actual load calculated by the flight model.

The model of course requires data to configure the blade as a specific type. In this case a McCutcheon blade was tested to derive the appropriate characteristics, [112]. The McCutcheon blade is used on the Montgomerie-Parsons gyroplane, so the simulation results are specific to that aircraft.

9.4   **Results**

Results are presented in the same form as that previously used for the parametric study and model validation. Figure 9.3 a) shows the airframe parameters in trim flight across the level flight speed range, Figure 9.3 b) the corresponding rotor parameters. Figure 9.3 c) shows comparison of the dynamic stability results in the context of the BCAR Section T boundaries. Figure 9.3 d) compares the response to the aft tilt control input used to demonstrate Section T compliance for the 40mph case. Above 40 mph both cases fail Section T compliance and become aperiodically unstable.

The lateral tilt of the rotor (directly proportional to the pilot's lateral stick input) is greater with the elastic torsion effect included, which improves correlation with flight, Figure 9.4. Correlation with flight-measured teeter angle, converted into lateral flapping, is also improved. In all other respects inclusion of this simple torsion model has a negligible impact on trim, stability and response. Note that the elastic distortion at the tip of a blade is relatively small, ±0.5 deg.

9.5   **Discussion**

These results tend to suggest that inclusion of a simple model of elastic twist will have a limited impact on prediction of trim, stability and control response. Whether considering dynamic stability (Figure 9.3 c)), which is pertinent to linearised or small perturbations from trim), or the large-amplitude non-linear response to a control input, Figure 9.3 d), the results suggest a negligible difference. In particular the small amount of torsion is insufficient to alter the rotorspeed response by a sufficient margin to present flight safety issue. Lateral control required for trim and the lateral flapping of the disc are, however, affected by a small amount that nonetheless improves correlation with flight experiment. The difference in lateral control is approximately 5%, at most, of the available lateral travel of the pilot's control column. A comparison of the stability and control derivatives has not been presented, but the only noticeable difference in evidence is in pitch/roll and roll/pitch cross-coupling.

These results are, however, specific to one blade type that is known to be torsionally stiff. A more definitive statement is not possible without similar comparisons of a dissimilar blade type which has not been possible. It must also be remembered that inclusion of this simple model can, at best, emulate only quasi-steady elastic behaviour, in this case of only one torsion mode. Coupling with a full aeroelastic model is a major undertaking but is required if the full time-varying nature of the dynamic behaviour is to be captured, to include other modes and coupling with bending. This has been one of the aims of a related study sponsored by the CAA, and a summary of results is presented in Addendum 3.
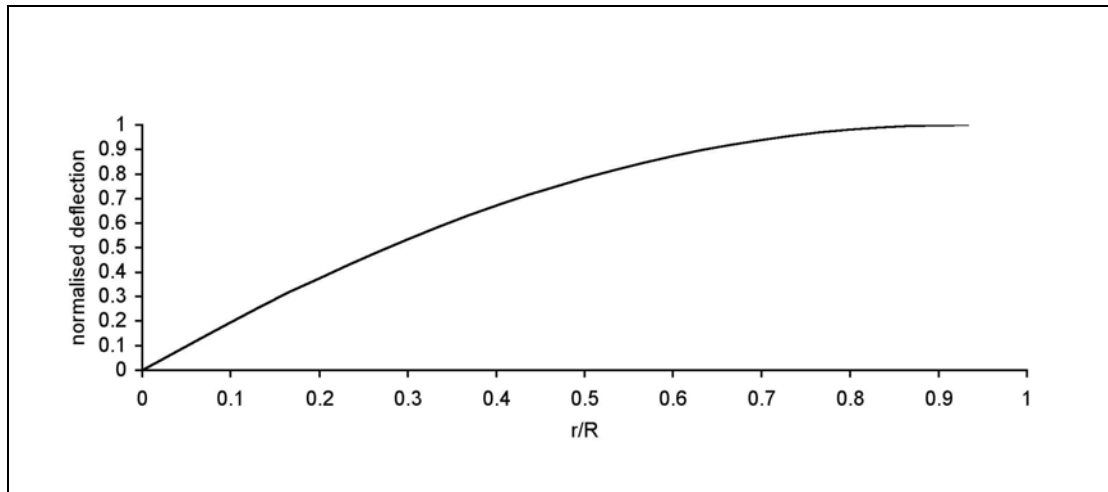
Figure 9.1   McCutcheon Blade Torsion Mode Shape
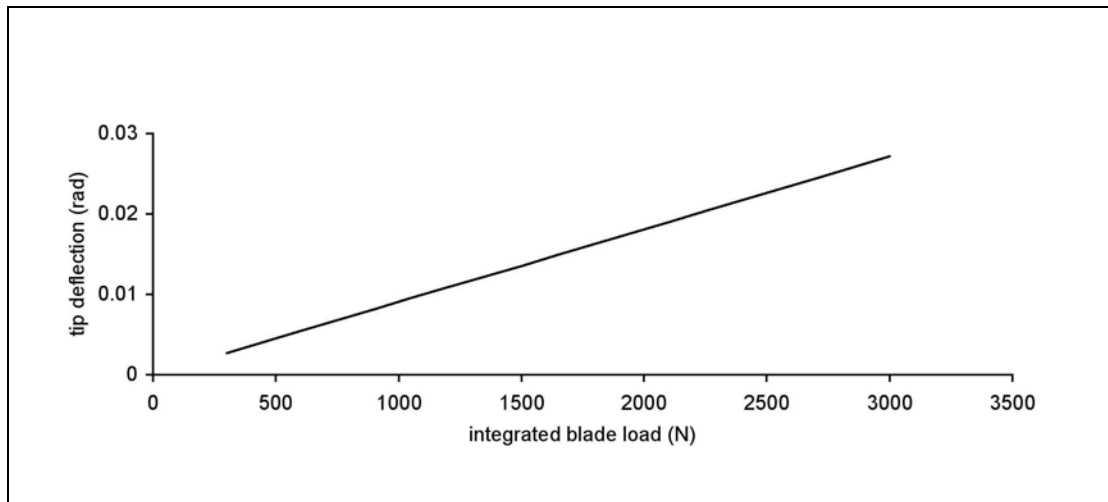
Figure 9.2   McCutcheon Blade Tip Torsional Deflection with Load
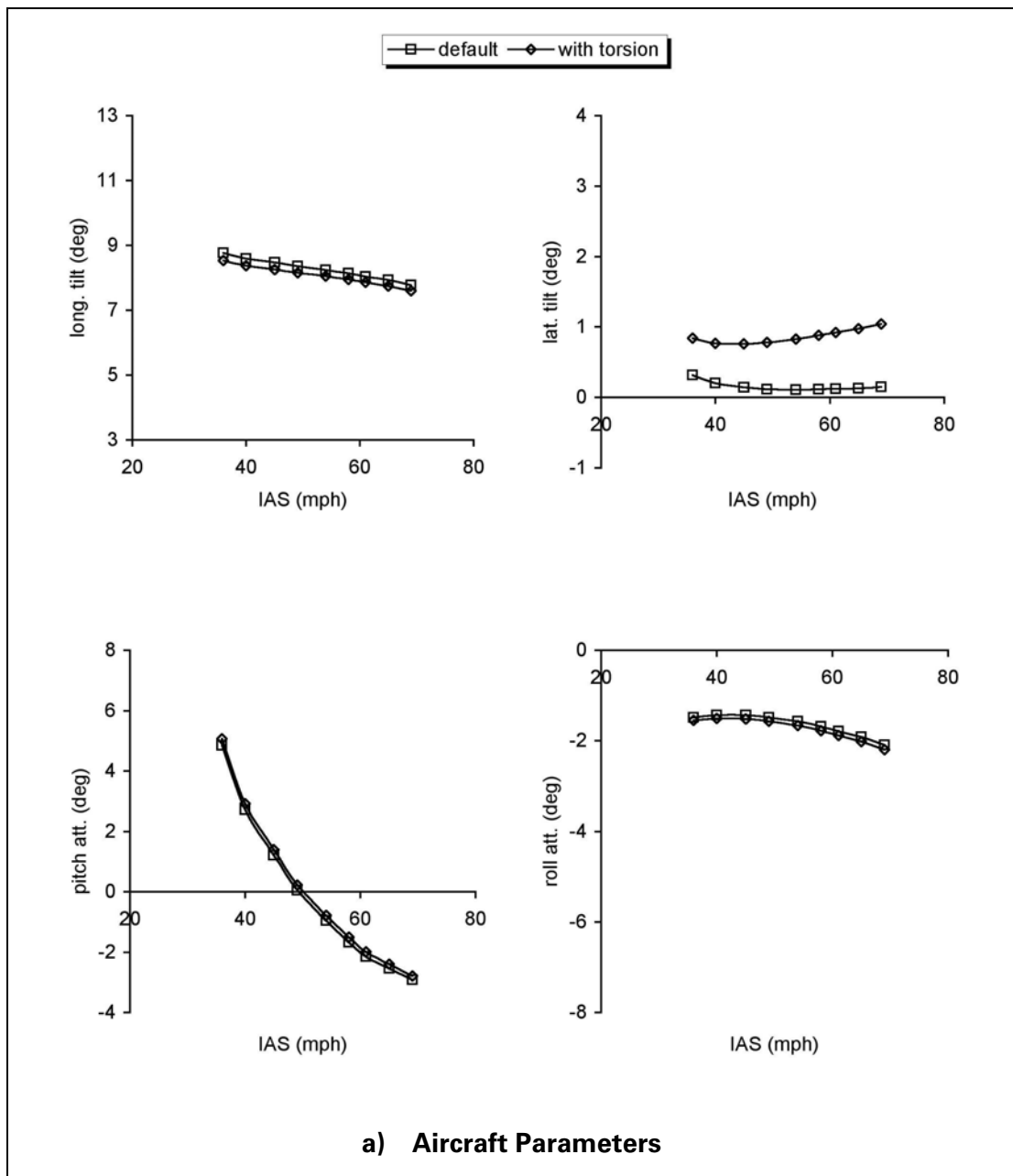
Figure 9.3   Effect of Including Simple Blade Torsional Model

b)   Rotor Parameters

Figure 9.3   Effect of Including Simple Blade Torsional Model (continued)

c)   **Dynamic Stability – Longitudinal Modes**

Figure 9.3   Effect of Including Simple Blade Torsional Model (continued)

d)   Response to BCAR Section T Compliance Demonstration Control Input
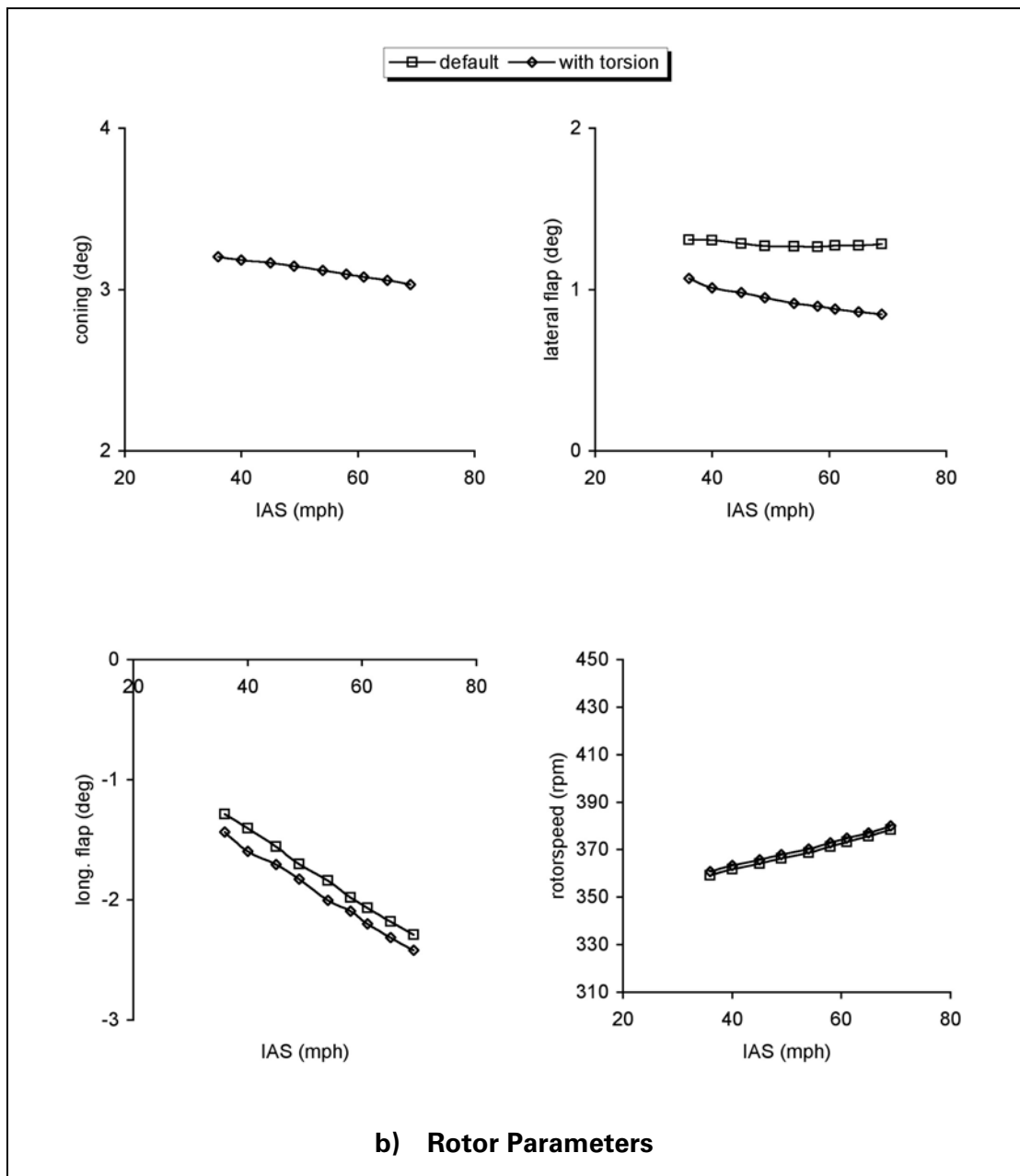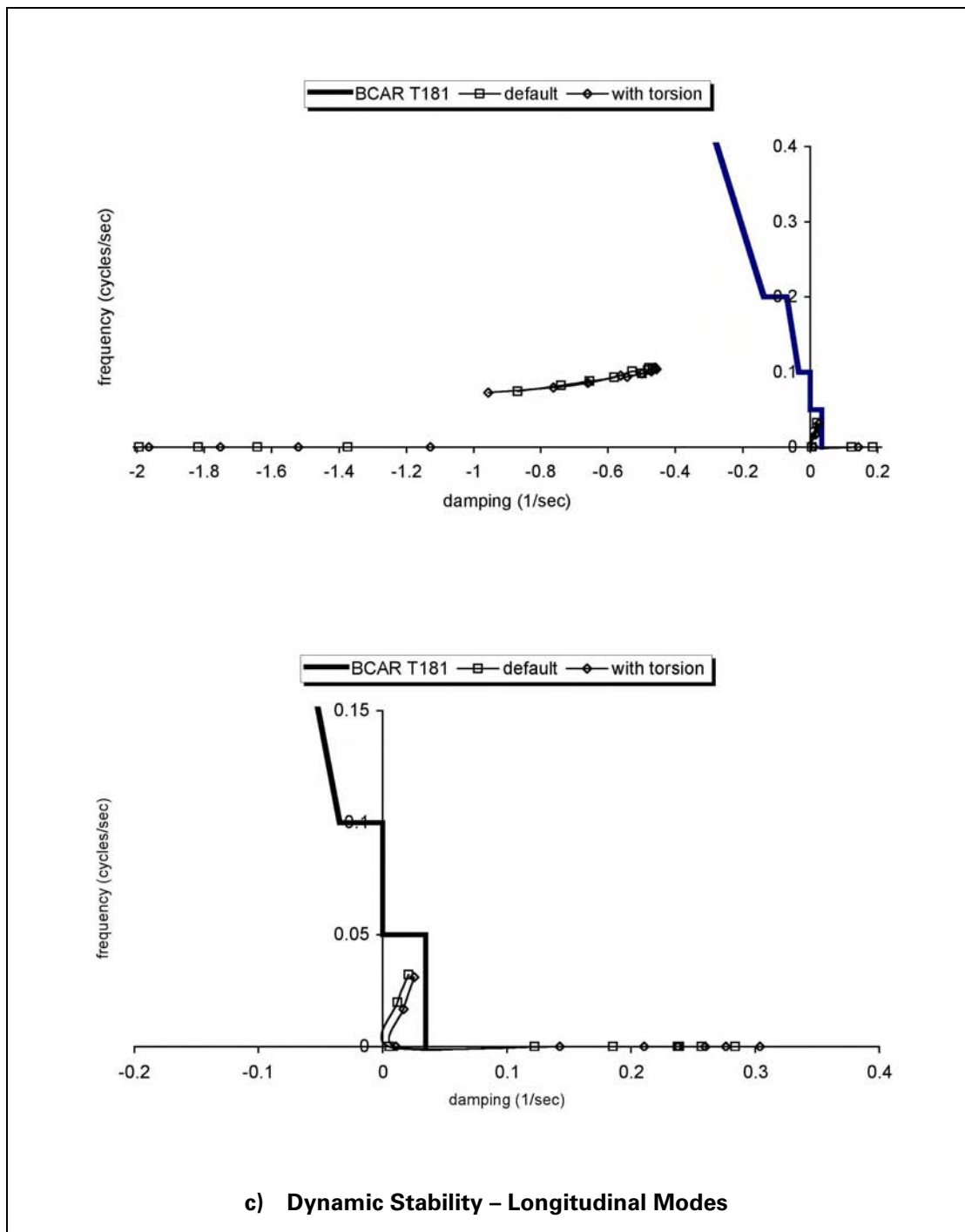
Figure 9.3   Effect of Including Simple Blade Torsional Model (continued)
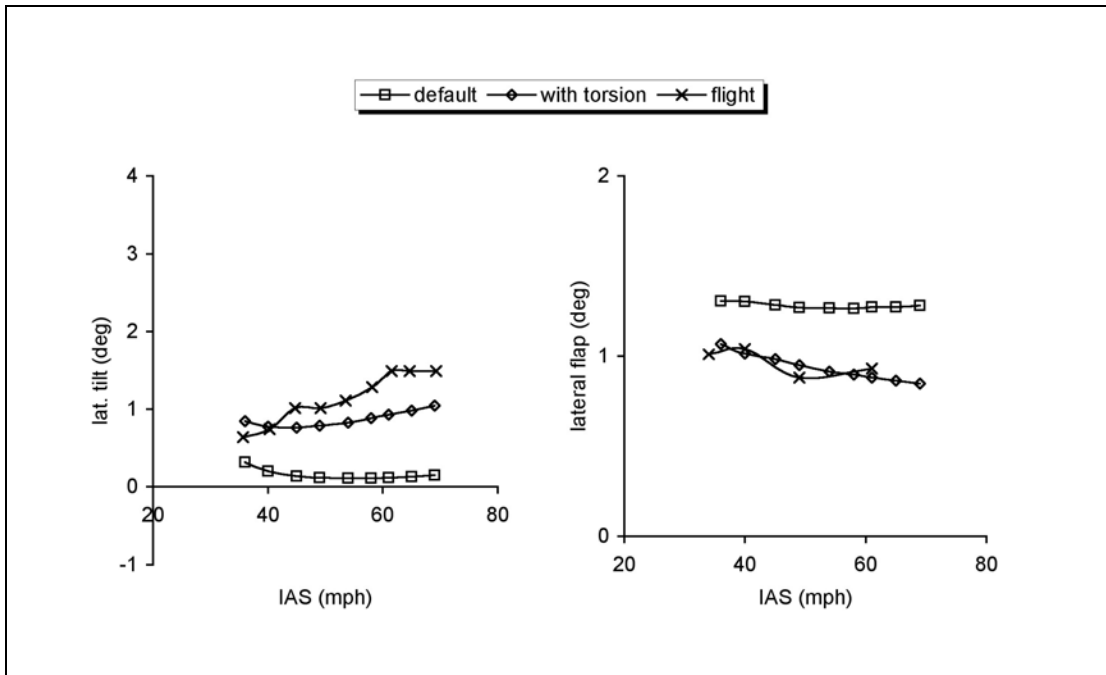
Figure 9.4   Correlation with Flight

10   A Simulation Study of Air Command Autogyros

10.1   Introduction

From the preceding chapters a general picture of gyroplane flight dynamics has been drawn, albeit with the focus on the test vehicles, a VPM M16, and a Montgomerie-Parsons. The successful validation of the RASCAL mathematical model against data from these aircraft allows its further use to predict the characteristics of other gyroplanes of the same class. Investigation of the Air Command series of gyroplane aircraft brings the work full circle, as it was a spate of fatal accidents to this type that initiated the study of gyroplane characteristics [1].

The essential result of the study is that, for the conventional light gyroplane operating at speeds up to 70 or 80 mph, only the vertical position of the centre-of-mass (c.g.) in relation to the propeller thrust line has a significant impact on the longitudinal characteristics of the aircraft across its speed range. Anecdotal evidence suggested that the effects of a low c.g. was consistent with experience in the pilot community. For example, one criticism of the Air Command was the low c.g. resulted in undesirable characteristics such as aft migration of the control column with increasing speed, reduced control margins at high speed and a substantial nose-down pitch change during low "g", high power manoeuvres.

Air Command analyses are, in a contemporary context, now only of academic interest as the type is no longer approved in the UK. However, the research reported in this section has an important objective, viz. to confirm that the correct relationship between propeller thrust line and c.g. location is the single most powerful design feature for endowing a gyroplane with good handling qualities that will satisfy BCAR Section T, across the speed range. Specific aims were first; to gather engineering data to allow RASCAL to be configured as single and two seat aircraft; second, to simulate both configurations and assess the results in the context of handling difficulties; finally, to assess the efficacy of the AAN modifications required to allow issue of a new Permit to Fly.

Full understanding of the impact of design changes on aircraft handling qualities can only be obtained if the reader is willing to grasp the concept of the stability derivative. Until this point in the report the stability derivative and its meaning have been consigned to appendices for the more curious reader to savour. However, in bringing the study of the aerodynamics of gyroplanes full circle it is necessary for the reader to grasp the physical importance of these mathematically abstract parameters. Classical fixed-wing modes of longitudinal motion are the phugoid and short-period. Helicopters can also exhibit similar behaviour, and Padfield [114] has presented and used appropriate approximations to these modes. These approximations emphasise the importance of the pitching moment stability derivatives M_u, M_w and M_q. The additional complicating factor with the gyroplane, to an extent that can only be quantified by the engineering model, is the rotorspeed degree of freedom. The rotorspeed, unlike the helicopter, is not governed but is free to vary with flight condition. It is therefore reasonable to assume that the derivative M_Ω might also have an impact on gyroplane longitudinal stability. Stabilising moments will be those for which:

$$M_u > 0$$
$$M_w < 0$$
$$M_q < 0$$
$$M_\Omega < 0$$

The latter derivative may not be familiar, even to helicopter flight dynamicists. The rationale for it to be stabilising if negative is as follows. Given an increase in rotorspeed, the rotor thrust will increase – if the aircraft then pitches nose-down, the reduced axial flow through the disc will in turn tend to reduce the rotorspeed.

The dominant forces and moments acting about the aircraft centre-of-mass are likely to be those of the main rotor and the propeller. In principle, rotor behaviour for a gyroplane will be the same as that for a helicopter, so the extensive theory of blade flapping behaviour developed for helicopters will also be applicable to the gyroplane.

For example, with a main rotor thrust line passing through the centre-of-mass in equilibrium flight, M_u will tend to be stabilising, and M_w destabilising. Simple rotor theory, e.g. Bramwell [83], explains that this is because a perturbation in u will result in the rotor disc flapping back and the thrust increasing, Figure 10.1. The tendency is therefore to pitch the aircraft up and hence to reduce the perturbation in u. Likewise, a perturbation in w will result in the rotor disc flapping back and the thrust increasing. The tendency is therefore to pitch the aircraft up and hence to increase the perturbation in w. A similar reasoning indicates that $M_\Omega>0$ would be destabilising.

However, with the gyroplane configuration the propeller thrust can be used to modify the location of the main rotor thrust line in relation to the centre-of-mass. For example, if the propeller thrust line is placed below the centre-of-mass, the consequent nose-up moment in equilibrium flight is balanced by placing the main rotor thrust line behind the centre-of-mass, Figure 10.2. The possibility then exists of producing a situation where M_w and M_Ω are now stabilising, with only M_u destabilising.

10.2   Analysis of Two-Seat Air Command G–BSSL

10.2.1   Flight Testing

The gradient of longitudinal stick position with speed is an important handling qualities parameter and, although derived from steady flight, is a measure of the dynamic stability derivative M_u. This derivative has been shown to have a significant impact on phugoid mode characteristics, particularly its frequency [114]. Hence one simple test can reveal much about static as well as dynamic stability. The two-seat Air Command, G-BOOJ similar to that shown in Figure 10.3, was used. The two-seater was chosen for reasons of availability and the additional safety afforded by having two crew. Measurements were averaged over two runs. Note that a different two seat Air Command, G-BSSL, was used for the static tests.

The geometry of the flight control system on this aircraft is such that fore and aft tilt of the rotor head is accomplished by, in effect, vertical movement of the stick, Figures 10.4 and 10.5. The quantitative measurements were taken simply with a 12 inch. ruler by the non-handling crew member. Figure 10.6 shows the stick position curves against speed, for an arbitrary datum (relative, rather than absolute data is all that is required for establishing gradient, and the datum of zero does not reflect a control limit, but rather the stick position in equilibrium flight at 40 mph). Conditions for the test were reported as flat calm.

A simple second order polynomial fit was made through these data, and differentiation of the polynomial with respect to airspeed then gives a linear equation representing stick gradient as a function of airspeed. This result is shown in Figure 10.7, together with results taken from Ref. 115. The VPM M16 results were obtained during the CAA-funded work using G-BWGI in 1996, and were recorded using the instrumentation system installed to support these tests. The RAF 2000 data was obtained in a similar manner to that for this Air Command exercise using G-BXDD. G-BOOJ data are converted to in/knot for consistency with Ref. 115. A stick/rotor tilt calibration was not available for the RAF 2000, hence VPM and Air Command flight results have been converted for consistency.

Airspeed calibration errors were unknown for both the Air Command and RAF 2000 aircraft and hence observations are difficult to compare directly. In general, however, the VPM demonstrates better speed stability than either of the other two aircraft at low to medium speeds. The Air Command and RAF 2000 speed stability is insensitive to airspeed changes, with the Air Command having better speed stability than the RAF 2000. However a previous study (Ref. 116) documents a single seat Air Command stick gradient of -0.045 inches/knot at 40 mph, but does not quantify the two seater result due to difficult test conditions, although this suggests that it is weaker that the single seat machine, i.e. less than -0.045 inches/knot. This is significantly dissimilar to the result presented in Figure 10.7 and serves to highlight the difficulty in reconciling different pilot opinion and assessment without on-board instrumentation.

10.2.2 Model Configuration

The aircraft is shown in Figure 10.8. Mass, c.g. and inertias were calculated from geometric measurements, wheel reactions and oscillation periods. Single point suspension was used for roll and pitch inertias, and a bifilar method [117] was used for yaw inertia calculation. The aircraft had zero fuel, and measurements were made with an 84 kg pilot on board. (Two sets of measurements were taken: with and without pilot. This allowed determination of pilot c.g., and hence calculation of weight and balance with the normal complement of two crew). The three methods used for determining single seat vertical c.g. could not be used with this aircraft, as with a pilot on board, it would not sit on its tailwheel. However, sufficient confidence has now been achieved with the incline method, that the result from a single test can be regarded as accurate. This method is now used at Glasgow University in preference to the single- or multi-point suspension for vertical c.g. calculation. The reaction at each of the three wheels is measured on a level surface allowing the longitudinal position of the c.g. to be found. The same measurements are then taken on an inclined surface which, by simple geometry, allows the vertical location also to be determined, see Appendix 3.

Table 10.1 presents the mass-related properties of the aircraft, together with the location of the propeller. The reference point for all measurements was one of the bolts through the mast plates approximately half-way up from the keel. The engine is inclined 3 deg downwards relative to the aircraft datum, resulting in the normal distance from the propeller axis to the c.g. being 4.5 in. Note that this configuration is an extrapolation of measurements taken with the 84kg pilot, but now assuming two crew, which gives the worst case in terms of vertical c.g. position.

Table 10.1   Calculated Mass and Inertia Properties, from Measurements

Quantity	Value
mass	310.2 kg
c.g. location	(0.2502,0,0.2590) m
propeller location	(-0.625,0,0.100) m
I_{xx}	73.0 kgm^2
I_{yy}	160.0 kgm^2
I_{zz}	90.0 kgm^2

Other measurements were taken to allow creation of a datafile for the RASCAL simulation program, which are summarised in Table 10.2. The lift curve slope for the various aerodynamic surfaces is based on previous experience with the VPM wind tunnel model. This may be of limited applicability for the pod, which unlike that of the single seat aircraft, is dissimilar to that of the VPM in terms of planform, shape and outline. The rotor blades are of NACA 8H12 section, data for which is published in Ref. 92. Note that rotor radius is increased relative to the single-seat aircraft.

Table 10.2   Measured Geometric Properties

Quantity	Value
rotor radius	3.8105 m
rotor location	(0,0,-0.877) m
pod frontal area	0.94 m^2
pod plan area	1.57 m$_2$
pod side area	1.57 m$_2$
fin area	0.69 m^2
tailplane area	0.47 m^2
pod drag coefficient	1.0
pod lift-curve slope	1.0 /rad
tailplane lift-curve slope	2.0 /rad
fin lift-curve slope	3.5 /rad

10.2.3 Results

Simulations were conducted in three configurations: the aircraft with both the pod and horizontal stabiliser fitted (compliant with the 1994 AAN produced to return the aircraft to flight following grounding); without these modifications (i.e. the configuration at the time of the fatal accidents); and finally without the AAN modifications but with the engine thrust line tilted down by 10 deg rather than 3 deg, the additional 7 deg. required to place the thrust line and c.g coincident. This may then be considered as an alternative modification to the AAN whose principle aerodynamic effect, inter alia, was to introduce a pod and tailplane. The results therefore quantify the effect of the principal changes arising from the modified AAN against a simple thrust line modification. Note that the simulations were configured for zero fuel and two crew, which as noted above gives the worst case in terms of c.g. position.

Figures 10.9, 10.10 and 10.11 show comparisons of the trim, principal longitudinal stability derivatives and stability roots, between 40 and 75 mph. The 1994 AAN modifications have little impact on the trim, stability and hence BCAR Section T compliance characteristics. However, simply tilting the engine thrust line down by 10 deg as opposed to 3 deg renders the aircraft stable in the phugoid (that is the real part of the eigenvalues are now negative), and Section T compliant across the speed range, that is the eigenvalues for the phugoid move from the right, non-compliant side of the boundary to the left compliant side.

The other main effect of the thrust line modification is on the trim of the aircraft. The model predicts that the hub tilt would be about 2 deg further forward, and pitch attitude about 2 deg more nose-up across the speed range. Again, M_u is reduced in magnitude, as predicted by elementary consideration of the rotor and propeller forces presented earlier in Section 10.1. Reduction in M_u will tend to reduce the frequency of the phugoid oscillation, i.e. increase the period. Note that M_w is rendered negative (stabilising) with the thrust line modification which will tend to improve the damping, i.e. reduce the instability. The pitching moment due to rotorspeed changes (M_Ω) is also more stabilising with the thrust line modification. The phugoid mode is now stable throughout the speed range, i.e. the eigenvalues remain to the right of the vertical axis within the stable region (as frequency is plotted against damping ratio - see Appendix 4) and with positive damping causing the amplitude of any oscillatory motion to decay. The modified aircraft would easily satisfy Section T.

10.3   Analysis of Single-Seat Air Command G–BRLB

10.3.1   Model Configuration

This aircraft is shown in Figure 10.12. Once again, mass, c.g. and inertias were calculated from geometric measurements, wheel reactions and oscillation periods. Single point suspension was used for roll and pitch inertias, and a bifilar method was used for yaw inertia calculation [117]. The aircraft had zero fuel, and all measurements were made with a 78 kg pilot on board. Three methods of measuring vertical c.g. were used: suspension; wheel reaction when sitting on an incline, nose-up; and wheel reaction when sitting on an incline, nose-down. The three methods produced a range in vertical c.g. position of $\pm$ 1.2 in, with the mean value being used in simulation. Note that three tests were performed to provide confidence in the final result however, subsequently it has been accepted that a single carefully conducted test using the inclination method should provide results with sufficient accuracy.

Table 10.3 presents the mass-related properties of the aircraft, together with the location of the propeller. The reference point for all measurements can be seen on Figure 10.4, as the top aft bolt on the engine suspension plate immediately behind the crew seat. This places the propeller 0.625 m behind and 0.1 m below the reference point, corresponding to a point mid-distance between the front and aft faces of the propeller hub. The engine is inclined 3 deg downwards relative to the aircraft datum, resulting in the normal distance from the propeller axis to the c.g. being 3-5 in, depending on measurement method.

Table 10.3   Measured Mass and Inertia properties

Quantity	Value
mass	240.5 kg
c.g. location	(0.1574,0,0.2376) m
propeller location	(-0.625,0,0.100) m
I_{xx}	70.8 kgm^2
I_{yy}	130.1 kgm^2
I_{zz}	60.0 kgm^2

Table 10.4   Measured Geometric Properties

Quantity	Value
rotor radius	3.5075 m
rotor location	(-0.0160,0,-0.877) m
pod frontal area	0.33 m^2
pod plan area	0.85 m$_2$
pod side area	0.65 m$_2$
fin area	0.47 m^2
tailplane area	0.38 m^2
pod drag coefficient	1.0
pod lift-curve slope	1.0 /rad
tailplane lift-curve slope	2.0 /rad
fin lift-curve slope	3.5 /rad

Other measurements were taken to allow the creation of a datafile for the RASCAL simulation program. These are summarised in Table 10.4. Note that the lift curve slope for the various aerodynamic surfaces is based on previous experience with the VPM wind tunnel model. The rotor blades are of NACA 8H12 section, data for which is published in [49].

Simulations were, again, conducted in three configurations: compliant with the 1994 AAN; the basic aircraft; and with the thrust line modification applied to the basic aircraft.

The single and two seat aircraft are almost identical geometrically apart from the pod, minor dimensional differences in the rotor head and, of course, the rotor diameter.

10.3.2   **Results**

Figure 10.13 shows the trim comparisons between 35 and 75 mph, the upper speed being some 10 mph faster than V_{ne}. It is clear that the pod and tailplane have an insignificant impact on trim. Note that the model predicts the aircraft to have positive speed stability, since the longitudinal tilt of the rotor spindle is increasingly forward with increasing speed.

Figure 10.14 shows the principal longitudinal stability derivatives across the same speed range. The positive speed stability is confirmed by M_u>0, but the angle of attack stability is negative, since M_w>0. The stability roots associated with the model put these derivatives in the context of dynamic stability and Section T compliance, Figure 10.15. In terms of dynamic stability, there are insignificant differences between the AAN-compliant version and unmodified aircraft other than at high speed where the modified aircraft is less unstable. However, both configurations fail to comply with Section T and, again, it is only the thrust line modified version that satisfies Section T.

10.4   **Discussion**

If the Air Command aircraft did have a handling qualities problem, it was likely to lie in poor phugoid mode characteristics. Simulation tends to suggest a very unstable mode, whether fitted with pod and tailplane as required by the current AAN or not. However, the instability is not too dissimilar to some unaugmented helicopters, e.g. the Lynx, and any pilot difficulty with the Air Command was likely to be due to either lack of currency, recency or experience, or the fact that the mode has a high natural frequency (almost 1 cycle every 10 sec) relative to other aircraft. Indeed, existing criteria for phugoid mode characteristics [100] were previously applied to the VPM M16 flight data, but these criteria do not extend to the relatively high frequency that is suggested by the Air Command simulation, so it is impossible to grade the aircraft in these terms.

However, the RASCAL mathematical model has known limitations in respect of simulation of the VPM M16, specifically with regard to the phugoid. This was isolated to the drag damping X_u which was significantly overestimated by simulation. (Phugoid damping is determined primarily by drag damping X_u although an increasingly positive M_w will tend to destabilise this mode). It is by no means certain that these limitations map directly across to validity in respect of other types. The model may be more or less valid for simulation of the Air Command types but, without a full validation exercise that is type-specific, this cannot be assessed. The simulation model is known to be optimistic in respect of the prediction of VPM M16 drag damping X_u, and this directly affects the damping of the mode of most concern to the Air Command problem. If this optimism reads across to the Air Commands, the degree of instability highlighted earlier will be even worse.

If there is concern regarding the applicability of the model for analysing the Air Command, the actual physical measurements of speed stability (weight, balance, inertia etc.), constitute valuable entities in their own right that communicate much about the real aircraft. For example, a low c.g. position will result in an arrangement of forces and resulting moments that will tend to be destabilising. Hence the low c.g. of both single and two-seat Air Commands points to a potential problem with pitch axis handling qualities, but will not, in isolation be sufficient to quantify this problem. The measurements from the very limited flight testing that was conducted are the most that can be attempted without instrumentation, but the results can be related directly to the prediction of speed stability and the derivative M_u. Speed stability is comparable to the VPM M16, and better than the RAF 2000.

The low c.g. position has a direct influence on the angle of attack stability M_w, as highlighted in Section 10.1 earlier. The simulation model has been demonstrated to be excellent for predicting VPM M16 M_w across the speed range. If this is also true for the Air Command aircraft, the impact on this derivative of increasing engine inclination from 3 to 10 deg has been accurately modelled. The stabilising influence of the modification will therefore also be accurately modelled.

A final point relates to observations of differences in control stick geometry. The two-seat variant was fitted with a 'pump-action' stick; perhaps they should have been fitted with a more conventional control stick that displaced in a fore-and-aft sense, rather than vertically. The already good speed stability might therefore have been translated into a conventional, and therefore readily interpreted form, for the pilot. It seems odd that pilots trained on the two-seater with one stick geometry, but had to progress onto the single-seater with fundamentally dissimilar control geometry.
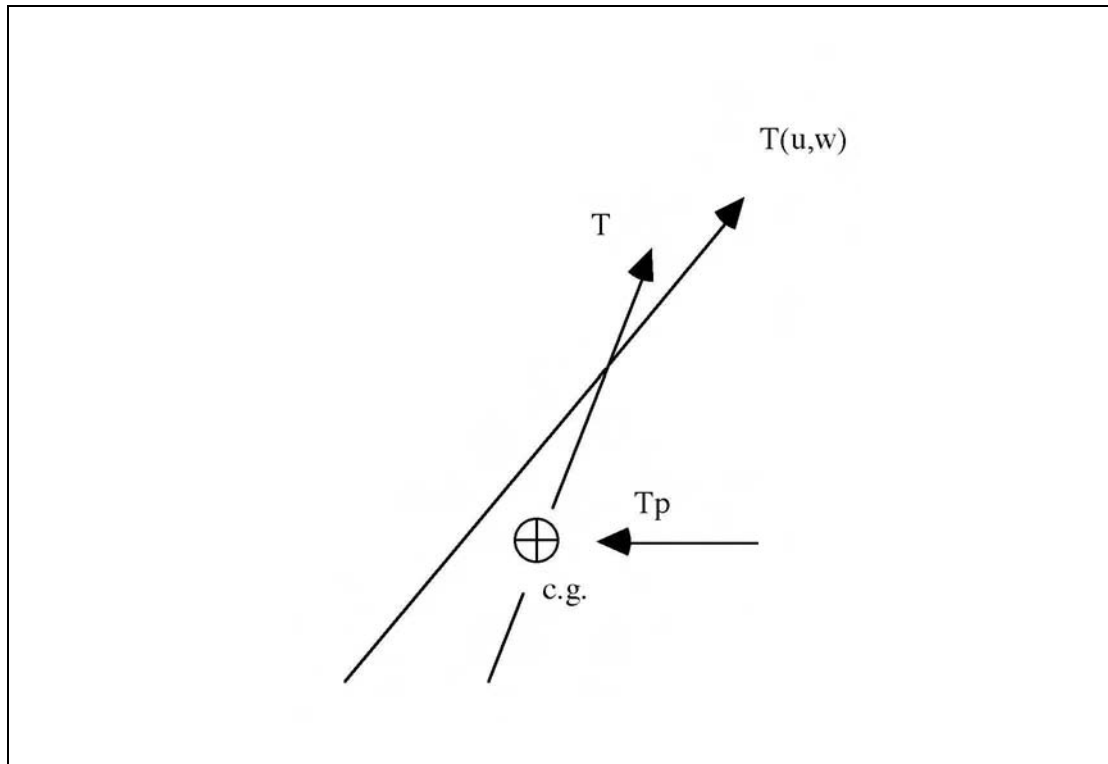
Figure 10.1   Schematic of Main Rotor Thrust Line Relative to c.g. in Undisturbed and Disturbed Flight - Propeller Thrust Line Passing Through c.g.
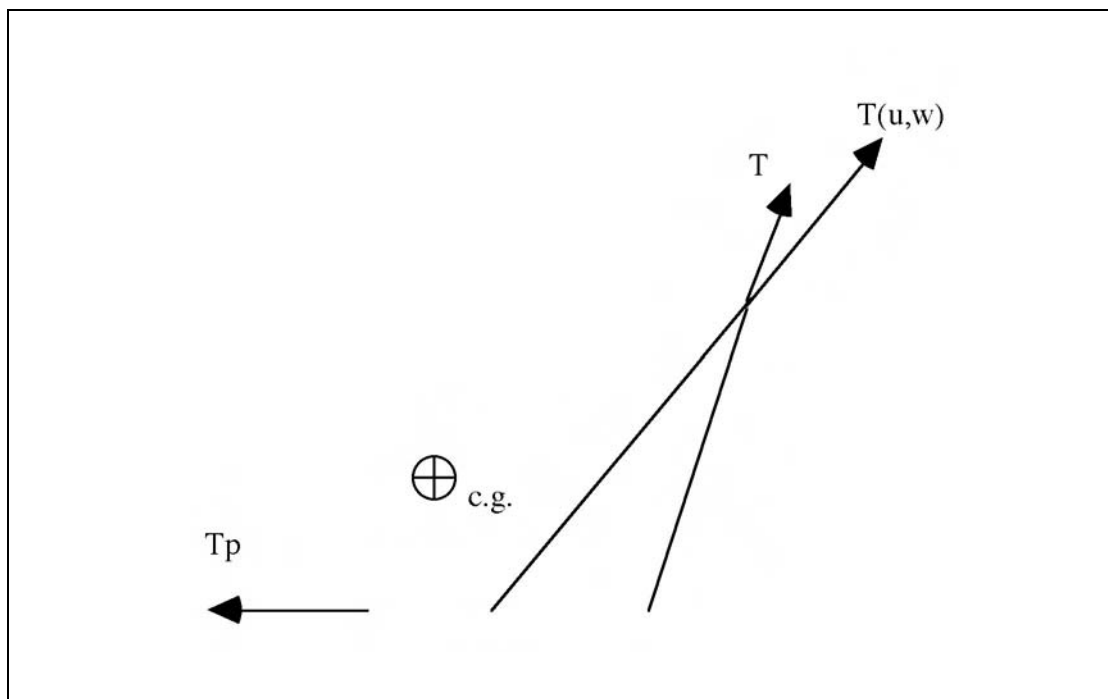
Figure 10.2   Schematic of Main Rotor Thrust Line Relative to c.g. in Undisturbed and Disturbed Flight - Propeller Thrust Line Passing Below c.g.

Figure 10.3 Two seat Air Command

Figure 10.4 Stick Fully Aft

Figure 10.5   Stick Fully Forward
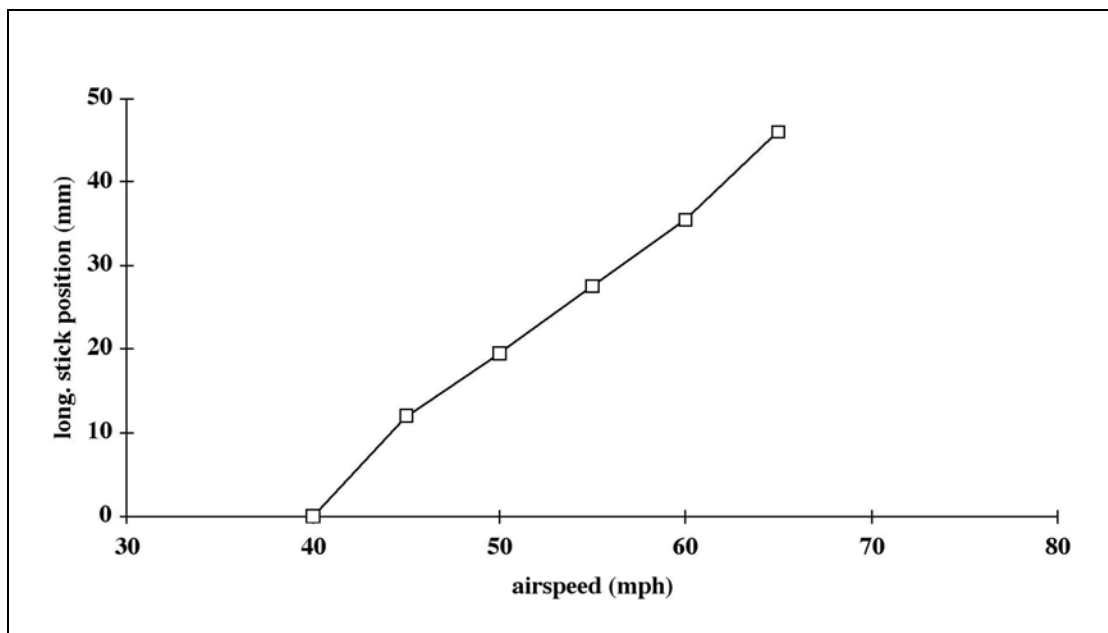
Figure 10.6   G-BOOJ Stick Position with Airspeed
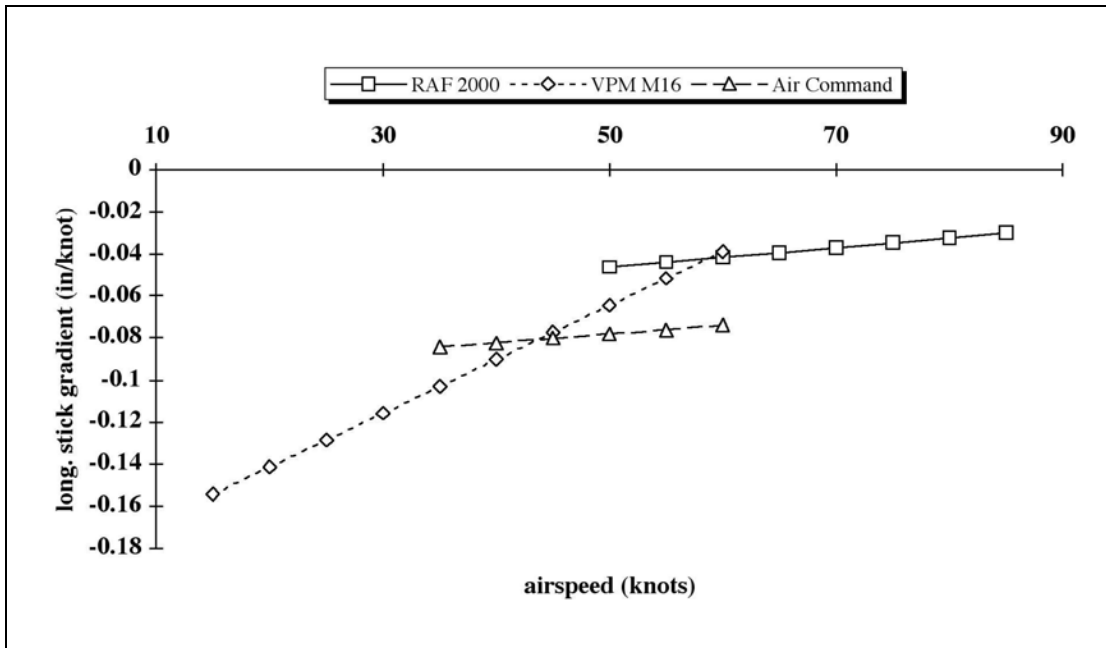
Figure 10.7   Stick Gradient Comparisons

Figure 10.8   Two Seat Air Command G-BSSL
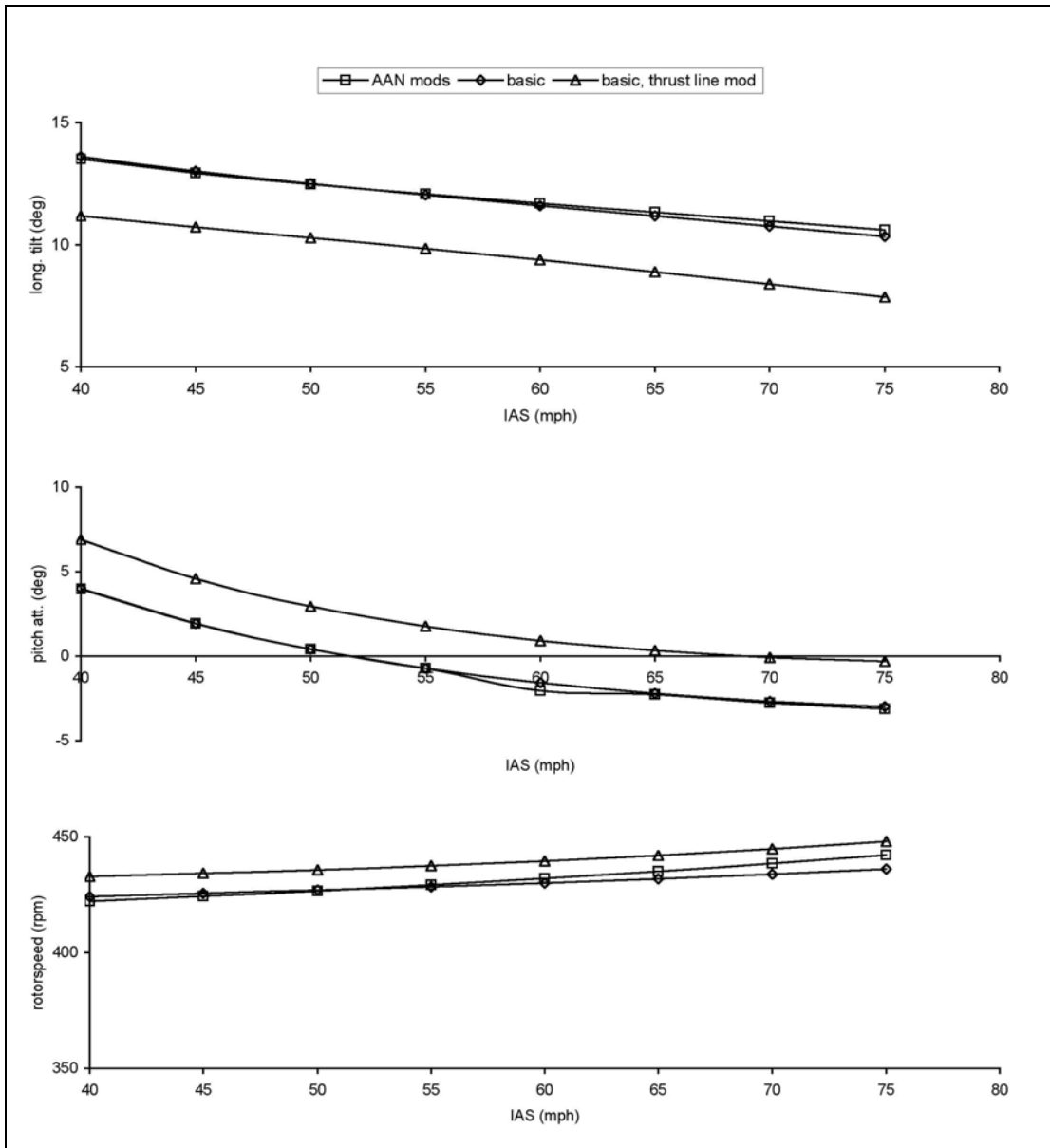
Figure 10.9   Trim Comparisons, Simulation of G-BSSL
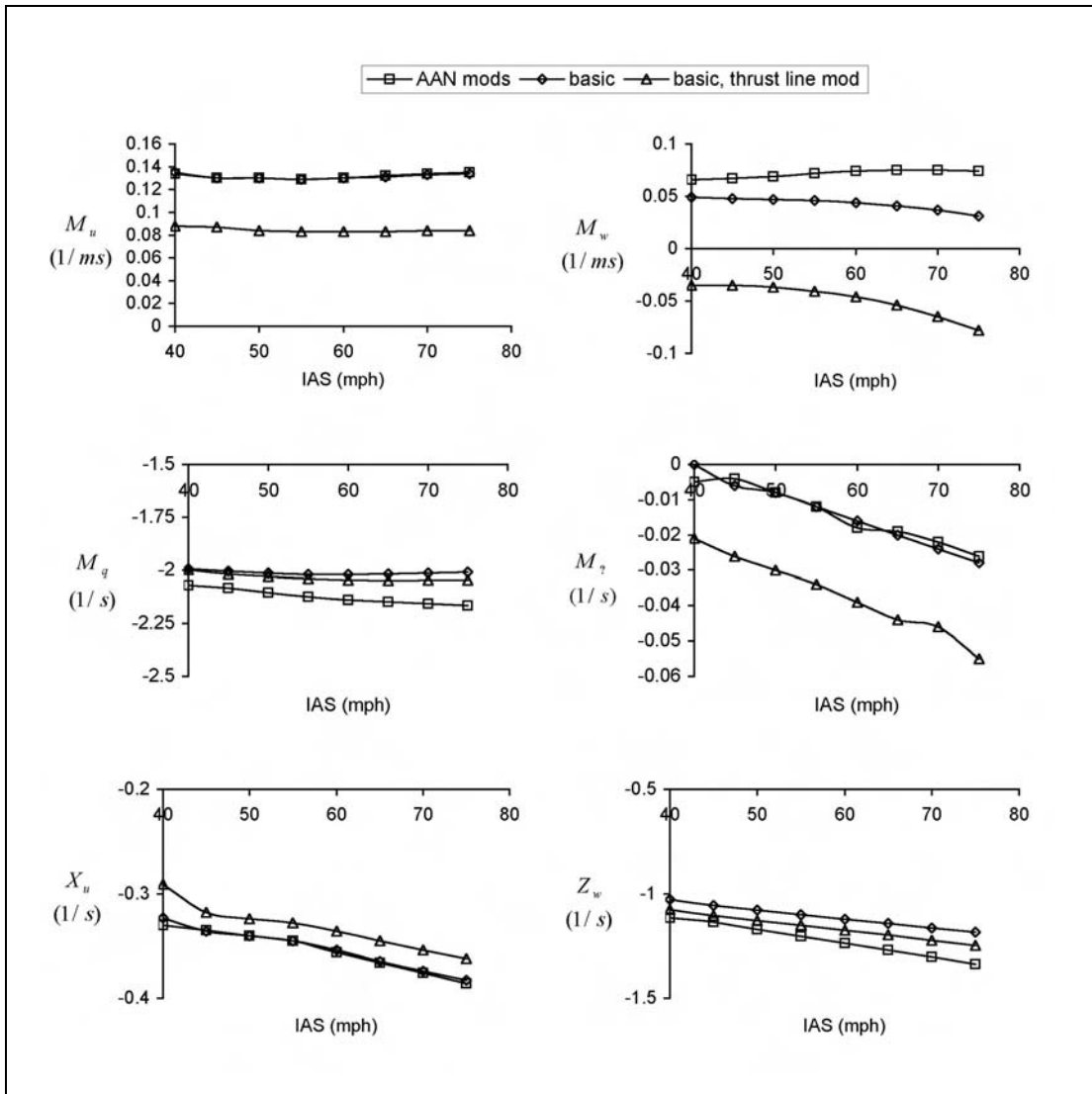
Figure 10.10 Derivative Comparisons, Simulation of G-BSSL
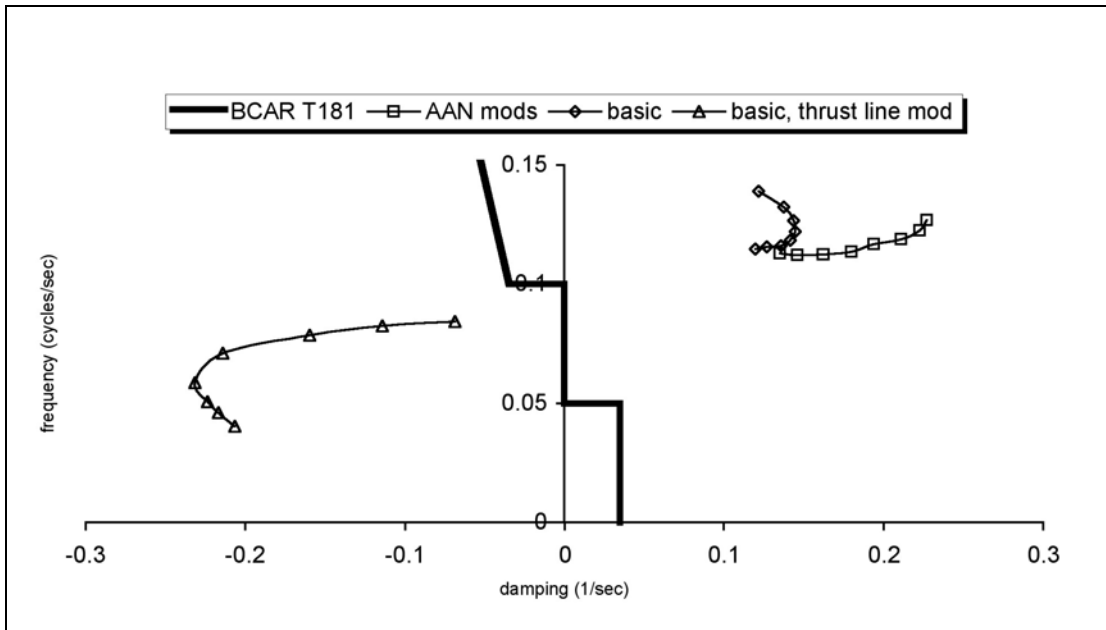
Figure 10.11   Comparison of Longitudinal Stability Roots

Figure 10.12   Single Seat Air Command G-BRLB
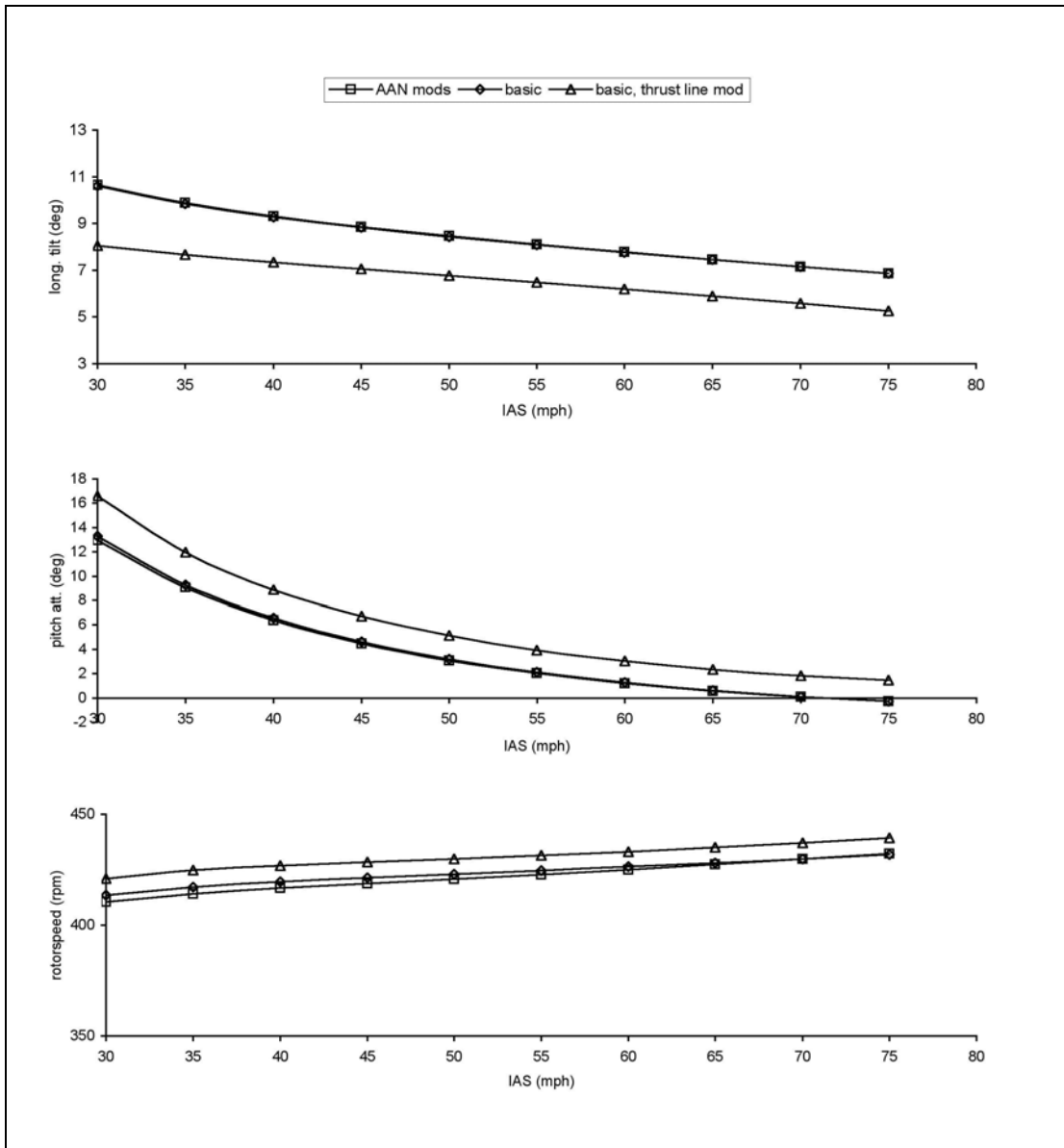
Figure 10.13 Trim Comparisons, Simulation of G-BRLB
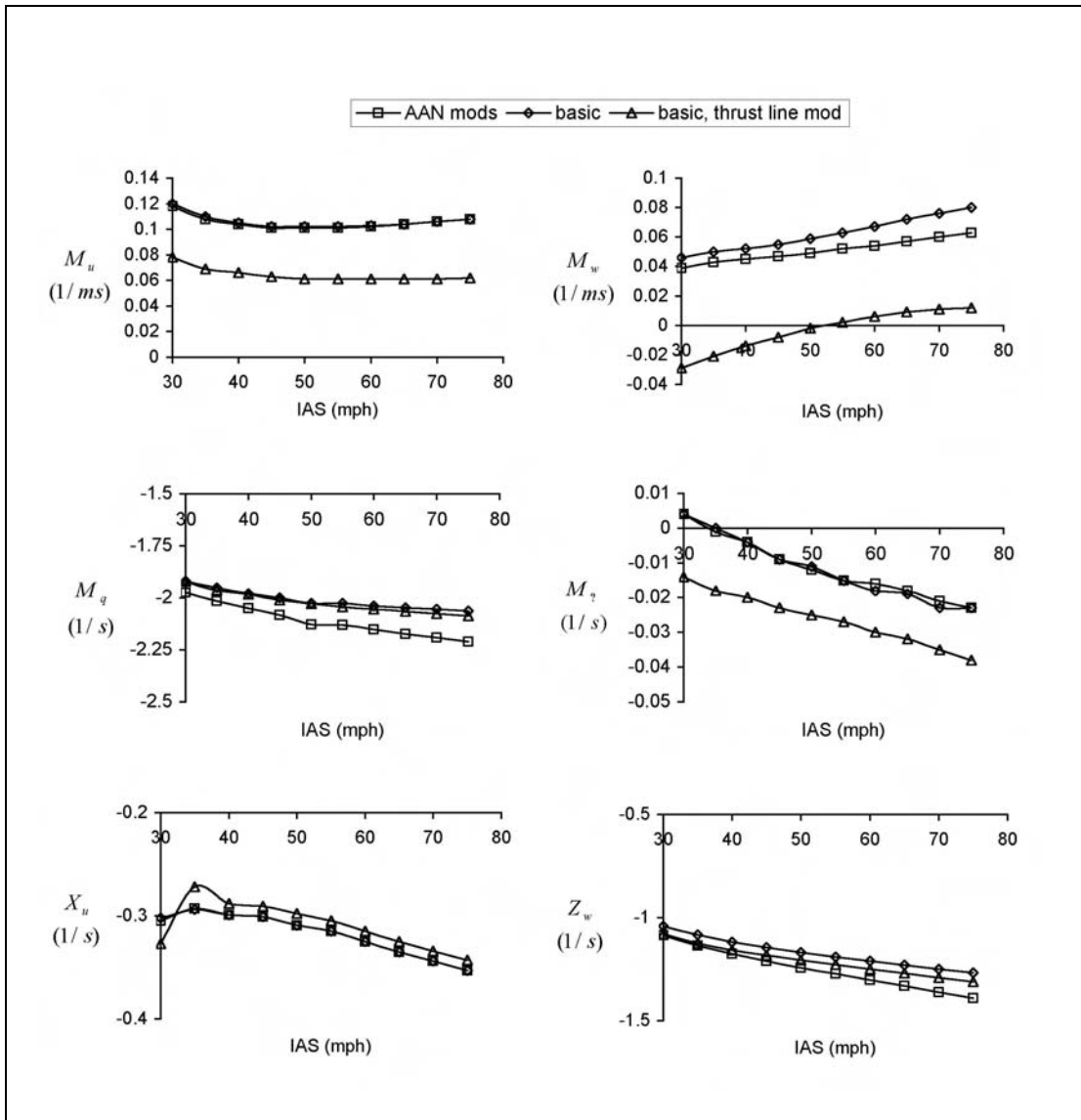
Figure 10.14 Derivative Comparisons, Simulation of G-BRLB
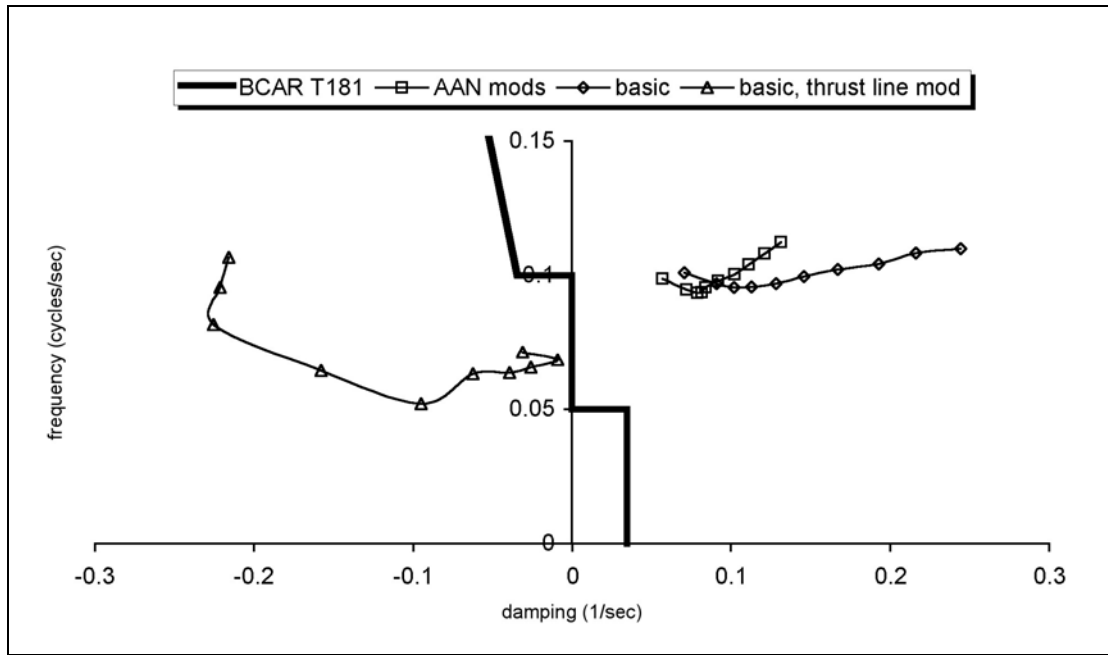
Figure 10.15 Stability Comparisons, Simulation of G-BRLB

11 Investigation of Gyroplane Rotor Teeter Motion

11.1 Introduction

Sufficient rotor teeter margin is a compliance demonstration requirement of BCAR Section T. This requires flight beyond the flight envelope boundary (V_{NE}) where nothing is known about teeter behaviour. Indeed teeter angle measurements have not previously been measured in flight. There is sufficient evidence (factual and anecdotal) to suggest that teeter angles can be excessive in certain circumstances, and can lead to blade strike with the propeller, pod or mast. There is therefore a need to take such measurements to establish just how significant teeter motion is, and whether it can have implications on aircraft safety. This will have secondary value both for use as further data for validation of the simulation model, and in the continued development of BCAR Section T.

11.2 Teeter Angle Measurements

One of the unique aspects of this series of flight tests was that this is the first time that a gyroplane rotor's teetering motion has been recorded. Detail of the experimental procedure is given in Section 5 of this report. Figure 11.1 shows the complete recording of teeter angle for flights 2 - 4 sampled at a rate of 200Hz. Note that the total recording time begins before the aircraft is started up and continues to record all data until the total record time has elapsed. For example, for flight no 2 the total recording time was 50mins (3000s), the first 500s (approx) represents the aircraft on the ground prior to engine start, and the final 500s (approx) is the aircraft back on the ground engine off. The very large teeter angles measured at the start and end of each recording are due to the rotor teetering due to wind or ground handling. Referring to the data for the remainder of the flight it is clear that the teeter angle remains small for most of the flight (less than ±5 degrees). The blade time histories shown in Figure 11.1 are referred purely to a time base and it is difficult to establish at which points on the azimuth that the peak values of teeter occur.

Figure 11.2 shows the disc tilt angle for flight 2. This shows the disc tilted aft (-ve) by about 1.5 - 2 degrees and by a similar amount to the right (+ve) over most of the flight. Figure 11.3 shows the disc tilt angles for flight 3. This particular flight was focused on dynamic testing with a series of pulse and step inputs applied. Despite this, the disc tilt angles are still small with the disc tilting slightly aft and to the right relative to the hub. Finally, the disc tilt angles for flight 4 are given in Figure 11.4, and, as before, small angles are observed for most of the flight.

11.3 Aircraft Response in Recovery from Large Amplitude Stick Displacement

Figures 11.1–11.4 show relatively small teeter angles during most of the flights. The exception to this observation is an event just before 1000s during Flight No. 4 (see Figure 11.1 and Figure 11.4). For a short period of time teeter angles of ±8 degrees were recorded. Figure 11.5 shows the teeter angle time history for the few seconds around this event. The very rapid increase in teetering is evident. This is a significant occurrence as the allowable range as quoted by the manufacturer is ±9 degrees. It should be noted that on the ground the physical restraint (i.e. the teeter stop) permits teetering motion beyond the manufacturer's quoted limits. This can be observed in Figures 11.1–11.4 where teeter angles of ±12 degrees (the design range of the sensor) are recorded in ground handling.

This occurrence corresponds to a recovery from a 1 inch step input of forward stick at a flight speed of 60mph. Although a 1 inch step was requested, evidence from the stick displacement transducer indicates a displacement somewhat larger than this. Given the rudimentary design of the aircraft cockpit it is extremely difficult to apply

control inputs of a particular amplitude with great accuracy. This event is presented in more detail by examining the 20s from 940s to 960s on the recording, Figure 11.6. The forward stick input is shown on the first plot which is, in effect, of shaft tilt angle, a forward stick input is applied which gives 4 degrees forward shaft tilt. The immediate effect is for the nose to pitch down to -20 degrees, airspeed to increase from a nominal 60mph to around 75 mph, and most surprisingly, rotorspeed increases dramatically from around 360rpm to 450rpm. The aircraft clearly has entered an uncomfortable flight state and the pilot has had to take rapid action to recover. The recovery involves a sudden chopping of power and an aft stick displacement equivalent to around 6 degrees of shaft tilt at roughly 950 seconds. The aircraft then begins to recover its attitude and airspeed, and rotor speed decays to its original values.

It is clear that the aircraft has experienced a severe manoeuvre, and that large teeter angles have been observed. The question arises as to where exactly the maximum teeter occurs in the azimuth. Figure 11.7 shows the teeter angle plotted against azimuth for the several revolutions of the blade during the period 948 - 952 seconds. It is clear that the peak value of teeter is occurring at around 220° of azimuth. The sensor is calibrated such that 180° is the rearmost position, and noting that the rotor is rotating in an anti-clockwise direction, the blade is reaching its maximum teeter in a location just over the pilot's right shoulder.

It should be noted that the teeter angle reaches a maximum of 7° in the 180° position raising the question of whether a propeller strike in flight is possible.

11.3.1   **Ground Checks on Propeller Clearance**

The results described above prompted a series of ground tests on the aircraft to determine propeller clearances in conditions where large teeter angles occurred. The first thing to note is that the strike plate which limits teetering motion is ineffective - with the stick fully aft the blade can be teetered through the plane of the propeller until its tip touches the ground, Figure 11.8. In this position there is still around 2cm of clearance between strike plate and under surface of the blade. To replicate the flight state observed during Event 1 of Flight 4, the stick was held in an aft position, and a teeter angle of 8° applied to the rotor, Figure 11.9. The clearance between the tip of the propeller and the under surface of the blade was 5cm. In comparing this with the actual event, it should be noted that in the ground test the stick was fully aft, and in flight there would be some coning of the blades providing additional clearance. Finally, the lowest position of the blade (i.e. maximum teeter occurs at around 220° of azimuth, Figure 11.7) which is to the side of the propeller disc. These three factors combined suggest that in flight the clearance is likely to have been a little greater than the 5cm measured on the ground.

The final test performed was to estimate the minimum teeter angle required to cause a blade strike on the propeller. The stick was held in its fully aft position to provide the worst possible situation. The blade was then teetered until it touched the tip of the propeller, Figure 11.10. The measured teeter angle was 11.1°. Again it should be stressed that this is the worst case - with the stick in a more central position, taking into account coning and the off-centre position for maximum teeter, a teeter angle in excess of 11.1° would likely be required to cause a strike in flight.

11.4   **Concluding Remarks**

The following three conclusions are based on the results presented in this paper, which were recorded during flight trials in the period 20-21st July 2005.

1   The rotor teeter angle is very small in all steady flight states.

2   In typical transient manoeuvres teeter angles equivalent to one third to one half of the allowable range are observed.

3   A single event indicates that gross manoeuvres can excite teeter motion such that the teeter angle can approach its limits. This has implications in recovery procedures from unusual flight states.

The data gathered has addressed a lack of knowledge of rotor teetering behaviour and has confirmed the applicability of a proposed change to BCAR Section T 143 (a) (Interpretive Material). The current issue of BCAR Section T (Issue 3) has interpretive material in support of T 143 (a) that states:

"The gyroplane's V_{NE} will normally be dictated by the need to have a positive teeter margin up to V_{NE}+15%".

Concern has been expressed that it is improper to relate an acceptance criteria to an airspeed 15% greater than V_{NE} and, hence, 4% greater than V_{DF}. Furthermore, available technology does not provide for a ready means of measuring rotor teeter angle and until the flight test programme described above, teeter angle had not been measured in flight. Following this work, alternative text requiring demonstration of satisfactory flight characteristics at speeds up to 1.11 V_{NE} has been drafted by the CAA.

Consequently, the CAA has proposed that the next issue of Section T should contain the following revised text for AMC T 143 (a):

"….. it will be expected that satisfactory flight characteristics have been demonstrated at speeds up to 1.11 V_{NE}. This demonstration must include satisfactory control margin and rotor clearance."
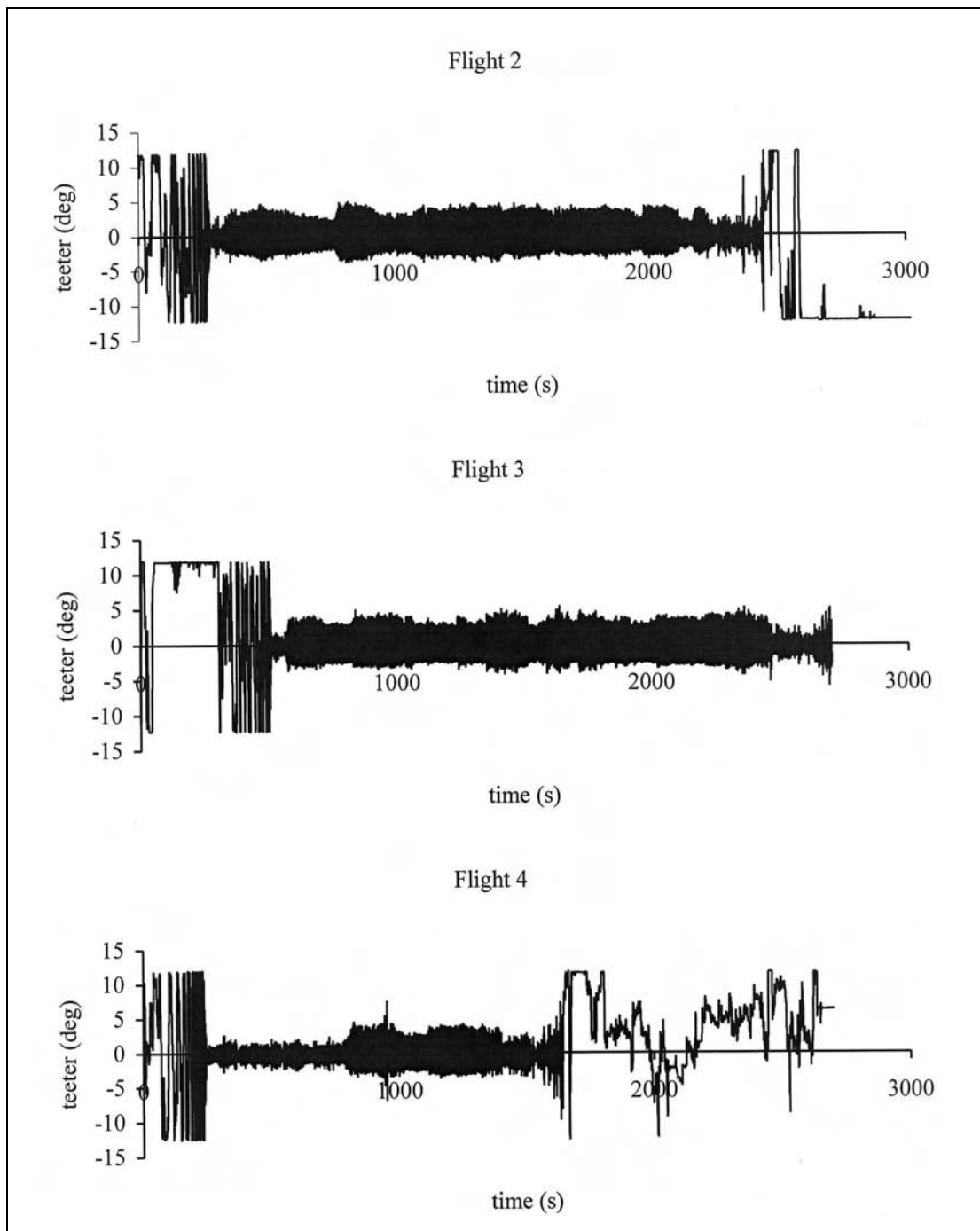
Figure 11.1   Blade Teeter Angles for all 3 Flights
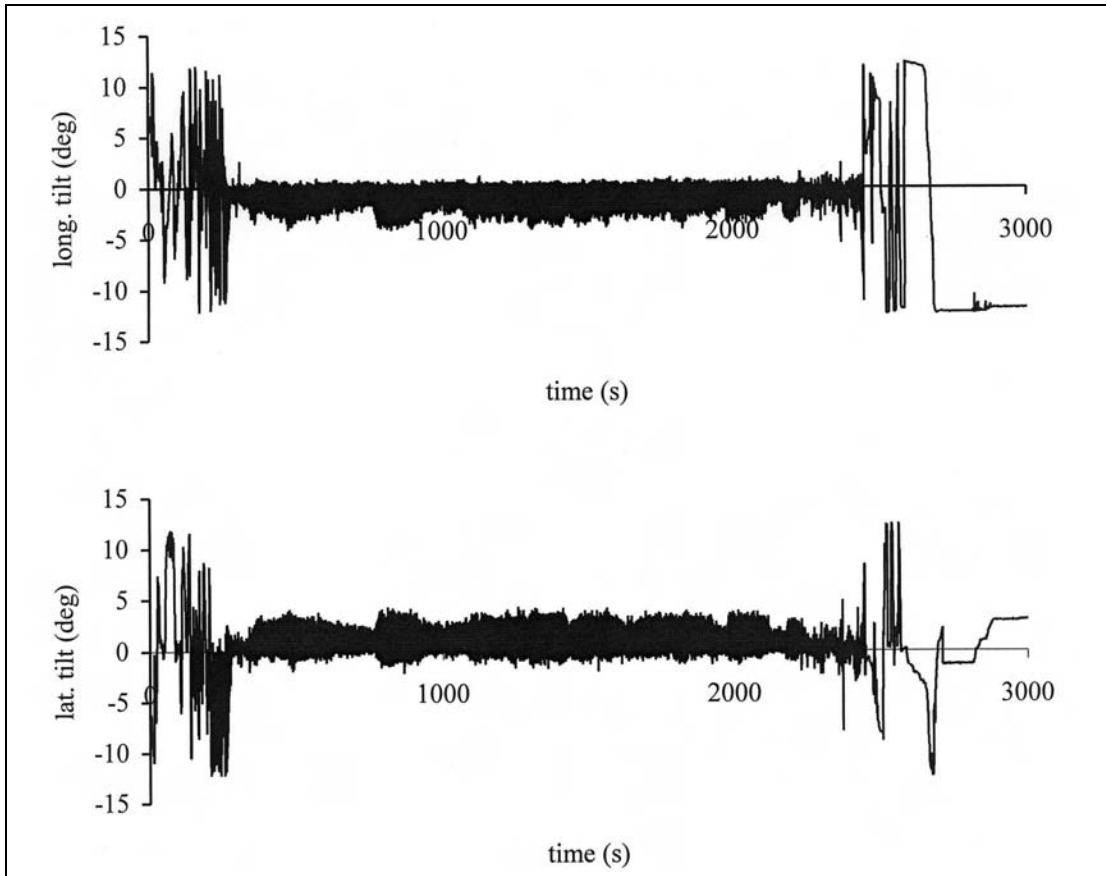
Figure 11.2   Blade Teeter Angles Expressed in Multi-blade Co-ordinates for Flight 2
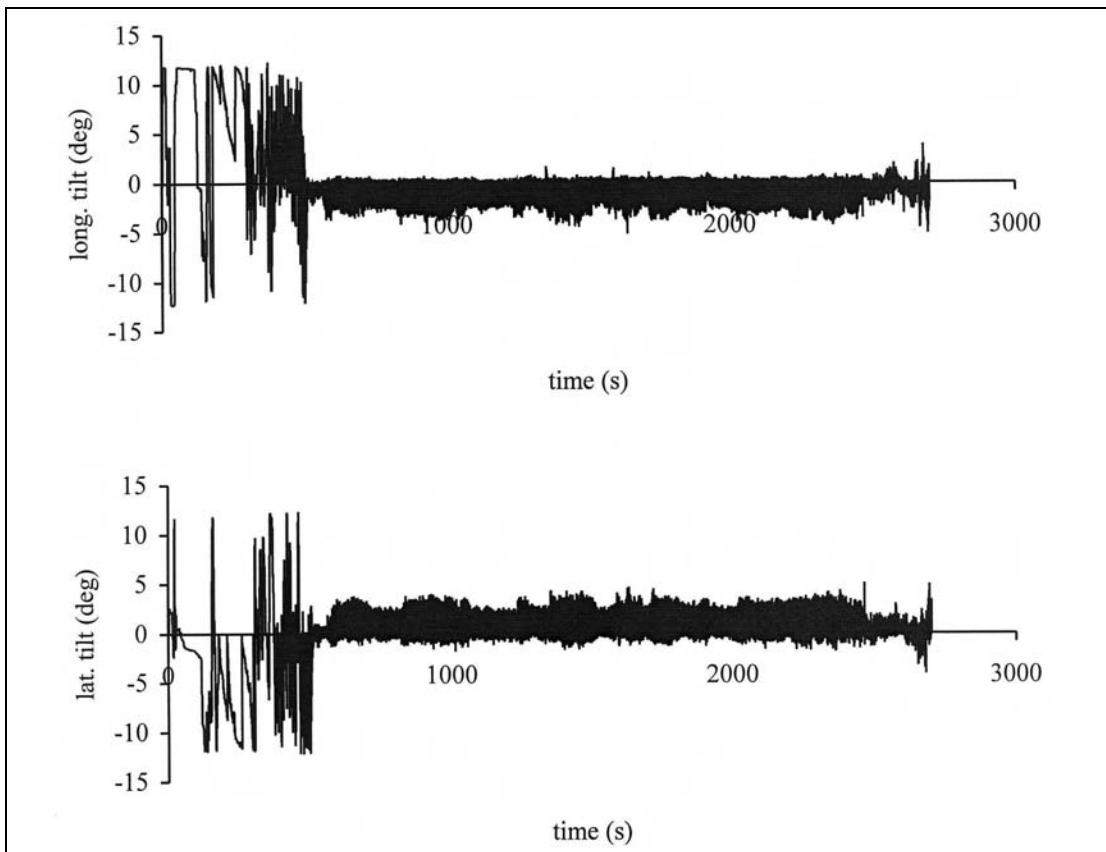
Figure 11.3   Blade Teeter Angles Expressed in Multi-blade Co-ordinates for Flight 3
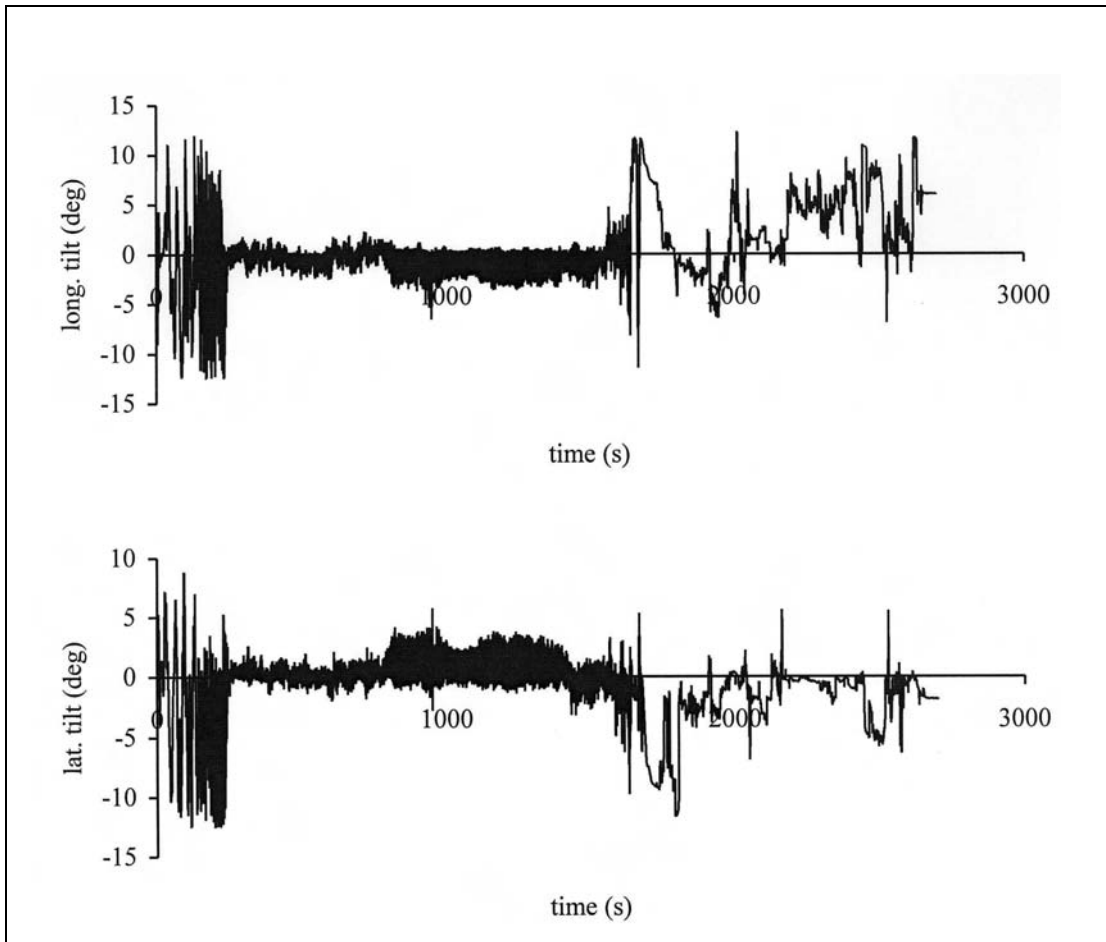
Figure 11.4   Blade Teeter Angles Expressed in Multi-blade Co-ordinates for Flight 4
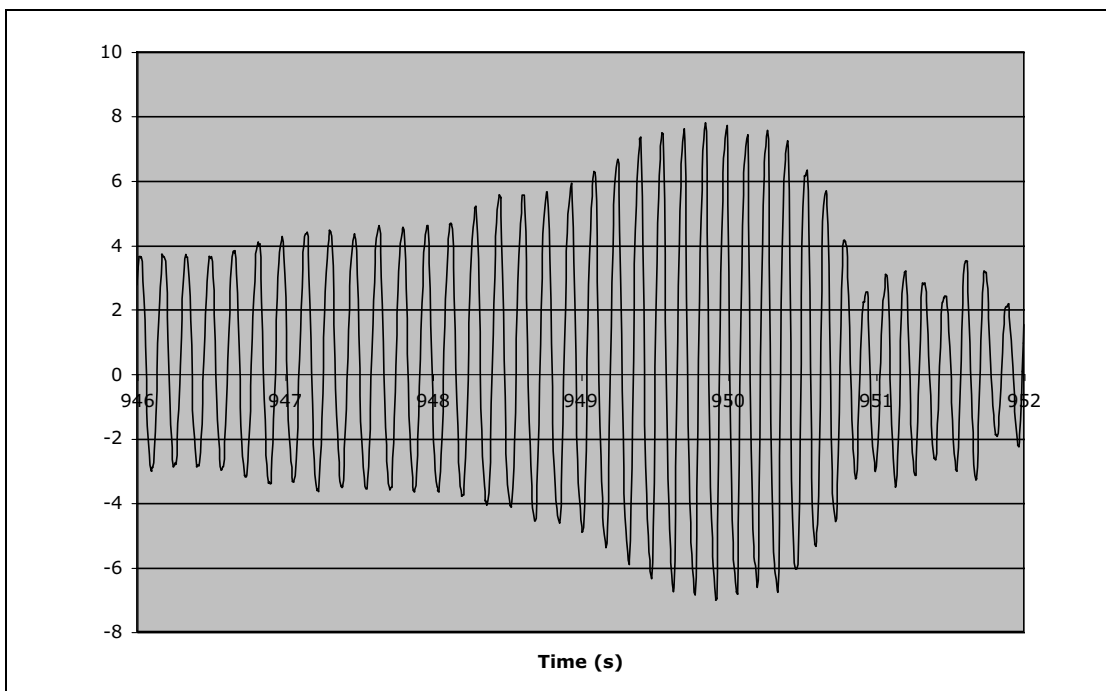
Figure 11.5   Teeter Angle During Recovery from Large Amplitude Input
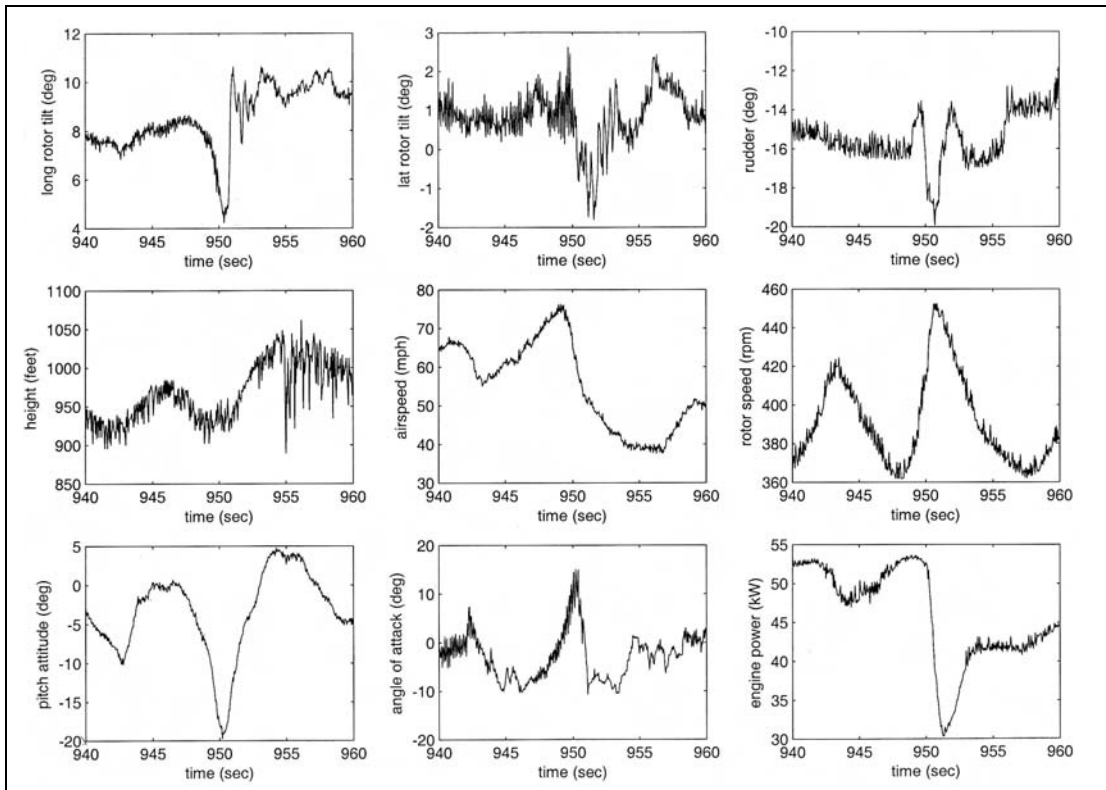
Figure 11.6   Time Histories for Recovery from Large Displacement Longitudinal
                   Stick Input
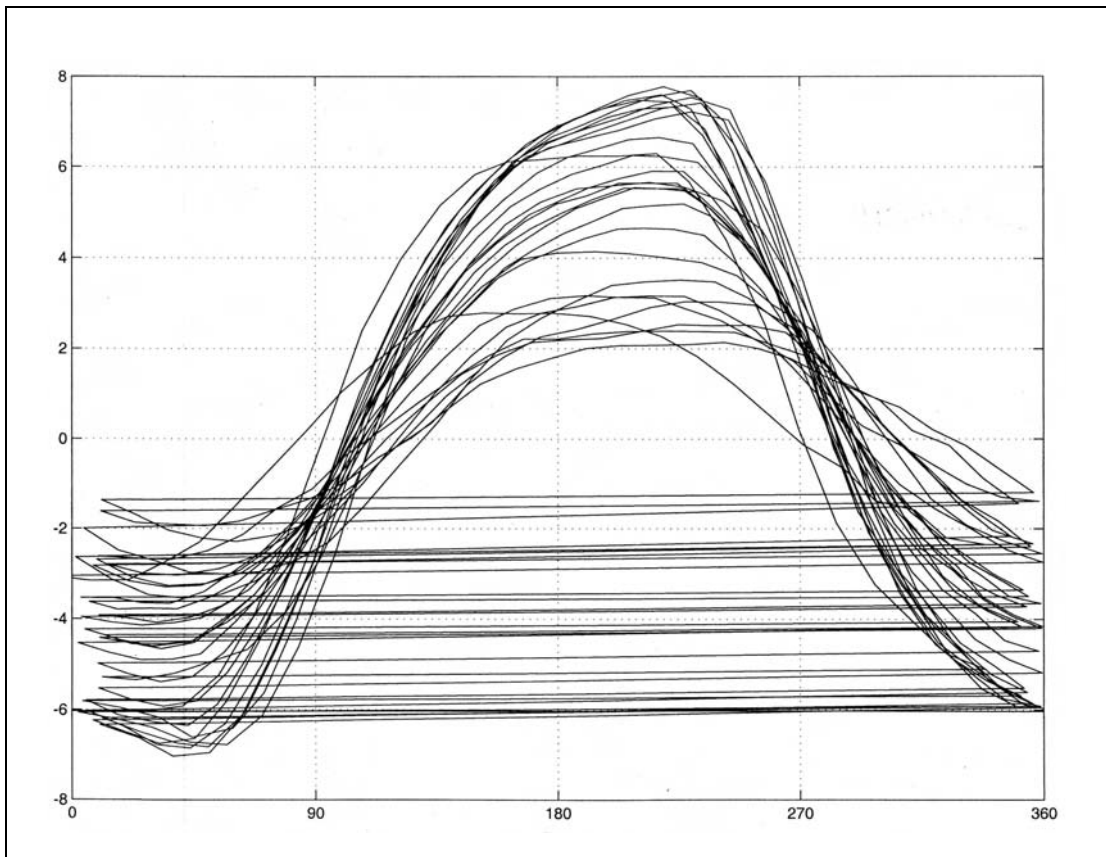
Figure 11.7   Teeter Angle vs. Azimuth for 948 - 952s of Flight 4
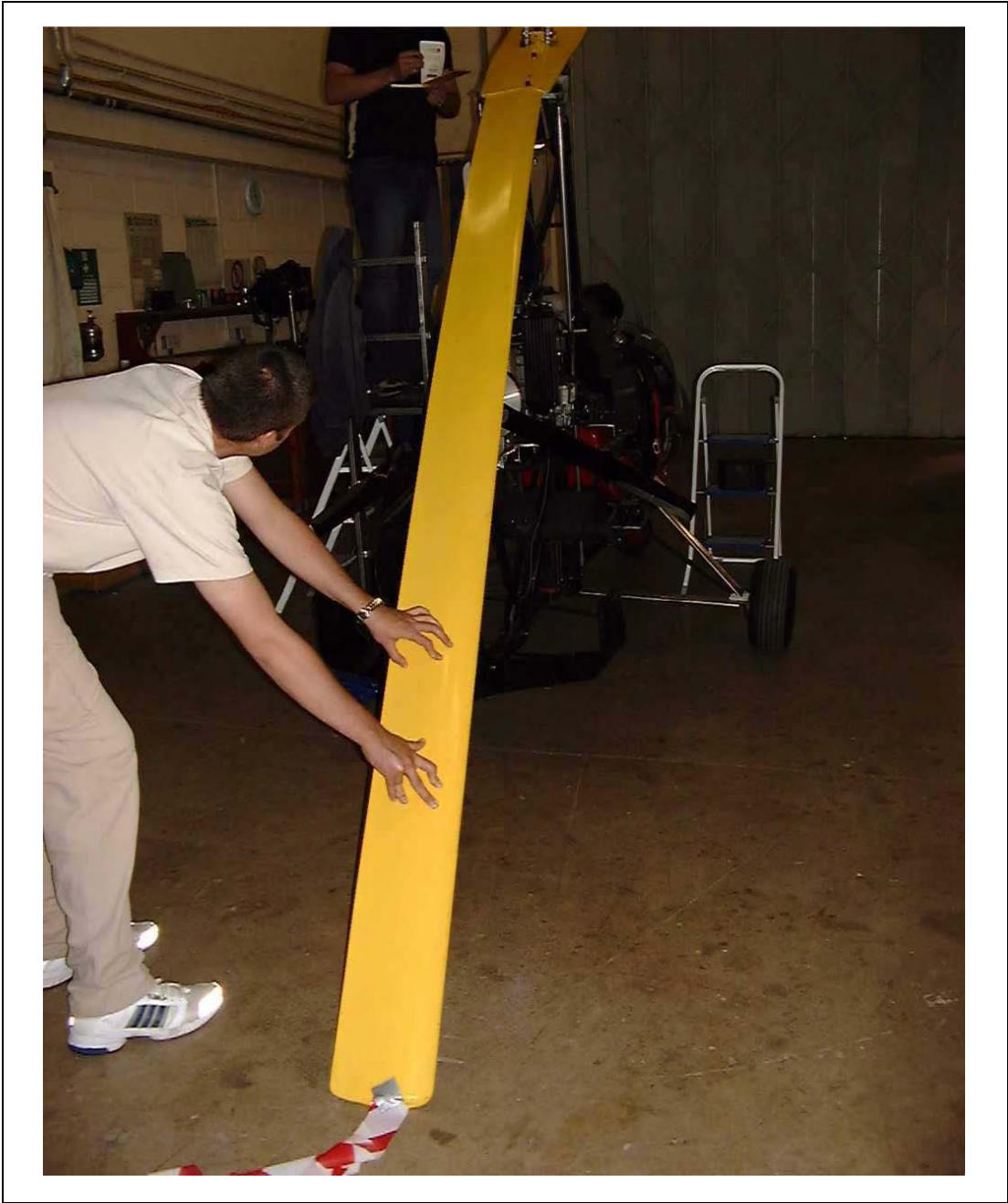
Figure 11.8   Stick Aft, Blade Teetered Through Propeller Disc
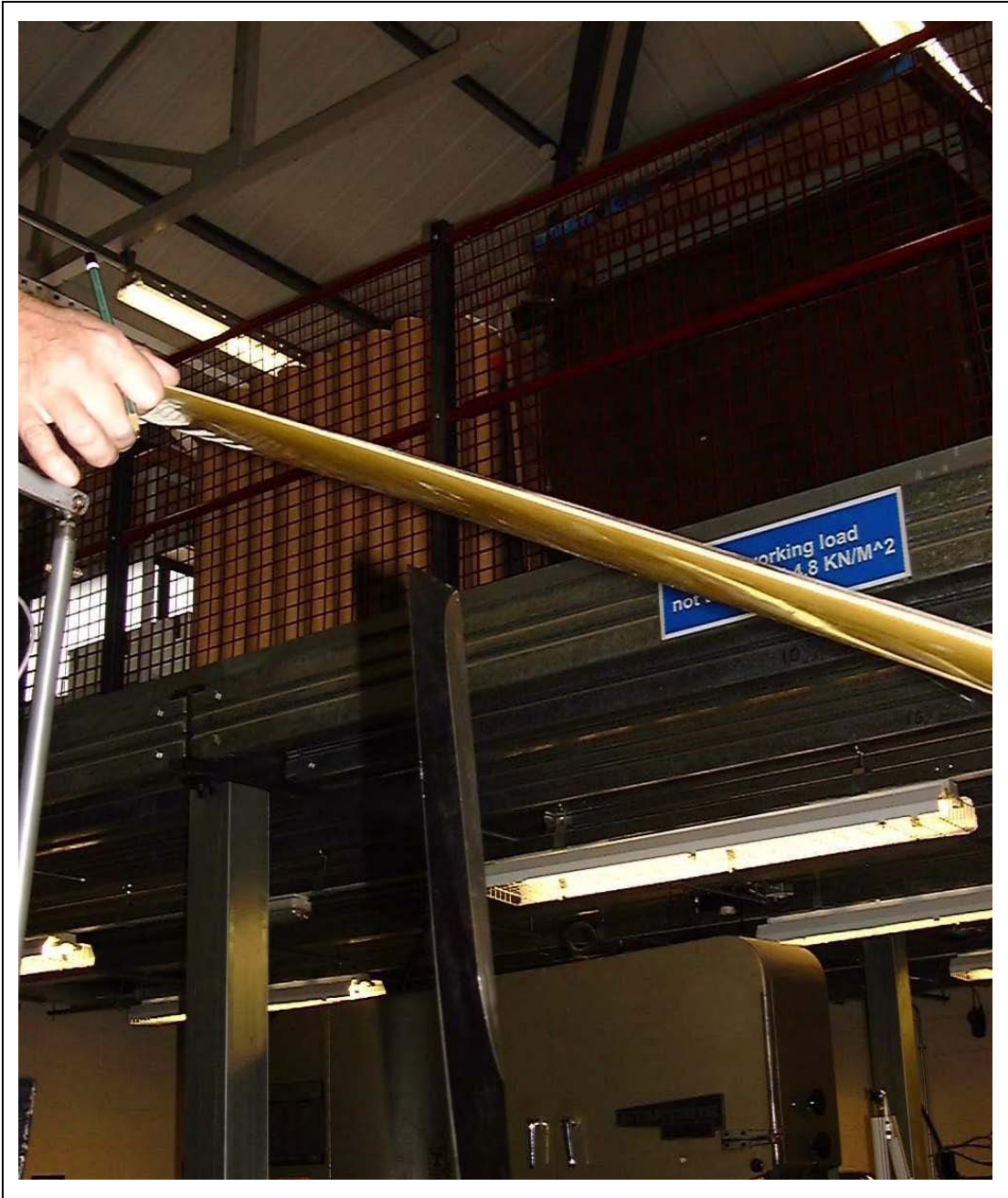
Figure 11.9   Stick Aft, 8° of Teeter
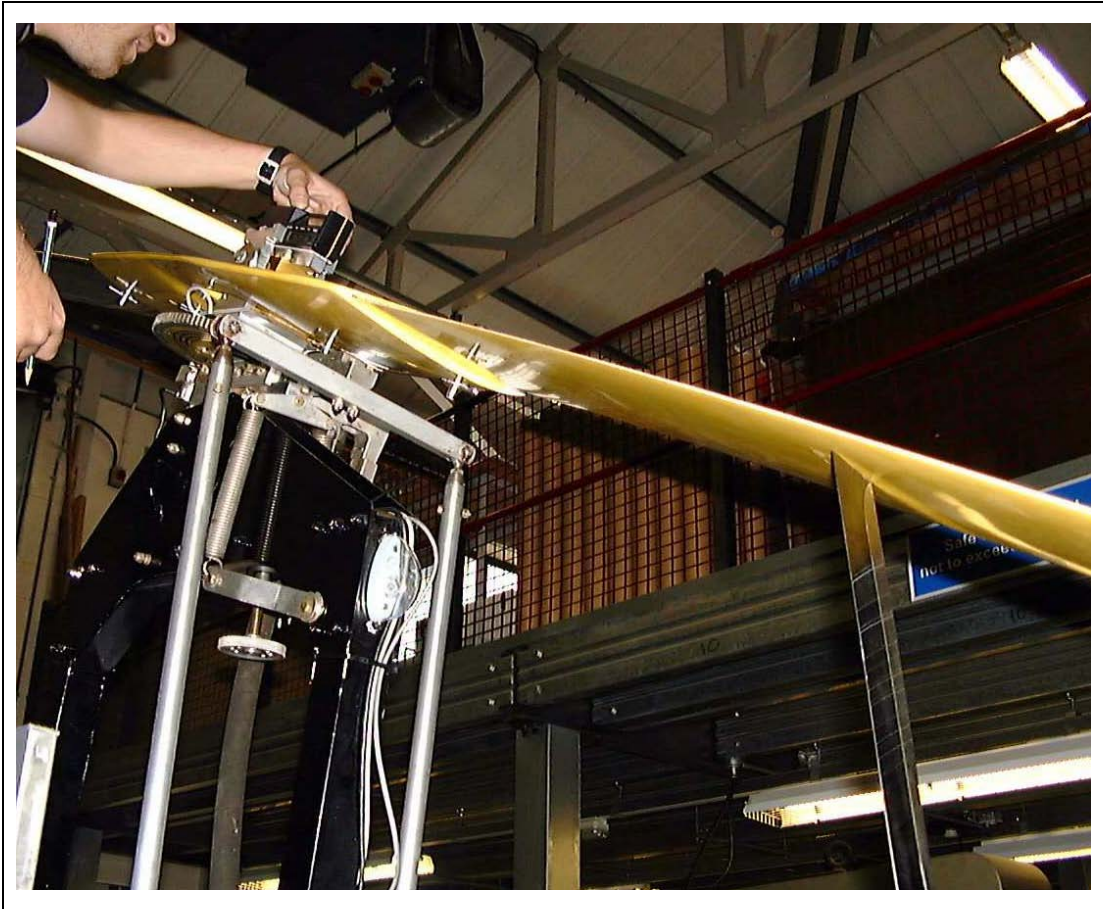
Figure 11.10　Teeter Measurement for a Propeller Strike

12   Overall Conclusions

Due to extremely poor accident statistics in the early 1990s, the AAIB recommended that the CAA undertake a research study into the aerodynamics of gyroplanes to address the lack of contemporary knowledge of this type of aircraft, and to provide the technical information required to update the airworthiness requirements for this class of aircraft, BCAR Section T. Research at the University of Glasgow has focused on supporting the UK Civil Aviation Authority to achieve these goals. The depth and breadth of knowledge on the flight characteristics of gyroplanes has without doubt been extended by this project. The following observations and conclusions can be drawn from the research.

a) At the outset of the project there was only a limited volume of archival documentation on the fundamental aerodynamic and dynamic properties of gyroplanes. Dissemination of the work reported in this document through journal articles, conference presentations and public lectures has gone some way to address this. Due to the interest generated by this project (both nationally and internationally), much more technical information is now available in the open literature.

b) Wind tunnel tests have shown that the aerodynamic properties of gyroplanes are relatively insensitive to configurational changes. Even at the high speed end of the range, the aerodynamic properties of the vehicle pod and tailplane have little influence.

c) The RASCAL mathematical model, both in its linear and nonlinear formulation, was validated using flight test data. Analysis of these results show that RASCAL provides a valid predictive tool for analysing gyroplane stability characteristics. Consistent results were obtained allowing the model's applicability and limitations to be defined. Certainly, in parametric studies where it is a trend in relation to changes in configurational parameters which is to be identified, RASCAL is as good as contemporary helicopter mathematical modelling practice.

d) In general gyroplanes exhibit a mix of stability characteristics typical of those from fixed wing aircraft and helicopters. Notably, they possess a lightly damped phugoid mode. The lateral/directional dynamics of the gyroplane are broadly similar to those of a conventional aircraft and are usually benign.

e) The single most significant factor in determining the longitudinal stability of gyroplanes is the vertical location of the centre of gravity relative to the propeller thrust line. It has been shown that a centre of gravity location below the propeller thrustline can destabilise the phugoid mode. Flight tests to demonstrate compliance with BCAR Section T can be difficult to perform, particularly without sophisticated measurement and data acquisition systems to provide objective documentation of aircraft performance. Locating the centre of gravity appropriately in location to the propeller thrust line then offers the best prospect for acceptable handling qualities across the speed range. Gyroplane stability is insensitive to changes in most other configurational parameters with the exception of the horizontal tailplane where gross changes in area (complete removal, for example) can influence the short period mode and hence the handling qualities of the aircraft.

f) Although the teeter motion of the rotor is generally of low amplitude, large scale inputs or severe manoeuvring can rapidly lead to large amplitude teeter oscillations with serious consequences for flight safety.

The work described in this Paper represents a substantial advance in the understanding of gyroplane flight dynamics. The development of the mathematical models now provide a significant predictive capability, and the data gathered in the flight tests, as well as being essential for validation purposes, has also provided insight into the flight characteristics of this vehicle type. The primary aim of the research was to improve gyroplane safety. This project has undoubtedly increased awareness of the issues associated with gyroplane configuration. Along with the redrafting of BCAR Section T, this project has contributed to a lower accident rate and so has fulfilled its main aim.

CAA Comment

Effect of tailplanes. The report also concludes that horizontal tailplanes are largely ineffective in improving the long term response of pitch dynamic stability (phugoid mode). This is the result of studies primarily on narrow tandem cockpit enclosures. CAA Flight Test Specialist qualitative evaluation of the effects of a horizontal tailplane on a single side-by-side configuration gyroplane type indicated a degree of improvement in the phugoid characteristics at higher speed. It is appreciated that in paragraph 8.3.1 (page 152) of the report it is stated that other factors can affect the phugoid mode.

Teeter Margins. Due to the possibility of excessive teeter angles under certain phases of flight, that can lead to blade strike with the prop, pod or mast, flight tests were undertaken. Flight instrumentation revealed small teeter angles in steady flight conditions, but in one instance during a particularly extreme manoeuvre, the angle reached 8 deg within an 11 deg safe envelope. Testing was limited, and it is difficult to draw meaningful conclusions from the data, other than to recognise that certain more extreme flight conditions will produce teeter angles that may go outside of the safe envelope, and so could lead to a strike on some part of the aircraft.

Advisory material to BCAR Section T.143 (a) is to be revised to require satisfactory control margin and rotor clearance up to 1.1Vne.

INTENTIONALLY LEFT BLANK

Acknowledgements

In over 15 years of research for this project the authors have sought advice from experts in all areas of gyroplane flight from owners, operators, manufacturers and those few individual researchers scattered over the globe who have at some point in their careers dared to investigate gyroplane flight. Their assistance was wide ranging and invaluable. There are too many to mention here in full, however the assistance of the following people was particularly valuable: Roger Savage, Jim Montgomerie, and the late Phil Barlow.

A major feature of the work was the flight testing of the gyroplane - a world first to the knowledge of the authors. This could not have been achieved without the invaluable assistance of Colin Handley and Vic Lockwood of FR Aviation. Also, the contribution of Colin Massey of GKN Westland Helicopters Ltd. in auditing the work on behalf of the CAA should not be overlooked. The authors would also like to acknowledge the professionalism and piloting skills of those who carried out the test flying: Chris Chadwick, Roger Savage and B. de Saar.

The authors would also wish to acknowledge the assistance provided by their colleagues, Prof. Frank Coton on the aerodynamic testing in the early stages of the project and, latterly, Dr Eric Gillies who has contributed significant expertise in the area of aeroelastic modelling. Particular credit must go also to Robert Gilmour, the Department's Research Technologist for all of his efforts in building, maintaining and operating the instrumentation on board G-UNIV. Tony Smedley and his technical staff should also be acknowledged for their contributions which were often above and beyond their job descriptions!

Finally, the authors wish to thank the Civil Aviation Authority for the support and funding for this research. It has given the University of Glasgow, and the authors particularly, the opportunity to be involved in an important and unique project. It is therefore appropriate here to list all of those who were involved: Robin Ablett, Dave Chapman, Julie Denning, Keith Dodson, Alistair Maxwell, Paul Spooner, Kevin Russell, Carl Thomas, Joji Waites, Jonathan Howes, Andrew Goudie, and Ray White. Particular acknowledgement of the efforts of Dave Howson who has borne the responsibility of managing the project should also be made.

INTENTIONALLY LEFT BLANK

References

[1]   Anon, "Airworthiness Review of Air Command Gyroplanes", Air Accidents Investigation Branch Report, Sept. 1991.

[2]   "British Civil Airworthiness Requirements, Section T, Light Gyroplane Design Requirements, " Civil Aviation Authority CAP 643, Issue 1, March 1995.

[3]   Glauert, H., "A General Theory of the Autogyro", ARC R and M No. 1111, Nov. 1926.

[4]   Lock, C.N.H., "Further Development of Autogyro Theory Parts 1 and 2", ARC and R and M No. 1127, March 1927.

[5]   Glauert, H., "Lift and Torque of an Autogiro on the Ground", ARC R and M No. 1131, July 1927.

[6]   Lock, C.N.H., Townend, H.C., "Wind Tunnel Experiments on a Model Autogyro at Small Angles of Incidence", ARC R and M No. 1154, March 1928.

[7]   Glauert, H., Lock, C.N.H., "A Summary of the Experimental and Theoretical Investigation of the Characteristics of an Autogyro", ARC R and M No. 1162, April 1928.

[8]   Wheatly, J.B., "Lift and Drag Characteristics and Gliding Performance of an Autogiro as Determined in Flight", NACA TR 434, 1932.

[9]   Wheatly, J.B., "Simplified Aerodynamic Analysis of the Cyclogiro Rotating Wing System", NACA TN 467, 1933.

[10]   Wheatly, J.B., "Wing Pressure Distribution and Rotor-blade Motion of an Autogiro as Determined in Flight", NACA TR 475, 1933.

[11]   Wheatly, J.B., "An Aerodynamic Analysis of the Autogiro Rotor with a Comparison Between Calculated and Experimental Results", NACA TR 487, 1934.

[12]   Wheatly, J.B., "The Aerodynamic Analysis of the Gyroplane Rotating Wing System" NACA TN 492, 1934.

[13]   Wheatly, J.B., Hood, M.J., "Full-Scale Wind Tunnel Tests of a PCA-2 Autogiro Rotor", NACA TR 515, 1935.

[14]   Wheatly, J.B., Influence of Wing Setting on the Wing Load and Rotorspeed of a PCA-2 Autogiro as Determined in Flight", NACA TR 523, 1935.

[15]   Wheatly, J.B., Windler, R., "Wind Tunnel Tests of a Cyclogiro Rotor" NACA TN 528, 1935.

[16]   Wheatly, J.B., Bioletti, C., "Wind Tunnel Tests of a 10-foot-Diameter Gyroplane Rotor", NACA TR 536, 1935

[17]   Wheatly, J.B., Bioletti, C., "Wind Tunnel Tests of a 10-foot-Diameter Autogiro Rotor", NACA TR 552, 1935

[18]   Wheatly, J.B., "A Study of Autogiro Rotor Blade Oscillations in the Plane of the Rotor Disk", NACA TN 581, 1936

[19]   Wheatly, J.B., Bioletti, C., "Analysis and Model Tests of Autogiro Jump Take-off", NACA TN 582, 1936

[20]   Wheatly, J.B., "An Analytical and Experimental Study of the Effect of Period Blade Twist on the Thrust, Torque, and Flapping Motion of an Autogyo Rotor", NACA TR 591, 1937.

[21]   Wheatly, J.B., "An Analysis of the Factors that Determine the Periodic Twist of an Autogiro Rotor Blade, with a Comparison of Predicted and measured Results", NACA TR 600, 1937.

[22]   Bailey, F.J. Jr., Gustafon, F.B., "Observations in flight of the region of stalled flow over the blades of an autogiro rotor", NACA-TN-741, 1939.

[23]   Bailey, F.J. Jr., "A Study of the Torque Equilibrium of an Autogiro Rotor", NACA-TR-623.

[24]   Breguet, L., "The Gyroplane – Its Principles and its Possibilities", Technical Memorandums, NACA, No. 816, 1937

[25]   Schrenk, M., "Static Longitudinal Stability and Longitudinal Control of Autogiro Rotors", Technical Memorandums, NACA, No. 879, 1938

[26]   Wallis, K.H., "Design and Construction of a low—cost Autogyro Aircraft and Detailed Prospects for Future Application", The Aeronautical Journal, Vol. 67, pp. 111 – 118, Feb. 1963.

[27]   Schad, J.L., "Small Autogyro Performance", Journal of the American Helicopter Society, Vol. 10, 1965.

[28]   Niemi, E.E. "Effect of Various Cabin Designs on the Performance of a Small Unstreamlined Autogyro", Master of Science Thesis Paper, Worcester Polytechnic Institute, January 1964.

[29]   Mouille, R., "The Turbogyre 330", Agard Report, Helicopter Development, 1966 (In French).

[30]   Smith, R.C., Levin, A.D., "The Unpowered Rotor: A Lifting Decelerator foor Spacecraft Recovery", Proceedings of AIAA Aerodynamic Deceleration Systems Conference, September 1968, AIAA-1968-969

[31]   Barzda, J.J., "Rotors for Recovery", AIAA Journal of Spacecraft and Rockets, Vol. 3, No. 1 pp 104 – 109, 1966.

[32]   Liss, A.I.U., "Consideration of Control Elasticity in Calculating the Deformation of Gyroplane Rotor Blades", Aviatsonnaia Tekhnika, Vol. 17, No. 1, pp 64 – 71, 1974.

[33]   Przybylski, J., Toms, R.L., Cheeseman, I.C., "The Investigation of Some Unusual Handling Characteristics of a Light Autogyro", Proceedings of the 2nd European Rotorcraft Forum, September 1976

[34]   Johnson, W., "Comparison of Calculated and Measured Helicopter Rotor Lateral Flapping Angles", Journal of the American Helicopter Society, Vol. 26, pp 46 – 50, April 1981.

[35]   Nicholls, J.M., Dymock, R.B., James, R.A., "Ultralight Aircraft and Gyrocopter Fatalities in South Australia", Medical Journal of Australia, Vol 149, Iss 2, p111, 1988.

[36]   McKillip, R.M., Chih, M.H., "Instrumented Blade Experiments Using a Light Autogiro", Proceedings of the 16th European Rotorcraft Forum, Glasgow, Sept. 1990.

[37]   Barnard, R.H., Philpot, D.R., "Aircraft Flight", p35-36, Longman Scientific and Technical, 1993, ISBN 0-582-00338-5

[38]   Kermode, A.C., "Mechanics of Flight", p191-196, Longman Scientific and Technical, 1991, 9th Edition, ISBN 0-582-42254-X

[39]   Prouty, R., "Helicopter Performance, Stability, and Control", p142, 154, 662, Krieger Publishing, 1990, ISBN 0-89464-457-2

[40]   Johnson, W., "Helicopter Theory", p10-11, 15-16, 301-302, Princeton University Press, 1980, ISBN 0-07917-691-4

[41]   Shippen, J., "Data Acquisition and Analysis of Service Loads in a Light Weight Autogyro", Proceedings of 52 Annual Forum of the American Helicopter Society, June 1996.

[42]   Shippen, J., "Measurement of Autogyro Control Forces", Proceedings of the I.Mech. E Part G. Journal of Aerospace Engineering, Vol. 212, No. 1, pp 57 – 60, 1998.

[43]   Lopez-Diez, J., Cuerno-Rejado, C., Lopez-Ruiz, J.L., "Directional Control of a Non-rudder Autogiro-Landing Manoeuvre of the C-30", Proceedings of the 24th European Rotorcraft Forum, pp. FM11.1 – FM11.9, September 1998

[44]   Lopez-Diez, J., Cuerno-Rejado, C., Lopez-Ruiz, J.L., "Study of Competitive Missions for Autogyros", Proceedings of the 25th European Rotorcraft Forum, September 1999.

[45]   Rapp, H., Wedemeyer, P., Teuber, C., "Measurement of in-Flight Rotor Blade Loads of an Autogyro". Proceedings of the 26th European Rotorcraft Forum, pp 101.1 – 101.8, September 2000.

[46]   Wang, H-J., Gao, Z., "Aerodynamic Virtue and Steady Rotary Speed of Autorotating Rotor", Acta Aeronautica et Astronautica Sinica, Vol. 22, No. 4, pp. 337 – 339, July 2001.

[47]   Kalmykov, A.A., "Realizable Combinations of Gyroplane Main Rotor Overload and Starting", Aviatsionnaya Tekhnika, No. 2, pp 6 – 10, April – June 2004.

[48]   McCormick, B.W., "A Numerical Analysis of Autogyro Performance", Proceedings of the Biennial International Powered Lift Conference and Exhibit, AIAA Paper No. AIAA-2002-5950, November 2002.

[49]   Traum, M.J., Carter, R.G., "Pitch Control Benefits of Elevators for Autogyros in Low-Speed Forward Flight", 43rd AIAA Aerospace Sciences Meeting and Exhibit, AIAA Paper No. AIAA 2005 – 26, January 2005.

[50]   Li, Y., DeLaurentis, D, Mavris, D., "Advanced Rotorcraft Concept Development and Selection Using a Probabilistic Methodology", Proceedings of the 3rd Annual AIAA Aviation Technology, Integration, and Operations Forum, Paper No. AIAA 2003-6759, November 2003.

[51]   Ahn, B-H, DeLaurentis, D., Mavris, D.N., "Advanced Personal Air Vehicle Concept Development Using Powered Rotor and Autogyro Configurations", Proceedings of the 2nd Annual AIAA Aviation Technology, Integration, and Operations Forum, October 2002.

[52]   Jensen, D.I., "Un-manned Autogyro for Cinematography and Reconnaissance", Proceedings of Aircraft, Technology Integration and Operations Forum, AIAA Paper No. AIAA-2001-5228, October 2001.

[53]   Lopez, C.A., Wells, V.L., "Dynamics and Stability of an Autorotating Rotor/Wing Unmanned Aircraft" AIAA Journal of Guidance, Control, and Dynamics, Vol. 27, Part 2, pp 258 – 270, 2004.

[54]   Somov, Y.I., Polyntsev, O.Y., "Nonlinear Dynamics and Robust Control of a Wind-milling Gyroplane Rotor", Proceedings of the International Conference on Physics and Control, August 2003.

[55]   Somov, Y.I., Polyntsev, O.Y., "Nonlinear Dynamics and Robust Control of a Gyroplane Rotor", Proceedings of the IFAC Congress, 2005.

[56]   Carter, J. Jr., "CarterCopter – A High Technology Gyroplane", Proceedings of the Vertical Lift Aircraft Design Conference, Jan. 2000.

[57]   Whitney, M.J., Shah, A.H., "Dynamic Analysis of the Hawk 4 Rotor Blade", Proceedings of the 43rd AIAA/ASME/ASCE/AHS/ASC Structures, Structural Dynamics and Materials Conference, Paper No. AIAA-2002-1605, April 2002.

[58]   Groen, D., "Gyroplane Technology", Proceedings of the International Air and Space Symposium and Exposition: The Next 100 Years, Paper No. AIAA-2003-2519, July 2003.

[59]   Gibbings, D., "The Fairey Rotodyne: Technology Before Its Time?", The Aeronautical journal, Vol. 108, No. 1089, pp. 565 – 574, 2004.

[60]   Leishman, J.G., "Development of the Autogiro: A Technical Perspective", AIAA Journal of Aircraft, Vol. 41, No. 4, July-August 2004.

[61]   Houston, S.S., Thomson, D.G., "A Study of Gyroplane Flight Dynamics", Paper No. VII-6, 21st European Rotorcraft Forum, St Petersburg, Russia, August 1995

[62]   Houston, S. S., "Longitudinal Stability of Gyroplanes", The Aeronautical Journal, Vol. 100 No. 991, 1996, pp. 1-6.

[63]   Houston, S.S., Thomson, D.G., "Flight Investigation of Gyroplane Longitudinal Flight Dynamics", Paper 108, Proceedings of the 23rd European Rotorcraft Forum, Dreseden, Germany, September 1997.

[64]   Houston, S.S., Thomson, D.G., "Identification of Gyroplane Stability and Control Characteristics", Proceedings of NATO Research and Technology Organisation Symposium 'System Identification for Integrated Aircraft Development and Flight Testing', Madrid, Spain, May 1998

[65]   Spathopoulis, V.M., Thomson, D.G., Houston, S.S., "Flight Dynamics Issues Relating to Autogyro Airworthiness and Flight Safety", Proceedings of the 54th American Helicopter Society Annual Forum, Washington, May 1998

[66]   Houston, S. S., "Identification of Autogyro Longitudinal Stability and Control Characteristics", Journal of Guidance, Control and Dynamics, Vol. 21, No. 3, 1998, pp. 391-399.

[67]   Houston, S. S., "Identification of Gyroplane Lateral/Directional Stability and Control Characteristics from Flight Test", Proc. Inst. Mech. Engrs, Part G, Vol. 212, 1998, pp. 271-285.

[68]   Coton, F., Smrcek, L., Patek, Z., "Aerodynamic Characteristics of a Gyroplane Configuration", AIAA Journal of Aircraft, Vol. 35, No. 2, 1998, pp.274-279.

[69]   Houston, S.S, Thomson, D.G., Spathopoulos, V.M., "Experiments in Autogyro Airworthiness for Improved Handling Qualities", Proceedings of 57th Annual Forum of the American Helicopter Society, May 2001.

[70]   Houston, S.S., "Analysis of Rotorcraft Flight Dynamics in Autorotation", AIAA Journal of Guidance, Control and Dynamics, Vol. 25, Vol. 1., pp 33 – 39, 2002.

[71]   Bagiev, M., Thomson, D.G., Houston, S.S., "Autogyro Inverse Simulation for Handling Qualities Assessment", Proceedings of the 29th ERF, Sept. 2003

[72]   Houston, S.S., "Modelling and Analysis of Helicopter Flight Mechanics in Autorotation", AIAA Journal of Aircraft, Vol. 40, No. 4, pp 675 – 682, 2003

[73]   Houston, S.S., Brown, R., "Rotor Wake Modelling for Simulation of Helicopter Flight Mechanics in Autorotation", AIAA Journal of Aircraft, Vol. 40, No. 5, 2003

[74]   Bagiev, M., Thomson, D.G., Houston, S.S., Autogyro Handling Qualities Assessment, Proc. of American Helicopter Society 60th Annual Forum, June 2004.

[75]   Thomson, D.G., Houston, S.S., "Experimental and Theoretical Studies of Autogyro Flight Dynamics", Proceedings of the 24th ICAS Congress, Sept. 2004

[76]   Thomson, D.G., Houston, S.S., "Application of Parameter Estimation to Improved Autogiro Simulation Model Fidelity", Special Issue on Parameter Estimation, AIAA Journal of Aircraft, Vol. 42, No. 1, Jan/Feb 2005.

[77]   Thomson, D.G., Houston, S.S, Spathopoulos, V.M., "Experiments in Autogyro Airworthiness for Improved Handling Qualities", Journal of American Helicopter Society, October 2005

[78]   Trchalik, J., Gillies, E., Thomson, D.G., "Aeroelastic Modelling of a Rotor in Autorotative, Axial Flight", Proceedings of the 32nd European Rotorcraft Forum, Maastricht, Netherlands, September 2006

[79]   Bailey, Roger, "The Role of the Test Pilot", *Aerogram*, Vol. 8, No. 3. Cranfield University (October 1996)

[80]   Tischler, M. B., "Identification Techniques, Frequency Domain Methods", AGARD LS178, pp. 6-1 to 6-4, October 1991.

[81]   Anon, AAIB Bulletin No: 4/95 Ref: EW/C95/1/5, April 1995

[82]   Leishman, J.G., "Principles of Helicopter Aerodynamics", Cambridge University Press, ISBN 0-521-85860-7, 2006

[83]   Done, G., Balmford, D., "Bramwell's Helicopter Dynamics", Butterworth Heinmann, ISBN 0-7506-5075-3, 2001.

[84]   Padfield, G., "Helicopter Flight Dynamics", Blackwell Science, ISBN 0-632-05607-X, 1996

[85]   Dreier, M., "Introduction to Helicopter and Tiltrotor Simulation", AIAA Education Series, ISBN 1-5637-873-0, 2007

[86]   Newman, S., "The Foundations of Helicopter Flight", Edward Arnold, ISBN 0-340-58702-4, 1994

[87]   Houston, S., "Rotorcraft Aeromechanics Simulation for Control Analysis - Mathematical Model Definition", University of Glasgow Dept. of Aerospace Engineering Report No. 9123, 1991.

[88]   Houston, S. S., "Validation of a Non-linear Individual Blade Rotorcraft Flight Dynamics Model Using a Perturbation Method," *The Aeronautical Journal*, Vol. 98 No. 977, 1994, pp. 260-266.

[89]   Houston, S. S., "Validation of a Blade-Element Helicopter Model for Large-Amplitude Manoeuvres", *The Aeronautical Journal*, Vol. 101 No. 1001, 1997.

[90]   Peters, D. A., HaQuang, N., "Dynamic Inflow for Practical Applications", *Journal of the American Helicopter Society*, Vol. 33, No. 4, 1988.

[91]   Houston, S., "Flight Mechanics of Gyroplanes", University of Glasgow, Dept. of Aerospace Engineering Report No. 9323, 1993.

[92]   Schaefer, R.F., Smith, H.A., "Aerodynamic Characteristics of the NACA 8-H-12 Airfoil Section at Six Reynolds Numbers". NACA Tech. Note 1998. December 1949.

[93]   Brotherhood, P., "Stability and Control of the Wallis W117 Autogyro", Royal Aircraft Establishment Technical Memorandum TM Aero. 1461, 1972.

[94]   Arnold, U. T. P., "Untersuchungen zur Flugmechanik eines Tragschraubers", Technische Universitat Braunschweig Diplomarbeit 88-5D, March, 1988.

[95]   Anon, "Helicopter Simulator Qualification", US Dept. of Transport Federal Aviation Administration Advisory Circular AC 120-63, Nov. 1994.

[96]   Tischler, M. B. (ed.), "Advances in Aircraft Flight Control", Taylor and Francis, 1996.

[97]   Tischler, M.B., "System Identification Methods for Handling Qualities Evaluation, Rotorcraft System Identification, AGARD LS 178, October 1991.

[98]   "British Civil Airworthiness Requirements, Section T, Light Gyroplane Design Requirements" Civil Aviation Authority Paper No. T 860 Issue 2, Jul. 1993.

[99]   Houston, S. S., "Review of BCAR Section T (issue 2)", The Aerodynamics of Gyroplanes CAA Contract No. 7D/S/1125, July 1997.

[100]   O'Hara, F., "Handling Criteria", Journal of the Royal Aeronautical Society, Vol. 71 No. 676, April 1967.

[101]   Anon, "Military Specification, Flying Qualities of Piloted Airplanes", MIL-F-8785C, Nov. 1980

[102]   Anon, "Handling Qualities Requirements for Military Rotorcraft", US Army Aeronautical Design Standard ADS-33D, July 1994.

[103]   "British Civil Airworthiness Requirements, Section T, Light Gyroplanes" Civil Aviation Authority CAP 643 Issue 3, Aug. 2005.

[104]   Houston, S. S., "Identification of Autogyro Longitudinal Stability and Control Characteristics From Flight Test", University of Glasgow Dept. of Aerospace Engineering Report No. 9701, 1997.

[105]   Anon, "Airworthiness Review of Air Command Gyroplanes", Air Accidents Investigation Branch Report, Sept. 1991.

[106]   Houston, S.S, Thomson, D.G., "Airworthiness Investigation of the Stability and Control of the Air Command Series of Gyroplane Aircraft", CAA Contract No. 7D/S/1125/1, Final Report, April 1999.

[107]   Houston, S. S., "A Survey of Gyroplane Centre-of-mass and Propeller Thrust Line Locations", Issue 2, Sept. 2005.

[108]   Talbot, N., White, W.F.R., "Montgomerie Bensen Autogyro Stability Investigation", CAA Internal Report Ref. 9/50/5/C66/1, Issue 3, Nov. 2005.

[109]   Chadwick, C. J., "Flight Test Report No. 2/93 on the VPM M16 Gyroplane G-BUPM Against the Requirements of BCAR Section T". Arrow Engines UK Flight Test Report No. 2/93. June 1993.

[110]   Przybylski, J., Toms, R.L., Cheeseman, I.C., "The Investigation of Some Unusual Handling Characteristics of a Light Autogyro", Proc. of the 2nd ERF, 1976.

[111]   Anon, 'Gyrocopter Rotor System Behaviour', Preliminary Aeronautical Report, Commonwealth of Australia, Department of Civil Aviation, Nov. 1972.

[112]   Trchalik, J., Gillies, E.A., Thomson, D.G., 'Development of an Aeroelastic Stability Boundary for a Rotor in Autorotation', Proceedings of the AHS Specialists Conference on Aeromechanics, San Francisco, Jan. 2008.

[113]   Turnour, S. R., Celi, R., 'Modeling of Flexible Blades for Helicopter Flight Dynamics Applications,' Journal of the American Helicopter Soc., Vol. 41, No. 1, 1996, pp.52-61

[114]   Padfield, G. D., "On the Use of Approximate Models in Helicopter Flight Mechanics", Vertica, Vol. 5, No. 3, 1981

[115]   Houston, S. S., "Investigation of the Longitudinal Stability Characteristics of RAF 2000 GTX-SE Gyroplane G-BXDD", University of Glasgow, Dept. of Aerospace Engineering Report No. 9718, Oct.1997.

[116]   Chadwick, C. J., "Flight Test Report No. CJC 01/94 on Modified Air Command Gyroplanes and the Modac 503 Gyroplane Against the Requirements of BCAR Section T". 12 March 1994.

[117]   Anon, "FRA Post Flight Report", No. M16-99-01

Appendix 1   Wind Tunnel Test Series

Table A1.1   Wind Tunnel Tests Conducted With Power On

MEASUREMENT NUMBER	β	δr	COWLING	TAIL
1	0	0	YES	YES
2	-30	0	YES	YES
3	-15	0	YES	YES
4	-7.5	0	YES	YES
5	7.5	0	YES	YES
6	30	0	YES	YES
7	15	0	YES	YES
8	15	-20	YES	YES
9	7.5	-20	YES	YES
10	0	-20	YES	YES
11	-7.5	-20	YES	YES
12	-15	-20	YES	YES
13	-15	20	YES	YES
14	-7.5	20	YES	YES
15	0	20	YES	YES
16	7.5	20	YES	YES
17	15	20	YES	YES
18	15	10	YES	YES
19	0	10	YES	YES
20	-15	10	YES	YES
21	-15	-10	YES	YES
22	15	-10	YES	YES
23	0	-10	YES	YES
24	0	-15	YES	YES
25	0	-5	YES	YES
26	0	5	YES	YES
27	0	15	YES	YES
28	0	15	NO	YES
29	0	10	NO	YES
30	0	5	NO	YES

Table A1.1   Wind Tunnel Tests Conducted With Power On (Continued)

MEASUREMENT NUMBER	β	δr	COWLING	TAIL
31	0	-5	NO	YES
32	0	-10	NO	YES
33	0	-15	NO	YES
34	0	-20	NO	YES
35	-15	-20	NO	YES
36	-7.5	-20	NO	YES
37	7.5	-20	NO	YES
38	15	-20	NO	YES
39	15	20	NO	YES
40	7.5	20	NO	YES
41	0	20	NO	YES
42	-7.5	20	NO	YES
43	-15	20	NO	YES
44	-15	0	NO	YES
45	-7.5	0	NO	YES
46	0	0	NO	YES
47	7.5	0	NO	YES
48	15	0	NO	YES
49	15	0	YES	NO
50	7.5	0	YES	NO
51	0	0	YES	NO
52	-7.5	0	YES	NO
53	-15	0	YES	NO
54	-15	20	YES	NO
55	-7.5	20	YES	NO
56	0	20	YES	NO
57	7.5	20	YES	NO
58	15	20	YES	NO
59	15	-20	YES	NO
60	7.5	-20	YES	NO
61	-7.5	-20	YES	NO
62	-15	-20	YES	NO

Table A1.1   Wind Tunnel Tests Conducted With Power On (Continued)

MEASUREMENT NUMBER	β	δr	COWLING	TAIL
63	0	-20	YES	NO
64	0	15	YES	NO
65	0	10	YES	NO
66	0	5	YES	NO
67	0	-5	YES	NO
68	0	-10	YES	NO
69	0	-15	YES	NO
70	0	0	NO	NO
71	15	0	NO	NO
72	30	0	NO	NO

Table A1.2   Wind Tunnel Tests Conducted With Power Off

MEASUREMENT NUMBER	β	δr	COWLING	TAIL
73	0	-15	YES	YES
74	0	-10	YES	YES
75	0	-5	YES	YES
76	0	-20	YES	YES
77	-7.5	-20	YES	YES
78	-15	-20	YES	YES
79	15	20	YES	YES
80	-7.5	20	YES	YES
81	0	20	YES	YES
82	0	0	YES	YES
83	-7.5	0	YES	YES
84	-15	0	YES	YES
85	-15	0	NO	YES
86	-7.5	0	NO	YES
87	0	0	NO	YES
88	0	20	NO	YES
89	-7.5	20	NO	YES

Table A1.2   Wind Tunnel Tests Conducted With Power Off (Continued)

MEASUREMENT NUMBER	β	δr	COWLING	TAIL
90	-15	20	NO	YES
91	-15	-20	NO	YES
92	-7.5	-20	NO	YES
93	0	-20	NO	YES
94	0	-15	NO	YES
95	0	-10	NO	YES
96	0	-5	NO	YES
97	0	-5	YES	YES
98	0	-15	YES	YES
99	0	-10	YES	YES
100	-15	-10	YES	YES
101	-15	10	YES	YES
102	-15	20	YES	YES
103	-7.5	20	YES	YES
104	0	20	YES	YES
105	0	-20	YES	YES
106	-7.5	-20	YES	YES
107	-15	-20	YES	YES
108	-15	0	YES	YES
109	-30	0	YES	YES
110	-7.5	0	YES	YES
111	0	0	YES	YES

Table A1.3   Additional Wind Tunnel Tests

MEASUREMENT NUMBER	β	δr	COWLING	TAIL	POWER	DESCRIPTION
112	0	0	YES	YES	NO	Standing Propeller
113	0	0	YES	YES	YES	Tail Boom Extended
114	0	0	YES	YES	NO	No End Plates on Tail

Appendix 2   Configurational Data

VPM M16 Gyroplane

Airframe reference point is the intersection of the projection of the mast centreline and the keel centreline with the x-body axis aligned with the keel. The rotor rotates in an anti-clockwise direction when viewed from above. The following represents the default data set used in the simulations presented in this report.

Gross Mass	450 kg	C_Y (Side Area)	-2.0 β
Moments of Inertia		C_Z (Plan Area)	2.0 α
I_{XX}	195 kg m^2		
I_{YY}	637 kg m^2	Tailplane Data:	
I_{ZZ}	4425 kg m^2	Area	0.9 m^2
I_{XZ}	-46 kg m^2	Lift curve Slope	3.5 /rad
		Setting Angle	0
Co-ordinates (in metres) for:			
Nominal Centre of Mass	(0.319, 0, -0.823)	Fin Data:	
Hub Plate Pivot Point	(0.0969, 0, -2.105)	Area	0.19 m^2
Propellor Hub	(-0.68, 0, -0.885)	Lift curve Slope	3.5 /rad
Fuselage C.P.	(1.2, 0, -0.3)	Setting Angle	0
Tailplane C.P.	(-1.52, 0, 0)		
Fin C.P.	(-1.4, 0, -0.3)	Endplate Data:	
End Plate C.P.	(-1.91, ±0.85, -0.13)	Area	0.18 m^2
Rudder C.P.	(-1.74, 0, -0.39)	Lift curve Slope	3.5 /rad
		Setting Angle	0
Rotor Blade Parameters:			
Radius	4.267m	Rudder Data:	
Chord	0.22m	Area	0.34 m^2
Mass	8.5 kg	Lift curve Slope	3.5 /rad
Flapping Inertia	51.6 kg m^2		
Lift Curve Slope	5.7 /rad	Propellor Data:	
Profile Drag Coeff.	0.015	Blade Radius	0.86 m
Shaft Length	0.15m	Blade Chord	0.1 m
		Blade Twist	0
Fuselage Data:		Blade Mass	0.9 kg
Side Area	1.4 m^2	Orientation of thrust line	2°
Plan Area	1.6 m^2	c.g. normal distance from thrust line	0.027m (below)
Frontal Area	0.59 m^2		
C_D (Frontal Area)	1.0		
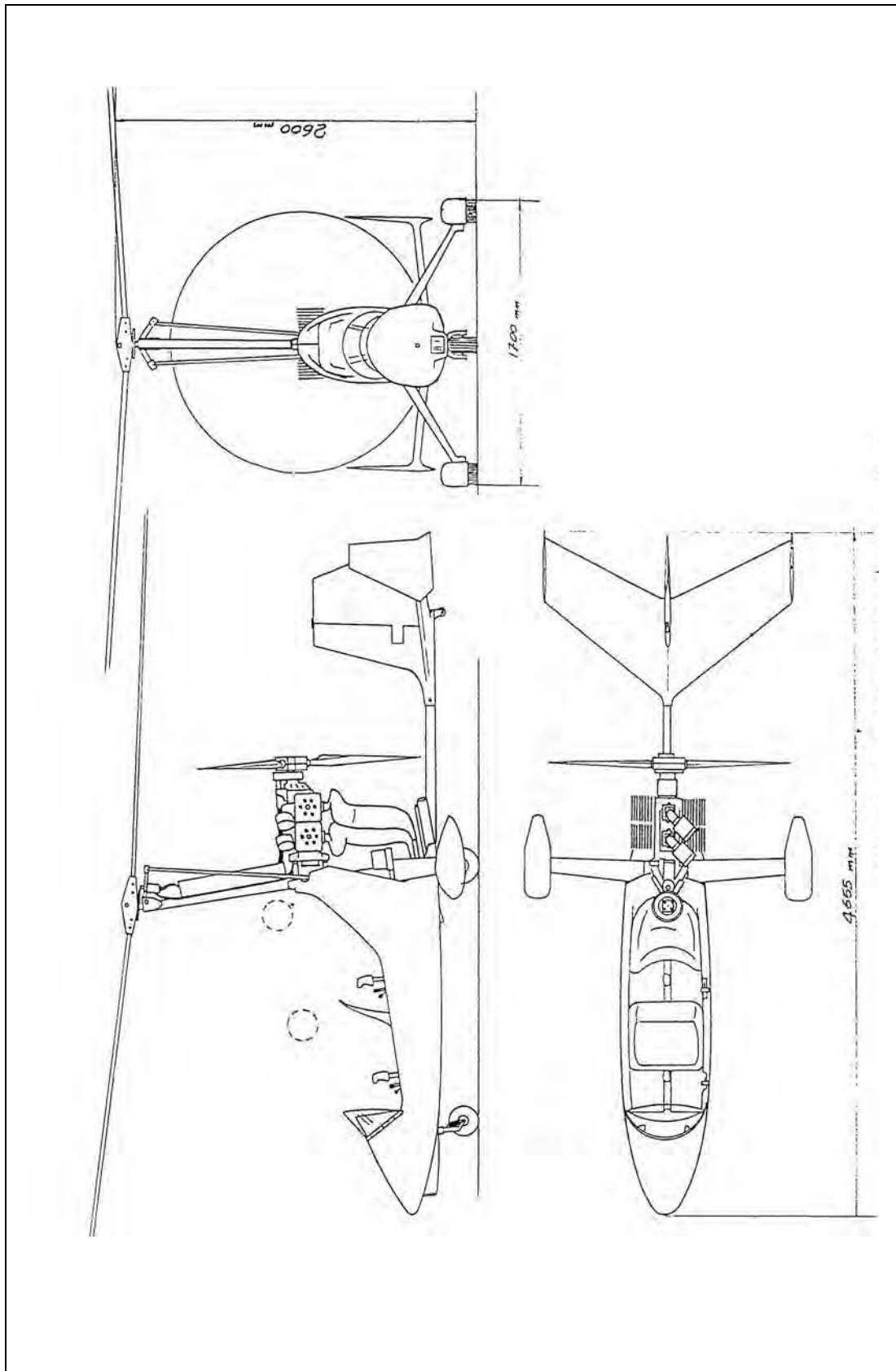
Figure A2.1 The VPM M16 Gyroplane

Montgomerie-Parsons Gyroplane G-UNIV

Airframe reference point is taken as the intersection of the projection of the mast centreline and the keel centreline with the x-body axis aligned with the keel. The rotor rotates in an anti-clockwise direction when viewed from above. The following represents the default data set used in the simulations presented in this report.

Gross Mass	355 kg	Tailplane Data:	
Moments of Inertia		Area	0.356 m^2
I_{XX}	72.96 kg m^2	Lift curve Slope	3.5 /rad
I_{YY}	297.21 kg m^2	Setting Angle	0
I_{ZZ}	224.25 kg m^2		
I_{XZ}	0 kg m^2	Fin Data:	
		Area	0.281 m^2
Co-ordinates (in metres) for:		Lift curve Slope	3.5 /rad
Nominal Centre of Mass	(0.199, 0, -0.757)	Setting Angle	0
Hub Plate Pivot Point	(-0.038, 0, -1.968)		
Propellor Hub	(-0.91, 0, -0.795)	Endplate Data:	
Fuselage C.P.	(1.626, 0, -0.48)	Area	0.107 m^2
Tailplane C.P.	(-1.02, 0, -0.057)	Lift curve Slope	3.5 /rad
Fin C.P.	(-1.0, 0, -0.268)	Setting Angle	0
End Plate C.P.	(-1.09, ±0.45, -0.063)		
Rudder C.P.	(-1.633, 0, -0.392)	Rudder Data:	
		Area	0.368 m^2
Rotor Blade Parameters:		Lift curve Slope	3.5 /rad
Radius	3.81m		
Chord	0.197m	Propellor Data:	
Mass	17.255 kg	Blade Radius	0.787 m
Flapping Inertia	83.492 kg m^2	Blade Chord	0.09 m
Lift Curve Slope	5.75 /rad	Blade Twist	0
Profile Drag Coeff.	0.011	Blade Mass	0.9 kg
Shaft Length	0.137m	Orientation of thrust line	1.0°
Shaft Offset	0.025m	c.g. normal distance from thrust line	0.018m (below)

Fuselage Data:	
Side Area	0.798 m^2
Plan Area	0.916 m^2
Frontal Area	0.448 m^2
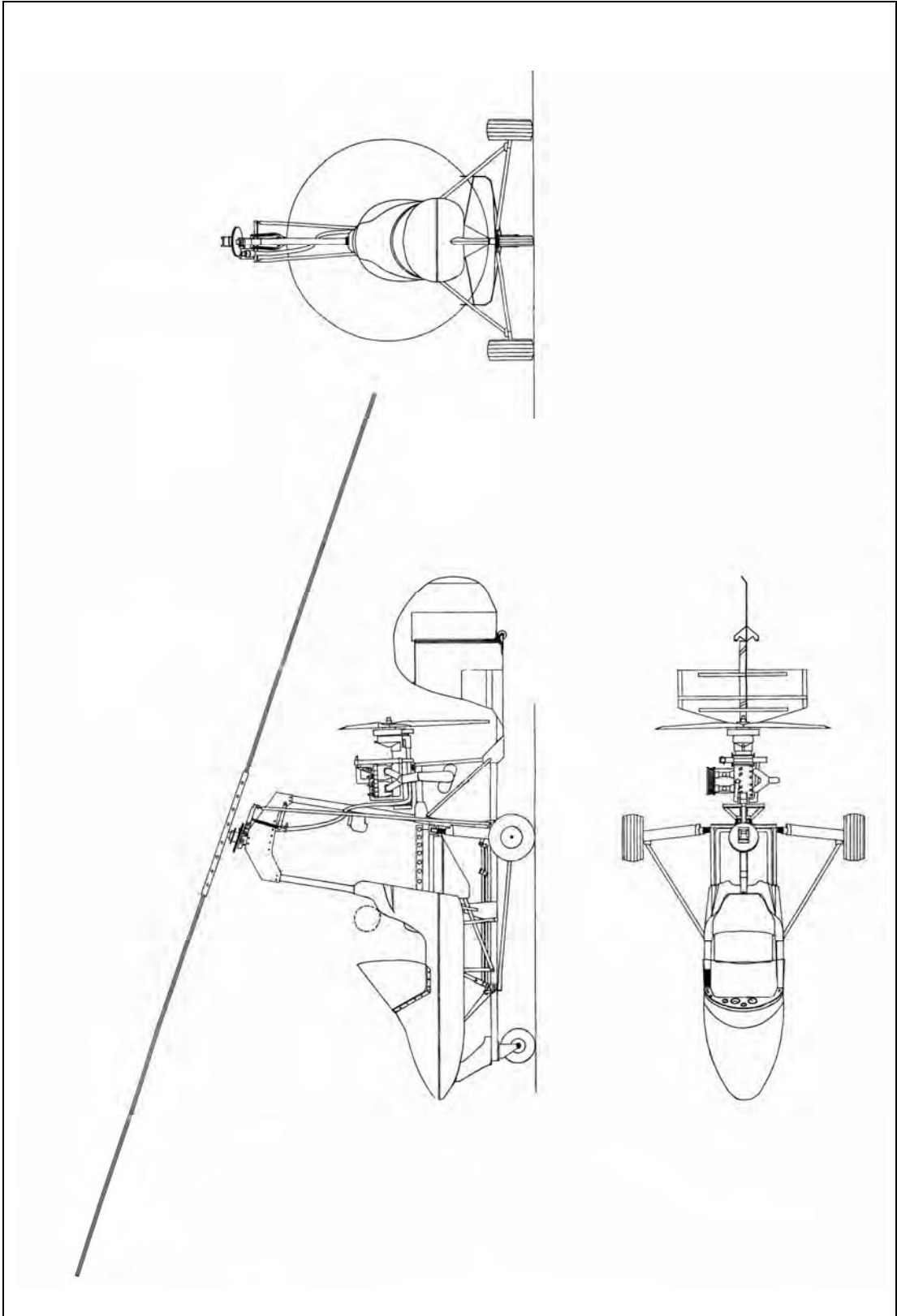
Figure A2.2   The Montgomerie-Parsons Two Persons Gyroplane

Appendix 3   Experimental Measurement of Centre of Gravity Position

Since the vertical location of the centre-of-gravity has been highlighted as an important design parameter for light gyroplanes, it is appropriate to consider a suitable method for determining this quantity. The method described here is easy to perform and provides robust results – most importantly error bounds on the calculated values are easily determined. Note that determination of c.g. position is not to replace the hang check – the hang check is really performed to determine if suitable control margins will be available, and is not really a weight and balance exercise in itself. A weight and balance exercise is therefore an additional item to be performed.

Equipment required includes three weight scales that each main wheel, plus nose (or tail) wheel is to rest upon. A tape measure is required to determine wheelbase, and a clinometer is necessary for measuring the pitch angle of the aircraft. The method is performed in two separate stages. First, the aircraft is placed on the scales as shown in Figure A3-1, on a level surface. The position of the vertical reference line is arbitrary, and is a matter of choice. For a symmetric aircraft, the left and right wheel reactions should be the same – if they are not, advice should be sought. The wheelbase should be measured, and then the longitudinal position of the c.g., with respect to the vertical reference line, is given by:

$$x_{cg} = \frac{W_{nose}}{W} \, l$$
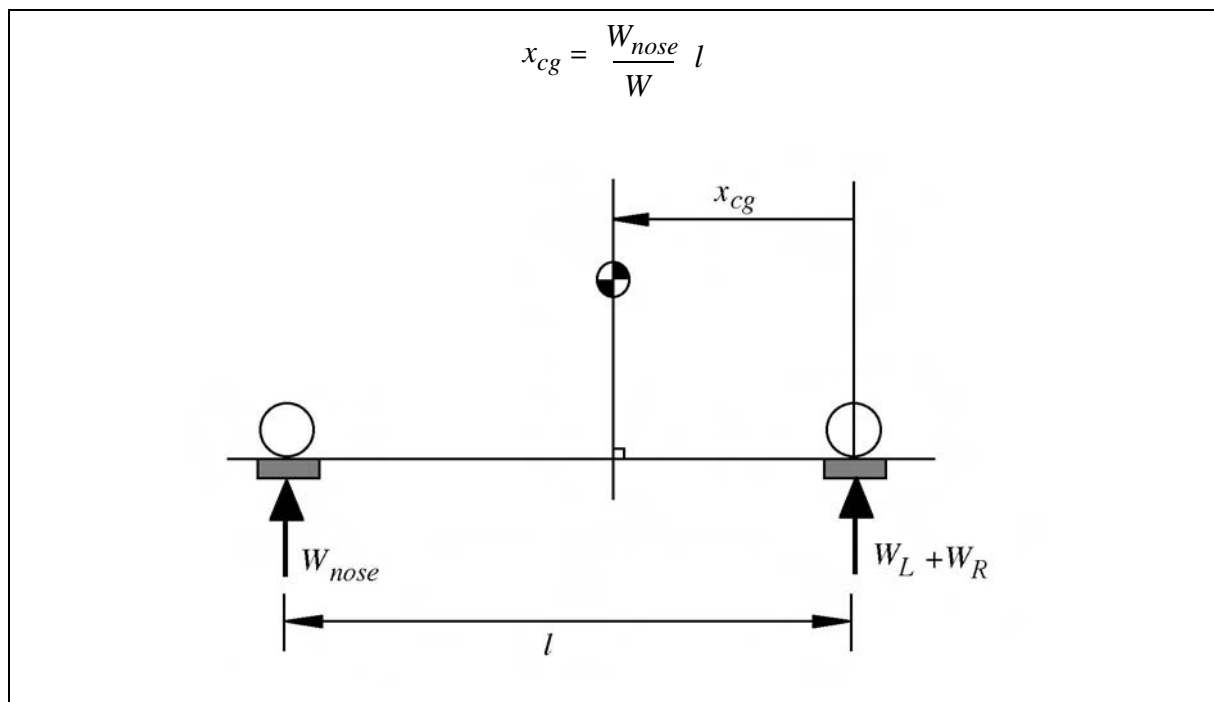
Figure A3.1   Measurement of Longitudinal c.g. Position

Note that W is the weight of the aircraft i.e. $W_L + W_R + W_{nose}$.

The nose of the aircraft should then be raised so that the keel is inclined no less than 5 deg to the level surface, and preferably 10 deg. Note that the scales should not be inclined, and are to remain level. From geometry shown in Figure A3.2, the vertical location of the c.g., relative to the original level surface, is given by:

$$z_{cg} = \frac{l(W_{nose} - W'_{nose})}{W \tan \theta}$$

where θ is the angle by which the keel has been raised. W_{nose} is the nose wheel reaction from stage 1, and W'_{nose} is the nose wheel reaction from the inclined test. It can be seen that only a few simple measurements need to be taken. However, the above equation emphasises the need for accuracy, especially in the measurement of the wheelbase. This is because of the tanq term. For inclined angles of around 5 deg, a 1 mm error in wheelbase will produce a 1 cm error in z_{cg}. For incline angles of 10 deg, this error is reduced by half, consequently angles greater than 10 deg. are desirable, however in practical terms aircraft handling can become difficult above this angle.
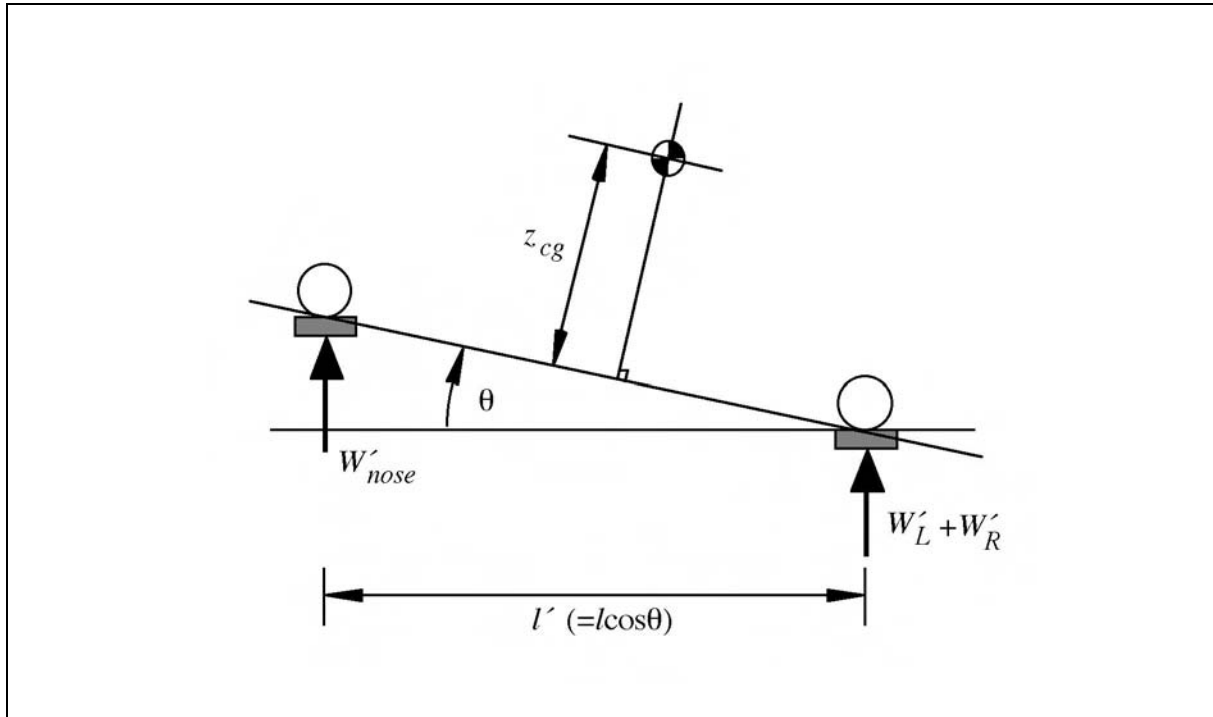
Figure A3.2   Measurement of Vertical c.g. Position

Appendix 4 Aircraft Dynamic Stability

The aim of this Appendix is to give the reader who is unfamiliar with theoretical flight dynamics some background and insight into the subject. For a more complete treatment, the reader is referred to the various textbooks on the subject which are widely available.

1   Aircraft Nonlinear Equations of Motion

A conventional fixed wing aircraft has 6 degrees of freedom (3 translational and 3 angular), and therefore, as described in Section 4 of this report, the aircraft nonlinear body equations of motion are given in the form of the Euler equations:

$$m(\dot{U} + QW - VR) = X - mg\sin\Theta$$
$$m(\dot{V} + RU - PW) = Y + mg\cos\Theta\sin\Phi$$
$$m(\dot{W} + PV - QU) = Z + mg\cos\Theta\cos\Phi$$

$$I_{xx}\dot{P} - I_{xz}\dot{R} + QR(I_{zz} - I_{yy}) - PQI_{xz} = L$$
$$I_{yy}\dot{Q} + RP(I_{xx} - I_{zz}) + (P^2 - R^2)I_{xz} = M$$
$$I_{zz}\dot{R} - I_{xz}\dot{P} + PQ(I_{yy} - I_{xx}) + QRI_{xz} = N$$

$$(A4.1)$$

In addition, the rotational kinematics are given by the expressions:

$$\dot{\Phi} = P + Q\sin\Phi\tan\Theta + R\cos\Phi\tan\Theta$$

$$\dot{\Theta} = Q\cos\Phi - R\sin\Phi$$

$$\dot{\Psi} = Q\sin\Phi\sec\Theta + R\cos\Phi\sec\Theta$$

$$(A4.2)$$

The various symbols used, and the sign convention for the state variables are given in convenient form in Table A4.1 and Figure A4.1.

For rotorcraft applications other degrees of freedom must be added: rotor speed, rotor inflow and most significantly, the blade degrees of freedom (flap, teeter, lag and pitch).

Table A4.1   State Variables for a Conventional 6 Degree of Freedom Aircraft Model

Aircraft Axis	TRANSLATIONAL			ANGULAR			
	Motion	**Velocity**	**force**	**Motion**	**Displacement**	**Rate**	**Moment**
x_b	Fore/Aft	U	X	Roll	Φ	P	L
y_b	Sidewards	V	Y	Pitch	Θ	Q	M
z_b	Heave	W	Z	Yaw	Ψ	R	N
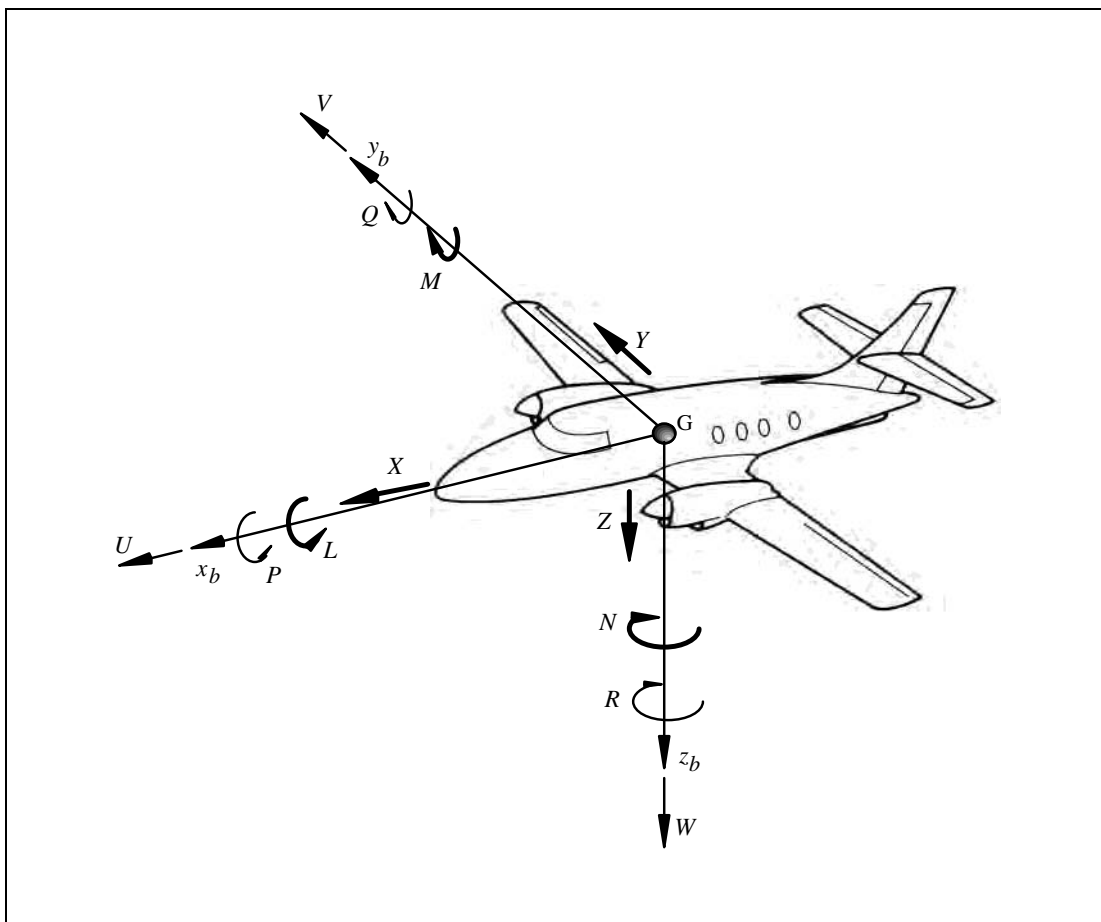
Figure A4.1   Conventions for Body Axes Set and State Variables

The mathematical model can then consist of a large set of nonlinear equations, often expressed in general form as:

$$\dot{\underline{x}} = f(\underline{x}, \underline{u})$$

(A4.3)

where $\underline{x}$ is the state vector which, for a conventional aircraft, will consist of the body states:

$$\underline{x} = \begin{bmatrix} U V W P Q R \Phi \Theta \end{bmatrix}^T$$

but supplemented by the various rotor states for a rotorcraft, for example:

$$\underline{x} = \begin{bmatrix} U V W P Q R \Phi \Theta \Omega v_0 v_{1_s} v_{1_s} \beta_1 \ldots \end{bmatrix}^T$$

The control vector, $\underline{u}$, is given for an aircraft with conventional controls (throttle, elevator, aileron, rudder) as:

$$\underline{u} = \begin{bmatrix} \delta_t \delta_e \delta_a \delta_r \end{bmatrix}^T$$

For a gyroplane with controls consisting of throttle, longitudinal and lateral stick, and rudder, we write the control vector as:

$$\underline{u} = \begin{bmatrix} \delta_t \eta_s \eta_c \delta_r \end{bmatrix}^T$$

The real modelling effort is in deriving analytical or empirical expressions for the external forces and moments (*X, Y, Z, L, M, N*). It is in the way these are calculated (and of course in the nature of the parametric data used) that different configurations may be simulated using basically the same equations. Equations (A4.3) are most often used to calculate the response of the aircraft, $\underline{x}$, due to a single or series of perturbations of the control vector, $\underline{u}$. Due to the complexity of the equations, a numerical algorithm such as the Runge-Kutta method is used for this calculation.

2   The Linearised Equations of Motion

The usual approach to determining the dynamic characteristics of a vehicle is to consider the linearised representation of the equations of motion. In these equations each state variable is considered to be composed of an equilibrium (trim) component and a small perturbation component, i.e. $U = U_e + u$ etc. The linearised equations become functions of the perturbations rather than the full values of the states. The major limitation of the linearised equations is that they are only valid for small perturbations from trim. For a fixed wing aircraft it is possible to linearise analytically, and for most aircraft types it is possible to decouple longitudinal and lateral directional dynamics. Written in state-space form:

$$\underline{\dot{x}} = \mathbf{A}\underline{x} + \mathbf{B}\underline{u}$$

(A4.4)

the two sets of equations are firstly, for longitudinal flight:

$$
\begin{bmatrix} \dot{u} \\ \dot{w} \\ \dot{q} \\ \dot{\theta} \end{bmatrix} = \begin{bmatrix} X_u & X_w & 0 & -g\cos\Theta_e \\ Z_u & Z_w & U_e & -g\sin\Theta_e \\ M_u^* & M_w^* & M_q^* & M_{\theta*} \\ 0 & 0 & 1 & 0 \end{bmatrix} \begin{bmatrix} u \\ w \\ q \\ \theta \end{bmatrix} + \begin{bmatrix} 0 \\ Z_{\delta_e} \\ M_{\delta_e} \\ 0 \end{bmatrix} [\delta_e]
$$

and then for the lateral/directional motion:

$$
\begin{bmatrix} \dot{v} \\ \dot{p} \\ \dot{r} \\ \dot{\phi} \\ \dot{\psi} \end{bmatrix} = \begin{bmatrix} Y_v & 0 & -U_e & g\cos\Theta_e & 0 \\ L_v^* & L_p^* & L_r^* & 0 & 0 \\ N_v^* & N_p^* & N_r^* & 0 & 0 \\ 0 & 1 & \tan\Theta_e & 0 & 0 \\ 0 & 0 & \sec\Theta_e & 0 & 0 \end{bmatrix} \begin{bmatrix} v \\ p \\ r \\ \phi \\ \psi \end{bmatrix} + \begin{bmatrix} Y_{\delta_r} & 0 \\ L_{\delta_r}^* & L_{\delta_a}^* \\ N_{\delta_r}^* & N_{\delta_a}^* \\ 0 & 0 \\ 0 & 0 \end{bmatrix} \begin{bmatrix} \delta_r \\ \delta_a \end{bmatrix}
$$

The terms in the equations such as X_u, X_w etc. are known as the "stability derivatives", and are defined as:

$$
X_u = \frac{\partial X}{\partial u}, X_w = \frac{\partial X}{\partial w} \quad \text{etc.}
$$

These are calculated (analytically or numerically) for a particular trim state and mathematically they are the first order terms in a Taylor series expansion representing an external force or moment (for example, $X = X_e + X_u u + X_w w + \ldots$). Physically they also have significance; for example X_u is the change in X-force experienced due to a small change in velocity, u. It is known as the "speed damping" derivative and plays an important role in the damping of the phugoid. An aircraft with a particularly small value for X_u will have insufficient phugoid damping, or even an unstable phugoid. Many of the other derivatives have important roles in stability analysis, and the reader is again referred to the standard textbooks for further information.

For the rotorcraft problem, the complexity of the forces and moments calculations, and the very strong coupling between longitudinal and lateral directional motion makes analytical derivation impossible, and a numerical method is used instead. To represent the longitudinal dynamics of the light gyroplane it is found that the rotor speed degree of freedom has to be included. The equations of motion can be written as:

$$
\begin{bmatrix} \dot{u} \\ \dot{w} \\ \dot{q} \\ \dot{\theta} \\ \dot{\Omega} \end{bmatrix} = \begin{bmatrix} X_u & X_w & X_q & X_\theta & X_\Omega \\ Z_u & Z_w & Z_q & Z_\theta & Z_\Omega \\ M_u & M_w & M_q & M_\theta & M_\Omega \\ 0 & 0 & 1 & 0 & 0 \\ Q_u & Q_w & Q_q & Q_\theta & Q_\Omega \end{bmatrix} \begin{bmatrix} u \\ w \\ q \\ \theta \\ \Omega \end{bmatrix} + \begin{bmatrix} X_{\eta_s} \\ Z_{\eta_s} \\ M_{\eta_s} \\ 0 \\ Q_{\eta_s} \end{bmatrix} [\eta_{1_s}]
$$

(A4.5)

3   Prediction of Dynamic Stability

Consider the state space equation, equation (A4.4) applied for the stick fixed situation (i.e. $\underline{u}$ = 0). We then have:

$$\underline{\dot{x}} = \mathbf{A}\underline{x}$$

(A4.6)

This equation represents a system of n first order, linear ordinary differential equations where n is the number of states and therefore degrees of freedom. This will have a general solution:

$$x_i = x_{0_i} e^{\lambda t}$$

(A4.7)

for i = 1, n, or in vector form:

$$\underline{x} = \underline{x_0} e^{\lambda t}$$

differentiating this and substituting in (A4.6):

$$\lambda \underline{x_0} e^{\lambda t} = \mathbf{A}\underline{x_0} e^{\lambda t}$$

Noting that this is a vector-matrix equation we can write:

$$\left(\lambda \mathbf{I} - \mathbf{A}\right)\underline{x_0} = 0$$

where $\mathbf{I}$ is the (nxn) identity matrix. In this expression $(\lambda \mathbf{I} - \mathbf{A})$ is an (nxn) matrix, while $\underline{x_0}$ is a vector of dimension (n). This equation has a trivial solution: $\underline{x_0}$ = 0, or the more useful solution that the determinant of $(\lambda \mathbf{I} - \mathbf{A})$ should be zero:

$$\left|\lambda \mathbf{I} - \mathbf{A}\right| = 0$$

(A4.8)

Equation (A4.8) is the characteristic equation which will be a polynomial of order n, and on factorisation its solution will yield n roots, or "eigenvalues", from which the stability of the system can be determined. Consider the general case of an eigenvalue being a complex number:

$$\lambda = \mathrm{Re}(\lambda) \pm i\,\mathrm{Im}(\lambda)$$

Substituting this into the general solution given by equation (A4.7):

$$x = x_0 e^{\lambda t} = x_0 e^{(\mathrm{Re}(\lambda)+i\,\mathrm{Im}(\lambda))t} = x_0 e^{\mathrm{Re}(\lambda)t} e^{i\,\mathrm{Im}(\lambda)t}$$

or

$$x = x_0 e^{\mathrm{Re}(\lambda)t} \big(\cos(\mathrm{Im}(\lambda)t) \pm i\sin(\mathrm{Im}(\lambda)t)\big)$$

(A4.9)

The response will therefore be oscillatory in nature with the imaginary part of the eigenvalue giving the frequency of the oscillation. If the real part of the eigenvalue is positive then the amplitude of the oscillations will increase exponentially, an unstable situation. Should however, the real part of the eignevalue be negative, then the amplitude will decay – a stable situation. Should the eigenvalue be real, then the solution is simply:

$$x = x_0 e^{\lambda t}$$

and the characteristic response will be exponential in form. If λ is negative then after a disturbance the aircraft's response will decay tending to return it to a steady state condition (a stable situation). Should λ be positive then the disturbance will grow and we have an unstable situation.

It is clear then that once the linearised equations are written in state space form, (A4.4), then it is possible to obtain the characteristic equation from (A4.8), the solution of which will give the aircraft's eigenvalues which can then be interpreted in order to predict its stability. The nature of the response can be quantified by calculating the damping and natural frequency of the mode from its eigenvalue. Consider a general eigenvalue:

$$\lambda = \sigma \pm i\omega$$

(A4.10)

This will have been derived from a quadratic factor of the characteristic equation (A4.8):

$$\lambda^2 - 2\sigma\lambda + \big(\sigma^2 + \omega^2\big) = 0$$

(A4.11)

that is:

$$(\lambda - \sigma - i\omega)(\lambda - \sigma + i\omega) = \lambda^2 - 2\sigma\lambda + \big(\sigma^2 + \omega^2\big)$$

Equation (A4.11) can be compared to the characteristic equation of a general 2nd order damped system. Consider first the general equation of motion for a damped 2nd order system:

$$\ddot{x} + 2\zeta\omega_n\dot{x} + \omega_n^2 x = 0$$

(A4.12)

where ζ is the damping ratio and ω_n is the undamped natural frequency. The undamped natural frequency is the frequency at which the system would oscillate without the presence of damping (essentially the frequency in simple harmonic motion). Making the substitution $x = x_0 e^{\lambda t}$ again, we get the characteristic equation:

$$\lambda^2 + 2\zeta\omega_n\lambda + \omega_n^2 = 0$$

This gives: $\omega_n^2 = \sigma^2 + \omega^2$ and $\zeta\omega = -\sigma$, or:

$$\omega_n = \sqrt{\sigma^2 + \omega^2} \text{ and} \zeta = \frac{-\sigma}{\sqrt{\sigma^2 + \omega^2}}$$

(A4.13)

It is therefore apparent that the damping and natural frequency associated with a dynamic mode can be derived directly from the real and imaginary parts of its eigenvalue. As there is damping present we require the damped natural frequency, ω_d, which in general is given by:

$$\omega_d = \omega_n\sqrt{1-\zeta^2}$$

or

$$\omega_d^2 = \omega_n^2\left(1-\zeta^2\right) = \omega_n^2 - \omega_n^2\zeta^2$$

Noting that $\zeta^2\omega_n^2 = \sigma^2$, we can write:

$$\omega_d^2 = \left(\sigma^2 + \omega^2\right) - \sigma^2 = \omega^2 \quad \text{or} \quad \omega_d = \omega$$

Hence, when a complex conjugate pair of eigenvalues $\lambda = \sigma \pm \iota\omega$ is present, the frequency of the resulting oscillation is given by the imaginary part of the eigenvalue, ω. This is also apparent on inspection of the general solution given by eqn (A4.9). The period of the oscillation is therefore given by:

$$T = \frac{2\pi}{\omega} = \frac{2\pi}{\text{Re}(\lambda)}$$

The way in which eigenvalues can be interpreted with respect to aircraft stability can be summarised, with reference to Figure A4.2, as follows:

λ Real and Negative :   This gives an aperiodic mode with an exponential decay or a "Convergence". This situation is indicative of static stability.

λ Real and Positive :   This gives an aperiodic mode with exponential growth or a "Divergence". This situation is indicative of static instability.

λ Complex -ve Real Part : This gives an oscillatory motion with a decreasing amplitude. This situation is indicative of dynamic stability.

λ Complex +ve Real Part : This gives an oscillatory motion with an increasing amplitude. This situation is indicative of dynamic instability.

4   Damping Ratio, ζ

Any force (or moment) acting on a system which is proportional to the velocity of the system is referred to as a "damping". The damping ratio relates the effective damping of the system, c, to its critical value:

$$\zeta = \frac{c}{c_{crit}}$$
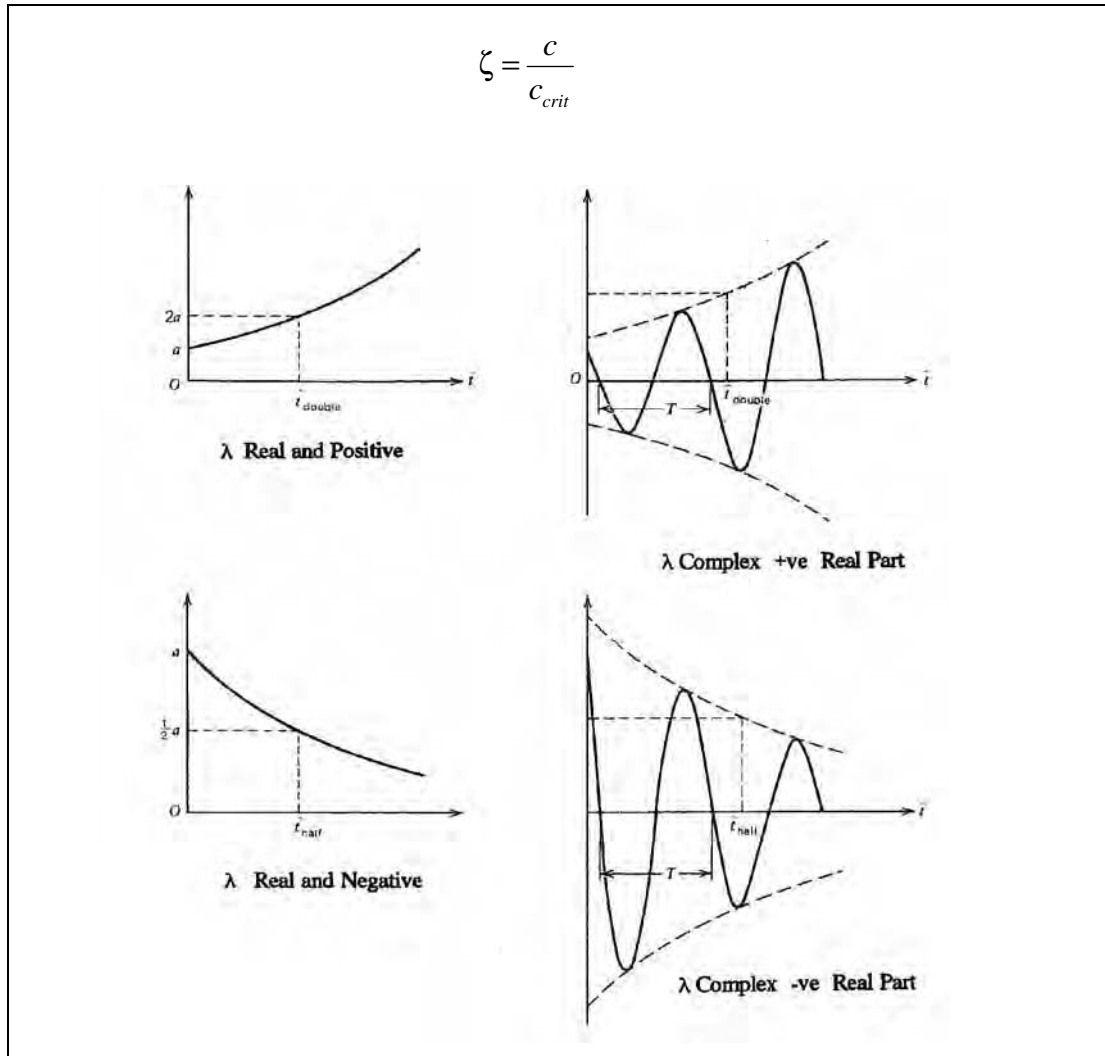
Figure A4.2   Characteristic Motions for Dynamic and Static Stability (Reproduced and Modified from Figure 6.1: "Dynamics of Flight", B. Etkin, 2nd Edition, Wiley, 1982)

The critical value of damping is best explained by considering the solution of (A4.12). The solution of this differential equation is dependent on the value of the damping ratio ζ.

i) $\zeta \leq 1$ (Underdamped Damped System)

This is the most common situation, and the solution of equation (A4.12) for an initial displacement x_0 is:

$$x(t) = x_0 e^{-\zeta \omega_n t} \left[\cos \omega_d t + \frac{\zeta}{\sqrt{1-\zeta^2}} \sin \omega_d t \right]$$

This gives an oscillation with damped natural frequency, ω_d, given by:

$$\omega_d = \omega_n \sqrt{1 - \zeta^2}$$

but with decaying amplitude, Figure A4.3
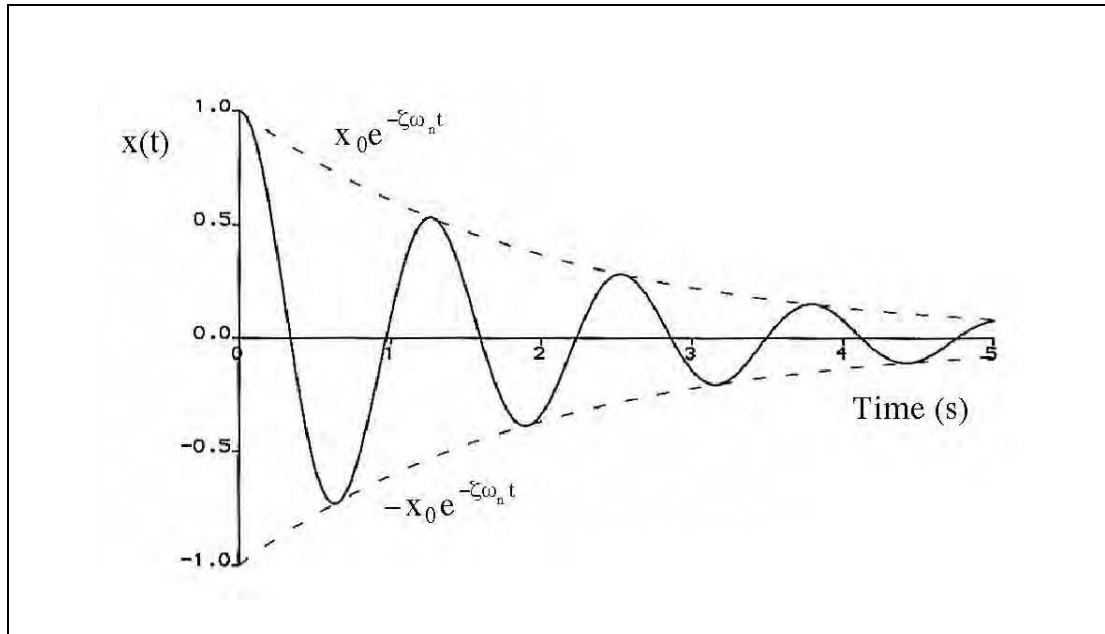
Figure A4.3   Free Vibration of an Underdamped 2nd Order System
($x_0 = 1.0$, $\omega_n = 5$ rad/s, $\zeta = 0.1$)

ii) <u>$\zeta > 1$</u> **(Overdamped System)**

Here the solution is:

$$x(t) = x_0 e^{-\zeta \omega_n t} \left[A e^{\left(\omega_n \sqrt{\zeta^2 - 1} \right) t} + B e^{-\left(\omega_n \sqrt{\zeta^2 - 1} \right) t} \right]$$

where A and B are constants related to the damping ratio, ζ. This gives an exponential response a indicated in Figure A4.3.

iii) <u>$\zeta = 1$</u> **(Critically Damped System)**

Critical damping is defined as $\zeta = 1$ or $c = c_{crit}$. For this particular case the response is again exponential and is given by:

$$x(t) = x_0 (1 + \omega_n t) e^{-\omega_n t}$$

$$x(t) = x_0(1 + \omega_n t)e^{-\omega_n t}$$
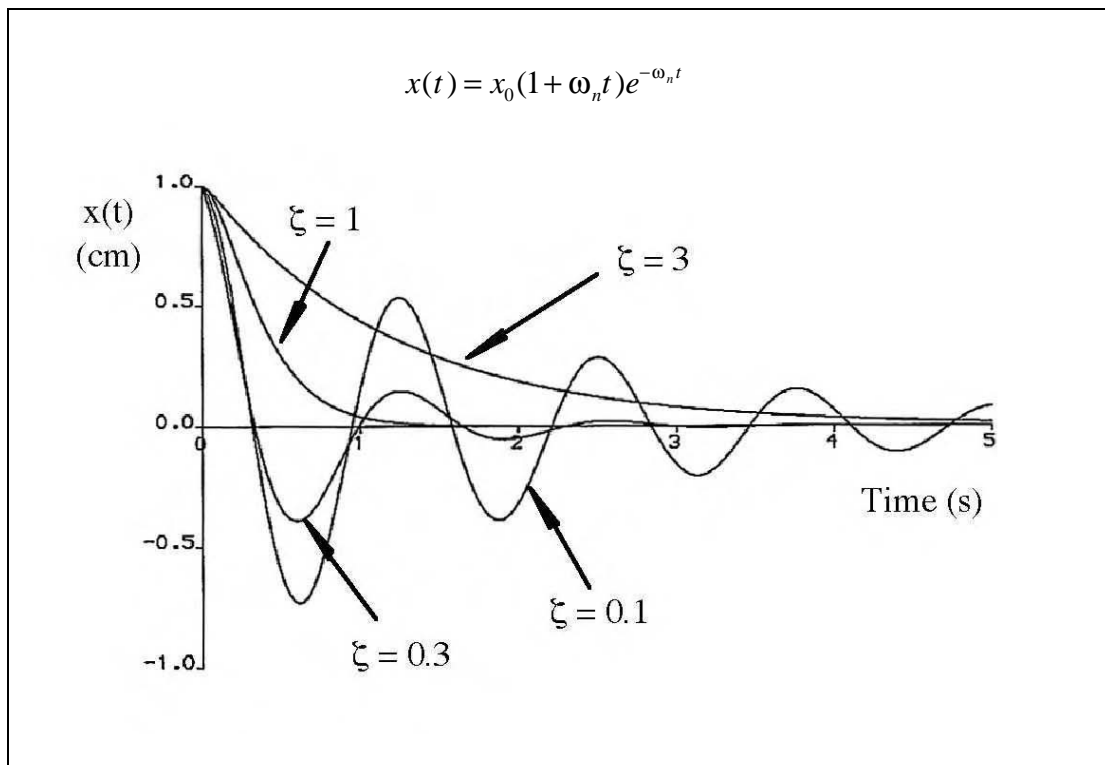
Figure A4.4   Effect of Damping Ratio on System Response
(x$_0$ = 1.0, ω_n = 5 rad/s)

The effect of damping on a second order system is presented in Figure A4.4. For all values of ζ < 1 the response will be oscillatory. The critical value is ζ = 1 after which the response is non-oscillatory and has exponential form. For stable, lightly damped systems (say 0 < ζ < 0.2) any disturbance will result in an oscillation which can take several cycles to settle, whilst moderately damped systems (say, 0.3 < ζ < 0.6) may only take a few cycles before settling on a new steady state. For heavily damped systems the nature of the response is determined by whether the system is under-damped or over-damped. For an under-damped system, in response to a disturbance, a heavily damping system (say, 0.7 < ζ < 1) would have a response which had perhaps only one or two cycles before settling. As damping is increased beyond the critical value (i.e. ζ > 1), the response type is exponential, and as damping is increased, the speed of the response drops so that systems with ζ >1 take a significant time to settle.

5   Representing Stability Characteristics on the Root Locus Plot

An aircraft's stability properties can vary with flight condition or with a configurational parameter (c.g. position or a control system gain, for example). Mathematically, the values of the stability derivatives change with flight condition and configurational parameter, and consequently so do the eigenvalues. As the eigenvalues are often complex numbers, it is convenient to plot them on a complex plane, Figure A4.3. The convention is to label the axes as the Real (part of the eigenvalue) versus the Imaginary (part of the eigenvalue). Referring to equation (A4.10) essentially, once the eigenvalue λ is calculated the real part σ is plotted against the imaginary part ω. The plot of a particular eigenvalue as a flight state or configurational parameter is varied is known as its "root locus". Any eigenvalue with a negative real part is of course stable,

and so any eigenvalue to the left of the imaginary axis indicates stability, any eigenvalue to the right (positive real part) instability. Any real eigenvalue will lie on the real axis, and again if this is to the left of the imaginary axis the mode is stable. Any complex eigenvalue appears as a conjugate pair and therefore the root locus diagram is symmetrical about the real axis, however conventionally only the top half of the plane is drawn. Examples of a root loci plots are given throughout this report, for example, Figure 4.3.

As demonstrated above, equation (A4.13), the damping and natural frequency of the mode may be derived from the real and imaginary parts, and so it is also possible to plot natural frequency vs damping ratio. It should be appreciated however that only complex eigenvalues (oscillatory modes) can be plotted, unlike the conventional root locus which includes real eigenvalues. Further, as a positive damping ratio indicates stability (that is decaying amplitude of oscillation), when eigenvalues are plotted as frequency vs damping ratio, values lying to the right hand side of the frequency axis indicate stable modes.
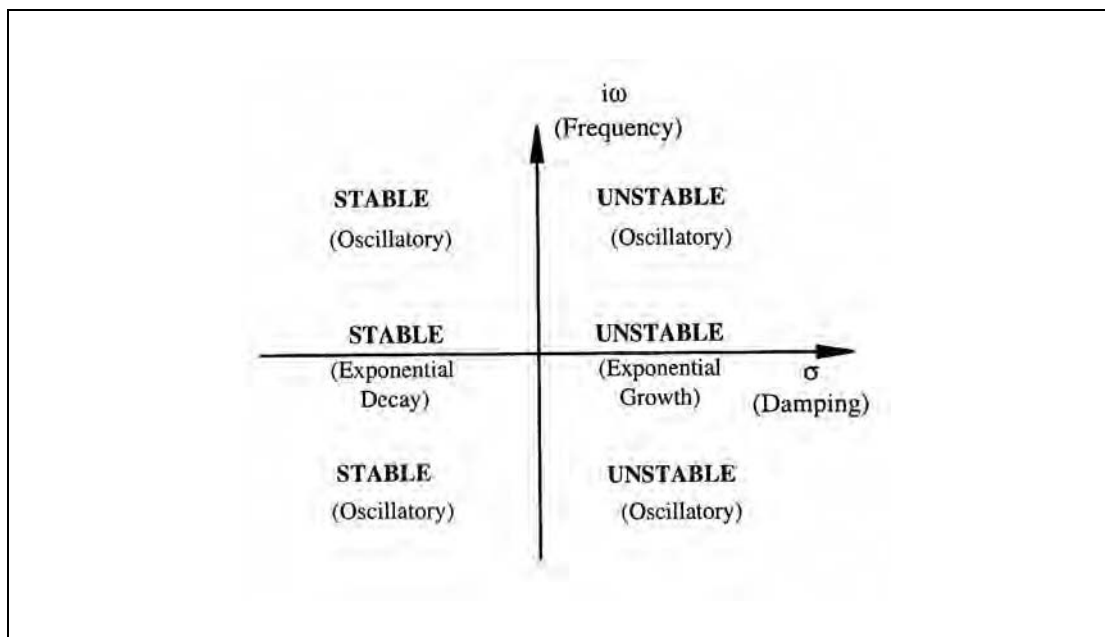
Figure A4.5   Stability Presented on Complex Plane

6   Quantitative Example

Referring to Section 4 of this report, the use of the RASCAL model is described, and calculations for the VPM M16 are presented. Trim calculations and time response results are shown. Here, for clarity, the way in which the eigenvalues for Figure 4.3 and 4.4 are calculated is presented. The model structure used is as in equation (A4.3), and expressing this in the form of equation (A4.4),that is for stick fixed flight, we have:

$$
\begin{bmatrix} \dot{u} \\ \dot{w} \\ \dot{q} \\ \dot{\theta} \\ \dot{\Omega} \end{bmatrix} = \begin{bmatrix} X_u & X_w & X_q & X_\theta & X_\Omega \\ Z_u & Z_w & Z_q & Z_\theta & Z_\Omega \\ M_u & M_w & M_q & M_\theta & M_\Omega \\ 0 & 0 & 1 & 0 & 0 \\ Q_u & Q_w & Q_q & Q_\theta & Q_\Omega \end{bmatrix} \begin{bmatrix} u \\ w \\ q \\ \theta \\ \Omega \end{bmatrix}
$$

Substituting the derivative values from the linearised RASCAL model for the 30mph flight condition we get:

$$
\begin{bmatrix} \dot{u} \\ \dot{w} \\ \dot{q} \\ \dot{\theta} \\ \dot{\Omega} \end{bmatrix} = \begin{bmatrix} -0.141 & -0.160 & 0.191 & -9.090 & 0.050 \\ -0.164 & -0.903 & 13.324 & -0.903 & 0.287 \\ 0.018 & -0.063 & -1.597 & 0.306 & 0.009 \\ 0 & 0 & 1 & 0 & 0 \\ -0.137 & -0.631 & 1.464 & 0.001 & -0.155 \end{bmatrix} \begin{bmatrix} u \\ w \\ q \\ \theta \\ \Omega \end{bmatrix}
$$

Applying equation (A4.8) we get the 5th order polynomial, characteristic equation:

$$
\lambda^5 + 2.796\lambda^4 + 2.8825\lambda^3 + 0.8643\lambda^2 - 0.1961\lambda + 0.07387 = 0
$$

When factorised this becomes:

$$
\left(\lambda^2 + 2.4408\lambda + 1.9625\right)\left(\lambda^2 - 0.078\lambda + 0.0869\right)\left(\lambda + 0.4331\right) = 0
$$

giving the eigenvalues:

$$
\lambda = -1.2204 \pm 0.6876\mathrm{i}
$$

$$
\lambda = 0.039 \pm 0.2922\mathrm{i}
$$

$$
\lambda = -0.4331
$$

The real part will have units of s^{-1}, whilst the imaginary part (i.e. the frequency) has units of rad/s. In referring to BCAR Section T where criteria are expressed in cycles/s the frequency is converted by dividing by 2π, and hence the final form of the eigenvalues is:

$$\lambda = -1.2204 \pm 0.1094i$$

$$\lambda = 0.039 \pm 0.0465i$$

$$\lambda = -0.4331$$

which correspond to the points on Figure 4.3 marked for the 30mph case.

The first of these eigenvalues is stable (real part is negative) and corresponds to the **short period** mode. This mode is characterised by a heavily damped pitching oscillation. In this case, the natural frequency, damping, and damped natural frequency are calculated as follows:

$$\omega_n^2 = 1.9625, \therefore \omega_n = 1.4 \text{rad/s} \, (= 0.1094 \text{cycles/s})$$

$$2\zeta\omega_n = 2.4408, \therefore \zeta = 0.8717$$

$$\omega_d = \omega_n\sqrt{1-\zeta^2}, \therefore \omega_d = 0.686 \text{rad/s} \quad (\text{or} \quad \omega_d = \text{Re}(\lambda))$$

The second mode is unstable (real part is positive) and corresponds to the phugoid which is a longer period oscillation in airspeed and altitude. The characteristic parameters are:

$$\omega_n^2 = 0.0869, \therefore \omega_n = 0.2948 \text{rad/s} \, (= 0.0465 \text{cycles/s})$$

$$2\zeta\omega_n = -0.078, \therefore \zeta = -0.1323$$

$$\omega_d = \omega_n\sqrt{1-\zeta^2}, \therefore \omega_d = 0.2922 \text{rad/s} \quad (\text{again}, \quad \omega_d = \text{Re}(\lambda))$$

The third mode is a <u>rotor speed</u> mode which is stable (negative real part). Aperiodic modes are characterised by the time to half amplitude (for a stable mode) or time to double amplitude (for an unstable mode). Here we have:

$$t_{\frac{1}{2}} = \frac{0.69}{\left|\text{Re}(\lambda)\right|}, \therefore \ t_{\frac{1}{2}} = 1.593\text{s}$$

The above calculation was repeated at a series of flight speeds to give the set of eigenvalues plotted on Figure 4.3 which shows the root locus of the aircraft over its normal flight range. Both the rotor speed and short period modes remain stable across the speed range, however the phugoid is unstable at low speed but stable at higher speeds (the root locus showing that the eigenvalue migrates from the right to the left hand half plane as airspeed increases).

The alternative presentation of the eigenvalues where frequency is plotted against damping ratio is presented in Figure 4.4. At 30 mph the phugoid mode, from above, gives the point (ζ, ω_n) as (-0.1323, 0.0465) which is unstable (negative damping indicating increasing amplitude) whilst the short period mode at 30 mph gives the point (0.8717, 0.1094) which lies on the right hand side of the axis, which is stable for this format of plot.

Appendix 5   Flight Test Instruction for Teeter Trials

Civil Aviation Authority

Flight Test Instruction

<u>Investigation of Gyroplane Teeter Margin Limits</u>

<u>Montgomerie-Parsons Gyroplane G-UNIV</u>

Prepared	- W F R White (Flight Test Engineer)	**Date**	- - - - - - - - - - - - - - -
Checked	- Dr S Houston (Trials Sponsor)	**Date**	- - - - - - - - - - - - - - -
Checked	- B de Saar (Trials Pilot)	**Date**	- - - - - - - - - - - - - - -
Authorised	- N Talbot (Deputy Chief Test Pilot)	**Date**	- - - - - - - - - - - - - - -

Distribution

<u>Glasgow University</u>

Dr S Houston

<u>CAA</u>

Mr N Talbot

Mr G Greene

Mr A Maxwell

Mr K Dodson

Mr B de Saar

<u>FR Aviation</u>

Mr C Handley

1   Introduction

An investigation into gyroplane stability by Glasgow University has been conducted using the RASCAL simulation model, validated by flight trials of 2 instrumentated gyroplanes, VPM M16, G-BWGI and Montgomerie-Parsons, G-UNIV. The investigation has concluded that degraded longitudinal stability characteristics are to be expected, should the thrust line be more than 2" higher than the vertical CG for contemporary light gyroplanes.

The model validation is, however, deficient in that it was not possible to instrument the rotor teeter (flapping) angle on either aircraft.

Review of BCAR Section T has identified that the definition of V_{NE} in terms of control margins is less than ideal, and compliance demonstration is very difficult, if not impossible without specialised instrumentation.

AMC T143: The gyroplane's V_{NE} will normally be dictated by the need to have a positive teeter margin up to V_{NE} + 15%.

Accordingly, a further flight trial has been proposed to investigate the teeter behaviour of the McCutcheon rotor of Montgomerie-Parsons, G-UNIV, the aim being:

a) To validate the model teeter behaviour with actual flight test data.

b) Review the results of the research investigation with the enhanced model.

c) To use the model with confidence to predict the stability characteristics of other light gyroplanes.

d) To support a technical review of the BCAR Section T definition of V_{NE} and associated control margins.

2   Aircraft Details

The trials aircraft will be the Glasgow University owned Montgomerie-Parsons 2-place, modified autogyro, G-UNIV.

The aircraft is equipped with a standard "Merlin" type cockpit nacelle for the forward seat. AAN27261 defines the installation of an instrumentation package. The rear seat/fuel tank has been replaced by an alternative tank with a faired mounting for a laptop computer which is used for flight test data acquisition.

A 25 ft McCutcheon rotor is installed. Engine is a Rotax 618, 75 hp, and propellor is an Ivoprop 3 blade 60".

3   Instrumentation

The following data are recorded on the on-board laptop PC:

- Control positions, longitudinal, lateral and yaw

- Pitch, Roll and Yaw attitudes

- 3 axis body rates and accelerations

- GPS position and x, y velocities

- Airspeed

- Altitude

- OAT

- Angle of attack

- Sideslip angle

- Rotor rpm

- Engine rpm

- Event number

- Voice

For this trial, a rotor teeter angle potentiometer is installed with the data transmitted over slip rings to the recording system. 360° rotor azimuth is also recorded.

The teeter angle instrumentation has been developed by Glasgow University with the support of the gyroplane manufacturer, JM Montgomerie, who has also been responsible for the reassembly of the modified rotor head.

4   Personnel

CAA	WFR White (Flight Test Engineer and co-sponsor)
	N Talbot (Deputy Chief Test Pilot)
CAA (under contract)	B de Saar (Trials Pilot)
Glasgow University	Dr S Houston (Trials Sponsor)
	Dr D Thomson (Head of Dept.)
	Mr R Gilmour (Responsible for Instrumentation Design and installation)

5   Operational Aspects

5.1   Trials Location

The trials will be conducted from Perth Aerodrome.

5.2   Trials Area

Test flights will be conducted away from built up areas, but where observation from the ground, by means of binoculars, as required to monitor aircraft behaviour and assist with pilot evaluation, is possible.

5.3   Communications

To facilitate the conduct of the trial, a dedicated trials frequency will be required.

5.4   Weather

Tests will be conducted in VMC by day only in as calm conditions as possible. No flights will be conducted in precipitation. Minimum cloudbase – 1000 ft, minimum visibility – 5 km, with good visual horizon.

5.5   Trials Management

Each test flight will be briefed thoroughly beforehand. A flight card (Figure A5-1) will be prepared during each briefing.

5.6   Trials Pilot

The trials pilot, Mr de Saar, is an experienced gyroplane pilot and instructor who has been given basic training in flight test techniques and who has already conducted a number of supervised handling and stability investigations on Bensen and Air Command gyroplanes.

Basic serviceability checks of the aircraft and instrumentation system prior to commencement of actual data gathering will ensure a suitable level of familiarisation with the type.

5.7   **Aircraft Servicing**

Normal aircraft serviceability checks will be performed by Mr de Saar as approved by the CAA AMSD. In the event that major maintenance action is required, additional approved engineering personnel will be engaged as required.

5.8   **Insurance**

No hull insurance is available. Third party liability is currently limited to £250,000.

6   Limitations

6.1   Tests will be conducted within the normal approved flight envelope of the aircraft, except that flight to V_{DF} ($1.11V_{NE}$) may be investigated.

6.2   The programme will be conducted incrementally. Basic analysis of data from each flight will be conducted before continuing the programme.

6.3   Sideslip tests will initially be limited to ±10°. Following preliminary analysis of flight test data, consideration will be given to progressively increasing the sideslip angle, particularly at lower airspeeds.

7   Safety of Flight Test

7.1   All test flying will be carried out in an incremental manner.

7.2   All manoeuvres involving a possible reduction of normal 'g' must be carried out in a very progressive manner. Account must be taken that nose up control inputs could lead to reductions of normal 'g', e.g. nose up input to establish phugoid behaviour is likely subsequently to result in nose down pitch rates greater than that generated by the initial nose up input.

7.3   Manoeuvres must be stopped if a noticeable reduction in normal 'g' or a rapid reduction in rotor rpm is perceived by the pilot.

7.4   Manoeuvres must be stopped if high or rapidly increasing pitch rates occur, particularly nose down.

7.5   Extreme attitudes are to be avoided. For guidance, pitch attitudes beyond ± 30 degrees with low pitch rates should be considered excessive. Lower pitch attitudes could be excessive with high pitch rates. Roll attitudes of greater than 60 degrees should be considered excessive

8   Test Programme

8.1   **Datum Flying**

A brief handling qualities evaluation will be conducted to assess the effect of the modified rotor head. This phase of testing will also be utilised to optimise the instrumentation system.

8.2   **Data Gathering**

The following flight conditions will be investigated:

8.2.1   **Airspeed Calibration**

The aircraft is equipped with an airspeed probe mounted on a boom. This will be used to calibrate the standard airspeed indicator during level flight constant speed runs.

8.2.2 **Steady State Conditions**

    a) Zero sideslip, trimmed, V_{min} to V_{NE}, in 5 mph increments.

    b) Min power speed, zero sideslip.

    c) Entry to, steady state and recovery from 30° turns at $V_{min\ power}$ and 65 mph.

    d) Entry to, steady state and recovery from 10° turns at V_{NE}.

    e) Max power climb, 50 mph.

    f) Cruise climb, 65 mph.

    g) Cruise descent, 65 mph.

    h) Idle descent, 65 mph.

    i) Idle descent, 50 mph.

    j) Min. control speed, idle power.

8.2.3 **Throttle slam**

From 65 mph and $V_{min\ power}$, with 1 sec pilot intervention time, and progressively increasing rates of power application.

8.2.4 **Throttle Chop**

From 65 mph, 40 mph and V_{min} with 1 sec pilot intervention time and progressively increasing rates of power reduction.

8.2.5 **Phugoid**

At $V_{min\ power}$, 60 and 65 mph, IAS. The phugoid will be investigated by means of an approximately 5° pitch disturbance, returning the cyclic to the trim position and recording the open loop response of the aircraft, stick fixed. Nose up inputs will be made first at each trim speed, and nose down inputs will be made with caution, and consideration of the response to the nose up input. In each case, the flight safety guidance detailed in paragraph 7 of this document will be observed.

8.2.6 **Control response**

Control response tests will be conducted at $V_{min\ power}$, 60 and 65 mph, IAS. An aft cyclic step input will be introduced and maintained, all other controls remaining fixed, and the aircraft response observed and recorded. Initially, the input will be approximately 1 cm (0.4"), sufficient to generate a pitch rate of approx 5°/sec. The amplitude of the cyclic input will be increased incrementally to generate an adequate pitch rate. In each case, the flight safety guidance detailed in paragraph 7 of this document will be observed particularly in determining the criteria for implementation of recovery action.

The tests will be repeated for left and right cyclic step inputs in turn.

Following analysis of aircraft response to the nose up inputs, consideration will be given to a cautious, progressive examination of the response to forward cyclic inputs.

8.2.7 **Steady Heading Sideslips**

Steady heading sideslips will be examined at $V_{min\ power}$, 60 and 65 mph IAS. Initially, ± 5° sideslip angles will be investigated and analysed before progressing to ± 10°. Following preliminary analysis of results, further testing may be conducted at greater sideslip angles. (see paragraph 7.4)

8.3   **Additional Tests**

Following analysis of the data gathered in paragraph 8.2, consideration will be given to investigating flight to V_{DF} (1.11 V_{NE}), and also turns on one control, pedal only.

8.3.1   **V_{DF}**

Flight to V_{DF} will only be undertaken following satisfactory exploration of the normal operating envelope to V_{NE}. In particular, satisfactory handling characteristics and adequate teeter margin will have been demonstrated.

For the actual test, the aircraft will be accelerated in level flight to the lesser of V_{NE} or V_H (maximum continuous power). Airspeed will then be progressively increased, initially by further throttle opening if available, then in a shallow dive to stabilise at V_{DF}. An instrumentation record will be taken and then a gentle deceleration to less than V_{NE} will be conducted by raising the nose as required and gently reducing power.

8.3.2   **Turns on 1 Control**

Turns on pedal only may be carried out to examine the rolling moment due to sideslip and the transient effect on lateral teeter margin. This test will only be conducted if examination of steady heading sideslips shows adequate lateral steady state teeter margin.

The aircraft will be stabilised at 60 mph level flight with zero sideslip. A pedal input sufficient to change heading by approx 5 - 10° will be introduced and maintained. Cyclic will be maintained in the trim position. The condition will be maintained until either a stable condition is achieved, or until flight safety considerations such as excessive roll or pitch attitude require a recovery. An instrumentation record will be taken throughout the manoeuvre. The test will be repeated for the opposite pedal input, and again at 65 mph and $V_{min\ power}$.

CAA FLIGHT TEST CARD

A/C TYPE:	Montgomerie Parsons	Reg:	G-UNIV

DATE		FLIGHT	

OBJECTIVE ....

ZFW:		TO FUEL:	
AUM		CG:	

CONFIGURATION ....

No.	TEST DESCRIPTION/REMARKS

FLIGHT TEST ENGINEER	TEST PILOT
TRAILS SPONSOR	

Figure A5.1   CAA Flight Test Card

INTENTIONALLY LEFT BLANK

Appendix 6   Kinematic Consistency

This Appendix is not intended as a tutorial on methods for analysing flight test data. The reader is referred to the excellent AGARD LS178 "Rotorcraft System Identification", [80] for detail on rotorcraft-specific applications. It is sufficient here to illustrate the approach taken by means of a trivial example.

If only pitching motion occurs, Euler's equations for kinematic angular motion reduce intuitively to:

$$\dot{\theta} = q$$

i.e. the rate of change of pitch angle is equal to the pitch rate. Given pitch rate from the rate gyroscope, integration of this signal should yield the pitch signal measured by the attitude gyroscope. If it does not, the data is kinematically inconsistent, and corrections need to be applied to the measured signals to render them consistent. This can be formalised as a least-squares optimisation problem, if the kinematic equation above is re-written as:

$$\dot{\theta} = kq + \delta$$

where k is a scale correction factor, and δ is a bias or offset correction. For a given k and δ, integration of this equation yields θ_{int}, the pitch attitude calculated from the rate information. Now if an error function is constructed as:

$$\varepsilon_\theta = \theta_{int} - \theta_m$$

where θ_m is the attitude gyroscope pitch information duly corrected itself for scale factor and bias, then a simple least-squares algorithm can be used to calculate the bias and scale factors required to minimise (to zero hopefully) the error ε_θ.

A similar process can be constructed for the air data and accelerometers - assuming still air conditions, integration of accelerometer information will give velocity components in aircraft body axes. The airspeed, sideslip and angle of attack can be used to calculate explicitly the corresponding velocity components, and exactly the same process as that described above can be applied to calculate scale factor and bias error corrections for these sensors.

Figure A6.1 shows attitude gyro roll and pitch outputs as measured during a phugoid test (70mph) using the VPM aircraft, and once corrected by the process described above. Of note is the fact that the scale factor in each case is close to 1, the principal corrections to render consistency with the rate information being to apply bias corrections. In roll, this gives an attitude more "left wheel down", and although difficult to see from the noisy pitch information, a more nose-down attitude. (The noisy pitch attitude was attributed to the gyroscope mechanism requiring maintenance).

All data used for analysis and model validation was subjected to kinematic consistency checking. For the purposes of demonstration only the technique for consistency checking angular parameters is presented here for clarity. The velocities and accelerations were treated in a similar manner. Results for all events in one particular flight are presented in Figures A6.2 and A6.3. In Figure A6.2, scale factor and bias errors are shown for the three rate gyroscopes. Note that most scale factors are clustered around 1, although most of the roll rate scale factors lie around 0.8. Bias errors are small, except in yaw rate, particularly towards the end of the flight. Attitude scale factors and biases are shown in Figure A6.3. Given the earlier statement regarding the noisy pitch attitude signal and the maintenance state of the attitude gyroscope

mechanism it is perhaps not surprising that the pitch attitude scale factors are not clustered around 1, although they are consistently about 0.6. Bias errors are consistently small. Figure A6.4 shows measured and corrected rates. Roll and pitch axes appear identical. The relatively large yaw rate bias error manifests itself in this case as a small shift in the yaw rate signal.

AGARD LS178 makes interesting reading regarding kinematic consistency. Results (in terms of biases and scale factor variations, event-to-event) can, in general, be variable and inconsistent. The problem is basically over-parameterised, i.e. so much flexibility is given to the matching process, least-squares or otherwise, that anything can be fitted to anything else. Techniques much more sophisticated than simple least squares can be employed, such as maximum likelihood methods, but experience has shown that this does little to improve confidence in the results. Indeed, one contributor to LS178 who employed a sophisticated matching algorithm, suggests that it is probably appropriate to filter data, and not apply kinematic consistency checking at all. Another reports that it is necessary to assume some scale factors are one, and biases zero, to get good, confident estimates of the remainder.

The view the authors take here is that if the basic data quality is good, and sound engineering judgement can be applied then meaningful results can be achieved from kinematic consistency checking. This despite its limitations and pitfalls and even using a simple algorithm as was the case here. It is judged that the results suggest that basic data quality is indeed good, but scale factors and biases as calculated need to be applied to the angular information.
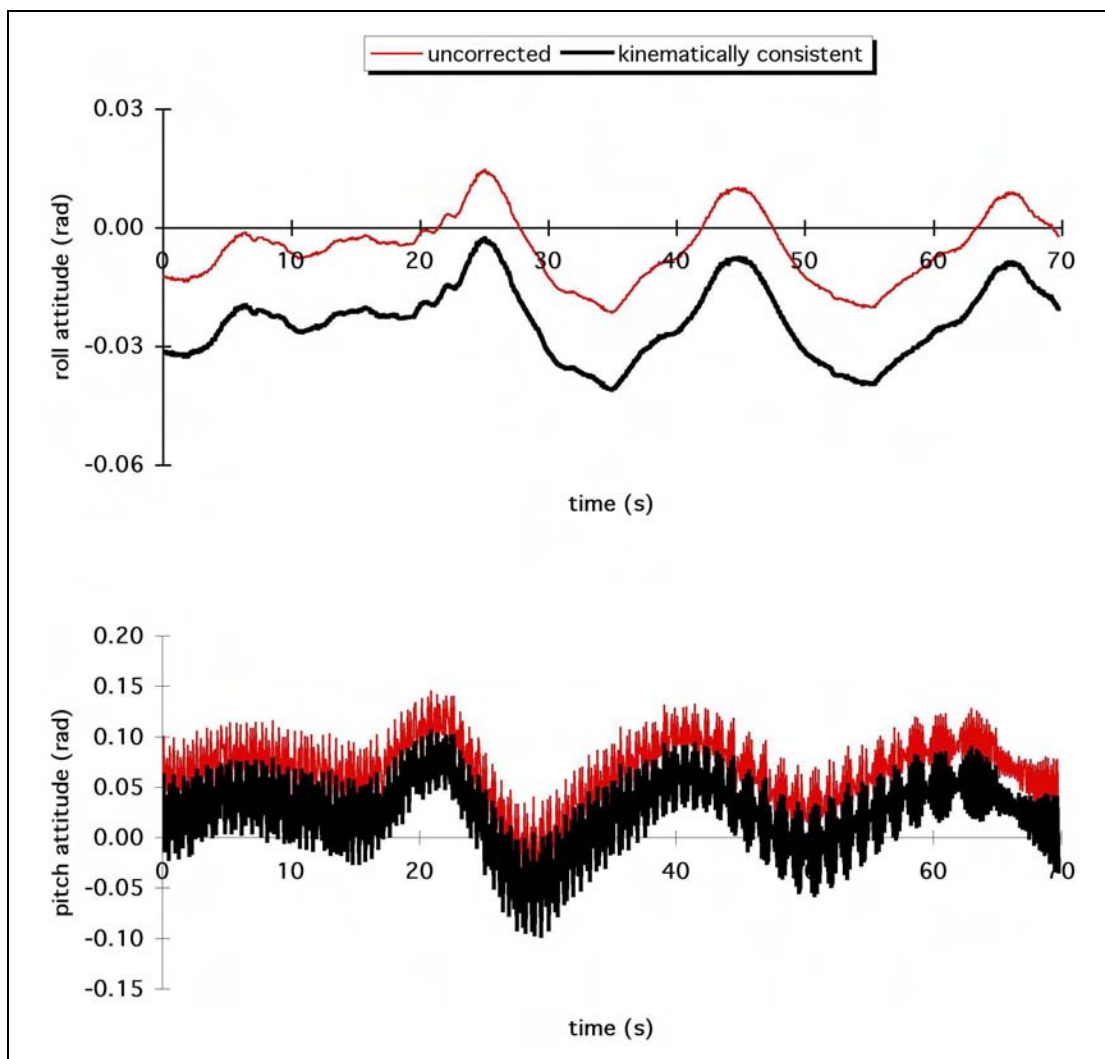
Figure A6.1   Attitude Angles During Phugoid Flight Test (70mph, VPM)
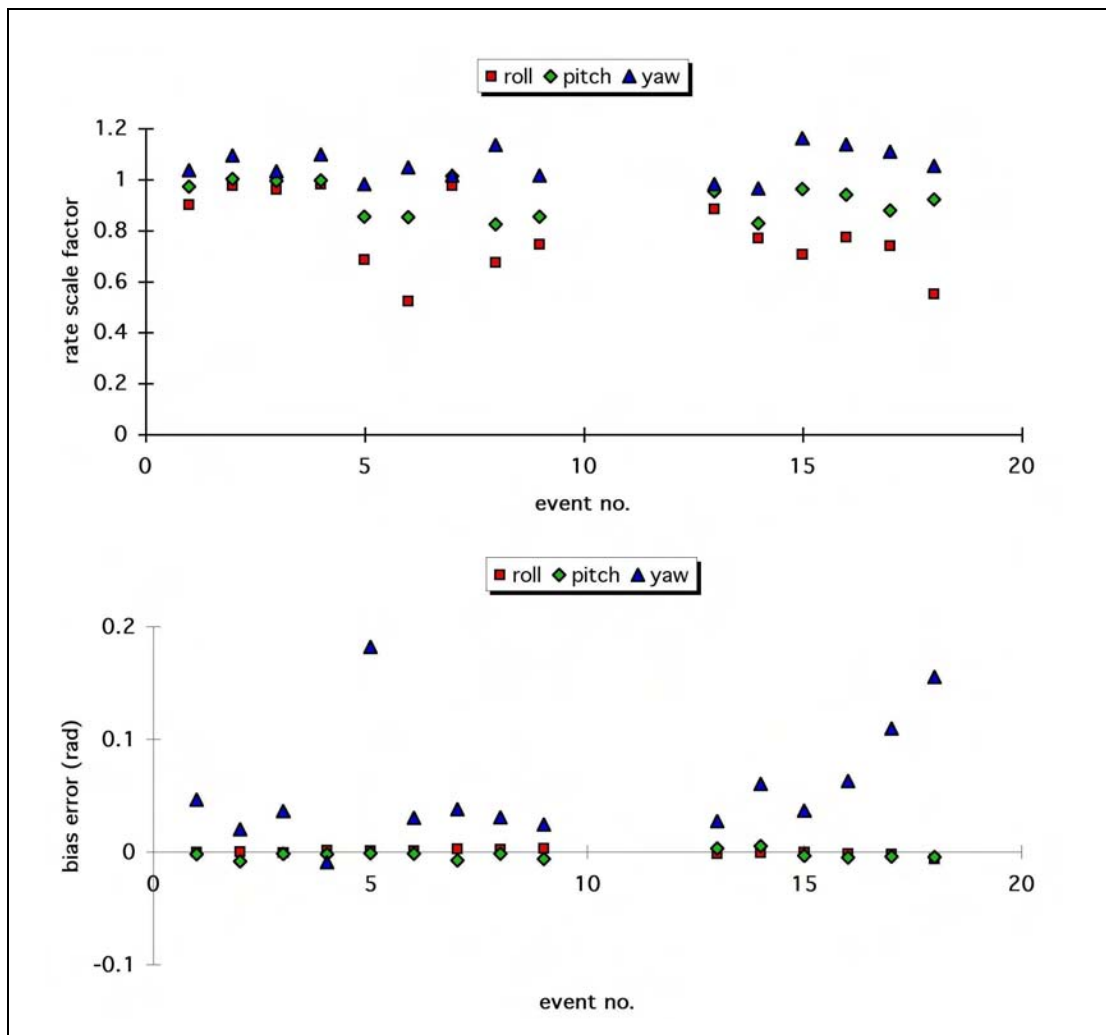
Figure A6.2   Summary of Rate Gyro Consistency Results (VPM)
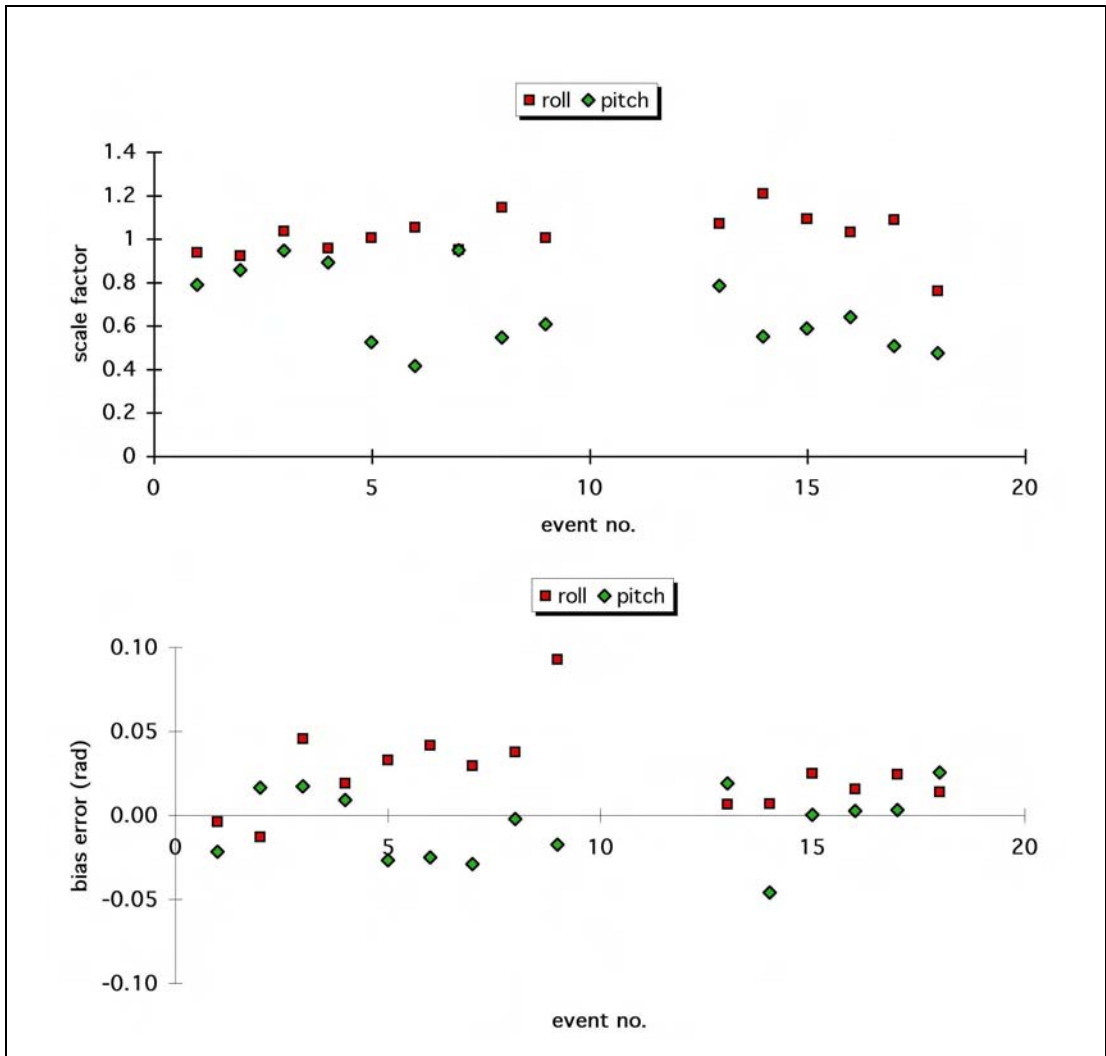
Figure A6.3   Summary of Attitude Gyro Consistency Results (VPM)
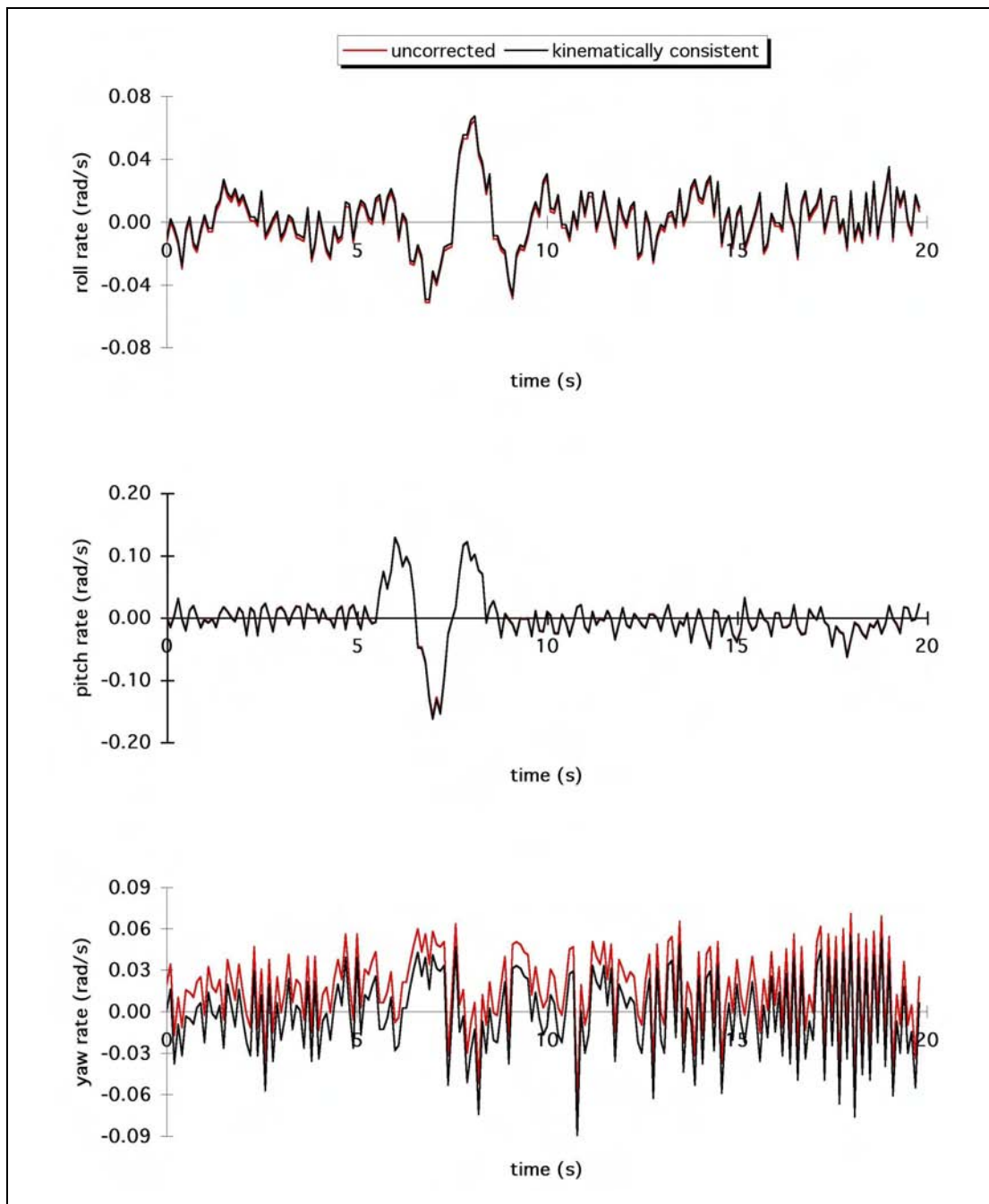
Figure A6.4   Attitude Rates Recorded During a fore/aft Doublet Input (VPM)

INTENTIONALLY LEFT BLANK

Appendix 7   Data Analysis and Model Synthesis

The model structure for which coefficients are to be identified, is of conventional state-space form, i.e.

$$\underline{\dot{x}} = \mathbf{A}\underline{x} + \mathbf{B}\underline{u}$$

(A7.1)

where

$$\mathbf{A} = \begin{bmatrix} X_u & X_w & X_q & X_\theta & X_\Omega \\ Z_u & Z_w & Z_q & Z_\theta & Z_\Omega \\ M_u & M_w & M_q & M_\theta & M_\Omega \\ 0 & 0 & 1 & 0 & 0 \\ Q_u & Q_w & Q_q & Q_\theta & Q_\Omega \end{bmatrix}, \quad \mathbf{B} = \begin{bmatrix} X_{\eta_s} \\ Z_{\eta_s} \\ M_{\eta_s} \\ 0 \\ Q_{\eta_s} \end{bmatrix}$$

(A7.2)

and

$$\underline{x} = [u \quad w \quad q \quad \theta \quad \Omega]^T, \quad \underline{u} = [\eta_s]$$

(A7.3)

This constitutes the longitudinal subset of the conventional 6 degree-of-freedom rigid-body flight mechanics model, with the important (and unique) addition of the rotorspeed degree of freedom. The rigid body states are taken to be with respect to a mutually orthogonal, right-handed frame of reference whose origin is at the centre of mass. The longitudinal and vertical axes are respectively parallel and normal to the keel of the aircraft.

The angular quantities in the state vector, and the control position, are all measured directly. The translational velocities   and   are obtained from airspeed, sideslip and angle of attack data measured at the nose-mounted boom, as follows:

$$u = u_{probe} - q(z_{vane} - z_{cg}) + r(y_{vane} - y_{cg})$$
$$w = w_{probe} - p(y_{vane} - y_{cg}) + q(x_{vane} - x_{cg})$$

(A7.4)

and

$$u_{probe} = \frac{V_f \cos \beta_{vane}}{\sqrt{1 + \tan^2 \alpha_{vane}}} \quad ; \quad w_{probe} = u_{probe} \tan \alpha_{probe}$$

(A7.5)

The time histories of each variable were then converted into frequency domain information using a Discrete Fourier Transform, [80], given by:

$$X(k\Delta f) = \Delta t \sum_{n=0}^{N-1} x_n e^{-i2\pi(kn)/N}; \quad k = 0,1,2,...,N-1$$

(A7.6)

which gives real and imaginary parts of X:

$$\mathrm{Re}[X(k\Delta f)] = \Delta t \sum_{n=0}^{N-1} x_n \cos(2\pi(kn)/N); \quad \mathrm{Im}[X(k\Delta f)] = -\Delta t \sum_{n=0}^{N-1} x_n \sin(2\pi(kn)/N)$$

(A7.7)

The quality of these frequency domain data can be enhanced by standard processing techniques such as applying overlapped and tapered windows to the data, as recommended by Tischler, [80].

Each degree of freedom can then be treated separately, and formulation as a linear regression problem allows estimation of the coefficients. The state-space description is converted to the frequency domain, i.e.

$$i\omega \, \underline{x}(\omega) = A\underline{x}(\omega) + B\underline{u}(\omega)$$

(A7.8)

Note that this assumes that any process noise is zero. The unknown coefficients of the A and B matrices are determined by solutions of the frequency domain equations:

$$-\omega \, \mathrm{Im}[\underline{x}(\omega)] = A(\mathrm{Re}[\underline{x}(\omega)]) + B(\mathrm{Re}[\underline{u}(\omega)])$$
$$\omega \, \mathrm{Re}[\underline{x}(\omega)] = A(\mathrm{Im}[\underline{x}(\omega)]) + B(\mathrm{Im}[\underline{u}(\omega)])$$

(A7.9)

This solution applies equal weighting to real and imaginary part errors, which is consistent with the standard weighting for system identification on a Bode plot. The pitching moment equation for example, is then expressed as the two equations:

$$-\omega \, \mathrm{Im}[q(\omega)] = M_u \, \mathrm{Re}[u(\omega)] + M_w \, \mathrm{Re}[w(\omega)] + M_q \, \mathrm{Re}[q(\omega)] + M_\theta \, \mathrm{Re}[\theta(\omega)]$$
$$+ M_\Omega \, \mathrm{Re}[\Omega(\omega)] + M_{\eta_s} \, \mathrm{Re}[\eta_s(\omega)]$$
$$\omega \, \mathrm{Re}[q(\omega)] = M_u \, \mathrm{Im}[u(\omega)] + M_w \, \mathrm{Im}[w(\omega)] + M_q \, \mathrm{Im}[q(\omega)] + M_\theta \, \mathrm{Im}[\theta(\omega)]$$
$$+ M_\Omega \, \mathrm{Im}[\Omega(\omega)] + M_{\eta_s} \, \mathrm{Im}[\eta_s(\omega)]$$

(A7.10)

The other degrees of freedom are in a similar form. Figure A7.1 shows the real and imaginary parts of the pitching moment equation in the above form, and the corresponding fit using the derivatives identified using the above process. This result is typical of that achieved in general for both VPM M16 and Montgomerie.
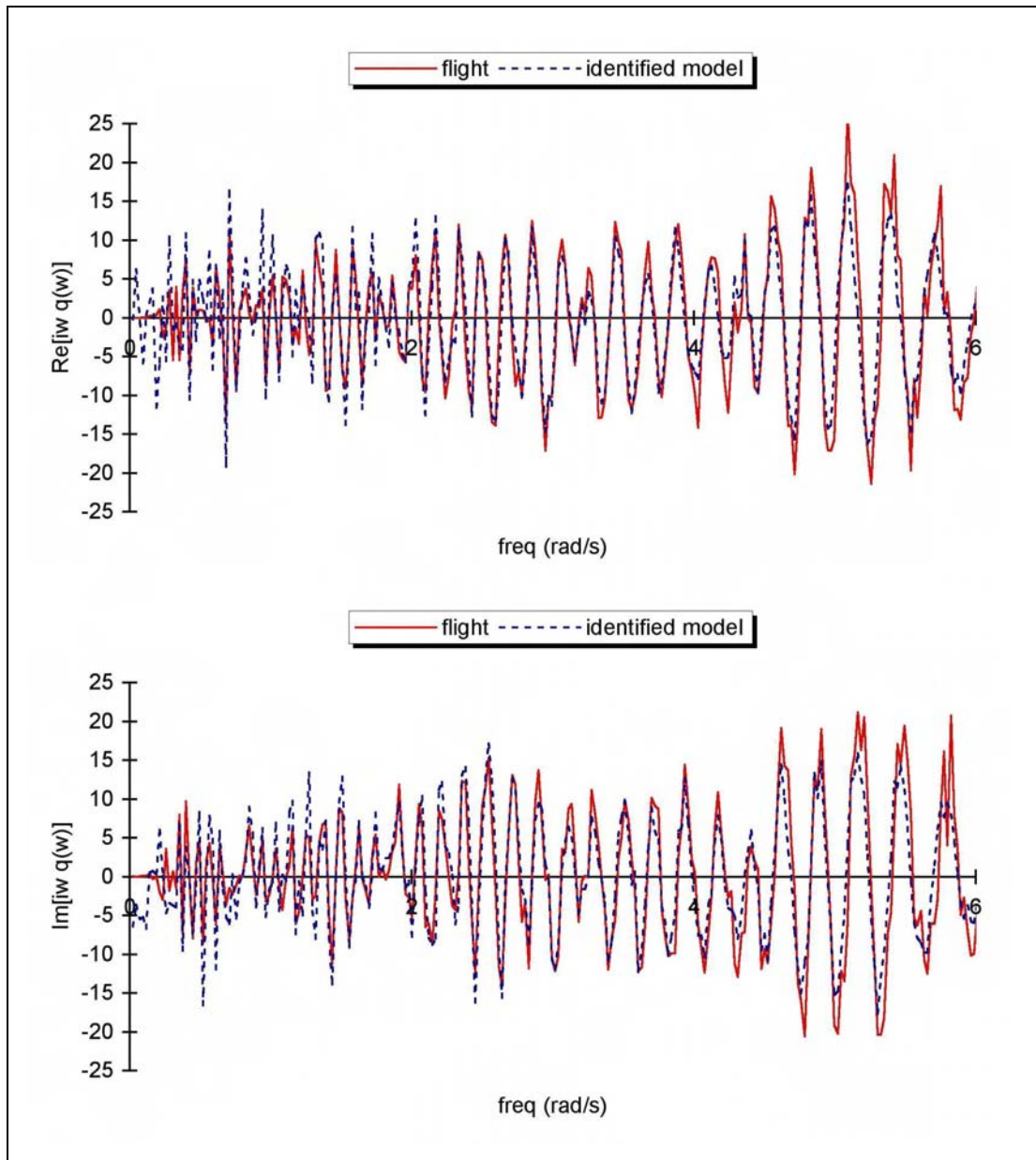
Figure A7.1   Fit Quality of Flight and Identified Model Pitching Moment Equation

INTENTIONALLY LEFT BLANK

Addendum 1   Technical Report

A Survey of Gyroplane Centre-of-mass and Propeller Thrust Line Locations

Dr Stewart Houston

Department of Aerospace Engineering University of Glasgow

Addendum 1   Technical Report

UNIVERSITY
of
GLASGOW

"A Survey of Gyroplane Centre-of-mass and Propeller Thrust Line Locations"

Report

(issue 2)

September 2005

Dr Stewart Houston

Dept. of Aerospace Engineering

James Watt Building, The University of Glasgow, Glasgow G12 8QQ

Tel. (0141)-330 6865; Fax. (0141)-330 5560

1   Introduction

The amendments and additions to BCAR Section T proposed by Glasgow University are based on criteria associated with the vertical position of the centre-of-mass. These criteria were developed from parametric studies using the RASCAL simulation model, and validated by flight test using the VPM M16 G-BWGI, and Montgomerie-Parsons G-UNIV. Limited supporting data from hearsay evidence associated with other types has helped to increase confidence in the proposed changes.

Five Bensen-type gyroplanes have been the subject of the CAA flight trials conducted to establish compliance demonstration against the dynamic stability requirements of BCAR Section T. This report documents the results of a weight and balance survey of these five aircraft. The objective is to provide a database of results that can be used to correlate flight compliance demonstration with c.g. location, and hence serve to validate the proposed limits between c.g. and propeller thrust line location.

2   Background

The role of the vertical location of the c.g. in relation to the propeller thrust line is a significant issue of which gyroplane pilots have always been keenly aware, but only in relation to the power-pushover phenomenon during flight with high power and at low rotor loading. However, its role in relation to static and particularly dynamic longitudinal stability has only recently been explored. Simulation studies highlighted the sensitivity of dynamic stability, particularly the phugoid-type mode, to vertical c.g. location in 1994 [1], and in 1997 a recommendation was made that the normal distance between the propeller thrust line and c.g. should not exceed ±2 in, [2]. In 1998 analysis of flight test data obtained using a VPM M16, which had a thrust line close to the 2 in limit, validated the simulation studies and postulated a simple mechanism that explained how raising the c.g. location would tend to improve stability [3].

The CAA recently undertook a series of flight tests using five Bensen-type gyroplanes, including compliance demonstration against the dynamic stability requirements of BCAR Section T. No quantitative weight and balance information was available for these aircraft, although one incorporated modifications claimed to place the propeller thrust in line with the c.g. This report documents results obtained from measurements taken using the same method with all five aircraft.

3   Analysis and experimental method

The analysis method chosen to calculate c.g. position is described in Appendix 3 of the main body of this report. It requires measurements of wheel reactions, wheelbase and airframe pitch attitude. It is accepted that it is not the only method of determining c.g. location and it is further accepted that the vertical position of the c.g. can be calculated with large error bounds. However it is practical and simple, and the errors are rigorously quantifiable. An alternative method, by suspension from multiple points, is illustrated in Figure 1 – the aircraft is G-BUJK, one of the subjects of this report, although the test shown in the figure was conducted over 10 years ago. It requires suspending the aircraft and hence the use of a winch or crane and it is argued that the photographs show this method is also prone to errors subject to interpretation and are therefore qualitative only. The preferred method here is widely accepted, and is perhaps the only means of dealing with large aircraft. The largest aircraft that this author has seen examined using multi-point suspension is Lynx

ZD559 (around 4 tonnes). In summary, it is argued that the practicalities of the chosen method outweigh disadvantages of accuracy, which are in any case controllable and quantifiable. Note that the results are calculated in Earth axes (Figure A3-1, main report), but can easily be transformed to airframe axes if required.

The experimental method was to roll the aircraft onto the load cells using the ramps provided. Depending on configuration and type, the aircraft would sit either on its tailwheel, or nosewheel and the load cell placed accordingly. A digital clinometer was used to measure the pitch attitude of the aircraft. Wheelbase was obtained by chalkmarking a rectangular box around each wheel and then measuring distances between box centroids.

It is important that no lateral force is placed on the load cells as this has been found to introduce bias errors, hence the importance of rolling the aircraft on and off. Lowering or lifting the aircraft onto the load cells, or even allowing the pilot to climb in once placed on the cells, has the potential to splay the main wheels or scrub the nosewheel laterally and hence introduce sideloads. Multiple tests of the same configuration were made to ensure repeatability and consistency. The aircraft was inclined by placing the cells on top of wooden pallets.

4   Results

Five aircraft were tested as detailed in Table 1. Each aircraft was examined in four configurations for which two sets of measurements were required to compute c.g. position (i.e. aircraft level, then inclined). This gave a total of 40 cases, most of which were repeated at least twice to address consistency.

Table 1   Aircraft surveyed

Aircraft	Date	Location	Appendix No.
Bensen B8MR G-YJET	25 May 2005	Barton	A2
Bensen B8MR G-BIHX	5 Jan 2005	North Coates	A3
Montgomerie-Bensen B8MR G-BZJR	6 Jan 2005	Shipdham	A4
Bensen B8MR G-BOZW	7 Jan 2005	Poole	A5
Montgomerie-Bensen B8MR G-BUJK	25 May 2005	RAF Benson	A6

The intention was to survey aircraft with zero fuel, and full fuel, although this was not possible and only G-BZJR was tested with full fuel. At each fuel state the aircraft would be assessed with and without pilot. A summary of configurations is given in Table 2. Note that G-BUJK was tested in the same configurations with a fuel load but G-YJET was only tested empty.

Centre of gravity positions were calculated for each aircraft, and the results are summarized in Table 3, as well as new data from the additional measurements taken using G-YJET and G-BUJK.

Table 2   Aircraft configurations

Aircraft	Pilot	Fuel	Wheel base (nose)	Wheel base (tail)	Wheel track
Bensen B8MR G-YJET	96.0 kg	0.0 kg (01)	1.192 m	1.214 m	1.627 m
Bensen B8MR G-BIHX	81.5 kg	15.0 kg (21 1)	1.268 m	1.152 m	1.567 m
Montgomerie-Bensen B8MR G-BZJR	74.0 kg	32.0 kg (45 1)	1.300 m	n/a	1.605 m
Bensen B8MR G-BOZW	92.5 kg	15.0 kg (21 1)	1.140 m	1.143 m	1.574 m
Montgomerie-Bensen B8MR G-BUJK	78.0 kg	14.5 kg (20 1)*	1.245 m	1.190 m	1.620 m
Mean (SD)	84.4 kg (9.5)	15.3 kg 11.3)	1.229 m (0.06)	1.175 m (0.03)	1.599 m (0.03)

* Estimated - no zero fuel configuration tested.

Table 3   Calculated c.g. locations, (x_{cg}, y_{cg}, z_{cg}) - m

Aircraft	Zero fuel, no pilot	Zero fuel, with pilot	Fuel, no pilot	Fuel, with pilot
Bensen B8MR G-YJET	-0.15,-0.03,-0.85	0.15,-0.03,-0.79	n/a	n/a
Bensen B8MR G-BIHX	-0.14,-0.01,-0.81	0.16,-0.02,-0.70	0.10,-0.02,-0.77	0.17,-0.01,-0.73
Montgomerie-Bensen B8MR G-BZJR	n/a	0.22,0.01,-1.02	0.07,0.01,-1.00	0.23,0.02,-0.99
Bensen B8MR G-BOZW	-0.19,0.01,-0.95	0.18,0.01,-0.84	-0.12,-0.02,-0.93	0.20,-0.01,-0.80
Montgomerie-Bensen B8MR G-BUJK	n/a*	n/a*	-0.11,0.01,-0.914	0.13,0.01,-0.78
Mean (SD)	-0.16,-0.01,-0.87 (0.026,0.020,0.072)	-0.18,-0.01,-0.84 (0.040,0.021,0.145)	-0.065,-0.01,-0.90 (0.090,0.017,0.097)	-0.18,-0.00,-0.83 (0.043,0.015,0.114)

* No zero fuel configuration tested.

The normal distance between the propeller thrust line and the c.g. can be calculated from:

$$d = (z_p - z_{cg})\cos(\gamma - \theta) - (x_p - x_{cg})\sin(\gamma - \theta)$$

where (x_p, y_p, z_p) is the position of the propeller hub in body axes, (x_{cg}, y_{cg}, z_{cg}) is the c.g. position, γ is the inclination of the propeller thrust line (positive down) and θ is the pitch attitude. The results are shown in Table 4. Positive values indicate c.g. below the thrust line.

Table 4   Distance of c.g. from propeller thrust line (m)

Aircraft	Zero fuel, no pilot	Zero fuel, with pilot	Fuel, no pilot	Fuel, with pilot
Bensen B8MR G-YJET	0.089	0.104	n/a	n/a
Bensen B8MR G-BIHX	0.030	0.072	0.081	0.047
Montgomerie-Bensen B8MR G-BZJR	n/a	-0.100	-0.083	-0.075
Bensen B8MR G-BOZW	0.024	0.042	0.052	0.077
Montgomerie-Bensen B8MR G-BUJK	n/a*	n/a*	0.030	0.130
Mean (SD)	0.048 (0.036)	0.030 (0.090)	0.062 (0.025)	0.045 (0.087)

Note: 2 inches = 0.0508 m   * No zero fuel configuration tested

The two podded machines appear to have the largest thrust line offset, of between 4-6 in above the c.g. The two open-frame aircraft have slightly smaller thrust line offsets of between 1.7-3 in. Only G-BZJR has a thrust line below the c.g., of between 3-4 in. This result appears consistent with Montgomerie's result, Figure 2, if the black line drawn on the pod to represent the propeller thrust line is discarded and a more appropriate line drawn that takes into account the engine tilt (which the line as drawn arguably does not).

5   Discussion

Four of the five aircraft surveyed displayed c.g. locations below the propeller thrust line, the average normal distance lying between 0.051 m (without pilot) and 0.078 m (with pilot). This is in excess of the 0.05 m (2 in) limit proposed for Section T, Ref. 2. However, one aircraft (G-BZJR) was designed to comply with Section T but does so only by having its c.g. 3-4 in above the thrust line. A large part of this characteristic is due not only to having a c.g. located considerably higher on the airframe relative to the other aircraft, but in also having the engine inclined downwards by 3.8 deg relative to the airframe, combined with a significantly further forward c.g. location which also makes a noticeable contribution to placing the thrust line below the c.g.

The two anomalous results discovered in earlier work have now gone as a direct consequence of the new data indicated earlier. G-BUJK does however remain worthy of discussion, as it has been the subject of a third weighing exercise to directly compare the method used here with a double-suspension point method proposed by the BRA and conducted at RAF Benson on 5 August 2005. On this occasion both methods gave identical results, with the propeller thrust line being a normal distance of 0.08 m above the c.g. Note that the result here gives 0.130 m. The difference can be attributed to the pilot sitting on foam cushion of substantial depth on the later exercise. Montgomerie's result for this aircraft with pilot does suggest a c.g. that is below the propeller thrust line, but not by 0.2 m, Figure 1.

Experience has shown that great care is required if accurate results are to be achieved. Primarily, no sideloads should be placed on the load cells, and consistent total loads should be obtained with the aircraft level and inclined. Inclinations of 5 deg seem to produce error bounds of 1-2 in, so consideration should be given to angles of 10 deg.

6   References

[1]   Houston, S., "The Aerodynamics of Gyroplanes CAA Contract No. 7D/S/1125 Phase 2 Interim Report". 5 May 1994.

[2]   Houston, S., "The Aerodynamics of Gyroplanes CAA Contract No. 7D/S/1125 Review of BCAR Section T (issue 2)". July 1997.

[3]   Houston, S., "Identification of Autogyro Longitudinal Stability and Control Characteristics". AIAA Journal of Guidance, Control and Dynamics Vol. 21 No. 3, pp. 391-399 (1998)
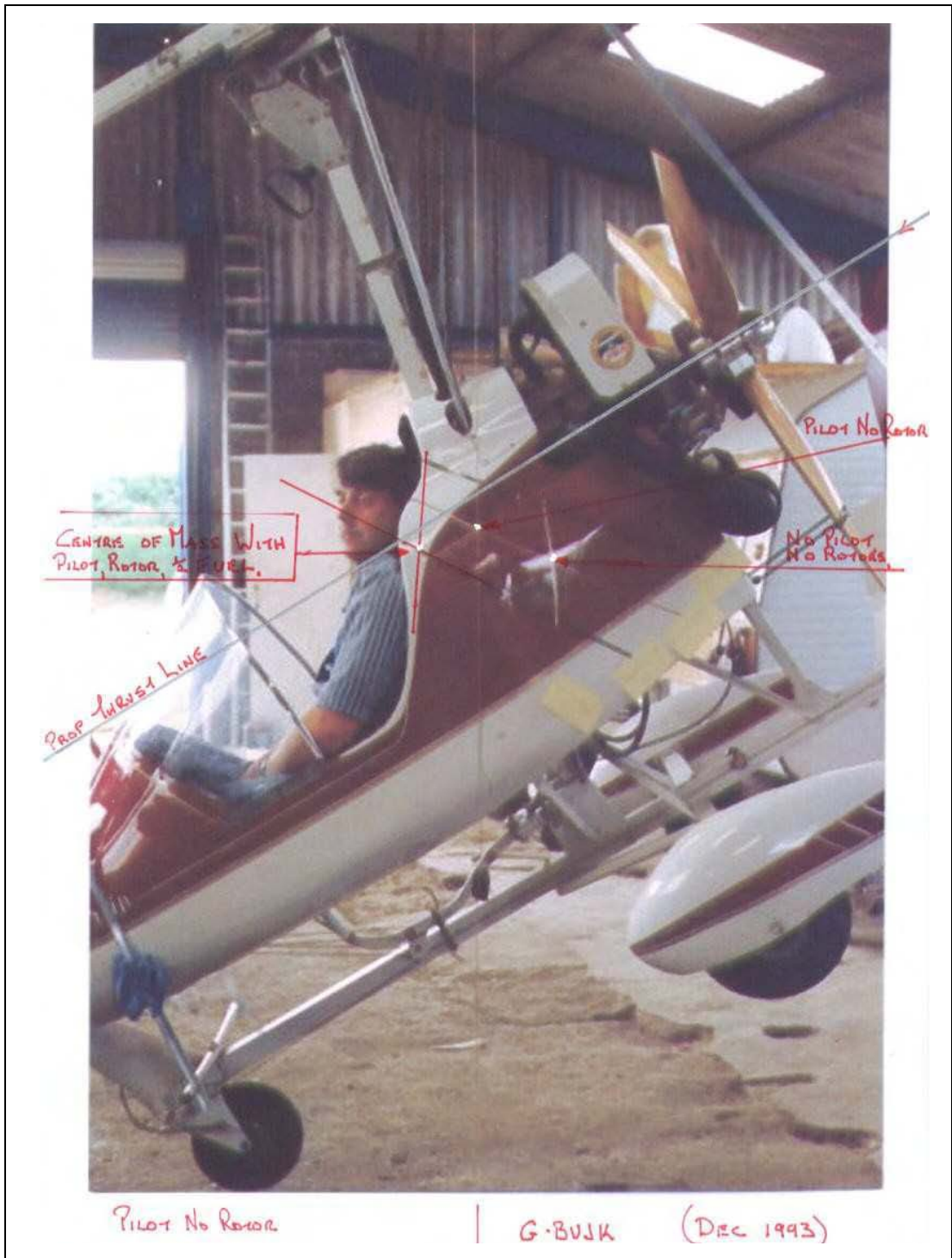
Figure 1

Figure 2

Addendum 2   Internal Report

Civil Aviation Authority
Safety Regulation Group

Montgomerie-Bensen Autogyro Stability Investigation

W.F.R. White
N. Talbot

1   Montgomerie Bensen Autogyro Stability Investigation

1.1   Introduction

Permit to Fly autogyros have the worst safety record of all types of flying machine. Based on the available evidence and AAIB reports, the record is up to 13 times worse than that for Microlight fixed wing aircraft (AAIB Bulletin No: 9/2004). Some other countries in which autogyros are allowed to fly would appear to have a similar situation.

A number of the accidents have been put down to the flight characteristics of this type of aircraft, combined with the ability of pilots to fly them satisfactorily which has lead to the question of whether the high accident rate is due to excessively demanding flight characteristics or to inadequate pilot training and ability.

In order to attempt to resolve this issue, and in response to AAIB Recommendations following fatal accidents to RAF 2000 G-CBAG and Ponsford Bensen G-BIGU, the CAA has carried out a number of evaluations of autogyro handling characteristics. Accident data showed that after the Air Command Elite 532, the Bensen B8MR series of autogyros has a significantly worse record than other types, so it was decided to investigate these first. A number of evaluations were required because the B8MR has been produced in a number of significantly varying configurations.

The evaluations were carried out by an experienced autogyro pilot and instructor who was also an experienced professional helicopter pilot, working under contract to the CAA. He was given basic instruction in flight test techniques. This was considered a good solution to avoid a heavy handed approach to recreational machines yet provide appropriate evaluation and help create a good flight evaluation capability within the autogyro industry for future use within a self regulatory context.

The aircraft evaluated so far, described in the next section, were all provided freely by the owners. Their generosity, support and interest in the evaluations was invaluable and is much appreciated by the CAA.

Some additional points from a Permit to Fly issue evaluation that was carried out on a Speich Air Command autogyro are also included.

1.2   Aircraft Tested

Five aircraft have been tested. The details of each are as follows:

Aircraft Type	Bensen B8MR
Aircraft No.	G-01-2003
Airframe Hrs.	95:45
Engine Type	Rotax 503
Engine No.	4154285
Rotor	22 ft Dragon Wings
Propeller	52 inch, 3 blade GSC
Built from plans	
Location	North Cotes

Figure 1   Aircraft Tested - G-BIHX

Aircraft Type	Bensen B8MR
Aircraft No.	G-01-1096
Airframe Hrs.	approx 200
Engine Type	Rotax 532
Engine No.	3722444
Rotor	22 ft RotorHawk (original type)
Propeller	52 inch, 3 blade GSC
Built from plans	
Location	Newton Peverill

Figure 2   Aircraft Tested - G-BOZW

Aircraft Type	Bensen B8MR
Aircraft No.	G-01-1211
Airframe Hrs.	164
Engine Type	Rotax 532
Engine No.	3798747
Rotor	22 ft RotorHawk
Propeller	60 inch, GSC TEC 3
Built and supplied by Montgomerie	
Location	Abingdon

Figure 3   Aircraft Tested - G-BUJK

Aircraft Type	Bensen B8MR
Aircraft No.	G-01-1072
Airframe Hrs.	180 approx
Engine Type	Rotax 582
Engine No.	
Rotor	22 ft Dragon Wings
Propeller	60 inch, Warp Drive
Built and supplied by Montgomerie	
Location	Barton

Figure 4   Aircraft Tested - G-YJET

Aircraft Type	Bensen B8MR
Aircraft No.	G-01-1320
Airframe Hrs.	
Engine Type	Rotax 582
Engine No.	
Rotor	22 ft Dragon Wings
Propeller	62 inch, Ivoprop
Built and supplied by Montgomerie	
Location	Shipdham

Figure 5   Aircraft Tested - G-BZJR

Each aircraft was in generally good condition and had been inspected by PFA immediately prior to the trial. G-YJET had not been flown for some time prior to the CAA visit and had a number of unserviceabilities, principally a failure of the prerotater engage cable and a cracked bracket for the radiator coolant header tank.

The final aircraft G-BZJR has been modified by Montgomerie Gyroplanes to raise the vertical c.g. position and lower the engine thrustline, but is otherwise virtually identical to G-BUJK.

1.3   **Test Programme**

Flight tests were conducted from the home airfield of each aircraft. The evaluation pilot was Mr B de Saar, and each exercise was managed/supervised by N Talbot and WFR White.

Table 1   Flight details

Aircraft	Date	Airfield	Total flight time
G-BIHX	14 June 2004	North Coates	1:10
G-BOZW	15 July 2004	Newton Peverill	1:30
G-BUJK	11 Aug 2004	Abingdon	2:20
G-YJET	18 Oct 2004	Barton	1:55
G-BZJR	10 Nov 2004	Shipdham	1:55

Weather conditions were acceptable for each exercise, with winds of 5-10kt.

The following tests were completed:

- Cockpit Assessment

- Ground Handling

- Take Off and Landing

- Airspeed Position Errors

- Longitudinal Static Stability

- Longitudinal Dynamic Stability

- Lateral and Directional Stability

- Power/attitude coupling.

1.4   **Initial Findings**

a) Cockpit Assessment

The cockpits of this class of aircraft fall into two main categories, being open or faired.

i) Open Frame Cockpits

The open frame cockpits are indeed completely open with no structure surrounding the pilot's seat (see photographs in previous section). Instruments were mounted in a binnacle in front of the pilot, generally low down and the predominant effect was of sitting in open space. There was clearly no protection from the elements, but more importantly, little or no structure to provide pitch reference.

It was also noticeable that the rotor tip path plane was very high in the normal flight condition, being 'flapped back' to substantially above the horizon, further removing cues to attitude that would, for example, be present in a helicopter.

Little effective instrumentation was generally provided. Most consisted of airspeed, altitude, a whiskey compass, with basic powerplant instruments, e.g. engine RPM and coolant temperature. Readability of airspeed and altimeters was generally poor with, sometimes, small scales covering large ranges. The accuracy of engine RPM gauges was questionable. There was typically no vertical speed indicator (VSI), or attitude indicator. Nr indications, where provided, were typically digital readouts of questionable accuracy especially at lower rpm and in general little use was made or importance placed on rotor speed.

The combined effect of the lack of pitch reference from structure, no attitude indicator, no VSI with, sometimes, very crude altimeter indications resulted in great difficulty in defining precise flight conditions for test purposes and undoubtedly contributed to the difficulty in maintaining stabilised flight. These factors may be influential in explaining the initial opinions on pitch dynamic stability between open and faired aircraft discussed later.

ii) Faired Cockpits

The 'faired' cockpits typically had a 'nose cone' shaped fairing with windscreen. The cockpit structure enclosed the pilot and seat up to just below shoulder height with the pilot sitting in the normal position (See photographs in previous section) but with very little space to spare. The sitting position in the faired cockpit aircraft was much more recumbent than the open framed machines owing to the rudder pedals being much higher.

The instrumentation standard was similar to that of the open frame machines. The primary difference from the open frame machines was that the cues to pitch attitude were somewhat improved by the greater amount of structure ahead of the pilot, although even this was of limited width.

iii) Cockpit Ergonomics

It was noted that some machines had poorly placed throttles that were difficult to use. Others had poor mechanical characteristics, i.e. high gearing or a tendency to create high gearing due to lack of arm support causing the throttle to be gripped close to it's fulcrum. These generally poor design features impeded smooth control of engine power in some cases particularly when combined with the non-linear power delivery characteristics of the Rotax 532 engine.

Furthermore, there was a lack of standardisation in the location of prerotater-engage and wheel brake controls and in some cases, the wheel brake lever was particularly poorly placed. Wheel brake, throttle and prerotater must be used simultaneously during initial rotor engagement and this poor cockpit layout made rotor engagement difficult.

b) Ground Taxy, Take-Off and Landing

i) Ground Taxy

Ground taxy did not present any particular problems, all the machines having wide track main wheels and powerful rudder effect from propeller slipstream. The characteristics of the nose wheel steering systems were variable. Braking was to the nosewheel only, either by means of a pad applied directly to the tyre, or by a conventional single leading shoe drum brake, which was somewhat more effective. Taxying over rough ground caused a significant amount of pitching due to the short-coupled semi-rigid nature of the undercarriage. The final aircraft examined, G-BZJR, had main gear suspension, but all operations were from paved surfaces, so no observation on rough ground handling was possible.

ii) Take-Off

The three faired aircraft had rotor pre-rotator mechanisms, allowing Nr to be increased before commencing the take-off run. The pre-rotator mechanisms were very prone to vibration and resonance during operation, and although this was only for a short period of time, and on the ground, it was plain from witness marks that damage was being caused to the main control rods on several of the aircraft due to contact with the airframe during pre-rotator operation.

Aircraft without a pre-rotator relied on natural wind or forward motion to spin up the rotor, and unless the natural wind was brisk, long take-off runs could result.

Without the general provision of Nr gauges, there was little definitive feedback to the pilot that Nr had risen adequately to achieve a take-off. Adequate Nr was judged by various methods, such as general 'feel', inability to count the passing blades, general experience, etc. Lack of adequate Nr during take-off results typically in a roll over accident, and these occur, at least anecdotally, quite frequently. Reliable useable Nr indications with proper operating handbook information could be influential in reducing this type of accident.

In other respects, take-offs were straightforward on smooth surfaces, but less so on rough surfaces. In this case, the short-coupled semi-rigid nature of the undercarriage resulted in quite severe pitching and associated difficulty in achieving smooth acceleration and Nr build up. Although manageable by experienced pilots, rough ground take-offs should be treated with caution and avoided where possible by less experienced pilots.

iii) Landing

Landings presented no particular problems with low speed, flared touchdowns possible, particularly with some wind.

c) Airspeed Calibrations

Detailed results are included in the individual flight test reports. There was a general trend for the airspeed indicator (ASI) to over read significantly at higher speeds, by up to 25% (see Figure 1 below). This appeared to be the case for both venturi and pitot type systems. The venturi systems had no obvious static source, which caused confusion as to how they functioned at all. The pitot systems typically had a static vent on the back of the ASI case, which clearly exposed the system to large potential errors depending on the location of the instrument. The large airspeed errors are perhaps one reason why some machines are felt to be more benign in their characteristics than others, in that these aircraft are never flown at higher actual speeds due to the indications.

Although it could be argued that gross over reading protects from exposure to poor high speed characteristics and is therefore a safety benefit, it would be more appropriate to have consistently accurate indications and correct maximum speed limitations. Consideration should be given to including airspeed calibration with appropriate accuracy requirements in Section T.
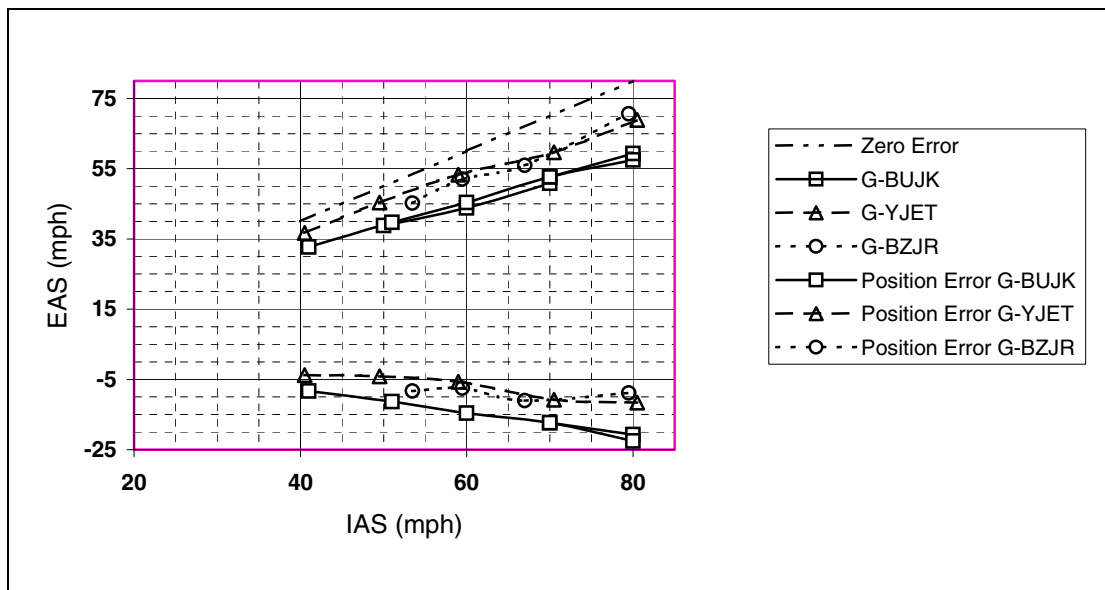
Figure 6　　Bensen B8MR Airspeed PE Calibration

d) Forward Flight Longitudinal Characteristics

Forward flight longitudinal characteristics were examined formally at two speeds, typically slow and fast cruise conditions in level flight. Details are given in the relevant flight test reports. A qualitative evaluation was carried out at Vne.

i) Controllability

Stick margins were adequate in all cases with relatively small amounts of the available range being required to maintain control. Power on yaw controllability was good at all speeds with propeller slipstream working on the large rudders, although large rudder offsets were required for many flight conditions to counter propeller slipstream asymmetric effects such as torque and thrust variation across the propellor disk due to varying blade angle of attack in very steep descents. A similar characteristic is apparent in high power steep ascents and, in particular, in nose-high throttle slams. Power off yaw controllability steadily degraded with reducing airspeed to a point at which it was no longer possible to maintain yaw control, typically 25mph (indicated). It follows that engine failures at or below this speed could be problematic and this is discussed later.

ii) Longitudinal Static Stability

Longitudinal static stability was typically positive, with good stick gradients as shown below in Figure 2 below. The results for G-BIHX are suspect owing to airflow effects on the spring tape used to measure stick position. Aircraft configuration, open frame or faired, with or without horizontal stabiliser did not make a significant difference.

Figure 7   Bensen B8MR Longitudinal Static Stability

iii) Longitudinal Dynamic Stability

Attempts were made to examine both stick fixed and stick free dynamic characteristics in the longitudinal axis. It was difficult to carry out stick free tests as most of the aircraft could not be trimmed due to a lack of an in-flight adjustable trim system, other than longitudinally at one speed and usually not laterally, i.e. it was not possible for the pilot to let go of the stick. It was equally dif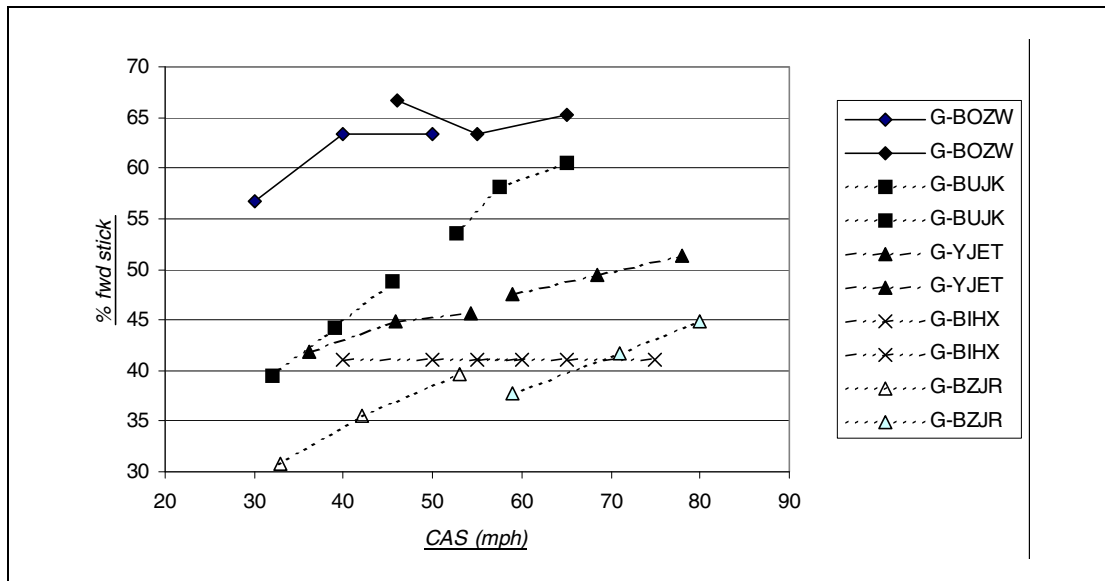ficult to carry out stick fixed tests due to the difficulty in returning the cyclic precisely to the original position once the disturbance had been made. The tests completed were therefore predominantly stick fixed but with a degree of variability. The dynamic stability tests were very dependant on pilot technique, and this developed and improved as the evaluations continued. Nevertheless, a good general impression of the longitudinal dynamic stability characteristics was obtained.

To summarise the characteristics, all the aircraft demonstrated dynamic instability at higher speeds, and at V_{NE} were reported to be noticeably 'twitchy,' based on general workload assessment. The open framed aircraft were less unstable than the faired cockpit aircraft, which could generate high nose up or nose down pitch rates on the first or second overshoot following an initial nose up disturbance, to the extent that the pilot was reluctant to make an initial nose down disturbance. Some aircraft had small, short coupled horizontal stabilisers, but as might be expected, these seemed to have no effect.

A potential anomaly was that initial impressions of stability during general flight were more favourable with the faired cockpit aircraft, whilst the formal examination of stability showed them to be worse. This is possibly explained by the additional references available from the cockpit structure allowing the pilot to detect and deal with the attitude changes caused by instability more quickly than with the open framed machines. (See also paragraph 4.a.(i) of this Addendum)

On more than one occasion, faired cockpit machines were seen to rotate rapidly nose down, giving the appearance of rotating about the centre of gravity. Such a manoeuvre can result in a considerable reduction in normal G and with less experienced pilots might induce large aft cyclic inputs with an increased probability of high flapping angles and rotor/airframe contact. Of equal concern

were the situations when the dynamic instability resulted in a rapid nose up departure with the potential for less experienced gyroplane pilots to respond with a sharp nose down cyclic input leading to G reduction, mast bumping and/ or rotor/airframe contact.

iv) Ability to Trim

As mentioned above, the ability to trim was generally poor, with no in-flight capability to reduce stick forces to zero. This resulted in permanent lateral forces and only one speed at which the aircraft would be trimmed longitudinally. No rudder trim was provided for and control force was invariably needed to maintain balanced flight. Such characteristics would not conventionally be acceptable and some form of in-flight trimming would reduce tendencies to flight path deviations and unstabilised flight. These characteristics would be positively dangerous in conditions of poor external visual cues, so it is fortunate that this class of machine is rarely flown in such conditions.

e) Forward Flight Lateral and Directional Characteristics

i) Lateral Static Stability

Lateral static stability, as might be expected, was neutral to occasionally negative with the faired cockpit aircraft exhibiting poorer characteristics in this respect. The lateral static stability characteristics observed are generally regarded as acceptable for VMC flight, but not for IMC or other cases of poor external visual references.

ii) Directional Stability

Steady Heading Sideslips and turns on cyclic were carried out power on and off, at various airspeeds. Directional stability was found to be weak but positive, becoming neutral at lower power off speeds. Combined with the high power-on yaw controllability, the weak yaw stability resulted in the ability to generate large yaw angles easily with a corresponding increase in pilot workload for the yaw control task. The directional characteristics could usefully be improved.

iii) Spiral Stability

Spiral characteristics could not be examined with any certainty owing to the trim characteristics, but there was no reported tendency to dutch roll, which confirms the results obtained from the lateral and directional tests.

f) Inter Axis Couplings

There was a certain amount of pitch to roll coupling, little yaw to roll coupling and some roll to yaw coupling, which reflect the basic stabilities of the aircraft. The predominant couplings were from power to yaw and power to pitch, with some power to roll effects.

i) Power to Yaw

Any changes in power resulted in sideslip due to the slipstream effects on the fin/rudder being in very close proximity to the propeller, with large sudden power changes having a correspondingly greater effect. Although there was adequate yaw control power to deal with this, the coupling effect and the poor directional stability resulted in significant attitude changes and high pilot workload during the attempts to maintain stabilised flight during power changes, e.g. manoeuvring flight or a go-around. The characteristics of the aircraft could be much improved by reducing the power to yaw coupling, e.g. by lengthening the fin/rudder moment arm and thereby increasing the separation of the fin/rudder from the propeller.

ii) Power to Pitch

The power to pitch coupling was found to be dependent on the relationship between propeller thrust line and vertical centre of gravity. For example, those aircraft with a high thrust line suffered significant nose down pitching with rapid power increase. This type of characteristic, when combined with longitudinal dynamic instability and poor pitch attitude references could be the precursor to an inability to maintain stabilised flight in the pitch axis.

Even without the pilot making power changes, some variation in thrust will occur in forward flight in turbulent conditions or whilst manoeuvring and such variations coupling into the pitch axis will tend to destabilise the aircraft.

It could be that aircraft with otherwise good pitch stability characteristics, could accommodate such power/pitch coupling, but for most of the aircraft evaluated, significant improvements could be made by either reducing the inherent disturbance and/or by improving the pitch stability characteristics.

The final aircraft evaluated in the series had been modified to bring the propeller thrust line/vertical c.g. offset within the ±2" recommended by the Glasgow University Autogyro Stability Research programme and this resulted in a significant reduction in power/pitch coupling and gave more docile handling characteristics generally. A similar result was also noted during the previous Permit to Fly Section T evaluation of the Speich Air Command Autogyro that had been similarly modified.

iii) Power to Roll

The torque effects from power variations caused roll disturbances that reflected the amplitude and rate of power change. Roll control power was adequate to deal with the attitude changes, but workload was increased.

g) Engine Handling, and Failures

i) Engine Handling

Engine handling was generally acceptable but with some tendency for power settings to vary for a fixed throttle position, particularly the Rotax 532. Furthermore, the Rotax 532 engine had rather non-linear power delivery characteristics which when combined with poor throttle characteristics could cause inexperienced pilots difficulty in setting and maintaining accurate and stabilised power. As mentioned previously, the physical and mechanical characteristics of some throttles' ergonomics did not enhance the ease of use, and improved design would be beneficial.

ii) Engine Failures

Formal evaluation of limiting Height/Velocity engine failure cases was not carried out, although the concept was established during the permit to fly testing of the Spieich Air Command. Introduction of appropriate methodologies for this into Section T would be beneficial to safety.

Engine failures were carried out at the minimum power on speed established during controllability testing. These resulted in significant height loss (circa 300ft) to re-establish forward flight, the height loss being very dependant on aircraft behaviour at the point of failure, and subsequent piloting techniques. For the high thrust line aircraft, there were significant pitch, roll and yaw attitude disturbances caused by the couplings mentioned above. In particular, a pitch up tendency caused speed to reduce which led to yaw control problems and increased height loss during recovery. The low thrust line aircraft tested last, did not suffer from the couplings to the same extent or the speed loss and the recovery was much more straightforward.

1.5   **Summary and Significant Findings**

- Successful evaluations were carried out of a range of B8MR aircraft configurations, including faired/open cockpit, high and low thrust line machines.

- The aircraft became progressively more difficult to fly as speed increases.

- The pitch dynamic characteristics are poor at higher speeds, leading to the possibility of unstabilised flight, large flapping angles and rotor/ airframe contact.

- Significant inter-axis coupling with the high thrust line aircraft exacerbated the poor pitch dynamic characteristics, significantly increasing workload and the ability to deal with adverse conditions.

- Tests on a low thrust line aircraft demonstrated much improved characteristics.

- Airspeed indicating systems were grossly inaccurate, and more precise definition of flight envelopes based on accurate airspeed could be beneficial in protecting against poor high-speed characteristics.

- Engine failure characteristics were significantly improved with a low thrust line.

- It was not generally possible to trim in flight.

- The lack of physical cockpit structure with the open framed aircraft degraded the ability of the pilot to control the aircraft precisely.

1.6   **Recommendations**

a) Section T should be modified taking into account the contents of this summary report and the detailed flight test results, to protect the situation for future autogyro designs.

b) Careful consideration needs to be made as to whether modifications should be required to the B8MR series of aircraft, considering that some owners fly successfully with no incentive to make changes. Possible options are:

  - Require modification to achieve a low thrust line;

  - Require open frame aircraft to have some attitude reference structure, e.g. T bar, rod antenna;

  - Improve airspeed indications and re-define V_{NE}s;

  - Apply minimum experience and greater training requirements for pilots wishing to fly unmodified aircraft.

1.7   **Future Work**

a) The relationship between thrust line and vertical c.g. position should be established for each of the aircraft tested during this investigation.

b) A number of Montgomerie Merlin aircraft, based on the B8MR type have been modified to use a 4 stroke Rotax 912 engine of increased power output. Consideration should be given to extending the test programme to investigate the stability characteristics of this modified variant in the light of the findings of this report.

N Talbot   WFR White

Deputy Chief Test Pilot   Flight Test Engineer

INTENTIONALLY LEFT BLANK

Addendum 3 ARB Scholarship Final Report

Aeroelastic Modelling of Gyroplane Rotors

Josef Trchalik
Dr Eric Gillies
Dr Douglas Thomson

August 2008

Air Registration Board Fellowship and Research Grant Scheme

CAA Contract No.905

Aeroelastic Modelling of Gyroplane Rotors

FINAL REPORT

Josef Trchalik

Dr Eric Gillies

Dr Douglas Thomson

Department of Aerospace Engineering

University of Glasgow

Glasgow

G12 8QQ

August 2008

1   Abstract

A mathematical Aeroelastic Model of a Rotor in Autorotation (AMRA) was created to simulate the aeroelastic behaviour of a rotor during autorotation. The model captures transverse bending and teeter, torsional twist and lag-wise motion of the rotor blade and hence it can be used to investigate couplings between blade flapping, torsion and rotor speed. Lagrange's method was used for the modelling of blade flapping and chord-wise bending. Torsional twist of the rotor blade was modelled with the aid of finite element method (FEM), and blade transverse bending could also be modelled in FEM. The model can switch between using a full FEM model for bending and torsion, or an FEM model for torsion and simple blade teeter, depending on the complexity that the user requires.

The AMRA model was verified against experimental data obtained during a CAA sponsored flight test programme and published results of modal analysis of helicopter rotor blades and other data published in open literature were used to validate the FEM model of the rotor blade. As a further verification of the modelling method, Aérospatiale Puma helicopter rotor blade data were compared on a Southwell plot showing comparison between experimental results and AMRA estimation.

The aeromechanical behaviour of the rotor during both axial flight and forward flight in autorotation was investigated. A significant part of the research was focused on investigation of the effect of different values of torsional and flexural stiffness, and the relative positions of blade shear centre/elastic axis and centre of mass of the blade on stability during the autorotation. The results obtained with the aid of the model demonstrate the interesting, and unique, characteristics of the autorotative regime – with instabilities possible in bending and torsion, but also in rotorspeed.

To conclude, the model is used to demonstrate that the requirements currently embedded in BCAR Section T are adequate and should provide a rotor free of the types of instabilities identified elsewhere in the report.

2 Nomenclature

a	Lift-curve slope	[1/rad]
a_L	Local lift-curve slope	[1/rad]
A	Rotor disc area	[m^2]
b	Blade length	[m]
c	Blade chord	[m]
c_D	Drag coefficient	[1]
c_L	Lift coefficient	[1]
c_M	Pitching moment coefficient	[1]
c_R	Resultant force coefficient	[1]
D	Drag force	[N]
$1/f$	Thrust coefficient based on descending velocity	[1]
$1/F$	Thrust coefficient based on resultant air velocity	[1]
G	Gravitational force	[N]
H	In-plane force	[N]
k_θ	Torsional Stiffness	[Nm^2/rad)
L	Lift force	[N]
m	Weight of the blade	[kg]
M	Weight of the vehicle	[kg]
M_c	Blade tip mass	[kg]
M_β	Blade forcing moment in flap	[N.m]
M_θ	Blade forcing moment in torsion	[N.m]
M_Ψ	Blade forcing moment in flap	[N.m]
N_B	Number of blades	[1]
Q	Blade torque	[N.m]
R	Rotor radius	[m]
S	Rotor blade area	[m^2]
t	time	[s]
T	Blade thrust	[N]
T	Kinetic energy	[J]
U	Inflow velocity	[m/s]
U_p	Vertical component of inflow velocity	[m/s]
U_t	Horizontal component of inflow velocity	[m/s]
V	Free-stream velocity	[m/s]
V	Potential energy	[J]

V_d	Speed of descent	[m/s]
v_i	Induced velocity	[m/s]
y_c	Chord-wise offset of aerodynamic centre from the elastic axis	[m]
y_g	Chord-wise offset of centre of gravity from the elastic axis	[m]
α	Blade angle of attack	[rad]
α_D	Rotor disc angle of attack	[rad]
β	Blade flapping angle	[rad]
ϕ	Inflow angle	[rad]
γ	Angle of descent/climb of the vehicle	[rad]
ι	Blade fixed angle of incidence	[rad]
λ, λ_p	Vertical inflow ratio	[1]
θ	Blade angle of induced twist	[rad]
ρ	Air density	[kg.m^{-3}]
τ	Blade geometric twist	[rad]
τ	Time constant matrix	
Λ	Dynamic inflow static gain matrix	
Ω	Rotor speed	[rad/s]
Ψ	Blade azimuth	[rad]

3   Introduction

The gyroplane represents the first successful rotorcraft design and it paved the way for the development of the helicopter during the 1940s. Further development of the gyroplane was ceased during the following decades as the helicopter became more successful. Interest in this type of aircraft as a recreational vehicle was resurrected in recent years thanks to the simplicity of its design and low operational costs.

Most gyroplanes use two-bladed teetering rotors for generation of lift. Unlike in helicopters, the rotor is not powered by an engine but rotor torque is generated by the aerodynamic forces and the rotor has to be pre-rotated before take-off. Gyroplanes do not need a tail rotor as there is no torque acting on their fuselage. Longitudinal and lateral tilt of the rotor disk is used for longitudinal and lateral control of the vehicle. Most gyroplanes use the combination of two-stroke or four-stroke engine and a propeller in pusher configuration, for thrust.

Unfortunately, autogyros, or gyroplanes, have been involved in a number of fatal accidents during the last two decades. Sudden loss of rotor speed or mechanical failures of the rotor blades as delamination were involved in many of the accidents. Very little data on gyroplane flight mechanics and handling qualities are available in the literature. Accordingly the UK Civil Aviation Authority (CAA) began investigation of these problems by contracting the Department of Aerospace Engineering, University of Glasgow to research the aerodynamics and flight mechanics of a gyroplane [1 - 4].

Much more is now understood on the flight dynamics and flying qualities of gyroplanes, however, rotor aeroelastic instability has not yet been investigated as a possible issue with regard to flight safety. The aim of the present work is to investigate this possibility.

The aim of the investigation is to identify flight conditions or configurations of the rotor that might have catastrophic consequences, and work out basic design criteria for gyroplane blades. The resulting aeromechanical model of gyroplane rotor blades can also be used for prediction of stability of new or modified gyroplane rotor configurations. The first stage of the investigation is to develop a suitable mathematical model of the rotor system.

4   Development of an Aeroelastic Model of a Gyroplane Rotor

4.1   Background – Autorotative Flight

There are substantial differences between dynamics of a helicopter rotor and dynamics of a rotor in autorotation. During autorotation, both torque and thrust are generated exclusively by flow through the rotor disc. Thus, in comparison with dynamics of a helicopter rotor, the system has one extra degree of freedom (i.e. rotor speed). Thrust and torque are functions of rotor speed and distribution of local angles of attack along the blade span. Further, angles of attack are dependent upon blade twist, rotor speed, speed of descent and induced velocity. It can be easily shown that both speed of descent and rotor angular velocity are strongly dependent upon rotor torque and rotor thrust. Therefore, simulation of the aeroelastic characteristics of a rotor in autorotation is iterative process that involves large number of algebraic loops. This makes modelling of autorotation significantly more challenging than powered flight.

During steady autorotation, overall torque generated by flow through the rotor disc is zero and rotor thrust is equal to the weight of the vehicle [5, 6]. There are several design parameters of the rotor that determine whether steady autorotation is possible. Perhaps the most important are blade incidence angle (i.e. angle of attack of the blade relative to the rotor disc plane) and blade torsional stiffness. Torque equilibrium can not be achieved for high incidence angles due to high value of blade drag. If torsional rigidity is too low, extensive blade twist has the same effect. The extra degree of freedom in rotor speed has significant implication for gyroplane rotor stability. Unlike helicopter rotors, gyroplane rotors can experience significant variations in rotor speed during changing torque generated at the rotor. Decrement of the rotor speed decreases centrifugal stiffness of the rotor and the resulting higher deflections in flap and twist generate more drag and cause further drop in rotor speed.

Conditions in which the rotor enters autorotative regime are also of great importance. If rotor speed during vertical descent is too low or even zero, the rotor does not autorotate, requiring pre-rotation to be included in the simulation. A constant value of torque is applied to the rotor in order to reach conditions that make autorotation possible.

4.2   An Overview of the Model

The most flexible and practical approach to developing the aeromechanical model of gyroplane rotor was to programme with the aid of the MATLAB - SIMULINK® computer package which offers powerful tools for modelling of complex mechanical systems. The model was named AMRA, which stands for 'Aeroelastic Model of a Rotor in Autorotation'.

A blade element method combined with quasi-steady aerodynamics (Theodorsen's Theory) is used for calculation of aerodynamic forces and moments generated by the rotor blade. The general arrangement of the blade model is shown in Figure 1. Two rotor blades and arbitrary number of blade span-wise elements can be used. The aerodynamic characteristics of the aerofoil for the full range of angles of attack are approximated with the aid of wind tunnel data [7]. A NACA 0012 aerofoil was chosen for the first version of the AMRA model since aerodynamic characteristics for the full range of angles of attack of the aerofoil are available [8]. A semi-empirical method of induced velocity calculation was used in the first versions of the AMRA model. The original calculation [9] was improved in order to capture blade stall and compressibility of the airflow. A simplified version of Peters – HaQuang inflow model replaced semi-empirical approach in the later versions of the AMRA model in order to improve fidelity of forward flight simulations.

Lagrangian equations of motion were used to describe dynamics of the rotor blade. Chord-wise locations of elastic axis (EA), centre of gravity (c.g.) and aerodynamic centre (AC) can be set in each span-wise station. Values of flexural and torsional rigidity of the blade can be set to investigate the behaviour of the rotor for different physical properties of the blades. The AMRA model also allows placement of single concentrated mass at any span-wise station of the blade.

4.3   Modelling the Aerodynamics of a Blade Element

The blade element method represents a widely used tool for description of the flow through a rotor disc. The theory has to be modified in order to capture the aerodynamics of a rotor in autorotation. During autorotation, the flow through the rotor has the opposite direction to that in the case of powered flight of a helicopter. Hence the blade aerodynamic angle of attack, α, can be expressed as [9 - 12]

$$\alpha = \phi + \theta$$

(1)

where θ is the angle of induced twist and ϕ is the inflow angle, Figure 2, given by:

$$\phi = \tan^{-1}\left(\frac{U_p}{U_T}\right)$$

(2)

where U_P is the component of flow normal to the blade element and U_T is the tangential component. The method of calculating normal and tangential and radial (U_R) components of velocity at a blade element is developed in Appendix 1. Local values of vertical and horizontal components of inflow velocity have to be calculated in order to determine aerodynamic angle of attack of any blade section. Inflow velocity is a function of angle of attack of the rotor disc, α_D, that is given by sum of incidence angle of the rotor disc ι (i.e. angle between rotor disc plane and the horizontal) and pitch angle of the vehicle here given the symbol γ. Note that during axial flight, rotor disc angle of attack is 90°. Using the symbols V_d and V_h to signify the vehicle body velocity components in the x and z directions, the disc angle of attack is given by:

$$\alpha_D = \iota + \gamma$$

(3)

where

$$\gamma = \tan^{-1}\left(\frac{V_d}{V_h}\right)$$

(4)

From Appendix 1, the result for axial flight is:

$$U_P = \Omega R\left(\lambda - \frac{d\beta}{d\psi}x - \theta\frac{d\theta}{d\psi}y\right)$$

(5)

$$U_T = \Omega R \left(x - \theta \frac{d\theta}{d\psi} y \right)$$

(6)

$$U_R = \Omega R \lambda \beta$$

(7)

where: Ω is the rotational speed of the rotor,

R is the rotor blade radius,

λ = non-dimensional inflow velocity ratio = $\dfrac{V_d - v_i}{\Omega R}$

v_i = inflow velocity,

β = blade flapping angle,

ψ = blade azimuth,

x = normalised radial position of element = $\dfrac{r}{R}$

y = non-dimensional chordwise position of aerodynamic centre with respect to elastic axis = $\dfrac{1}{R} \left(\dfrac{3}{4} c - y_{EA} \right)$

The equations above allow the angle of attack and velocity at each blade element to be determined and hence, given appropriate data for the particular blade section, aerodynamic loads can be found. An assumption of a linear lift curve and parabolic drag curve is often used in order to simplify the model and speed up computations. However, this approach does not allow the effects of blade stall, drag divergence and most importantly air compressibility to be captured. Since the aerodynamic characteristics of rotor blade elements depend upon local values of angle of attack and Mach number, it is convenient to express aerodynamic characteristics of the blade aerofoil as functions of these two variables. This can be achieved by expressing aerodynamic characteristics of the blade in terms of polynomial functions of angle of attack and Mach number [5].

It was shown by Prouty [7] that it is possible to obtain full-range angle of attack aerodynamic data of an aerofoil with the aid of polynomial fit. Prouty uses the example of the NACA 0012 aerofoil in his book [7]. Prouty's empirical equations were derived from data published in Carpenter [13]. Since full-range AOA aerodynamic data for the same aerofoil are available from numerous sources [8, 14], Prouty's approach was amended and incorporated into the AMRA model. Figures 3 and 4 show the variation of lift and drag coefficient of a NACA 0012 section obtained using the polynomial representations suggested by Prouty.

When the values of aerodynamic coefficients at all span-wise stations are obtained, the forces generated by the blade elements can be calculated:

$$dL = \frac{1}{2} \rho U^2 C_L c\, dx \qquad dD = \frac{1}{2} \rho U^2 C_D c\, dx \qquad dM_{c/4} = \frac{1}{2} \rho U^2 C_M c^2\, dx$$

It can be seen from equations (5) – (7) that inflow velocity does not depend upon azimuth in axial flight. This symmetry makes modelling of axial flight much easier since model of single blade can be created and resulting aerodynamic forces can be obtained by integrating the elemental loads across the blade span and multiplying by the number of blades (N_B). In forward flight, inflow angle of the blade is a function of azimuth. Therefore, assumption of uniform rotor disc loading cannot be made.

4.4 Dynamic Inflow Calculation

Many models of helicopter aerodynamics utilise momentum theory for computation of induced velocity. However, for small negative values of speed of climb, momentum theory fails to estimate induced velocity correctly (see Figure 5). Therefore, classical momentum theory cannot be used for calculation of induced velocity of autorotating rotor. Instead, a modified version of Peters - HaQuang inflow model that was introduced by Houston [15] was used. In forward flight induced velocity is assumed to vary radially and around the blade azimuth and can be expressed as:

$$v_i = v_{i_0} + x\left(v_{i_s} \sin\psi + v_{i_c} \cos\psi\right)$$

(8)

These components of the induced velocity are calculated from the following system of differential equations [16]:

$$[\tau]\begin{bmatrix} \dot{v}_{i_0} \\ \dot{v}_{i_s} \\ \dot{v}_{i_c} \end{bmatrix} + \begin{bmatrix} v_{i_0} \\ v_{i_s} \\ v_{i_c} \end{bmatrix} = [\Lambda]\begin{bmatrix} T \\ L \\ M \end{bmatrix}$$

(9)

Matrix τ is the time constant matrix and is defined as [17]:

$$[\tau] = \begin{bmatrix} \dfrac{4R}{3\pi V_T C_0} & 0 & \dfrac{-R\tan(\chi/2)}{12U_m} \\[3mm] 0 & \dfrac{64R}{45\pi U_m(1+\cos\chi)} & 0 \\[3mm] \dfrac{5R\tan(\chi/2)}{8V_T} & 0 & \dfrac{64R\cos\chi}{45\pi U_m(1+\cos\chi)} \end{bmatrix}$$

(10)

whilst matrix Λ is defined as the dynamic inflow static gain matrix and is given by:

$$[\Lambda] = \begin{bmatrix} \dfrac{R}{2V_T} & 0 & \dfrac{15\pi\tan(\chi/2)}{64U_m} \\[3mm] 0 & -\dfrac{4}{U_m(1+\cos\chi)} & 0 \\[3mm] \dfrac{15\pi\tan(\chi/2)}{64V_T} & 0 & -\dfrac{4\cos\chi}{U_m(1+\cos\chi)} \end{bmatrix}$$

(11)

In the equation (9) T, L and M are rotor thrust, rolling moment and pitching moment. If V_x, V_y and V_z are component free-stream velocities, the remaining variables form equation (9) are given as follows:

$$U_m = \frac{V_x^2 + V_y^2 + (2u_{mom} - V_z)(u_{mom} - V_z)}{V_T}$$

$$V_T = \sqrt{V_x^2 + V_y^2 + (V_z - u_{mom})^2}$$

$$u_{mom} = \sqrt{\frac{T}{2\rho A}}$$

$$\chi = \tan^{-1}\left(\frac{\sqrt{V_x^2 + V_y^2}}{u_{mom} - V_z}\right)$$

$$C_0 = \frac{8}{3\pi}$$

(12)

From the system of equations (9), only the first equation was used in the simulation and the remaining two components of induced velocity were assumed to be negligible. This modification decreases computing time and reduces complexity of the AMRA model significantly. The equation below shows the solution for the rate of change of vertical component of induced velocity.

$$\dot{v}_{i0} = -\frac{3C_0\left(2\pi\rho R^2 v_{i_0}\sqrt{V_x^2 + V_y^2 + V_z^2} - \sqrt{2}V_z\sqrt{\frac{T}{\rho\pi R^2} + \frac{T}{2\rho\pi R^2}} - T\right)}{8\rho R^3}$$

(13)

Hence, the value of induced velocity during forward autorotative flight can be obtained by integration of the above equation according to time.

$$v_i \approx v_{i_0} = \int \dot{v}_{i_0}\, dt$$

(14)

4.5   **Modelling Blade Dynamics**

The AMRA model can use Lagrange's equations of motion or the finite element method (FEM) for modelling of rotor blade structural dynamics in bending, teeter and torsion. Alternatively, combinations of both approaches can be used. This allows comparison of differences between results obtained with the aid of models with different levels of complexity. In Lagrange's method, the blades are assumed to be perfectly rigid and blade stiffness is modelled with springs located at the root of each blade. Bending and torsional deflections are assumed to be constant along the blade span. This requires less computational time but it does not provide a full picture of the dynamics of the system since it is significantly simplified. Finite element analysis (FEA) of coupled bending-torsion of the blade on the other hand is highly complex and requires significantly higher computational time.

4.5.1   **Blade Dynamics Using Lagrange's Method**

Lagrange's method is an elegant way of obtaining the equations of motion and it is useful for modelling of complex dynamics of rotorcraft rotor blades. In order to use span-wise distributions of blade physical properties and also allow coupling of Lagrange's equations of motion with FEA of blade dynamics, each rotor blade is discretized into a number of lumped masses. Lagrange's equations of motion are generated for each lumped mass. Linearized and simplified versions of equations of motion for coupled torsion-flap of a rotor blade are published in the open literature [18]. Further details of the development of these equations is given in Appendix 2.

4.5.2   **Galerkin's Method – Development of Finite Element Approach to Blade Dynamics**

Galerkin's method of solution is used in the AMRA model. The model can perform dynamic FEA of blade torsion or blade bending for teetering rotors. Alternatively, FEA of coupled bending-torsion dynamics with inclusion of teeter can be used. A 1D FEA was used in order to reduce complexity of the model. Each blade element has two nodes and number of degrees of freedom differs from one (torsion only) to three (torsion with flap-wise bending). Differential equation of blade torsion can be written in following form [19]

$$\frac{\partial w_f}{\partial r} GJ \frac{\partial \theta}{\partial r} + w_f i_x \ddot{\theta} + w_f A_T - w_f q = 0$$

(15)

The term A_T represents sum of terms that represent the effect of coupling of blade torsional dynamics with degrees of freedom in flap and rotation.

Although solution of the differential equation of blade torsion with the aid of FEM does not require shape functions of higher order and linear shape functions can be used, cubic shape function was chosen for modelling of blade torsion in AMRA. Cubic shape function is defined as [19]

$$H_1 = 3(x_{i+1} - x)^2 - 2(x_{i+1} - x)^3$$

$$H_2 = 1 - H_1 = 3(x - x_i)^2 - 2(x - x_i)^3$$

(16)

Corresponding mass and stiffness matrices and forcing vector are as follows [19]

$$[K_i] = GJ \begin{bmatrix} \dfrac{-6}{5l_i} & \dfrac{6}{5l_i} \\ \dfrac{6}{5l_i} & \dfrac{-6}{5l_i} \end{bmatrix}$$

(17)

$$[M_i] = i_x \begin{bmatrix} \dfrac{13l_i}{35} & \dfrac{9l_i}{70} \\ \dfrac{9l_i}{70} & \dfrac{13l_i}{35} \end{bmatrix}$$

(18)

$$\{f_i\} = f_i \begin{Bmatrix} \dfrac{l_i}{2} \\ \dfrac{l_i}{2} \end{Bmatrix}$$

(19)

Alternatively, diagonal (or diagonally lumped) mass matrix can be used. It speeds up the computations as inversion of this mass matrix is much easier than in case of consistent mass matrix [19]

$$[M_i] = i_x \begin{bmatrix} \dfrac{l_i}{2} & 0 \\ 0 & \dfrac{l_i}{2} \end{bmatrix}$$

(20)

The finite element model of blade bending has two nodes per element but in contrary to the FEM model of blade torsion it requires two degrees of freedom per node - vertical displacement and flap-wise rotation. Differential equation of blade bending is shown below [19].

$$\frac{\partial^2 w_f}{\partial r^2} EI \frac{\partial^2 w}{\partial r^2} + w_f \mu_b \ddot{w} + w_f A_B - w_f t = 0$$

(21)

Again, the term A_B in the above equation represents a sum of all coupling terms.

Unlike FEA of blade torsion, modelling of blade bending with the aid of FEM requires shape functions of higher order. Hence, two different shape functions have to be used in order to describe distribution of both vertical displacement of blade nodes and slope of blade elements over a blade element. These shape functions are called Hamiltonian shape functions and they are based on the cubic shape function described in equation (16) [19]. Application of Hamiltonian shape functions results in the following forms of stiffness matrix, consistent mass matrix and forcing vector [19].

$$[K_i] = \frac{EI}{l_i^3} \begin{bmatrix} 12 & 6l_i & -12 & 6l_i \\ 6l_i & 4l_i^2 & -6l_i & 2l_i^2 \\ -12 & -6l_i & 12 & -6l_i \\ 6l_i & 2l_i^2 & -6l_i & 4l_i^2 \end{bmatrix}$$

(22)

$$[M_i] = \mu_i \frac{l_i}{420} \begin{bmatrix} 156 & 22l_i & 54 & -13l_i \\ 22l_i & 4l_i^2 & 13l_i & -3l_i^2 \\ 54 & 13l_i & 156 & -22l_i \\ -13l_i & -3l_i^2 & -22l_i & 4l_i^2 \end{bmatrix}$$

(23)

$$\{f_i\} = \frac{f_i}{12} \begin{Bmatrix} 6l_i \\ l_i^2 \\ 6l_i \\ -l_i^2 \end{Bmatrix}$$

(24)

A diagonal form of mass matrix is more convenient for dynamic analysis. Parameter has to be a positive number smaller than 50. Kwon et al [19] recommends $\alpha_M = 1/78$, which is used in AMRA.

$$[M_i] = \mu_i l_i \begin{bmatrix} \frac{1}{2} & 0 & 0 & 0 \\ 0 & \alpha_M l_i^2 & 0 & 0 \\ 0 & 0 & \frac{1}{2} & 0 \\ 0 & 0 & 0 & \alpha_M l_i^2 \end{bmatrix}$$

(25)

5   Experimental Measurement of Blade Properties

Since the majority of gyroplane rotor blades are manufactured by small private companies, it is relatively difficult to get any information of structural properties of these blades. A pair of blades from the Montgomerie-Parsons gyroplane were subjected to a series of experiments in order to assess its physical properties and mass distribution. Data gathered during the experiments were used as input values of the simulations.

The first blade was cut up into 20 sections and each was measured and weighed so as to ascertain span-wise mass distribution of the blade. Chord-wise position of centre of gravity was also estimated for each blade element from the arrangement of internal structure of each blade section (i.e. position and size of the spar, thickness of the skin and distribution of potential filling material). Figure 6 shows the internal structure of the blade at blade root and at the tip. It can be seen that both mass distribution and chord-wise positions of c.g. are mainly given by span-wise distribution of the spar. Span-wise distributions of blade mass and c.g. locations that were obtained from the experiments are depicted in Figure 7 and Figure 8.

Experimental measurements accomplished with use of second Montgomerie-Parsons gyroplane rotor blade were focused on structural properties of the blades. Torsional stiffness and chord-wise positions of elastic axis of the blade were measured at three span-wise stations. Span-wise positions of these the stations were x = 0.25 (quarter-span), x = 0.5 (half-span) and x = 0.75. The rotor blade was firmly fixed at the root and clamped into outboard clamp at the appropriate span-wise station. The outboard clamp was then used for loading of the blade with a torsional moment. Constant weight was used and loading moment was changed by shifting of the weight along the clamp arm. Consequent measurements of blade angular deflections allowed calculation of appropriate stiffness coefficients.

$$k_\theta = \frac{M_\theta}{\theta}$$

(26)

Angular deflections of the blade in pitch were determined with the aid of calibrated angle measuring instruments that were fixed to the upper surface of the clamp. The arrangement of the equipment during the experiment is shown in Figure 9. Measurements were carried out for different values of torque at each span-wise station to increase higher accuracy of stiffness estimation. Graphical interpretations of the results are given in Figure 10. Torsional stiffness was determined for each span-wise station of the blade (see Table 1 below).

Table 1   Locations of elastic axis and torsional stiffness as obtained during the experiment

Span-wise station [1]	0.25	0.5	0.75
Location of EA [%c]	35.5	25.3	27.24
GJ [N.m^2/rad]	1534	1443	1409

Measurement of the first flexural natural frequency of the blade was used to estimate flexural stiffness of the blade. Determination of blade flexural stiffness that was used during the experiment is described below.

$$f = \frac{1}{T} = \frac{N_{cycles}}{t} \quad \omega = 2\pi f \quad EI \approx \frac{\omega^2 R^3 \int_0^1 mx^4 dx}{4}$$

(27)

Data gathered during the experiment are shown in Table 2 below.

Table 2   Characteristics of oscillations in flap of Montgomerie-Parsons rotor blade

Number of oscillations	Time [s]	T [s]	f (Hz)	ω [rad/s]
60	47.63	0.793833	1.25971	7.914993
60	47.62	0.793667	1.259975	7.916655
60	47.67	0.7945	1.258653	7.908352

The resulting estimated value of flexural stiffness is **EI = 1166.2 N.m^2.**

6   Model Verification and Validation

Although the AMRA model is fully functional standalone model of rotor aeromechanics in autorotation, its main purpose was to test model of blade dynamics in autorotation so that it can be incorporated into a rotorcraft flight mechanics model. Therefore, the main objective of the validation phase of the project was to make sure that blade dynamics are computed correctly by the AMRA model. FEM model of blade torsion represents the key block of AMRA and extra care was taken during its validation. Values of teetering angle predicted by the AMRA model were verified against G-UNIV gyroplane flight data. Estimations of flight performance during flight in autorotation were also successfully compared with experimental data published in open literature [6, 18].

6.1   Verification in Axial Flight

A series of simulations of aeromechanical behaviour of a gyroplane rotor in axial autorotative flight was performed as a simple method of model verification. The input parameters of the simulations can be found in Table 3. Simulations of a gyroplane rotor in steady autorotative descent have revealed that the AMRA model captures all key features of the system. The rotor speed has to be increased by application of external torque during pre-rotation. Once the rotor speed reaches sufficient value, the external torque is removed and the system enters autorotative regime. Both acceleration of the rotor from lower rotor speed and transition from helicopter regime (i.e. deceleration from higher rotor speed, see Figure 11) can be demonstrated by the simulation (see Figure 12). Note that rotor speed always stabilises at the same value once steady autorotation is established since its configuration did not change.

It should be noted that rotor speed in autorotation is much lower than rotor speed of helicopter rotor during flight. It can be seen from Figure 11 that the rotor speed is stabilized and the system reaches torque equilibrium within few seconds. At this point, the total thrust of the rotor is in balance with the weight of the vehicle and the value of speed of descent is approximately 11.5m/s (see Figure 13). The value of speed of descent agrees with the results of experimental flight measurements that were carried out by NACA and several other research bodies [5, 6]. Equation (28) below shows empirical relationship of disc loading of a gyroplane and speed of descent that was derived from the experimental results [5, 6].

Table 3   Input parameters of the simulations

PARAMETER	VALUE
Blade length (R)	3.63 m
Blade chord (c)	0.2 m
Chord-wise position of EA (y_{EA})	0.08 m = 40%c
Chord-wise position of c.g. (y_{cg})	0.066 m =33%c
Chord-wise position of AC (y_{AC})	0.05 m = 25%c
Offset of c.g. from EA (y_g)	0.014 m
Offset of AC from EA (y_c)	0.03 m
Blade weight (m)	13 kg
Number of blades (N_B)	2

Table 3   Input parameters of the simulations (Continued)

PARAMETER	VALUE
Blade fixed incidence angle	0 rad
Span-wise distribution of blade geometric twist	$\varepsilon = 0$ rad
Weight of the gyroplane (M)	400 kg
Blade torsional stiffness coefficient (k_θ)	$1600 \text{N.m}^2/\text{rad}$
Blade flexural stiffness coefficient (k)	1200N.m^2
Blade section geometry	NACA 0012
Torque used for pre-rotation (Q_{PR})	2000N.m

$$V_d \approx 1.212\sqrt{T/A}$$

(28)

The weight of the vehicle is M = 400kg and rotor radius is R = 3.63m, hence rotor disc loading is T/A = 96N.m^{-2} and equation (28) gives speed of descent V_d = 11.8m/s.

A characteristic span-wise distribution of blade torque for a rotor in the autorotative regime is observed. The inboard part of the blade generates positive torque and the outboard part of the blade generates negative torque. In steady autorotation, the total value of torque generated by the blade is zero. Figure 14 shows a comparison of span-wise distribution of torque obtained from the simulation and torque distribution as described in open literature [5, 6]

The so-called coefficient of resultant force is another important characteristic of autorotative regime [5, 6]. It is defined by

$$c_R = \frac{2R}{\rho V^2 A}$$

$$R = \sqrt{L^2 + D^2}$$

$$V = \sqrt{V_h^2 + V_d^2}$$

(29)

Previous research involving experimental flight measurements [5, 6] found that C_R on typical rotor of a gyroplane during steady autorotative flight at large rotor disc angles of attack (α_D > 30deg) is about 1.25. It is important to realize that the majority of gyroplane rotors have very small or zero fixed blade angle of incidence (in effect a collective pitch setting, in helicopter jargon). Figure 15 shows a comparison of experimental values of c_R [5, 6] and the outcome of the simulation. The AMRA model predicts value of C_R to be 1.19.

6.2   **Verification in Forward Flight**

Since gyroplanes operate mostly in forward flight regime, modelling of forward autorotative flight represents the key task in investigation of aeroelastic behaviour of a gyroplane rotor blade. In comparison to the simulation of axial autorotative flight, simulation of forward flight in autorotation induces some complication. Both direction and value of the inflow velocity are functions of azimuth if horizontal speed is not zero (see equations (A1.2) and (A1.3)). This means that there is no torque equilibrium during steady forward flight and the value of torque oscillates around the zero value (see Figure 16). The amount of vibrations induced by the rotor blade during steady forward flight is therefore significantly higher than in axial descent. In addition, free-stream velocity at the advancing side of the rotor disc is higher, and thus the values of the forcing moments are higher too. It can be expected that gyroplane rotor blade in the forward flight regime is more prone to undergo aeroelastic instability than the same blade during axial autorotative flight.

6.3   **Validation of the AMRA Model**

a) Teeter Motion

Data gathered during the CAA sponsored series of flight test of the University of Glasgow Montgomerie-Parsons gyroplane (G-UNIV) were used for validation of model of blade teeter that is included in the AMRA model. AMRA uses a NACA 0012 airfoil that has different aerodynamic characteristics in comparison with NACA 8-H-12 that are used in McCutcheon rotor blades. The NACA 8-H-12 is normally chosen due to its speed stability properties however in this case a complete and reliable set of aerodynamic data was required, and hence the 0012 profile was chosen. In order to reach similar flight conditions during simulations (i.e. rotor speed and speed of descent), rotor speed was set to mean value of rotor speed measured during the flight tests. Two different regimes of steady level flight were chosen for the validation. Predictions of the model were found to be in a good agreement with teeter angles measured during flight trials as it can be seen from Figures 17 and 18. Table 4 summarizes the results of validation of AMRA model of blade teeter.

Table 4   Comparison of predictions of rotor blade teeter and G-UNIV experimental data

CASE	V_H	Ω	β_{exp}	β_{AMRA}
	[m/s]	[rad/s]	[rad]	[rad]
A	14	38	0.031	0.026
B	27	41	0.058	0.056

b) Validation of FEM Model of Blade Torsion

Deflections of beams of several lengths and with different torsional stiffness that were loaded statically by a torsional moment at the tip were computed by the AMRA FEM model of blade torsion. The results were then compared with analytical estimations of beam tip torsional deflections according to the St. Venant theory and were found to be in very good agreement. Mean relative deviation was less than 2%.

The shape of the first torsional mode predicted by the FEM model was also compared to corresponding torsional mode shapes that were published in open literature [18]. Predictions of the model are in good agreement with published data.

Comparison of the first torsional mode shape computed by the FEM model of blade torsion with data published in open literature, Bielawa [18], is depicted in Figure 19.

Since the span-wise distribution of blade torsion has a strong influence on blade aerodynamics, it is absolutely crucial that it is modelled correctly and the aerodynamic forcing of the blade is estimated realistically. Figures 20 and 21 depict a qualitative comparison of distribution of torque generated by rotor blade over the rotor disk as predicted by the AMRA model and qualitative sketch of torque distribution reproduced in open literature [6].

Comparisons of the first natural frequencies in torsion and bending of two different rotor blades with results of experimental measurements and predictions of other models of blade dynamics represent another phase of AMRA validation. Data obtained during experimental measurements of physical properties of the McCutcheon blade along with comprehensive data on physical properties of Aérospatiale SA330 Puma helicopter rotor blade were used [21]. A Southwell plot of the McCutcheon rotor blade is shown in Figure 22. Although first natural frequency in torsion is slightly under-predicted by the AMRA model, general agreement with experimental data is good. Simple dynamic model of blade bending using spring stiffness and rigid blades was used during testing of the FEM model of blade torsion. Predictions of first natural frequency in bending of McCutcheon rotor blade is consistent with both theory and published shake tests of similar rotor blades [22, 23].

As can be seen from Figure 23 predictions of first natural frequency in bending of Puma rotor blade is in reasonable agreement with results of METAR/R85. CAMRAD and RAE/WHL models predict lower values of the first natural torsional frequency than both METAR/R85 and AMRA. Bousman et al [21], however, describes estimations of modal frequencies of METAR/R85, CAMRAD and RAE/WHL models as consistent.

c) Validation of FEM Model of Blade Bending

A coupled FEM model of blade torsion and bending was validated in similar manner as the FEM model of blade torsion. Predictions of both static and dynamic loading of the blade were compared with analytical predictions, experimental measurements and results of other structural analysis codes.

Predictions of static bending as obtained from the AMRA model are in good agreement with analytical predictions. Values of blade vertical displacement obtained with the model are roughly by 5% lower than analytical predictions and relative deviation of blade gradients is roughly 6% and these values do not change with loading, blade flexural stiffness or blade length.

Estimations of blade bending behaviour were validated against the same set of data that was used for validation of the FEM model of blade torsion [21]. The conclusion can be made that both static and dynamic behaviour of AMRA structural dynamics block was validated and that the model is likely to give realistic estimations of both rotor blade torsion and bending. Figures 24 and 25 depict distribution of torsional deflections and flexural vertical displacements over the rotor disc during forward flight.

7 Aeroelastic Stability of a Rotor in Autorotation

Unlike helicopter rotors, rotors in autorotation can experience significant variations in rotor speed during manoeuvres. Decrement of the rotor speed decreases centrifugal stiffness of the rotor and the resulting higher deflections in flap and twist generate more drag and may cause further drop in rotor speed. It is clear that thrust and torque of the rotor are functions of rotor speed and distribution of local angles of attack along the blade span. Further, angles of attack are dependent upon blade twist, rotor speed, descent rate and induced velocity. It can be easily shown that both descent rate and rotor angular velocity are strongly dependent upon rotor torque and rotor thrust. The AMRA model has shown that the extra degree of freedom in rotor speed has significant effect on the aeromechanics and aeroelastic stability of an autorotating rotor.

A series of parametric studies that was carried out with the aid of the model [24] shows that blade induced twist (torsion), fixed angle of incidence of the blade and blade geometric twist have by far the strongest influence on the aeromechanical behaviour of a rotor in autorotation.

AMRA simulations were performed for three different levels of model complexity. The simplest configuration of the model used perfectly rigid rotor blades in both bending and torsion and blade flexibility was modelled with the aid of spring stiffness located at blade root. The second configuration of AMRA employed the FEM model of blade torsion while only spring stiffness was used for modelling of blade bending. The most complex variant of the model utilized coupled FEM models of both torsion and bending. Comparison of results obtained for these three model configurations allowed assessment of the effect of complexity of the structural dynamics model on performance and fidelity of AMRA simulations. In order to investigate rotor stability boundary in torsion, AMRA simulations for various values of torsional stiffness and chord-wise positions of centre of gravity (c.g.) were carried out.

The results of the simulations have revealed that low torsional stiffness of the blade leads to an aeroelastic instability (flutter) that manifests as coupled rotor speed / pitch / flap oscillations. These oscillations result in catastrophic decrease of rotor speed. This is a demonstration of strong rotor speed / pitch / flap coupling that exists only during autorotation.

Decrement of the rotor speed decreases centrifugal stiffness of the rotor and the resulting higher deflections in flap and twist generate more drag and cause further drop in rotor speed. This type of flutter is unique for rotors in autorotation since it differs from both helicopter rotor flutter and flutter of a fixed wing.

7.1 Aeroelastic Stability of a Rotor in Axial Autorotative Flight

Since blade aerodynamic forcing during steady axial autorotative flight is not dependent upon blade azimuth, it becomes constant after the rotor reaches equilibrium state. During steady vertical autorotation, overall torque generated by flow through the rotor disc is zero and rotor thrust is equal to the weight of the vehicle. The rotorspeed converges towards its steady value during torsional equilibrium. A characteristic span-wise distribution of blade torque for a rotor in the autorotative regime is observed. The inboard part of the blade generates positive torque and the outboard part of the blade generates negative torque [5, 6]. The AMRA model describes all major features of aerodynamics of a rotor in autorotative axial descent very well [24].

Results of the AMRA simulations obtained for different levels of complexity of the model show that torsion is the most important parameter to compute accurately; torsion therefore requires a FEM. The aeroelastic behaviour of the rotor for two different levels of model complexity is shown in Figures 26 and 27. In Figure 26, the simplified model of blade dynamics using equivalent spring stiffness for modelling both torsion and bending is usued, whilst the full FEM model was used to calculate the results shown in Figure 27. As it can be seen in the figures, reduction of rotor speed from a steady value to zero takes only few seconds. Speed of descent increases to unacceptable value during this time due to dramatic decrease of rotor thrust. Parametric studies carried out with an earlier generation of the model [24] had shown that chord-wise position of c.g. seems to have much stronger influence on the stability of autorotation than chord-wise position of EA. Note that the c.g. location in Figures 26, 27, 28, and 29 is destabilising, as it is 8% after the elastic axis.

7.2   Aeroelastic Stability of a Rotor in Forward Autorotative Flight

Since gyroplanes operate mostly in the forward flight regime, modelling of forward autorotative flight represents the key task in investigation of aeroelastic behaviour of a gyroplane rotor blade. Since both direction and value of the inflow velocity are functions of azimuth if horizontal speed is not zero there is no torque equilibrium during steady forward flight and the value of torque oscillates around the zero value. The amount of vibration induced by the rotor blade during steady forward flight is therefore significantly higher than in axial descent. In addition, free-stream velocity at the advancing side of the rotor disc is higher than at the retreating side, and thus the values of the forcing moments are higher and also asymmetrical.

Since aerodynamic forcing of the blade during steady forward flight has harmonic character, blade motion in both bending and torsion has harmonic components too. As in case of axial flight, simplification of the model of blade torsion seems to significantly degrade predictions of the model. Only small changes in behaviour are seen when bending is modelled by an equivalent spring stiffness rather than a FEM.

Similarly as in case of axial flight in autorotation, simulations for various torsional stiffness and chord-wise positions of centre of gravity were performed. Computations carried out with the aid of the AMRA model have shown that the rotor suffers of aeroelastic instability if c.g. lies aft EA. Aeroelastic behaviour of the rotor for all three different levels of model complexity has very similar character to the aeroelastic instability predicted in autorotative vertical descent and it is shown in Figures 28 and 29. The resulting aeroelastic stability boundary can be found in Figure 30 which is a plot of the blade torsional stiffness at which instability occurs, $k_{\theta crit}$, for specific chord-wise location of c.g., y_{cg}. It can be seen from the figure that position of c.g. aft EA is destabilizing, similar to fixed wing classical flutter and helicopter pitch flap flutter.

8   Investigation of Aeroelastic Stability Boundaries of Gyroplane Rotors – Impact on BCAR Section T

8.1   Background

The poor safety record of the gyroplane in the UK in the early 1990s led to a review of the airworthiness requirements of the type, BCAR Section T [25]. From the mid-1990s the Civil Aviation Authority has funded a series of research programmes in the University of Glasgow in support of the development of BCAR Section T including simulation, wind tunnel testing and flight testing. The results of this work have fed directly into certain key areas of BCAR Section T, notably the requirements for dynamic stability [2, 3]. The current work reported here has been to study the aeroelastic properties of gyroplane rotors, and from the previous section it is clear that instabilities do exist. The aim of the work reported in this section is to further the aeroelastic stability boundary, carrying out parametric studies to identify if particular design features might lead to an unstable rotor system. The aim is to verify (or otherwise) that the requirements for chordal balance currently in BCAR Section T are appropriate.

8.2   Analysis of BCAR Section T Chordal Balance Requirement

BCAR Section T (light gyroplanes) paragraph T659 states:

Mass balance

a) ......

b) The chordwise balance of the blades must be at, or forward, of the 25% chord. The chordwise balance of each blade in a pair must be the same, or within a tolerance to be agreed with the CAA.

This paragraph is similar to the requirement which achieves pitch-flap flutter stability for helicopter rotors, where it may be shown (see for example Bramwell's Helicopter Dynamics, by Done and Balmford, 2nd Ed, Chapter 9, section 9.3 [26]) that flutter and divergence stability for a helicopter blade may be assured, regardless of the control system stiffness, if the blade chordwise c.g. is ahead of the collinear pitch axis and quarter chord point. A linear stability analysis shows that the flutter boundary for a rigid blade, pitching, about the feather hinge at the quarter chord point, and flapping about a flap hinge, is a hyperbola, as shown in Figure 31. The divergence boundary is linear, and is usually below the flutter boundary. Note that Figures 30 and 31 are similar, however the detail is different as Figure 31 shows the boundary for a helicopter blade pitching around the quarter chord position and is generated by a linear model, whilst Figure 30 is generated by a nonlinear model of a gyroplane blade twisting about the elastic axis.

The dashed line in Figure 31 is the maximal aft position of c.g. that assures flutter stability regardless of control system stiffness, and this always lies at, or slightly aft of the quarter chord. This is only strictly true for a blade pitch axis coincident with the aerodynamic centre. The linearized, non-dimensional model used to elucidate this stability boundary is

$$
\begin{bmatrix} 1 & 0 \\ -I_x^* & I_\theta^* \end{bmatrix} \begin{bmatrix} \ddot{\beta} \\ \ddot{\theta} \end{bmatrix} + \begin{bmatrix} 1 & 0 \\ -I_x^* & I_\theta^*(\omega_\theta^2 + 1) \end{bmatrix} \begin{bmatrix} \beta \\ \theta \end{bmatrix}
$$

(30)

for the mass and stiffness matrices, which are added to the following aerodynamic terms (developed using thin aerofoil, and Theodorsen's theory):

$$
\begin{bmatrix} \dfrac{\gamma}{8}C(k) & 0 \\ 0 & \dfrac{\gamma}{32}\dfrac{1}{AR^2} \end{bmatrix}\begin{bmatrix} \dot{\beta} \\ \dot{\theta} \end{bmatrix} + \begin{bmatrix} 0 & -\dfrac{\gamma}{8}C(k) \\ 0 & 0 \end{bmatrix}\begin{bmatrix} \beta \\ \theta \end{bmatrix}
$$

(31)

Rotorspeed does not enter into these linearized, non-dimensional equations of motion.

To elucidate the stability properties of a gyroplane, a similar linearized model is developed here and is compared to time marched results of a non-linear Finite Element Model (FEM) of an existing gyroplane rotor. Modifications to the helicopter model are required to account for the different hub design of a gyroplane to that of a helicopter, and, in the FEM case, the inclusion of rotorspeed as a degree of freedom. The results are only pertinent to conventional two bladed teetering light-gyroplane hubs with no blade feather hinge.

A gyroplane hub has a slightly different construction to a helicopter rotor hub: the gyro blades are usually mounted to the hub bar at the quarter chord point, but do not have a separate pitch degree of freedom, and also have a rotorspeed degree of freedom. The blades pitch about the quarter chord when they are fore and aft (0/180° azimuth), but pitch about an offset axis, due to the offset hinge on the gyro hub (an introduction of Igor Bensen in 1948 to provide stick free pitch stability). This offset hinge arrangement is shown in Figures 32(a) and 32(b).

A rigid blade model (similar to the above linearized equations of motion for a helicopter blade) of a gyroplane hub therefore has flap and pitch blade degrees of freedom, with the pitch axis moving cyclically about the quarter chord. Alternatively, the blade degrees of freedom can be expressed as a lateral disc tilt about the centre of rotation and a longitudinal disc tilt slightly ahead of the centre of rotation. An oscillation in flutter would therefore manifest itself as an oscillatory disc tilt.

As a result of this pitch about an axis unequal to the quarter chord, extra terms come into the aerodynamic matrices for the gyro flutter boundary. The aerodynamic terms for a single flapping gyro blade become:

$$
\begin{bmatrix} \dfrac{\gamma}{8}C(k) & 0 \\ \dfrac{\gamma}{12}\dfrac{1}{AR}\left(\dfrac{1}{2}-\bar{x}\right)C(k) & \dfrac{\gamma}{32}\dfrac{1}{AR^2}\left(\dfrac{1}{2}-\bar{x}\right) \end{bmatrix}\begin{bmatrix} \dot{\beta} \\ \dot{\theta} \end{bmatrix} + \begin{bmatrix} 0 & -\dfrac{\gamma}{8}C(k) \\ 0 & -\dfrac{\gamma}{12}\dfrac{1}{AR}\left(\dfrac{1}{2}+\bar{x}\right)C(k) \end{bmatrix}\begin{bmatrix} \beta \\ \theta \end{bmatrix}
$$

(32)

For the teetering gyro rotor as a whole, the mass and stiffness matrices become:

$$
2\begin{bmatrix} 1 & 0 \\ -I_x^* & I_\theta^* \end{bmatrix}\begin{bmatrix} \ddot{\beta} \\ \ddot{\theta} \end{bmatrix} + 2\begin{bmatrix} 1 & 0 \\ -I_x^* & I_\theta^*(\omega_\theta^2+1) \end{bmatrix}\begin{bmatrix} \beta \\ \theta \end{bmatrix}
$$

(33)

and the aerodynamic terms for both blades sum together to become:

$$
\begin{bmatrix} \dfrac{\gamma}{8}C(k) & 0 \\[2ex] 0 & \dfrac{\gamma}{32}\dfrac{1}{AR^2} \end{bmatrix}
\begin{bmatrix} \dot{\beta} \\[1ex] \dot{\theta} \end{bmatrix}
+ 2\begin{bmatrix} 0 & -\dfrac{\gamma}{8}C(k) \\[2ex] 0 & 0 \end{bmatrix}
\begin{bmatrix} \beta \\[1ex] \theta \end{bmatrix}
$$

(34)

i.e., the extra aerodynamic terms for the offset pitch axis average out to zero (one blade has a rear pitch axis, and the other a forward pitch axis- the net effect is zero). Again it should be noted that rotorspeed does not enter in to these linearized equations of motion. The flutter stability boundary for the gyro blade is therefore equivalent to the boundary for a helicopter rotor blade and so, for axial flight, and based on a linear stability analysis, BCAR Section T should produce a rotor free from 'pitch-flap' flutter and divergence.

The stability boundary for the gyro rotor is shown in Figure 33. For forward flight, however, the offset pitch axis terms in the aerodynamic matrices do not cancel out because of the added asymmetry in local velocity on the rotor disc at a particular advance ratio. The effect of non-zero advance ratio, for a typical hub pitch offset is shown in Figure 34 to be stabilizing when the blades are not at the 0/180° azimuth. This means a c.g. further aft is permissible when the blades are not at the 0/180° position. The critical blade mass balance condition is the same as for axial flight, however, which we have shown to be equivalent to that of a helicopter blade (despite the different hub design). Linear theory therefore suggests that compliance with BCAR T 659 will assure flutter stability in forward or axial flight.

The critical case is in axial flight, which is never encountered in operation. In forward flight, the hub offset is slightly stabilizing. The flutter, or divergence, boundary for the rotor is always furthest left (at its lowest x_{cg}/c) at low (but usually non-zero) values of control system stiffness. However, it should be remembered that the results of this stability analysis assume a control system with zero friction. A small amount of friction is undoubtedly present in actual gyroplane control linkages. When friction is added to the blade pitch terms in the system of equations it is stabilizing, meaning that a farther aft c.g. is tolerable. It is, however, difficult to quantify the amount of friction present in an actual gyroplane- to give a conservative flutter boundary, it is usual in aeroelastic analyses to assume zero friction, although, in the 1940s, Theodorsen found that small amounts of friction added to flutter equations often produced more realistic results than for systems without friction [27].

The rigid blade equations, used for this linear stability analysis were time integrated, to confirm that a small amount of friction in the control system was stabilizing. The effect of changing C_{M_0} was also investigated using this model. For gyroplanes, positive C_{M_0} is often added to the aerofoil section in order to prevent rotor overspeed. For a single blade, positive C_{M_0} is slightly destabilizing in the model and negative C_{M_0} slightly stabilizing. For a rotor as a whole, however, the pitching moment arising from C_{M_0} on one blade is counteracted by that of the other blade and so a change to C_{M_0} has no effect on the linear stability boundary for the gyroplane rotor.

The predicted flutter frequency for low stiffness control systems is of the order of 1/rev.

8.3   **Parametric Analysis**

A finite element analysis was undertaken for a gyroplane rotor model to confirm the conclusions of the linear stability analysis. 10-20 finite elements were used to model blade torsion and bending (on top of teeter), rotorspeed was included in the model as a degree of freedom, and blades could either pitch about the control system, or about their own elastic axes. A thin aerofoil, Theodorsen, strip theory aerodynamic model was used in the analysis. Moreover, non-zero C_{M_0} was added to the model. Various blade c.g. positions were input to the model, together with varying torsional stiffness, and the solution time-marched in order to see if the rotor model was stable. The results are summarized below. As time marching is computationally intensive, points on the flutter boundary were calculated for c.g.s at 0.28, 0.36, 0.40 and 0.46 chord and polynomials fit, in a least squares sense, to the data. Linear polynomials provided the best fit. The flutter boundaries are similar in character to the linear stability analyses.

The results of varying C_{M_0} are shown in Figure 35. These results are for blades twisting about their elastic axes (i.e. each blade has its own twist degree of freedom). Positive C_{M_0} is seen to be slightly de-stabilizing (it shifts the boundary to the left) and negative C_{M_0} is predicted to be slightly stabilizing. Unlike the case where blades are pitching about the control system axis, the blade elastic torsion degree of freedom is associated with significant stiffness (in fact, gyro blades are often much stiffer than helicopter blades). Again, BCAR T 659 should provide a rotor safe from flutter, given that actual measured blade stiffness' are high.

Bending stiffness did not affect the stability of the rotor in any of our simulations, but only small deflections were considered in the model, and no off-axis bending was modelled. It is noted, however, that off-axis bending is a mechanism by which an apparently low torsional stiffness can be achieved.

Figure 36 shows the effect of modelling the blade pitch to be about the control system (the lowest stiffness DOF) or about the blade elastic axes. This figure shows two boundaries, one for a blade pitching about the quarter chord (i.e. the pitch control axis) and one for a blade twisting at a nominal value of the elastic axis (at 32% chord in the figure). At zero stiffness, the destabilizing effect of pitching about the elastic axis is more pronounced due to the dominant effect of the extra aerodynamic coupling introduced by the elastic axis/quarter chord offset. This effect is only of academic interest, however, as the blade elastic axis is always associated with a high stiffness.

8.4   **Concluding Remarks**

In conclusion, BCAR T 659 provides a safe rotor, in terms of pitch flap flutter and divergence, for conventionally designed light gyroplanes with teetering rotors. In addition, the offset gyroplane hub is seen to be slightly stabilizing in forward flight. The predicted flutter frequency for low stiffness control systems is around 1/rev. This low frequency, and the fact that the dominant (low stiffness) degrees of freedom are longitudinal and lateral disc tilt, means that any flutter phenomenon arising from an aft c.g. will manifest itself as a 1/rev varying disc tilt.

9 Conclusions

An aeromechanical model of a gyroplane rotor AMRA was developed in the MATLAB programming language and used in predicting the aeroelastic behaviour of a rotor. Two regimes were investigated – autorotative axial flight (vertical descent) and forward flight in autorotation. Simulations have shown that autorotation is a complex aeromechanical process with auto-stabilizing characteristics. In order to obtain input parameters for the structural model of the blade, a series of experimental measurements were carried out on a typical gyroplane blade. Blade mass distribution, position of elastic axis, span-wise distribution of c.g. and torsional and flexural stiffness was determined during the experiments.

Results from the AMRA model were verified and found to be in reasonable agreement with experimental measurements. Several parametric studies were performed so as to gain more knowledge on the effect of blade geometry and structural properties on performance of the rotor during autorotation.

It was found that blade twist / bending / rotor speed coupling has major effect on the stability of autorotation when the rotor is in a stable configuration. Computations were performed for three different levels of complexity of the model of blade structural dynamics. Results of the AMRA simulations have shown that detailed modelling of rotor blade torsion (i.e. blade induced twist) has major influence on aeromechanics of a rotor in autorotation. It has been demonstrated that it is sufficient to model only first bending mode, i.e. to assume constant span-wise distribution of flap angle. The conclusion can be made that any aeroelastic simulation of a rotor in autorotation should contain model that gives realistic predictions of blade dynamics in torsion.

Occurrence of a type of flutter that is unique for autorotating rotors was predicted by the model both during axial descent in autorotation and autorotative forward flight. This aeroelastic instability is driven by blade pitch / bending / rotor speed coupling and differs from both flutter of a helicopter rotor and flutter of a fixed wing. The instability results in catastrophic decrease of the rotor speed and significant increase of speed of descent.

Finally, the research undertaken in this project was applied to a review of elements of BCAR Section T, and it was found that BCAR T 659 provides a safe rotor, in terms of pitch flap flutter and divergence, for conventionally designed light gyroplanes with teetering rotors.

CAA Comment

CAA accepts this finding yet notes that the stabilising affect of a number of other parameters was not exhaustively investigated during this limited research. As such the CAA would consider accepting blades that do not meet this single parametric requirement, as long as blade stability could be demonstrated by other means. This would allow for CAA acceptance of alternate means of compliance that demonstrate an equivalent level of safety to this requirement for blade stability.

---

10   References

1   Thomson, D.G., Houston, S.S., Spathopoulos, V. M., "Experiments in Autogiro Airworthiness for Improved Handling Qualities", Journal of American Helicopter Society, Pg. 295, No. 4, Vol. 50, October 2005.

2   Houston, S. S., "Longitudinal Stability of Gyroplanes", The Aeronautical Journal, Vol. 100 (991), 1996, pp. 1-6.

3   Houston, S. S.: "Identification of Autogiro Longitudinal Stability and Control Characteristics", Journal of Guidance, Control and Dynamics, Vol. 21, No. 3, 1998, pp. 391-399.

4   Coton, F., Smrcek, L., Patek, Z., "Aerodynamic Characteristics of a Gyroplane Configuration", Journal of Aircraft, Vol. 35, No. 2, 1998, p. 274 - 279.

5   Leishman, J.G., The Development of the Autogiro: A Technical Perspective, Journal of Aircraft, Vol. 41, (2), 2004, pp. 765-781.

6   Leishman, J.G., Principles of Helicopter Aerodynamics, Cambridge University Press, 2nd Edition, 2006, ISBN 0-521-85860-7.

7   Prouty, R. W., Helicopter Performance, Stability and Control, Robert E. Krieger Publishing Co., Malabar, FA, USA, 1990.

8   Sheldahl, R. E., Klimas, P. C., Aerodynamic Characteristics of Seven Aerofoil Sections Through 180 Degrees Angle of Attack for Use in Aerodynamic Analysis of Vertical Axis Wind Turbines, SAND80-2114, Sandia National Laboratories, Albuquerque, New Mexico, USA, 1981.

9   Nikolsky, A.A., Seckel, E., An Analytical Study of the Steady Vertical Descent in Autorotation of Single-Rotor Helicopters, NACA TN 1906, Washington, 1949.

10   Wheatley, B., Bioletti, C., Wind-Tunnel Tests of a 10-foot-diameter autogyro Rotor, NACA TR 536.

11   Wheatley, J.B., The Aerodynamic Analysis of the autogyro Rotating-Wing System, NACA TN 492, Langley Memorial Aeronautical Laboratory, 1934.

12   Wheatley, J.B., An Aerodynamic Analysis of the Autogiro Rotor with a Comparison between Calculated and Experimental Results, NACA TR 487, 1934.

13   Carpenter, P.J., Lift and Profile-drag Characteristics of an NACA 0012 Airfoil Section as Derived from Measured Helicopter-rotor Hovering Performance, NACA TN 4357, Langley Memorial Aeronautical Laboratory, Langley Field, VA, USA, 1958.

14   www.cyberiad.net/foildata.htm, visited in the fall 2005

15   Houston, S. S., Modelling and Analysis of Helicopter Flight Mechanics in Autorotation, Journal of Aircraft, Vol. 40, No. 4, 2003.

16   Chen, R. T. N., A Survey of Nonuniform Inflow Models for Rotorcraft Flight Dynamics and Control Applications, NASA TM 102219, Ames Research Centre, California, USA, 1989.

17   Houston, S. S., Brown, R. E., Rotor Wake Modelling for Simulation of Helicopters Flight Mechanics in Autorotation, Journal of Aircraft, Vol. 40, No. 5, 2003.

18   Bielawa, R. L., Rotary Wing Structural Dynamics and Aeroelasticity, Second edition, AIAA Education series, 2006. ISBN 1-56347-698-3

19   Kwon, Y. W., Bang, H., The Finite Element Method Using MATLAB, Second Edition, CRC Press, 2000, ISBN 0-8493-0096-7.

20   Sissingh, G., "Contribution to the Aerodynamics of the Rotating Wing Aircraft", NACA 921.

21   Bousman, W.G., Young, C., Toulmany, F., Gilbert, N.E., Strawn, R.C., Miller, J.V., Maier, T.H., Costes, M., A Comparison of Lifting-Line and CFD Methods with Flight Test Data from a Research Puma Helicopter, NASA TM 110421, Ames Research Center, Moffett Field, CA, USA, 1996

22   Friedman, P. P., Rotary-Wing Aeroelasticity: Current Status and Future Trends, AIAA Journal, Vol. 42, No. 10, October 2004.

23   Wilkie, W.K., Mirick P.H., Langston, Ch.W., Rotating Shake Test and Modal Analysis of a Model Helicopter Rotor Blade, NASA TM 4760, ARL TR 1389, Langley Research Center, Hampton, VA, USA, 1997.

24   Trchalík, J., Gillies, E.A., Thomson, D.G., Aeroelastic Behaviour of a gyroplane Rotor in Axial Descent and Forward Flight, 32nd European Rotorcraft Forum, Maastricht, Netherlands, October 2006.

25   Anon, "British Civil Airworthiness Requirements, Section T, Light Gyroplanes" Civil Aviation Authority CAP 643 Issue 3, Aug. 2003.

26   Bramwell, A.R.S., Done, G., Balmford, D., 'Bramwell's Helicopter Dynamics', 9th Edition, Butterworth Heineman, Oxford, 2001

27   Theodorsen, T. and Garrick, I., "Flutter calculations in three degrees of freedom' NACA TN-741, 1941

11 Acknowledgments
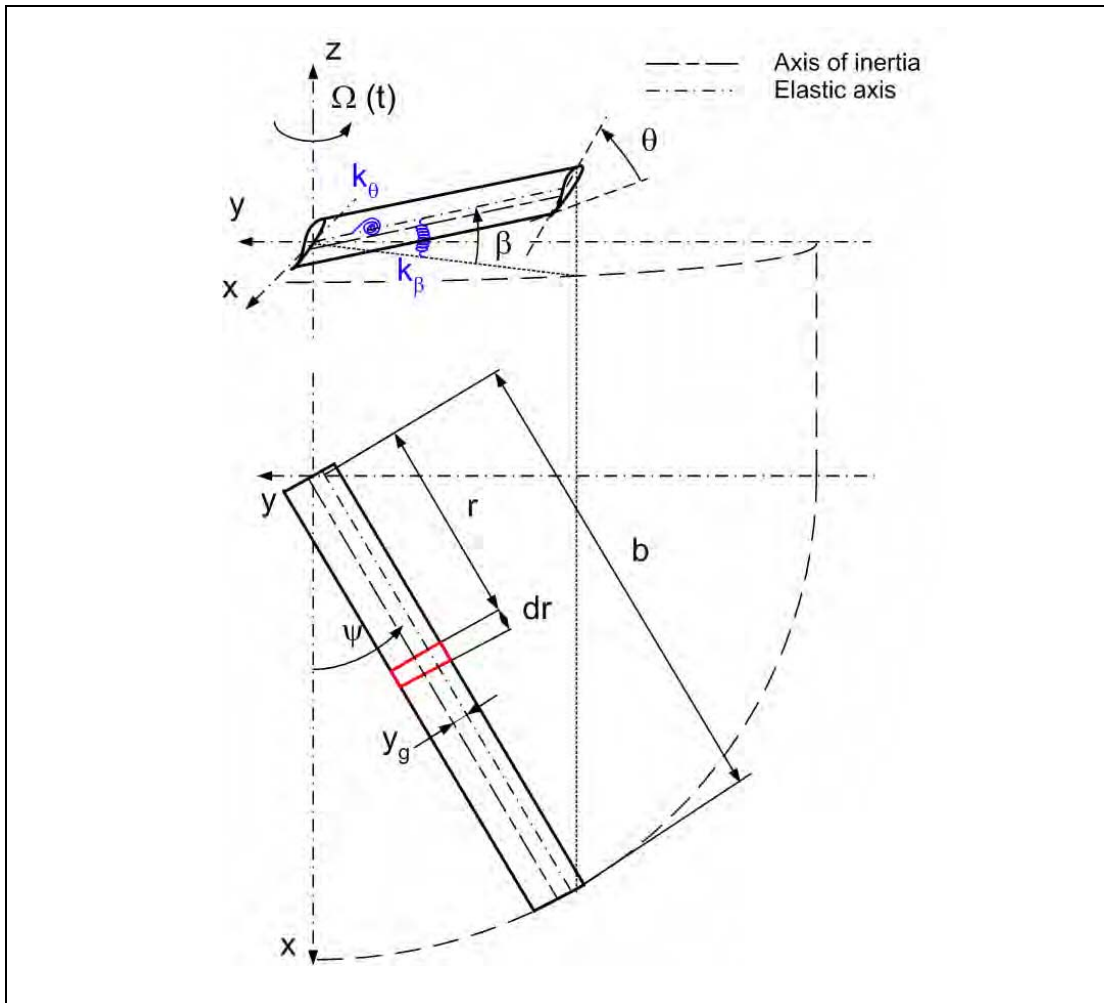
Figure 1   General arrangement of the AMRA gyroplane rotor blade model
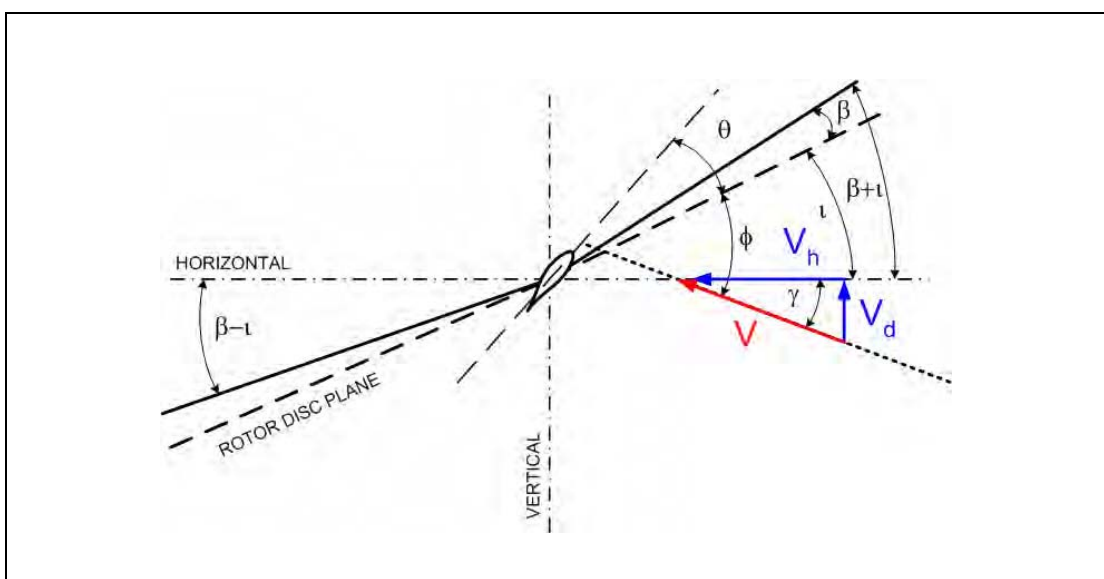
Figure 2   Relation of blade twist, flap and inflow angle of a rotor in autorotation
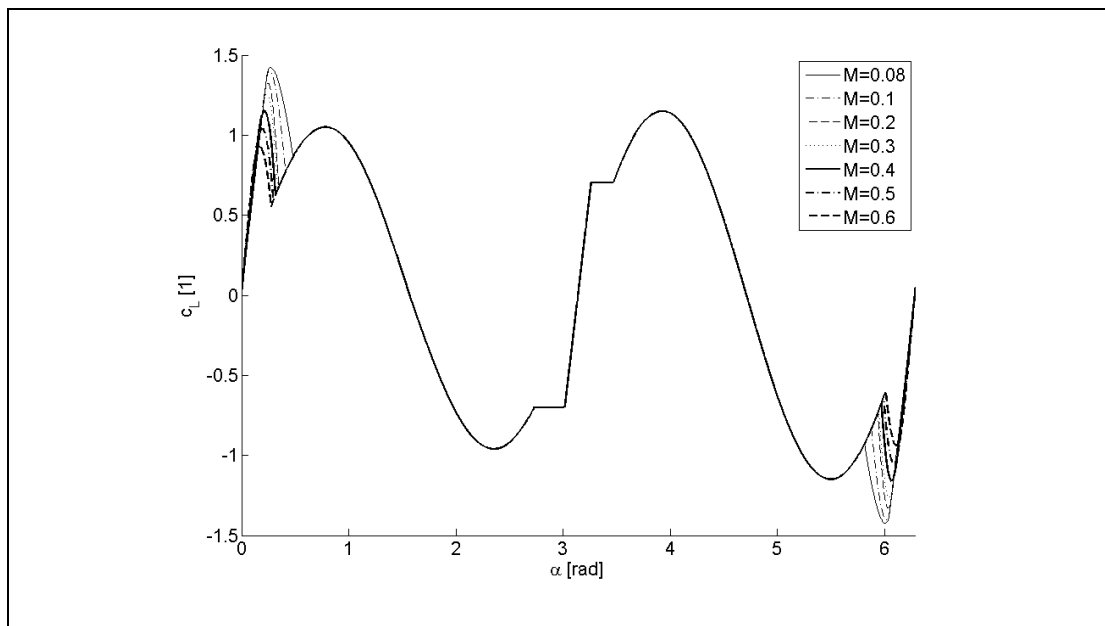
Figure 3   Trends of NACA 0012 lift coefficient obtained for different values of Mach number. Obtained with the aid of approach described in Ref.5
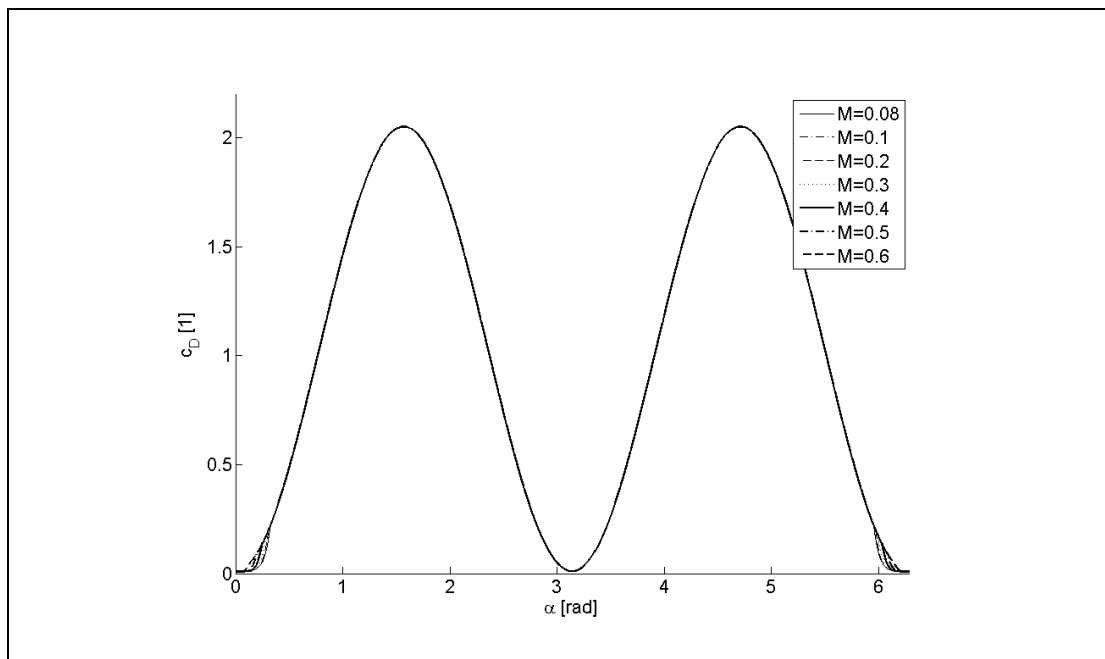
Figure 4   Trends of NACA 0012 drag coefficient obtained for different values of Mach number. Obtained with the aid of approach described in Ref. 5
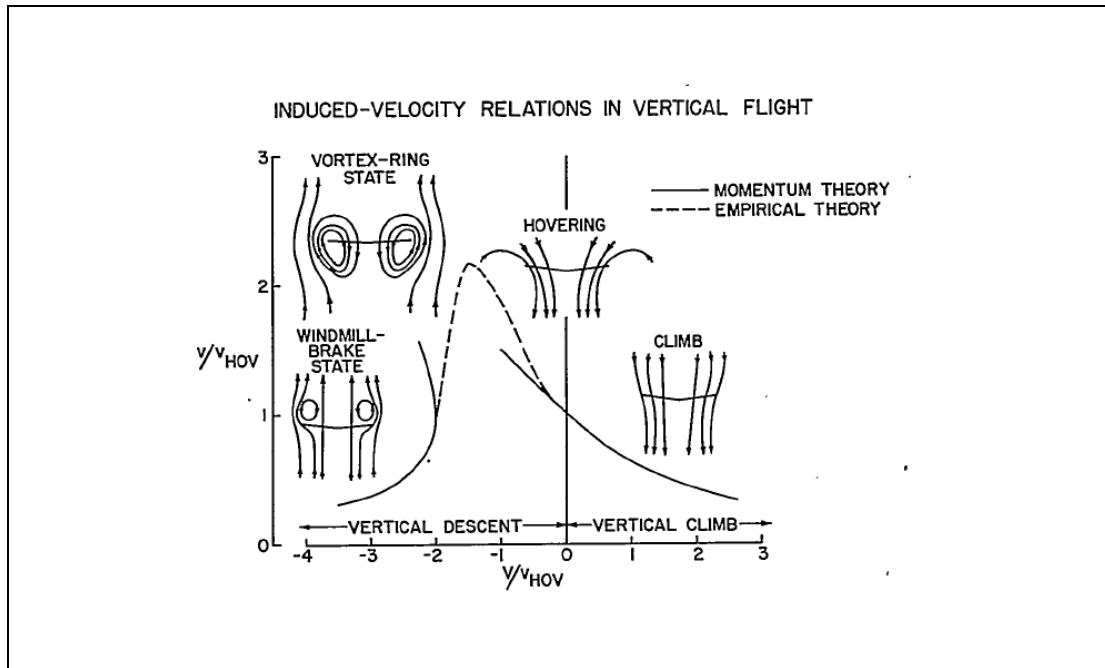
Figure 5   Induced velocity relations in vertical flight (speed of climb on the x-axis, induced velocity on the y-axis). Reproduced from Ref. 23

Figure 6   Internal structure of the rotor blade from Montgomerie-Parsons research Gyroplane. Left section comes from the root of the blade while the right one was located close to the tip of the rotor blade
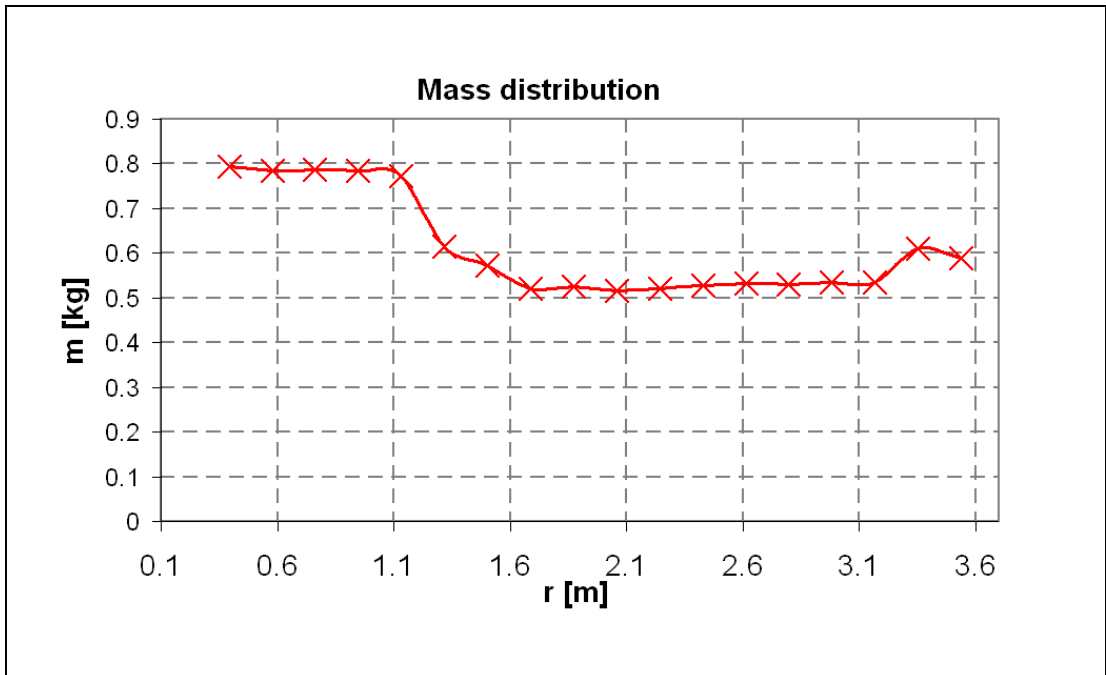
Figure 7   Span-wise mass distribution of the blade. The total weight of one blade was 11.95kg
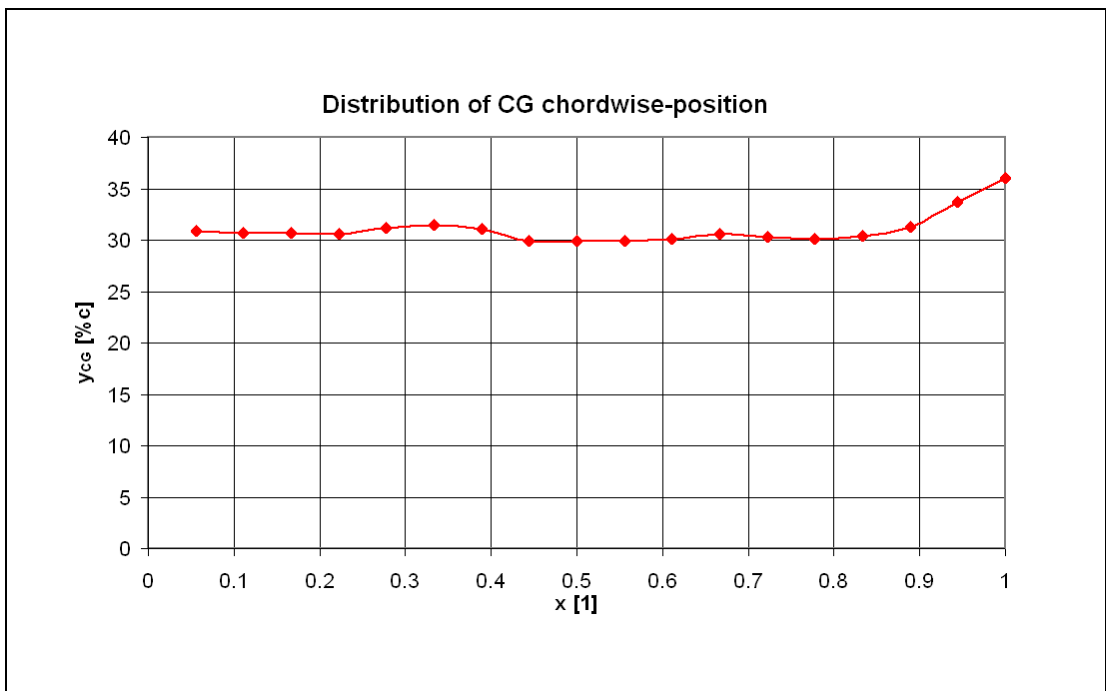
Figure 8   Span-wise distribution of blade c.g.

Figure 9   Arrangement of the experimental measurements of EA position and
torsional stiffness of the blade
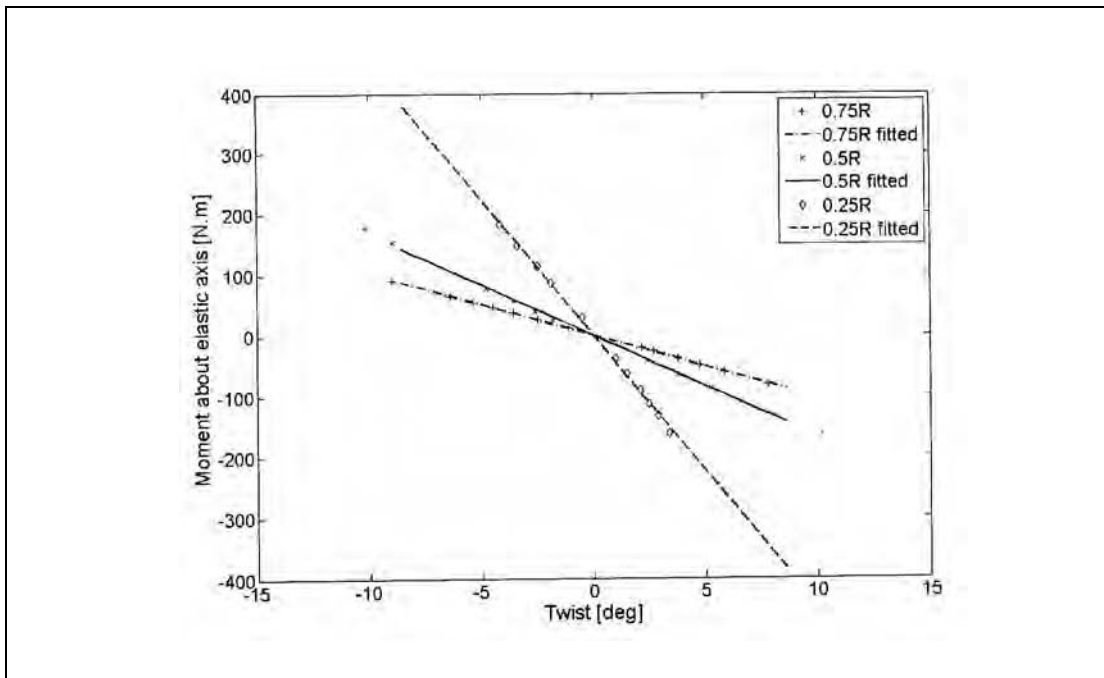
Figure 10   Dependence of blade twist upon torsional loading at three span-wise
stations
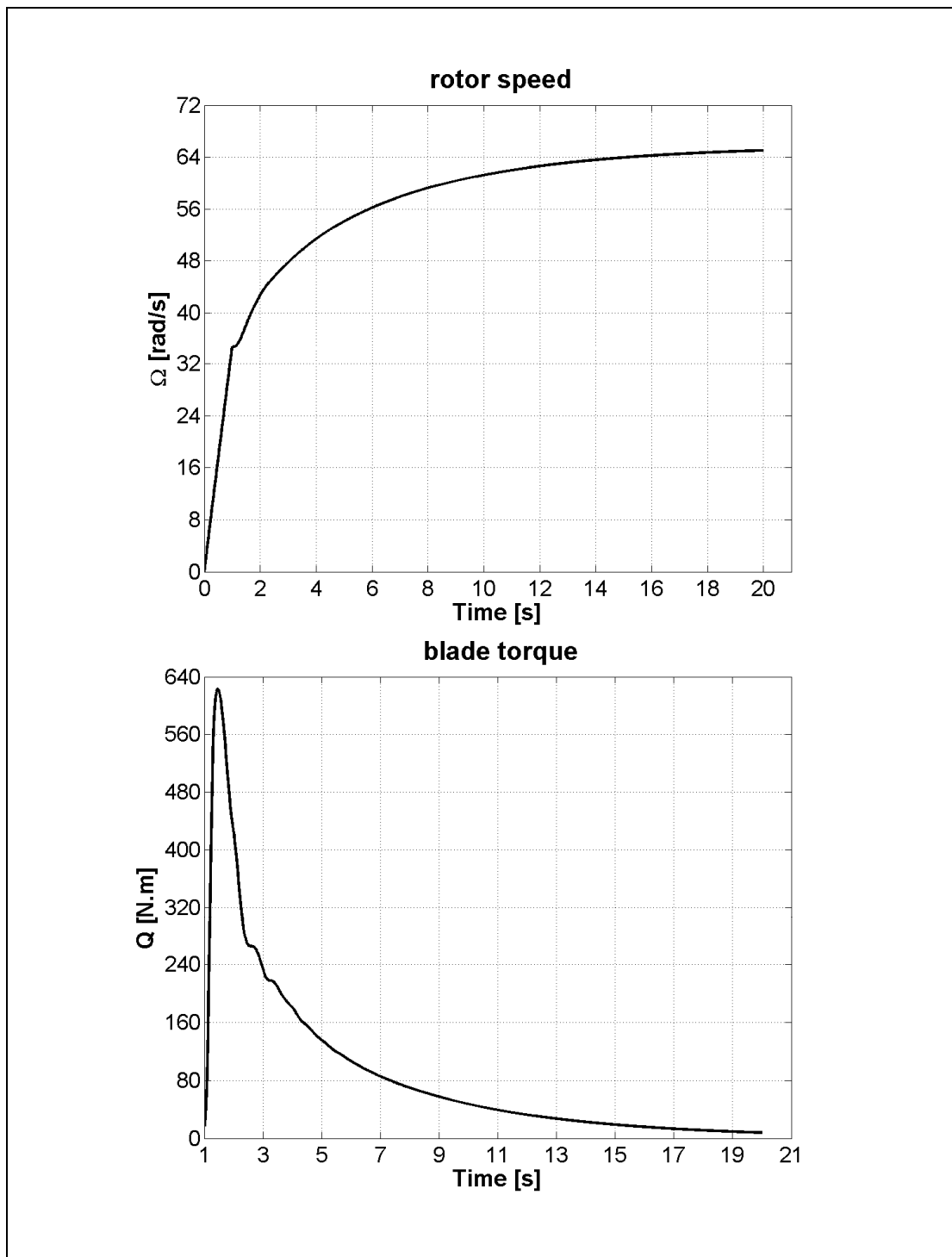
Figure 11 Stabilization of rotor speed and corresponding torque equilibrium during steady axial autorotative flight
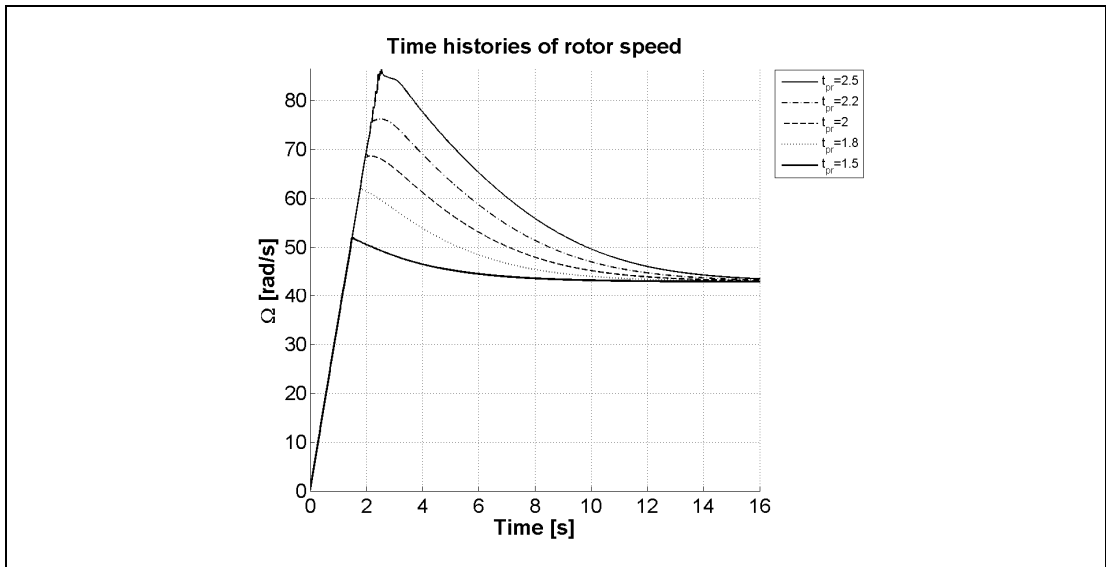
Figure 12 Time behaviour of rotor speed for different lengths of pre-rotation
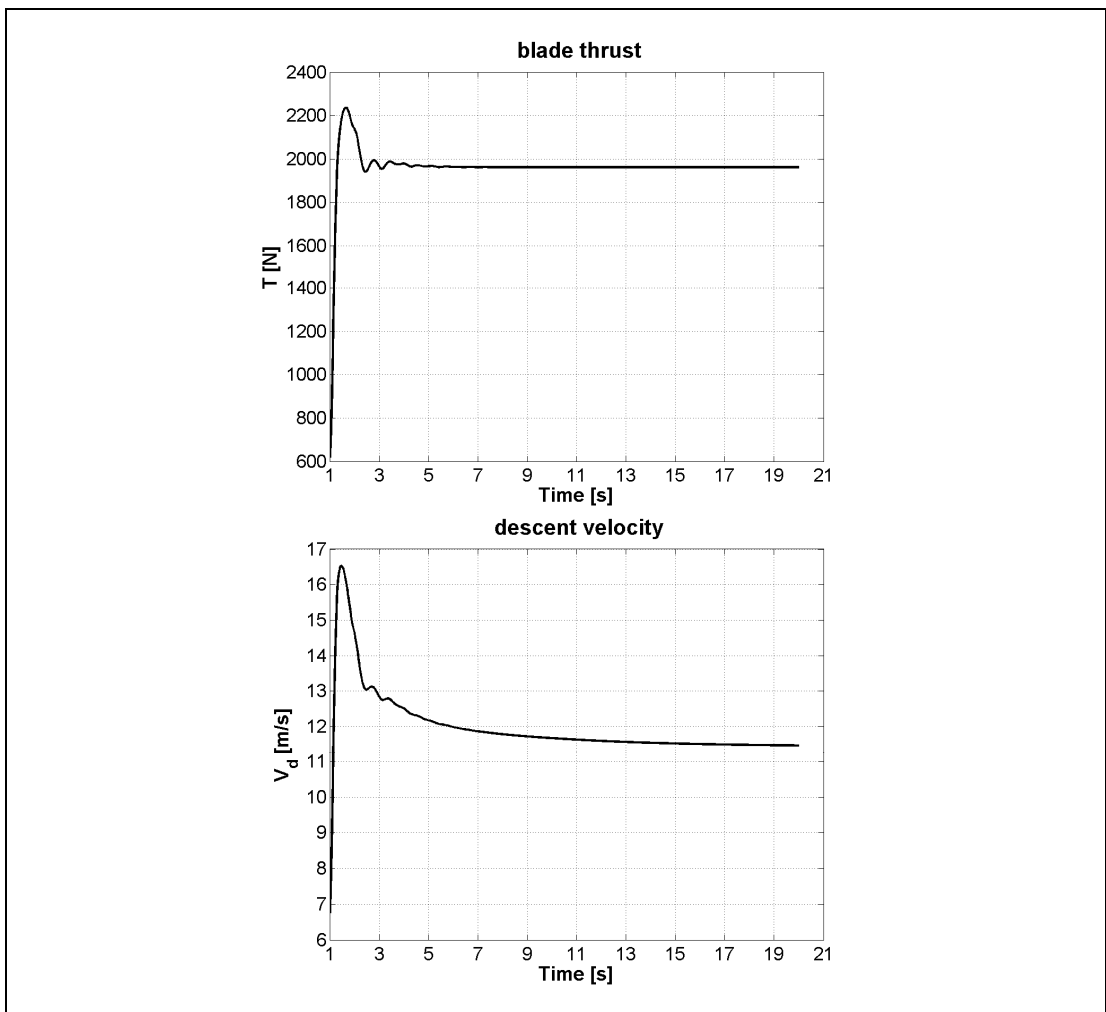
Figure 13 Trends of thrust (for single blade) and speed of descent during steady autorotative descent
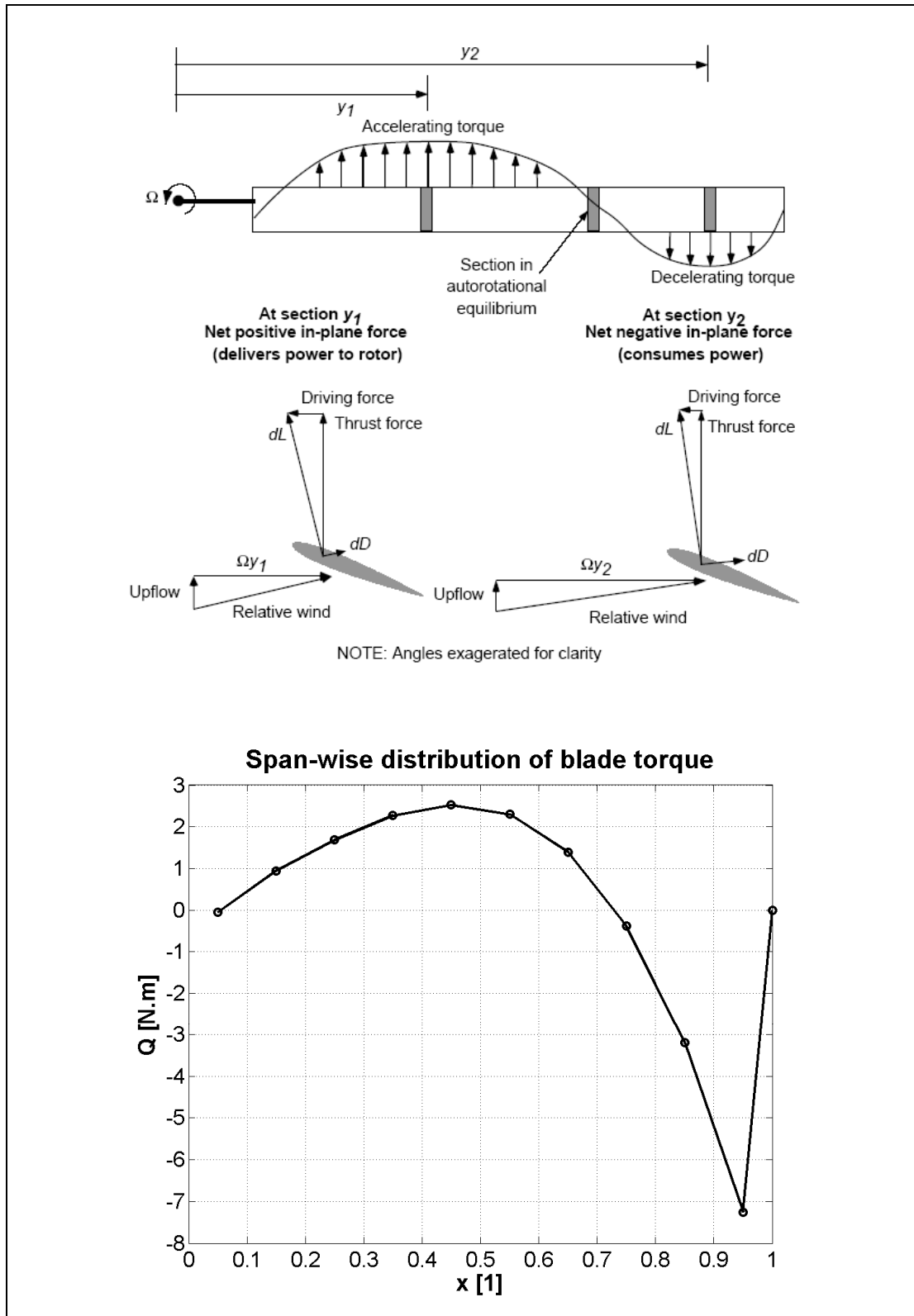
Figure 14   Span-wise distribution of torque during steady autorotation. The right-hand side figure was reproduced from Ref. 14 and Ref. 20
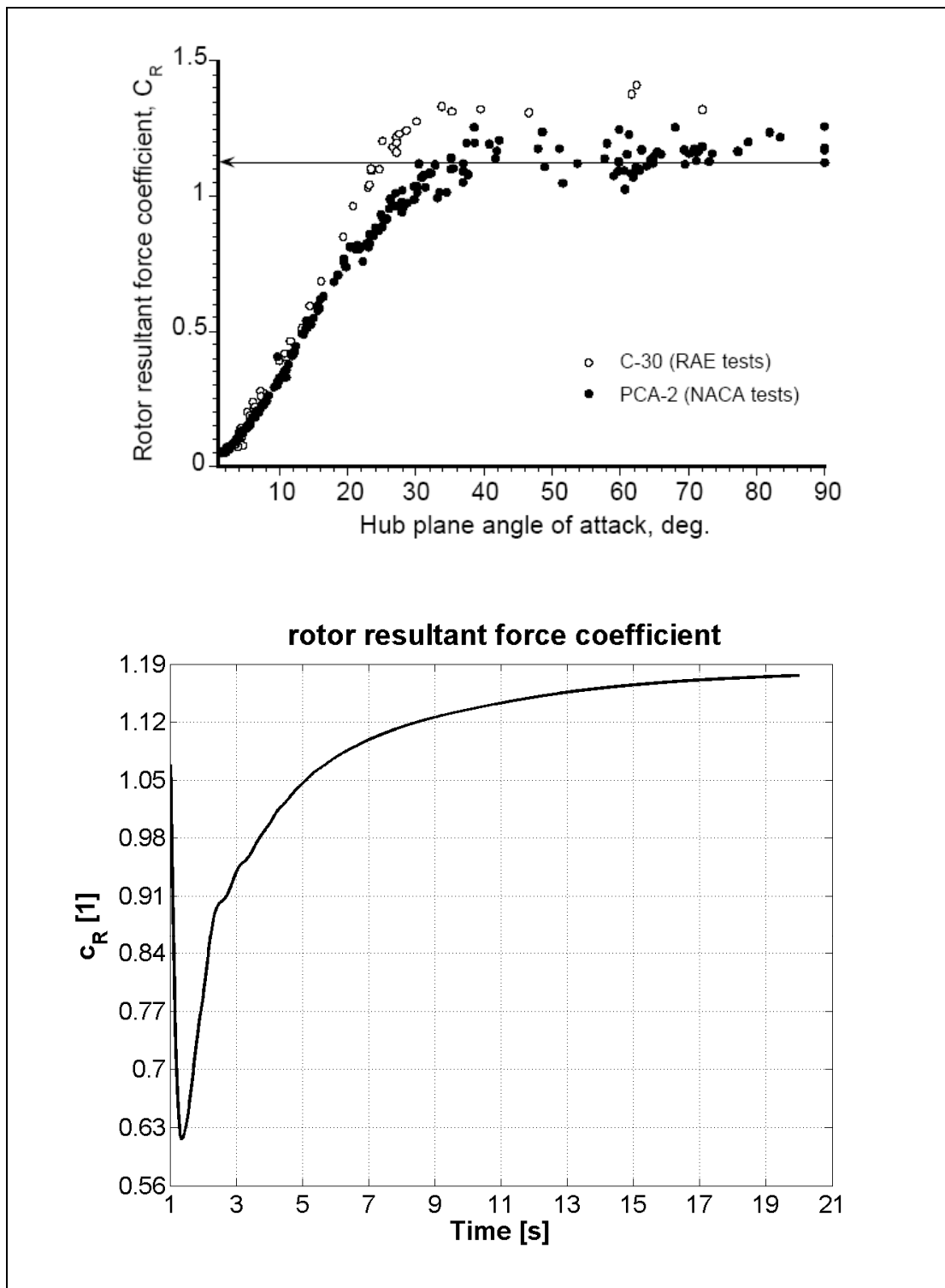
Figure 15 Comparison of values of resultant force coefficient as a function of rotor disc angle of attack obtained by experimental flight measurements (top) and value of c_R predicted by the simulation for axial flight (i.e. $\alpha_D = 90\text{deg}$) and zero blade incidence angle. The figure on the top was reproduced from Ref. 14 and Ref. 20
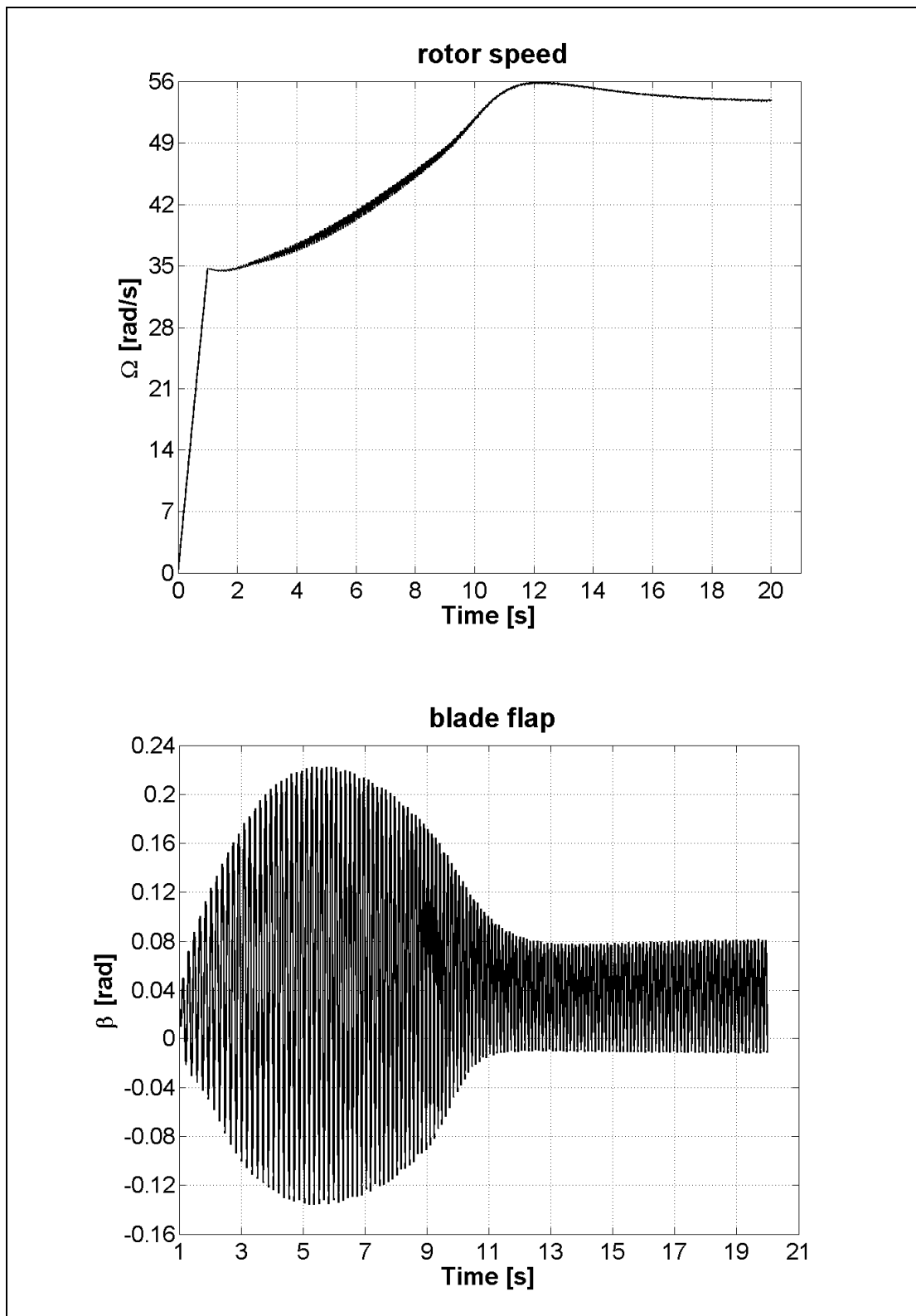
Figure 16   Rotor speed and blade flap angle in stable forward flight
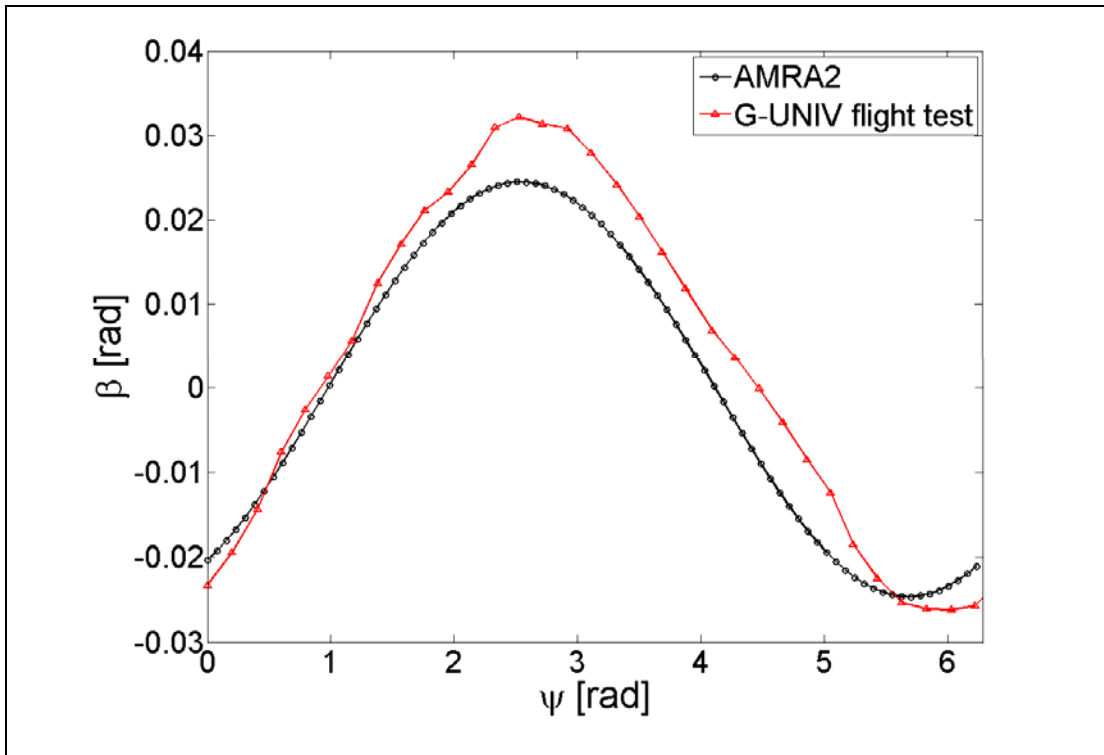
Figure 17   Comparison of predictions of rotor blade teeter and G-UNIV experimental
data
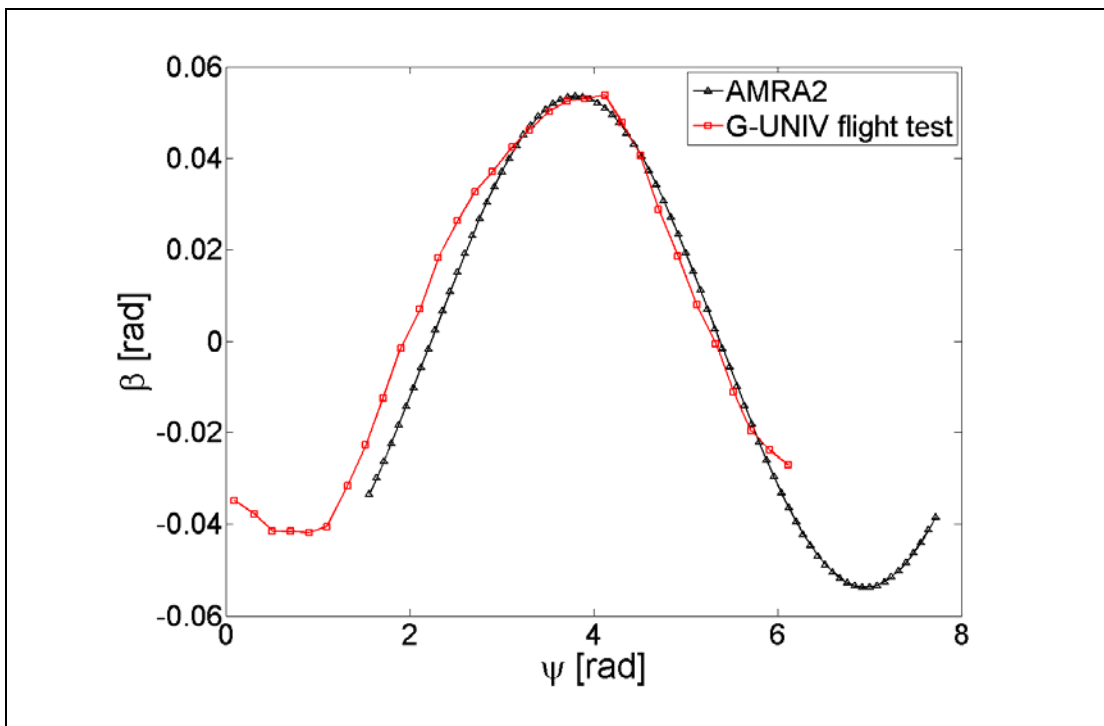
Figure 18   Comparison of predictions of rotor blade teeter and G-UNIV experimental
data
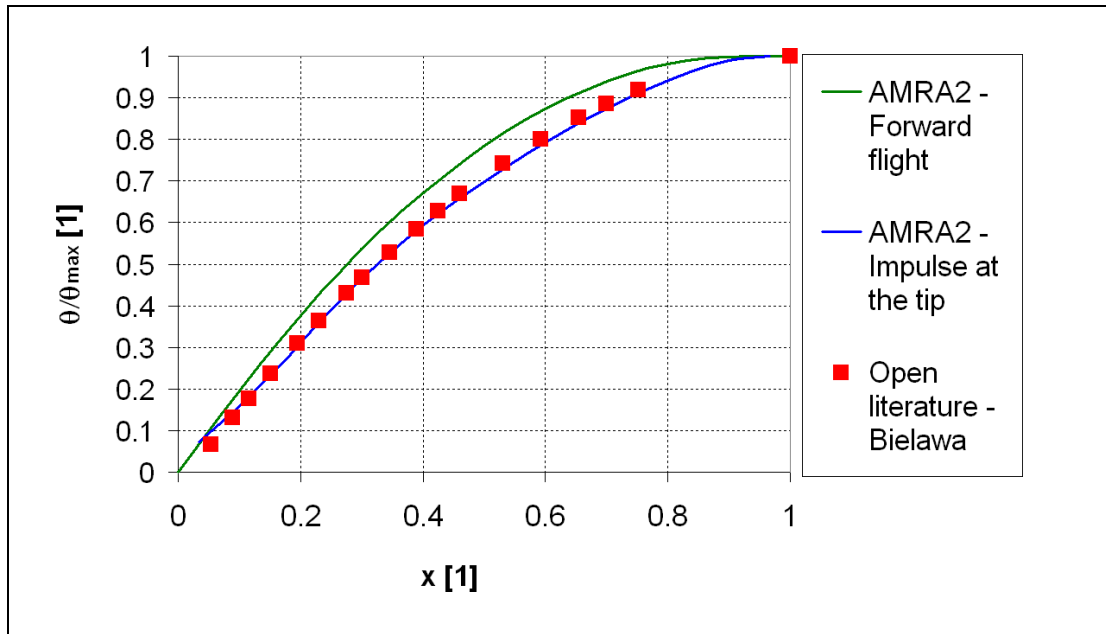
Figure 19   Comparison of the first torsional mode shape computed by the AMRA and published data
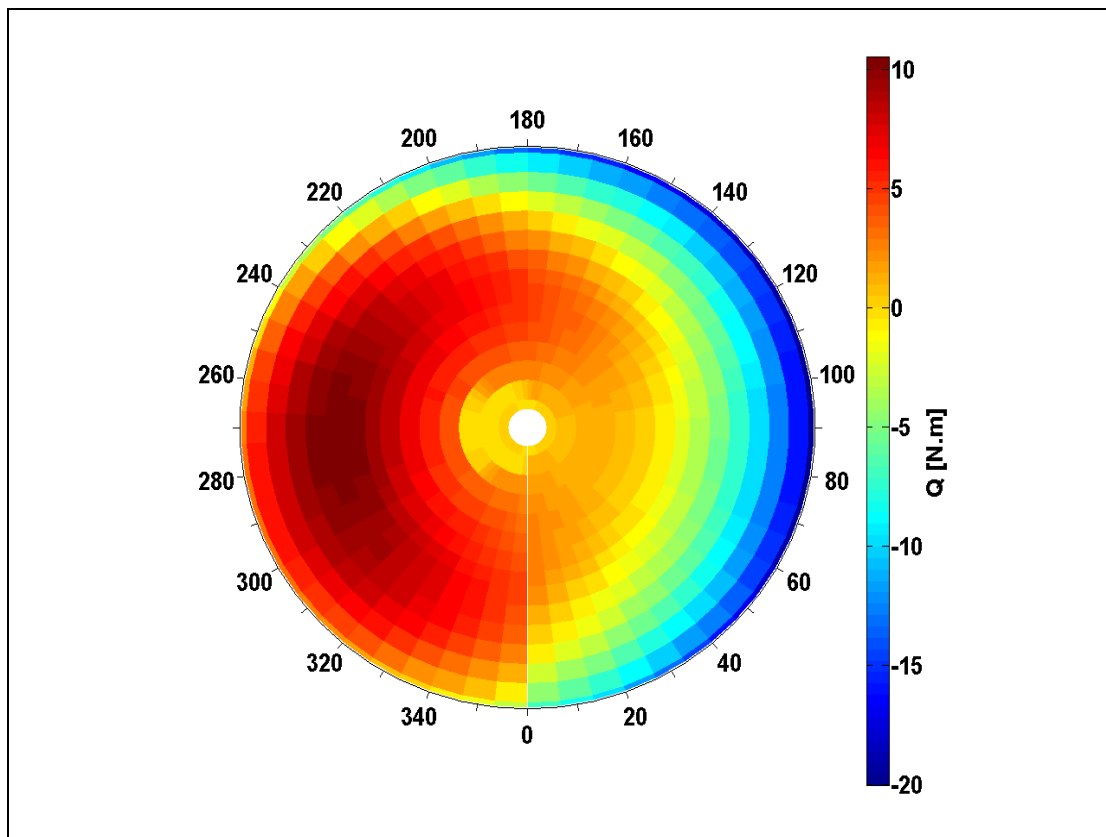
Figure 20   Distribution of blade torque over rotor disk during steady forward flight in autorotation estimated by AMRA
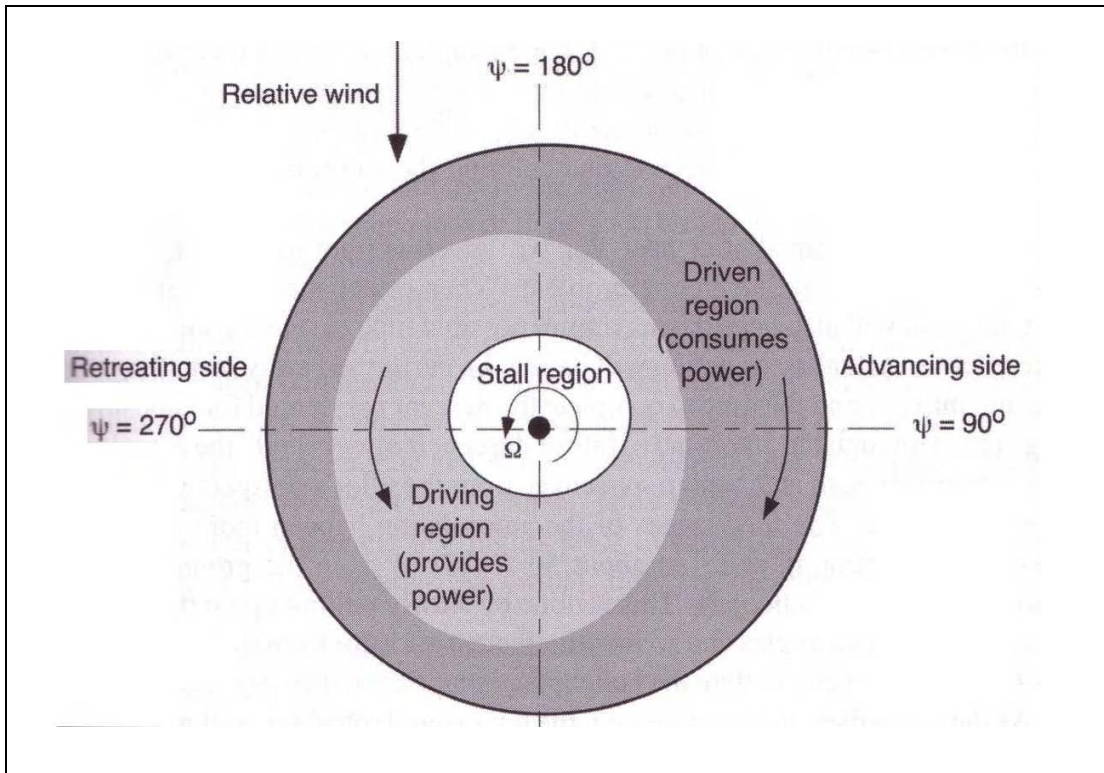
Figure 21   Distribution of blade torque over rotor disk during steady forward flight in
autorotation published by Leishman [Ref. 6, pg 247]
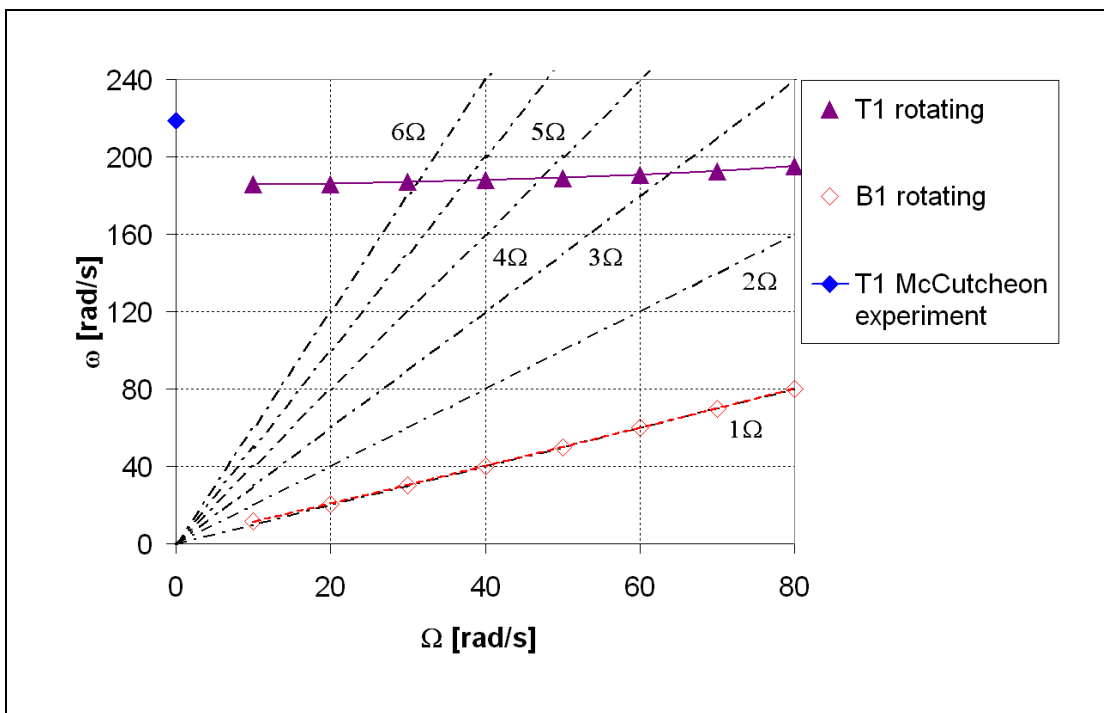
Figure 22   Southwell plot of McCutcheon rotor blade showing correct qualitative
behaviour
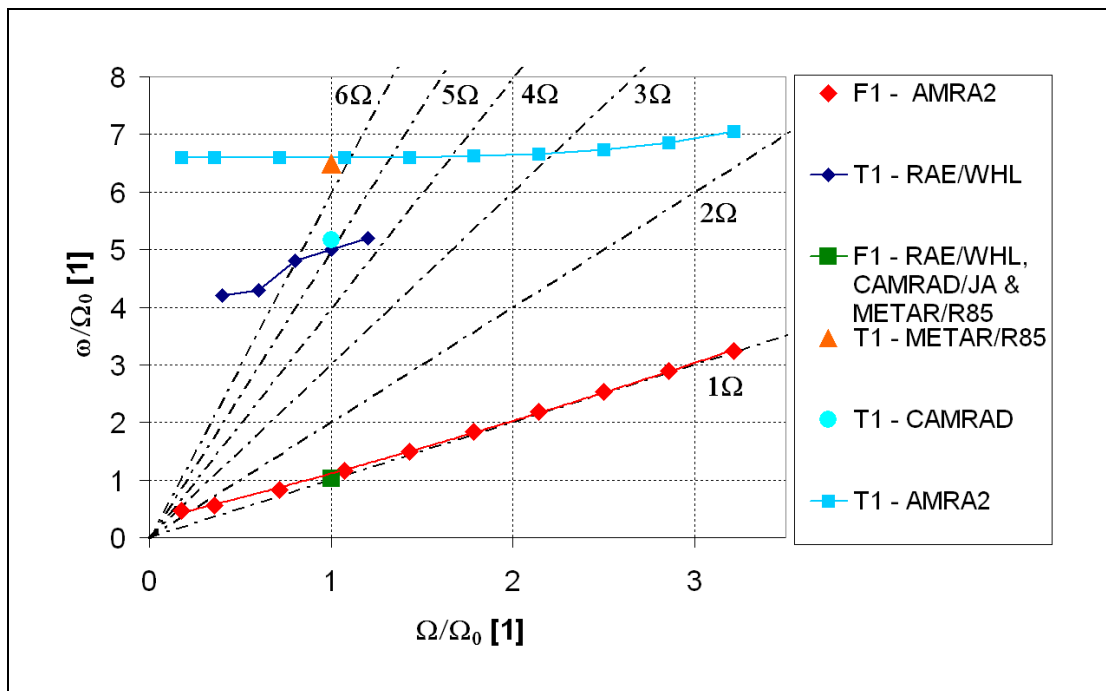
Figure 23 Southwell plot Aérospatiale SA330 Puma helicopter rotor blade showing correct qualitative behaviour. Data in the plot are non-dimensionalised with Ω = 28rad/s
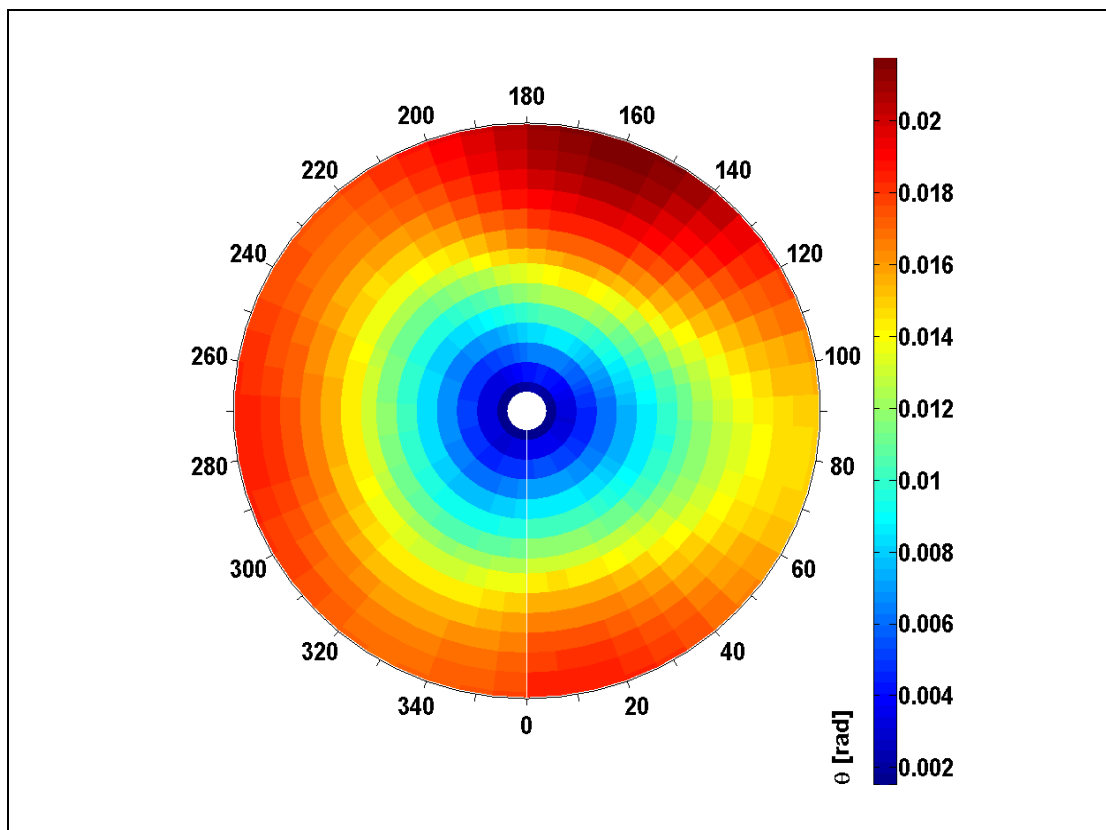
Figure 24 Distribution of blade torsional deflection obtained with the aid of AMRA
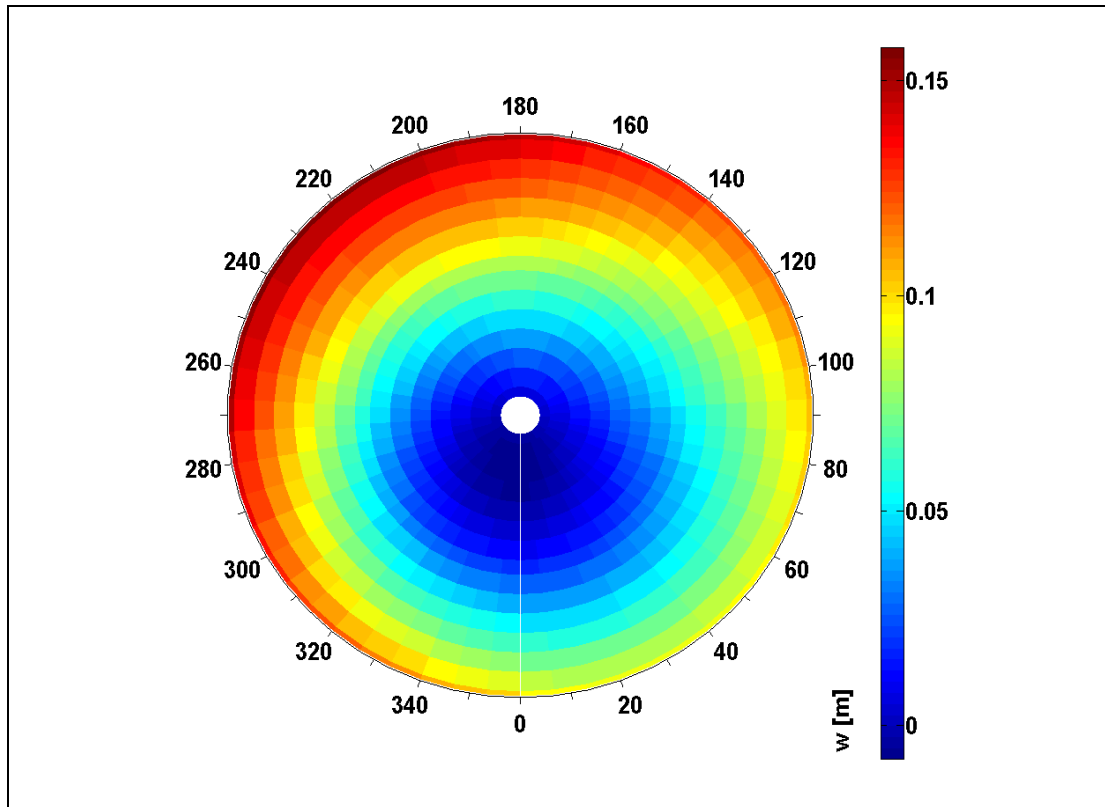
Figure 25   Distribution of blade vertical displacement in bending obtained with the aid of AMRA
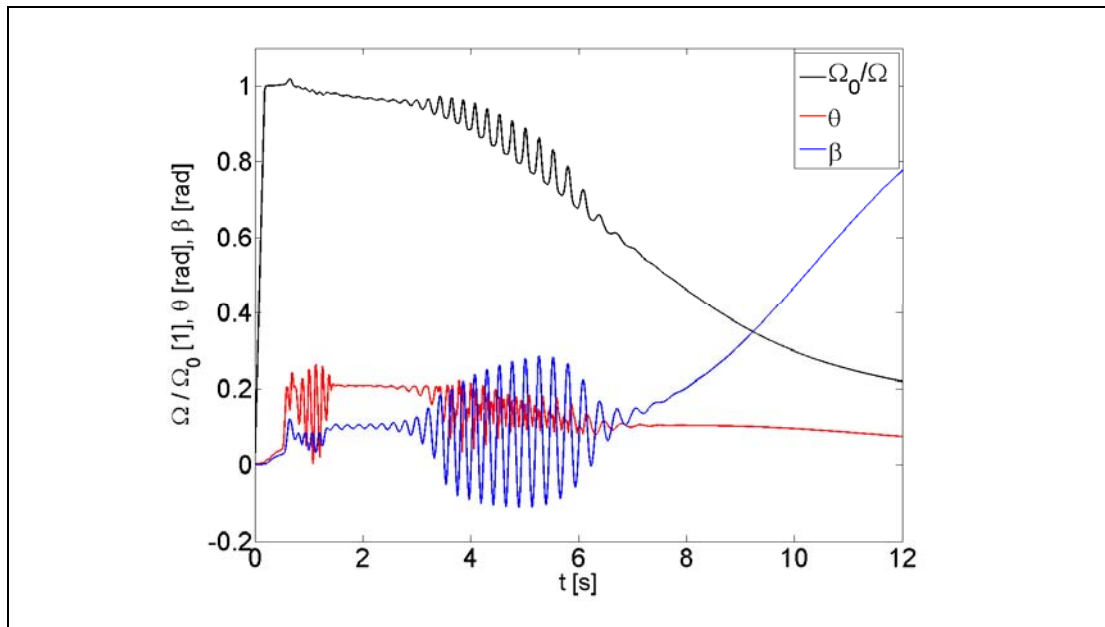
Figure 26   Aeroelastic instability during axial flight in autorotation as predicted by AMRA with simplified model. Data used: blade torsional stiffness of 100N.m^2/rad, elastic axis at 32%, and blade centre of gravity at 40% of blade chord
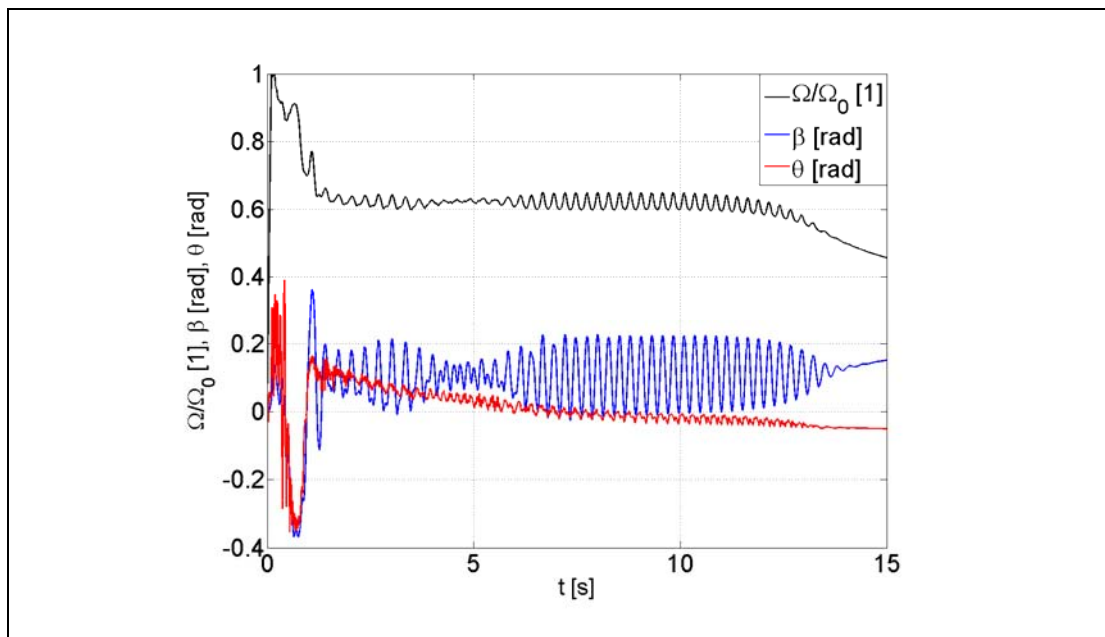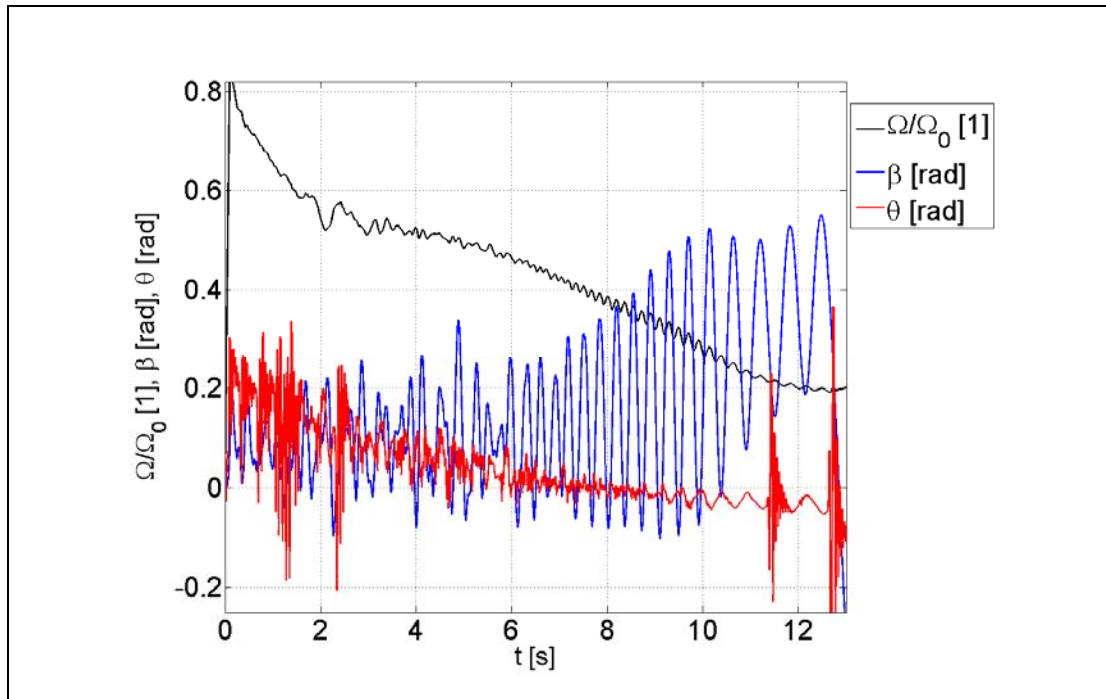
Figure 27 Aeroelastic instability during axial flight in autorotation as predicted by AMRA. Coupled FEM model of blade torsion and bending used. Data used: blade torsional stiffness of 400N.m^2/rad, elastic axis at 32%, and blade centre of gravity at 40% of blade chord
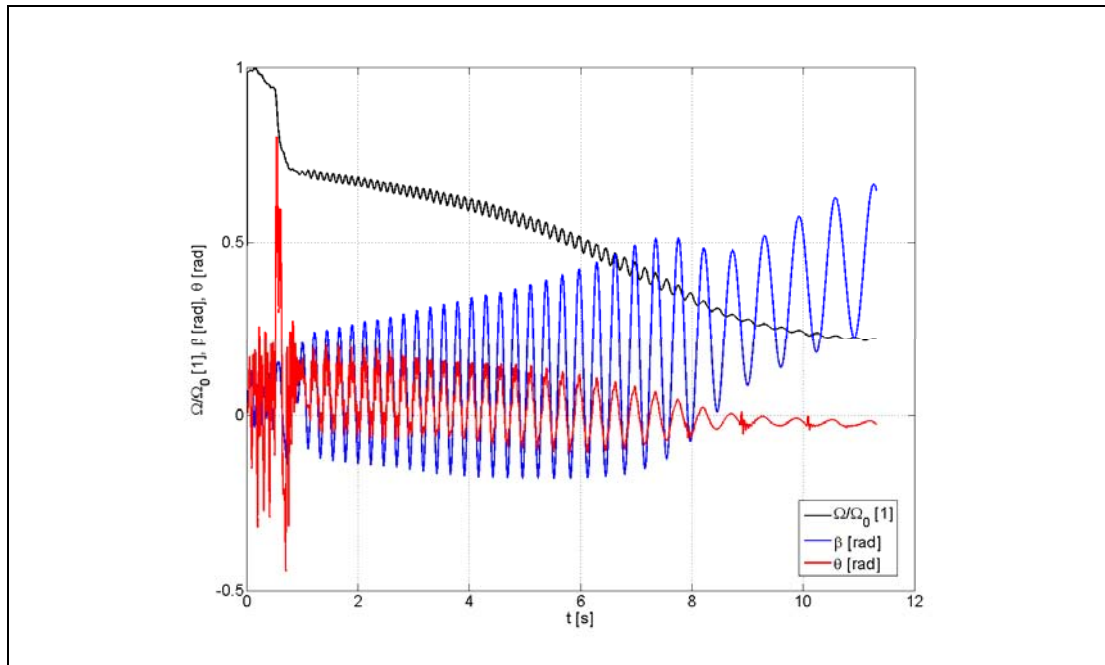
Figure 28 Aeroelastic instability during forward flight in autorotation as predicted by AMRA. Simplified model of blade dynamics (equivalent spring stiffness for modelling both torsion and bending). Data used: blade torsional stiffness of 300N.m^2/rad, elastic axis at 32%, and blade centre of gravity at 40% of blade chord

Figure 29   Aeroelastic instability during forward flight in autorotation as predicted by the AMRA. Coupled FEM model of blade torsion and bending used. Data used: blade torsional stiffness of 600N.m^2/rad, elastic axis at 32%, and blade centre of gravity at 40% of blade chord
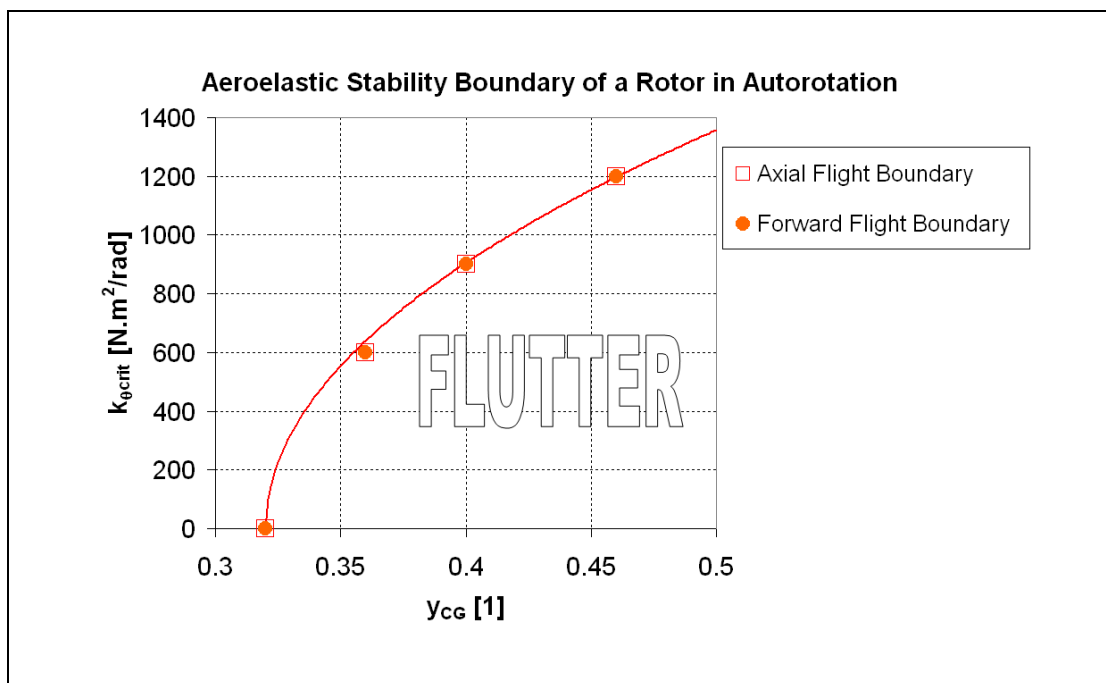

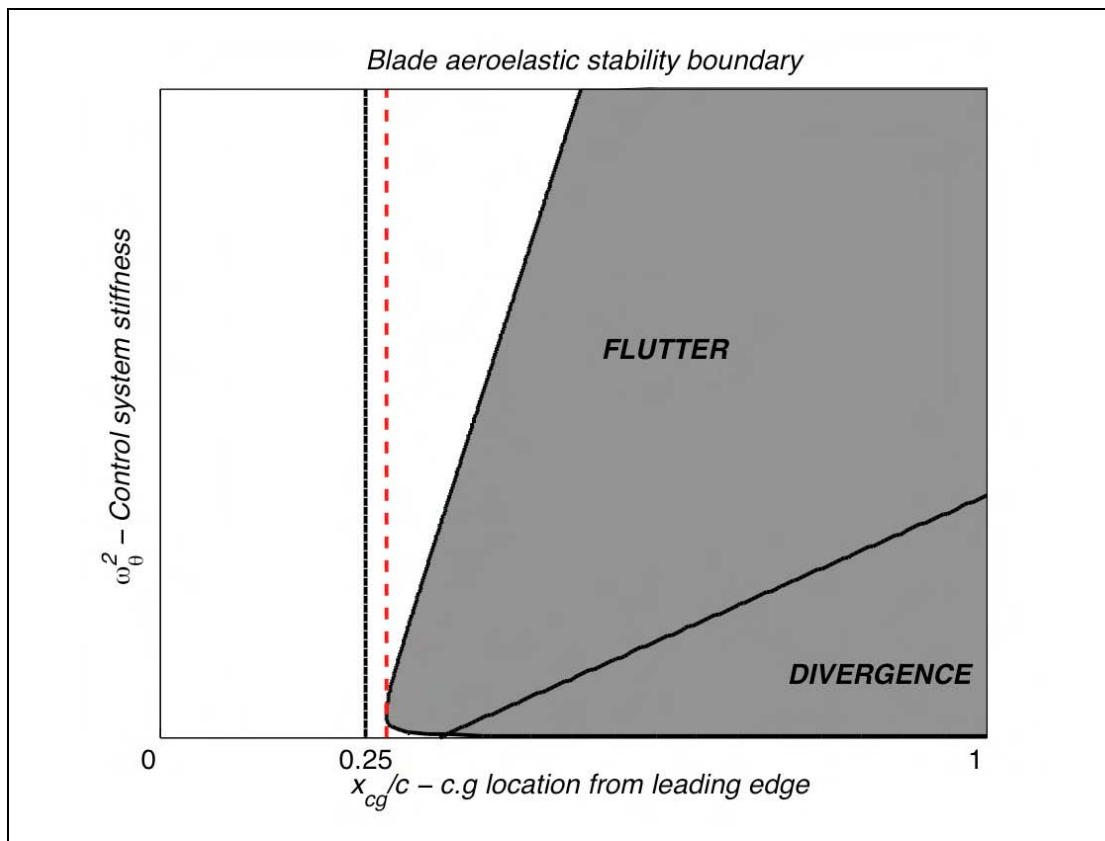
Figure 30   Stability boundary for autorotative flight

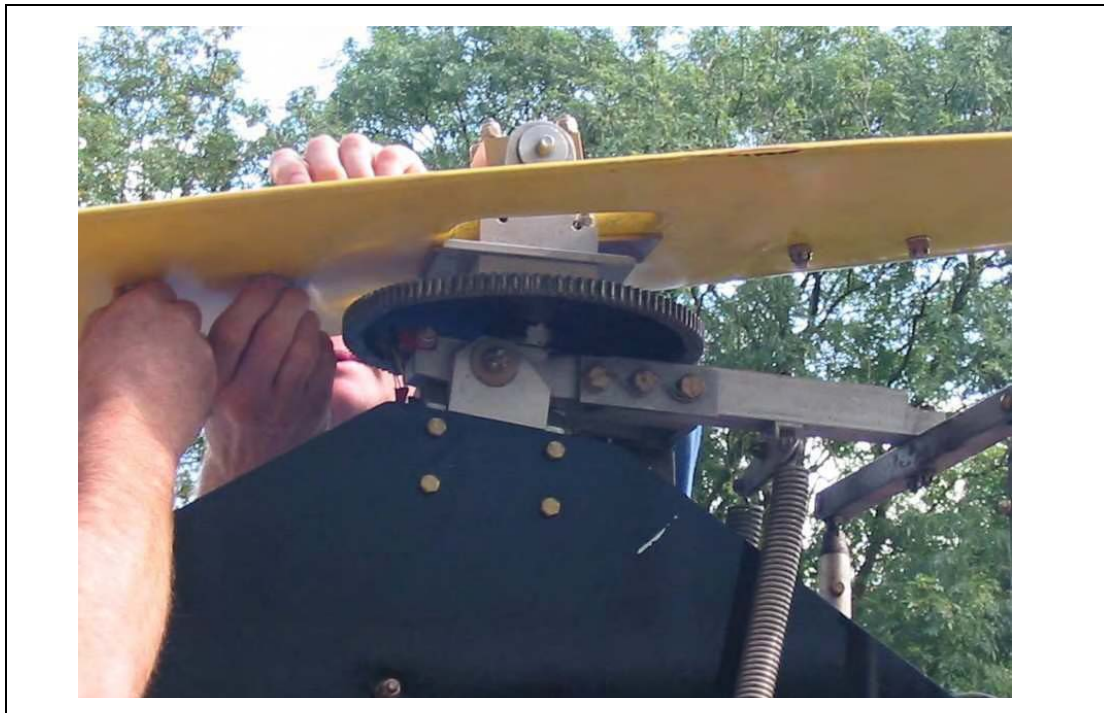**Figure 31**   Flutter Boundary for a Helicopter Rotor Blade
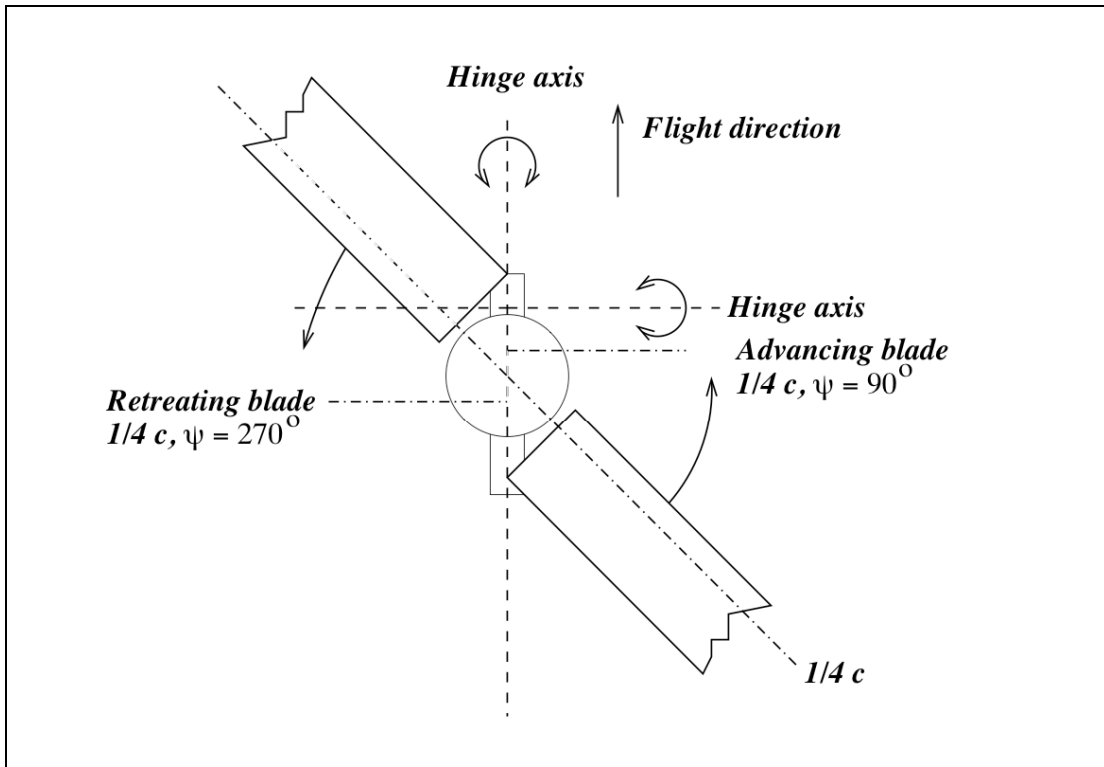

Figure 32a)   Offset Hinge
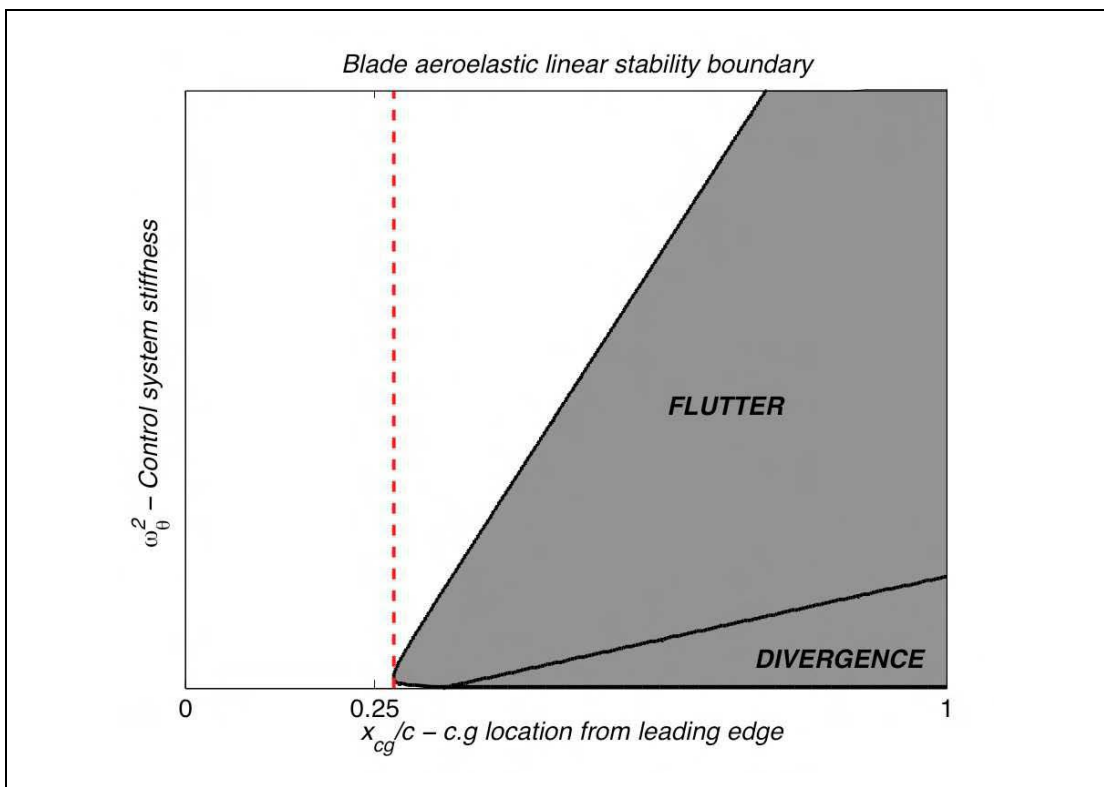
Figure 32b)   Hub offset sketch

Figure 33   Stability boundary for a gyroplane rotor in axial flight
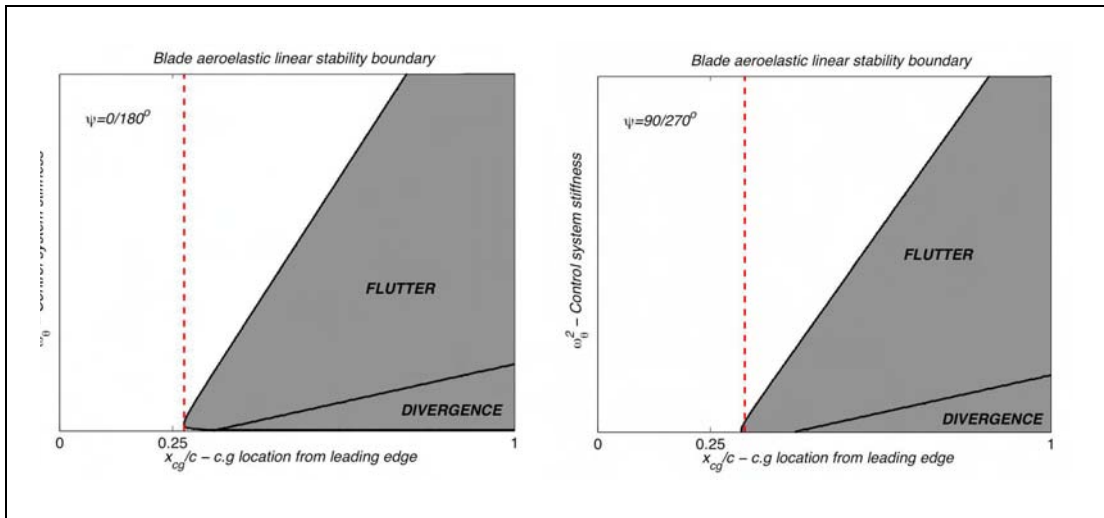
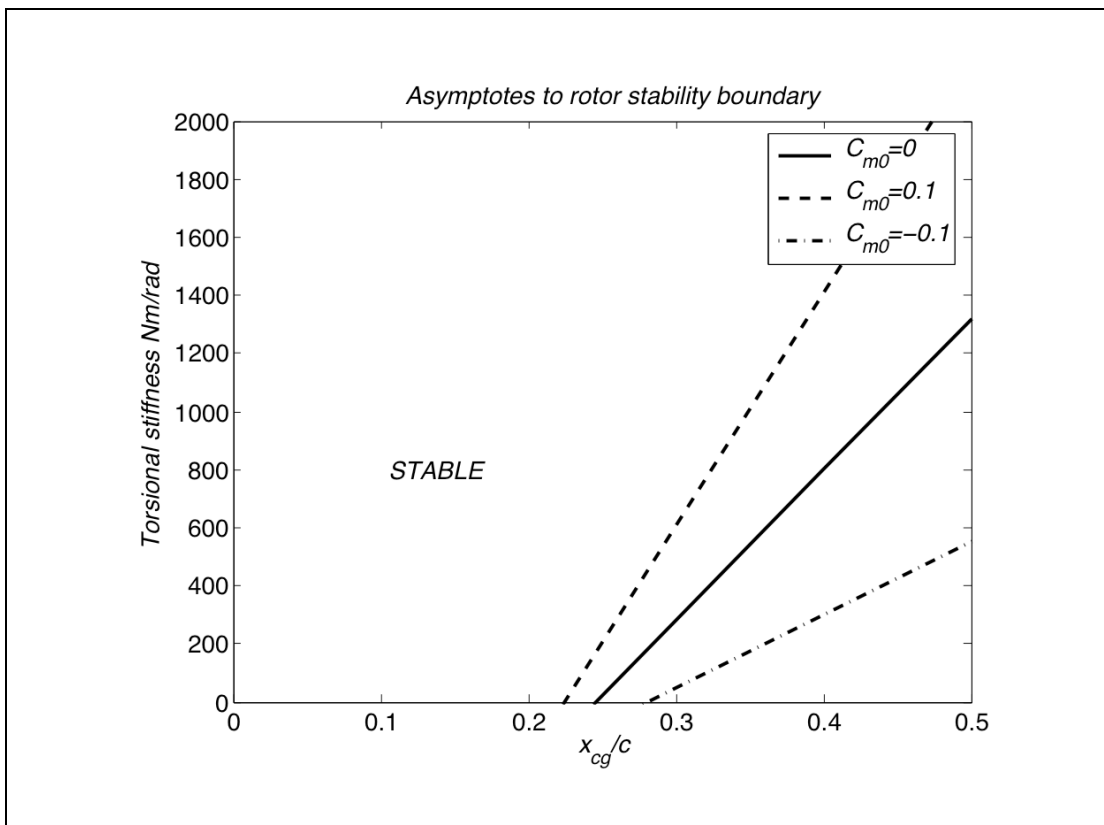**Figure 34** Gyroplane rotor stability boundary at advance ratio 0.2

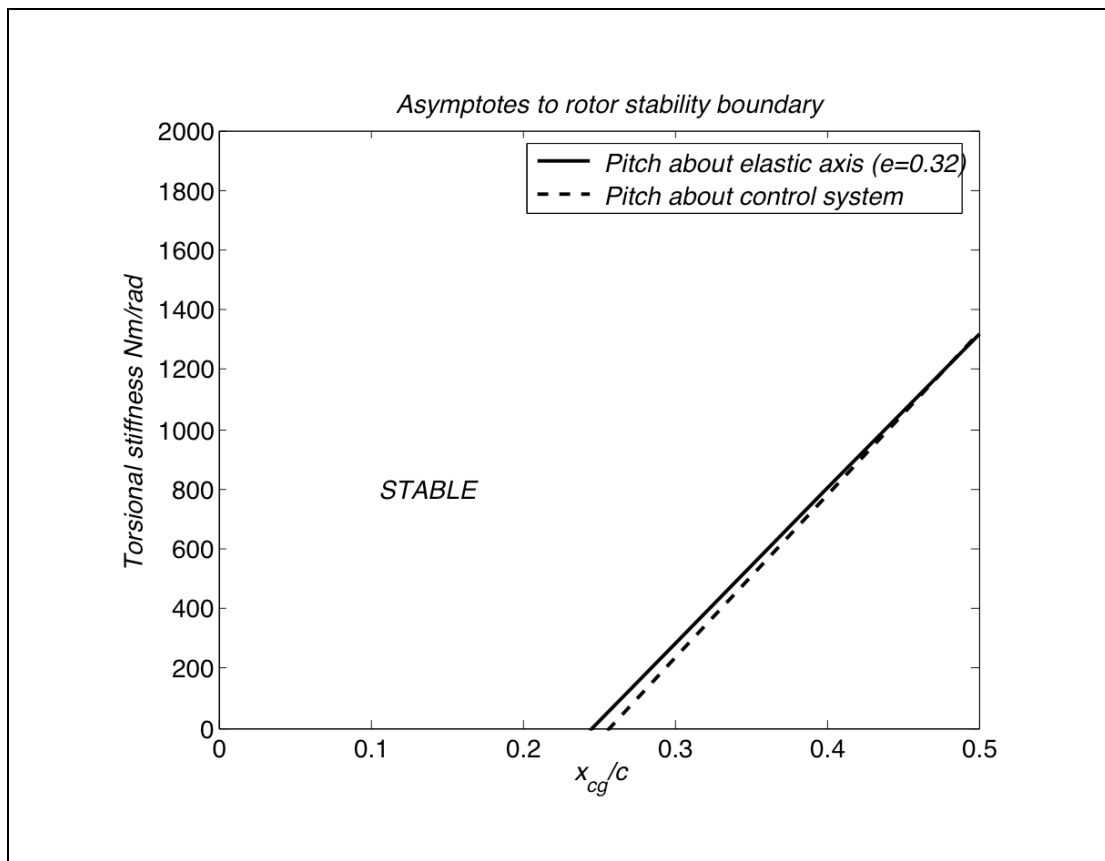**Figure 35** FEM stability boundary

Figure 36 Effect of pitch axis

Appendix 1 - Calculation of Blade Element Velocities

Referring to Figure2, if i is the incidence angle of the rotor disc, the angle between the blade longitudinal axis and the horizontal plane can be expressed as:

$$i_B = \beta - i\cos\psi$$

(A1.1)

therefore, the vertical component of the inflow velocity can be expressed as

$$U_P = V_d\cos(\beta - i\cos\psi) + V_h\sin(\beta - i\cos\psi)\cos\psi - v_i\cos\beta - \dot{\beta}r - \dot{\theta}\left(\frac{3c}{4} - y_{EA}\right)\cos\theta$$

(A1.2)

The horizontal component of inflow velocity is given by the following equation.

$$U_T = (V_h\cos i - V_d\sin i)\sin\psi + \Omega r\cos\beta - \dot{\theta}\left(\frac{3c}{4} - y_{EA}\right)\sin\theta$$

(A1.3)

Component of inflow velocity that is tangential to the rotor disc and parallel with blade axis is usually neglected, especially if axial flight is considered. It is given below.

$$U_r = V_h\cos(\beta - i\cos\psi)\cos\psi + V_d\sin(\beta - i\cos\psi) - v_i\sin\beta$$

(A1.4)

The above equations describe inflow velocity components for general flight conditions and they were used in AMRA model of a gyroplane rotor. However, the equations can be modified and simplifying assumptions can be made when describing axial flight or high speed forward flight. In axial flight, horizontal speed is negligible and $\alpha_D = \gamma = \frac{\pi}{2}$ rad. Thus, $i = \alpha_D - \gamma = 0$ and:

$$U_P = V_d\cos\beta - v_i\cos\beta - \dot{\beta}r - \dot{\theta}\left(\frac{3c}{4} - y_{EA}\right)\cos\theta$$

$$U_T = \Omega r\cos\beta - \dot{\theta}\left(\frac{3c}{4} - y_{EA}\right)\sin\theta$$

$$U_r = V_d\sin\beta - v_i\sin\beta$$

(A1.5)

If both flapping angle and pitch angle of the blade are small, equations (A1.5) can be rewritten.

$$U_P = -v_i + V_d - \dot{\beta}r - \dot{\theta}\left(\frac{3c}{4} - y_{EA}\right)$$

$$U_T = \Omega r - \dot{\theta}\theta\left(\frac{3c}{4} - y_{EA}\right)$$

$$U_r = V_d\beta - v_i\beta$$

(A1.6)

Components of inflow velocity can be expressed in different if following substitutions are made[13]

$$x = \frac{r}{R} \quad \lambda = \frac{V_d - v_i}{\Omega R} \quad y = \frac{1}{R}\left(\frac{3}{4}c - y_{EA}\right)$$

$$\frac{V}{\Omega R}\cos\alpha_D = \mu \Rightarrow \mu\Omega R = V\cos\alpha_D$$

(A1.7)

Hence, equations (A1.7) can be written in different form

$$U_P = \Omega R\left(\lambda - \frac{\dot{\beta}}{\Omega}x - \frac{\dot{\theta}}{\Omega}y\right)$$

$$U_T = \Omega R\left(x - y\frac{\dot{\theta}}{\Omega}\theta\right)$$

$$U_r = \Omega R\lambda\beta$$

(A1.8)

The above equations can be further modified with the aid of the equation below

$$\frac{1}{\Omega}\frac{d}{dt} = \frac{dt}{d\psi}\frac{d}{dt} = \frac{d}{d\psi}$$

(A1.9)

Using the above transformation, we get

$$U_P = \Omega R \left(\lambda - \frac{d\beta}{d\psi} x - \theta \frac{d\theta}{d\psi} y \right)$$

$$U_T = \Omega R \left(x - y \frac{d\theta}{d\psi} \theta \right)$$

$$U_r = \Omega R \lambda \beta$$

(A1.10)

In case of high speed forward flight, rotor disc incidence (i) is very small and hence the assumption can be made that $\alpha_D \approx Y$. Therefore, equations, (A1.2 - 1.4) can be rewritten in the following manner:

$$U_P = V_d \cos \beta + V_h \sin \beta \cos \psi - v_i \cos \beta - \dot{\beta} r - \dot{\theta} \left(\frac{3c}{4} - y_{EA} \right) \cos \theta$$

$$U_T = V_h \sin \psi + \Omega r \cos \beta - \dot{\theta} \left(\frac{3c}{4} - y_{EA} \right) \sin \theta$$

$$U_r = V_d \beta + V_h \cos \beta \cos \psi - v_i \sin \beta$$

(A1.11)

Since rotor disc incidence is negligible, horizontal and vertical components of free-stream velocity are $V_h = V \cos \alpha_D$ and $V_d = V \sin \alpha_D$. Further simplifications in the above equations can be made with the aid of the assumption that flapping angle (β) and blade twist (θ) are small.

$$U_P = V_d - v_i - \dot{\beta} r - \dot{\theta} \left(\frac{3c}{4} - y_{EA} \right) \cos \theta + V \beta \cos \alpha_D \cos \psi$$

$$U_T = \Omega r - \dot{\theta} \left(\frac{3c}{4} - y_{EA} \right) \theta + V \cos \alpha_D \sin \psi$$

$$U_r = V_d \beta + V_h \cos \psi - v_i \beta$$

(A1.12)

Ignoring negligible terms, it follows from (A1.7), that:

$$U_P = \Omega R \left(\lambda - \frac{x}{\Omega} \dot{\beta} - \frac{y}{\Omega} \dot{\theta} + \mu \beta \cos \psi \right)$$

$$U_T = \Omega r (x + \mu \sin \psi)$$

$$U_r = \Omega R (\lambda \beta + \mu \cos \psi)$$

(A1.13)

Finally, transformation shown in (A1.9) yields in the equations below.

$$U_P = \Omega R \left(\lambda - x \frac{d\beta}{d\psi} - y \frac{d\theta}{d\psi} + \mu \beta \cos \psi \right)$$

$$U_T = \Omega r (x + \mu \sin \psi)$$

$$U_r = \Omega R (\lambda \beta + \mu \cos \psi)$$

(A1.14)

Appendix 2 - Blade Equations of Motion Using a Lagrangian Approach

The rotor blades are modelled as perfectly rigid beam, which means that both flap and twist of the blade are constant along the blade span. The blade has three degrees of freedom - in flap, torsion and rotor speed. Lagrangian equations of motion were used for the dynamic model of the blade. The system of equations consists of three differential equations that describe dynamic behaviour of the blade in pitch (twist), flap and rotation. General arrangement of blade equation motion is shown below.

$$\frac{d}{dt}\left(\frac{\partial T}{\partial \dot{\beta}}\right) - \frac{\partial T}{\partial \beta} + \frac{\partial V}{\partial \beta} = M_\beta$$

$$\frac{d}{dt}\left(\frac{\partial T}{\partial \Omega}\right) - \frac{\partial T}{\partial \psi} + \frac{\partial V}{\partial \psi} = M_\psi$$

$$\frac{d}{dt}\left(\frac{\partial T}{\partial \dot{\theta}}\right) - \frac{\partial T}{\partial \theta} + \frac{\partial V}{\partial \theta} = M_\theta$$

(A2.1)

In the above equations, T is blade kinetic energy and V is potential energy of the blade and M_β, M_ψ and M_θ are forcing moments. The potential energy of the blade consists of a component due to flexibility of the blade (V_F) and a component due to mass of the blade (V_M). Span-wise mass distribution of the blade was assumed to be homogenous during derivation of the equations of motion. Hence, T and V of a gyroplane rotor having weight m, length b, flexural stiffness k_β, torsional stiffness k_θ and offset of elastic axis from centre of gravity y_g are as follows:

$$T = \frac{m}{2b}\int_0^b \dot{\underline{r}}.\dot{\underline{r}}\, dr$$

$$V = V_F + V_H$$

$$V_F = \frac{1}{2}k_\beta \beta^2 + \frac{1}{2}k_\theta \theta^2 \quad V_H = \frac{mg}{R}\int_0^R y_g(1+\sin\theta)dr + \frac{mg}{R}\int_0^R r(1+\sin\beta)dr$$

(A2.2)

After integration, equations describing kinetic and potential energy of the blade give

$$T = \frac{1}{6}mb^2\dot{\beta}^2 + \frac{1}{2}my_g^2\dot{\theta}^2 - \frac{1}{2}mby_g\dot{\beta}\dot{\theta}\cos\theta + \frac{1}{2}my_g^2\dot{\beta}^2\sin^2\theta - my_g^2\Omega\dot{\beta}\sin\theta\cos\theta\cos\beta$$

$$- my_g^2\Omega\dot{\theta}\sin\beta + \frac{1}{2}mby_g\dot{\beta}\Omega\sin\beta\cos\theta + \frac{1}{2}my_g^2\Omega^2(\cos^2\theta + \sin^2\beta\sin^2\theta)$$

$$- \frac{1}{2}mby_g\Omega\dot{\theta}\sin\theta\cos\beta + \frac{1}{6}mb^2\Omega^2\cos^2\beta + \frac{1}{2}mby_g\Omega^2\sin\theta\sin\beta\cos\beta$$

(A2.3)

$$V = \frac{1}{2}\left(k_\beta \beta^2 + k_\theta \theta^2\right) + mg\left(\frac{R}{2}\left(1 + \sin\beta\right) + y_g\left(1 + \sin\theta\right)\right)$$

<div align="right">(A2.4)</div>

Both blade kinetic energy and the final form of Lagrange's equations of motion were verified with the aid of MAPLE$^{\circledR}$ and MATLAB$^{\circledR}$ software packages. Forcing moments of the blades are computed from the output of the aerodynamic model of the blade. Each blade is divided into ten span-wise elements and aerodynamic forces and physical properties of the blade are defined in the middle of each element (see Fig.A2.1). Thrust, in-plane force, torque and pitching moment of the j-th span-wise blade element can be calculated using equations below. Boundaries of the element of the blade are defined by dimensionless span-wise coordinates x_{j-1} and x_j. Variable y_c is the offset of aerodynamic centre of the blade element from its centre of gravity and R is blade length (i.e. radius of the rotor).

$$dT_j = dL_j \cos\phi + dD_j \sin\phi$$

$$dH_j = dL_j \sin\phi - dD_j \cos\phi$$

$$dQ_j = R\left(\frac{x_j + x_{j-1}}{2}\right)dH_j$$

$$dM_j = \left(\frac{y_{c_j} + y_{c_{j-1}}}{2}\right)\left(dL_j \cos\alpha + dD_j \sin\alpha\right) - dM_{c/4,j}$$

<div align="right">(A2.5)</div>

Using the variables defined in the previous equation, forcing moments in system of equations (A2.1) are

$$M_\beta = R\sum_{j=1}^{n}\left(\frac{x_j + x_{j-1}}{2}\right)dT_j$$

$$M_\psi = \sum_{j=1}^{n} dQ_j$$

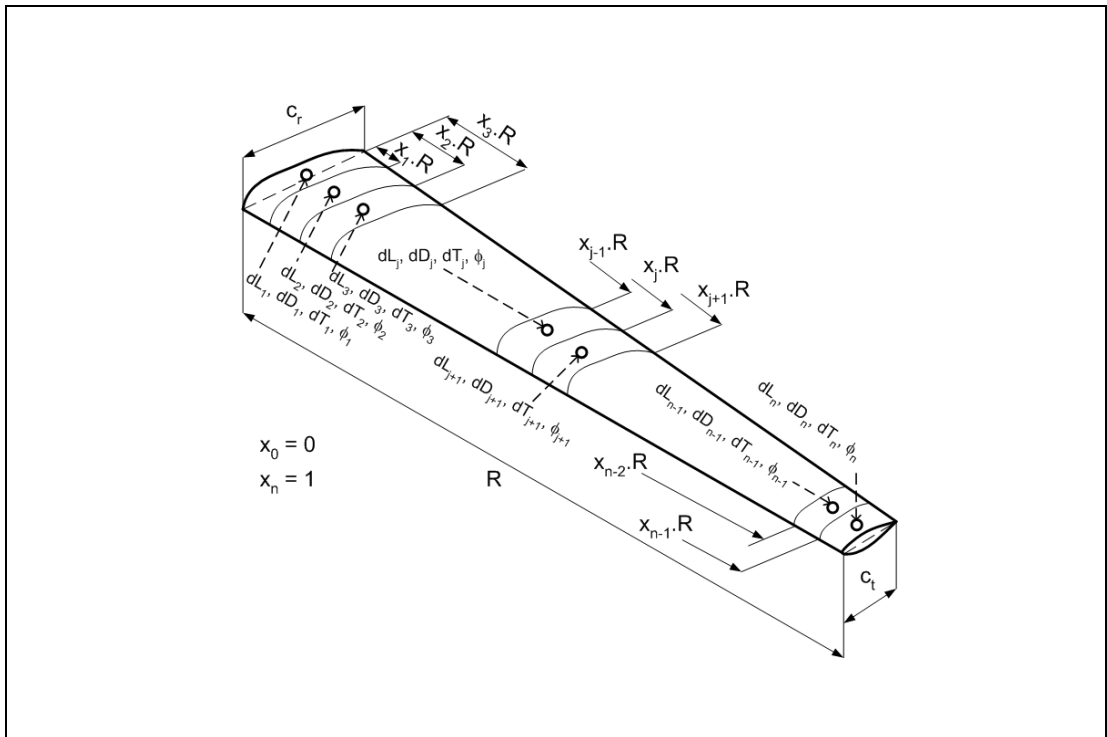$$M_\theta = \sum_{j=1}^{n} dM_j$$

<div align="right">(A2.6)</div>

Figure A2.1   Blade Element Arrangement